



HAL
open science

**EMISSION DE CENDRES PENDANT L'ACTIVITE
EXPLOSIVE DES VOLCANS ITALIENS EN ZONE
DISTALE : ESTIMATION, CARACTERISATION
PHYSICO-CHIMIQUE ET CONTRUCTION D'UNE
BASE DE DONNEE POUR MIEUX EVALUER LES
ALEAS VOLCANIQUES DANS LE SUD DE L'ITALIE.**

Benoît Caron

► **To cite this version:**

Benoît Caron. EMISSION DE CENDRES PENDANT L'ACTIVITE EXPLOSIVE DES VOLCANS ITALIENS EN ZONE DISTALE: ESTIMATION, CARACTERISATION PHYSICO-CHIMIQUE ET CONTRUCTION D'UNE BASE DE DONNEE POUR MIEUX EVALUER LES ALEAS VOLCANIQUES DANS LE SUD DE L'ITALIE.. Sciences de la Terre. Università degli studi di Pisa; Université Paris Sud - Paris XI, 2010. Français. NNT: . tel-00545633

HAL Id: tel-00545633

<https://theses.hal.science/tel-00545633>

Submitted on 10 Dec 2010

HAL is a multi-disciplinary open access archive for the deposit and dissemination of scientific research documents, whether they are published or not. The documents may come from teaching and research institutions in France or abroad, or from public or private research centers.

L'archive ouverte pluridisciplinaire **HAL**, est destinée au dépôt et à la diffusion de documents scientifiques de niveau recherche, publiés ou non, émanant des établissements d'enseignement et de recherche français ou étrangers, des laboratoires publics ou privés.

Università di Pisa

Dipartimento di Scienze della Terra

Université de Paris Sud 11

*Interactions et Dynamique
des Environnements de Surface*

Doctor's degree in Earth Science

Final dissertation

**CONTRIBUTION OF DISTAL ASH DEPOSITS TO THE
KNOWLEDGE OF EXPLOSIVE ACTIVITY OF
ITALIAN VOLCANOES INSIGHTS FOR HAZARD
ZONATION.**

Benoît Caron

Advisor:

Prof. Roberto Santacroce

(Univ. di Pisa, Italia)

Co-advisor:

Dr. Giuseppe Siani

(Univ. Paris Sud, France)

Commission:

Dr. Martine Paterne (LSCE, France)

Prof. Mauro Rosi (Univ. di Pisa, Italia)

Prof. Raffaello Cioni (Univ. di Cagliari, Italia)

Referee:

Dr. Martine Paterne (LSCE, France)

Prof. Costanza Bonadonna (Univ. de Genève, Suisse)

Pisa, December 2009



This PhD project is co-supported by Vinci program of **Università Italo-Francese** and of SETCI from region of **Île-de-France**. ^{14}C AMS of the sediment core MD 90-918 were supported by **ARTEMIS**.

This PhD project was in collaboration with **Dr. Martine Paterne** (Laboratoire des Sciences du Climat et de l'Environnement, LSCE, Gif-sur-Yvette, France), **Dr. Roberto Sulpizio** (Dipartimento Geomineralogico, Univ. di Bari, Italy) and **Dr. Giovanni Zanchetta** (Dipartimento di Scienze della Terra, Univ. di Pisa, Italy).

Abstract

In addition to the destruction of the sites close to the volcanoes, the accumulation of volcanic ash in distal zones can cause damage to buildings (i.e. roof collapses), the interruption of lifelines (roads, railroads, etc), closure of airports and disturbance to the communications and powerlines. These effects surely occurred in the past in the Neapolitan area and in wide part of southern Italy, affected by the deposition of ash mainly from Neapolitan volcanoes, but the evaluation of the related hazard is not fully addressed in present day mitigation plans.

The detailed study of the dispersion, joined with the physical and geochemical characterization, of distal pyroclastics deposits produced by explosive eruption of Italian volcanoes during late Quaternary was the focus of the presented PhD project. In the investigated time span, which mainly encompasses Upper Pleistocene and Holocene, explosive activity occurred at Somma-Vesuvius, Phlegrean Fields, Aeolian Islands, Mount Etna, Pantelleria, Ischia and Procida volcanoes. The distal deposits from these volcanoes were investigated through the tephrostratigraphic study of three lacustrine cores from Lake Shkodra (Albania), and Albanian side of Lake Ohrid (Macedonia/Albania border), and one marine core from the northern Ionian Sea.

As a whole, twenty-two tephra layers were recognised, all from explosive eruptions of south Italy volcanoes. Their multidisciplinary study includes stratigraphy, stable isotope ($\delta^{18}\text{O}$), AMS ^{14}C datings, paleomagnetism, content of organic carbon and geochemistry. Seventeen tephra layers were correlated with terrestrial proximal counterparts and with both marine and lacustrine tephra layers already known in the central Mediterranean area.

A total of nine tephra layers were recognised in the cores from Lake Shkodra, which were correlated with six different Holocene explosive eruptions: A.D. 472 and Avellino (ca. 3.9 cal. ka BP) from Somma-Vesuvius, FL (ca. 3.4 cal. ka BP) from Mount Etna, Astroni (ca. 4.2 cal. ka BP), Agnano Monte Spina (ca. 4.5 cal. ka BP) and Agnano Pomici Principali (ca. 12.3 cal. ka BP) from Phlegrean Fields.

Five tephra layers were recognised in the core from the Albanian side of Lake Ohrid, and correlated to P11 tephra layer (131 ka) from Pantelleria Island, X6 (107 ka) of generic Campanian origin, Campanian Ignimbrite-Y5 and SMP1-Y3 (39 and 31 ka, respectively) from Phlegrean Fields, and FL (ca. 3.4 cal ka BP) from Etna Volcano.

Eight tephra layers were recognised in the marine core. The oldest one was tentatively correlated to the Monte Guardia eruption (ca. 22 ka BP) from Lipari Island., which was the source of other two tephra layers recognised in the core and correlated to the Gabelotto-Fiumebianco (E-1 tephra layer, ca. 8.6 cal ka BP) and to the Monte Pilato (A.D. 1200) eruptions. The other five tephra layers have all Na-phonolitic composition, which clearly indicates the Somma-Vesuvius as the source. This unique composition indicates the Mercato deposits (ca. 8.9 cal ka BP) as proximal counterparts, but poses some problems with correlation of tephra layers deposited over 2000 years with a single eruption. This suggests the occurrence of interplinian activity between the eruptions of Mercato (ca. 8.9 cal ka BP) and Avellino (ca. 3.9 cal ka BP), which is poorly documented in the proximal stratigraphic succession.

All the data from the studied cores were collated into a Geographic Information System of the Central Mediterranean, and integrated with existing literature data. This data-base implemented in a GIS environment allows a significant improvement in the knowledge of the ash dispersal in the Central Mediterranean area, with a significant enlargement of the previous assessed dispersal areas. The GIS data-base represents an useful tool for the improvement of volcanic hazard mitigation in southern Italy and central Mediterranean area.

Remerciements

J'ai tenu à écrire mes remerciements dans ma langue natale afin de pouvoir choisir mes mots et exprimer pleinement toute ma gratitude aux nombreuses personnes qui m'ont permis de réaliser cette thèse.

En tout premier lieu, je tiens à remercier le Professeur Roberto Santacroce qui m'a accordé toute sa confiance. Il m'a m'orienté dans mes recherches et a toujours été disponible pour répondre aux questions que je me posais. Il a partagé sa connaissance et son expérience des volcans italiens et ses remarques pertinentes et constructives m'ont permis d'avancer tout au long de ce travail. Je l'en remercie profondément.

Je remercie aussi Giuseppe Siani, sans qui cette thèse n'aurait pas pu voir le jour. L'aventure a commencé en 2006 lorsqu'il m'a m'orienté vers l'Università di Pisa où je suis allé passer un concours à l'issue duquel j'ai obtenu un financement de thèse. Grâce à lui, une fructueuse collaboration s'est mise en place entre l'Italie et la France. Il est aussi à l'origine de la collaboration entre différentes équipes pour l'étude des sites de Shkodra et Ohrid. Je le remercie pour nos discussions scientifiques et son aide précieuse notamment pour les observations sous microscope binoculaire.

Merci à Martine Paterne qui m'a accueilli chaleureusement au sein de son équipe du LSCE. Elle s'est montrée d'une grande disponibilité et m'a toujours donné de précieux conseils. Je remercie aussi Giovanni Zanchetta et Roberto Sulpizio. Ils m'ont tous les deux suivi, aidé, guidé depuis le début. Que ce soit en laboratoire, en campagne, derrière un ordinateur ou en partageant un déjeuner, ils m'ont donné la motivation et les moyens pour avancer.

J'adresse également mes remerciements à Costanza Bonadonna, Martine Paterne, Raffaello Cioni et Mauro Rosi, pour l'intérêt qu'ils ont porté à mon travail en tant que referees et membres du Jury.

Je tiens maintenant à remercier toutes les personnes qui m'ont permis d'obtenir l'ensemble des données de cette thèse et avec qui j'ai apprécié de travailler :

- toutes les personnes du LSCE et plus particulièrement Fabien Devilde pour sa compétence et sa rigueur concernant les isotopes stables (^{18}O et ^{13}C), Christine Katté et Caroline Gauthier pour les études du Carbone Organique, Gulay Isguder pour son aide en laboratoire et François Guichard pour ses enrichissantes discussions.

-
- Franco Colarieti pour les préparations d'échantillons et sa gestion du SEM de Pisa, et Michel Fialin et Frederic Couffignac du service CAMPARIS.
 - Elena Zanella, Edivokia Tema et Roberto Lanza de m'avoir accueilli au "Alpine Laboratori of Paleomagnetism" de Pederagno. Merci aussi pour leur grande contribution.
 - Marina Bisson et à Glaria Isola de l'INGV de Pisa pour leurs conseils en matière de GIS.
 - Donnatela Insinga (IAMC, Napoli) pour m'avoir permis d'embarquer sur la campagne océanographique de janvier 2008 à bord de l'Urania.
 - Anne-Marie Lézine, Soumaya Belmecheri et Amandine Bordon (LSCE), Sonia La Felice (Univ. di Palermo) et Aurélien van Welden (LGCA) pour leurs collaborations et discussions concernant les carottes des lacs d'Ohrid et de Skhodra (Albanie).
 - Virginie Metrot et Renato Papa pour leur aide informatique.
 - Mesdames Burchianti, Raboux et Ho pour leur gentillesse et leur aide administrative.

Cette thèse était co-financée par l'Université franco-italienne grâce au Programme Vinci et par la région Île-de-France grâce au programme SETCI. Les datations ^{14}C AMS de la carotte sédimentaire MD 90-918 ont été financées par ARTEMIS.

Ces trois dernières années ont été partagées entre l'Italie et la France, Paris et Pisa, universités, laboratoires et institutions. J'ai par conséquent rencontré énormément de personnes avec qui j'ai pu travailler, discuter, partager un bureau ou un simple café. La liste est bien trop longue mais je les remercie tous pour leur sympathie, leur bonne humeur et leur amitié.

Puis, et pas le moindre, je tiens à remercier toute ma famille et tous mes amis de Daux, Toulouse, Paris, Pisa, Castrovillari (là aussi la liste est très très longue), qui m'ont accompagné jour après jour. Merci à mes parents qui m'ont toujours soutenu tout au long de mon parcours et qui m'ont permis de m'épanouir dans ma passion. À mon frère sur qui j'ai toujours pu compter. J'ai aussi une pensée particulière et un souvenir ému de mon grand-père.

À toi, qui m'a soutenu et encouragé, qui m'a poussé et motivé. Nous avons partagé des moments forts. Nous avons traversé cette épreuve. Et La Vache Miou-Miou....



INTRODUCTION:	17
----------------------------	-----------

I. CHAPTER I: VOLCANIC GENERALITY, CENTRAL MEDITERRANEAN GEODYNAMIC CONTEXT AND VOLCANIC ACTIVITY..... 23

I.1. VOLCANO HISTORY	25
I.1.1. <i>Why to reconstruct the history of a volcano?</i>	25
I.1.2. <i>How to study a volcano? How to reconstruct the volcanoes history?</i>	26
I.2. TEPHROSTRATIGRAPHY & TEPHROCHRONOLOGY:	31
I.2.1. <i>Geochemical tephra identification</i>	32
I.2.2. <i>Relationship between tephra and chronology methods</i>	34
I.2.3. <i>Campanian Ignimbrite Y-5 example:</i>	35
I.3. FROM THE GENERAL GEODYNAMIC CONTEXT OF MEDITERRANEAN BASIN TO THE ITALIAN	36
I.4. CENTRAL MEDITERRANEAN VOLCANISM:	45
I.4.1. <i>Campanian Province</i>	47
I.4.1.1. The Mount Somma-Vesuvius	48
I.4.1.2. Phlegrean Fields	53
I.4.1.3. Island of Ischia	57
I.4.1.4. Island of Procida-Vivira	58
I.4.2. <i>Roman province</i>	59
I.4.2.1. Alban Hills	60
I.4.2.2. Sabatini Volcanic District	60
I.4.3. <i>Aeolian province</i>	61
I.4.3.1. Island of Lipari	62
I.4.3.2. Island of Vulcano	64
I.4.3.3. Island of Stromboli	66
I.4.3.4. Island of Salina	68
I.4.4. <i>Sicilian province</i>	68
I.4.4.1. Mount Etna	69
I.4.5. <i>Sicily Channel</i>	72
I.4.5.1. Pantelleria	72
I.4.6. <i>Resumed volcanic activity of Italian volcanoes</i>	73
I.5. DISTAL RISKS AND HAZARDS	78

II. CHAPTER II: MATERIAL AND METHODS 83

II.1. PISTON CORE DRILLING LOCATIONS	85
II.1.1. <i>Shkroda</i>	86
II.1.2. <i>Ohrid JO-2004</i>	86
II.1.3. <i>MD 90-918</i>	88
II.2. CORES DESCRIPTION AND SAMPLING	88
II.2.1. <i>Shkroda</i>	88
II.2.2. <i>Ohrid JO-2004</i>	89
II.2.3. <i>MD 90-918</i>	90
II.3. ISOTOPIC STUDIES	91
II.3.1. <i>MD 90-918</i>	91
II.4. CHRONOLOGY	93
II.4.1. <i>Shkroda</i>	95
II.4.2. <i>Ohrid JO-2004</i>	95
II.4.3. <i>MD 90-918</i>	96
II.5. MAGNETIC SUSCEPTIBILITY	97
II.5.1. <i>Shkroda</i>	97
II.5.2. <i>Ohrid JO-2004</i>	97
II.5.3. <i>MD 90-918</i>	98
II.6. CARBON ORGANIC CONTENT	99
II.6.1. <i>MD 90-918</i>	99

II.7.	TEPHROSTRATIGRAPHY	100
II.7.1.	<i>Shkroda</i>	101
II.7.2.	<i>Ohrid JO-2004</i>	101
II.7.3.	<i>MD 90-918</i>	101
II.8.	GEOCHEMICAL ANALYSES	102
II.8.1.	<i>Geochemical analyse instruments</i>	102
II.8.2.	<i>Intercalibration of analyse instruments</i>	103
II.8.3.	<i>Tephra's classification</i>	106
II.9.	GEOGRAPHIC INFORMATION SYSTEM (GIS)	106

III. CHAPTER III: THE HOLOCENE TEPHROSTRATIGRAPHIC RECORD OF LAKE SHKODRA (ALBANIA AND MONTENEGRO) 115

III.1.	ABSTRACT	119
III.2.	INTRODUCTION	119
III.3.	SITE DESCRIPTION	120
III.4.	MATERIALS AND METHODS	121
III.5.	LITHOSTRATIGRAPHY AND MS OF THE CORE SEDIMENTS	122
III.6.	GLASS AND MINERAL COMPOSITION OF THE TEPHRA LAYERS	122
III.7.	DISCUSSION	123
III.7.1.	<i>Correlation with proximal deposits and other distal archives.</i>	123
III.7.2.	<i>Deposition environment and sedimentation rates</i>	126
III.8.	CONCLUSION	128
III.9.	REFERENCES	129
III.10.	APPENDIX	131

IV. CHAPTER IV: THE LATE HOLOCENE TO PLEISTOCENE TEPHROSTRATIGRAPHIC RECORD OF LAKE OHRID (ALBANIA) 139

IV.1.	ABSTRACT - RESUME	144
IV.2.	INTRODUCTION	145
IV.3.	SITE DESCRIPTION	145
IV.4.	MATERIALS AND METHODS	146
IV.5.	RESULTS	148
IV.5.1.	<i>Cryptotephra JO-941</i>	148
IV.5.2.	<i>Cryptotephra JO-575</i>	148
IV.5.3.	<i>Cryptotephra JO-244</i>	148
IV.5.4.	<i>Cryptotephra JO-187</i>	149
IV.5.5.	<i>Cryptotephra JO-42</i>	149
IV.6.	DISCUSSION	149
IV.6.1.	<i>Correlation of tephra layers</i>	149
IV.6.1.1.	<i>Cryptotephra JO-941</i>	149
IV.6.1.2.	<i>Cryptotephra JO-575</i>	150
IV.6.1.3.	<i>Tephra JO-244</i>	151
IV.6.1.4.	<i>Tephra JO-187</i>	151
IV.6.1.5.	<i>Cryptotephra JO-42</i>	152
IV.6.2.	<i>Significance of tephra layers in Lake Ohrid</i>	152
IV.7.	CONCLUSION	153
IV.8.	ACKNOWLEDGEMENTS	155
IV.9.	REFERENCES	156
IV.10.	FIGURE CAPTIONS.....	164
IV.10.	FIGURES.....	168

V. CHAPTER V: LATE PLEISTOCENE-HOLOCENE TEPHROSTRATIGRAPHIC RECORD FROM THE IONIAN SEA: INSIGHTS FOR THE EXPLOSIVE ACTIVITY OF ITALIAN VOLCANOES.	181
ABSTRACT.....	186
V.1. INTRODUCTION	187
V.2. MATERIAL AND ANALYTICAL METHODS	188
<i>V.2.1. Tephrostratigraphy and chemical analysis</i>	<i>188</i>
<i>V.2.2. Stable isotope analysis</i>	<i>190</i>
<i>V.2.3. Radiocarbon datings</i>	<i>190</i>
<i>V.2.4. Magnetic sampling and measurements</i>	<i>191</i>
V.3. CHRONOLOGICAL FRAMEWORK	191
V.4. RESULTS	192
<i>V.4.1. Rock-magnetism</i>	<i>192</i>
<i>V.4.2. Tephra layers</i>	<i>193</i>
V.5. DISCUSION	195
V.6. CONCLUSIONS.....	199
ACKNOWLEDGEMENTS:.....	200
REFERENCES	200
FIGURE AND TABLE CAPTIONS	210
FIGURE.....	212
VI. CHAPTER VI: CONCLUSION AND PERSPECTIVES.....	235
REFERENCES.....	245
ANNEXES	277

Introduction:

The Central Mediterranean area is at high volcanic risk, because it is densely inhabited and with many vulnerable infrastructures. Beyond the hazard and risk in areas close to the volcanic centers, the accumulation of volcanic ash in distal zones often represents an underestimated hazard. Ash accumulation can cause important damage to building roofs, interruptions of lifelines (motorways, roads, railways, etc.), closure of airports, and disturbance to communications and power lines. Airborne fine particles affect human and animal health causing respiratory problems, the pollution of water resources, and pasture contamination. Therefore, a better estimate of volcanic ash dispersal would greatly improve the volcanic hazard mitigation plans.

In the last thirty years, many tephrostratigraphic studies were carried out in the Central Mediterranean zone, but the data presented in this study cover gaps in the geographic distribution of studied sites, since three of the studied cores are from Balkan lakes and the fourth from the north Ionian Sea.

The studies presented in this PhD manuscript are the result of a three-year work in close collaboration between the Dipartimento di Scienze della Terra (University of Pisa, Pisa, Italy), the Dipartimento Geomineralogico (University of Bari, Bari, Italy), the Interactions et Dynamique des Environnements de Surface laboratory (CNRS – University of Paris Sud XI, Orsay, France) and the Laboratoire des Sciences du Climat et de l'Environnement (CNRS – CEA – UVSQ, Gif-sur-Yvette, France). Moreover, various collaborations were developed with the Laboratoire de Géodynamique des Chaînes Alpines (University of Savoie, Le Bourget du Lac, France), the LSCE of Orme des Merisiers (Saclay, France), the Alpine Laboratory of Paleomagnetism (University of Torino, Peveragno, Italy), Camparis laboratory (Paris, France) and the Istituto per l'Ambiente Marino Costiero (CNR, Napoli, Italy).

During these three years PhD thesis I have studied 3 sites in the Central Mediterranean area, with the aim to estimate the dispersal of volcanic ash from the various Italian volcanoes. This is an invaluable tool for supporting the volcanic hazard related studies and stratigraphy of continental, lacustrine and marine environments during Quaternary. The study of tephra layers requires a multidisciplinary approach, and in this manuscript they are characterised by physical, chemical or chronological points of view.

The presentation of this work is thus articulated on six chapters.

To complete successfully this research project, we need the best possible knowledge of ash deposition in the past, which represents the key for predicting future behaviour. Most of the information about ash dispersal in the past comes from the available literature, and is summarised in the first chapter of this manuscript.

In the second chapter is described the materials and methods which were used during this research. The used techniques include geochemistry, stable isotopes, chronology, tephrostratigraphy, and palaeomagnetism. All the collected data from both literature and the study of the three new cores were collated into a Geographical Information System (GIS), which represent a large data base of ash dispersal in the Central Mediterranean area.

The three successive chapters are dedicated at the study of the main sites that were studied during this PhD: Lake Shkodra (Montenegro/Albania border), Lake Orhid (Albania/Macedonia border) and the north part of the Ionian Sea. Four sedimentary cores were studied for tephra layers and cryptotephra. These chapters represent articles that were accepted or submitted to international journals.

Finally in the last chapter I present a general conclusion of the PhD manuscript and the perspectives.



I. Chapter I: Volcanic generality, Central Mediterranean geodynamic context and volcanic activity.

I.1. Volcano History

I.1.1. Why to reconstruct the history of a volcano?

Story of a volcano is composed of accumulation of building and destructing phases. These phases can be dangerous and can cause several damages to human population and to infrastructures. So, to understand how is dangerous a volcano, we need to know the history of the volcano. Better is the knowledge of a volcano, better will be the management of the risk and the danger which it represents. The good knowledge of volcano's story is the key to anticipate the future eruption and to protect in priority the population and the infrastructures.

In present, there are more than 1300 volcanoes all around the Earth and less of the half (600) in the earth's surface (**Figure 1-1**). Millions of persons live in close zones volcanoes.

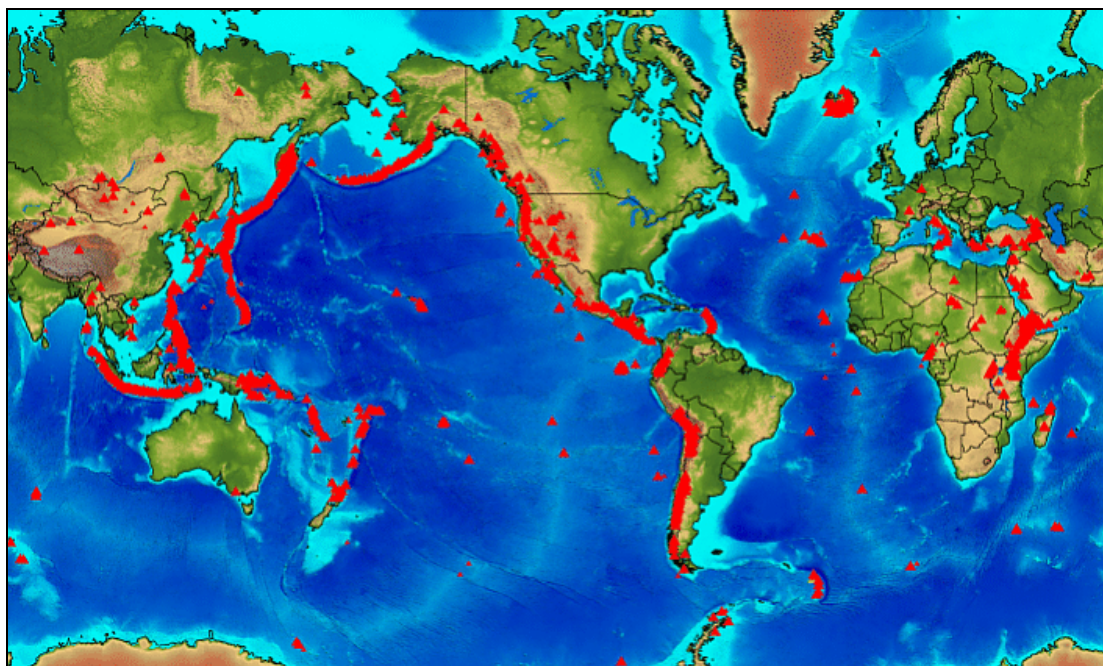


Fig. 1-1: Location of volcanoes all over the world (from United States Geological Survey website at <http://www.usgs.gov/>).

For this PhD research project, I have focusing on the Central Mediterranean area. This area is considered as one of the most geodynamically active, with a large number of volcanoes which frequently produced intense explosive eruption (*Peccerillo, 2005; Beccaluva et al., 2007; Oppenheimer and Pyle, 2009*). Even if there are various volcanic complex all

around the Mediterranean, I have focused my research close the Italy and by consequence on the Italian volcanic activities. To reconstruct the volcanic history and the volcanic ash dispersions of this area, I have searched volcanic deposits far from the aim volcanic sources, using the tephrostratigraphy methods. Tephrostratigraphy is a powerful tool that is widely applied to volcanology, Quaternary sciences, palaeoceanography or archaeology. This is particularly true in the central Mediterranean region, which bore witness to frequent and powerful volcanic explosive activity during both Holocene and Late Pleistocene (*Keller, 1978; Paterne et al., 1988, 1990; Mahood and Hildreth, 1986; Poli et al., 1987; Santacroce, 1987; Vezzoli, 1988; Pappalardo et al., 1999; Coltelli et al., 2000; De Vivo et al., 2001; Siani et al., 2004; Sulpizio et al., 2003; Wulf et al., 2004; Di Vito et al., 2008; Santacroce et al., 2008*). Moreover, the evaluation of the hazard associated with the ash deposition is not fully addressed in present day mitigation plans of the Mediterranean Central Zone (*Cioni et al., 2003; Sulpizio, 2005*).

So, to understand the volcanic hazard and to allow the development of mitigation plan to protect the populations and the infrastructures, we have to study these edifices and more especially the related complex history.

1.1.2. How to study a volcano? How to reconstruct the volcanoes history?

The life of a volcanic edifice can last several hours or can last several millions of years. During its live, it will know various eruptive styles which will change the morphology of the edifice. The effusive and the explosive styles are a consequence of an overpressure within the volcano complex but the effusive style generates lava flows or domes, while the explosive style generates pyroclastic material.

The Central Mediterranean geodynamic context is extremely complex (*e.g. Turco and Zupetta, 1998; Gueguen et al., 1998; Cadoux et al., 2007*) and volcanoes extremely active (*Keller, 1978; Paterne et al., 1988, 1990, 2008; Wulf et al., 2004, 2008; Santacroce et al., 2008*).

The Central Mediterranean is the place of an intense and varied volcanic activity since the Quaternary. The majority part of the various eruptive activities has affected this area (*Pyle et*

al., 2006; Sulpizio et al., 2009). The volcanic products of these eruptive activities were able to scatter in all this area.

The story and the evolution of magma affect the eruptive style and also the eruptive activity. In fact, the volcano eruptive styles are subdivided in a classification of several eruptive activities. The mains eruptive activities are: Hawaiian, Strombolian, Vulcanian Subplinian, Plinian, Ultraplinian, Surtseyan and Phreatoplinian (**Figure 1-2**; *Walker, 1973*).

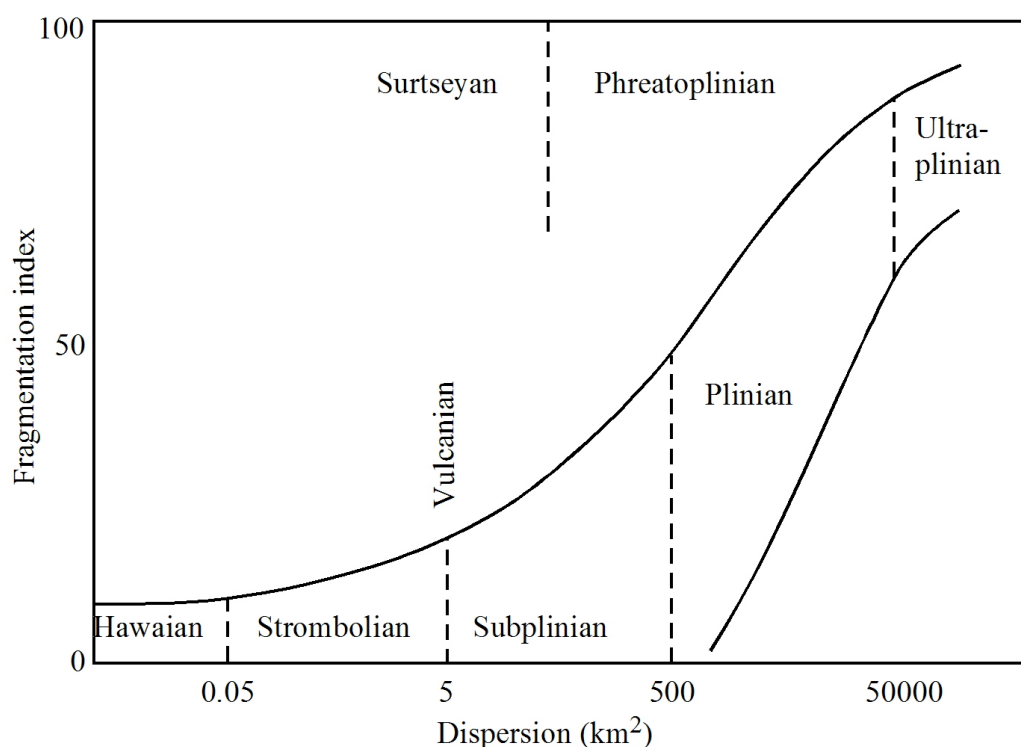


Fig. 1-2: Dispersal area (D in km²) vs fragmentation index (F%) from Walker (1973).

All the eruptive activities product volcanic ash which will be dispersed far from the origin sources.

In the case of less powerful explosive eruptions, the generated plumes carry material at weak heights. The dispersal ash area can cover few km² and the products fall near the origin event for the less intensive activity (e.g. Strombolian activity of Paricutin 1943-1952, over 10 km², *Pioli et al., 2008*). Concerning the more intensive eruption, the generated plumes can be some ten kilometers height and the ash particles can be dispersed over considerable distances can cover some thousands km² (e.g. the Y-5 Campanian Ignimbrite from Phlegrean Fields (39.3 ka) has cover area between 1.5 to 3.10⁶ km², *Barberi et al., 1978; Pyle et al., 2006*).

Walker (1973) had classified the height of eruption column in relation with the explosiveness and the eruption activities (**Figure 1-3**). Some of the most frequent eruptive activities are described quickly in the next paragraphs.

The Hawaiian eruptive activities are named after the predominant style of activity observed at the currently active volcanoes of the Hawaiian Island. Hawaiian eruptions are characterized by their lava fountain (**Figure 1-4 a**) which are ejected from the vent at speeds of around 100 m.s^{-1} and typically rise to heights of a ten to hundreds of meters above the vent (**Figure 1-3**). The lava has a very high temperature ($> 1100^\circ\text{C}$) and a geochemical composition poor in silica. Lava flows are generated by this eruptive activity.

The Strombolian eruptive activities are characterized by consist discrete explosions of short duration (**Figure 1-4 b**). It is named after the volcanic island Stromboli in Mediterranean Sea. Each explosion generates a small ash plume which is usually of some hundreds high (**Figure 1-3**) and throws out large incandescent blocks. The volume of material produced by each explosion is small, some cubic meters.

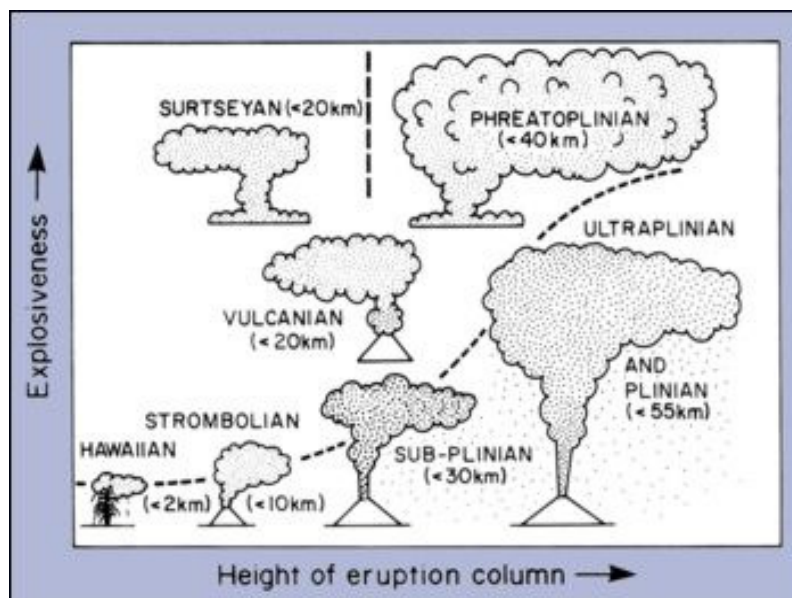


Fig. 1-3: Plume classification from Walker (1973).

The Plinian eruptive activities are subdivided into sub-Plinian, Plinian and ultra-Plinian style of activities which are based on their mass flux and plume heights (**Figure 1-4 c1 and c2**). This activity type is named after Pliny the Younger who wrote an account of the

79 A.D. eruption of the Mount Somma-Vesuvius. In eruptions of this kind a jet of gas and magma clasts emerges from the vent at speeds of around $100\text{-}600\text{ m.s}^{-1}$ and forms a convecting plume in the atmosphere (**Figure 1-3**). These plumes rise to heights of several kilometers to many tens of kilometers. Larger clasts are carried upwards only a short distance and fall to the ground close the vent. The smallest are carried to greater heights and fall out further from the vent. Generally, Plinian eruptions involve magmas which are relatively rich in silica and in dissolved gas, are very viscous and have a low temperature. Moreover, this eruptive activities generate pyroclastic current density called too pyroclastic flow or pyroclastic surge or nuée ardente. They are the aim consequences of an unstable eruptive column which collapses. They are destructive and have devastating effects. Pyroclastic flow is a hot cloud of volcanic ash and blocks, magmatic gas and air which flows along the ground at a very high speed (*Lacroix, 1904*).

The Vulcanian eruptive activities are characterized by discrete or transient explosions (**Figure 1-4 d**). They are more evolved magmas than those causing by Strombolian eruption. Typically, Vulcanian explosions last a number of seconds or minutes and often occur in sequences with repose times between explosions varying from tens of minutes to hours. Vulcanian explosions can be extremely violent events with velocities range between 200 and 400 m.s^{-1} . They can eject blocks a few meters size out to distance of some km to the vent. The generated eruption plumes by the Vulcanian eruptions carry finer material to heights of several kilometers (**Figure 1-3**).

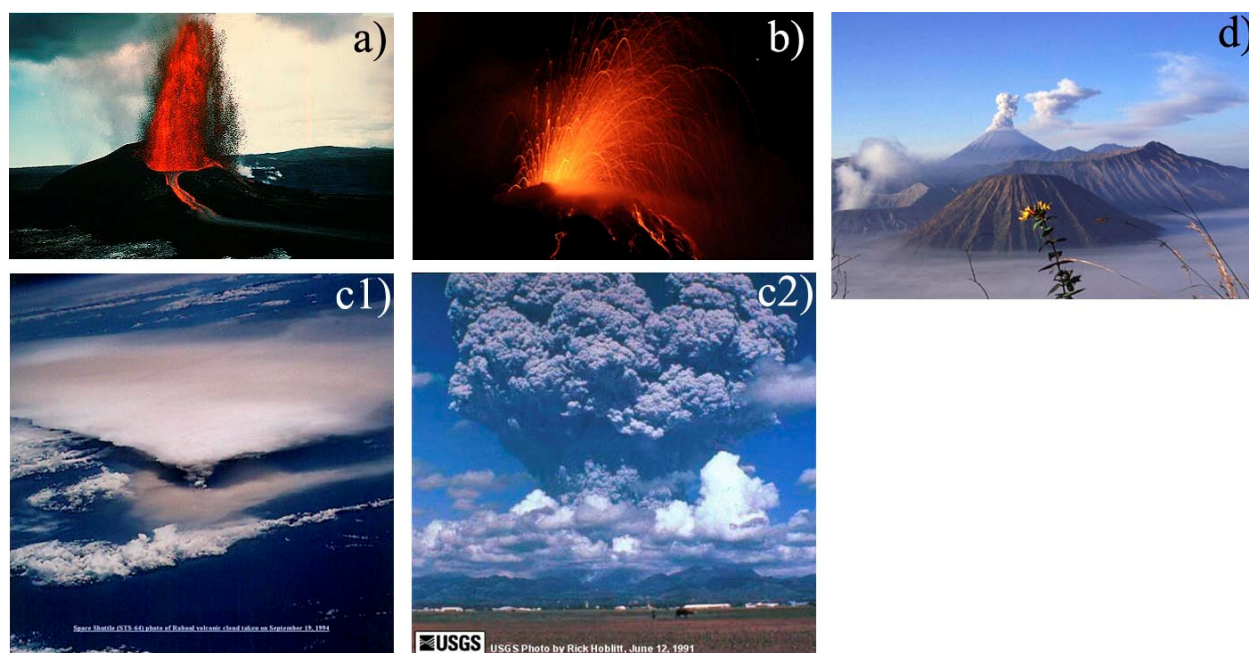
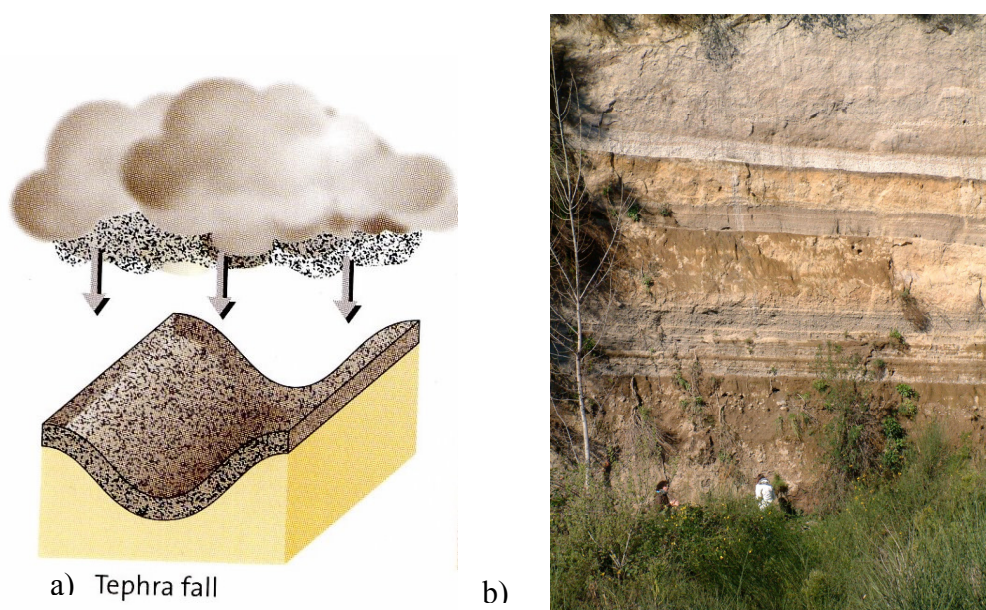


Fig. 1-4: Pictures of some eruptive activities: a) Hawaiian (Hawaii, 1983), b) Strombolian (Stromboli, 2008), c1) Subplinian (Rabaul, 1994), c2) Plinian (Pinatubo, 1991), d) Vulcanian (Semeru, 2003).

In the Quaternary period, all the mains eruptive activities have affected the Central Mediterranean zone. So, to complete successfully this research project, we have to keep in mind that all volcanic products can be the consequence of various eruptive activities.



a) Tephra fall

b)

Fig. 1-5: a) Sketch of tephra fall deposit and b) picture of fallout deposits from the Mt Somma-Vesuvius.

So, close the volcano or in proximal areas is possible to study the volcanic deposit to reconstruct its story with geological stratigraphic studies (**Figure 1-5**). But this reconstruction is sometimes difficult or incomplete because of vegetation cover, erosion activity, building phase of the volcano which cover the oldest deposit, destructing phase of volcano which cancel a part of the story. For example, one study reveals that several phonolitic-trachytic tephra layers recognised in the Sulmona paleo-lake and dated between ca. 7,600 and 4,800 cal yr BP (*Giaccio et al., 2009*) have been interpreted as products of the Somma-Vesuvius activities. This correlation contradicts the proximal data.

Only a combination between the proximal and the distal studies allows the more complete reconstruction of a volcanic complex.

I.2. Tephrostratigraphy & tephrochronology:

Deciphering a complete eruption record from onshore geology is commonly problematic, due to burial by deposits from younger events, dense vegetation which obscures the geologic deposits, erosion, and catastrophic removal of deposit by flank collapse events. During explosive eruption, the volcanic deposits (i.e. pumice or glass shards, **Figure 1-6**) can be transported on very long distances and deposited thousands kilometers far from their sources. Then, these volcanic fallout deposits are integrated in marine or lake sediments and preserved. Tephra records in sediment cores collected by piston, gravity or vibrocoreing extend volcanic histories back by several tens of thousands of years (*Scheiddeger, 1973; Scheiddeger et al., 1980; Kennett and Thunell, 1975; Kennett et al., 1977; Thunnell et al., 1979; Keller et al., 1978; Sigurdsson et al., 1980; Paterne, 1985; Paterne et al., 1986, 1988, 2008; Le Friant et al., 2008*).

Distal tephra studies aim mainly at finding, at recognizing and at characterizing the tephra layers deposited far from their volcanic source and interbedded in sedimentary successions to correlate them with event eruptive known and dated. A tephra layer which is over wide areas and chronologically constrained, represents an isochronous marker layers that provide a useful tool for correlating sedimentary successions in different environments. Most of the tephrostratigraphic researches deal with lacustrine or deep sea sediments successions which represent very preservative environments for fine grained distal tephra layers.

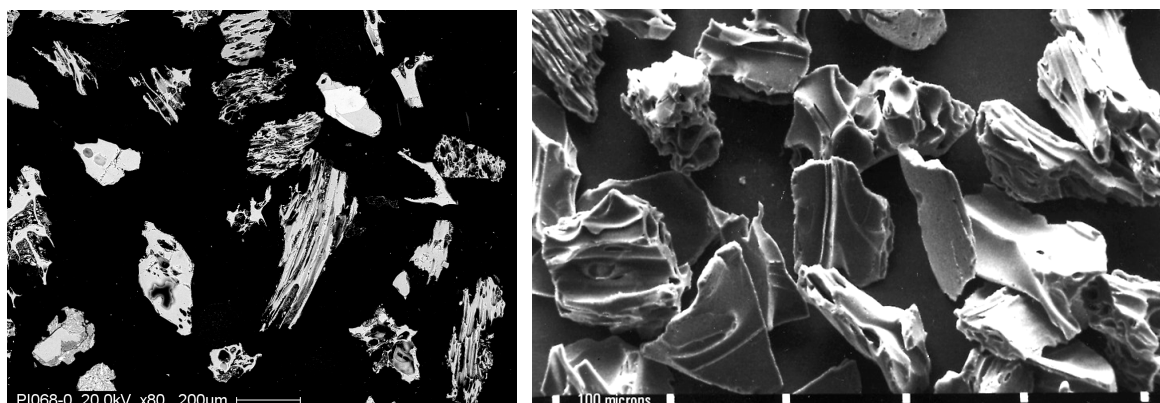


Fig. 1-6: SEM pictures of Y3 tephra.

In the last decades the tephrostratigraphy and tephrochronology works knew an important development and in a more consequent way these last years. To obtain the strongest correlation of tephra layers, a careful inspection of possible volcanic sources was required (*Paterne et al., 1988, 2008; Siani et al., 2004; Wulf et al., 2004, 2008*). We have to take in account the distance between the various volcanic sources and the studied sites, the eruption type, the wind directions and the magmatic chemistry from the sources.

Many papers were published aiming at identifying tephra marker layers in the Mediterranean area, both on land in lacustrine successions (*Narcisi, 1996; Munno et al., 2001; Wulf et al., 2004, 2008; Munno and Petrosino, 2006*) and in the Tyrrhenian, Ionian and Adriatic seas (*Keller et al., 1978; Paterne et al., 1986, 1988, 1990, 2008; Calanchi et al., 1998; Siani et al., 2004; Marciano et al., 2008*).

1.2.1. Geochemical tephra identification

Each volcanic complex possesses a specific mineralogical and geochemical signature (*Keller et al., 1978; Paterne, 1985; Paterne et al., 1986, 1988*) which depends per example of nature volcanism, of volcanic complex situation or of magma evolution. The analysis of major and trace elements allow identifying the source or more especially the eruption thanks the correlation with terrestrial deposits. For example and concerning the Italian volcanoes, *Wulf et al. (2008)* have reported many of them in a Total Alkali Silica (*Le Bas et al., 1986; Figure 1-7*). It is possible to shown several geochemical different compositions with major element. Here, *Wulf et al. (2008)* have defined several fields in correspondence of each volcanic source

with geochemical major elements of the glass composition. In this diagram, only SiO_2 , K_2O and Na_2O are considered but other major elements are important to discriminate geochemically the magmatic source or the different eruptions from a same volcanic complex like *Santacroce et al. (2008)* shown in the **Figure 1-8**.

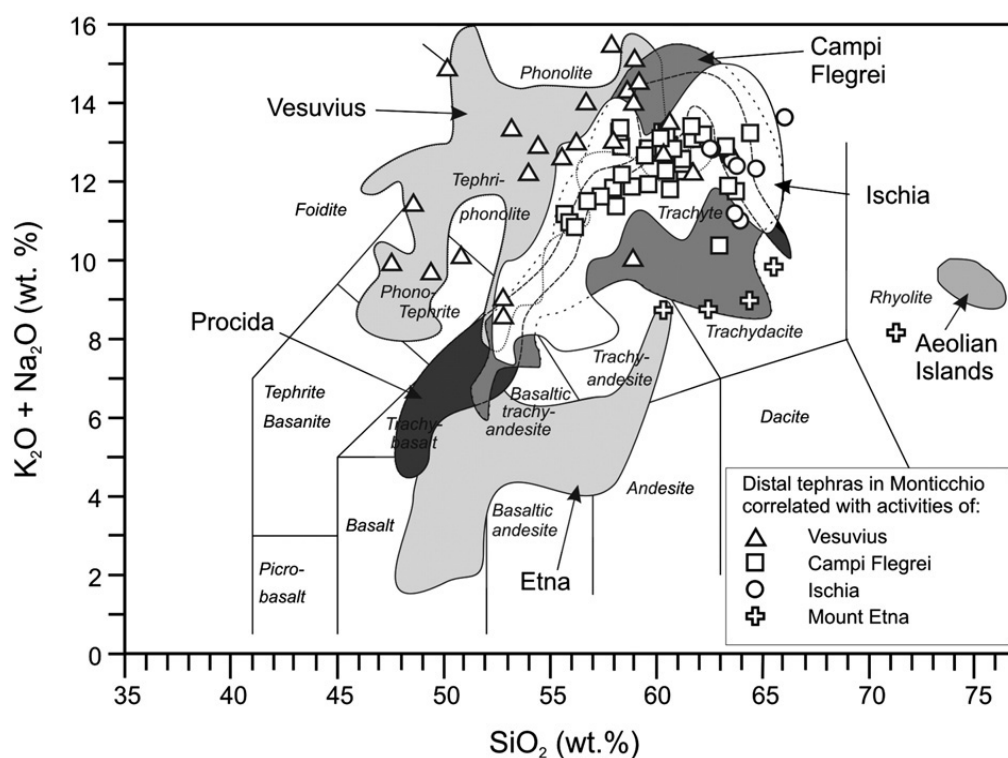


Fig. 1-7: Total alkali silica (TAS) plot of distal tephra (< 20,000 yr BP) occurring in the Lago Grande di Monticchio record from *Wulf et al. (2008)*.

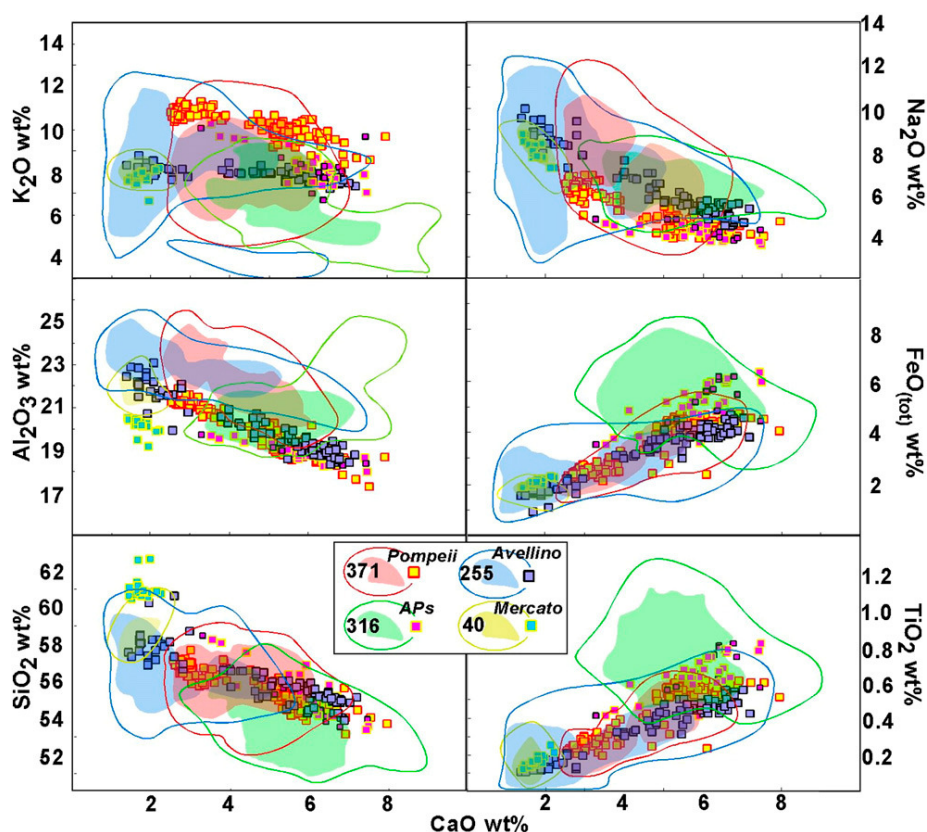


Fig. 1-8: Example of graphic element vs. element plots of whole rocks and glasses variation fields from the main explosive eruptions of the 8900 cal yr BP – A.D. 79 period, from Santacroce et al., (2008).

The tephrostratigraphic studies allow knowing the historic activity of each volcanic complex. The explosive volcano activities of the South of Italy or of Aegean Arc were studied from ash layers recognised in many marine cores of Mediterranean Sea or in many lacustrine cores of Italy, Balkans, Greece...) (e.g. Keller et al., 1978; Thunnell et al., 1979; Paterne et al., 1988; Paterne et Guichard, 1993; Siani et al., 2004; Wulf et al. 2004, 2008; Magny et al., 2007; Margari et al., 2007; Sulpizio et al 2008; Wagner et al., 2008b).

1.2.2. Relationship between tephra and chronology methods

The tephrochronological studies were developed with dating methods which represent important tools (e.g. Keller et al., 1978; Paterne et al., 1986, 1988). Indeed the ^{14}C , $^{40}\text{Ar}/^{39}\text{Ar}$, U/Th, varve studies, isotopic studies of ^{18}O or ^{13}C methods had given discriminated indications to obtain good correlation. The chronology of a tephra layers is obtained indirectly with the core rate sedimentation or on the core sediments close the tephra layer (Paterne,

1985). If the tephra layer is correlated to a well-known eruption, the dating of the terrestrial out-crops can be correlated to the core tephra layer.

Concerning the important volcanic eruptions, they can product important quantity of tephra which are dispersed over considerable area. So, when this event is recorded in a drilling core, and if it is turned out that the stratigraphic position in the core is just, then the tephra represents a strong chronological marker (e.g. *Ninkovich et Heezen, 1965, 1967; Keller et al., 1978; Thunnel et al., 1979; Paterne 1985; Paterne et al., 1986, 1988, 2008; Sulpizio et al., 2003, 2009; Wulf et al., 2004, 2008; Pyle et al., 2006*). In some cases, the other proxies (e.g. isotopic stratigraphy, pollen studies, ^{14}C dating...) cannot give the chronological scale for various reasons. So, the tephra layers of well-known eruption were using like chronological markers to build the chronological scale and permit to obtain the sediment rate of the sedimentary core.

1.2.3. Campanian Ignimbrite Y-5 example:

The Phlegrean Fields are the origin event of this eruption which has developed an eruptive column estimated at 44-45 km of altitude (*Rosi et al., 1999*). The volcanic deposits were found at more than 2,500 km far from the source (*Pyle et al., 2006*) and were recorded in around twenty drilling marine and lacustrine cores. From the Campanian Volcanic Zone to the Est part of the Mediterranean basin (core TR172-19, *Margari et al., 2007*), to the North of the Greece (e.g. *Cornell et al., 1983; Paterne, 1993*) and to the North part of the Black Sea (*Pyle et al., 2006*), the dispersed tephra area was estimated between 1.5 to 3.10^6 km² (**Figure 1-9; Pyle et al., 2006**). The Campanian Ignimbrite Y-5 eruption is dated at 39.3 ± 0.1 ka BP, using $^{40}\text{Ar}/^{39}\text{Ar}$ chronological method on crystals (*De Vivo et al., 2001*). Moreover, the Campanian Ignimbrite Y-5's tephra have a particular geochemical composition (trachyte to phonotrachyte) and morphology (*Vezzoli, 1991; Civetta et al., 1997; Signorelli et al., 2001; Pappalardo et al., 2002a*).

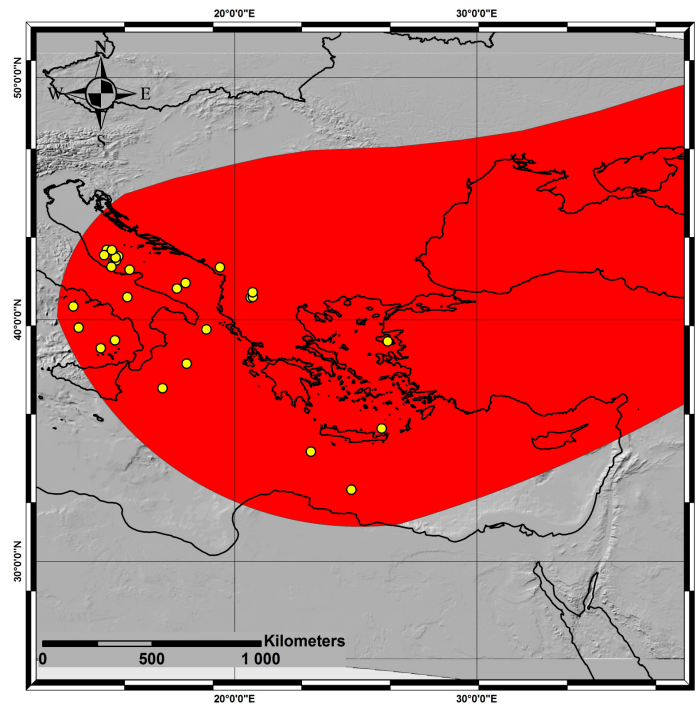


Fig. 1-9: General distribution of ash Y5 Campanian Ignimbrite, modified from Pyle et al. (2006).

This eruption, which is the most important of the last 100,000 years and has covered an important part of the Eastern Europe (Barberi et al., 1978; Pyle et al., 2006), represents a strong chronological marker due to his characteristics. It was the case for the Orhid core (Albania) study of this PhD research project (Chapter 4).

I.3. From the general geodynamic context of Mediterranean basin to the Italian

The arrangement of the Mediterranean area essentially results from the subduction of the African plate below the Eurasian one. This induced since the late Cretaceous, the progressive closure of the Tethys ocean basin, whose remnant is the Mediterranean Sea (Santacroce et al., 2003). In addition to Africa and Eurasia, other microplates are involved in Mediterranean tectonics.

For the geodynamic reconstructions, the Mediterranean area has always been a complicated puzzle. The main geodynamic factor controlling Mediterranean tectonics has

usually been considered to the relative motion of Africa and Europe as a consequence of different spreading rates along the Atlantic oceanic ridge. The Alpine orogen was considered to relate to collision between the Adriatic or African promontory and Europe (*Argand, 1916*). *Gueguen et al.* propose in 1998 four steps for the Neogene to recent overall tectonic evolution of the western Mediterranean area. He says that the opening of western Mediterranean mainly took place in the last 30 Ma, with genesis of irregular basins which migrated in age from west to east and not only over the influence of general N-S convergence which was responsible for the eastward escape of the Apennines (*e.g. Tapponnier, 1977; Boccaletti and Dainelli, 1982*).

The extension in the western Mediterranean and the growth of the Apenninic arc developed in the general frame of slow convergence between Africa and Europe, mainly after a terminal collisional episode in the Pyrenees at 20 Ma (**Figure 1-10**; *Mattauer and Séguret, 1971; Viallard, 1978, 1979; Gueguen et al., 1998*).

The geodynamic framework shows that the absolute plates motion directions of Europe and Africa are north-east oriented (*Smith et al., 1994; Ward, 1994*) and so the western Mediterranean was initiated during the Late Oligocene as the west-directed Apennines–Maghrebides subduction started (*Robertson and Grasso, 1995*). At this time, the main east-directed Alpine subduction had reached the continental collision stage leading to the flip of the subduction zone along the back-thrust belt of the Alpine orogen area where remnants of the oceanic Tethys were still present (*Dogliani et al., 1998*).

Guegen (1995) shows that during the 25–10 Ma time period, the Corsica–Sardinia block rotated 60° anticlockwise around a pole located at 42.7°N and 9.6°E (**Figure 1-11**). During the late Burdigalian, the Calabrian and Peloritani massifs began to separate from the Sardinia block with the opening of the Tyrrhenian area (i.e. Vavilov basin). At this time the Valencia trough was still opening, even if compression was still operating in the Balearic Islands. Due to the rotations of the continental blocks, the length of the Apenninic arc increased, leading to the break-up of the arc between the Balearic Islands and Sardinia and to the formation of an oceanic domain corresponding to an area of fan-shaped magnetic anomalies that can be observed in an aeromagnetic map of the Algerian basin (*Galdeano and Rossignol, 1977*). From the Late Oligocene, the North Algerian basin started to open by dislocation of its internal zones.

Then, from 10 to 5 Ma, the Liguro–Provençal basin, the Valencia trough and the North Algerian basin were almost completely opened at 10 Ma. The Numidian trough was closed and the Kabylia blocks were attached to Africa. During the opening of the North Algerian basin, coeval closure of the Numidian trough by roll-back of the subduction zone absorbed all of the convergence of Africa with respect to Europe. The northern arm of the arc (i.e. the Apenninic and Tyrrhenian area) was affected by eastward migration of compression in the eastern margin of the arc and extension followed immediately to the west. The Vavilov basin progressively reached the oceanisation stage during the Late Miocene–Early Pliocene, while the Marsili basin started to open (**Figure 1-12**), and Calabria was also affected by extensional tectonics. This jump in the extension process was marked by a change in direction of opening from N120° to N140°. This was probably controlled by the fact that the only oceanic domain in the foreland allowing easy subduction roll-back was (and still is) the Ionian Sea.

From 5 Ma to present, the Vavilov basin in the Tyrrhenian domain was almost completely opened and new oceanic crust began to form in the Marsili basin during the Late Pliocene (**Figure 1-13**). In the southern Apennines, interference of the subduction zone with thicker continental crust of the Apulian platform halted migration of the subduction hinge, whereas in the central and northern Apennines subduction of thin Adriatic oceanic lithosphere allowed continuing roll-back of the hinge. Owing to these different roll-back rates the velocity of the Apenninic slab retreat was split in two ‘sub-arcs’ separated by the Tremiti line (*Dogliani et al., 1994*).

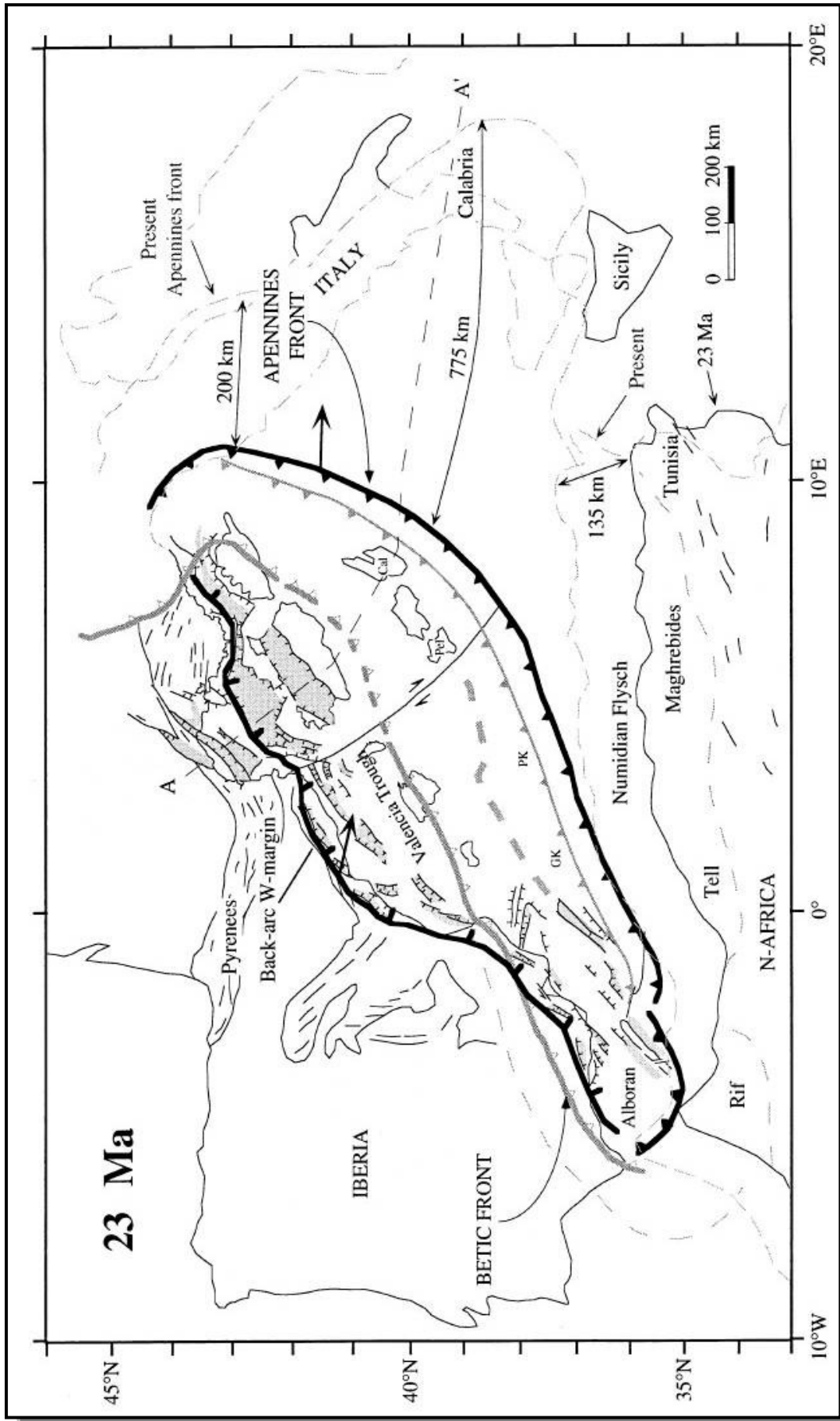


Fig. 1-10: Early Miocene palaeotectonic reconstruction of the western Mediterranean showing the extensional system (Provenc. al-Valencia-Alboran), considered as the back-arc basin of the west-directed Apenninic subduction (in black). *Gueguen et al. (1998).*

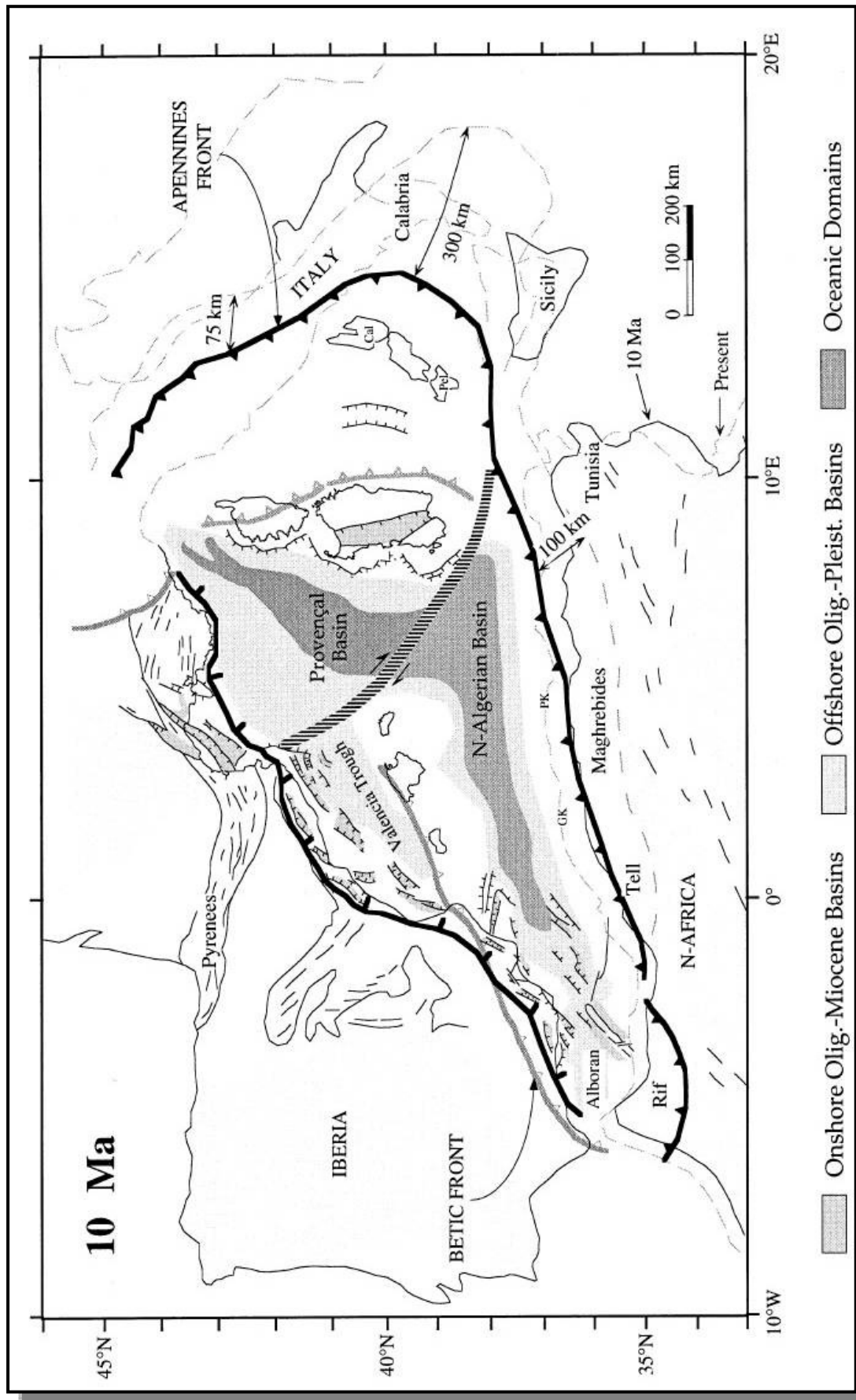


Fig. 1-11: Most of the western Mediterranean basins had already opened during Tortonian times. Both the trench of the Apennine subduction and related focus of back-arc extension continued to migrate eastwards. *Gueguen et al. (1998).*

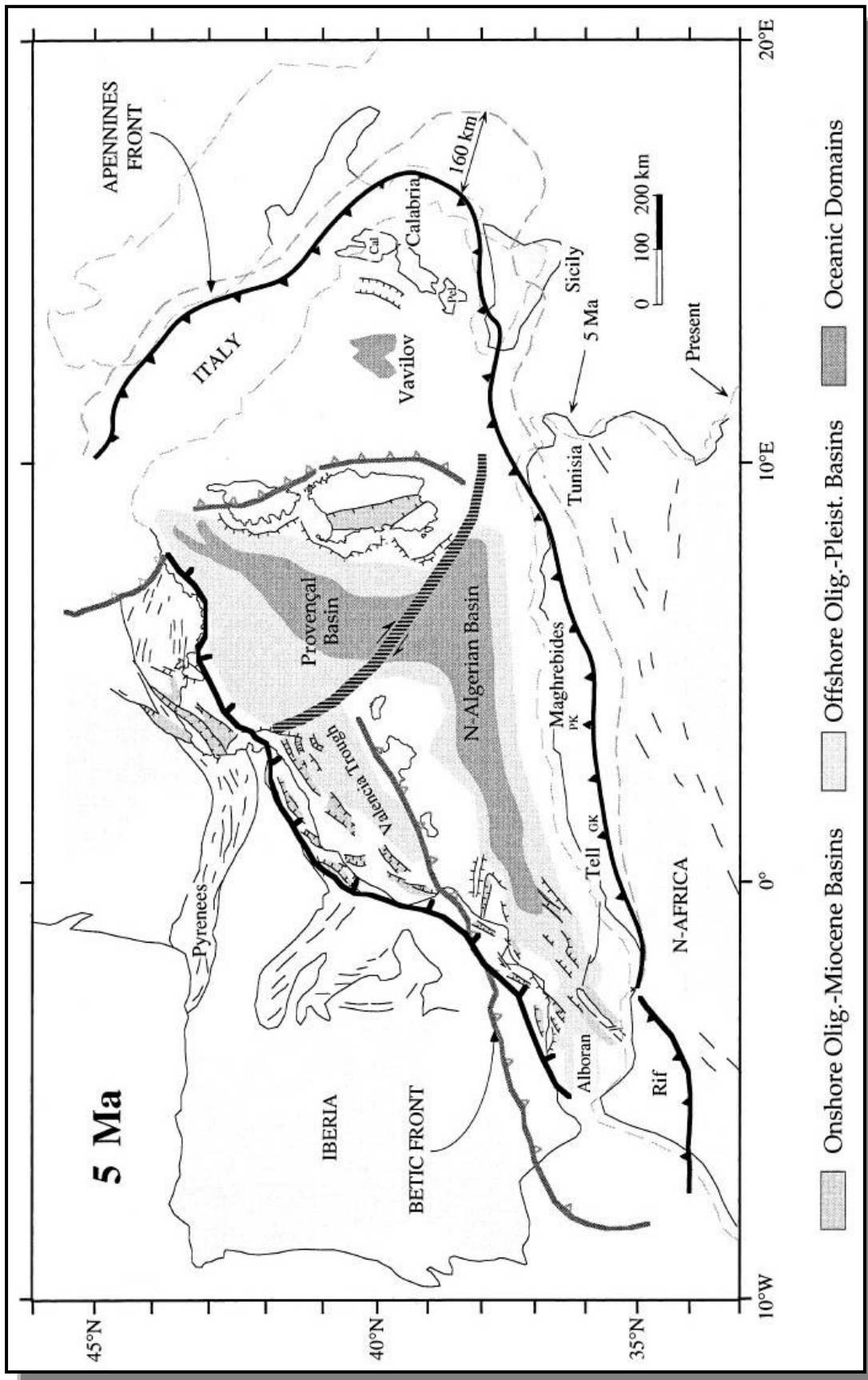


Fig. 1-12: Early Pliocene palaeotectonic reconstruction. The Tyrrhenian basin began to develop oceanic crust in the Vavilov area. The entire system associated with the Apenninic subduction migrated eastward at rates up to 50 mm/year. *Gueguen et al. (1998).*

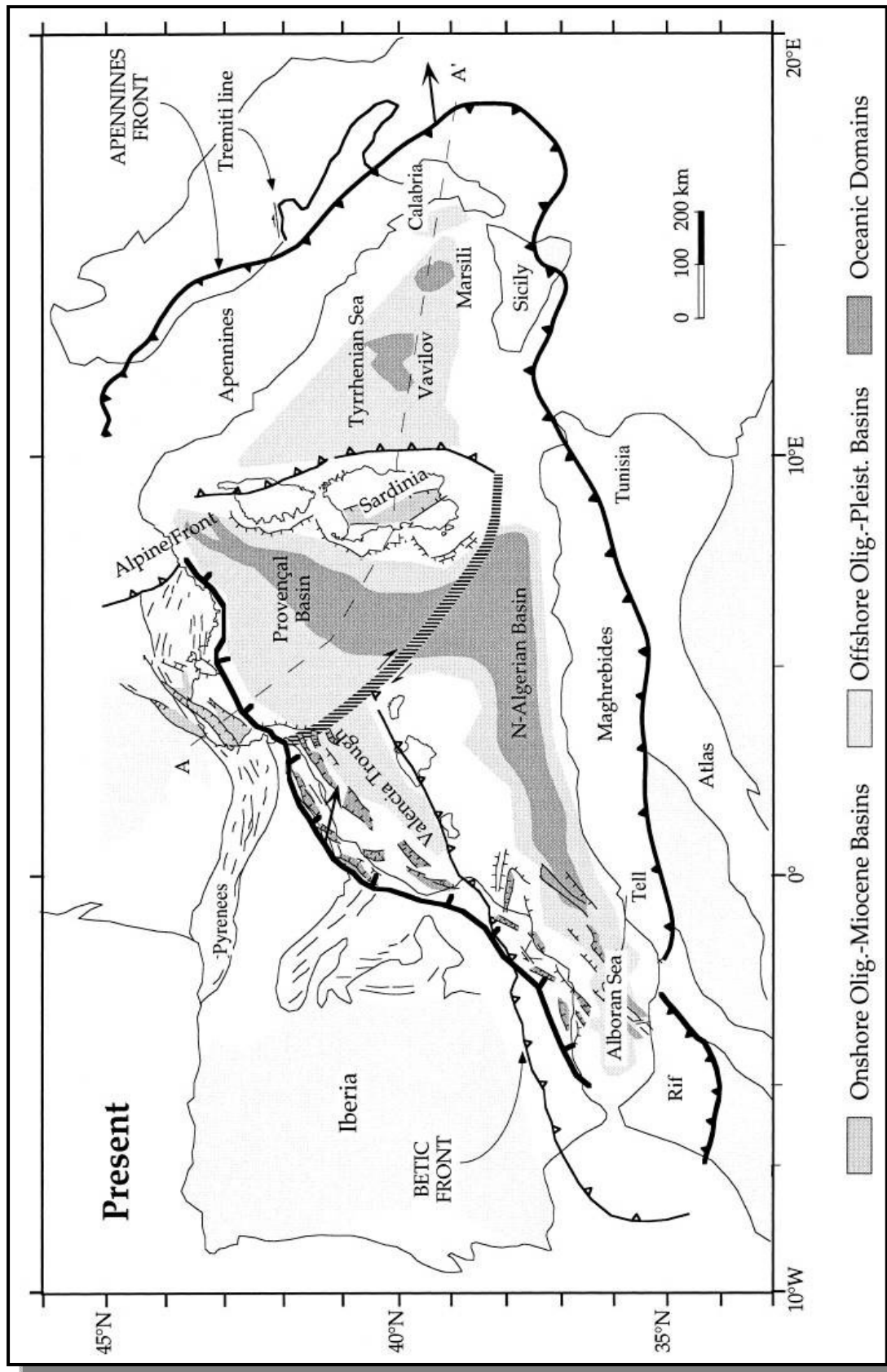


Fig. 1-13: The western Mediterranean is composed of sub-basins becoming younger from west to east. They developed in the hanging wall of the 'eastward' retreating Apenninic subduction, as back-arc basins, during the last 30 Ma. Gueguen et al. (1998).

The evidence of subduction rollback in the Tyrrhenian-Apennine system derives from the distribution of subduction-related magmatism, which indicates movement of the magmatic arc consistent with rollback of the subduction hinge toward the east and the southeast (**Figure 1-14**). These events produced a regional rise of the mantle, with a maximum at the center of Tyrrhenian Sea, and caused an intense phase of volcanism on thinned continental crust along the Italian peri-Tyrrhenian border, specifically in some subsided areas.

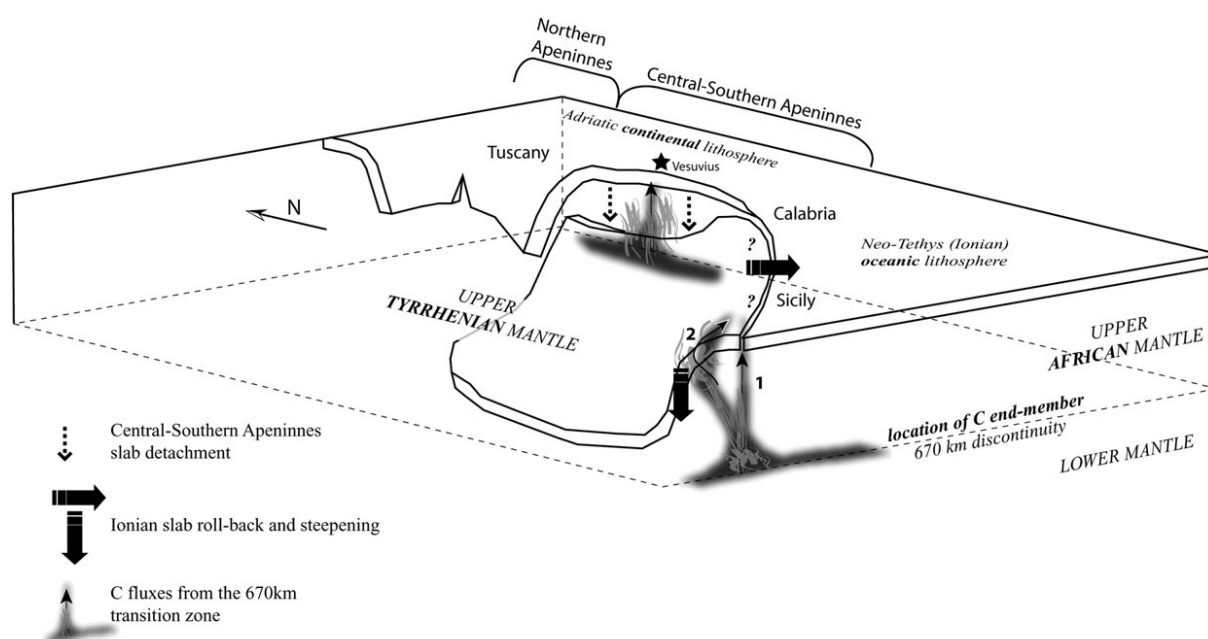


Fig. 1-14: Sketch of possible geodynamic model for Italian magmatism, from Cadoux et al. (2007) and modified from Spakman and Wortel (2004).

The central Mediterranean volcanism which is mainly localised in Italy, is subdivided in five areas which will be presented later. On the structural sketch of Tyrrhenian Sea and Apennines from *Turco and Zupetta (1998)* (**Figure 1-15**), it is possible to see the tectonic structures of the thrust belt and the localisation of Italian volcanoes.

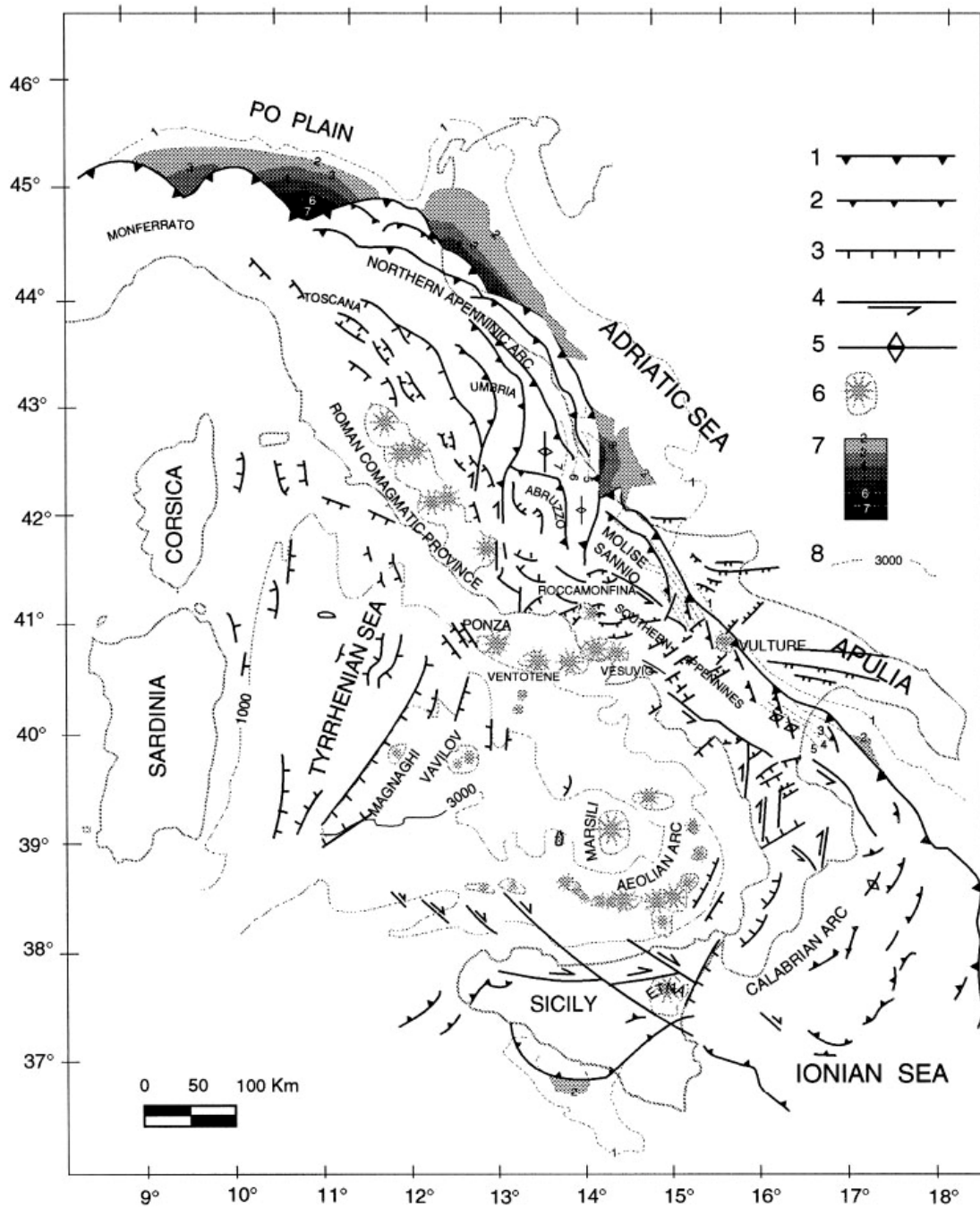


Fig. 1-15: Structural sketch of the Tyrrhenian Sea and Apennines from [Turco and Zupetta \(1998\)](#); 1 = front of the Apenninic thrust belt; 2 = surface and subsurface main thrust; 3 = extensional faults; 4 = strike-slip faults; 5 = fold axes; 6 = volcanoes; 7 = base of Pleistocene isobaths (km); 8 = Tyrrhenian isobaths (m).

I.4. Central Mediterranean volcanism:

From several million of years, the Central Mediterranean area knew a high volcanic activity from several regions like Massif Central in France, Eifel in Germany, Hellenic Arc in Greece, Central Anatolia in Turkey or like Italy. On this study, I am focusing only on the Italian volcanoes. Indeed the French volcanism has known important explosive eruptions, they are too old (more than 250 ka, *Boivin et al., 1991*) to be recorded in the different drilling core of this PhD project. The Eifel volcanic complex has produced phonolitic Laacher See tephra at $12,900 \pm 560$ yrs, which is widespread only in central and northern Europe (*van den Bogaard, 1995; Schmincke et al., 1999*). The fallouts from Hellenic Arc and from Anatolia are mainly calc-alkaline composition and were deposited in the eastern part of Mediterranean area (*Keller, 1978; Druitt et al, 1995*).

The Central Mediterranean area, and more specially the Italy, has been the site of vigorous volcanic activity since Oligocene (**Figure 1-16**; *Keller, 1978; Paterne, 1985; Santacroce et al., 2003, 2008; Peccerillo, 2005*).

Currently at least five areas can be considered active:

1. the Campanian Volcanic Zone (CVZ) and its offshore area, hosting Mount Somma-Vesuvius, Phlegrean Fields, Ischia and Procida islands
2. Roman Province with Alban Hills and Sabatini Volcanic District
3. the Aeolian archipelago and its extension into the Tyrrhenian Abyssal Plain, persistently active Stromboli and with historical eruption at Vulcano and Lipari
4. Mount Etna, persistently active
5. Sicily Channel where sporadic submarine eruptions occurred in 1831 (Ferdinanda/Graham), 1891 (Foerstner, offshore of Pantelleria) and Pantelleria Island.

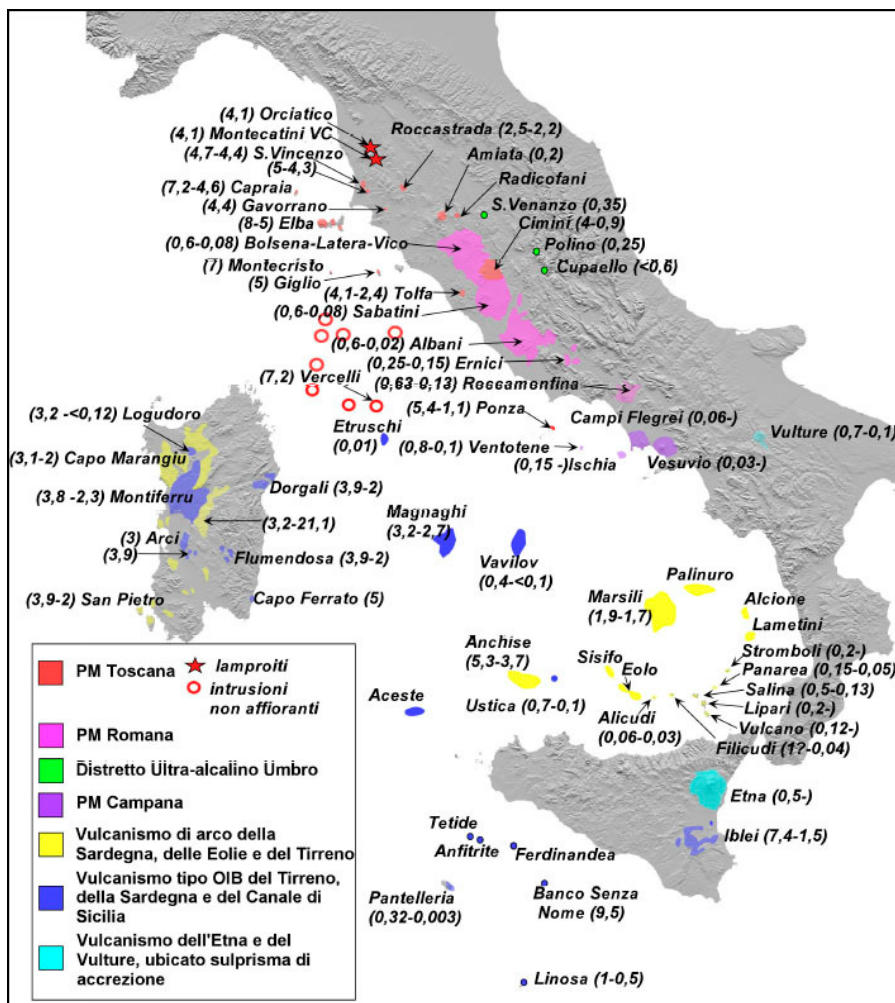


Fig. 1-16: Plio-Quaternary volcanism in Italy with dating in Ma modified from Peccerillo (2005).

In the next pages, there are the presentation and the activity of the most active and the most important Italian volcanic complex. It is important to have a good idea of the last volcanic activity because the found tephra in the drilling core can be correlated to one of these volcanic activities.

I.4.1. Campanian Province

The Campanian Province (CP) is a tectonic depression, consequence of stretching and thinning of the western border (*Scandone, 1980*) during the opening of the Tyrrhenian Sea. This depression is composed of carbonate platforms (about 5 km thick, *Ippolito et al., 1973*) and upper is covered with alluvial sediment and volcanic deposits.

The mains Quaternary volcanic of the CP are Somma–Vesuvius and the Phlegrean Fields. The Phlegrean Fields include the islands of Procida and Ischia, as well as submarine vents in the north-western Gulf of Naples. It is one of the main volcanic areas in the CP and consists of a NE–SW active volcanic ridge and displays the largest, most recent and best exposed NE–SW fractures (**Figure 1-17**).

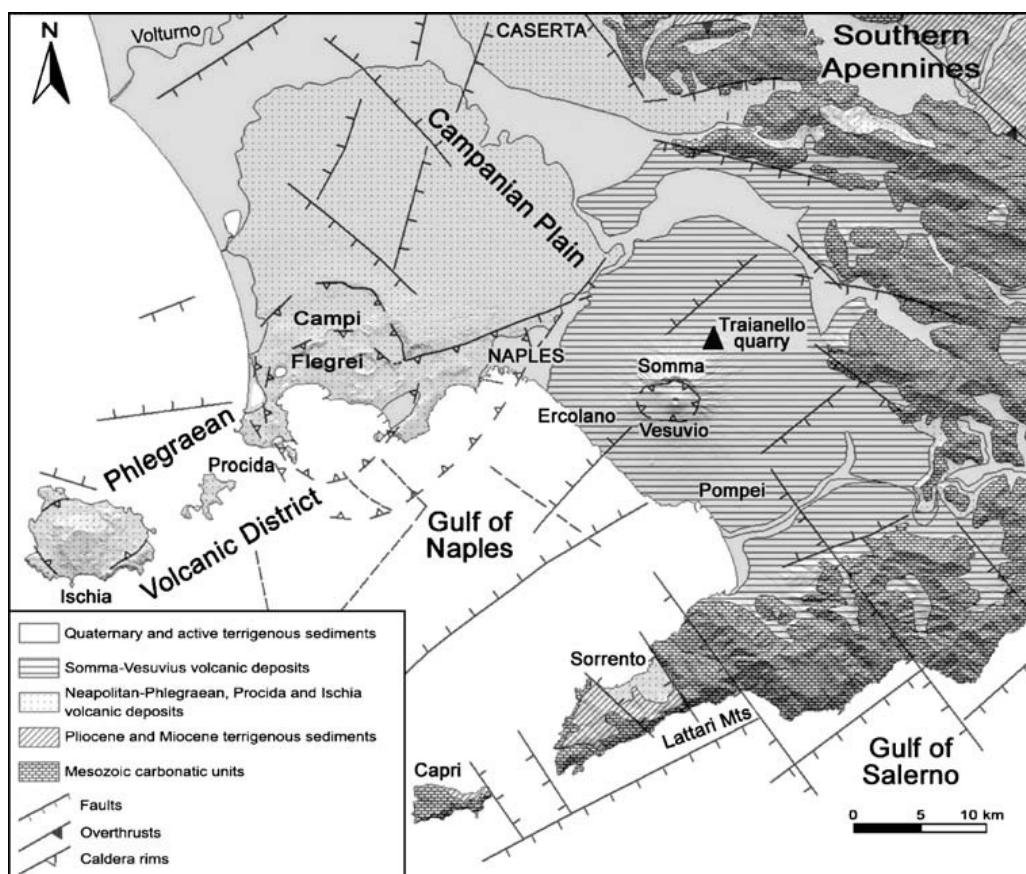


Fig. 1-17: Structural sketch map of the Phlegrean Fields caldera, from *Aulinas et al. (2008)* modified from *Orsi et al. (2004)*.

I.4.1.1. The Mount Somma-Vesuvius

The Somma-Vesuvius volcanic complex is located 20 km east of Naples. This complex consists of an older volcano dissected by a summit caldera, Mt. Somma, and a recent cone, Vesuvius, that grew within the caldera after the 79 A.D. Pompeii eruption. The volcano is relatively young: the Mt Somma stratocone most probably postdates the 39-ka old Campanian Ignimbrite eruption of Phlegrean Fields (*Bocchini et al., 2001; Santacroce and Sbrana, 2003; Di Renzo et al., 2007*) and stopped activity at about 20 ka. It consists of a pile of thin lava flows interbedded with spatter and cinder deposits (Kbasalt- trachybasalt to K-tephrite-phonotephrite) (*Johnson Lavis, 1884; Rittman and Ippolito, 1962; Santacroce, 1987; Santacroce et al., 2003, 2008*). About 22 ka ago the style of activity changed: after a long quiescence a large Plinian eruption (Pomici di Base) ejected K-trachytic to K-latic magmas (*Delibrias et al., 1979; Cioni et al., 1999; Andronico et al., 1995*). Then follows the second largest event of this period: Pomici Verdoline or Greenish Pumice ca. 20 ka (*Delibrias et al., 1979; Santacroce et Sbrana, 2003; Santacroce et al., 2008*). In the following 16 ka, three other Plinian eruptions occurred, each preceded by long rest periods: Mercato (8 ka, K-phonolite; *Johnston Lavis, 1884; Walker, 1977; Delibrias et al., 1979; Cioni et al., 1999*), Avellino (3.4 ka; *Lirer et al., 1973; Arnò et al., 1987; Cioni et al., 2000*), and Pompeii (A.D. 79; *Sigurdsson et al., 1985; Cioni et al., 1992*), both K-phonolite-tephriphonolite, while effusive activity was limited to a few lava flows from lateral vents (approx. 17 ka). In between the four major Plinian events, 8–10 minor explosive eruptions occurred, Subplinian to Vulcanian in style. After A.D. 79, the recent cone began to form (*Andronico et al., 1995*). It grew discontinuously during periods of persistent Strombolian and effusive activity occurred in the Ist–IIIrd, V–VIIIth (after A.D. 472 Pollena eruption), X–XIIth centuries and in 1631–1944. A dozen explosive eruptions alternated with the open conduit activity, each preceded by long (100–300 years) rest. The largest eruptions of this last period of activity occurred in A.D. 472 and 1631 and were Subplinian in size and dynamics (*Delibrias et al., 1979; Rosi et al., 1993; Rosi and Santacroce, 2003*).

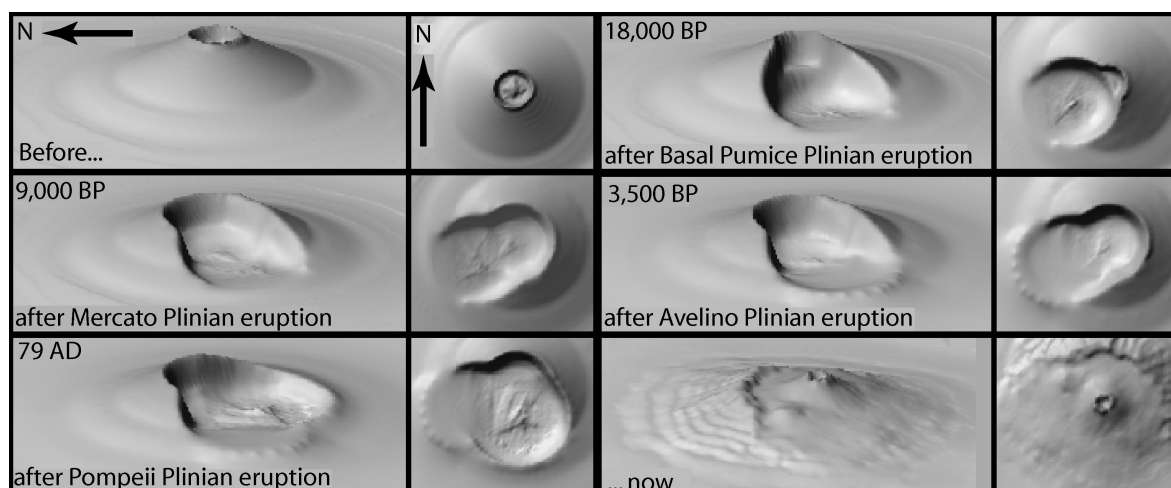


Fig. 1-18: Schematic reconstruction of the morphological evolution of Somma-Vesuvius caldera from [Santacroce et al. \(2003\)](#).

Mt. Somma is a nested, polyphased caldera related to the emptying of shallow reservoirs during large eruptions. Four caldera forming events have been recognized (**Figure 1-18**; [Santacroce et al., 1987](#); [Cioni et al., 1999](#); [Santacroce and Sbrana, 2003](#)), occurred during Plinian eruptions. The structural collapses constantly accompanied the final phreatomagmatic phases common to all four events. The geometry of the caldera did not suffer significant modifications related to the Interplinian volcanic activity until the post A.D. 79 reconstructing period, whose products covered and mostly obliterated the seaward lower rim of the caldera.

The eruptive history of Vesuvius reflects a plumbing system characterized by the constant presence of shallow magma chambers and alternating periods of open and obstructed conduit conditions ([Santacroce et al., 1994](#); [Cioni et al., 1997](#)).

When the conduit is open, the reservoir is continuously tapped through persistent Strombolian activity. The periodic arrival of fresh magma in the full plumbing system results in either quiet lava effusions and moderate growth of the magma chamber (<3 km depth) or in explosive-effusive poly-phased eruptions whose dynamics induce the complete emptying of the reservoir. After short quiescent periods (reflecting the system recharge), Strombolian conditions are restored, initiating a new cycle.

When the conduit is obstructed the magma chamber grows until, after quiescent intervals of variable length, an explosive eruption is initiated. The increasing volume is accompanied by changes in the aspect ratio of the chamber as well as in the compositional layering: (1) initial stage, high aspect ratio chamber, moderate volume (0.01–0.1 km³), almost homogeneous mafic melt; (2) young stage, medium aspect ratio chamber, medium volume

(0.1–0.5 km³), almost continuous gradient from mildly evolved to felsic melt; (3) mature stage, low aspect ratio chamber, large volume (0.5–5 km³), two fold layering with stepwise gradient separating a lower, convective, mildly evolved portion from an upper, statically stratified, felsic portion.

Many eruptions younger than 22,000 cal yrs BP (**Figure 1-19**) are characterized by a marked compositional zoning, which gives them a unique signature. The geochemical and chronological framework presently available for Somma-Vesuvius activity is resumed in the **Table 1-1** from *Santacroce et al. (2008)*. The Vesuvius pyroclastics display variability from the saturated (trachytes-phonolites) changing with the time to highly under saturated high-potassic rocks (leucitic phonolites to tephrites) (*Santacroce, 1987; Santacroce et al., 2008*).

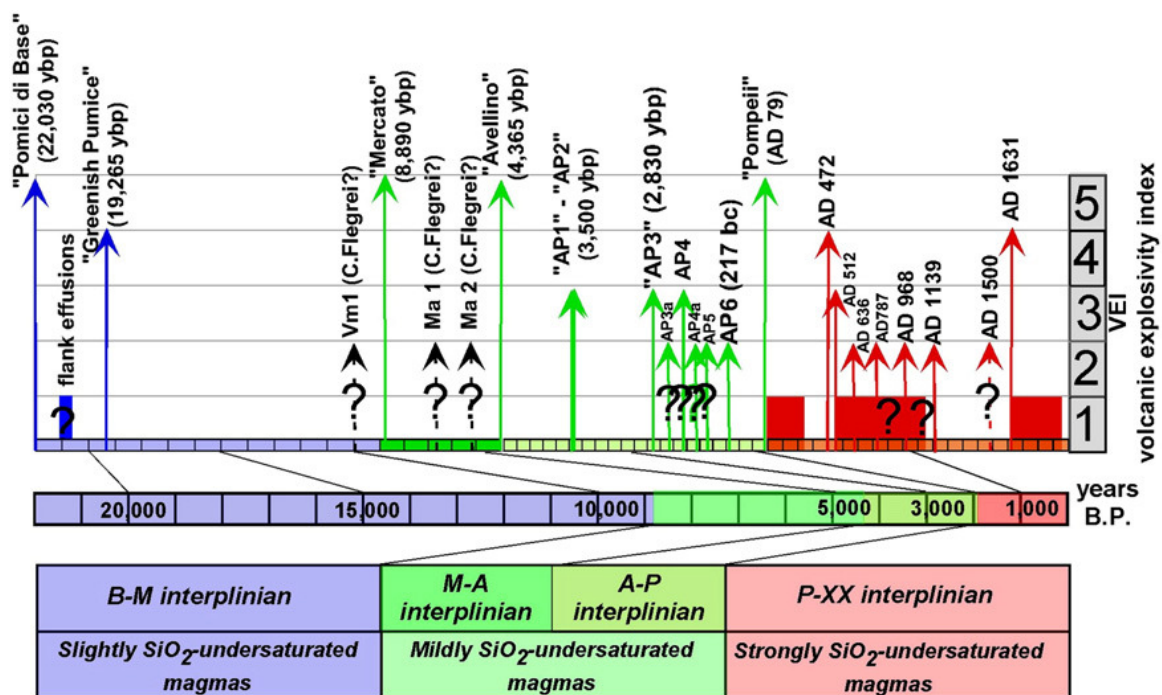


Fig. 1-19: Synthetic eruptive history of the last 22,000 years of Mt Somma-Vesuvius (calibrated ages) as recorded by the stratigraphic successions and selected historical sources from *Santacroce et al. (2008)*.

Eruption	Proximal deposits	Lithology	Isopach maps
AD 1631	<p><i>PFD</i>: Basal, few cm-thick layer of light grey scoria followed by an upper layer of dark grey scoria. Final fine ash of phreatomagmatic origin.</p> <p><i>PDC deposits</i> abundant only on western and southern slopes of the volcano, at top of the main fallout beds.</p>	<p><i>Light grey scoria</i>: highly to moderately vesicular, porphyritic (lc + cpx + san) Tephri- phonolite. Glassy groundmass</p> <p><i>Dark grey scoria</i>: moderately to incipiently vesicular, highly porphyritic (lc + cpx + bt). Phono-tephrite. Microlite-rich groundmass.</p> <p><i>Lithic fragments</i>: lc-bearing lava, intrusive and skarn rocks; rare carbonate rocks</p> <p><i>Loose crystals</i>: abundant (lc + cpx)</p>	
AD 512 (AS1)	<p><i>PFD</i>: complex stratified sequence of scoria lapilli (from light brown, to dark brown to black) beds with minor ash interlayerings.</p> <p>Minor <i>PDC deposits</i> at the base of the sequence, only dispersed in very proximal sectors</p>	<p><i>Brown scoria</i>: moderately to highly vesicular, crystal-poor (cpx + lc + bt), glassy scoria. Phono-teprite.</p> <p><i>Dark brown to black scoria</i>: moderately to poorly vesicular, crystal-poor (cpx + bt), ipocrystalline groundmass (mainly lc-microlites). Phono-tephrite.</p> <p><i>Lithic fragments</i>: lc-bearing lava</p> <p><i>Loose crystals</i>: rare</p>	
AD 472 (Pollena)	<p><i>PFD</i>: Complex stratified sequence. Basal layer of greenish-grey pumice followed by several layers of dark grey scoriae. Thin ash interbeds between the lapilli beds. Fine ash beds at top</p> <p><i>PDC deposits</i> widely dispersed all around the the volcano</p>	<p><i>Greenish-grey pumice</i>: highly vesicular, porphyritic (lc + cpx + san + amph + gt), glassy groundmass. Tephri- phonolite to phonolite.</p> <p><i>Dark grey scoria</i>: moderately to incipiently vesicular, highly porphyritic (lc + cpx + bt + dav). Leuciticitephrite ÷ phonolite. Cryptocrystalline groundmass.</p> <p><i>Lithic fragments</i>: lc-bearing lava, intrusive and skarn rocks; rare carbonate rocks</p> <p><i>Loose crystals</i>: abundant (lc + cpx + bt)</p>	
AD 79 (Pompeii Pumice)	<p><i>PFD</i>: Compositionally zoned, two-fold pumice lapilli deposit. White pumice basal bed followed by a grey pumice upper bed. Four ash interlayers in the grey pumice. Thickly bedded fine ash at top of the sequence.</p> <p><i>PDC deposits</i> interlayered in the grey pumice bed and at top of it, dispersed all around the volcano and in the plain nearby</p>	<p><i>White pumice</i>: highly to extremely vesicular, porphyritic (san + cpx + gt + amph + bt); lc-bearing, microlite-rich groundmass. P Phonolite.</p> <p><i>Grey pumice</i>: highly vesicular, porphyritic (san + cpx + bt); lc-bearing, microlite-rich groundmass. Tephri- phonolite.</p> <p><i>Lithic fragments</i>: lc-bearing lava, tuffs, intrusive and skarn rocks; abundant carbonate rocks (limestones and marbles).</p> <p><i>Loose crystals</i>: present (san + amph + cpx + gt + bt ± lc)</p>	
AP6	<p><i>PFD</i>: stratified sequence of four alternate light- to dark-grey scoria lapilli and ash beds.</p>	<p><i>Light grey scoria</i>: highly to moderately vesicular, subaphyric (lc + cpx ± bt). Microlite-rich groundmass (lc + cpx ± bt).Tephri-phonolite</p> <p><i>Dark grey scoria</i>: moderately to poorly vesicular, subaphyric (lc + cpx ± bt). Microlite-rich groundmass</p> <p><i>Lithic fragments</i>: lc-bearing lava</p> <p><i>Loose crystals</i>: rare</p>	
AP5	<p><i>PFD</i>: thinly stratified scoria lapilli bed, from dark brown to reddish at top. Violet coloured, lithic-rich, bt-bearing, coarse ash bed at top.</p>	<p><i>Dark brown scoria</i>: poorly vesicular, subaphyric (cpx + bt ± plag). Glassy groundmass with leucite microphenocrysts (+ cpx + bt + san + plag). Tephri-phonolite.</p> <p><i>Lithic fragments</i>: lc-bearing lava</p> <p><i>Loose crystals</i>: abundant bt flakes in the ash beds</p>	
AP4	<p><i>PFD</i>: complex sequence of three main beds. Stratified, ash and lapilli bed at the base, followed by a thinly stratified, coarse to fine scoria lapilli bed, topped by an accretionary lapilli-bearing, fine ash bed</p>	<p><i>Dark brown scoria</i>: poorly vesicular, subaphyric (cpx + bt + plag ± san). Glassy groundmass with leucite microphenocrysts (+ cpx + bt + san + plag). Tephri-phonolite.</p> <p><i>Lithic fragments</i>: lc-bearing lava, very minor carbonate rocks</p> <p><i>Loose crystals</i>: rare</p>	
AP3	<p><i>PF</i> main dark brown scoria, stratified, scoria lapilli bed sandwiched between two stratified, fine to coarse ash, accretionary lapilli beds.</p>	<p><i>Dark brown scoria</i>: poorly vesicular, subaphyric (cpx + bt + plag ± san). Glassy groundmass with leucite microphenocrysts (+ cpx + bt + san + plag). Tephri-phonolite.</p> <p><i>Lithic fragments</i>: lc-bearing lava, very minor carbonate rocks</p> <p><i>Loose crystals</i>: rare</p>	
AP2	<p><i>PFD</i>: two main lapilli beds separated by an accretionary lapilli-bearing fine ash bed. Basal, light-grey pumice bed and grey to dark green, lithic-rich, stratified scoria lapilli bed. Accretionary lapilli-bearing ash bed at top.</p> <p><i>PDC deposits</i> only present as stratified surge beds proximal to the vent area. These deposits are interbedded between the two main lapilli beds</p>	<p><i>Light grey pumice</i>: highly vesicular, subaphyric (plg + san + cpx + bt). Glassy, lc-bearing, poorly crystalline groundmass. Phonolite</p> <p><i>Grey to dark green scoria</i>: poorly to highly vesicular, subaphyric (plg + cpx + bt). Glassy, lc-bearing (+ san + cpx + bt), microlite-rich groundmass. Tephri-phonolite</p> <p><i>Lithic fragments</i>: lc-bearing lava, intrusive and skarn rocks; carbonate rocks (limestones and marbles).</p> <p><i>Loose crystals</i>: rare</p>	

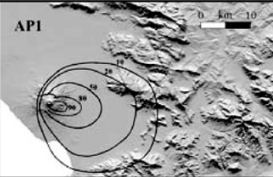
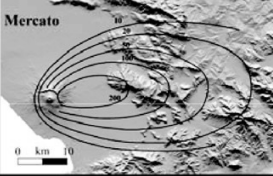
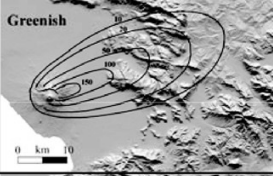
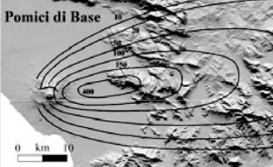
Eruption	Proximal deposits	Lithology	Isopach maps
AP1	<p><i>PFD</i>: two main lapilli beds separated by an accretionary lapilli-bearing, fine ash bed. Basal, light-grey pumice bed and dark green, thinly stratified, scoria lapilli bed. Accretionary lapilli-bearing ash bed at top.</p> <p><i>PDC deposits</i> only present as stratified surge beds proximal to the vent area. These deposits are interbedded between the two main lapilli beds</p>	<p><i>Light grey pumice</i>: highly vesicular, banded, subaphyric (san + cpx + amph + bt ± plag). Characteristic bt flakes. Glassy, lc-bearing groundmass. Phonolite</p> <p><i>Dark green scoria</i>: moderately vesicular, porphyritic (plg+cpx+bt ± san). Glassy, lc-bearing groundmass. Tephri-phonolite</p> <p><i>Lithic fragments</i>: lc-bearing lava, intrusive and skarn rocks; carbonate rocks (limestones and marbles).</p> <p>Loose crystals: bt</p>	
Mercato Pumice	<p><i>PFD</i>: three main well-sorted, light-coloured pumice lapilli beds, interlayered with pinkish-brown massive ash beds. The upper bed is lithic-rich.</p> <p><i>PDC deposits</i> are mainly dispersed in the main valleys on the volcano slopes.</p>	<p><i>White pumice</i>: highly to extremely vesicular, almost aphyric (san + cpx ± gt ± amph). Glassy, microlite-poor groundmass. Fine-sized, round vesicles and abundant tubular pumice. Phonolite</p> <p><i>Lithic fragments</i>: lc-bearing lava, intrusive and skarn rocks; carbonate rocks (limestones and marbles).</p> <p>Loose crystals: rare</p>	
Greenish Pumice	<p><i>PFD</i>: complex alternation of fine to coarse lapilli and ash layers. Different types of juvenile fragments mixed in the same stratigraphic level. Light-brown pumice and dark-green to brown scoria. Pumice lapilli only present in the basal lapilli bed.</p> <p><i>PDC deposits</i> are scarce and are mainly present on northern slopes of Mount Somma</p>	<p><i>Light-brown pumice</i>: highly vesicular, almost aphyric (san + amph + gt). Glassy, microlite-free groundmass. Trachyte</p> <p><i>Dark-green to brown scoria</i>: highly to moderately vesicular, almost aphyric (san + amph + gt). Glass-bearing to completely crystalline groundmass (san + minor cpx and amph). Trachyte</p> <p><i>Lithic fragments</i>: lc-bearing lava; marl; carbonate rocks (limestones and marbles).</p> <p>Loose crystals: rare</p>	
Pomici di Base	<p><i>PFD</i>: white to grey pumice basal layer followed by a black scoriae upper layer.</p> <p><i>PDC deposits</i> are poorly exposed and crop out mainly on northern slopes of Mount Somma</p>	<p><i>White to grey pumice</i>: highly vesicular, almost aphyric (san + cpx + amph). Phenocrysts mainly assembled in glomerophyres. Glassy, microlite-free groundmass. Trachyte</p> <p><i>Black scoria</i>: moderately vesicular, subaphyric (san + cpx). Microlite-rich, glass-poor to glass-free groundmass (san + plag + minor cpx) Latite to shoshonite.</p> <p><i>Lithic fragments</i>: lc-bearing lava; rare carbonate rocks (limestones and marbles).</p> <p>Loose crystals: rare</p>	

Table 1-1: Main features and dispersal areas of pyroclastic deposits from the Somma-Vesuvius eruptions, table from Santacroce et al. (2008).

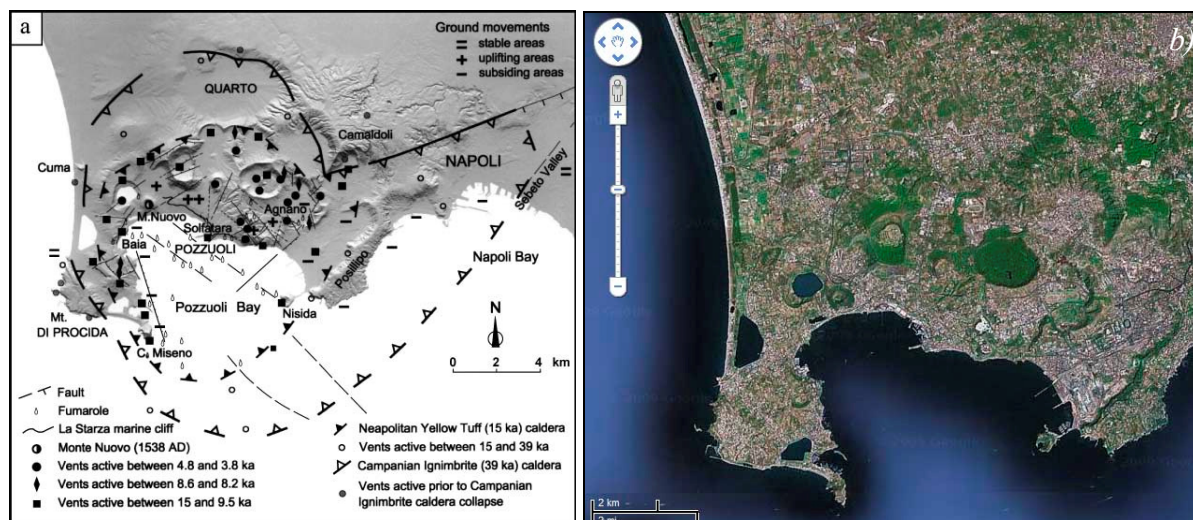
I.4.1.2. Phlegrean Fields

Fig. 1-20: a) Structural map of the Phlegrean Fields caldera from [Santacroce et al. \(2003\)](#); b) Satellite image of Phlegrean Fields zone (© Google earth).

The Phlegrean Fields are localised on the border west of Naples with continental and submerged parts (**Figure 1-20 a and b**). The Phlegrean Fields are composed of a large number from volcanic edifices, like monogenic volcanoes and calderas. The volcanism commenced more than 60 ka and was characterised by explosive phase ([Rosi and Sbrana, 1987](#); [Orsi et al., 1996](#); [Pappalardo et al., 1999](#)). [Orsi et al. \(1992, 1996\)](#), on the basis of the results of surface and subsurface geological investigations, and of geochronological and geophysical data, suggested that the Phlegrean Fields caldera has been generated by at least two major collapses (**Figure 1-21**). Those collapses were related to the Campanian Ignimbrite Y-5 (CI Y-5; 39 ka; [Barberi et al. 1978](#); [Fisher et al. 1993](#); [Rosi et al. 1996, 1999](#); [Civetta et al. 1997](#); [De Vivo et al. 2001](#); [Fedele et al. 2002, 2003](#); [Pappalardo et al. 2002a](#)) and Neapolitan Yellow Tuff (NYT; 15 ka; [Orsi et al. 1992, 1995](#); [Scarpati et al. 1993](#); [Wohletz et al. 1995](#); [Deino et al. 2004](#)) eruptions respectively.

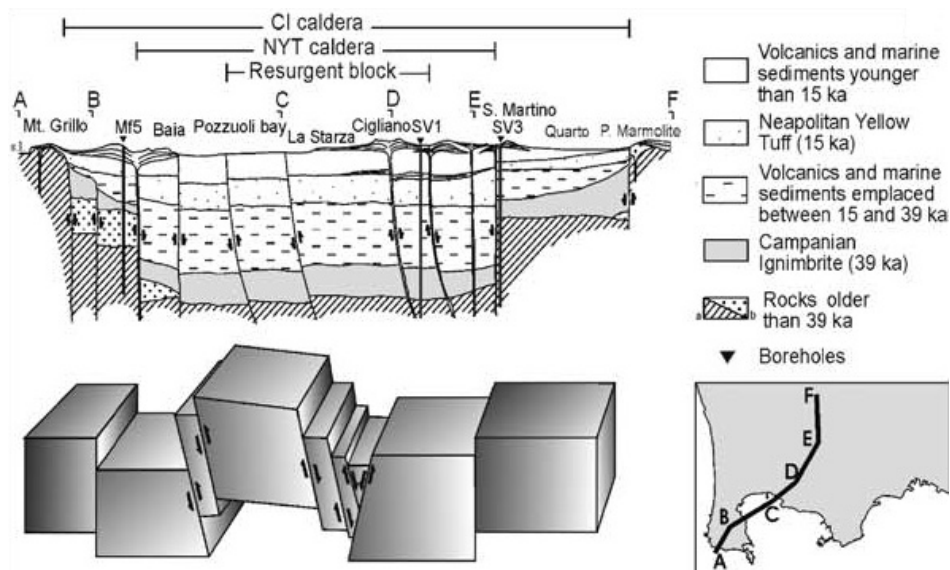


Fig. 1-21: Geological cross section through the Phlegrean Fields caldera and illustration of the proposed dynamic model from Orsi et al. (2004) and modified after Orsi et al. (1991, 1996).

The Campanian Ignimbrite Y-5 eruption, the largest of the Mediterranean area over the past 200 ka, extruded a volume of dense magma estimated between 105 and 210 km³ and with a minimum surface of 2.10⁶ km² (Pyle et al., 2006) of trachytic to phonolitic-trachytic magma. The caldera collapse affected the area which at present includes the Phlegrean Fields, Naples, the bay of Pozzuoli and part of the bay of Naples. The subsequent volcanism was concentrated within the CI Y-5 caldera.

The NYT phreatoplinian eruption, the second largest of the Campanian area, extruded about 40 km³ of alkali-trachyte to latite magma (Orsi et al., 1992; Wohletz et al., 1995). The caldera related to this eruption was nested within the CI Y-5 caldera, centred on the present Phlegrean Fields.

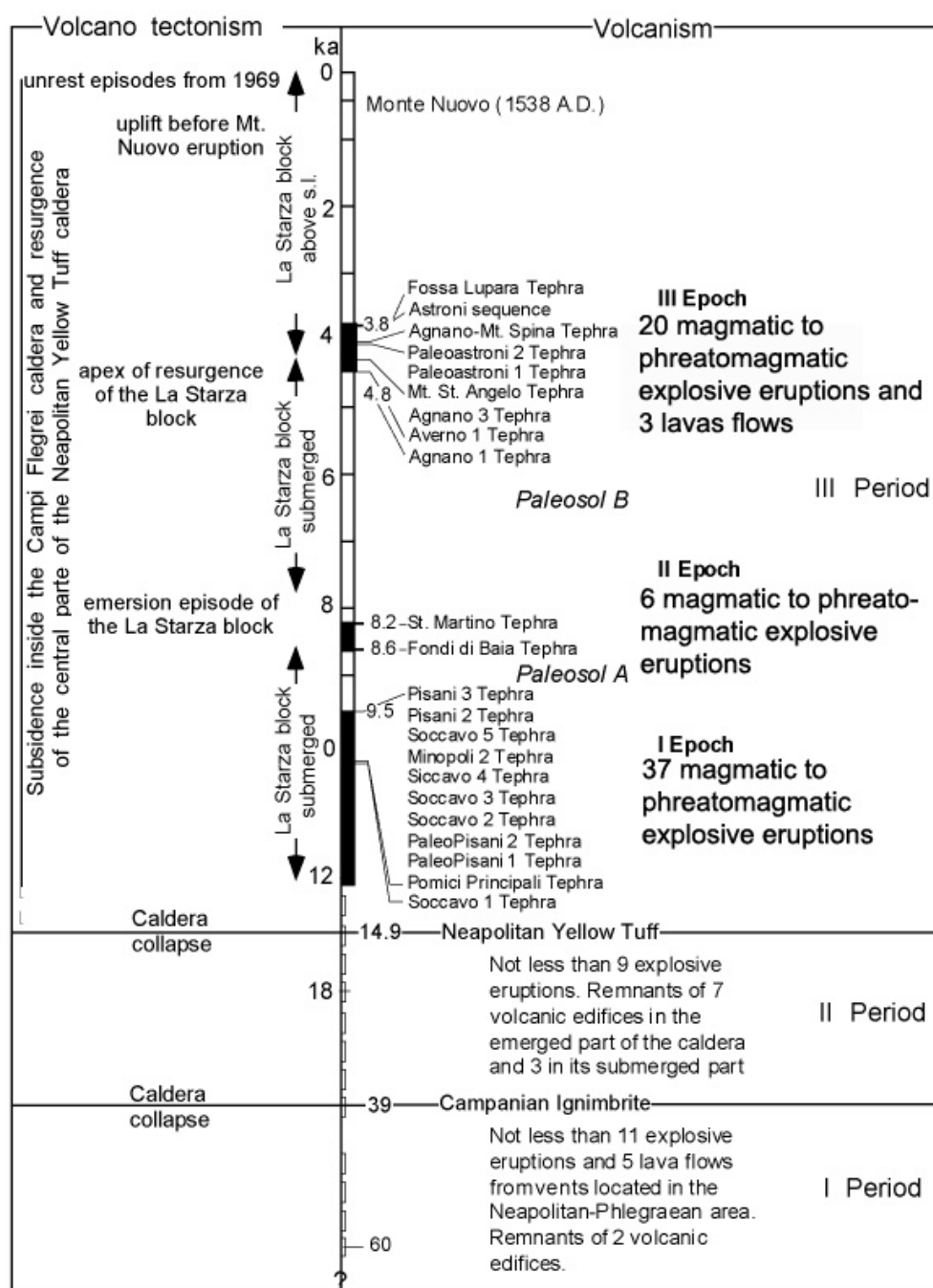


Fig. 1-22: Stratigraphic sequence for the Phlegrean Fields volcanic activity from Orsi et al. (2004).

The results of petrological studies shown that the magma system of the Phlegrean Fields caldera is very complex (D'Antonio et al., 1999; Pappalardo et al., 1999, 2002b; Marianelli et al., 2003; Orsi et al., 2004). The Phlegrean Fields pyroclastic products are characterised by a typical high-K-trachytic to phonolitic (Rosi and Sbrana, 1987; Wulf et al., 2004).

In the **Figure 1-22**, *Orsi et al. (2004)* made the hypothesis that the magmatic system of the Phlegrean Fields caldera includes a shallow, large-volume trachytic reservoir periodically refilled by new magma batches rising from a storage zone located between depths of 10 and 15 km. The shallow reservoir has been the site of differentiation processes. From 60 to 44 ka, the reservoir was growing due to input of new magma batches, while from 44 to 39 ka, it was an isotopically homogeneous, large-volume, zoned system, whose evolution culminated in the CI Y-5 eruption. Arrival of new magma batches formed an apparently independent, large-volume reservoir which fed the NYT eruption (*Orsi et al., 1992*). In the past 15 ka, three isotopically and geochemically distinct magmatic components were erupted as either homogeneous or mixed magma batches (*D'Antonio et al., 1999*). One component is similar to the CI Y-5 trachytic magma, the second is similar to the NYT latitic-alkalitrachytic magma and the third is a trachybasalt never erupted before. It has been hypothesized that the CI Y-5 and NYT components represent residual portions of older, large-volume magma reservoirs which have fed eruptions since about 60 and 15 ka, respectively (*Orsi et al., 2004*). The least-evolved component, erupted through vents located on a NE-SW regional fault system, likely represents the deeper seated magma tapped by regional faults.

Volcanism of the past 15 ka has concentrated in three “Epochs of Activity” separated by quiescence (*Di Vito et al., 1999*). It has generated mostly explosive eruptions, variable in magnitude and generally characterised by alternating magmatic and phreatomagmatic explosions. During each Epoch, eruptions occurred at intervals of about 60 years, on average. During the I Epoch (12.0–9.5 ka), out of 37 explosive eruptions, only the Pomici Principali (10.3 ka; *Lirer et al., 1987; Di Vito et al., 1999; Orsi et al., 2004*) was a high-magnitude event. The II Epoch (8.6– 8.2 ka; *Orsi et al., 2004*) generated 6 low-magnitude explosive eruptions. The III Epoch (4.8 – 3.8 ka) produced 20 explosive and 3 effusive eruptions (*Orsi et al., 2004*). During this Epoch the only high-magnitude event was the Agnano- Monte Spina eruption (4.1 ka; *de Vita et al., 1999; Dellino et al., 2001*). The first two periods of quiescence lasted 1.0 and 3.5 ka, respectively, while the last, begun at the end of the III Epoch, was interrupted in 1538 A.D. by the Monte Nuovo eruption (*Orsi et al., 2004*).

I.4.1.3. Island of Ischia

Fig. 1-23: Satellite image of the Ischia Island (© Google earth).

The island of Ischia (**Figure 1-23**) is a volcanic field of about 42 km², composed of volcanic rocks, landslide deposits and subordinate terrigenous sediments. The volcanic rocks range in composition from trachybasalt to latite, trachyte and phonolite; the most abundant are trachyte and alkali-trachyte. The volcano is located at the intersection of NESW and NW-SE regional fault systems (Vezzoli, 1988). A caldera collapse accompanied the Mt. Epomeo Green Tuff (MEGT) eruption (Rittmann, 1930) and was later deformed by a simple shearing block resurgence, which has generated a net uplift of the Mt. Epomeo block by about 900 m over the past 30 ka (Gillot et al., 1982; Vezzoli, 1988; Orsi et al., 1991; Tibaldi and Vezzoli, 1998). The beginning of volcanism on the island is not precisely known. The oldest exposed rocks, not dated, are the remnant of a complex volcanic edifice. The volcanism which followed the construction of this volcano (150–74 ka, Poli et al., 1987; Vezzoli, 1988) produced mainly trachytic and phonolitic lava domes and subordinately alkali-trachytic pyroclastic deposits. For the period between 75 to 55 ka, Brown et al. (2008) indicate that this period bore witness to the largest eruptions recorded on the island. The deposits of at least 10 explosive phonolite to basaltic-trachyandesite eruptions have been described and interpreted. They record a diverse range of explosive volcanic activity including voluminous fountain-fed ignimbrite eruptions, fallout from sustained eruption columns, block-and-ash flows, and phreatomagmatic eruptions. The following caldera forming phase is MEGT eruption, dated at about 55 ka (Gillot et al., 1982; Poli et al., 1987; Vezzoli, 1988). The volcanic and magmatic history of Ischia in the past 55 ka has been subdivided in three periods of activity. The first

period, initiated with the MEGT eruption, continued up to 33 ka with hydromagmatic and magmatic explosive eruptions (*Orsi and Chiesa, 1988; Orsi et al., 1991*). An early trachytic magma was followed by trachytic-to-alkalitrachytic magmas with increasing degree of differentiation and constant isotopic composition through time, suggesting that the magma chamber was differentiating mostly through fractional crystallisation processes. The trachybasaltic eruption of Grotta di Terra, at about 28 ka, marked the beginning of the second period, which continued until 18 ka with sporadic explosive (alkalitrachytic) and effusive (trachytic) eruptions. The erupted magmas varied through time from trachybasalt to alkalitrachyte with increasing incompatible elements and Sr isotope ratio, suggesting arrival of new magma, progressive differentiation and mixing with the resident alkalitrachytic magma. Lava effusions were followed by phreatomagmatic and magmatic explosive eruptions (*Vezzoli, 1988*). During the last period, which began at about 10 ka (*Poli et al., 1987*), volcanism was mostly concentrated within the eastern portion of the island, where normal faults were generated in response to the extensional stress regime induced by resurgence. Reactivation of regional faults, likely determined the reappraisal of volcanism also in the north-western corner of the island, outside the resurgent area, at about 6.0 ka. After a period of quiescence, volcanism resumed again in the eastern portion of the island at about 5.5 ka (*Orsi et al., 1991, 1996; de Vita et al., 2006*). The following repose was interrupted at about 2.9 ka by a very intense phase of activity (35 eruptions) which ended in 1302 A.D. with the last eruption on the island (*Poli et al., 1987; Vezzoli, 1988*). A decrease in Sr isotope ratio of the magma erupted at the beginning of this period suggests the arrival of a geochemical distinct magma into the system (*Civetta et al., 1991*). Mostly trachytic and subordinately latitic magmas were erupted during this period. Compositional variations, isotopic and mineralogical disequilibria suggest mixing among compositionally different magmas (*Piochi et al., 1999*). Although Ischia is still an active volcano and home for 50,000 people, no risk mitigation action have been planned as yet.

I.4.1.4. Island of Procida-Vivara

Volcanic activity of the double-island of Procida-Vivara in the Gulf of Naples was restricted between 70 and 14 ka BP (*De Astis et al., 2004*). This activity is characterized by low-energetic explosive eruptions (*Scandone et al., 1991*). The only Fiumicello (considered older than 55 ka and 31 ka) and Solchiaro (between 19 and 14 ka) eruptions are more

widespread (Rosi et al., 1988; Scandone et al., 1991; De Astis et al., 2004). The composition of these volcanic products is restricted at a trachybasaltic field.

I.4.2. Roman province

The Roman province is composed of two aim volcanic districts: the Monti Sabatini and the Alban Hills (Figure 1-24). The both are characterized by a high and sometimes discontinuous K enrichment relative to silica (Rogers et al., 1985; Karner et al., 2001). These two volcanic districts belong to the silica-undersaturated potassic Roman Comagmatic Province (Washington, 1906).

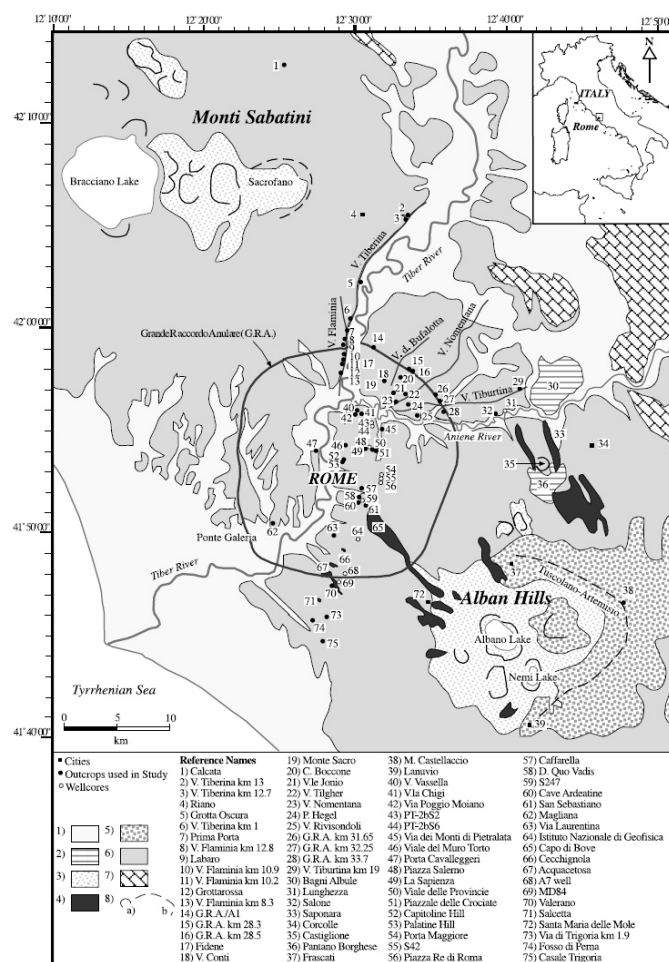


Fig. 1-24: Simplified geologic map of the Monti Sabatini and Alban Hills volcanoes, from Karner et al. (2001).

Monti Sabatini			Alban Hills			
Mattias & Ventriglia (1970)	De Rita et al. (1993)	Karner et al. (2001)		Marra & Rosa (1995) De Rita et al. (1995)	De Rita et al. (1988a)	Fornasieri et al. (1963)
	Hydromagmatic Phase	Hydromagmatic Activity	Peperino di Marino (Lapis Albanus) 36±1 ka*		Final Hydromagmatic Phase	
Tufo di Bracciano	Pizzo Prato, Bracciano, Vigna di Valle Pyroclastic Flow Units					
Tufo Giallo di Sacrofano	Sacrofano Upper Pyroclastic Flow Unit	Tufo Giallo di Sacrofano 285±1 ka*				
			Capo di Bove, Saponara Flowe 277±2, 277±2 ka		Campi di Annibale Edifice (=Faete) Phase	
Tufo Stratificati Varicolori di La Storta	Pyroclastic Fall Products from Sacrofano and local Scoria Cones	Tufo Stratificati Varicolori di La Storta ca. 410 ka	Villa Senni Eruptive Sequence 355±2 ² ; 357±2; 351±3 ka	Villa Senni Eruption	Fourth Tuscolano-Artemisio pyroclastic flow unit (Pozzolanelle; Tufo di Villa Senni)	Tufo di Villa Senni
						Pozzolane Superiori (=Pozzolanelle, Tufo di Giulianello)
			Pozzolane Nere 407±4 ka*	Pozzolane Nere	Third T.A. pyro. flow unit (Pozz. Nere= Tufo Lionato)	Tufo Lionato
			Conglomerato Giallo	San Paolo Unit (=Stage 1)		Pozzolane Nere (Pozzolane d. Tre Fontane)
Tufo Rosso a Scorie Nere (=Tufo Grigio Sabatino)	"Red Tuff with Black Scoria" Pyroclastic Flow Unit	Tufo Rosso a Scorie Nere 449±1 ka*	Pozzolane Rosse 457±4 ka	Pozzolane Rosse	Vallerano Lava Second T.A. pyro. flow unit	Conglomerato Giallo
			Vallerano Lava 460±4 ka*			Pozzolane Rosse (Pozzolane di San Paolo)
Tufo Stratificati Varicolori di Sacrofano (Tufo Antichi, Tufo Pisolitici, Tufo Terrosi, Tufo Granulari)	Pyroclastic Fall Products from Sacrofano and local Scoria Cones	Tufo Terroso con Pomici Bianche 488±2 ka*				Lave dell'Acquacetosa, Vallerano, Selcetta
		Grottarossa Pyroclastic Sequence 514±5; 518±5 ka				
			Tufo di Bagni Albule			Tufo Antichi, Tufo Pisolitici, Tufo Terroso, Tufo Granulare Grigio, Peperino Grigio
Tufo Giallo della Via Tiberina	Sacrofano Lower Pyroclastic Flow Unit	Tufo Giallo di Prima Porta 514±3 ka	Tufo del Palatino 520±8; 528±1 ka	Palatino Unit	Lava dell'Acquacetosa First Tuscolano-Artemisio pyroclastic flow unit	
		Upper Tufo Giallo della Via Tiberina 548±4 ka				
		Lower Tufo Giallo della Via Tiberina 561±1 ka*	Tufo Pisolitico di Trigona 561±1 ka	Tor de' Cenci Unit		
	Pyroclastic Fall Products from Morlupo Edifice	First Ash Fall Deposits 800-590 ka				Tufo Cimeritico Grigio (=Tufo Pisolitico Grigio)

Table 1-2: Eruptive activities of the Monti Sabatini and Alban hills volcanoes, from *Karner et al. (2001)*.

I.4.2.1. Alban Hills

The activities of the Alban Hills volcanic complex (**Table 1-2**) are characterized by ignimbrite eruptions occurred between 500 and 350 ka (*Marra et al., 2003; Freda et al., 2006; Carapezza et al., 2007*) followed by a large caldera collapse. Then, the activity continued with a progressive reduction in volume of emitted magma, until a late hydromagmatic phase which is at the origin of a large number of maar craters, which were accompanied by small-volume basic ignimbrite eruptions (*Trigila, 1995; De Rita et al., 1995; Freda et al., 2006*).

I.4.2.2. Sabatini Volcanic District

The Sabatini Volcanic District (SVD) is localised 30 km north-west of Rome. The activity between 514 and 449 ka (**Table 1-2**) of this volcanic complex, was characterised by highly explosive eruptions that produced widespread Subplinian and Plinian fall deposits

(Sottili *et al.*, 2004). Later on, the ignimbrite eruption of Tufo Giallo di Sacrofano, 285 ka, and produced phonotrachytic pyroclastic flows and surges (Karner *et al.*, 2001). The final activity was mainly a hydromagmatic activity (De Rita *et al.*, 1993; Karner *et al.*, 2001).

I.4.3. Aeolian province

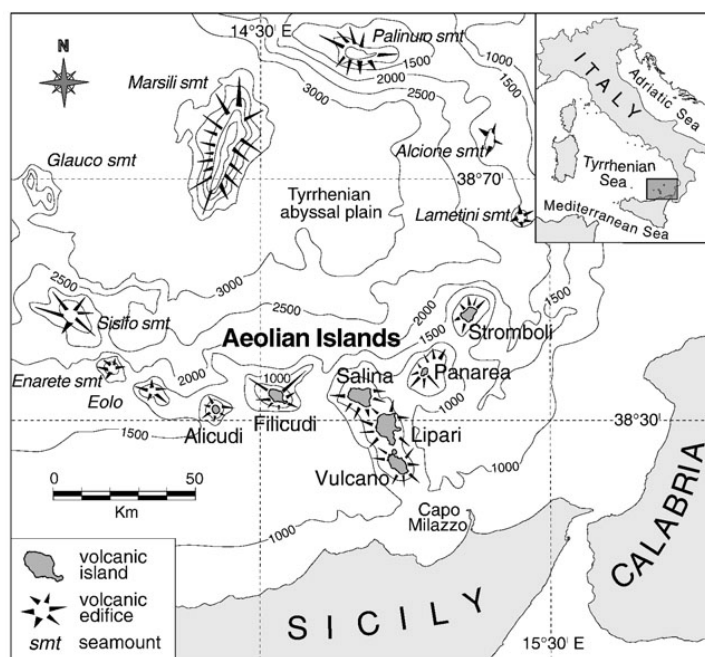


Fig. I-25: Bathymetry of the Southern Tyrrhenian Sea where the location of the Aeolian Islands is outlined, from Lucchi *et al.* (2008) modified from Beccaluva *et al.* (1985).

The Aeolian Islands are the emerged volcanoes of the Aeolian Volcanic District, a complex volcanic region located in the southern border of the Tyrrhenian Sea, which also includes several seamounts (Figure 1-25). The subaerial portion of the seven mainly calc-alkaline volcanic edifices has developed (under strong control of regional stress fields) from ~400 ka BP on Salina and Filicudi up to historical and present times on Lipari, Vulcano and Stromboli islands (Keller, 1980a, 1980b; Capaldi *et al.*, 1985; Gillot, 1987; Gillot and Keller, 1993; Hornig-Kjarsgaard *et al.*, 1993; Tranne *et al.*, 2002a,b; De Rosa *et al.*, 2003; Lucchi *et al.*, 2003, 2007; De Astis *et al.*, 2006).

Together with Salina, the islands of Lipari and Vulcano form a NNW-SSE alignment which is orthogonal to the volcanic arc. The development of these volcanic islands is linked to the presence of an active crustal discontinuity (*Barberi et al., 1994; Ventura, 1994*), corresponding to the NNW-SSE trending dextral strike-slip fault system named Tindari-Letojanni (*Ghisetti, 1979*).

I.4.3.1. Island of Lipari

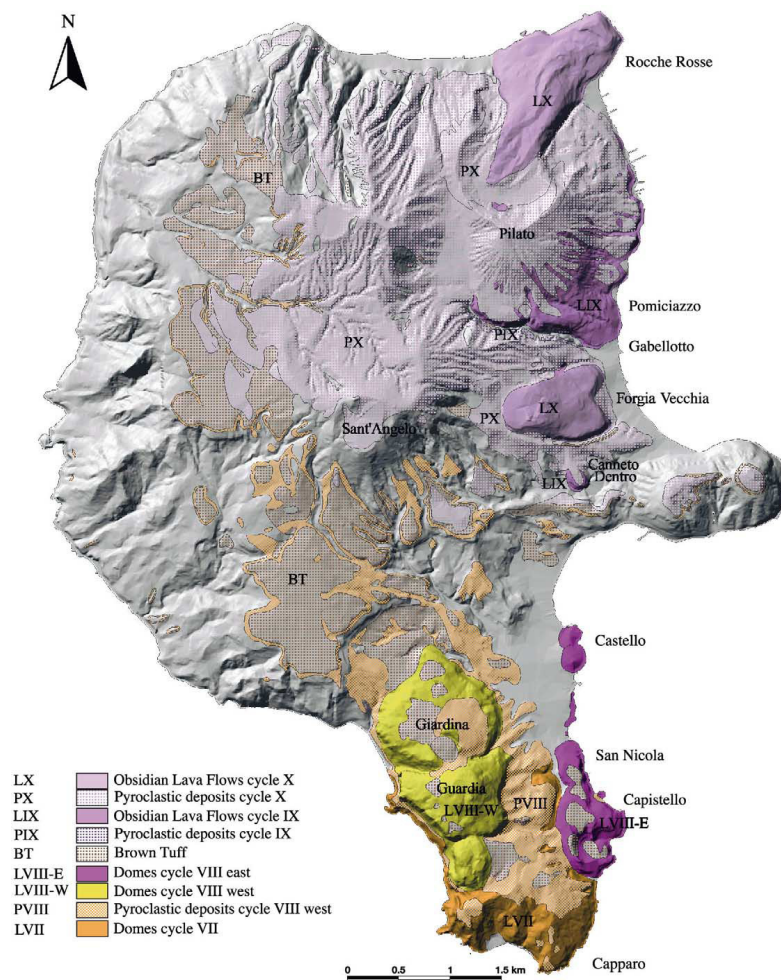


Fig. 1-26: Schematic geological map of Lipari Island for the post-42 ka products, from Gioncada et al. (2003) modified after Pichler (1980) and Crisci et al. (1983).

Subaerial volcanic activity at Lipari (**Figure 1-27**) dates back to around 220 ka (*Crisci et al., 1991*), with andesitic products of high-K calc-alkaline affinity. After the growth of Mt.

Sant'Angelo volcano in the central sector of Lipari, which lasted until 98 ka BP (*Crisci et al., 1991*), a relatively long period of quiescence occurred. The activity resumed at about 42 ka on the southernmost part of the island, with changed composition. The first Lipari products resting on the deposits of Mt. Sant'Angelo consist of rhyolitic lava domes and pyroclastic deposits. These overlie a brown ash layer with juvenile glass shards having shoshonitic composition, that was erupted by offshore vents between the islands of Lipari and Vulcano (Brown Tuff; *Crisci et al., 1983; Losito, 1989*). The K/Ar determinations carried out on the lowest rhyolitic lava domes gave an age of 42 ka (*Crisci et al., 1991*). Three further Brown Tuff ash flow deposits are interbedded in the post-42 ka rhyolitic lava domes and pyroclastic products. The rhyolitic lavas and pyroclastic products below the Brown Tuff are dated at 23.5 ka by *Crisci et al. (1991)*. After 23.5 ka, explosive activity in the southern part of the island gave rise to rhyolitic fall and surge deposits followed by the extrusion of endogenous lava domes (Monte Guardia and Giardina; *Crisci et al., 1991*). These products are capped by a Brown Tuff layer dated at 16.8 ka. The most recent volcanic activity on Lipari shifted northward (*Cortese et al., 1986; Sheridan et al., 1987*) and several rhyolitic eruptions took place following the emplacement of the upper ash flow unit at 16.8 ka. The rhyolitic eruptions occurred from distinct vents aligned along N-S direction, representing the northward continuation of the San Nicola-Castello alignment (*Gioncada et al., 2003*). The successive rhyolitic explosive phase, Gabelotto-Fiumebianco, is dated ca. 8.6 ± 1.5 ka (*Crisci et al., 1991*). The latest phase gave rise to the pyroclastic deposits and lava flow of the Forgia Vecchia centre, to a pumice cone (Monte Pilato) and ended with an obsidian lava flow (Rocche Rosse). Historical reports indicate the date of A.D. 729 for the latest volcanic activity on Lipari (*Cortese et al., 1986*) while the archeo-magnetism methods indicate age between A.D. 1030-1528 (*Zanella, 2006*) or at A.D. 1200-1240 (*Arrighi et al., 2006*).

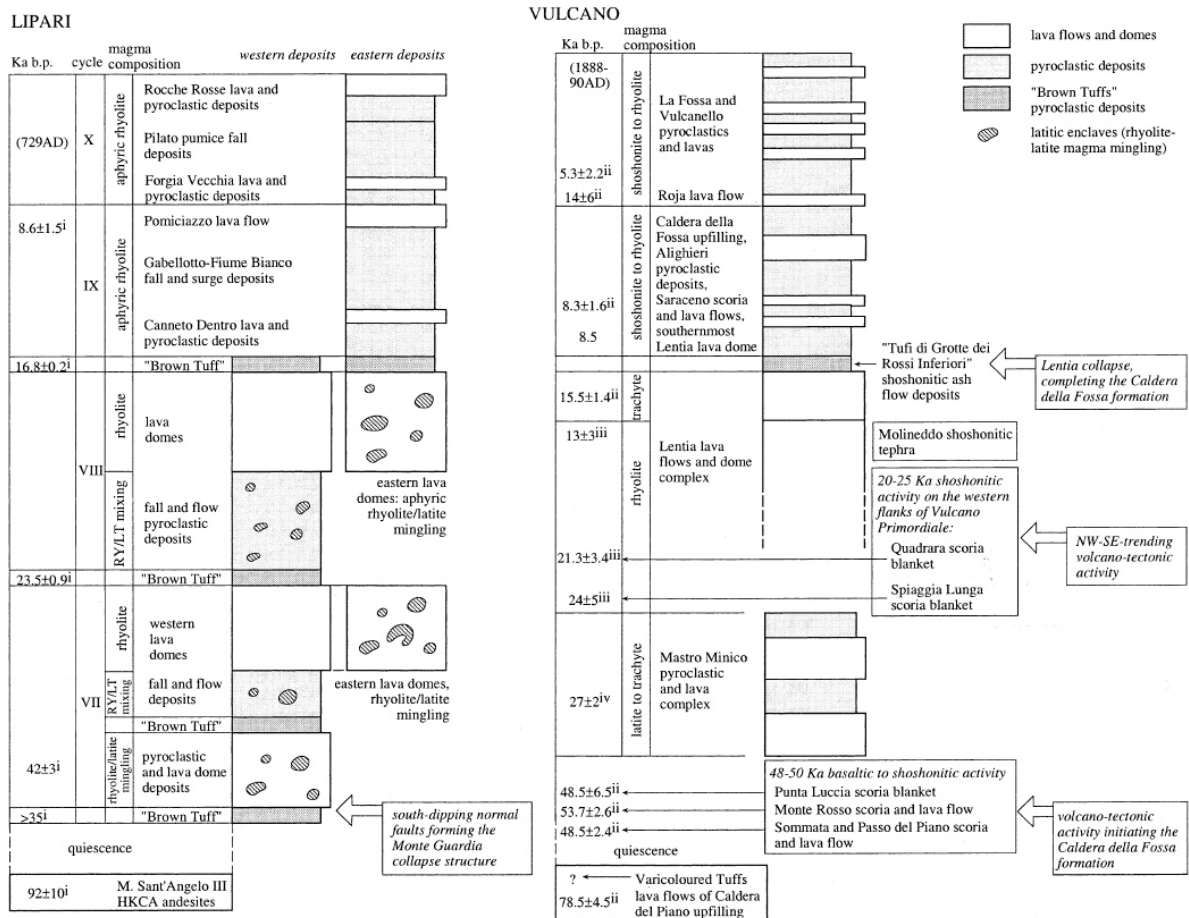


Fig. 1-27: Composite schematic stratigraphic columns of the Lipari and Vulcano deposits in the post-50 ka period from Gioncada et al. (2003).

I.4.3.2. Island of Vulcano

The Vulcano oldest subaerial products (Figure 1-27) date back to 120 ka and belong to a shoshonitic stratovolcano termed Vulcano Primordiale (120-100 ka; Keller, 1980b), forming the southern part of the island (Figure 1-28; Gioncada et al., 2003). At around 100 ka, the edifice was dissected by arcuate faults forming a caldera structure (Caldera del Piano), filled by later volcanic activity (De Astis et al., 1989). Around 50 ka ago north-dipping normal faults affected the northern part of the old edifice, initiating the formation of the subsidence basin called Caldera della Fossa (De Astis et al., 1989; Gioncada and Sbrana, 1991), and basaltic to shoshonitic eruptions occurred (scoria deposits and lava flows of Sommata, Monte Rosso, Punta Luccia, Piano Luccia). A second important volcano-tectonic phase occurred around 25 ka (Votaggio et al., 1997), in coincidence with shoshonitic eruptions along NNW-SSE trending faults (Spiaggia Lunga and Quadrara scoria blankets).

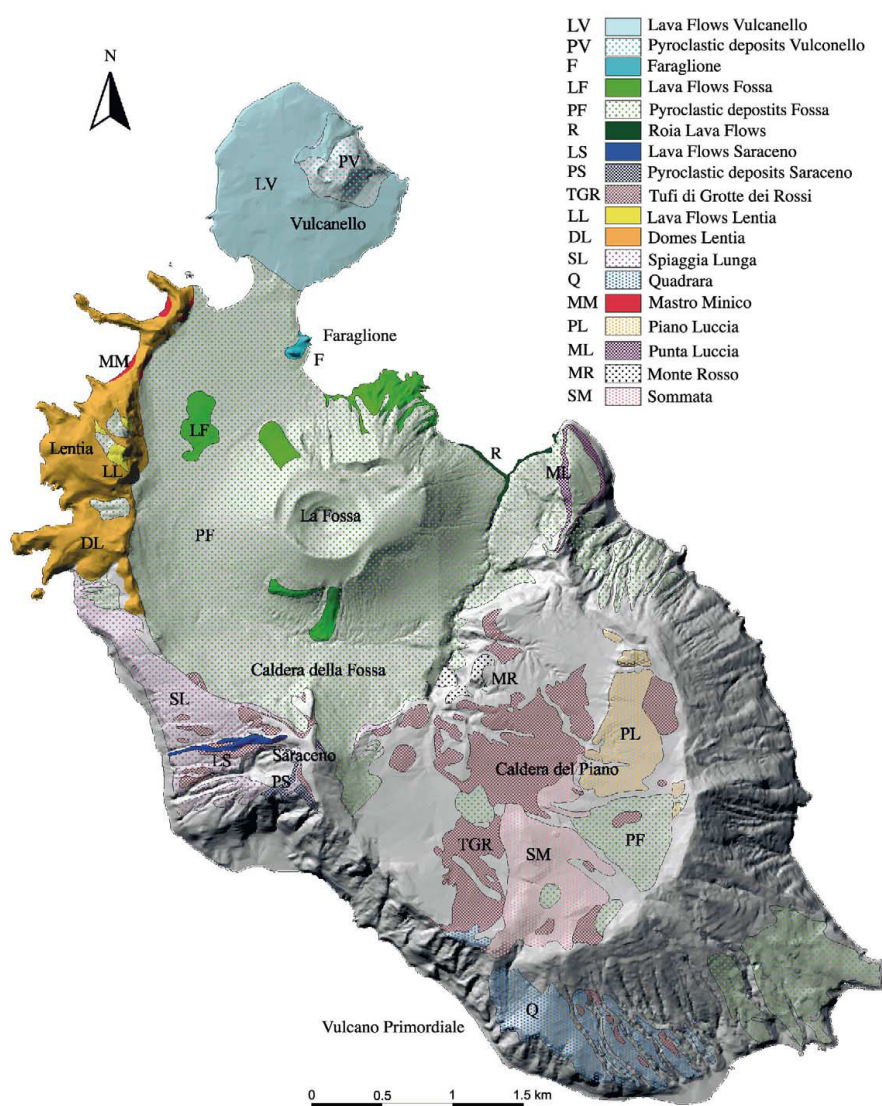


Fig. 1-28: Schematic geological map of Vulcano Island, from Gioncada *et al.* (2003) modified after Keller (1980b).

In the meantime, latite to rhyolite products were erupted in the northern sector of Vulcano Island (Mastro Minico-Lentia complex). The Mastro Minico sequence consists of an alternation of latitic to trachytic lava and pyroclastic products, dated at the base to 27.9 ka (Soligo *et al.*, 1999). This is followed by a series of rhyolitic lava domes, closed by trachytic lava flows (Lentia, 13-15 ka). At about 15 ka (Frazzetta *et al.*, 1984), the Lentia complex was affected by an important collapse, which completed the formation of the Caldera della Fossa structure with its N-S trending western fault. This coincided with the huge eruption of the Tufi di Grotte dei Rossi, having its source area located inside the Caldera della Fossa volcano-tectonic depression, which could be correlated to the Brown Tuffs capping the rhyolitic domes on southern Lipari (De Astis *et al.*, 1997; Losito, 1989). After 15 ka, the activity

concentrated in the northern sector of the island, and shoshonitic and latitic products filled the depression. *Soligo et al. (1999)* report a small rhyolitic dome, immediately south of Lentia, dated at 8.5 ka. Several vents activated along a N-S alignment (Saraceno, Fossa, Vulcanello), coinciding with the direction of the contemporaneous activity at Lipari. La Fossa cone building went on for 6,000 years (*Frazzetta et al., 1984*); the last eruption occurred in 1888-1890 and the volcano is still active with fumarolic activity. The composition of the products erupted at La Fossa varies from latitic to rhyolitic, with minor shoshonites.

I.4.3.3. Island of Stromboli

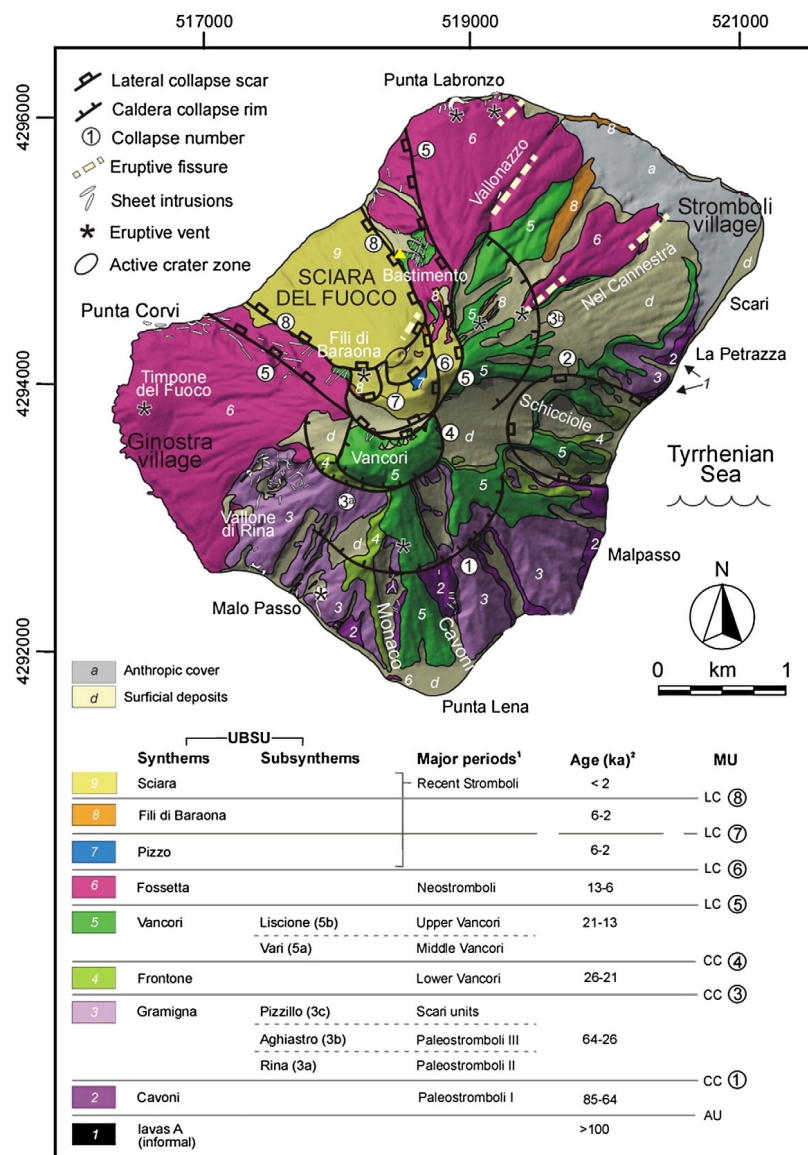


Fig. 1-29: Schematic geological map of Stromboli Island from *Casagli et al. (2009)*.

Stromboli Island represents the 976 m high emerged portion of a volcanic cone located in the Tyrrhenian Sea 60 km North of Sicily (Italy). The island rises from a depth of about 2,500 m below sea level. All the rocks of Stromboli are volcanic in origin and probably formed within the last 100 ka. They consist of subaerial lava flows, pyroclastic materials and subordinate volcanoclastic sediments. Dykes and sills are exposed on the eroded slopes of the volcano. Products of Stromboli have been referred to cycles which are separated by important structural events. The products of the old activity of the main island consist of lavas and pyroclastics with calc-alkaline affinity and age of about 100 ka (*Gillot, 1984; Francalanci et al., 1986, 1988 1989; Francalanci, 1987*). The lava plug of Strombolicchio is also calc-alkaline with an even older 200 ka. The post-100 ka evolution of the volcano has been subdivided into four periods (**Figure 1-29**): Paleostromboli (100–26 ka), Vancori (26–13 ka), Neostromboli (13–6 ka), recent Stromboli (6 ka-present) (*Gillot and Keller, 1993; Keller et al., 1993; Santacroce et al., 2003; Casagli et al., 2009*). Products of Neostromboli consist of K-rich basalts often bearing small phenocrysts of leucite (Lc-shoshonites). Lavas and pyroclastics of the Vancori period are evolved andesites of the high potassium calc-alkaline suite. In present, the activity of Stromboli volcano is characterized by very low energy explosions, occurring every 10–20 min, throwing out lava above the crater rim. The typical activity of Stromboli consists of intermittent mild explosions ejecting scoriaceous bombs, lapilli and ash from vents where glowing lava stands at high level in an open conduit. The explosions occur when large bubbles of compressed gas burst at the surface of the magma column resulting in the formation of a jet of hot gas and incandescent lava fragments. Although the volcanic activity of Stromboli has been known since the Classic Age, historical sources older than 1,000 A.D. are not accurate enough to assess if the activity was exactly the same as we see today.

On average two or three mid-scale explosions per year occurred over the past 100 years. Less frequently much more violent explosions occur. They produce showers of incandescent scoriae and spatter within a distance of several kilometers from the craters sometimes affecting the two villages on the coast (Stromboli and Ginostra) like in 2003 or 2007 (*Rosi et al., 2006; Scandone et al., 2009*).

I.4.3.4. Island of Salina

The geology and the evolution of the island have been studied by *Keller (1980)*, who distinguishes two main cycles of volcanic activity. The older cycle (from 430 to 127 ka) is characterized by the eruption of high-alumina basalts from four stratovolcanoes (Capo Rivi, Corvo, Fossa delle Felci) with dacites and andesites as the final products. The younger cycle (100-13 ka) built up the andesitic cone of Monte dei Porri and ended with the formation of the explosion crater of Pollara on the north-western edge of the island (*Calanchi et al. 1988; De Rosa et al. 1990*). In the last 30 ka the volcanic activity resumed at least three times within the Pollara depression. It began with the effusion of the andesitic to dacitic lava flows of Punta di Perciato (30 ka) and was followed by two explosive eruptions Lower and Upper Pollara pyroclastics 24 and 13 ka respectively (*Keller, 1980; Calanchi et al., 1993; De Rosa et al., 2002*) whose deposits built up a complex tuff-ring structure which represents one of the most impressive morpho-tectonic features of Salina.

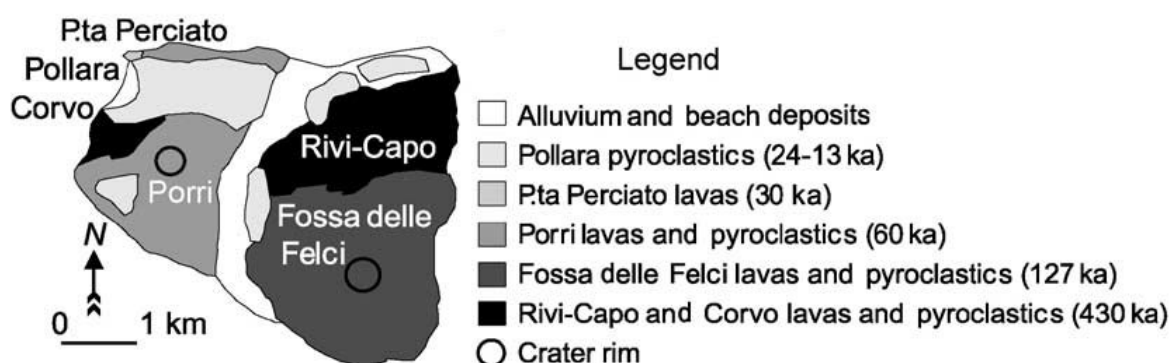


Fig. 1-30: Schematic geological map of Salina Island from *De Rosa et al. (2002)* modified from *Barca and Ventura (1991)*.

I.4.4. *Sicilian province*

The Sicilian province (**Figure 1-31**) is composed of the Mount Etna localised in the East part of the Sicily Island.



Fig. 1-31: Satellite image of Aeolian Islands, Mount Etna and Pantelleria Island (© Google earth).

I.4.4.1. Mount Etna

Mount Etna is the largest active volcano in Europe, reaching 3,350 m a.s.l. and covering a surface about 1,260 km². Mount Etna started its activity at about 600 ka, after the end of Upper Pliocene to Pleistocene subaqueous and subaerial eruptions at the north-western edge of the Iblean Plateau. Mt. Etna is a stratovolcano, consisting of edifices centred on distinct eruptive axes, of whom the most recent ones may be still recognized.

Etnean magmas rise up from a mantle source into the crust, subject to strong extensional stresses, and the volcano is actually placed at the intersection of two major regional fault systems, trending respectively NNW-SSE (Iblean-Maltese) and NNE-SSW, along the coastline between Taormina and Messina.

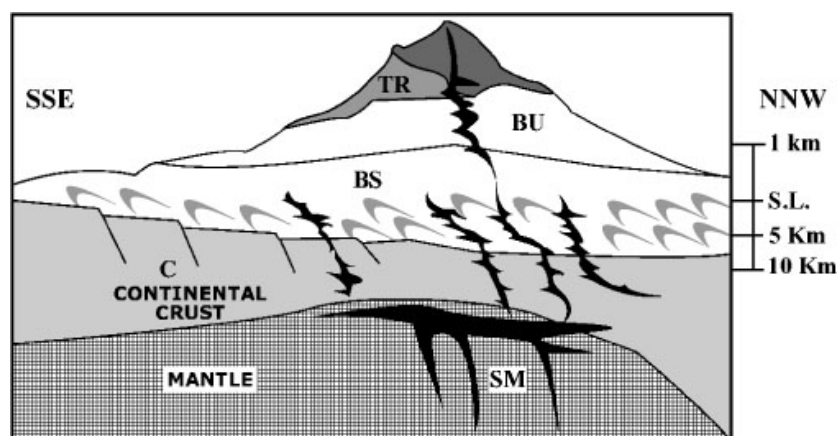


Fig. 1-32: Sketch NNW-SSE section of Mount Etna from Santacroce *et al.*, (2003). Note the different scale of elevations above and below sea level (lm). MB: Mongibello Unit; TR: Trifoglietto Unit; UB: Basal volcanic Units (older than 80 ka); BS: sedimentary Basement Successions; SM: main magma reservoirs.

Data on mineral phases, fluid and melt inclusions and some seismological evidence suggest a 20 to 15 km deep plexus of magma-filled fractures and of shallower and smaller chambers, where magma resides, differentiates and eventually gives rise to the activity of the various centers which have followed each other in time (**Figure 1-32**). The oldest (600 ka) volcanic centers are submarine tholeiitic to transitional basalts, erupted on the sea floor (ca. 500 m depth) of a wide gulf, extending between the northern mountain chain and the Iblean Plateau to the south. After a strong regional uplift, subaerial tholeiites were erupted (ca. 300 ka): they currently outcrop only in the south-western sector, but probably covered much wider areas. Central volcanoes, fed by Na-alkaline magmas, started to develop (200 ka) above the earliest volcanic levels. The younger period than 200 ka was characterised by: strombolian to plinian eruption (ca. 100 ka, *Coltelli et al.*, 2000), plinian benmoreitic activity (80 to 100 ka, *Coltelli et al.*, 2000), strombolian to Subplinian from basaltic to mugearitic activity (80 to 16 ka, *Coltelli et al.*, 2000). The most recent Mongibello activity (< 30 ka) was characterized by recurrent, significant explosive activity until a few thousands of years ago. Paroxysmal eruptions gave origin to calderas, still recognizable, although largely filled by younger products (“Ellittico caldera”, 15 ka, ca. 4.5 km across; Piano caldera, 122 B.C., *Kieffer, 1979; Cortesi et al., 1988; Gillot et al., 1994; Coltelli et al., 2000*). During the last centuries explosive activity of Mongibello was quite mild, semi-persistent at the summit vents to sporadic from lateral vents. Intensity of summit vent phenomena is very variable (quiet steam emission to Strombolian explosions and lava fountains), infrequently combined with small

lava effusions, lasting few hours up to several months or even years. At present there are several vents in the top region, each behaving independently and suggesting a complex feeding system for their activity. Peripheral vents can open also at low elevations (down to 300 m a.s.l.), even outside the edge of the volcanic cover (Gravina di Catania, Mojo Alcantara). The summer 2001 and winter 2002 eruptions are to be ascribed to this last type of fairly explosive events. This activity lasts from a few days to several months, exceptionally for years. In the last 350 years, around 70 eruptions occurred, irregularly distributed in time and space.

Romano (1982)	Guest et al. (1984)		Kieffer (1985)	Chester et al. (1987)		Coltelli et al. 2002
RECENT MONGIBELLO			MODERN MONGIBELLO	RECENT MONGIBELLO		UNIT E and Milo lahar
UPPER TUFFS AND LAHARS	MILO LAHAR	UPPER TEPHRA 5-6 ka BP	UPPER UNIT yellow ash and lapilli layers (strombolian activity similar to the present) LOWER UNIT yellow ash with scattered basaltic lapilli (unique phreatomagmatic eruption)	UPPER TEPHRA	UPPER UNIT	13 ka BP to the Present
	yellow ash and scoria layers (several eruptions) 8.7 - 2.4 ka BP				LOWER UNIT	
BIANCAVILLA MONTALTO IGNIMBRITE 15.5 - 15 ka BP			BIANCAVILLA IGNIMBRITES 14180 a BP	BIANCAVILLA - MONTALTO IGNIMBRITES about 15 ka BP		UNIT D 15.5 - 15 ka BP
LOWER TUFFS AND LAHARS yellow ashes	LOWER TEPHRA	UPPER UNIT yellow ash with scattered scoria lapilli (unique phreatomagmatic eruption)		LOWER TEPHRA	UPPER UNIT	UNIT C 80 - 15 ka BP
		MIDDLE UNIT basaltic scoria lapilli and ash layers (unique phreatomagmatic eruption with strombolian episodes)			MIDDLE UNIT	
	LOWER UNIT yellow ash with scattered hawaiitic lapilli (unique phreatomagmatic eruption with strombolian episodes) 26.4 ka BP	MILO LAHAR	LOWER UNIT			
lahars of S. Tecla pumice and volcanogenic sediments in Acireale area						UNIT B 100- 80 ka BP
						UNIT A ~100 ka BP
				ACIREALE TEPHRA AND LAHARS S. Caterina ashes and lahars S. Tecla lahars 150 - 70 ka BP		

Table 1-3: Eruptive activities of the Mount Etna from *Coltelli et al. (2000)*.

I.4.5. Sicily Channel

I.4.5.1. Pantelleria

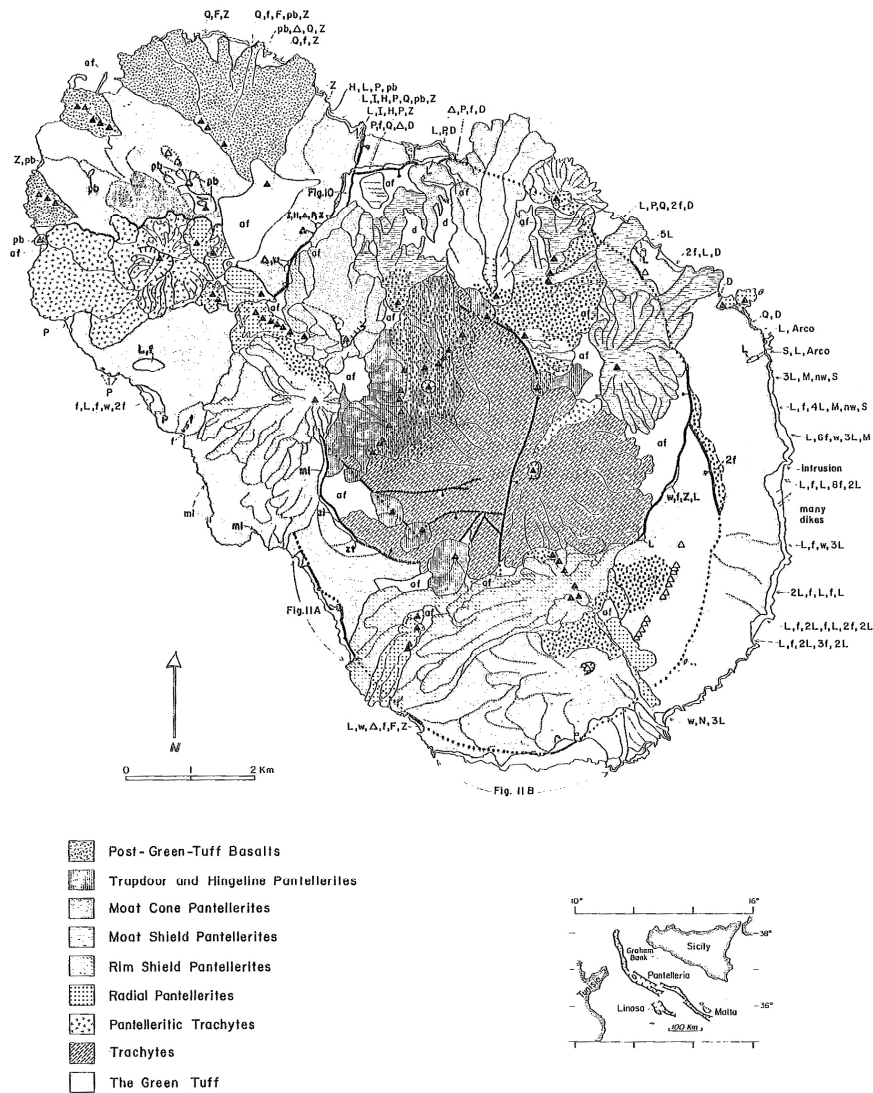


Fig. 1-33: Map of Pantelleria from *Mahood and Hildreth (1986)*.

The 13x8 km pear shaped Island of Pantelleria is situated in a submerged continental rift in the Strait of Sicily and Tunisia (**Figure 1-33**). Pantelleria is a volcanic island with subaerial eruptive history longer than 300 ka (*Cornette et al., 1983; Civetta et al., 1984; Mahood and Hildreth, 1986*). The activity of Pantelleria volcano in this period is mainly composed of explosive eruptions and less effusive eruptions. Some of tephra layer from

Pantelleria were yet found all over the Mediterranean area (e.g. Keller, 1978; Paterne et al., 2008). One of the most widespread corresponds to the Green Tuff eruption with a 6 km-wide caldera collapse (45 ka, Wright, 1980; Cornette et al., 1983; Civetta et al., 1984; Mahood, 1984; Mahood and Hildreth, 1983, 1986).

The aim geochemical particularity of explosive phase deposits is an excess of alkalies and alumina in the peralkaline magma (Mahood and Hildreth, 1986; Paterne, 1985; Paterne et al., 2008).

The effusive activity inside and extra caldera are composed of voluminous trachytic lava flows (Mahood and Hildreth, 1986). The most recent activity was a basaltic submarine eruption 4 km north-west of Pantelleria Island in 1891.

I.4.6. Resumed volcanic activity of Italian volcanoes

In the **Figure 1-34** and **1-35** (next pages) is resumed the main volcanic activities of the main Italian volcanoes.

Fig. 1-34: Main volcanic activity of Mt Somma-Vesuvius (from Santacroce, 1987; Santacroce et al., 2003, 2008; Giaccio et al., 2009); Ischia Island (from Gillot et al., 1982; Poli et al., 1987; Vezzoli, 1988; Orsi and Chiesa, 1988; Orsi et al., 1991; Tibaldi and Vezzoli, 1998; de Vita et al., 2006; Brown et al., 2008); Phlegrean Fields (from Barberi et al., 1978; Rosi et Sbrana, 1987; Orsi et al., 1992, 1996, 2004; Wohletz et al., 1995; Pappalardo et al., 1999; De Vivo et al., 2001); Procida-Vivara (from Rosi et al., 1988; Scandone et al., 1991; De Astis et al., 2004) and Roman Province (from Tragila, 1995; De Rita et al., 1995; Karner et al., 2001; Marra et al., 2003; Freda et al., 2006; Carapezza et al., 2007).

Fig. 1-35: Main volcanic activity of Lipari Island (from Pichler et al., 1980; Crisci et al., 1983, 1991; Cortese et al., 1986; Sheridan et al., 1987, Losito et al., 1989; Gioncada et al., 2003); Vulcano Island (from Keller et al., 1980; Frazzetta et al., 1984; De Astis et al., 1989; Gioncada and Sbrana, 1991; Voltaggio et al., 1997; Soligo et al., 1999; Gioncada et al., 2003); Stromboli Island (from Gillot, 1984; Gillot and Keller, 1993; Keller et al., 1993; Casagli et al., 2009); Salina Island (from Keller, 1980; Calanchi et al., 1988, 1993; De Rosa et al., 2002); Mt Etna (from Cortesi et al., 1988; Gillot et al., 1994; Coltelli et al., 2000); and Pantelleria Island (from Mahood and Hildreth, 1986).

Fig. I-34:

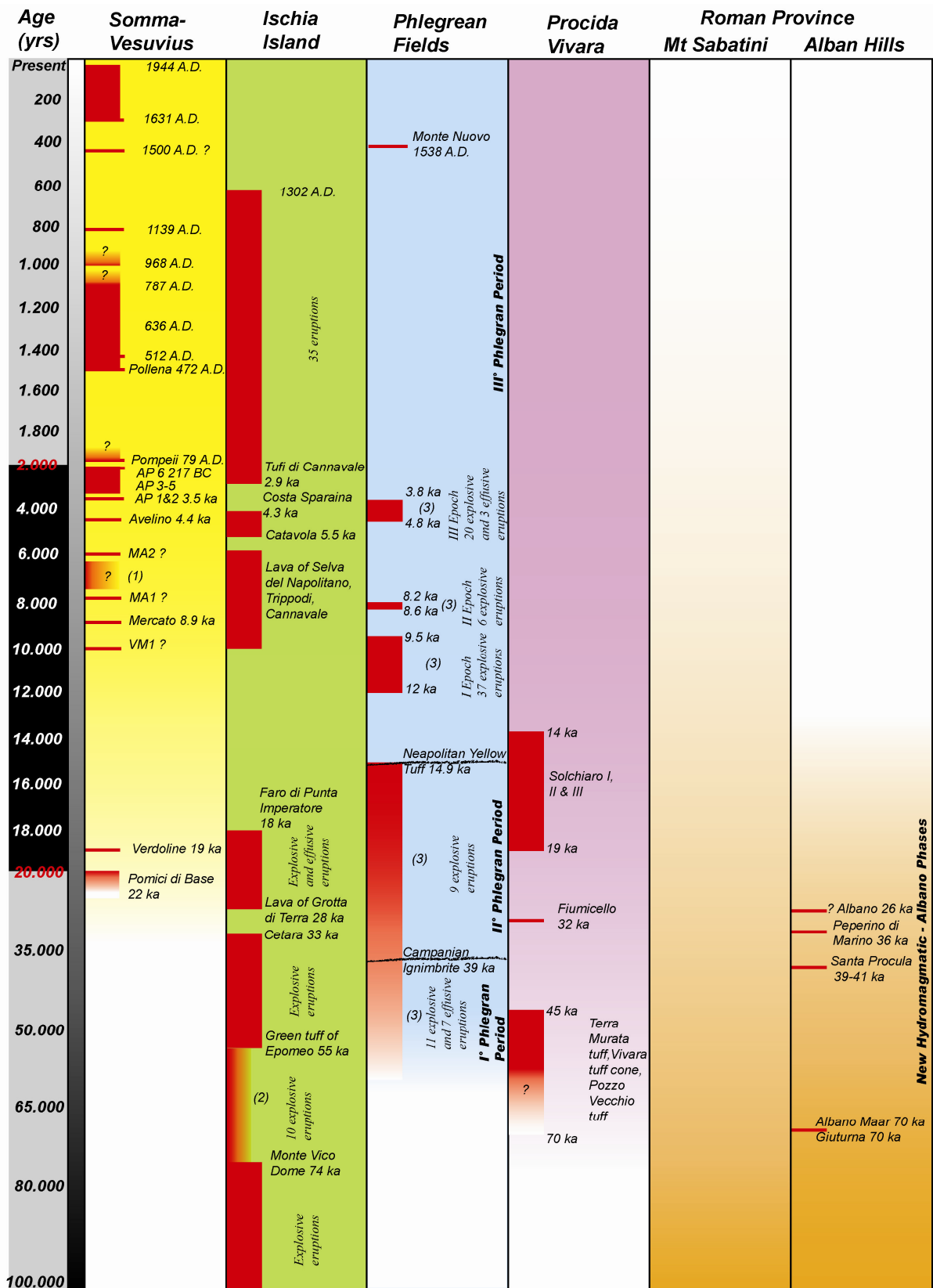


Fig. 1-34 continued:

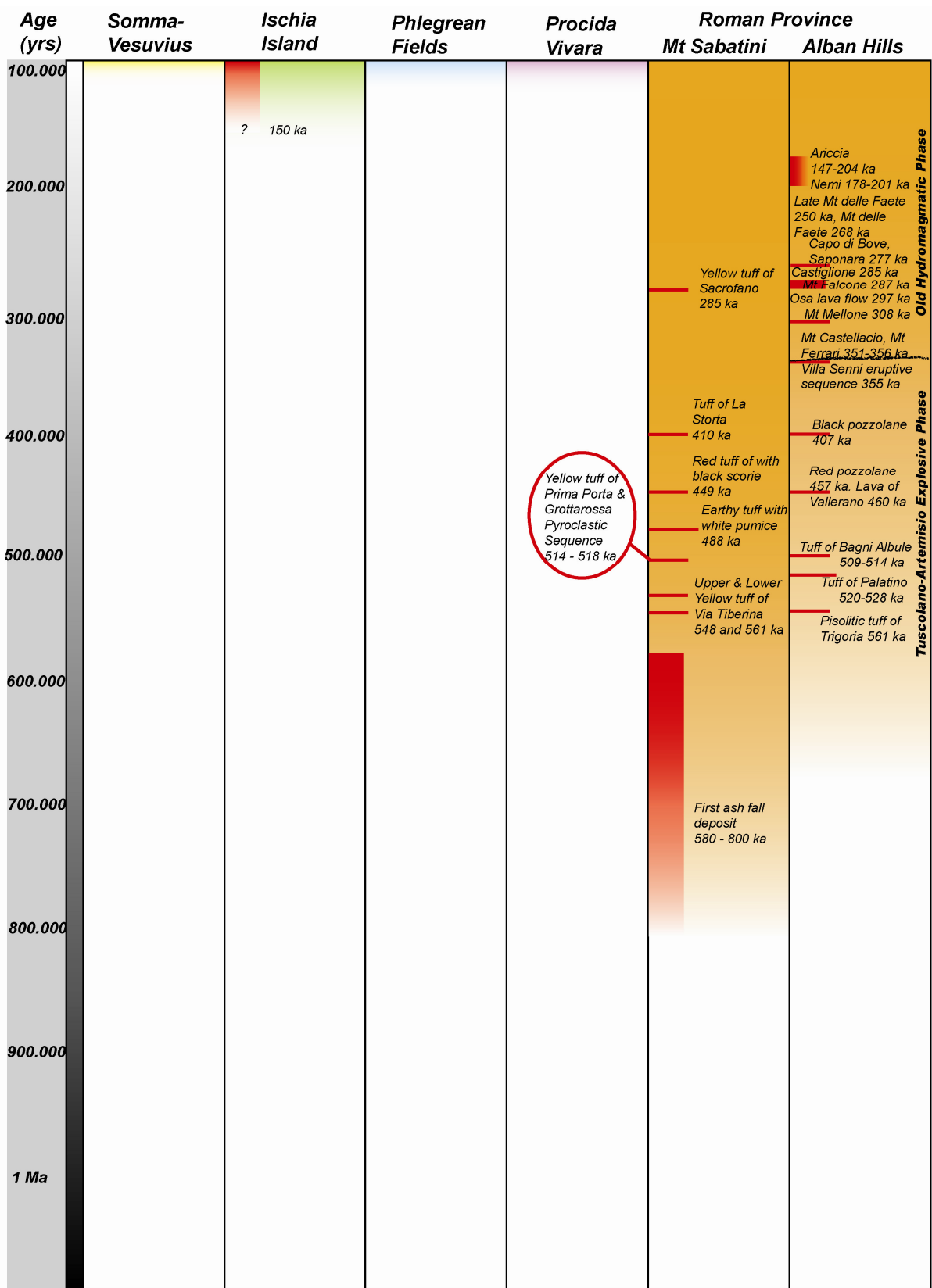


Fig. 1-35:

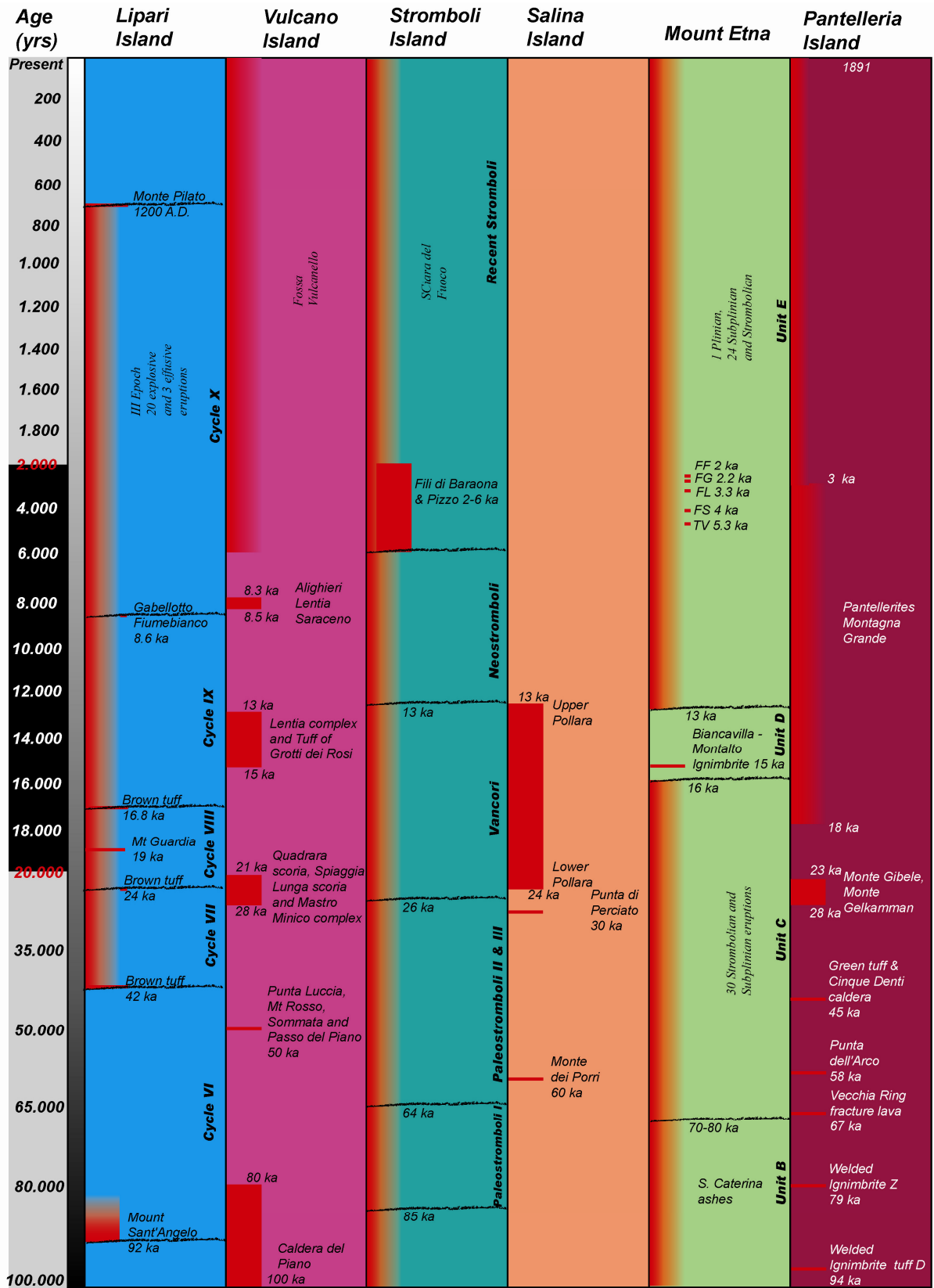
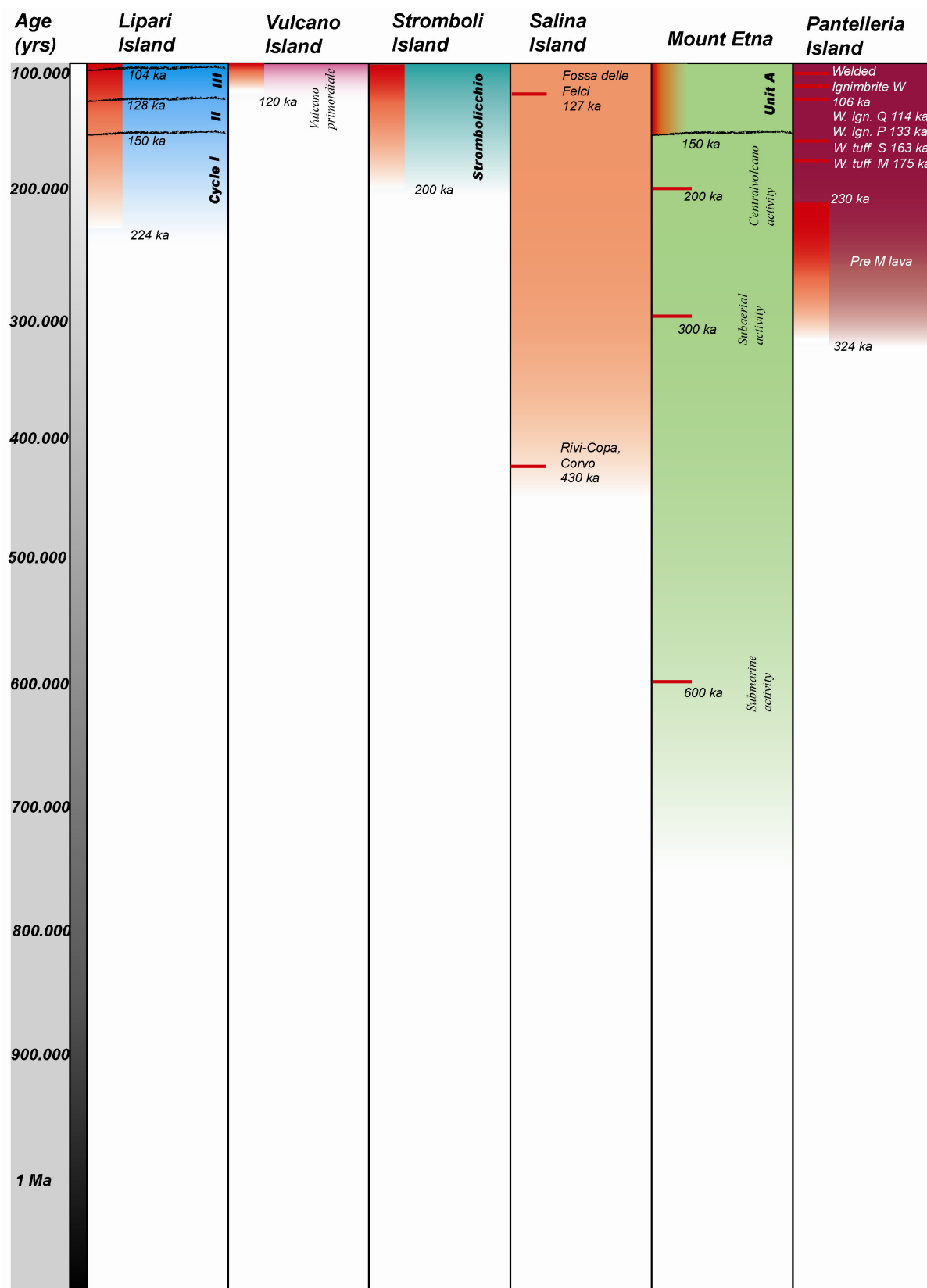
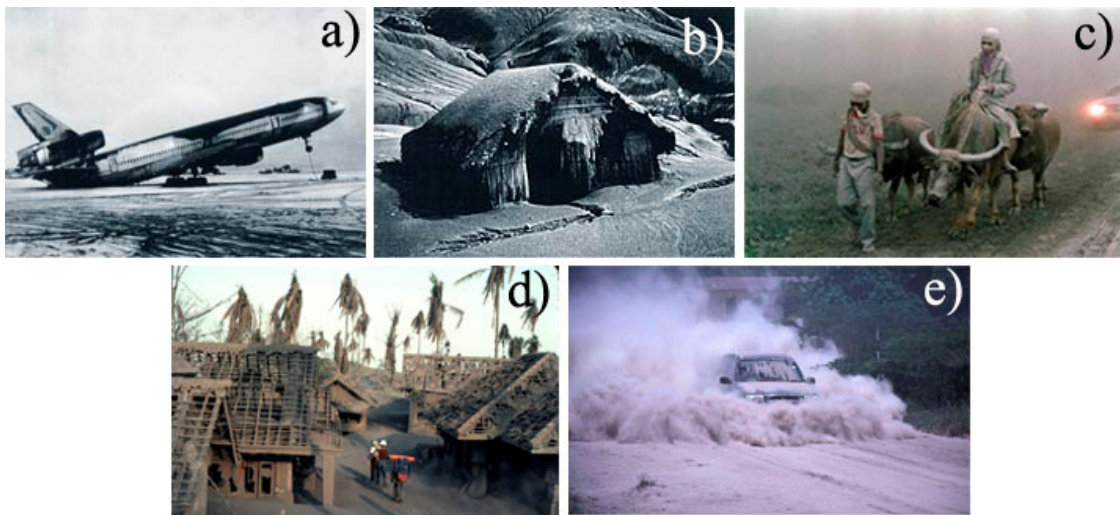


Fig. I-35 continued:



I.5. Distal risks and hazards

Several European settlements are at risk from the impact of explosive volcanic eruptions. Plinian and Subplinian eruptions can be accompanied by tephra fall many last hours or days, posing threats to people, building and economic activity. Ash is not soft, but is hard and abrasive consisting mostly of pulverized rock and silica. It does not dissolve in water, is mildly corrosive, and conducts electricity when wet. Winds can carry ash vertically and horizontally great distances, and thus can create economic and health hazards in unexpected areas. Numerous historical examples exist of tephra damage and tephra casualties (*Blong, 1981; Spence et al., 2005a, 2005b*). For some distance from the source, up to tens of kilometres, tephra falls can accumulate to sufficient depth to cause roof collapse, causing further death and injury. Tephra can also be disruptive to agriculture, transport, communications and industry. These sectors can be impacted even in regions distal to the main volcanic plume (**Figure 1-36**).



Fig; 1-36: a) DC-10 airplane recovered of Pinatubo's products, 1991 (U.S. Navy photo by R.L. Rieger); b) ash fall on native hut, Pinatubo, 1991 (USGS photo by R.P. Hoblitt); c) Village evacuation, Pinatubo, 1991, (AP Photo); d) destroyed village, Galunggung, 1982, (USGS photo by J. Lockwood); e) Soufriere Hills eruption, 2001 (Horwell and Baxter, 2006).

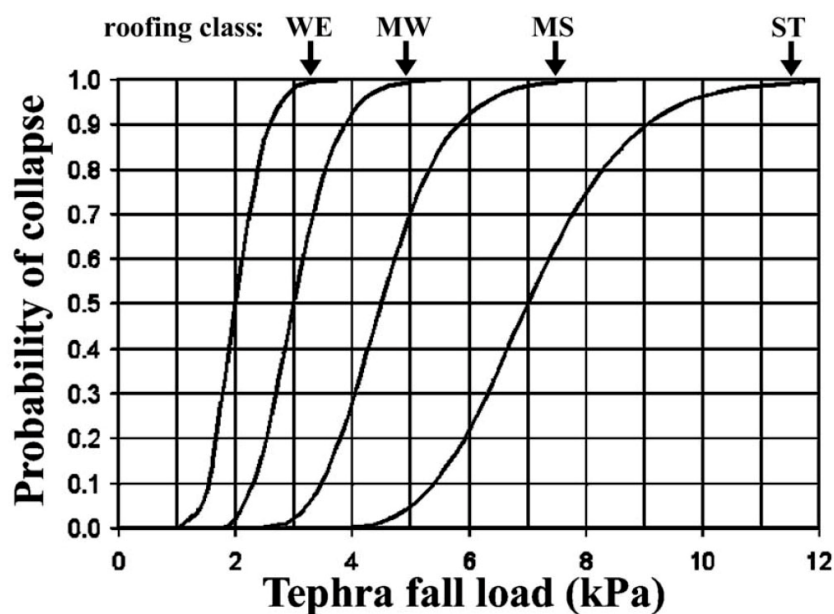


Fig. 1-37: Graphic of the probability roof collapse vs. the tephra fall load from Spence et al. (2005a, 2005b). Tephra load = ρgh with g = Gravitational Acceleration (9.81m/s^2); h = tephra thickness (m) and ρ = tephra density (kg/m^3).

Roof Class	Description	Typical design load range	Mean collapse load
WE (weak)	Sheet roofs, old or in poor condition. Tiled roof, old or in poor condition. Masonry vaulted roof.	Pre-design code, or no design code.	2.0 kPa
MW (medium weak)	Sheet roof on timber; average quality; average or good quality tiled roof on timber rafters or trusses. Steel or precast reinforced concrete joists and flat terrace roof.	1–2 kPa	3.0 kPa
MS (medium strong)	Flat reinforced concrete roof not all above characteristics; sloping reinforced concrete roof. Sheet roof on timber rafters or trusses, good quality and condition, designed for cyclone areas.	2–3 kPa	4.5 kPa
ST (strong)	Flat reinforced concrete roof designed for access; recent, good quality construction, younger than 20 years.	>3 kPa	7.0 kPa

Table 1-4: Roof type classification in relation with the fig. 1-33, from Spence et al. (2005a, 2005b).

The pattern of initial deposition depends on the nature of the eruption, the dynamics of the different particles, and the weather, especially wind and precipitation, at the time of the eruption. Dry tephra densities can range from ca. 400 kg/m^3 to ca. $1,600\text{ kg/m}^3$ (e.g. Blong, 1981) depending on the compaction. The composition, depth, density and particle size distribution of the tephra deposit can vary widely from volcano to volcano and from place to place affected by a single eruption.

For example the eruption of Tambora in 1815 which causes several collapse with less 10 cm of uncompacted tephra thick (*Blong, 1981*) or the most recent Cerro Negro eruption in 1992 which caused at least 2 deaths and 146 injured from building collapse with a tephra fallout thick of 4 cm (*Connor et al., 2001*). Such tephra fall can cover an extensive area with a tephra thickness sufficient to cause serious damage to building (**Figure 1-37; Table 1-4**) and massive disruption to human activity.

The size of respirable material is $< 4\mu\text{m}$ (*Horwell and Baxter, 2006*) and represents a significant quantity of products, even in the case of distal fallout. In the **Table 1-5** (*Horwell and Baxter, 2006*), there are some examples of the quantity of respirable material present in proximal and distal volcanic deposits of some eruptions. The respirable materials represent short-term (e.g. asthma, bronchitis) and long-term (e.g. silicosis, chronic obstructive pulmonary disease) health effects and risks for the populations (*Horwell and Baxter, 2006*).

Volcano	Eruption date	Distance from vent	Respirable material (cumulative volume %)	Volcanic explosivity index
Merapi, Indonesia	11–19 Jul 1998	200 m	12.7	2
Soufrière Hills, Montserrat	5 June 1999	4 km	10.7	3
Sakurajima, Japan	1 Jan 1994	4 km	0.9	3
Vesuvius, Italy	24 Aug AD79	6 km	16.9	5
Etna, Italy	4 Nov 2002	~11 km	1.8	3
Pinatubo, Philippines	4 July 1991	20 km	9.8	6
Cerro Negro, Nicaragua	30 Nov 1995	20 km	0.6	2
El Reventador, Ecuador	3 Nov 2002	90 km	4.9	4
Mt. St. Helens, USA	18 May 1980	378 km	11.7	5

Table 1-5: Variations in respirable material ($<4\ \mu\text{m}$ diameter) with volcano, distance from vent and explosivity, from Horwell and Baxter (2006).

If the eruption type is known, then it becomes possible to provide a better prediction of the nature of the tephra likely to be experienced at a certain distance from the vent for different wind scenarios (*Spence et al., 2005a, 2005b*).

Concerning the Monte Somma-Vesuvius complex, the present 60-year long quiescence departs from the pattern of open conduit conditions and after 1944 eruption the conduit remained obstructed. The volume of magma entered the chamber since then could be in the order of $2.10^8\ \text{m}^3$. If totally ejected during a single explosive event, it could result into a

Subplinian eruption, similar to the last of this kind (A.D. 1631). Such an eruption has been therefore taken as reference event for the presently Maximum Expected Eruption whose scenario, from field and historical data, was included in the Emergency Plan established by the Civil Defense.

Concerning Phlegrean Fields, the persistent state of activity of the caldera and its intense urbanization make the volcanic risk very high. To mitigate such high risk, an emergency plan is in preparation by the Department of Civil Defense. Presently the area at highest risk, that is the one which could be affected by pyroclastic currents (Red Zone), has been defined and evacuation of the population (350,000 people) before the beginning of the eruption, is planned.

Marra et al. (2003) considers that the Alban Hills should not be considered an extinct volcanic district and a detailed re-assessment of the volcanic hazard for the area of Rome is in order.

Concerning Etna's proximal risk almost 60% of the Etnean region has been covered by at least one lava flow since the 13th century, including even some densely populated sectors at low elevations. Even if the recent activity is moderately hazardous for human life, it seriously threatens all human activities in this densely populated area, due to complete destruction in the lava flooded surface, remaining barren for centuries.

II. Chapter II: Material and Methods

II.1. Piston core drilling locations.

For this work, we have chosen to study areas downwind of the Italian volcanoes where the probability to find distal tephra is higher because of prevailing seasonal wind direction. Three main sites were studied (**Figure 2-1**). The first one, lake of Shkroda (or Scutari or Skadar) is located between Montenegro and Albania borders. The second one, still in the Balkans, is the lake Ohrid, near the between Macedonia and Albania. Finally the last one is located in the Ionian Sea, south of S. Maria di Leuca cape. With these three new sites and the previous reported in literature, we consider to present a sufficient geographical cover to reconstruct a very precise picture of the dispersal of volcanic ash as well as a good (hopefully complete), record of the explosive activity of Italian volcanoes at least for the last thousands of year.

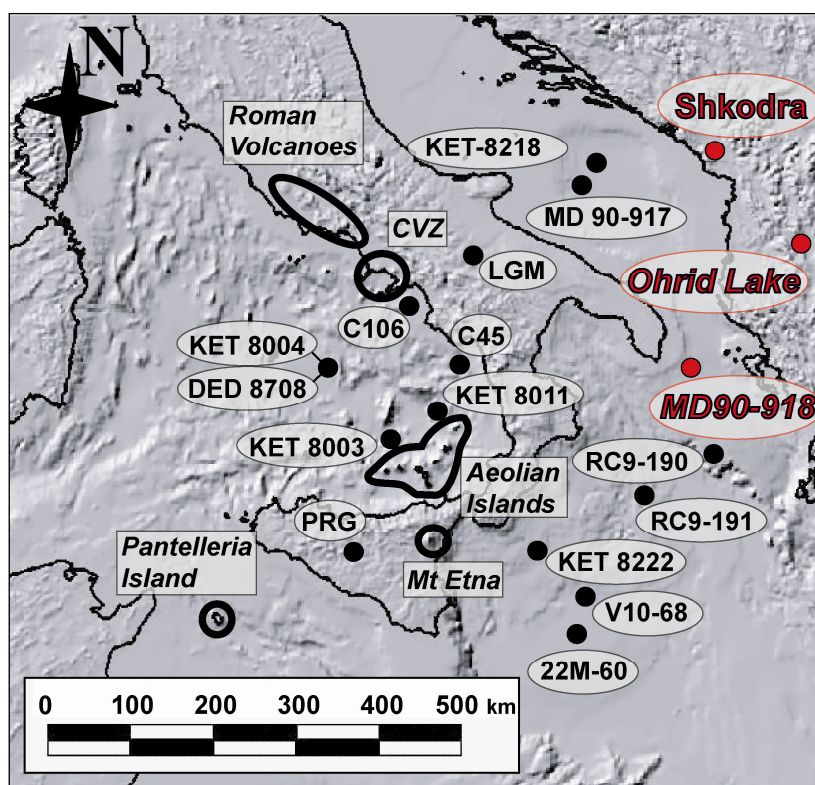


Figure 2-1: Location of main drilling sites in the Mediterranean area. CVZ = Campanian Volcanic Zone (Campi Flegrei, Vesuvio, Ischia and Procida), PRG = Lake of Pergusa, LGM = Lago Grande di Monticchio.

II.1.1. Shkroda

The Holocene sediments filling Lake Shkroda ($42^{\circ} 10' N$; $19^{\circ} 24' E$, 5 m a.s.l.; **Figure 2-2**) were sampled by Christian Beck team (Laboratoire Géodynamique des Chaînes Alpines, University of Savoie, France) in September 2003, with a UWITECTM platform and coring device (*van Welden et al., 2008*) within the frame of a NATO project “Science for Peace”. The main target of that project was devoted for seismological studies. A piston corer was used to take cores composed of 3 m-long sections with about 0.5 m overlap. All core liners have a 6 cm internal diameter. Several cores were drilled but we have focused our interest on core SK19 (5.8 m, coastal domain), and core SK13 (7.8 m, central domain).

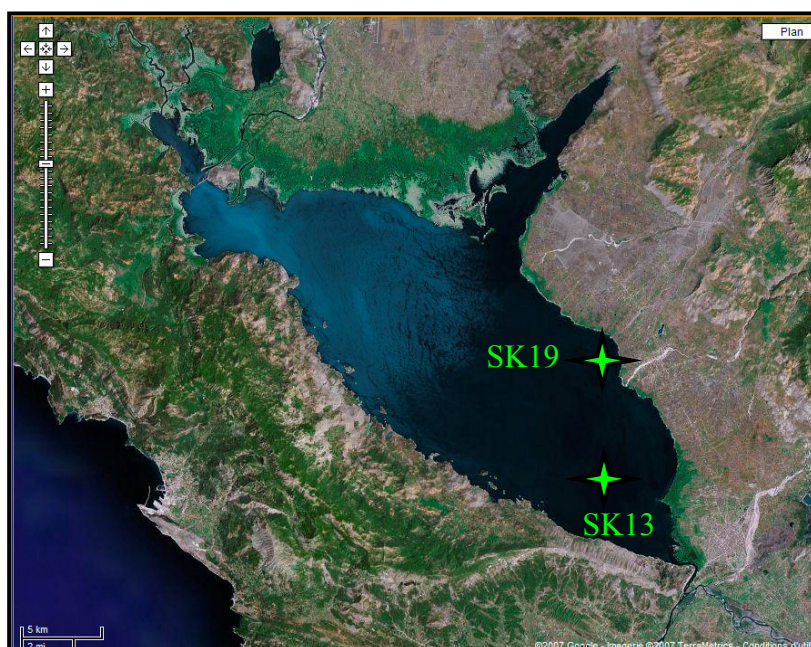


Figure 2-2: Location of SK13 and SK19 cores on the satellite view of the Shkodra Lake.

II.1.2. Ohrid JO-2004

Two series of piston cores (JO 2004-1 and JO 2004-1a) were drilled by the team of Anne-Marie Lezine (LSCE, France) in the southwest part of the Lake Ohrid ($40^{\circ} 55,000' N$; $20^{\circ} 40,297' E$; 705 m a.s.l.; **Figure 2-3**, *Belmecheri et al., 2009*; *Lezine et al., 2010*). This work was supported by CNRS grants from the French ECLIPSE program. The uppermost sediments (approx. 10 m) were recovered using a cable-operated piston-core (63 mm in diameter and 3 m long; Niederreiter Corer). In order to obtain a continuous sediment record,

four sections (labelled A, B, C and D respectively from the top to the base) were cored from a first drilling site (JO 2004-1). Three sections (A, B and C) were cored from a second site (JO 2004-1a) with a planned depth offset of 1.5 m from a second drilling site located at about 5 m of distance from the first.

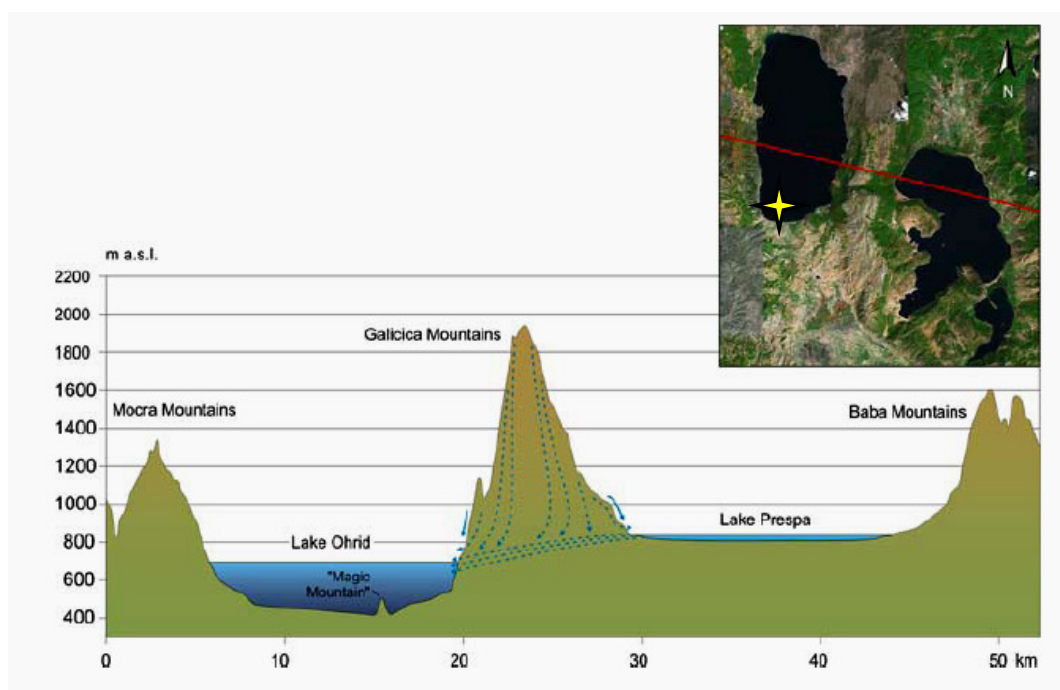
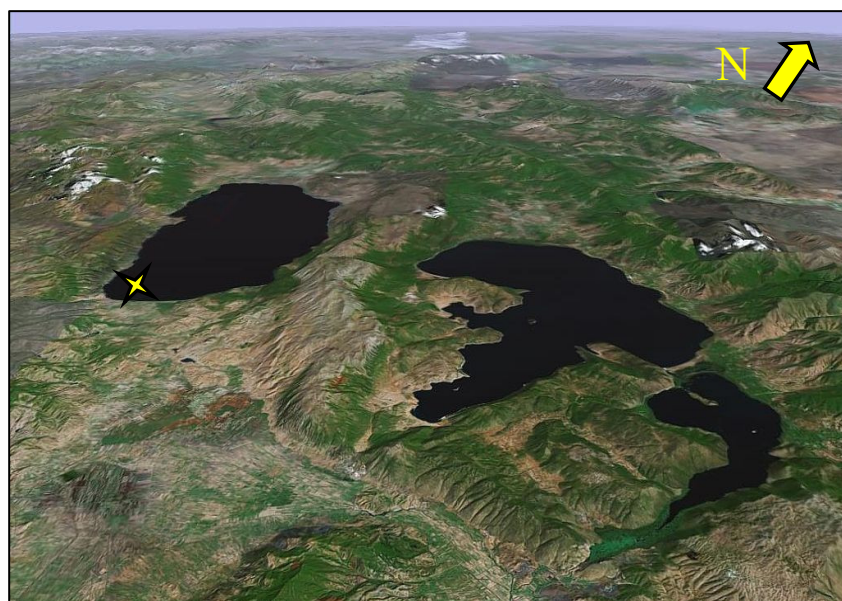


Figure 2-3: Satellite view and bathymetry of the Ohrid and Prespa lakes.

II.1.3. MD 90-918

The MD 90-918 deep-sea marine core is located in the Ionian Sea ($39^{\circ} 35,64' N$; $18^{\circ} 50,43' E$; 695 m b.s.l.; **Figure 2-4**) and has been collected during the PROMETE II cruise in 1990 by Martine Paterne (LSCE, France) on the French N/O Marion Dufresne. The MD 90-918 deep sea core is composed by 10 sections and presents a total length of 14.77 m.

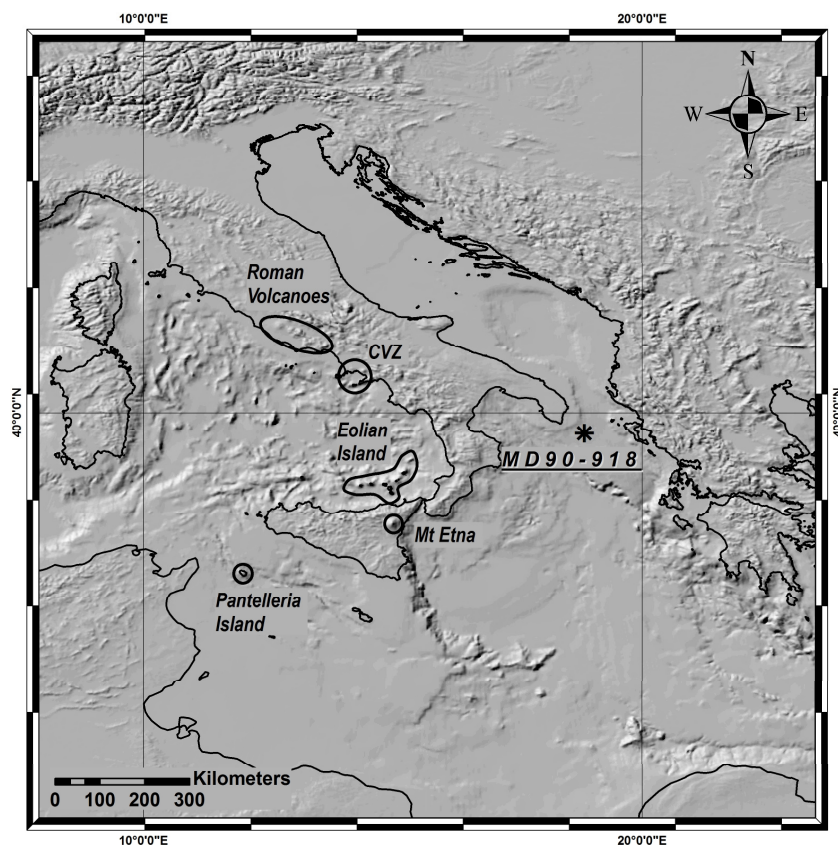


Figure 2-4: Location map of the deep sea core MD 90-918.

II.2. Cores description and sampling.

II.2.1. Shkroda

Two long cores were studied (**Figure 2-5**): SK19 (5.8 m long, coastal domain), and SK13 (7.8 m long, central domain). Sediments are mostly fine-grained, massive light-brown calcareous muds containing rare shell debris. Sampling in this core was mainly driven by magnetic susceptibility measurement and by naked eyes inspection. Sampling was performed by Aurélien van Welden (Univ. of Savoie), Roberto Sulpizio (Univ. of Bari) and Giovanni

Zanchetta (Univ. of Pisa) as collaboration project on ash dispersal within Mediterranean funded by Italian civil protection and Istituto Nazionale di Geofisica.

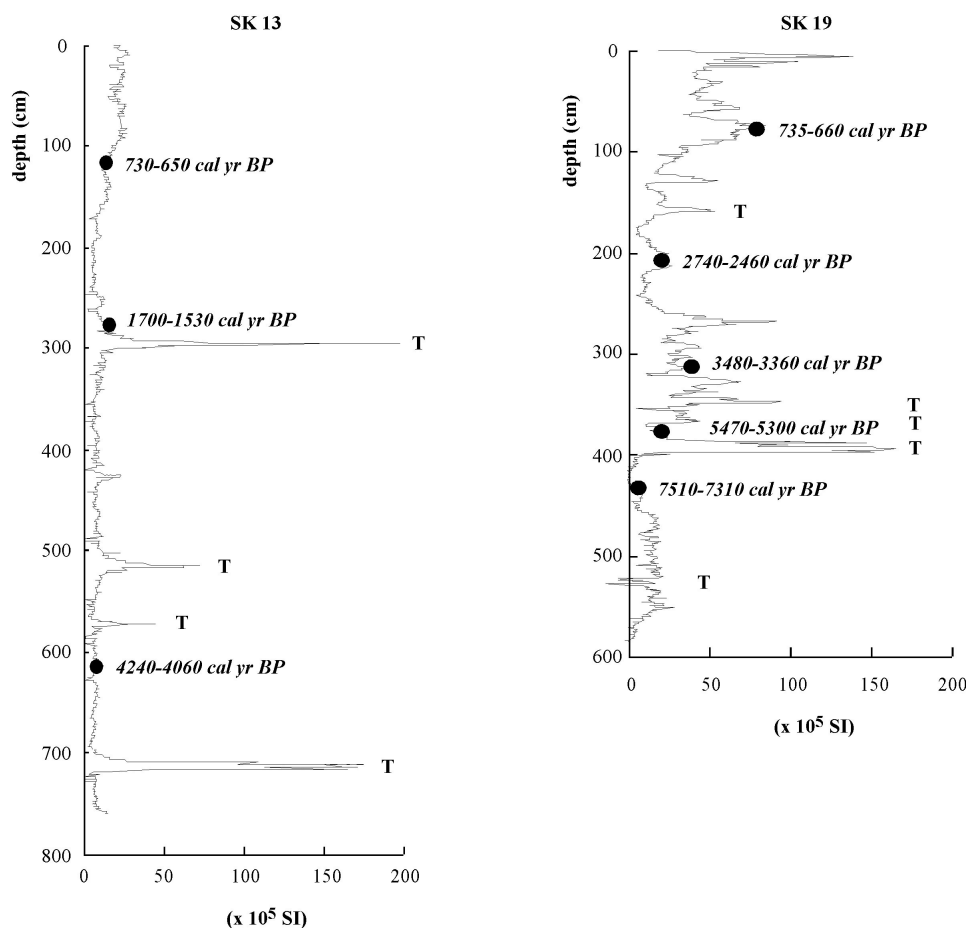


Figure 2-5: Magnetic susceptibility and calibrated AMS ^{14}C ages of the SK13 and SK19 cores from the Shkodra Lake.

II.2.2. Ohrid JO-2004

The overlapping of the sections were correlated using marker layers clearly identified in both cores and the resulting composite profile checked for consistency using the magnetic susceptibility record (**Figure 2-6**). The composite profile of the JO 2004-1 core was continuously sampled at 1 cm interval. Each sample was washed and sieved at 125, 63 and 40 μm using distilled water. The different grain size fractions were dried in an oven at 50 $^{\circ}\text{C}$ over 24h. Less 3,000 samples were analysed.

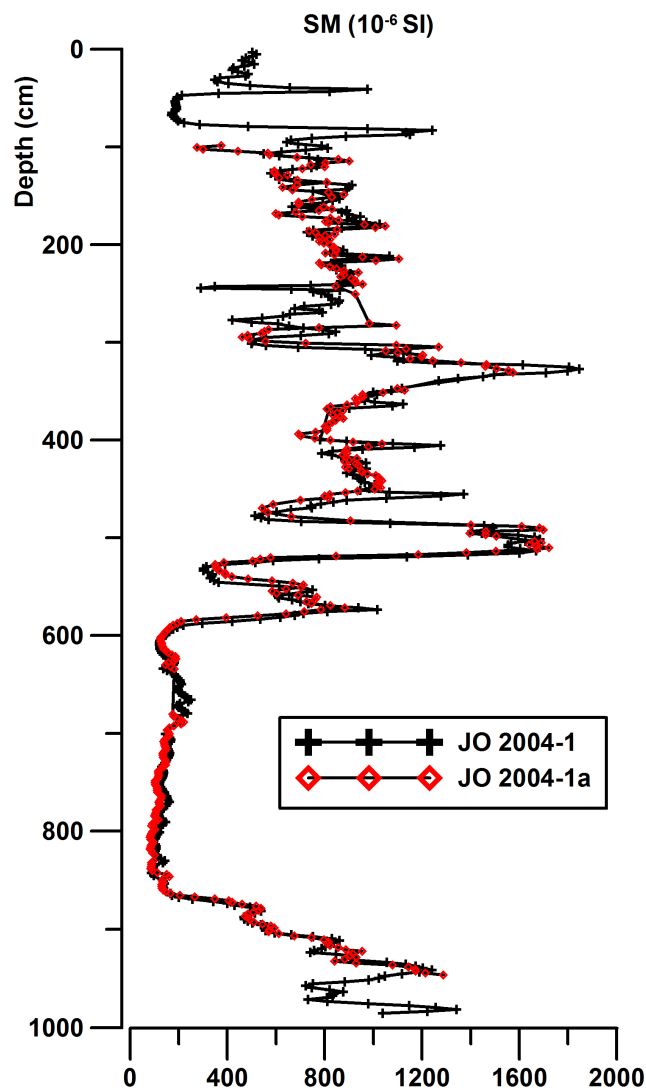


Figure 2-6: Magnetic susceptibility curve of the JO-2004-1 and JO-2004-1a cores from the Ohrid Lake.

II.2.3. MD 90-918

The sediments consist of grey to brown clays, including black layers in the upper part of the core (between 203 and 231 cm depth) identified to be the Sapropel S1 deposit (**Figure 2-7**). Moreover, at 992 cm depth, we note the presence of a turbidite layer ca 20 cm thick (**Figure 2-7**). Samples 2 cm-thick were taken every 5 cm all along the core, while close to and within the Sapropel S1, sample resolution was increased to 1 cm. Each sample was washed and sieved at 125 and 40 μm using distilled water. The different grain size fractions were dried in an oven at 50 $^{\circ}\text{C}$ over 24h.

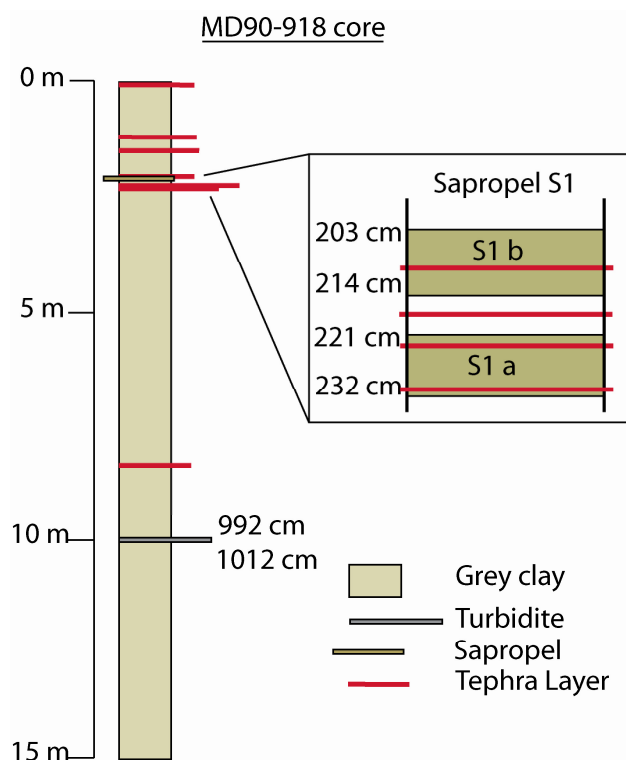


Figure 2-7: MD 90-918 deep sea core stratigraphy and tephrostratigraphy.

II.3. Isotopic studies

II.3.1. MD 90-918

An isotopic stratigraphy, performed along the MD 90-918 marine core, reconstructed the variation of the oxygen stable isotopes ($\delta^{18}\text{O}$). The comparison of this record with others similar deep sea cores of the Mediterranean basin allows to define the various paleoclimatic events and their chronology.

Oxygen isotope measurements, expressed in ‰ versus VPDB (Vienna Pee Dee Belemnite standard) were obtained on the planktonic foraminifera *Globigerinoides ruber* sampled every 10 cm along the core MD 90-918. Analyses were performed at the LSCE (Gif-sur-Yvette, France) on Finnigan $\Delta+$ mass spectrometer (**Figure 2-8**). Following [Coplen \(1988\)](#), V-PDB is defined with respect to NBS-19 and NBS-18 carbonated standards. The

mean external reproducibility (1σ) of carbonate standards is $\pm 0.05\text{‰}$ for the determinations; measured NBS-18 $\delta^{18}\text{O}$ is $-23.2 \pm 0.1\text{‰}$ V-PDB.



Figure 2-8: Finnigan $\Delta+$ mass spectrometer (LSCE).

Between 6 to 10 shells of planktonic foraminifera *Globigerinoides ruber* were picked in the 250-315 μm size range. The samples were cleaned in a methanol ultrasonic bath during a few seconds then roasted under vacuum at 380°C for 45 minutes, prior to isotopic analyses. The $\delta^{18}\text{O}$ curve is shown in the **Figure 2-9** and the data are in the annexe 1.

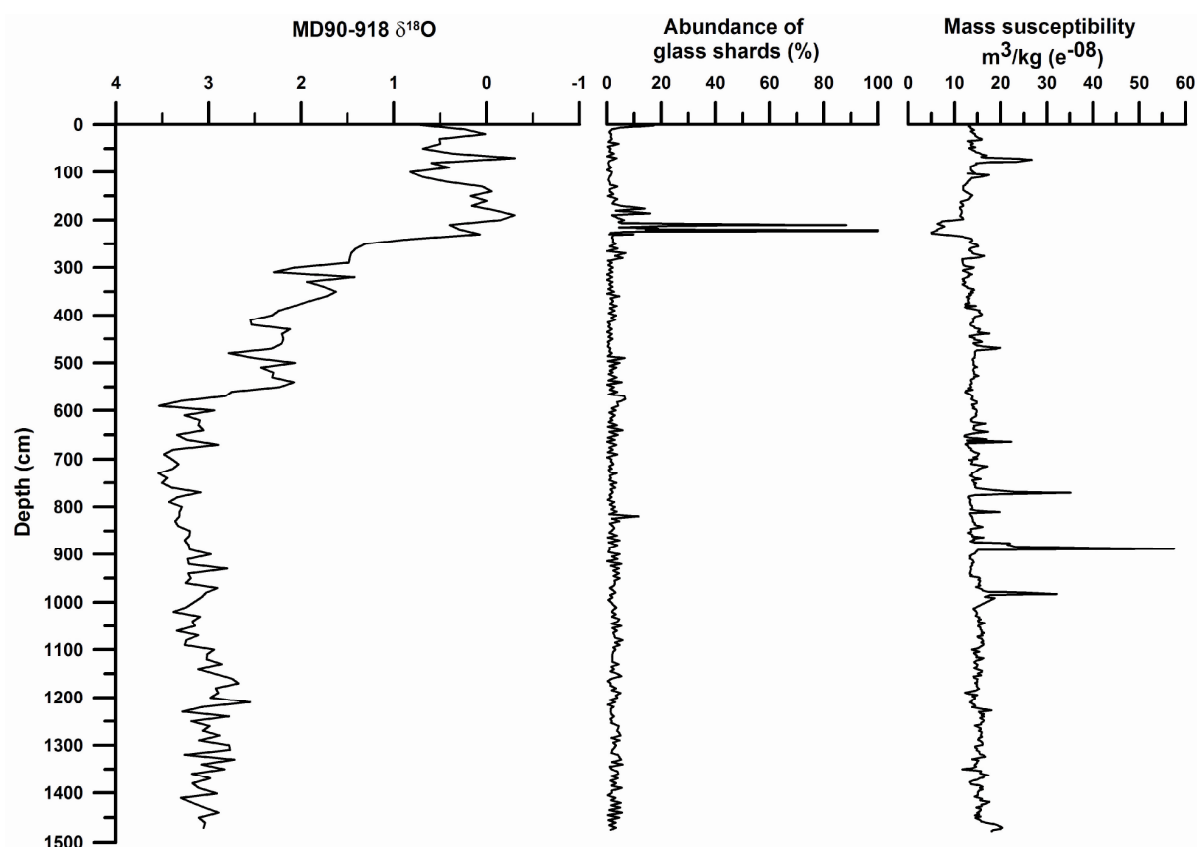


Figure 2-9: $\delta^{18}\text{O}$ curve, glass counting and MS curve of the MD 90-918 sea core.

II.4. Chronology

The establishment of a precise chronology of the marine or lacustrine sediment cores is a fundamental aspect for both tephrochronological and tephrostratigraphic purpose, but on the other hand, tephra layers yield the unique opportunity to correlate and date sediment, especially beyond the limit of radiocarbon. In correlation with the ^{14}C ages, these studies allow to establish chronological age models and to obtain the sedimentation rate of the studied sedimentary sequences. Then, the age of the undated portion core will be based on the measurement of the sedimentation rate, which is usually assumed to be constant between two dated samples (*Paterne, 1985*).

The ^{14}C dating method is the most common method employed for dating sediment layers for the last ca. 50 ka. Indeed, for this PhD project research, we have only use the ^{14}C dating method which is described in detail in the annexe 2.

In order to calculate accurate ages, any atmospheric ^{14}C fluctuations must be corrected using a calibration curve (*Bard et al., 2004*). Several approaches have been devised to construct the ^{14}C calibration curves. For the Holocene period, abundant fossil trees have been used to produce a high-resolution atmospheric curve by comparing ^{14}C levels and tree-ring counts forming the tree section (*Stuiver et al., 1998; Kromer and Spurk, 1998*).

A new calibration curve for the conversion of radiocarbon ages to calibrated (cal) ages has been constructed and internationally ratified to replace INTCAL98 which extended from 0-24 ka cal BP (Before Present, 0 cal BP = A.D. 1950). The new calibration dataset for terrestrial samples extends from 0 to 26 ka cal BP, with much higher resolution beyond 11.4 ka cal BP than INTCAL98. Dendrochronologically dated tree-ring samples cover the period from 0 to 12.4 ka cal BP. Beyond the end of the tree-rings, data from marine records (corals and foraminifera) are converted to the atmospheric equivalent with a site-specific marine reservoir correction to establish a common chronological framework for marine and continental paleoproxies. A substantial enhancement relative to INTCAL98 is the introduction of a coherent statistical approach based on a random walk model, which takes into account the uncertainty in both the calendar age and the radiocarbon age to calculate the underlying calibration curve (*Reimer et al., 2004*).

For most non-marine radiocarbon samples from the Northern Hemisphere, the INTCAL04 curve is the preferred choice (*Stuiver et al., 2005*).

For ^{14}C ages older than 26 ka BP, *van der Plicht et al. (2004)* advice not to use INTCAL04. So, for the range of ^{14}C ages between 26 and 50 cal ka BP, we will use the polynomial equation of *Bard et al. (1998)* or Calpal software (*Weninger and Jöris, 2008*).

One additional tool is the isotope stratigraphy based on $\delta^{18}\text{O}$ analyses on monospecific planktonic foraminifera. This method is very useful for correlation and to obtain further chronological constraints. Thanks to the isotopic stratigraphy, it is possible to correlate different cores with some stacked and well dated isotopic marine records.

As several time mentioned along this thesis, once a tephra is unequivocally identified and its age is well known the tephra event also constitute an important chronologic and stratigraphic markers. However, an unknown tephra preserved within a stratigraphic succession is a suitable material to be dated either directly using argon isotope, fission track

dating, or indirectly by radiocarbon dating of organic material associated with the tephra layer (Walker, 2005).

II.4.1. Shkroda

The chronological framework is defined by a set of eight ^{14}C AMS measurements on terrestrial macrofossils (TM) which were performed in Poznan laboratory. Five of them have been performed on core SK19 and three on SK13 (Figure 2-5; Table 2-1; van Welden et al., 2008). The ^{14}C ages have been calibrated using INTCAL04 (Reimer et al., 2004). No reservoir effect correction on ages of terrestrial macrofossils deposited into the lake was applied in view of permanent exchange between atmospheric CO_2 and lake and continuous water column mixing (very shallow depth and lack of thermal stratification, van Welden et al., 2008).

Core	Lab. No.	Material	Depth (cm)	^{14}C age yr (BP)	2σ range (yr BP)
SK13	SacA	TM	17	200±30	305-0
SK13	Poz-15211	TM	115	745±30	728-661
SK13	Poz-15212	TM	288	1695±30	1684-1535
SK13	Poz-15214	TM	614	3760±35	4238-3990
SK19	Poz-9251	TM	81	775±30	735-669
SK19	Poz-9201	TM	207	2500±30	2732-2467
SK19	Poz-9252	TM	311	3220±35	3555-3368
SK19	Poz-9199	TM	370	4645±35	5469-2306
SK19	Poz-9250	TM	435	6510±40	7497-7322

Table 2-1: AMS ^{14}C dating for the SK13 and SK19 lacustrine cores from the Shkodra Lake.

II.4.2. Ohrid JO-2004

Seven ^{14}C AMS radiocarbon datings were performed on terrestrial organic matter (OM) (Table 2-2). The ^{14}C activity was determined by UMS-ARTEMIS (Pelletron 3MV) AMS facilities (France, Saclay). Raw radiocarbon measurements (Lezine et al., 2010) were converted to calibrated ages using the INTCAL04 method (Reimer et al., 2004) for the ^{14}C age younger than 26 ka BP and the Bard method for the only one ^{14}C age older than 26 ka BP (Bard et al., 2004).

Mean Composite Depth (cm)	Material	¹⁴ C age	error	age cal BP	error 1 σ
20.5	OM	1285	30	1253	30
59.5	OM	5840	35	6680	66
74	OM	6130	80	7048	156
78.5	OM	7800	80	8550	139
85.5	OM	7850	40	8622	52
100.5	OM	8275	40	9407	121
307.6	OM	39100	1200	44812	1055

Table 2-2: AMS¹⁴C dating for the JO2004-1 lacustrine core from the Ohrid Lake.

II.4.3. MD 90-918

The chronology of the MD 90-918 deep sea core is based on seven ¹⁴C AMS dates. All dates were obtained from test of *Globigerina ruber* (> 150 μ m) out the level at 470-472 cm, which was obtained from test of *Globigerina bulloides* (> 150 μ m) and levels 820-822 and 1475-1477 cm depth which were obtained from test of a mixing of *Globigerina bulloides* (ca. 80%, >150 μ m) and of *Globorotalia inflata* (ca. 20%, >150 μ m) (**Table 2-3**). The ¹⁴C analyses were performed at the ARTEMIS laboratory in CNRS Center of Gif-sur-Yvette (France). A marine reservoir correction (R(t)) of 400 ¹⁴C years was used throughout the entire record except for the last deglaciation where a R(t) increase by a factor of 2 (*Siani et al. 2001*). Ages were calibrated using INTCAL04 (*Reimer et al., 2004*) for ¹⁴C age younger than 26 cal ka BP and Calpal software for age older than 26 cal ka BP (*Weninger and Jöris, 2008*).

Depth (cm)	Species	¹⁴ C age	error	¹⁴ C yr cal BP	Error $\pm 1\sigma$
0-6	<i>G. ruber</i>	960	35	615	20
175-177	<i>G. ruber</i>	6535	45	6989	57
210-212	<i>G. ruber</i>	7900	50	8342.5	56
230-232	<i>G. ruber</i>	8470	50	9004.5	42
470-472	<i>G. bulloides</i>	13740	60	15823	267
820-822	<i>G. bulloides</i> + <i>G. inflata</i>	16610	70	19391	110
1475-1477	<i>G. bulloides</i> + <i>G. inflata</i>	22710	110	26925	563

Table 2-3: Reservoir-corrected AMS¹⁴C dating for the MD 90-918 deep sea core from the Ionian Sea.

II.5. Magnetic susceptibility

II.5.1. Shkroda

Magnetic susceptibility (MS) was performed by Aurélien van Welden and first measured along all cores using a Bartington 72-mm-diameter loop sensor to assess core retrieval and establish preliminary lateral correlations. After core splitting, new detailed MS profiles were performed using a Bartington MS2 contact sensor with a 5 mm measuring interval (**Figure 2-5**; *van Welden et al., 2008*; *Sulpizio et al., 2009*). The prevailing calcareous matrix makes MS precise enough for the identification of the most prominent tephra layers.

II.5.2. Ohrid JO-2004

Core sections were sub-sampled with U-channels at the core repository of the LSCE (Gif-sur-Yvette, France). Then, Natural Remnant Magnetization (NRM) and bulk magnetic parameters were measured at high resolution by Alain Mazaud (LSCE). Bulk magnetic parameters are the volume low field susceptibility (K), the Anhyseretic Remnant Magnetization (ARM), and the Isothermal Remnant Magnetization (IRM). K is determined by the amount, nature and grain size of ferromagnetic and paramagnetic minerals. ARM and IRM are remnant magnetizations; therefore solely depend on the fraction of ferro/ferri-magnetic minerals, not paramagnetic minerals. ARM is principally linked to small magnetic grains, with a size of $\sim 0.1\text{--}5\ \mu\text{m}$, while IRM is sensitive to a wider spectrum of grain sizes (*Verosub and Roberts, 1995*). ARM was acquired along the axis of the U-channel using a 100 m T AF field and a 50 μTesla DC field. It was demagnetized using the same steps than those used for the NRM. IRM was acquired in 6 steps up to 1T using a 2G-pulsed IRM solenoid. IRM1T was stepwise demagnetized. ARM and IRM were determined with pass-through cryogenic magnetometers designed for long-core measurements (*Weeks et al., 1993*). Measurements of K were performed using a small-diameter Bartington sensor loop mounted in line with a track system designed for U-channels. The MS curve obtained has allowed the reconstructing of a composite profile of JO-2004-1 core (**Figure 2-6**). According to preliminary tephrostratigraphic studies, *Wagner et al. (2008a, 2008b)* noted that MS was unable to describe tephra occurrences owing to the very high component of high Magnetic clastic component.

II.5.3. MD 90-918

The core was sampled by inserting non magnetic cubic plastic boxes (2x2x2 cm size) oriented with respect to the top of the core. A total of 539 samples were obtained from the 14.77 m long core. We note that before sampling, the MD 90-918 core was staying some ten years in horizontal position that may engender a rotation of magnetic minerals in the part the richest of water which can degrade the original magnetic signal.



Figure 2-10: AGICO KLY-3 kappabridge of Peveragno (Univ. Torino).

In the laboratory Alpine Laboratory of Paleomagnetism, Peveragno (ALP), measurements were performed by Elena Zanella and Evdokia Tema (Univ. of Torino) with the following scheme:

- the magnetic susceptibility (k_m) on the whole of the samples and anisotropy of magnetic susceptibility (AMS) with a spacing of about 20 cm, using an AGICO KLY-3 device (**Figure 2-10**);
- the NRM using a 2G Enterprises cryogenic magnetometer;
- the AF demagnetization mostly up to 50 mT; a 80 mT peak-field was imparted to pilot specimens;
- the ARM with 80 mT AF magnetic field, 0.1 mT bias magnetic field and ARM25 after demagnetization at a peak-field of 25 mT along z-axis;

- the IRM: firstly a 1T field was given to get the saturation of the IRM (the SIRM), then two back-fields, of 0.1 and 0.3 T, to compute the S-ratio ($S_{0.1T} = \text{IRM}_{0.1T}/\text{SIRM}$, $S_{0.3T} = \text{IRM}_{0.3T}/\text{SIRM}$) using a Bussi impulse magnet;
- samples were dried and the weight was used to normalize the volume susceptibility and get the mass susceptibility (κ).

All these data, which were measured in laboratory, allow obtaining the various magnetic parameters which are resumed in the **Figure 2-11** and in the annexe 3.

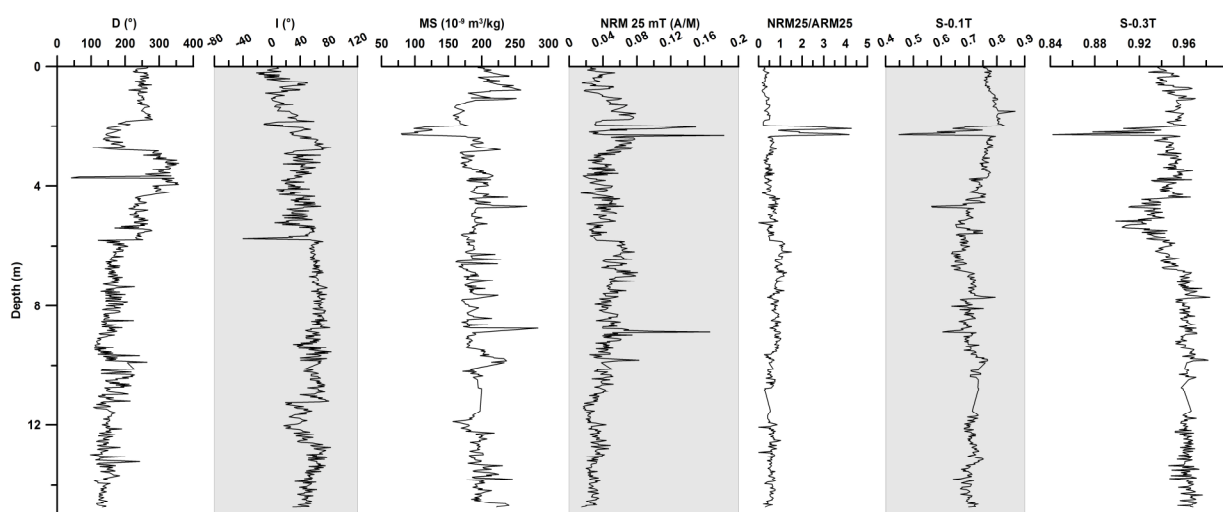


Figure 2.11: Results of the complete study of the paleomagnetism of the MD 90-918 core with declinaison (D), inclinaison (I), MS, NRM, NRM25/ARM25, saturation of IRM at 0.1T and 0.3T.

II.6. Carbon Organic Content

II.6.1. MD 90-918

The Sapropel deposit is enriched in organic matter compared to “normal” Mediterranean sediments. The determination of the % of the organic carbon in the sediment sample permits to obtain the Sapropel position in the MD 90-918 deep sea core (**Figure 2-12**, annexe 4). The organic carbon measurements were performed at the LSCE (Gif-sur-Yvette, France). For that, 33 samples of 1–2 g of sediment between 195 and 243 cm were collected, and afterwards dried at 50 °C for a maximum of 2 days. This step permits good preservation of organic matter, minimizing the influence of possible bacterial degradation. The sediment was decarbonated with a preparation of HCl 1% (non-hydrolysis of organic matter with this

concentration was checked), soaked, dried at 50 °C in oven, and homogenized. The analysed sample weights were comprised between 4.7 and 10 mg. The sample is combusted in a Fisons Instrument NA 1500 Element Analyzer and carbon content determined by the Eager software. An acetanilide standard (71.07 wt. % of carbon) is inserted every 10 samples. Organic carbon content in bulk sediment is deduced by assuming that mineral carbon exists only as CaCO₃. Results are reported in % weight of organic carbon in the bulk sediment (the completed protocol is described in [Gauthier et al., 2008](#)).

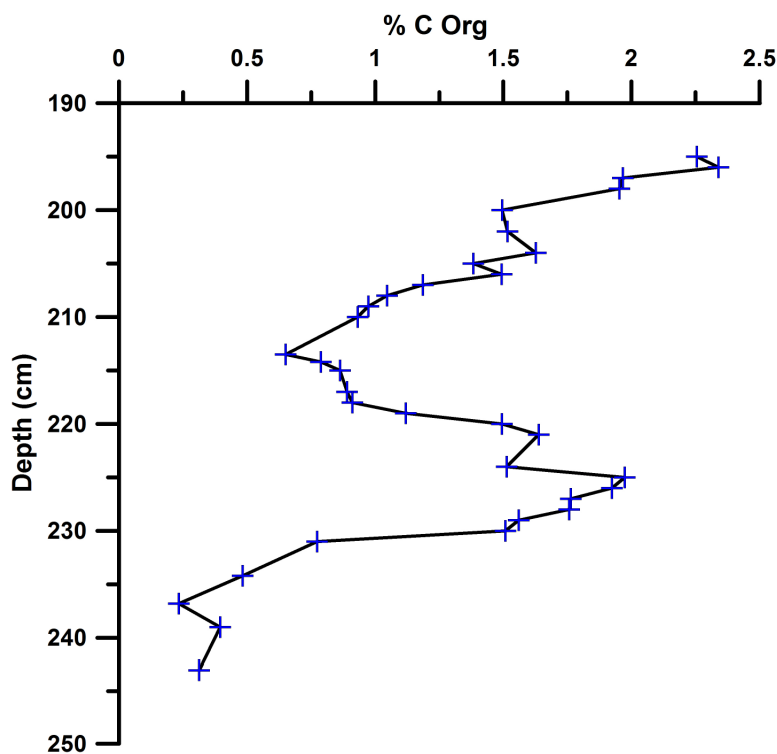


Figure 2-12: Organic Carbon curve of the MD 90-918 deep sea core.

II.7. Tephrostratigraphy

After washing the sediment, a counting of about 400 grains was performed on each sample of the core. This method permits, though time consuming, to evaluate the proportion of volcanics particles (i.e. glass shards, pumice, magmatic crystals, volcanic lithics), crystals and lithics fraction on the sample fraction > 40 µm ([Fretzdorff et al., 2000](#)). Moreover, this procedure allows the recognition of cryptotephra formed by pure glass-shards, which are

usually undetectable using magnetic susceptibility. The abundance curve of the volcanic material allows the identification of peaks which correspond to phases of ash deposition.

II.7.1. Shkroda

Nine tephra layers were recognised in the two cores, and in most cases there was coincidence with peaks in the magnetic susceptibility curve (**Figure 2-5**). All the tephra layers were visible to the naked eye, and were sampled and wet-sieved at 40 μm .

II.7.2. Ohrid JO-2004

Due to the very high component of highly magnetic clastic component, the MS cannot help us to localise tephra horizon. So, the three sediment fractions 125, 63 and 40 μm were carefully inspected under the stereo-microscope, looking for volcanic particles. In samples with volcanic glass in excess of 10 %, glass shards and micro-pumice fragments were picked and sealed in resin beads. Five tephra layers were recognised (**Figure 2-12**). They were then polished to avoid compositional variations caused by surface alteration processes.

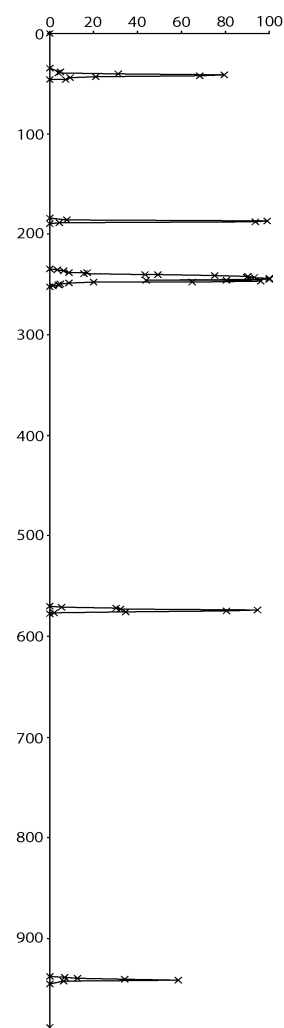


Figure 2-12: Glass counting curve of the JO-2004 core.

II.7.3. MD 90-918

The sediment fractions were carefully inspected under the stereo-microscope too. In the MD 90-918 marine core, only peaks of abundance larger than two times the background, calculated at 4.7% for the 323 counted samples, was considered as tephra events. Glass shards or micropumice were morphologically described under stereo-microscope. Between 230 and 200 cm depth, the tephra abundance values are high and the very high resolution glass

counting brings to light two different types glasses of morphology from distinct eruptions. Then, and in addition of the tephra counting, the morphological study of the various glasses allowed us to identify with extreme precision the position of each tephra layer. Therefore it was assumed that the tephra layer position corresponds at the depth of maximum abundance of glass shards coupled with homogeneous morphology and composition of glass fragments. Instead, the bell-like shape of glass abundance probably reflects the bioturbation effect and the sampling procedures. Eight tephra layers were recognised along the MD 90-918 core (**Figure 2-9**).

II.8. Geochemical analyses.

The glass shards or pumice sample were picked in each abundance peak and were mounted on epoxy resin beads. Then, they were polished in order to avoid compositional variations due to the surface alteration processes. Two different instruments were used to determinate the major element composition of the pumice or glass shard.

II.8.1. Geochemical analyse instruments

The first one was an Electron Probe Micro-Analyser (EPMA) on a CAMECA-SX 100 (Camparis, Paris, France). Analyses were performed with an acceleration voltage of 15 kV and a beam current of 4 nÅ. The analytical data of individual tephra layers have been normalized then to 100 wt%. Usually chemical data show closure > 97%, which indicate a good preservation of the original composition of the glass shards. The chemical data < 95% of closure, when present, were excluded.

The second one using an EDAX-DX micro-analyser (EDS analyses) mounted on a Philips SEM 515 (University of Pisa, Pisa, Italy). Operating conditions were: 20 kV acceleration voltage, 1 nÅ beam current, (100 s live counting, beam diameter \approx 500 μ m, 2100 shots per second), ZAF correction. The ZAF correction procedure does not include natural or synthetic standards for reference, and requires the analyses normalization at a given value

(which is chosen at 100%). Instrument calibration and performance are described in *Marianelli and Sbrana (1998)*.

II.8.2. Intercalibration of analyse instruments

Ninety-nine analyses from 5 distinct levels, which were performed on these two instruments, were compared to obtain an instrument intercalibration. All these analyses were exposed in on table (annexe 5) and were resumed in the **Table 2-4**.

Table 2-4 (next page): Intercalibration data between SEM of the University of Pisa and the microprobe of Camaparis. A set of 99 analyses of five distinct tephra layers (5; 175; 185; 219 and 820 respectively) is resumed here with: 1) the mean of all analyses from the two instruments; 2) the mean of the micropobe analyses; 3) the mean of the SEM analyses; 4) the difference between the means of the analyses from the two instruments; 5) the standard deviation of between the means of the analyses from the two instruments; 6) the variance in % of the means of analyses from the two instruments. Finally at the bottom of the table, the average of variance from all analysed layers.

	SiO ₂	TiO ₂	Al ₂ O ₃	FeO _{tot}	MnO	MgO	CaO	Na ₂ O	K ₂ O	P ₂ O ₅	ClO
Level 5											
Mean of all analyses from the level 5	74.81	0.05	13.41	1.51	0.05	0.05	0.78	4.02	4.95	0.01	0.37
Mean from the microprobe analyses	75.18	0.06	13.22	1.52	0.07	0.04	0.79	3.98	4.76	0.02	0.38
Mean from the SEM analyses	74.44	0.05	13.61	1.49	0.03	0.06	0.78	4.05	5.14	0.00	0.36
Difference between the two means	0.74	0.01	-0.39	0.03	0.04	-0.02	0.01	-0.07	-0.38	0.02	0.02
Sd of the two means	0.52	0.01	0.27	0.02	0.03	0.01	0.00	0.05	0.27	0.01	0.01
% variance of the two means from both instrument	0.98	15.42	2.91	2.06	59.28	48.92	0.70	1.88	7.95	100.00	4.58
Level 175											
Mean of all analyses from the level 175	58.92	0.14	21.53	1.72	0.20	0.10	1.65	8.45	6.71	0.02	0.57
Mean from the microprobe analyses	59.01	0.15	21.28	1.71	0.20	0.08	1.68	8.58	6.69	0.03	0.59
Mean from the SEM analyses	58.79	0.13	21.87	1.74	0.19	0.13	1.60	8.28	6.73	0.00	0.55
Difference between the two means	0.22	0.03	-0.59	-0.03	0.01	-0.05	0.08	0.30	-0.05	0.03	0.05
Sd of the two means	0.16	0.02	0.42	0.02	0.01	0.04	0.05	0.21	0.03	0.02	0.03
% variance of the two means from both instrument	0.38	16.87	2.77	1.49	6.51	64.84	4.62	3.46	0.70	100.00	7.86
Level 185											
Mean of all analyses from the level 185	58.74	0.15	21.43	1.69	0.18	0.11	1.59	8.86	6.65	0.01	0.59
Mean from the microprobe analyses	58.91	0.16	21.19	1.68	0.18	0.07	1.61	8.90	6.64	0.01	0.64
Mean from the SEM analyses	58.48	0.15	21.80	1.72	0.19	0.17	1.56	8.78	6.65	0.00	0.51
Difference between the two means	0.43	0.01	-0.61	-0.04	-0.01	-0.10	0.06	0.12	0.00	0.01	0.14
Sd of the two means	0.30	0.01	0.43	0.03	0.01	0.07	0.04	0.08	0.00	0.01	0.10
% variance of the two means from both instrument	0.73	4.94	2.90	2.46	4.79	138.13	3.57	1.35	0.07	100.00	21.23
Level 219											
Mean of all analyses from the level 219	74.80	0.07	13.21	1.48	0.07	0.05	0.84	3.92	5.20	0.01	0.34
Mean from the microprobe analyses	74.95	0.07	13.08	1.50	0.07	0.03	0.84	3.91	5.16	0.01	0.37
Mean from the SEM analyses	74.58	0.07	13.40	1.46	0.06	0.07	0.83	3.95	5.28	0.00	0.31
Difference between the two means	-0.37	0.00	0.31	-0.04	-0.01	0.03	-0.01	0.04	0.13	-0.01	-0.07
Sd of the two means	0.26	0.00	0.22	0.03	0.01	0.02	0.01	0.03	0.09	0.01	0.05
% variance of the two means from both instrument	0.49	5.93	2.37	2.90	11.86	101.85	1.29	1.01	2.43	100.00	18.15
Level 820											
Mean of all analyses from the level 820	68.97	0.30	16.08	2.27	0.13	0.47	1.49	4.57	5.36	0.03	0.33
Mean from the microprobe analyses	69.31	0.27	15.79	2.29	0.13	0.43	1.50	4.59	5.29	0.07	0.32
Mean from the SEM analyses	68.74	0.32	16.27	2.27	0.13	0.49	1.48	4.56	5.40	0.00	0.33
Difference between the two means	0.57	-0.05	-0.48	0.02	0.01	-0.06	0.02	0.03	-0.11	0.07	-0.01
Sd of the two means	0.40	0.04	0.34	0.02	0.00	0.04	0.02	0.02	0.08	0.05	0.00
% variance of the two means from both instrument	0.82	20.18	3.03	1.05	5.11	13.85	1.61	0.68	2.07	100.00	1.82
average of the % variance	0.68	12.67	2.80	1.99	17.51	73.52	2.36	1.68	2.65	100.00	10.73

The variance of analytical precision between the two instruments was calculated using the mean of the analyses from the 5 tephra layers. The geochemical compositions of these 5 tephra layers are rhyolitic or phonolitic. This difference of composition has not incidence on the variance between both instruments.

- The variance of the SEM relatively to the microprobe instrument is:

- 1) 0.68 % for the SiO_2 (abundance > 59 wt. %),
- 2) 2.80 % for the Al_2O_3 (abundance between 13 and 22 wt. %),
- 3) between 1.7 and 2.7 % for Na_2O , K_2O , FeO_{tot} and CaO (abundance between 1 and 9 wt. %),
- 4) 10.73 % for ClO (abundance ca. 0.4 wt. %)
- 5) moderate and strong with 13, 18 and 74 % for TiO_2 , MnO and MgO respectively (abundance is close to the limit detection of both instruments),
- 6) not calculated for the P_2O_5 which is under limit detection of the SEM of the University of Pisa.

The intercalibration shows that the compatibility of the SEM of the University of Pisa and the microprobe of Camparis, has to be considered strong and faithful.

II.8.3. Tephra's classification

The composition of tephra was classified using the Total Alkali vs. Silica diagram (TAS, Figure 2-13; *Le Bas et al., 1986*).

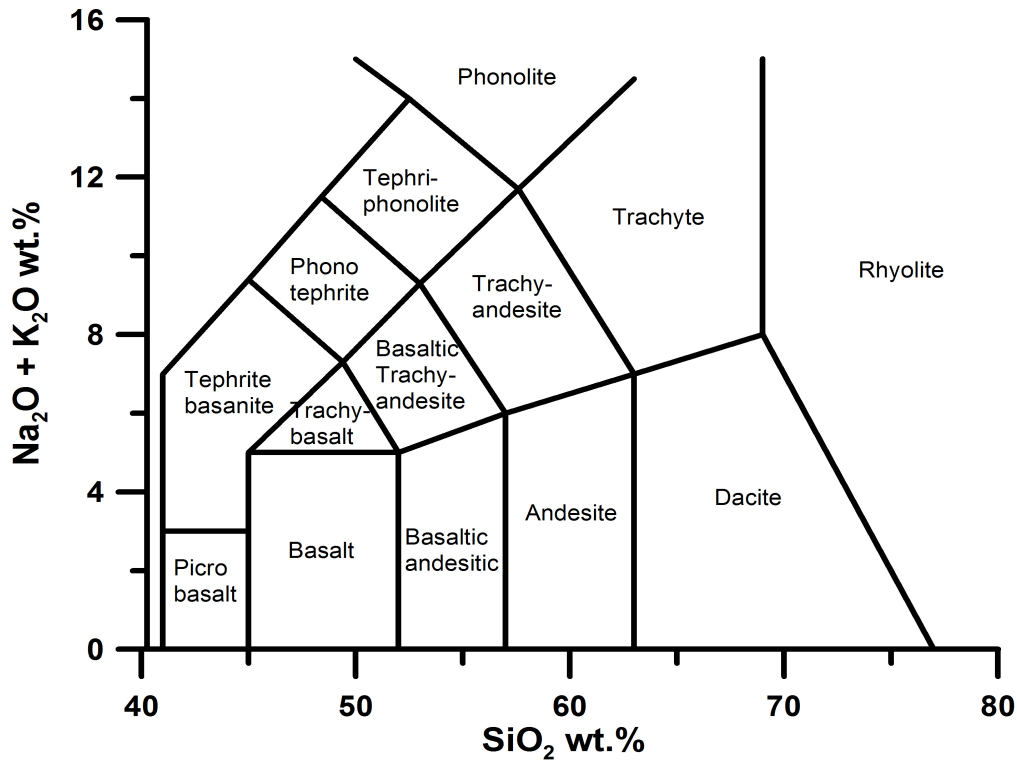


Figure 2-13: Total Alkali vs Silica from *Le Bas et al. (1986)*.

II.9. Geographic Information System (GIS)

A Geographic Information System (GIS) integrates hardware, software, and data for capturing, storing, editing, sharing, analyzing, and displaying all forms of geographically referenced information.

GIS allows us to analyze spatial information, edit data or maps, understand, question, interpret, and visualize data in many ways that reveal relationships, patterns, and trends in the form of maps, globes, reports, and charts.

A GIS helps you answer questions and solve problems by looking at your data in a way that is quickly understood and easily shared.

Concerning this PhD project, to develop a GIS was motivated by two main goals:

1) create a data base on the volcanic activities of the Central Mediterranean area. The rich literature was the main source as well as the results obtained during this PhD.

2) develop a tool to obtain geo-referenced dispersal maps of volcanic products. The geo-referencing is important to obtain faithful distances and surfaces which are the bases to calculate physical characteristics of volcanic eruption.

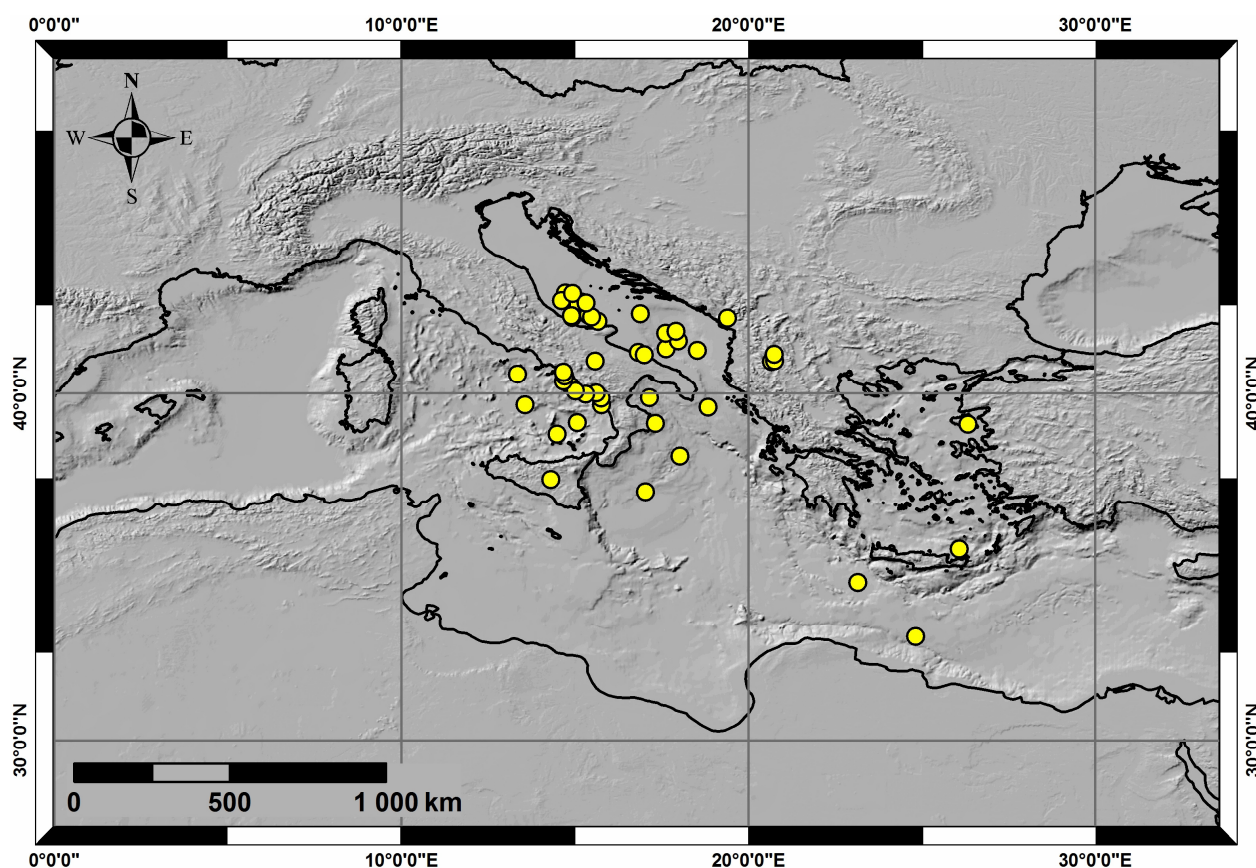


Figure 2-14: Map of location of the various lacustrine and marine cores included in the data base of the Geographic Information System.

A very long work was performed to build this GIS. Presently, more than 40 marine or lacustrine cores from the Central Mediterranean area are integrated in the data base which represents more than 300 tephra layers (**Figure 2-14**).

The information and data included in the data base are (**Figure 2-15**, the detailed table of the data base used in the GIS is in the annexe 6):

- UTM localisation
- core name
- literature reference (first author + publication year)
- name of the location studied site
- origin of the studied site (lake or sea or outcrops)
- altitude or marine depth of the core
- reference or name of the tephra layer
- depth in the core of the tephra layer
- thickness of the tephra layer
- colour of the tephra layer
- geochemistry of the tephra layer
- dating method used
- age without correction (yr)
- age calibrated (cal yr BP)
- age error
- volcanic complex origin correlated
- eruption correlated
- observation

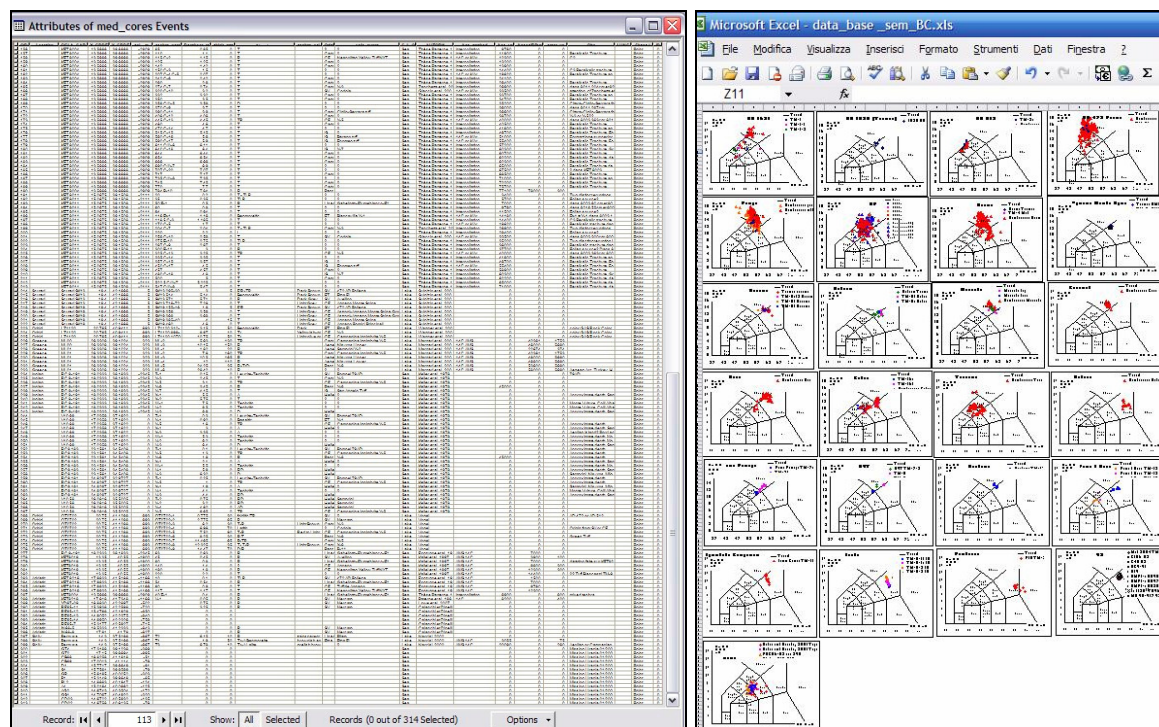


Figure 2-15: a) table of the date base of the various tephra layers (left); b) geochemistry data base of the data in a TAS of the various tephra layers (right).

The GIS is a powerful tool that allows studying all referenced data quickly.

It is possible to select all tephra layers which are correlated at a specific eruption, a particular volcano, an age, a geochemistry...

In the **Figure 2-16**, were select all tephra layers which were correlated to the Ignimbrite Campanian / Y-5 eruption (line in blue).

OID	Location	SIGLA_CARO	X_GREC	Y_GREC	asl_m	tephra_nam	Depthcor_m	thick_mm	Chemistry	tephra_col	Origin	volc_event	S_L_O	AUTORH	Aqe_methc	
82		RF53-77	15 11650	42 4435	-152	797	7.97	0	T		Campanian	C-20	Sea	Calanchi et al., 1998		
98		CM92-42	15 20122	42 82294	-161	710	7.1	0	T		Campanian	C-20	Sea	Calanchi et al., 1998		
58	Monticchio	monticchio	15 58333	40 93333	656	TM-18	24 950001	257	Tr-P	Beige Grey	CF	Campanina Ignimbrite Y-5	Lake	Wulf et al., 2004	varve	
102		CM92-42	15 20122	42 82294	-161	400	4	0	Tr-P		CF	Campanina Ignimbrite Y-5	Sea	Calanchi et al., 1998		
120	Orhid	JO 2004	20 67162	40 91667	705	JO244		2.44	0	TP	CF	Campanina Ignimbrite Y-5	Lake	Caron et al., 2009		
225	Orhid	LZ1120	20 785	40 94111	693	LZ1120 1070-10		10.75	50	Tr	CF	Campanina Ignimbrite Y-5	Lake	Wagner et al., 2009 J		
226	Greece	MIL00	26 33096	39 10247	323	ML-2		5.63	130	TP	CF	Campanina Ignimbrite Y-5	Lake	Margari et al., 2007	14C AMS	
229	Greece	MIL01	26 33096	39 10247	323	ML-2		7.6	160	TP	CF	Campanina Ignimbrite Y-5	Lake	Margari et al., 2007	14C AMS	
236	Ionian	RC 9-191	18 03333	38 18333	-2345	Y-5		3.1	0	TP	CF	Campanina Ignimbrite Y-5	Sea	Keller et al., 1978		
246		V10 69	17 03583	37 16222	0	Y-5		1.6	0	TP	CF	Campanina Ignimbrite Y-5	Sea	Keller et al., 1978		
253		RC9 183	23 15611	34 54083	0	Y-5		1.3	0	TP	CF	Campanina Ignimbrite Y-5	Sea	Keller et al., 1978		
260		RC9 181	24 62972	32 97278	0	Y-5		1	0	TP	CF	Campanina Ignimbrite Y-5	Sea	Keller et al., 1978		
267		V10 59	26 08167	35 50656	0	Y-5		6.65	0	TP	CF	Campanina Ignimbrite Y-5	Sea	Keller et al., 1978		
272	Orhid	OTO702	20 75	41 12889	693	OTO702-5		7.52	90	Tr-P	CF	Campanina Ignimbrite Y-5	Lake	Vogel		
6	Monticchio	monticchio	15 58333	40 93333	656	TM-2-1		2.53	0.1	Tr	IS	Cannavale/Chiaro	Lake	Wulf et al., 2008	varve	
79	Adriatic Sea	MD90-917	17 63	41 28333	-1010	275		2.75	0	T	South Tyrrh	Capo Palinuro	Sea	Siani et al., 2004	14C G. bulliodes	
23	Monticchio	monticchio	15 58333	40 93333	656	TM-4-2		7.26	0.2	Tr-P	CF	Casse	Lake	Wulf et al., 2005	varve	
171		KET 8004	13 58667	39 66683	-2909	390 C-11		3.9	0	T	Campanian	Ciglio-Serrara tuff	Sea	Thèse Parterne, 198	Interpollation	
50	Monticchio	monticchio	15 58333	40 93333	656	TM-16a		16.51	16	Tr-P	SV	Codola	Lake	Wulf et al., 2004	varve	
51	Monticchio	monticchio	15 58333	40 93333	656	TM-16b		17.1	68	Tr-P	SV	Codola	Lake	Wulf et al., 2004	varve	
131		KET 8003	14 45417	38 817	-1900	290-300 C-10		3	100	T	SV	Codola	Sea	Giacco et al., 2008	14C	
166		KET 8004	13 58667	39 66683	-2909	320 C-10		3.2	0	T	SV	Codola	Sea	Giacco et al., 2008	14C or KI/Ar	
201		KET 8011	15 0675	39 15083	-2111	258 C-10		2.58	0	T	SV	Codola	Sea	Giacco et al., 2008	14C or KI/Ar	
271	Orhid	OTO702	20 75	41 12889	693	OTO702-4		6.98	70	Latic	?	Codola	Lake	Vogel		
140		KET 8003	14 45417	38 817	-1900	562 C-17		5.62	0	T	IS	Epomeo tuff	Sea	Thèse Parterne, 190	KI/Ar	
178		KET 8004	13 58667	39 66683	-2909	590 C-17		5.9	0	T	IS	Epomeo tuff	Sea	Thèse Parterne, 198	14C or KI/Ar	
208		KET 8011	15 0675	39 15083	-2111	450 C-17		4.5	0	T	IS	Epomeo tuff	Sea	Thèse Parterne, 198	14C or KI/Ar	
118	Orhid	JO 2004	20 67162	40 91667	705	JO42		0.42	0	Benmoreitic - Mugearitic	Dark Brown	ET	Etna FL	Lake	Caron et al., 2009	
215	Scutari	Scutari SK13	19.4	42 16667	5	SK13 514		5.14	0	Benmoreitic	Dark Brown	ET	Etna FL	Lake	Sulpizio et al., 2009	
223	Orhid	LZ1120	20 785	40 94111	693	LZ1120 310-315		3.15	50	Benmoreitic	Dark	ET	Etna FL	Lake	Wagner et al., 2009 J	

Figure 2-16: Example of attribute table with the selected cores of the Ignimbrite Campanian / Y-5 eruption, highlighted in blue.

In the table of attributes are indicated all information associated at these tephra layers. It appears directly too, on the GIS map, the selected cores which are highlighted in blue (Figure 2-17).

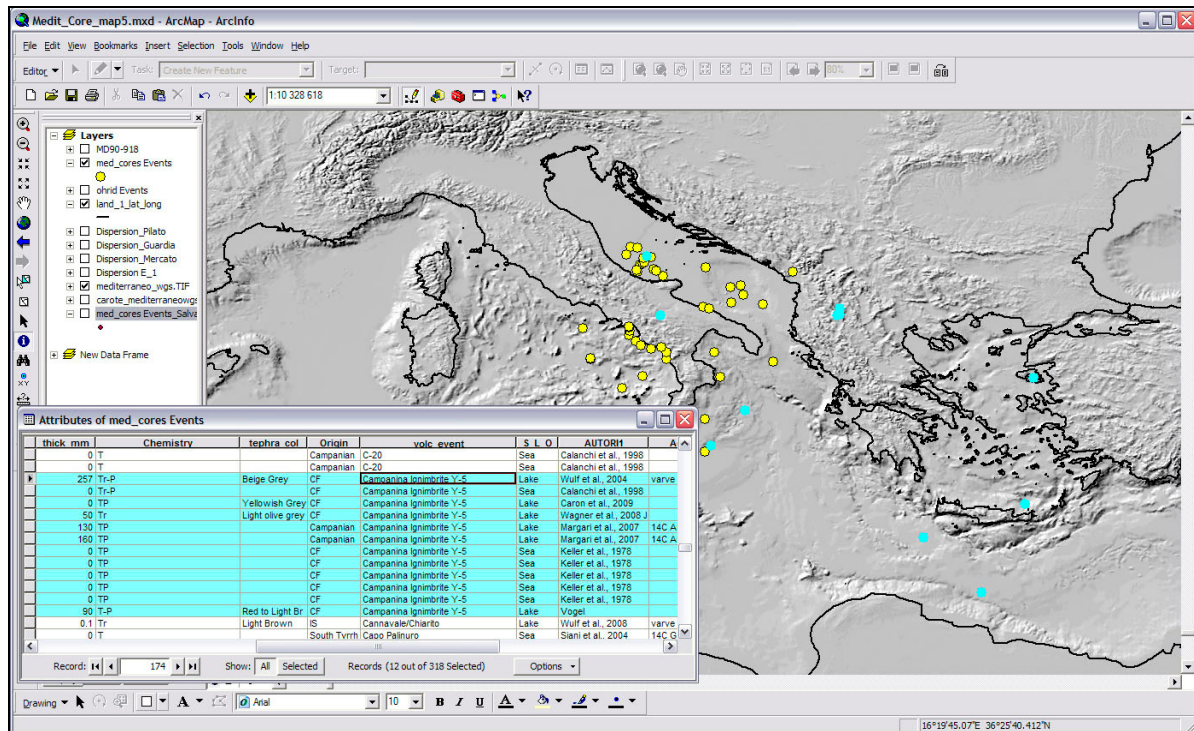


Figure 2-17: Screenshot of attribute table and GIS map with the selected cores of the Ignimbrite Campanian / Y-5 eruption, highlighted in blue.

An other possibility is selecting the cores directly on the map of the GIS to obtain the information of the selected cores. For example, were selected some cores around Italy in the **Figure 2-18**. On the right of this screenshot, there is the informative table where is indicated the list of the selected cores and all information related to the list selected core.

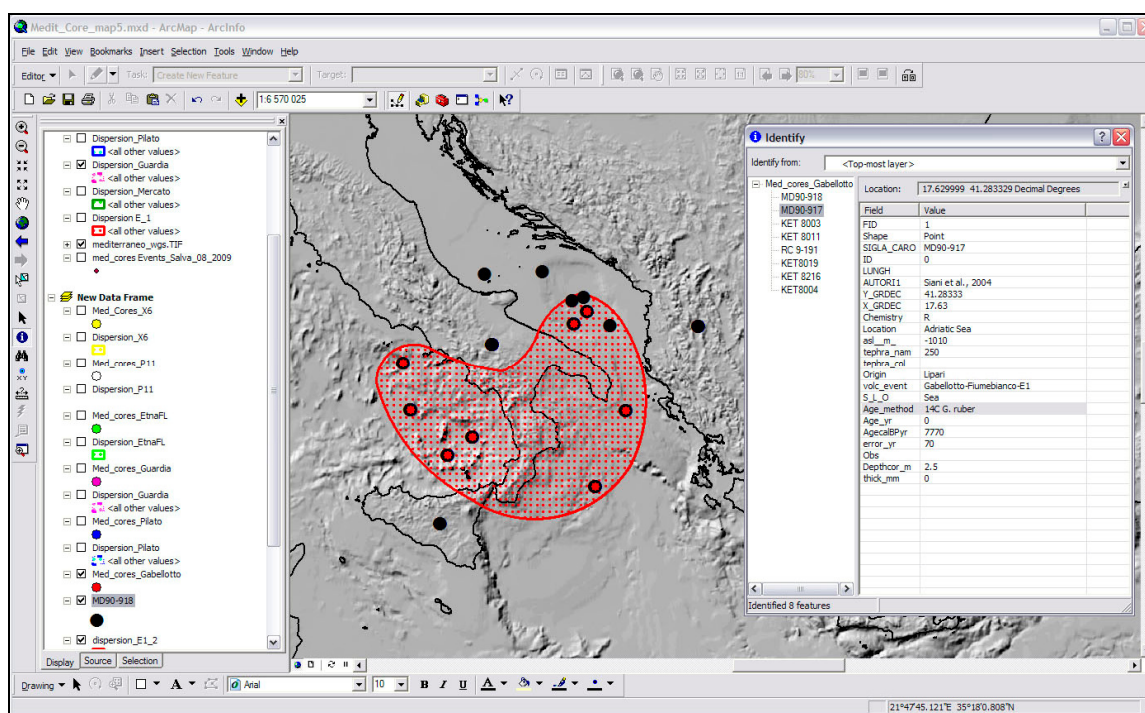


Figure 2-18: Screenshot of selected cores (highlighted in red) from the GIS map and of an informative table related to the selected cores.

Once all cores of the same eruption selected, it becomes possible drawing an estimated dispersal area of the tephra (**Figure 2-19**). In a second step, an informative table is created and informs on the surface of this dispersal ash area (informative table on the right of the screenshot, **Figure 2-19**).

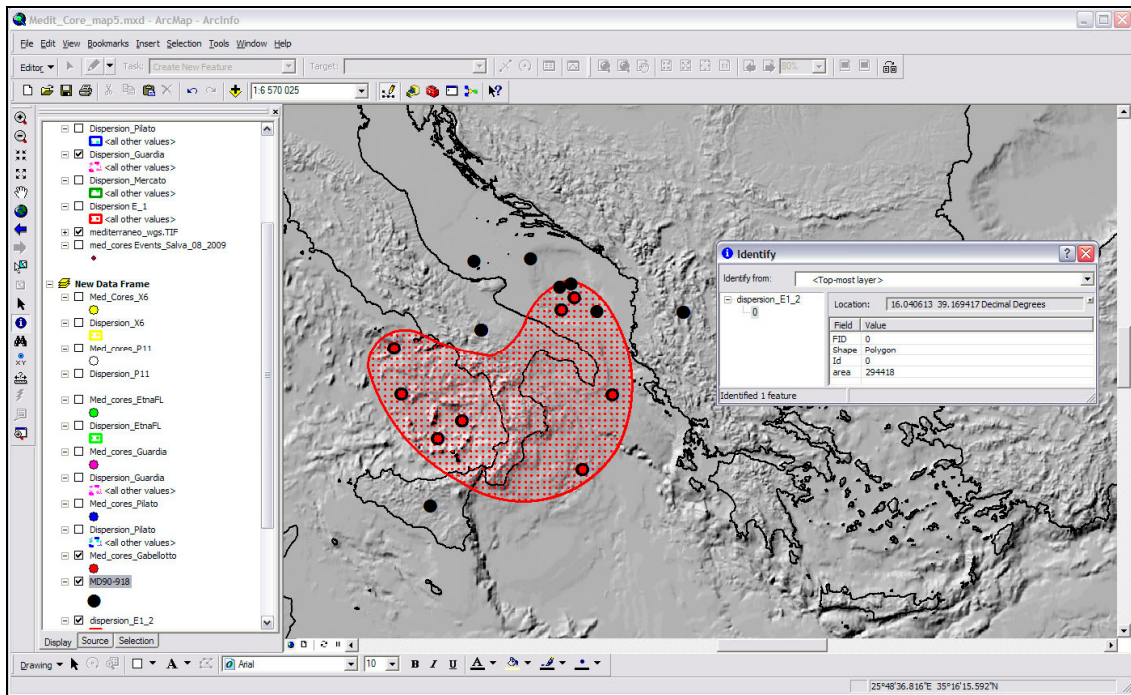


Figure 2-19: Screenshot of a drawn dispersal area associated with an informative table.

The ultimate step is export the map in image format (Figure 2-20) with coordinate grid, kilometers scale and North direction.

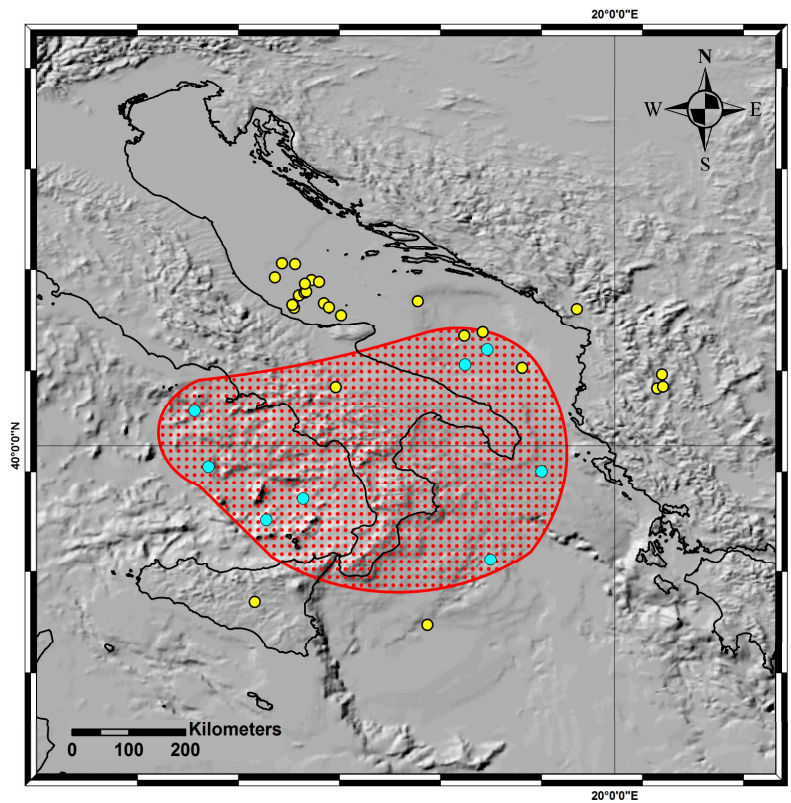


Figure 2-20: Image of a map exported from the GIS.

Moreover, the GIS allows studying several dispersal areas in the same image (**Figure 2-21**). With the image of accumulated dispersal ash areas, the identification of zones which are regularly cover by the volcanic products are easily identifiable.

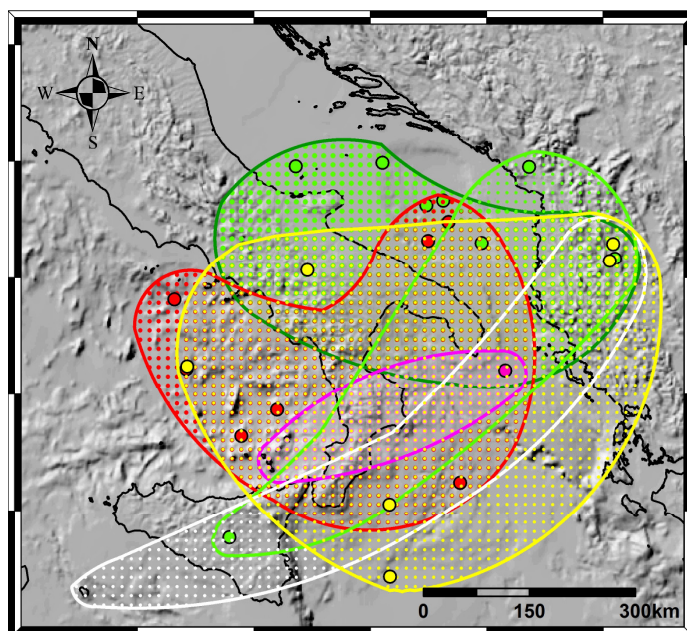


Figure 2-21: Image the accumulated dispersal areas map exported from the GIS.

All these results depend of the quality and quantity of the data which are included in the data base of the GIS. This data base must be update usually possible with cheked and certified data. Finally, the results from the GIS could significantly improve the estimation of volcanic hazard in Central Italy, and more generally in the Mediterranean basin. The results could be useful to responsible institutions for the mitigation of volcanic risks and hazard in the Italian zone.

III. Chapter III: The Holocene tephrostratigraphic record of Lake Shkodra (Albania and Montenegro)

An Albanian-French NATO project (Science For Peace 977 993) was dedicated to seismic hazards assessment, combining morphotectonic, seismological, and GPS geodetic surveys, with an attempt to search possible earthquake response recorded within the lacustrine sedimentary archive. Shkodra Lake (Albania) coring was initiated and managed by Prof. F. Jouanne at Laboratoire de Géodynamique des Chaînes Alpines (LGCA). Moreover C. Beck and J.L. Mugnier of LGCA, and R. Koci and S. Bushati from Albanian institutions have made coring possible.

A. van Welden (LGCA) studied the last 500 years of sedimentation in Lake Shkodra and has developed a chronological and a magnetic frame of the cores for investigation on paleo-earthquakes. He showed ([van Welden et al., 2008](#)) that this period was characterised by undisturbed sedimentation of fine-grained material. Destructive earthquakes affected the area in 1905 and 1979, but did not induce any visible perturbation of the lacustrine archive. On the contrary, human activity (damming, change in agricultural practices) and climate (i.e. catastrophic floods occurred in 1962–1963 and the Little Ice Age between A.D. 1650 and 1820) had an imprint on lake sedimentation ([van Welden et al., 2008](#)).

The collaboration with R. Sulpizio (Univ. of Bari), A. van Welden (Univ. of Savoie) and G. Zanchetta (Univ. of Pisa) allows developing a tephrostratigraphic study on two lacustrine cores from the Shkodra Lake. The core processing for layer recovering and geochemical analyses was carried out at the Dipartimento di Scienze della Terra (University of Pisa). The results of these researches were submitted at Journal of Quaternary Science and the scientific article is in press ([Sulpizio et al., 2009](#)).

The Holocene tephrostratigraphic record of Lake Shkodra (Albania and Montenegro)

ROBERTO SULPIZIO,^{1*} AURELIEN VAN WELDEN,^{2†} BENOIT CARON³ and GIOVANNI ZANCHETTA³

¹ CIRISIVU, c/o Dipartimento Geomineralogico, Bari, Italy

² Laboratoire de Géodynamique des Chaînes Alpines, UMR 5025, Le Bourget du Lac, France

³ Dipartimento di Scienze della Terra, Pisa, Italy

Sulpizio, R., Van Welden, A., Caron, B. and Zanchetta, G. The Holocene tephrostratigraphic record of Lake Shkodra (Albania and Montenegro). *J. Quaternary Sci.*, (2009). ISSN 0267-8179.

Received 9 September 2008; Revised 24 June 2009; Accepted 9 July 2009

ABSTRACT: Two cores were recovered in the southeastern part of Lake Shkodra (Montenegro and Albania) and sampled for identification of tephra layers. The first core (SK13, 7.8 m long) was recovered from a water depth of 7 m, while the second core (SK19, 5.8 m long) was recovered close to the present-day shoreline (water depth of 2 m). Magnetic susceptibility investigations show generally low values with some peaks that in some cases are related to tephra layers. Naked-eye inspection of the cores allowed the identification of four tephra layers in core SK13 and five tephra layers in core SK19. Major element analyses on glass shards and mineral phases allowed correlation of the tephra layers between the two cores, and their attribution to six different Holocene explosive eruptions of southern Italy volcanoes. Two tephra layers have under-saturated composition of glass shards (foiditic and phonolitic) and were correlated to the AD 472 and the Avellino (ca. 3.9 cal. ka BP) eruptions of Somma-Vesuvius. One tephra layer has benmoreitic composition and was correlated to the FL eruption of Mount Etna (ca. 3.4 cal. ka BP). The other three tephra layers have trachytic composition and were correlated to Astroni (ca. 4.2 cal. ka BP), Agnano Monte Spina (ca. 4.5 cal. ka BP) and Agnano Pomice Principali (ca. 12.3 cal. ka BP) eruptions of Campi Flegrei. The ages of tephra layers are in broad agreement with eight ¹⁴C accelerator mass spectrometric measurements carried out on plant remains and charcoal from the lake sediments at different depths along the two cores. The recognition of distal tephra layers from Italian volcanoes allowed the physical link of the Holocene archive of Lake Shkodra to other archives located in the central Mediterranean area and the Balkans (i.e. Lake Ohrid). Five of the recognised tephra layers were recognised for the first time in the Balkans area, and this has relevance for volcanic hazard assessment and for ash dispersal forecasting in case of renewed explosive activity from some of the southern Italy volcanoes. Copyright © 2009 John Wiley & Sons, Ltd.



Supporting information may be found in the online version of this article.

KEYWORDS: tephrostratigraphy; tephrochronology; Italian volcanoes; Lake Shkodra; Albania; Montenegro.

Introduction

Application of tephrochronology to volcanology, Quaternary science, palaeoceanography and archaeology has an exceedingly high potential in the Mediterranean region, owing to the intense explosive volcanic activity that occurred over the last 200 ka (Keller *et al.*, 1978; Thunnell *et al.*, 1979; McCoy, 1981; Paterne *et al.*, 1986, 1988, 1990; Poli *et al.*, 1987; Rosi and Sbrana, 1987; Calanchi *et al.*, 1998; Narcisi and Vezzoli, 1999; Pappalardo *et al.*, 1999; Siani *et al.*, 2004; Peccerillo, 2005; Di Vito *et al.*, 2008; Santacrose *et al.*, 2008; Turmey *et al.*, 2008). In the last 30 years, Quaternary tephra layers have been used

extensively to develop a high-resolution event stratigraphy for the Late Pleistocene and Holocene across the central and eastern Mediterranean (e.g. Keller *et al.*, 1978; Federman and Carey, 1980; Pateme *et al.*, 1988; Narcisi and Vezzoli, 1999; Siani *et al.*, 2004; Lowe *et al.*, 2007; Margari *et al.*, 2007). While early work focused mainly on samples from marine cores, recent work on terrestrial archives (including Italian, Greek and Turkish lakes, and Bulgarian, Greek and Italian cave sites; e.g. St Seymour and Christianis, 1995; Narcisi and Vezzoli, 1999; St Seymour *et al.*, 2004; Wulf *et al.*, 2004; Frisia *et al.*, 2008; Giaccio *et al.*, 2008) has considerably advanced the development of a long, high-resolution tephrostratigraphy that will link marine and terrestrial records of Holocene–Pleistocene age across the Mediterranean region and mainland Europe. Nevertheless, there are some areas in the central Mediterranean in which volcanological and Quaternary studies are still at the beginning, and the link to the general tephrostratigraphic Mediterranean network is lacking. The Balkans

*Correspondence to: R. Sulpizio, CIRISIVU, c/o Dipartimento Geomineralogico, via Orabona 4, 70125, Bari, Italy.
 E-mail: sulpizio@dst.unipi.it

†Present address: Geological Survey of Norway (NGU), Trondheim, Norway.

area across Macedonia, Albania and Montenegro is one in which tephrostratigraphic and tephrochronological studies are in their infancy, although preliminary studies on lacustrine settings appear extremely promising (e.g. Lake Ohrid and Lake Shkodra; van Welden, 2007; Wagner *et al.*, 2008). For these areas both tephrostratigraphic and tephrochronological studies can offer invaluable stratigraphic support for sedimentological, palaeoclimatic, palaeoenvironmental and volcanological studies.

In this paper we present a study of tephra layers recognised in Holocene sediments of Lake Shkodra (Albania–Macedonia border; Fig. 1). The lake is located downwind of most of the Italian volcanoes that were active during the late Quaternary (Roman and Campanian volcanoes, Aeolian Islands, Mount Etna, Pantelleria Island). The products of explosive activity of these volcanoes have been extensively recognised in Adriatic and Ionian sea cores (Keller *et al.*, 1978; Paterne *et al.*, 1988; Fontugne *et al.*, 1989; Siani *et al.*, 2004; Lowe *et al.*, 2007; Calanchi and Dinelli, 2008), and, less frequently, in Macedonian, Greek and Bulgarian sites (St Seymour and Christianis, 1995; Narcisi and Vezzoli, 1999; St Seymour *et al.*, 2004; Pyle *et al.*, 2006; Margari *et al.*, 2007; Wagner *et al.*, 2008). In this framework, Lake Shkodra has a strategic position that potentially links the very distal sites of the Aegean Sea and Greece mainland with the Adriatic and Ionian marine cores and the inland Italian sites. From a volcanological point of view, the tephra layers recognised in Lake Shkodra yield crucial information about ash dispersal during explosive eruptions, and can be useful for improving volcanic hazard mitigation in the Mediterranean region.

Site description

Lake Shkodra (also known as Skadar or Scutari) is a large (45 km length, 15 km width) and shallow (5 m mean depth) lake crossed by the Albania/Montenegro border. It covers part of a wide, flat depression surrounded by NW–SE elongated relief (up to 2750 m a.s.l.) in a tectonically complex folded and faulted region (Lasca *et al.*, 1981). The present-day lake surface is 5 m a.s.l. The catchment area mainly consists of carbonate rocks (limestones and dolomites), with only two minor exposures of terrigenous rocks that supply siliciclastic sediments to the main tributary (Moraca River; Beeton and Karaman, 1981; van Welden *et al.*, 2008). The unique outlet of the lake is the Bojana (also known as Buna river in Montenegro), which flows directly to the Adriatic Sea.

The Mediterranean precipitation/evaporation regime with occurrence of flash floods, combined with a relatively high catchment/lake ratio (=11) and bathymetry, control significant lake-level fluctuations (up to 5 m in the Montenegrin part between 1956 and 1970, according to Lasca, 1981). Bloesch (1995) and Lövested and Hargeby (2005) emphasised the importance of wind on a shallow non-thermally stratified lake. According to modelling by Lee (1981), moderate (3 m s^{-1}) northeasterly winds should induce a negligible rise of a few millimetres on the coastal zone after 20 h (Lee, 1981). Wavelengths and wave base effects, which represent a potential reworking factor, were not reported by Karaman and Beeton (1981). Therefore, it can be concluded that wind-

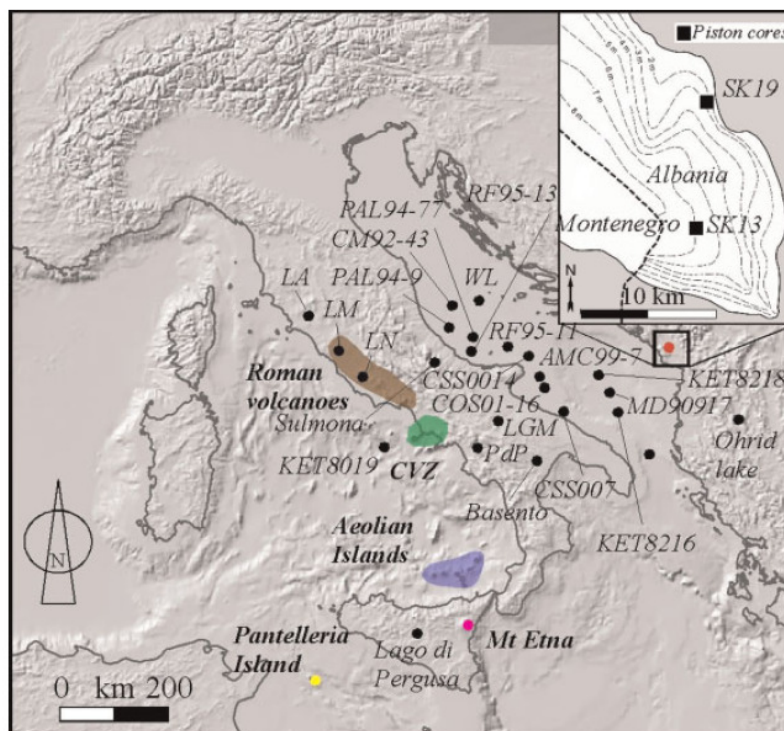


Figure 1 Location map of the study area. In the framework in the upper right angle the locations of the two studied cores are shown. Shaded areas and dots indicate the main Italian volcanoes: CVZ, Campanian volcanic zone (Campi Flegrei, Somma-Vesuvius, Ischia and Procida islands). Black dots indicate the cores used for tephra correlations: LA, Lago dell'Accesa (Magny *et al.*, 2006); LM, Lago di Mezzano; PdP, Pian di Pecore, Basento (Sulpizio *et al.*, 2008); LN, Lago di Nemi (Calanchi *et al.*, 1996), Lake Ohrid (Wagner *et al.*, 2008), Lago Grande di Monticchio (Wulf *et al.*, 2004, 2008), Sulmona (Giaccio *et al.*, 2009), PAL94-77, RF95-13, CM92-43, PAL94-9, RF95-11, AMC99-7, CSS0014, COS01-16, CSS007, WL (Lowe *et al.*, 2007); KET82-18, KET80-19, KET82-16 (Paterne *et al.*, 1988); MD90-917 (Siani *et al.*, 2004). This figure is available in colour online at www.interscience.wiley.com/journal/jqs

induced sediment reworking is negligible for Lake Shkodra deposits.

van Welden *et al.* (2008) studied the last 500 a of sedimentation in Lake Shkodra and showed that this period was characterised by undisturbed sedimentation of fine-grained material. Destructive earthquakes affected the area in 1905 and 1979, but did not induce any visible perturbation of the lacustrine archive. On the contrary, human activity (damming, change in agricultural practices) and climate (i.e. catastrophic floods occurred in 1962–1963 and the Little Ice Age between AD 1650 and 1820) had an imprint on lake sedimentation (van Welden *et al.*, 2008).

Materials and methods

The Holocene sediment fill of Lake Shkodra was sampled in September 2003, with a UWITEC™ platform and coring device. A piston corer was used to take cores composed of 3 m long sections with about 0.5 m overlap. All core liners have a 6 cm internal diameter. Two long cores were studied (Fig. 1(b)): SK19 (5.8 m long, coastal domain), and SK13 (7.8 m long, central domain). Sediments are mostly fine-grained and light-brown, and usually contain shell debris of bivalves. Magnetic susceptibility (MS) was first measured along all cores using a Bartington 72 mm diameter loop sensor to assess core retrieval

and establish preliminary lateral correlations. After core splitting, new detailed MS profiles were performed using a Bartington MS2 contact sensor with a 5 mm measuring interval (Fig. 2). The chronological framework is defined by a set of nine ^{14}C accelerator mass spectrometry (AMS) measurements (Poznan laboratory and 'Laboratoire de Mesure du Carbone 14' at Gif-sur-Yvette), obtained from terrestrial macrofossils. Five samples are from core SK19, and four from core SK13 (Appendix Table 1 and Fig. 2; van Welden, 2007). The obtained ^{14}C ages were calibrated using the IntCal 04 curve (Reimer *et al.*, 2004). Hard water and reservoir effects can induce a large array of errors and quality insurance issues on ^{14}C measurements on lake sediments with low organic carbon content taken from lakes with long water residence times (e.g. Wohlfarth 1996; Lowe and Walker, 1997). However, Lake Shkodra is a shallow lake without thermal-induced water stratification (Bloesch, 1995; Löfstedt and Hargeby, 2005), and this reduces the possibility of an important influence of reservoir effects on ages of organic material deposited into the lake. The hard water effect is more difficult to estimate, but the selection of terrestrial macrofossil remains allows to partially overcome this concern.

Nine tephra layers were recognised in the two cores, and in most cases there was coincidence with peaks in the MS curve (Fig. 2). All the tephra layers were visible to the naked eye, and were sampled and wet-sieved at 40 μm . No cryptotephra were recognised in coincidence with the MS peaks that not coincide with the sampled tephra layers.

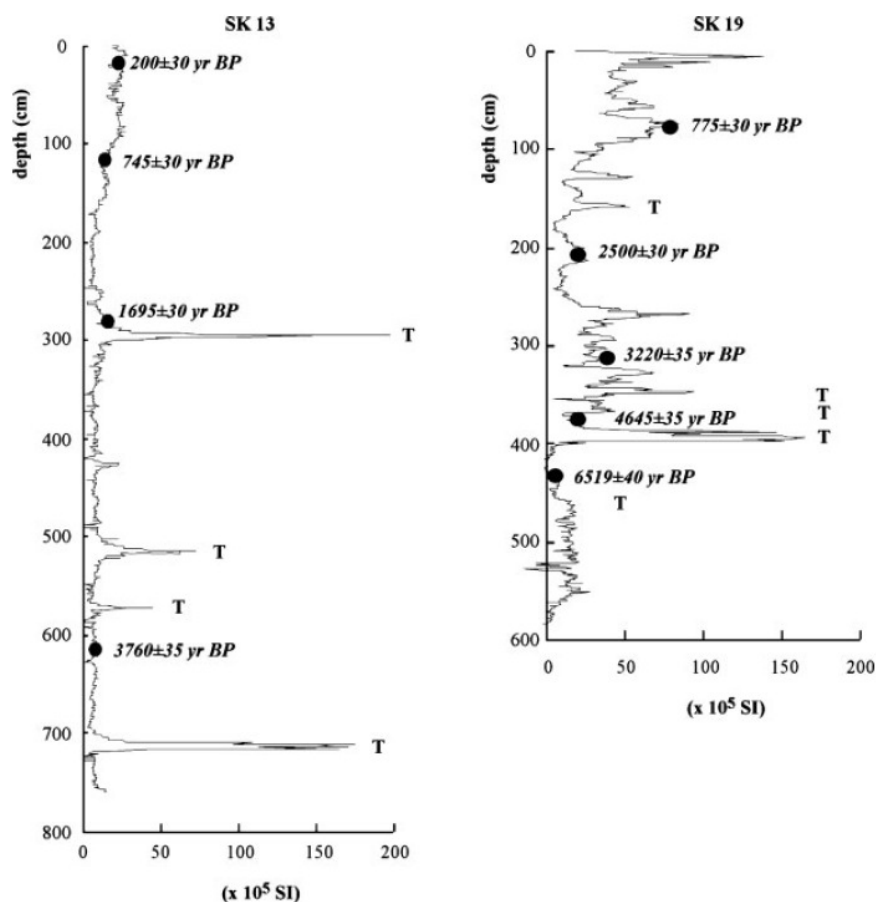


Figure 2 Magnetic susceptibility curves for cores SK13 and SK19. The letter T indicates the occurrence of a tephra layer. The ^{14}C ages obtained from plants and woods remains within the sediments are also reported

Energy-dispersive spectrometry (EDS) analyses of glass shards and glasses from micro-pumice fragments were performed at the Dipartimento di Scienze della Terra (University of Pisa), using an EDAX-DX micro-analyser mounted on a Philips SEM 515 (operating conditions: 20 kV acceleration voltage, 100 s live time counting, 200–500 nm beam diameter, 2100–2400 shots per second, ZAF correction). The ZAF correction procedure does not include natural or synthetic standards for reference, and requires analysis normalisation at a given value (which is chosen at 100%). Analytical precision is 0.5% for abundances higher than 15 wt%, 1% for abundances around 5 wt%, 5% for abundances of 1 wt% and less than 20% for abundances close to the detection limit (around 0.5 wt%). Interlaboratory standards include ALV981R23 (basalt), CFA47 (trachyte), KE12 (pantellerite; Cioni *et al.*, 1998; Appendix Table 2) samples. Some further comparisons of wave dispersion spectroscopy (WDS) microprobe analyses carried out at Geoforschungszentrum (GFZ, Potsdam, Germany), and at CAMPARIS service (CMP, Paris, France) on trachyte to rhyolite glass shards are shown in Appendix Table 2, confirming the full comparability of EDS analyses from Pisa laboratory with respect to WDS data. Accuracy of measurement is around 1%, a value analogous to that obtained using WDS, as tested by Marianelli and Sbrana (1998). Comparison of EDS and WDS micro-analyses carried out on the same samples has shown differences of less than 1% for abundances greater than 0.5 wt%.

Lithostratigraphy and MS of the core sediments

According to ^{14}C measurements, core SK13 records the last 5 ka of sedimentation in Lake Shkodra. Calcareous clayey silts dominate the sedimentary facies of this core. The overall colour of the sediments is light-brown with three noticeable greyish layers at 670 cm, 400 cm and 270 cm. Naked-eye inspection of cored sediments shows the presence of four tephra layers between 295 and 300 cm, at 514 and 571 cm, and between 716 and 726 cm (Fig. 2). The MS curve shows almost constant values around $20\text{--}30 \times 10^{-5}$ SI, which are exceeded only at the depth of the four tephra layers (peaks of MS up to 200×10^{-5} SI; Fig. 2).

The SK19 core records more than 8 ka of sedimentation in Lake Shkodra. Sedimentary facies vary strongly along the SK 19 core. White to light-brown, very fine-grained sediments with about 30% carbonate content characterise the base of the core (van Welden, 2007). Between 560 cm and 450 cm, sediments progressively become darker, organic content increases and carbonate content decreases (less than 5%). Organic matter is prevalent at 450 cm, reaching up to 30% by volume. The upper sediments (from 450 cm to the top) have near-constant sedimentology facies with silty-clayey particles composed of ~7% organic matter and ~20% carbonates. Bioclasts are often present and greyish levels can be observed at 400 cm and 350 cm depth. No erosion surfaces or gravity-driven structures (i.e. sediment slumpings) were observed along the core at the sharp contact at 450 cm between organic-rich and carbonate-rich layers. Naked-eye inspection of cored sediments shows the presence of five tephra layers between 155 and 160 cm, at 356 and 368 cm, between 385 and 400 cm, and at 460 cm (Fig. 2). The magnetic susceptibility curve shows several peaks along the core, in which only three cases (155–160 cm, 356 cm and 385–400 cm) are related to the occurrence of tephra layers (Fig. 2).

Glass and mineral composition of tephra layers

Chemical composition of glass shards and micro-pumice fragments (Appendix Table 3(a) and (b)) was classified using the silica vs. total alkali diagram (TAS; Le Bas *et al.*, 1986; Fig. 3). Composition of mineral phases was obtained through EDS analysis, and recalculated according to IMA (1988) (Appendix Tables 4–7; Fig. 4 and Supporting Information).

Four tephra layers were recognised along core SK13, between 295 and 300 cm, at 514 and 571 cm, and between 716 and 726 cm (Appendix Table 8). The sample at 295–300 cm is dark-brown and contains moderately vesicular micro-pumice fragments. Scanning electron microscopy (SEM) image analysis of micro-pumice shows they have circular bubbles with thick glassy walls (Fig. 5(a)) and a porphyritic texture, with crystals of leucite up to several tens of microns in diameter. The groundmass contains abundant acicular micro-crystals of sanidine and clinopyroxene (Fig. 5(a)). The glass composition is mostly foiditic to phonolitic, with few analyses that plot in the tephri-phonolitic field (Appendix Tables 3(a) and 8; Fig. 3). Mineral phases contain K-rich sanidine (Or79-92; Appendix Table 4; Fig. 4(a)), exotic clinopyroxenes (Fe- and Al-rich diopside and essenite) with $\text{Mg}/\text{Mg}+\text{Fe}_{\text{tot}}$ ratio around 0.5 (Appendix Table 5) and amphiboles (Appendix Table 6).

The sample at 514 cm is dark brown and contains poorly vesicular juvenile fragments (Appendix Table 8). SEM image analysis show a porphyritic texture, with crystals of plagioclase and clinopyroxene up to some tens of microns (Fig. 5(b)). The groundmass contains abundant acicular micro-crystals of plagioclase and clinopyroxene (Fig. 5(b)). Many fragments have a crystalline groundmass, without or rare interstitial glass. When present, the glass shows mostly benmoreitic composition, with few analyses plotting in the trachytic, tephritic and phonolitic fields (Appendix Table 3(a); Fig. 3).

Mineral phases comprise mainly andesine-labradorite plagioclase (An42-60; Appendix Table 4), diopside and augite clinopyroxenes with $\text{Mg}/\text{Mg}+\text{Fe}_{\text{tot}}$ ratio around 0.7 (Appendix Table 5) and olivine (Fo62-73; Appendix Table 7).

The sample at 571 cm is dark grey and mainly comprises micro-pumice fragments (Appendix Table 8). SEM image analysis shows highly vesicular juvenile fragments, with coalescent bubbles of irregular shape (Fig. 5(c)). They have porphyritic texture with crystals of clinopyroxene and sanidine up to 100 μm (Fig. 5(c)). The groundmass contains abundant acicular micro-crystals of sanidine and clinopyroxene (Fig. 5(c)). The glass composition is phonolitic (Appendix Table 3(a); Fig. 3). Mineral phases contain feldspars (sanidine, rare plagioclase and a ternary feldspar; Appendix Table 4; Fig. 4(a)), scapolite (Appendix Table 4), clinopyroxenes of variable composition (Appendix Table 5; Fig. 4(b)) and amphiboles (Appendix Table 6). Apatite occurs as accessory mineral.

The sample at 716–726 cm is light grey and contains micro-pumice fragments and glass shards (Appendix Table 8). SEM image analysis shows vesicular juvenile fragments with an almost glassy groundmass (Fig. 5(d)). The composition of glass is trachytic (Appendix Table 3(a); Fig. 3). Rare micro-crystals of clinopyroxene sometimes occur (Appendix Table 5; Fig. 4(b)).

Tephra layers were recognised between 155 and 160 cm, at 356 and 368 cm, between 385 and 400 cm, and at 460 cm along core SK19 (Appendix Table 8). All the tephra layers are visible as discrete sandy-silty layers (coarse to fine ash). The tephra at 155–160 cm is dark-brown, and has the same textural and petrographic characteristics as that at 295–300 cm in the SK13 core (Fig. 5(a)), the same foiditic-phonolitic composition (Appendix Table 3(b)), and are therefore assumed to be deposits

HOLOCENE TEPHROSTRATIGRAPHIC RECORD OF LAKE SHKODRA

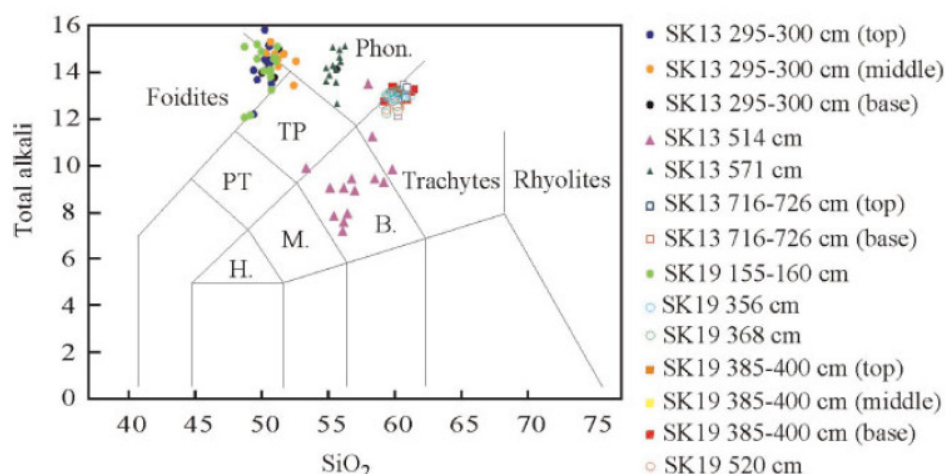


Figure 3 Total alkali vs. silica diagram (Le Bas *et al.*, 1986) of glass compositions of the recognised tephra layers. If more than one analysis was performed for a given tephra layers the position of sampling is indicated in parentheses. Phon., phonolites; TP, tephri-phonolites; PT, phono-tephrites; B, benmoreites; M, mugearites; H, hawaiites

of the same eruption. The two tephra layers at 356 and 368 cm are light grey, and mainly comprise elongated and convoluted glass shards with a glassy, crystal-free groundmass (Fig. 5(e)) and a trachytic composition (Appendix Table 3(b); Fig. 3). The sample at 385–400 cm is light grey, and has the same textural and petrographic characteristics of that at 716–726 cm in the SK13 core (Fig. 5(d)), the same trachytic composition (Appendix Table 3b), and are assumed to be deposits from the same eruption.

The tephra at 460 cm is light-grey and contains micro-pumice fragments (Appendix Table 8). SEM image analysis shows they are vesicular, with a glassy groundmass and with trachytic composition (Appendix Table 3(b); Fig. 3). Rare, acicular, sanidine crystals sometimes occur (Fig. 5(f)).

Discussion

Correlation with proximal deposits and other distal archives

The ^{14}C measurements performed on organic matter from cores SK13 and SK19 indicate the sediments are Holocene in age,

which constrains the search for the source of parent eruptions of tephra layers to the explosive activity of Mediterranean volcanoes during this period. All the recognised tephra layers show alkaline affinity, and can be roughly separated into under-saturated (phonolites and foidites) and saturated (benmoreites and trachytes) glass compositions (Appendix Table 3(a) and (b); Fig. 3). The composition and geochemical affinity limit their sources to Italian volcanoes, since the sources in the Aegean area during the Holocene have calc-alkaline affinity (e.g. Keller *et al.*, 1990). Sources from Massif Central (France) and Eifel (Germany) are probably too far, since their deposits have never been recognised close to the study area.

The geochemical data indicate Somma-Vesuvius as a source for tephra layers SK13 295–300 cm (and SK19 155–160 cm) and SK13 571 cm. In particular, the foiditic–phonolitic composition of tephra layer SK13 295–300 cm (and SK19 155–160 cm) matches well that of the AD 472 (Pollena) eruption (Appendix Table 9; Fig. 6; Rosi and Santacroce, 1983; Santacroce, 1987; Sulpizio *et al.*, 2005; Santacroce *et al.*, 2008), although the distal deposits show a slight lower mean content in MgO than the proximal ones (Appendix Table 9). The composition of mineral phases, which comprise K-rich sanidine, amphibole and Al- and K-rich clinopyroxenes (Appendix Tables 4–6), replicates the mineral assemblage

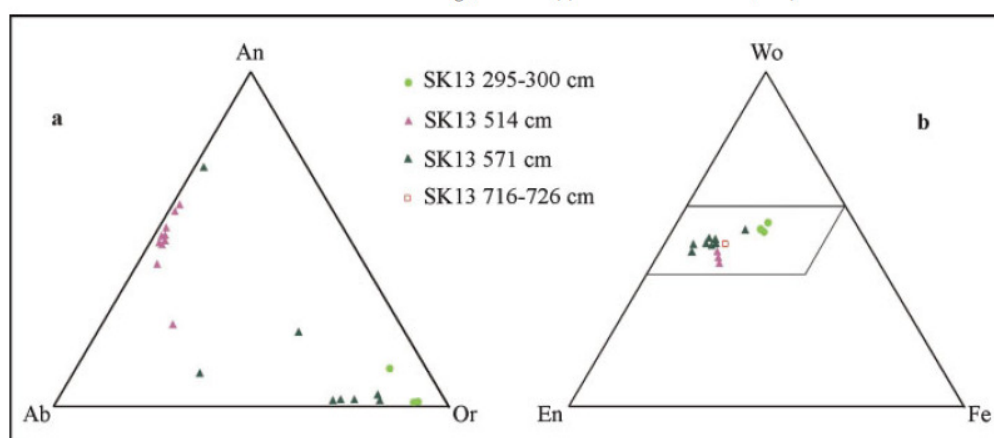


Figure 4 Triangular diagrams for classification of mineral phases. (a) albite–anorthite–orthose diagram for classification of feldspars; (b) wollastonite–ferrosillite–enstatite diagram for classification of pyroxenes

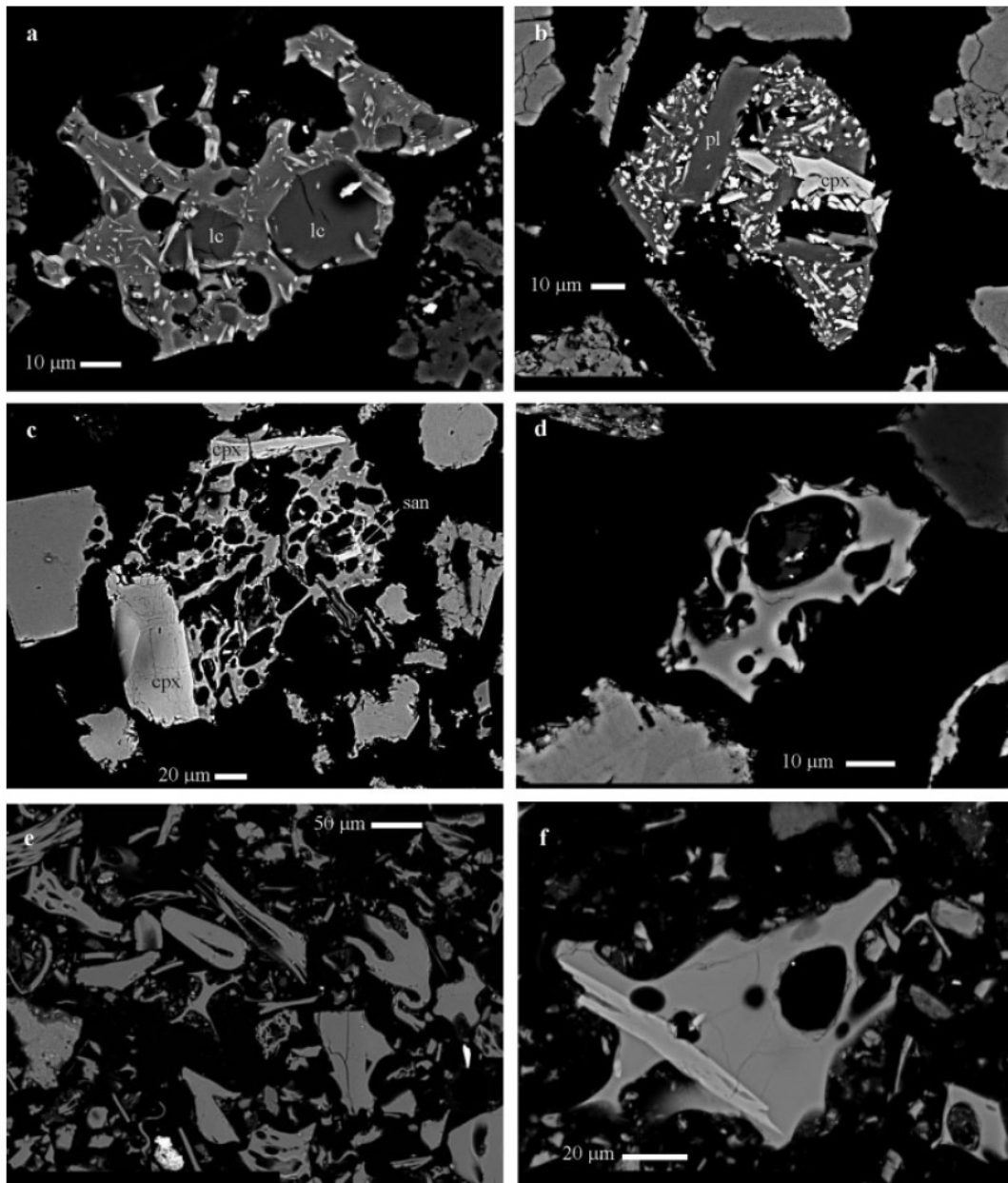


Figure 5 SEM images of the recognised tephra layers. (a) Sample from AD 472 (Pollena) tephra. lc, leucite. (b) Sample from FL tephra layer. pl, plagioclase; cpx, clinopyroxene. (c) Sample from Avellino tephra layer. cpx, clinopyroxene; san, sanidine. (d) Sample from Agnano Monte Spina tephra layer. (e) Samples from Astroni tephra layers. (f) Sample from Agnano Pomici Principali tephra layer

described for proximal deposits of the AD 472 eruption (Rosi and Santacroce, 1983; Santacroce, 1987; Sulpizio *et al.*, 2005). Also the ^{14}C ages, which indicate a time window around 1500–1700 cal. a BP (Fig. 2; Appendix Table 1), are in good agreement with the age of the eruption. The recognition of ash related to the AD 472 eruption in Lake Shkodra (located more than 440 km from the Somma-Vesuvius) is the first report of this tephra as a discrete layer in the Balkan area, since it was recently reported in Lake Ohrid sediments (Albania–Macedonia border; Vogel *et al.*, 2009) but as a cryptotephra probably mixed with the products of the following AD 512 eruption from Somma-Vesuvius. The area of dispersion of AD 472 products is

significantly enlarged to the east (Fig. 7(a)). It is noteworthy that the recognition of this tephra layer in Lake Shkodra is in good agreement with hagiographic documents, which reported ash fallout on Constantinople in AD 472 (Rosi and Santacroce, 1983).

The other Somma-Vesuvius tephra at 571 cm in core SK 13 is slightly younger than 4240–4060 cal. a BP (Fig. 2) and shows a phonolitic composition (Appendix Table 3(a)). In the last 4 ka, tephri-phonolitic to phonolitic magmas fed several explosive eruptions at Somma-Vesuvius. In particular, the period that includes the Avellino (best age between 3.9 and 4.1 cal. ka BP; Santacroce *et al.*, 2008) and Pompeii (AD 79) eruptions was characterised by glass compositions similar to the SK13 571 cm

HOLOCENE TEPHROSTRATIGRAPHIC RECORD OF LAKE SHKODRA

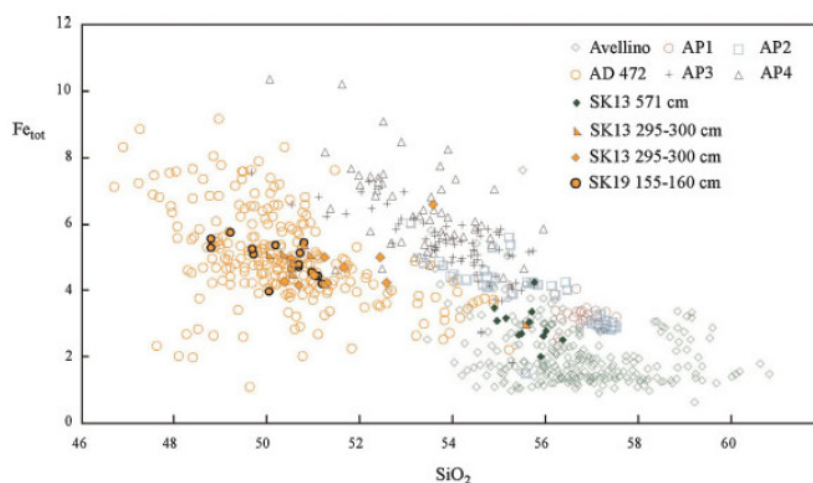


Figure 6 SiO_2 vs. FeO_{tot} diagram of glass composition of Avellino and AD 472 (Pollena) tephra layers. The glass compositions of other Vesuvian proximal deposits (Santacroce *et al.*, 2008) are also plotted for supporting the correlation of the two tephra layers

tephra layer (Santacroce *et al.*, 2008). While the inferred age rules out a correlation with the AD 79 (Pompeii) eruption, it may be difficult to discriminate among the Avellino and some of the interplinian eruptions which occurred in the Avellino–Pompeii time span (AP eruptions; Andronico and Cioni, 2002). However, when plotted on a FeO_{tot} vs. SiO_2 diagram (Fig. 6), the SK13 571 cm analyses show a good match with the Avellino glass compositions. The correlation with the Avellino eruption is also strengthened by the mineral assemblage of the SK13 571 cm tephra, which contains sanidine (Appendix Table 4), clinopyroxenes (Appendix Table 5), amphiboles (Appendix Table 6) and, most important, rare scapolite crystals (Appendix Table 4), which is an exotic mineral phase exclusive of Avellino products (Cioni *et al.*, 2000; Sulpizio *et al.*, 2008). Both the composition and morphology of the ash particles indicate the SK13 571 cm tephra belongs to the EU3 (grey fallout) magmatic Plinian deposits of the Avellino eruption, which also has a different area of dispersion with respect to the phreatomagmatic ash of the Avellino eruption (Fig. 7(c); Sulpizio *et al.*, 2008). The SK13 571 cm tephra represent the first recognition of the Avellino tephra in the Balkan area, and enlarges the dispersion area of the magmatic deposits of the eruption to more than 440 km east of Somma-Vesuvius (Fig. 7(c)).

The benmoreitic composition of tephra at 514 cm in core SK13 constrains the source of the activity to Mount Etna, which is the only known source of this magma type in the central Mediterranean area active during the Holocene (e.g. Kieffer, 1979; Cristofolini and Romano, 1982; Coltelli *et al.*, 2000). According to its age (younger than 4240–4060 cal. a BP; Fig. 2), composition, and mineral assemblage (Appendix Tables 4, 5 and 7), it can be correlated to a tephra layer recognised in the Holocene sediments of Lake Ohrid (Albania–Macedonia border; Fig. 1; Wagner *et al.*, 2008; Vogel *et al.*, 2009) and Lago di Pergusa (central Sicily; Fig. 1; Sadori and Narcisi, 2001; Appendix Table 9), which was correlated with the deposits of FL eruption from Etna volcano (3440–3300 cal. a BP; Coltelli *et al.*, 2000; Wagner *et al.*, 2008). The recognition of FL tephra in the Lake Shkodra sediments confirms the regional importance of this tephra layer, and enlarges its dispersion to the north (Fig. 7(b)).

The other four tephra layers recognised at 356 and 368 cm in core SK19, at 716–726 cm in core SK13 (and 385–400 cm in core SK19) and at 460 cm in core SK19 have very similar trachytic–phonolitic composition (Fig. 3). During the Holocene

a trachytic–phonolitic composition of glass characterised the explosive activity of Campi Flegrei caldera (Civetta *et al.*, 1991; Santacroce *et al.*, 2008; Turney *et al.*, 2008; Fig. 1). In particular, the SK19 356 cm, SK19 368 cm and SK19 385–400 cm (and SK13 716–726 cm) can be correlated to the Astroni–Agnano Monte Spina–Averno eruptions (Rosi and Sbrana, 1987; Di Vito *et al.*, 1999), which form an almost compositional homogeneous cluster of tephra layers in other archives of the central Mediterranean area (i.e. Lago Grande di Monticchio; Fig. 1; Wulf *et al.*, 2004, 2008; Adriatic Sea core MD90-917; Siani *et al.*, 2004; Fig. 1). The cluster has been dated between 4290–4050 and 5430–5130 cal. a BP in the Adriatic Sea core MD90-917 (Fig. 1; Siani *et al.*, 2004), which is in agreement with ^{14}C ages reported for proximal deposits (3820 ± 50 to 4530 ± 50 ^{14}C BP; between 4330–4150 and 5280–5080 cal. a BP; Di Vito *et al.*, 1999). This time window is compatible with ages on both core SK13 (older than 4240–4060 cal. a BP; Fig. 2) and core SK19 (5470–5300 cal. a BP; Fig. 2). Furthermore, the stratigraphic data of core SK19 can shed light on the sedimentology of these tephra layers in Lake Shkodra. Despite their geochemical homogeneity (Appendix Table 3(a) and (b)), the three tephra layers recognised in core SK19 are separated by lake sediments with thickness of several centimetres, which indicate different times of deposition, confirming they are from different eruptions. It is also worth noting that the basal tephra layer (385–400 cm) is the thickest, shows homogeneous grain size, and comprises almost 100% glass particles, testifying to a rapid and undisturbed sedimentation. This stratigraphic evidence may indicate the occurrence of a large-magnitude eruption, able to spread centimetre-thick ash deposits over large areas. If we take into account the proximal deposits of the Astroni–Agnano Monte Spina–Averno group, the most probable correlation of the 385–400 cm tephra layer is with the Agnano Monte Spina eruption, which is the highest-magnitude event in the group (Di Vito *et al.*, 1999). Therefore, the correlation of tephra layers SK19 356 cm, SK19 368 cm and SK19 385–400 cm (and SK13 716–726 cm) to the Astroni–Agnano Monte Spina succession is here proposed on the basis of stratigraphy, homogeneity in major oxides composition and stratigraphy. This implies that the basal age of the 385–400 cm tephra layers corresponds to that of Agnano Monte Spina eruption. The age of this tephra is debated. De Vita *et al.* (1999) suggested a best age of 4500–3700 cal. a BP, obtained



Figure 7 Dispersal areas of the recognised tephra layers. Black and white ellipses indicate the dispersal of coarse-grained fallout deposits of the different eruptions. In the case of Avellino tephra layer the two areas with different shading indicate dispersal of ash from the magmatic (right) or phreatomagmatic (left) phases of the eruption (Sulpizio *et al.*, 2008). This figure is available in colour online at www.interscience.wiley.com/journal/jqs

by the integration of ^{14}C and $^{40}\text{Ar}/^{39}\text{Ar}$ dates. The varve-supported age of TM5c tephra layer at Lago Grande di Monticchio is 5660–5120 cal. a BP (Wulf *et al.*, 2004, 2008). Blockley *et al.* (2008) indicated an age between 4690 and 4300 cal. a BP based on Bayesian analysis of available ages (95% confidence), which appears the most convincing considering field evidence and available radiometric ages on proximal deposits.

The AMST represents a common stratigraphic marker for central Italy and the Adriatic sea (Fig. 7(d); e.g. Calanchi *et al.*, 1998; Siani *et al.*, 2004; Wulf *et al.*, 2004, 2008; Lowe *et al.*, 2007; Calanchi and Dinelli, 2008).

The tephra layer at 460 cm in core SK 19 is older than 7510–7310 cal. a BP (Fig. 2), and this, combined with glass composition, indicates a correlation with the Agnano Pomici Principali eruption from Campi Flegrei caldera (Rosi and Sbrana, 1987; Di Vito *et al.*, 1999). Blockley *et al.* (2008) suggested a best age of 12 380–12 140 cal. a BP based on Bayesian analysis of available ages (95% confidence). This

tephra layer has been recognised in some other central Mediterranean archives, including the Lago Grande di Monticchio core (TM-7b tephra layer; Wulf *et al.*, 2004), Tyrrhenian and Adriatic sea cores (C1 tephra layer; Paternò *et al.*, 1988; Siani *et al.*, 2004; Fig. 7(e)), and Lago dell'Accesa (central Italy, Fig. 1; Magny *et al.*, 2006). The recognition in Lake Shkodra is the first in the Balkan area, and enlarges the recognition area of the Agnano Pomici Principali deposits up to more than 440 km east of Campi Flegrei caldera (Fig. 7(e)).

Deposition environment and sedimentation rates

Although limited to only two cores, the succession of sedimentary facies along the SK13 and SK19 cores may be tentatively used for gaining information about the palaeoenvironmental evolution in two different locations of Lake Shkodra. Core SK13

HOLOCENE TEPHROSTRATIGRAPHIC RECORD OF LAKE SHKODRA

is dominated by silty to muddy lithofacies, which indicate sedimentation from a lacustrine environment over the last 5.3 cal. ka BP. By contrast, lithofacies association of core SK19 shows organic-rich sediments below 450 cm depth, and calcareous mud lithofacies above this point. This lithofacies association, the presence of broken shells and the absence of diatoms suggest a lagoon-like palaeoenvironment until about

7.4 cal. ka BP (450 cm of depth), whereas between 7.4 cal. ka BP and the present day the SK19 area hosted a lake with no significant modification in sedimentation dynamics. The two different lithofacies associations of cores SK13 and SK19 indicate that the lake level may have been at least 2 m lower between 13–12 cal. ka BP and about 7.4 cal. ka BP, during which the present-day near-shore region was dominated by a

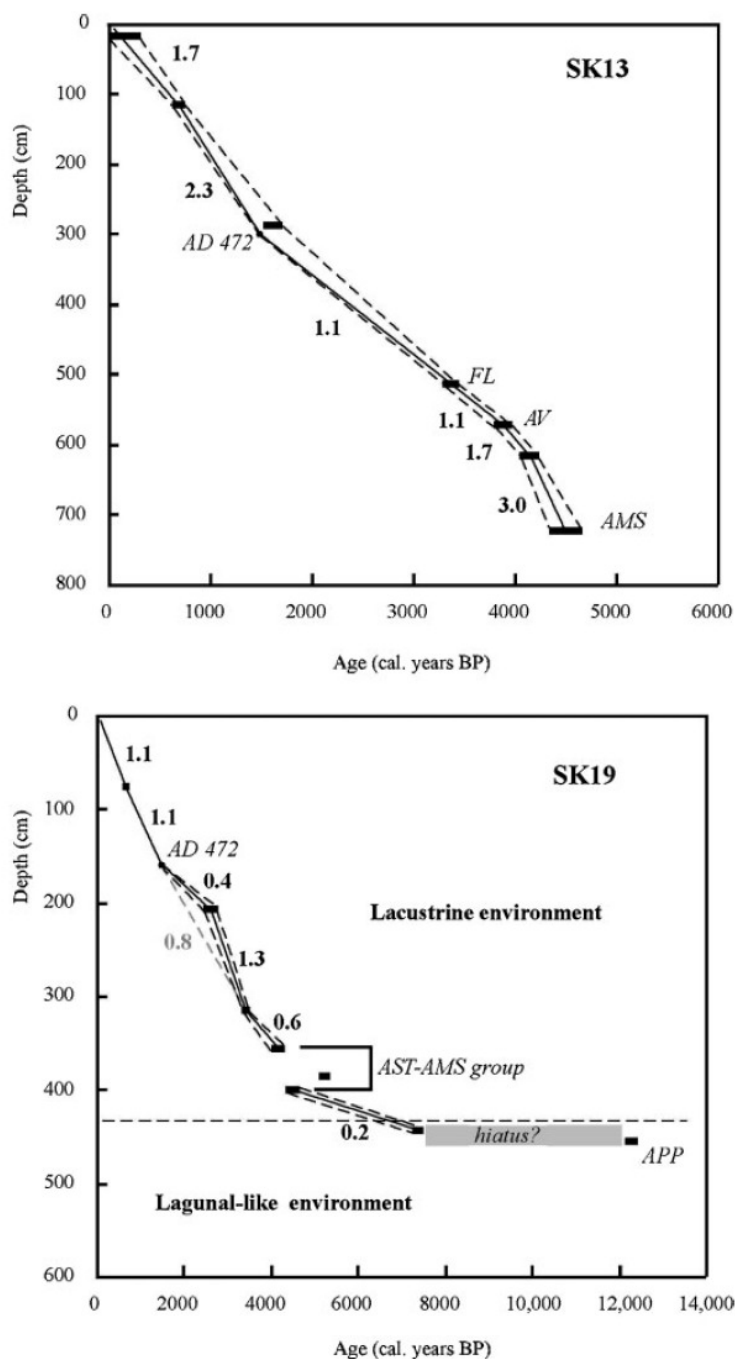


Figure 8 Age–depth relationship for cores SK13 and SK19 using ^{14}C ages and tephra layers. The latter are labelled with the correspondent tephra layer: AV, Avellino; AMS, Agnano Monte Spina; AST, Astroni; APP, Agnano Pomici Principali. The width of black bars indicates 2σ calibration values. The dashed lines indicate the 2σ range of both ^{14}C and tephra ages. Bold numbers indicate the calculated sedimentation rate based on simple extrapolation between two ages

lagoonal-like environment. The level of the lake in the Shkodra depression started to rise before the deposition of the Agnano Monte Spina tephra layer, with sedimentation of fine-grained deposits in both cores.

Based on available ^{14}C ages and dated tephra layers, sedimentation curves can be traced for both cores. Since the profile of a sedimentation curve critically depends on the chosen age model, some comments are needed about the reference ages of the tephra layers. Apart from the AD 472 tephra layer, which has a precise historical age (Rosi and Santacroce, 1983), and the FL tephra layer, which has only two published ages (one on a terrestrial deposit, Coltelli *et al.*, 2000; and the other from lacustrine sediment, Sadori and Narcisi, 2001), the available ages of Avellino, Agnano Monte Spina–Astroni and Agnano Pomici Principali tephra layers have some uncertainties. This is particularly true for the age of the Avellino tephra, which has a wide range between 3.6 and 4.4 cal. ka BP (Santacroce *et al.*, 2008). However, the younger age (Vogel *et al.*, 1990) is a weighted average of Avellino ages and data from charcoal from the soil underneath the following eruption (AP1; e.g. see Santacroce *et al.*, 2008, for a recent review), while the older age is from humic acids from a black palaeosol developed on the alluvial plain east of the Somma–Vesuvius edifice (Santacroce *et al.*, 2008). Therefore, these end members of the Avellino age range can be considered as the upper and lower limits for the most probable age of the eruption. Here, we used the age of 3940–3860 cal. a BP, obtained from charcoal collected in the very top part of a palaeosol underneath the Avellino fallout deposits on the volcano slopes (Andronico *et al.*, 1995), and thus assumed to represent an age very close to the deposition.

The Agnano Monte Spina and Astroni ages share similar uncertainties with the Avellino eruption, which mainly derive from the use of different dating methods (^{14}C and $^{40}\text{Ar}/^{39}\text{Ar}$ ages; Rosi and Sbrana, 1987; Di Vito *et al.*, 1999). The age framework is further complicated by the complexity of the eruptive successions of both eruptions (Di Vito *et al.*, 1999; Isaia *et al.*, 2004), which produced deposition of distinct tephra layers with different ages in distal areas (e.g. Lago Grande di Monticchio; Wulf *et al.*, 2004, 2008; Adriatic deep sea core MD90-918; Siani *et al.*, 2004). For the Agnano Monte Spina eruption, here we used the ^{14}C age of 4690–4300 cal. a BP (95%) obtained applying Bayesian statistics to the available ages (Blockley *et al.*, 2008). The top age of Astroni tephra was assumed to be 4170 ± 120 cal. a BP, which corresponds to the glass peak at 140 cm depth in core MD90-917 (Siani *et al.*, 2004). Since glass shards (which mark the onset of tephra deposition) and foraminifera (from which the age is obtained) were deposited at the same time, we assumed that this age is the best available for the end of the Astroni activity. ^{14}C ages of Agnano Pomici Principali are rather scarce, and indicate ages between 11 and 13 cal. ka BP (Rosi and Sbrana, 1987; Di Vito *et al.*, 1999; Siani *et al.*, 2004). Similar to the Astroni eruption, we assume here the age of 12 380–12 140 cal. a BP (Blockley *et al.*, 2008) to be the best available, taking also into account the good agreement of this age with the marine age of 12 540–12 180 cal. a BP (305–310 cm depth; Siani *et al.*, 2004) and the terrestrial age of 12 340–12 060 cal. a BP obtained from charcoal just underneath proximal deposits (Di Vito *et al.*, 1999).

Core SK13 shows a quite constant sedimentation rate (comprised between 1.1 mm a^{-1} and 1.7 mm a^{-1}) for most of its length, the only exception being the periods between 115 cm and AD 472 and between 614 cm and Agnano Monte Spina tephra, when the sedimentation rate increased up to 2.3 mm a^{-1} and to 3 mm a^{-1} , respectively (Fig. 8).

The sedimentation curve of core SK19 shows a trend similar to the core SK13 between the present day and AD 472 tephra

layer (1.1 mm a^{-1} ; Fig. 8(b)). A sharp change in slope of the curve below this tephra layer seems to indicate a lowering of the sedimentation rate, but a less sharp decrease in the slope of the curve is obtained if we consider that the age at 207 cm is too old and interpolate between 160 cm and 311 cm (grey dashed line in Fig. 8(b)). The sedimentation rate returns to values of 1.3 mm a^{-1} between 311 and 356 cm (4170–3420 cal. a BP; Fig. 8(b)), but constantly decline below 400 cm (Fig. 8(b)). It is worth noting that the Agnano Pomici Principali tephra layer (12380–12140 cal. a BP) occurs a few centimetres below the date of 7510–7310 cal. a BP. This indicates the probable occurrence of a sedimentary hiatus between 443 and 460 cm (Fig. 2), which is in agreement with the observed change between organic-rich lithofacies and calcareous mud lithofacies around 450 cm of depth. The changes in sedimentation rate, when combined with lithofacies association, support the hypothesis of transition from a lagoonal-like environment during the Younger Dryas to a purely lacustrine environment afterwards. This transition in sedimentary facies is in accordance with contemporaneous lacustrine depositional successions studied in the Balkan area or in Italy (e.g. Lago dell'Accesa; Magny *et al.*, 2006).

Conclusion

The recognition of six tephra layers in the Lake Shkodra sediments has relevance for both volcanology and Quaternary science. From a volcanological point of view, five of the tephra layers (AD 472, Avellino, Astroni, Agnano Monte Spina and Agnano Pomici Principali) have been recognised for the first time in the Balkan area, enlarging to the east the previously assessed dispersal areas. The FL tephra layer from Mount Etna has already been recognised in the Balkan area (lake Ohrid, southeast of Lake Shkodra; Fig. 1), but these new data enlarge its dispersal area to the north and represent the most distal finding of this Etnean tephra layer. The enlargement of tephra distributions confirms the high mobility of ash from explosive eruptions of Italian volcanoes during the Holocene (e.g. Sulpizio *et al.*, 2008), irrespective of whether they are from high-intensity (Plinian) or intermediate-intensity (sub-Plinian) eruptions. This poses new challenges for research devoted to volcanic hazard mitigation in case of renewed explosive activity from some of these in the near future. In particular, the wide dispersal of these Holocene tephra layers requires more sophisticated and accurate numerical models of ash dispersal, capable of forecasting the areas likely to be affected by ash deposition far beyond the present-day distributions, which today are limited to a few tens of kilometres around the volcanic source (Cioni *et al.*, 2003; Costa *et al.*, 2008).

From a Quaternary research point of view the recognition of the six tephra layers in the Holocene sediments of Lake Shkodra provides time constraints for sedimentary succession and permits the establishment of the first, robust, physically based correlation with natural archives of the adjacent region. In particular, Avellino and Agnano Pomici Principali tephra layers have particular relevance due to their age of deposition. The Avellino tephra links the Lake Shkodra archive to the Adriatic Sea and lakes of central (Lago dell'Accesa, Lago di Nemi, Lago di Mezzano; Fig. 1) and southern Italy (Lago Grande di Monticchio), during a key period for Holocene palaeoclimatic evolution in the central Mediterranean area (e.g. Sadori and Narcisi, 2001; Drysdale *et al.*, 2006; Magny *et al.*, 2007). The Agnano Pomici Principali tephra layer links the Lake Shkodra sediments to Adriatic Sea and lacustrine archives of southern

(Lago Grande di Monticchio) and central Italy (Lago dell'Accesa), and physically confirms the Younger Dryas period in these different archives.

Acknowledgements Shkodra lake coring was funded by NATO Science for Peace project (SFP 977 993), which was initiated and managed by Prof. François Jouanne at Laboratoire de Géodynamique des Chaînes Alpines' (LGCA). The authors wish to thank their colleagues who made the coring possible, especially C. Beck and J. L. Mugnier at LGCA, and R. Koci and S. Bushati from Albanian institutions. This research has been partially supported by INGV-DPC 2005–2007 projects (V-3 subproject on explosive activity of Somma-Vesuvius). Simon Blockley and Stefan Wastergard improved the quality of the manuscript with their careful revisions. We thank Russel Drysdale for the editing of the English text.

References

- Andronico D, Cioni R. 2002. Contrasting styles of Mount Vesuvius activity in the period between the Avellino and Pompeii Plinian eruptions, and some implications for assessment of future hazards. *Bulletin of Volcanology* **64**: 372–391.
- Andronico D, Calderoni G, Cioni R, Sbrana A, Sulpizio R, Santacroce R. 1995. Geological map of Somma-Vesuvius volcano. *Periodico di Mineralogia* **64**: 77–78.
- Beeton A, Karaman GS. 1981. General summary. In *The Biota and Limnology of Lake Skadar*. Smithsonian Institution: Washington, DC; 429–436.
- Blockley SPE, Bronk Ramsey C, Pyle DM. 2008. Improved age modelling and high-precision age estimates of late Quaternary tephras, for accurate palaeoclimate reconstruction. *Journal of Volcanology and Geothermal Research* **177**: 251–262.
- Bloesch J. 1995. Mechanisms, measurement and importance of sediment resuspension in lakes. *Marine Freshwater Research* **46**: 295–304.
- Calanchi N, Dinelli E. 2008. Tephrostratigraphy for the last 170 ka in sedimentary successions from the Adriatic sea. *Journal of Volcanology and Geothermal Research* **177**: 81–95.
- Calanchi N, Dinelli E, Lucchini F, Mordenti A. 1996. Chemostratigraphy of the Late sediments from Lake Albano and Central Adriatic Sea cores (PALICLAS project). *Memorie Istituto Italiano di Idrobiologia* **55**: 247–263.
- Calanchi N, Cattaneo A, Dinelli E, Gasparotto G, Lucchini F. 1998. Tephra layers in Late Quaternary sediments of the central Adriatic Sea. *Marine Geology* **149**: 191–209.
- Cioni R, Levi S, Sulpizio R. 2000. Apulian Bronze Age pottery as a long-distance indicator of the Avellino Pumice eruption (Vesuvius, Italy). In *The Archaeology of Geological Catastrophes*, McGuire WG, Griffiths DR, Hancock PL, Stewart IS (eds). Geological Society of London; Special Publication 171; 159–177.
- Cioni R, Marianelli P, Santacroce R. 1998. Thermal and compositional evolution of the shallow magma chambers of Vesuvius: evidence from pyroxene phenocrysts and melt inclusions. *Journal of Geophysical Research* **103**: 18277–18294.
- Cioni R, Longo A, Macedonio G, Santacroce R, Sbrana A, Sulpizio R, Andronico D. 2003. Assessing pyroclastic fall hazard through field data and numerical simulations: the example from Vesuvius. *Journal of Geophysical Research* **108**: ECV2.1–ECV2.11.
- Civetta L, Carluccio E, Innocenti F, Sbrana A, Taddeucci G. 1991. Magma chamber evolution under Phlegraean Fields during the last 10 ka: trace element and isotope data. *European Journal of Mineralogy* **3**: 415–428.
- Coltelli M, Del Carlo P, Vezzoli L. 2000. Stratigraphic constraints for explosive activity in the past 100 ka at Etna volcano, Italy. *International Journal of Earth Sciences* **89**: 665–677.
- Costa A, Dell'Erba F, Di Vito M, Isaia R, Macedonio G, Orsi G, Pfeiffer T. 2008. Tephra fallout hazard assessment at the Campi Flegrei caldera (Italy). *Bulletin of Volcanology* **71**: 259–273.
- Cristofolini R, Romano R. 1982. Petrologic features of the Etnean volcanic rocks. *Memorie della Società Geologica Italiana* **23**: 99–115.
- de Vita S, Orsi G, Civetta L, Carandente A, D'Antonio M, Deino A, di Cesare T, Di Vito MA, Fisher RV, Isaia R, Marotta E, Necco A, Ort M, Pappalardo L, Piochi M, Southon J. 1999. The Agnano–Monte Spina eruption (4100 years BP) in the restless Campi Flegrei caldera (Italy). *Journal of Volcanology and Geothermal Research* **91**: 269–301.
- Di Vito MA, Isaia R, Orsi G, Southon J, de Vita S, D'Antonio M, Pappalardo L, Piochi M. 1999. Volcanism and deformation since 12,000 years at the Campi Flegrei caldera (Italy). *Journal of Volcanology and Geothermal Research* **91**: 221–246.
- Di Vito MA, Sulpizio R, Zanchetta G, D'Orazio M. 2008. The late Pleistocene pyroclastic deposits of the Campanian Plain: new insights into the explosive activity of Neapolitan volcanoes. *Journal of Volcanology and Geothermal Research* **177**: 19–48.
- Drysdale RN, Zanchetta G, Hellstrom J, Maas R, Fallick AE, Pickett M, Cartwright I, Piccini L. 2006. Late Holocene drought responsible for the collapse of Old World civilizations is recorded in an Italian flowstone. *Geology* **34**: 101–104.
- Federman AN, Carey SN. 1980. Electron microprobe correlation of tephra layers from Eastern Mediterranean abyssal sediments and the island of Santorini. *Quaternary Research* **13**: 160–171.
- Fontugne M, Paterne M, Calvert SE, Murat A, Guichard F, Arnold M. 1989. Adriatic deep water formation during the Holocene: implication for the reoxygenation of the deep Eastern Mediterranean sea. *Paleoceanography* **4**: 199–206.
- Frisia S, Borsato A, Susini J. 2008. Synchrotron radiation applications to past volcanism archived in speleothems: an overview. *Journal of Volcanology and Geothermal Research* **177**: 96–100.
- Giaccio B, Isaia R, Fedele FG, Di Canzio E, Hoffecker J, Ronchitelli A, Sinityn A, Anikovich M, Lisitsyn SN. 2008. The Campanian Ignimbrite and Codola tephra layers: two temporal/stratigraphic markers for the Early Upper Palaeolithic in southern Italy and eastern Europe. *Journal of Volcanology and Geothermal Research* **177**: 210–228.
- Giaccio B, Messina P, Sposato A, Voltaggio M, Zanchetta G, Galadini F, Gori S, Santacroce R. 2009. Tephra layers from Holocene lake sediments of the Sulmona basin, central Italy: implications for volcanic activity in Peninsular Italy and tephrostratigraphy in the central Mediterranean area. *Quaternary Science Reviews*, doi: 10.1016/j.quascirev.2009.06.009
- Isaia R, D'Antonio M, Dell'Erba F, Di Vito M, Orsi G. 2004. The Astroni volcano: the only example of closely spaced eruptions in the same vent area during the recent history of the Campi Flegrei caldera (Italy). *Journal of Volcanology and Geothermal Research* **133**: 171–192.
- Karaman GS, Beeton A. 1981. *The Biota and Limnology of Lake Skadar*. Smithsonian Institution: Washington, DC/Univerzitet Veljko Vlahvic.
- Keller J, Ryan WBF, Ninkovich D, Alther R. 1978. Explosive volcanic activity in the Mediterranean over the past 200,000 years as recorded in deep-sea sediments. *Geological Society of America Bulletin* **89**: 591–604.
- Keller J, Rehren T, Stadtbauer E. 1990. Explosive volcanism in the Hellenic Arc: a summary and review. In *Thera and the Aegean World III*, Hardy DA, Keller J, Galanopoulos VP, Flemming NC, Druitt TH (eds). Thera Foundation: Santorini, Greece; 13–26.
- Kieffer G. 1979. L'activité de l'Etna pendant le dernier 20,000 ans. *Comptes Rendù de l'Académie des Sciences Paris* **288D**: 1023–1026.
- Lasca NP, Radulovic V, Ristic RJ, Cherkauer DS. 1981. Geology, hydrology, climate and bathymetry of Lake Skadar. In *The Biota and Limnology of Lake Skadar*. Smithsonian Institution: Washington, DC; 17–38.
- Le Bas MJ, Le Maitre RW, Streckeisen A, Zanettin B. 1986. A chemical classification of volcanic rocks based on the Total Alkali–Silica diagram. *Journal of Petrology* **27**: 745–750.
- Lee KK. 1981. Application of mathematical modelling in studying of Lake Skadar circulation patterns. In *The Biota and Limnology of Lake Skadar*. Smithsonian Institution: Washington, DC; 56–65.
- Lövstedt CB, Hargeby A. 2005. Seasonal variation in resuspension in a shallow Swedish lake: potential factors. In *15th International North-*

- ern Research Basin Symposium and Workshop, Lulea to Kvikkjokk, Sweden; 101–109.
- Lowe JJ, Walker MJC. 1997. *Reconstructing Quaternary Environments*. Pearson Prentice Hall: London.
- Lowe JJ, Blockley S, Trincardi F, Asioli A, Cattaneo A, Matthews IP, Pollard M, Wulf S. 2007. Age modelling of late Quaternary marine sequences in the Adriatic: towards improved precision and accuracy using volcanic event stratigraphy. *Continental Shelf Research* **27**: 560–582.
- Magny M, de Beaulieu JL, Drescher-Schneider R, Vanni ere B, Walter-Simonnet AV, Millet L, Bossuet G, Peyron O. 2006. Climatic oscillations in central Italy during the Last Glacial–Holocene transition: the record from Lake Accesa. *Journal of Quaternary Science* **21**: 311–320.
- Magny M, de Beaulieu JL, Drescher-Schneider R, Vanni ere B, Walter-Simonnet AV, Miras Y, Millet L, Bossuet G, Peyron O, Brugiapaglia E, Leroux A. 2007. Holocene climate changes in the central Mediterranean as recorded by lake-level fluctuations at Lake Accesa (Tuscany, Italy). *Quaternary Science Review* **26**: 1736–1758.
- Margari V, Pyle DM, Bryant C, Gibbard PL. 2007. Mediterranean tephra stratigraphy revisited: results from a long terrestrial sequence on Lesbos Island, Greece. *Journal of Volcanology and Geothermal Research* **163**: 34–54.
- Marianelli P, Sbrana A. 1998. Risultati di misure di standard di minerali e di vetri naturali in microanalisi a dispersione di energia. *Atti Societ  Toscana di Scienze Naturali Memorie Serie A* **105**: 57–63.
- McCoy FW. 1981. Areal distribution redeposition and mixing of tephra within deep-sea sediments of the Eastern Mediterranean Sea. In *Tephra Studies*, Self S, Sparks RSJ (eds). Reidel: Dordrecht; 245–254.
- Narcisi B, Vezzoli L. 1999. Quaternary stratigraphy of distal tephra layers in the Mediterranean: an overview. *Global Planetary Change* **21**: 31–50.
- Pappalardo L, Civetta L, D’Antonio M, Deino A, Di Vito M, Orsi G, Carandente A, de Vita S, Isaia R, Piochi M. 1999. Chemical and Sr-isotopic evolution of the Phlegrean magmatic system before the Campanian Ignimbrite and the Neapolitan Yellow Tuff eruptions. *Journal of Volcanology and Geothermal Research* **91**: 179–214.
- Pappalardo L, Civetta L, de Vita S, Di Vito M, Orsi G, Carandente A, Fisher RV. 2002. Timing of magma extraction during the Campanian Ignimbrite eruption (Campi Flegrei Caldera). *Journal of Volcanology and Geothermal Research* **114**: 479–497.
- Paterne M, Guichard F, Labeyrie J, Gillot PY, Duplessy JC. 1986. Tyrrhenian Sea tephrochronology of the oxygen isotope record for the past 60 000 years. *Marine Geology* **72**: 259–285.
- Paterne M, Guichard F, Labeyrie J. 1988. Explosive activity of the south Italian volcanoes during the past 80,000 years as determined by marine tephrochronology. *Journal of Volcanology and Geothermal Research* **34**: 153–172.
- Paterne M, Labeyrie J, Guichard F, Mazaud A, Maitre F. 1990. Fluctuations of the Campanian explosive volcanic activity (south Italy) during the past 190,000 years as determined by marine tephrochronology. *Earth and Planetary Science Letters* **98**: 166–174.
- Peccerillo A. 2005. *Plio-Quaternary Volcanism in Italy*. Springer: Berlin.
- Poli S, Chiesa S, Gillot PY, Guichard F. 1987. Chemistry versus time in the volcanic complex of Ischia (Gulf of Naples, Italy): evidence of successive magmatic cycles. *Contributions to Mineralogy and Petrology* **95**: 322–335.
- Pyle DM, Ricketts GD, Margari V, van Andel TH, Sinitsyn AA, Praslov N, Lisitsyn S. 2006. Wide dispersal and deposition of distal tephra during the Pleistocene ‘Campanian Ignimbrite/Y5’ eruption, Italy. *Quaternary Science Review* **25**: 2713–2728.
- Reimer PJ, Baillie ML, Bard E, Bayliss A, Beck JW, Bertrand CJH, Blackwell PG, Buck CE, Burr GS, Cutler KB, Damon PE, Edwards RL, Fairbanks RG, Friedrich M, Guilderson TP, Hogg AG, Hughen KA, Kromer B, McCormac G, Manning S, Bronk-Ramsey C, Reimer RW, Remmele S, Southon JR, Stuiver M, Talamo S, Taylor FW, van der Plicht J, Weyhenmeyer CE. 2004. IntCal04 terrestrial radiocarbon age calibration, 0–26 cal kyr BP. *Radiocarbon* **46**: 1029–1058.
- Rosi M, Sbrana A. 1987. *Phlegraean Fields*. Vol. 114(8), CNR Quaderni della Ricerca Scientifica, Rome.
- Rosi M, Santacroce R. 1983. The A.D. 472 ‘Pollena’ eruption, volcanological and petrological data for this poorly known plinian-type event at Vesuvius. *Journal of Volcanology and Geothermal Research* **17**: 249–271.
- Sadori L, Narcisi B. 2001. The postglacial record of environmental history from Lago di Pergusa, Sicily. *Holocene* **11**: 655–670.
- Santacroce R. 1987. *Somma-Vesuvius*, Vol. 114(8), CNR Quaderni della Ricerca Scientifica, Rome.
- Santacroce R, Cioni R, Marianelli P, Sbrana A, Sulpizio R, Zanchetta G, Donahue DJ. 2008. Age and whole rock-glass compositions of proximal pyroclastics from the major explosive eruptions of Somma-Vesuvius: a review as a tool for distal tephrostratigraphy. *Journal of Volcanology and Geothermal Research* **117**: 1–18.
- Siani G, Sulpizio R, Paterne M, Sbrana A. 2004. Tephrostratigraphy study for the last 18,000 ¹⁴C years in a deep-sea sediment sequence for the South Adriatic. *Quaternary Science Review* **23**: 2485–2500.
- St Seymour K, Christianis K. 1995. Correlation of a tephra layer in Western Greece with a late Pleistocene eruption in the Campanian province of Italy. *Quaternary Research* **43**: 46–54.
- St Seymour K, Christianis K, Bouzinos A, Papazisimou S, Papatheodorou G, Moran E, Denes G. 2004. Tephrostratigraphy and tephrochronology in the Philippi peat basin, Macedonia, Northern Hellas (Greece). *Quaternary International* **121**: 53–65.
- Sulpizio R, Mele D, Dellino P, La Volpe L. 2005. A complex, Subplinian-type eruption from low-viscosity, phonolithic to tephri-phonolithic magma: the AD 472 (Pollena) eruption of Somma-Vesuvius (Italy). *Bulletin of Volcanology* **63**: 743–767.
- Sulpizio R, Bonasia R, Dellino P, Di Vito MA, La Volpe L, Mele D, Zanchetta G, Sadori L. 2008. Discriminating the long distance dispersal of fine ash from sustained columns or near ground ash clouds: the example of the Pomici di Avellino eruption (Somma-Vesuvius, Italy). *Journal of Volcanology and Geothermal Research* **177**: 263–276.
- Thunnell R, Federman A, Sparks S, Williams D. 1979. The age, origin and volcanological significance of the Y-5 ash layer in the Mediterranean. *Quaternary Research* **12**: 241–253.
- Turney CSM, Blockley SPE, Lowe JJ, Wulf S, Branch NP, Mastrolorenzo G, Swindle G, Nathan R, Pollard AM. 2008. Geochemical characterization of quaternary tephras from the Campanian province, Italy. *Quaternary International* **178**: 288–305.
- van Welden A. 2007. *Enregistrements s dimentaires imbriqu s d’une activit  sismique et de changements pal oenvironnementaux. Comparaison entre diff rents sites: Golfe de Corinthe (Gr ce), Lac de Shkodra (Albanie/Mont n gro) et Golfe de Cariaco (V n zuela)*. PhD dissertation, LGCA, Le Bourget du Lac, France.
- van Welden A, Beck C, Reyss JL, Bushati S, Koci R, Jouanne F, Mugnier JL. 2008. The last 5000 year of sedimentation in Shkodra Lake (Albania/Montenegro): paleoenvironmental evolution and potential for paleoseismicity studies. *Journal of Paleolimnology* **40**: 619–633.
- Vogel JS, Cornell W, Nelson DE, Southon JR. 1990. Vesuvius Avellino, one possible source of seventeenth century BC climate disturbance. *Nature* **344**: 534–537.
- Vogel H, Zanchetta G, Sulpizio R, Wagner B, Nowaczyk N. 2009. A tephrostratigraphic record for the last glacial-interglacial cycle from Lake Ohrid, Albania and Macedonia. *Journal of Quaternary Science* (in press). DOI: 10.1002/jqs.1311
- Wagner B, Sulpizio R, Zanchetta G, Wulf S, Wessels M, Daut G, Nowaczick H. 2008. The last 40 ka tephrostratigraphic record of Lake Ohrid, Albania and Macedonia: a very distal archive for ash dispersal from Italian volcanoes. *Journal of Volcanology and Geothermal Research* **177**: 71–80.
- Wohlfarth B. 1996. The Chronology of the last termination: a review of radiocarbon-dated, high-resolution terrestrial stratigraphies. *Quaternary Science Reviews* **15**: 267–284.
- Wulf S, Kraml M, Brauer A, Keller J, Negendank JFW. 2004. Tephrochronology of the 100 ka lacustrine sediment record of Lago Grande di Monticchio (southern Italy). *Quaternary International* **122**: 7–30.
- Wulf S, Kraml M, Keller J. 2008. Towards a detailed distal tephrostratigraphy in the Mediterranean: the last 20 kyrs record of Lago Grande di Monticchio. *Journal of Volcanology and Geothermal Research* **177**: 118–132.

HOLOCENE TEPHROSTRATIGRAPHIC RECORD OF LAKE SHKODRA

APPENDIX

Table 1 List of ^{14}C ages performed on plants and wood remains along the cores SK13 and SK19. Calibration (2σ) of ^{14}C data was performed using IntCal04 calibration curve (Reimer et al., 2004)

Core	Lab. no.	Depth (cm)	^{14}C age (a BP)	2σ range (a BP)
SK13	SacA	17 cm	200 ± 30	305–0
SK13	Poz-15211	115 cm	745 ± 30	728–661
SK13	Poz-15212	288 cm	1695 ± 30	1694–1535
SK13	Poz-15214	614 cm	3760 ± 35	4238–3990
SK19	Poz-9251	81 cm	775 ± 30	735–669
SK19	Poz-9201	207 cm	2500 ± 30	2732–2467
SK19	Poz-9252	311 cm	3220 ± 35	3555–3368
SK19	Poz-9199	370 cm	4645 ± 35	5469–5306
SK19	Poz-9250	435 cm	6510 ± 40	7497–7322

Table 2 Comparison of the EDS device used in this study in comparison with WDS microprobes from Geoforschungszentrum (GFZ, Potsdam, Germany), from CAMPARIS service (CMP, Paris, France) and from Saclay (France; Cioni et al., 1998). Reference material comprises volcanic glasses with a chemistry ranging from basalt to rhyolite. ALV981R23, CFA47 and KE12 samples from Cioni et al. (1998)

	ALV981R23 (basalt)		CFA 47 (trachyte)		KE 12 (pantellerite)		SMP1-a (trachyte)		CA1-a (trachyte)		Mercato (phonolite)		Aeolian rhyolite																
	EDS	Saclay	EDS	Saclay	EDS	Saclay	EDS	GFZ	EDS	GFZ	EDS	CMP	EDS	CMP															
SiO_2	49.56	0.14	49.79	0.19	61.39	0.27	61.94	0.33	70.80	0.23	70.83	0.22	60.29	0.16	60.17	0.17	58.41	0.45	58.67	0.39	58.48	0.25	58.89	0.30	74.58	0.25	74.93	0.63	
TiO_2	1.3	0.07	1.28	0.05	0.48	0.09	0.42	0.05	0.31	0.06	0.28	0.02	0.48	0.07	0.46	0.03	0.53	0.09	0.48	0.01	0.15	0.10	0.15	0.11	0.07	0.08	0.07	0.06	
Al_2O_3	16.57	0.13	16.67	0.08	18.61	0.11	18.62	0.16	7.92	0.16	7.82	0.03	19.23	0.10	19.40	0.09	19.24	0.18	18.96	0.07	21.80	0.19	21.18	0.18	13.40	0.10	13.07	0.29	
FeO	8.44	0.22	8.46	0.09	2.76	0.12	2.66	0.15	8.41	0.06	8.67	0.20	3.01	0.08	3.15	0.05	3.95	0.24	4.22	0.14	1.72	0.09	1.68	0.10	1.46	0.05	1.50	0.11	
MnO	0.22	0.03	0.14	0.06	0.24	0.13	0.18	0.04	0.38	0.07	0.29	0.03	0.29	0.13	0.26	0.04	0.18	0.09	0.14	0.03	0.19	0.10	0.18	0.05	0.06	0.08	0.08	0.06	
MgO	8.82	0.16	8.73	0.11	0.58	0.08	0.42	0.02	0.10	0.04	0.00	0.00	0.22	0.06	0.36	0.02	0.99	0.15	1.01	0.10	0.17	0.08	0.07	0.03	0.07	0.05	0.03	0.03	
CaO	11.84	0.25	11.87	0.11	1.83	0.08	1.85	0.06	0.36	0.07	0.35	0.01	1.67	0.06	1.87	0.05	3.22	0.25	3.50	0.23	1.56	0.11	1.61	0.08	0.83	0.07	0.84	0.09	
Na_2O	3	0.18	2.9	0.04	5.43	0.08	5.40	0.12	7.10	0.19	7.23	0.25	6.65	0.23	6.34	0.17	4.28	0.20	4.27	0.10	8.78	0.26	8.90	0.24	3.95	0.09	3.90	0.33	
K_2O	0.1	0.05	0.05	0.01	8.14	0.04	8.02	0.16	4.29	0.07	4.19	0.15	7.23	0.21	7.10	0.08	8.60	0.29	8.21	0.26	6.65	0.19	6.64	0.14	5.28	0.11	5.15	0.38	
P_2O_5	—	—	—	—	—	—	—	—	—	—	—	—	0.00	0.00	0.00	0.00	0.00	0.00	0.00	0.00	0.00	0.00	0.01	0.03	0.00	0.00	0.00	0.02	
Cl	—	—	—	—	—	—	—	—	—	—	—	—	0.92	0.05	0.90	0.02	0.60	0.06	0.55	0.03	0.51	0.07	0.64	0.05	0.31	0.02	0.37	0.04	
S	0.14	0.04	0.12	0.00	0.54	0.08	0.49	0.01	0.32	0.08	0.33	0.00	—	—	—	—	—	—	—	—	—	—	—	—	—	—	—	—	—

Table 3 (a) Mean EDS data of tephra layers from core SK13; (b) mean EDS data of tephra layers from core SK19. All the analyses are water-free with sum at 100%. The suffixes base, middle and top indicate multiple analyses at different stratigraphic heights of the same sample. In the case of SK13 514 cm depth tephra layer the terms *a* and *b* indicate two different compositions of glass

	SK13 295–300 top			SK13 295–300 middle			SK13 295–300 base			SK13 514 cm (a)			SK13 514 cm (b)			SK13 571 cm			SK13 716–726 cm top			SK13 716–726 cm base			
	<i>n</i> = 9	SD		<i>n</i> = 9	SD		<i>n</i> = 10	SD		<i>n</i> = 11	SD		<i>n</i> = 3	SD		<i>n</i> = 12	SD		<i>n</i> = 4	SD		<i>n</i> = 10	SD		
SiO ₂	51.16	1.69	1.03	51.52	1.03	0.54	50.25	0.54	0.13	57.10	1.60	55.73	2.36	55.59	0.44	55.59	0.44	60.11	0.26	59.76	0.58	59.76	0.26	59.76	0.58
TiO ₂	0.49	0.13	0.13	0.52	0.13	0.13	0.63	0.13	0.13	1.04	0.21	1.84	0.54	0.36	0.11	0.36	0.11	0.49	0.06	0.52	0.10	0.52	0.06	0.52	0.10
Al ₂ O ₃	22.25	0.24	0.43	22.10	0.43	1.04	22.00	1.04	21.56	1.37	16.74	16.74	0.69	21.79	0.65	21.79	0.65	19.10	0.32	19.40	0.51	19.40	0.32	19.40	0.51
FeO _{tot}	4.59	0.71	0.72	4.74	0.72	0.82	5.14	0.82	3.85	1.08	1.08	8.58	2.85	2.98	0.56	2.98	0.56	3.58	0.34	3.56	0.23	3.56	0.34	3.56	0.23
MnO	0.17	0.08	0.06	0.13	0.06	0.17	0.17	0.13	0.07	0.07	0.07	0.16	0.15	0.14	0.06	0.14	0.06	0.12	0.04	0.10	0.07	0.10	0.04	0.10	0.07
MgO	0.55	0.10	0.40	0.66	0.40	0.36	0.67	0.36	0.96	0.27	2.92	2.92	2.38	0.59	0.40	0.40	0.59	0.08	0.83	0.91	0.15	0.91	0.08	0.91	0.15
CaO	5.53	0.71	0.64	5.66	0.64	0.80	5.83	0.80	5.93	1.38	2.84	2.84	0.96	3.78	0.78	3.78	0.78	2.52	0.29	2.63	0.17	2.63	0.29	2.63	0.17
Na ₂ O	8.13	0.75	1.66	7.79	1.66	0.94	8.11	0.94	6.40	0.31	5.57	5.57	2.39	6.49	0.68	6.49	0.68	4.15	0.51	4.17	0.44	4.17	0.51	4.17	0.44
K ₂ O	6.23	0.81	0.71	6.00	0.71	0.84	6.21	0.84	2.68	1.00	4.62	4.62	0.95	7.74	0.34	7.74	0.34	8.52	0.43	8.46	0.34	8.46	0.43	8.46	0.34
P ₂ O ₅	—	—	—	—	—	0.01	0.01	0.02	0.15	0.09	0.58	0.58	0.23	—	—	—	—	—	—	—	—	—	—	—	—
ClO	0.90	0.16	0.11	0.89	0.11	0.13	0.98	0.13	0.26	0.09	0.43	0.43	0.11	0.54	0.04	0.54	0.04	0.59	0.04	0.54	0.08	0.54	0.04	0.54	0.08
Total	100.01	—	—	100.00	—	100.00	100.00	—	100.00	—	100.00	100.00	—	100.00	—	100.00	—	99.99	—	100.04	—	100.04	—	100.04	—
Total alk.	14.37	—	—	13.79	—	14.32	14.32	—	9.09	—	10.19	10.19	—	14.23	—	14.23	—	12.66	—	12.63	—	12.63	—	12.63	—
K ₂ O/Na ₂ O	0.77	—	—	0.77	—	0.77	0.77	—	0.42	—	0.83	0.83	—	1.19	—	1.19	—	2.05	—	2.03	—	2.03	—	2.03	—

	SK19 155–160			SK19 356 cm			SK19 368 cm			SK19 385–400 cm top			SK19 385–400 cm middle			SK19 385–400 cm base			SK19 520 cm				
	<i>n</i> = 16	SD		<i>n</i> = 11	SD		<i>n</i> = 9	SD		<i>n</i> = 10	SD		<i>n</i> = 10	SD		<i>n</i> = 10	SD		<i>n</i> = 6	SD			
SiO ₂	50.28	0.83	0.59	59.91	0.47	59.37	59.87	0.47	59.37	0.60	59.56	59.56	0.28	60.37	0.66	60.37	0.66	59.81	0.35	59.81	0.35	59.81	0.35
TiO ₂	0.55	0.11	0.10	0.51	0.09	0.55	0.54	0.09	0.55	0.09	0.51	0.51	0.12	0.45	0.07	0.45	0.07	0.51	0.04	0.51	0.04	0.51	0.04
Al ₂ O ₃	22.64	0.62	0.31	19.09	0.09	18.91	18.98	0.09	18.91	0.13	18.99	18.99	0.16	18.91	0.13	18.91	0.13	19.11	0.18	19.11	0.18	19.11	0.18
FeO _{tot}	4.91	0.53	0.24	3.52	0.19	3.88	3.54	0.19	3.88	0.35	3.72	3.72	0.17	3.40	0.23	3.40	0.23	3.57	0.22	3.57	0.22	3.57	0.22
MnO	0.17	0.07	0.08	0.14	0.09	0.12	0.12	0.09	0.12	0.10	0.11	0.11	0.09	0.07	0.07	0.07	0.07	0.11	0.07	0.11	0.07	0.11	0.07
MgO	0.65	0.29	0.16	0.80	0.16	0.94	0.87	0.16	0.94	0.14	0.84	0.84	0.11	0.72	0.15	0.72	0.15	0.94	0.06	0.94	0.06	0.94	0.06
CaO	5.69	0.67	0.27	2.63	0.27	2.95	2.58	0.27	2.95	0.33	2.79	2.79	0.17	2.43	0.27	2.43	0.27	2.70	0.11	2.70	0.11	2.70	0.11
Na ₂ O	8.32	1.02	0.26	4.07	0.26	3.89	4.23	0.26	3.89	0.21	4.06	4.06	0.17	4.43	0.26	4.43	0.26	4.03	0.18	4.03	0.18	4.03	0.18
K ₂ O	5.82	0.92	0.28	8.85	0.28	8.86	8.67	0.28	8.86	0.23	8.87	8.87	0.14	8.60	0.24	8.60	0.24	8.66	0.34	8.66	0.34	8.66	0.34
P ₂ O ₅	0.02	0.03	0.01	0.01	0.00	0.00	0.00	0.00	0.00	0.00	0.00	0.00	0.00	0.00	0.00	0.00	0.00	0.00	0.00	0.00	0.00	0.00	0.00
ClO	0.97	0.10	0.07	0.57	0.06	0.53	0.61	0.06	0.53	0.03	0.56	0.56	0.08	0.62	0.05	0.62	0.05	0.58	0.06	0.58	0.06	0.58	0.06
Total	100.00	—	—	100.10	—	99.99	100.00	—	99.99	—	100.00	100.00	—	100.00	—	100.00	—	100.01	—	100.01	—	100.01	—
Total alk.	14.14	—	—	12.93	—	12.75	12.89	—	12.75	—	12.79	12.79	—	12.79	—	12.79	—	12.79	—	12.79	—	12.79	—
K ₂ O/Na ₂ O	0.70	—	—	2.17	—	2.28	2.05	—	2.28	—	2.31	2.31	—	2.31	—	2.31	—	2.31	—	2.31	—	2.31	—

Table 5 EDS analyses and recalculations of pyroxenes from some of the recognised tephra layers

	SK13 295–300 cm			SK13 514 cm			SK13 571 cm					SK13 716–726 cm			
	d	d	es	d	au	au	d	d	d	j	ae	j	ae	ae	d
SiO ₂	40.25	41.33	43.62	48.31	50.72	49.56	46.86	48.17	49.04	52.28	48.99	52.18	48.67	47.69	49.33
TiO ₂	2.46	2.96	2.11	2.08	1.76	1.93	1.90	1.42	1.30	0.65	1.46	0.56	1.21	0.93	1.05
Al ₂ O ₃	11.63	12.92	12.91	5.36	3.23	4.16	8.27	6.89	8.74	2.57	6.62	3.71	6.63	6.28	7.39
Fe _{tot}	12.9	12.16	11.55	9.22	9.22	10.12	7.45	7.57	6.80	5.38	6.47	4.90	6.65	11.28	8.72
MnO	0.27	0.11	0.27	0.25	0.29	0.29	0.10	0.13	0.00	0.24	0.13	0.09	0.10	0.12	0.32
MgO	7.09	7.69	6.84	13.08	13.46	13.56	12.79	13.55	12.41	16.46	13.38	15.67	14.17	9.84	11.25
CaO	24.15	22.45	20.22	21.53	20.78	20.24	22.14	22.08	20.67	22.42	22.71	22.90	22.57	23.81	20.66
Na ₂ O	0.54	0.19	0.58	0.16	0.41	0	0.00	0.00	0.26	0.00	0.00	0.00	0.00	0.00	0.55
K ₂ O	0	0.18	1.85	0	0.03	0.03	0.04	0.09	0.67	0.00	0.15	0.00	0.00	0.00	0.74
Total	99.29	99.99	99.95	99.99	99.90	99.89	99.55	99.90	99.89	100.00	99.91	100.01	100.00	99.95	100.01
<i>Recalculation on the basis of 6 oxygens</i>															
Si	1.54	1.57	1.65	1.81	1.90	1.86	1.75	1.79	1.82	1.92	1.82	1.91	1.80	1.81	1.84
Ti	0.07	0.08	0.06	0.06	0.05	0.05	0.05	0.04	0.04	0.02	0.04	0.02	0.03	0.03	0.03
Al IV	0.46	0.43	0.35	0.19	0.10	0.14	0.25	0.21	0.18	0.08	0.18	0.09	0.20	0.19	0.16
Al VI	0.07	0.15	0.23	0.04	0.04	0.04	0.11	0.09	0.20	0.03	0.11	0.07	0.09	0.09	0.16
Fe ³⁺	0.29	0.13	0.13	0.05	0.00	-0.01	0.03	0.05	-0.04	0.02	0.00	-0.02	0.05	0.05	0.01
Fe ²⁺	0.13	0.26	0.23	0.24	0.29	0.33	0.20	0.19	0.25	0.15	0.20	0.17	0.15	0.31	0.26
Mn	0.01	0.00	0.01	0.01	0.01	0.01	0.00	0.00	0.00	0.01	0.00	0.00	0.00	0.00	0.01
Mg	0.41	0.44	0.39	0.73	0.75	0.76	0.71	0.75	0.69	0.90	0.74	0.86	0.78	0.56	0.63
Ca	0.99	0.91	0.82	0.86	0.83	0.81	0.89	0.88	0.82	0.88	0.90	0.90	0.89	0.97	0.83
Na	0.04	0.01	0.04	0.01	0.03	0.00	0.00	0.00	0.02	0.00	0.00	0.00	0.00	0.00	0.04
K	0.00	0.01	0.09	0.00	0.00	0.00	0.00	0.00	0.03	0.00	0.01	0.00	0.00	0.00	0.04
Wo	54.78	52.65	52.18	45.88	44.49	43.06	48.39	47.13	47.80	45.27	48.97	47.19	47.54	51.42	47.91
En	22.38	25.10	24.56	38.79	40.10	40.14	38.90	40.25	39.93	46.25	40.15	44.93	41.53	29.57	36.30
Fs	22.84	22.26	23.26	15.33	15.41	16.80	12.71	12.61	12.27	8.48	10.89	7.88	10.93	19.01	15.78
Mg/Mg+Fe _t	0.49	0.53	0.51	0.72	0.72	0.70	0.75	0.76	0.76	0.85	0.79	0.85	0.79	0.61	0.70

d, diopside; es, essenite; au, augite; j, jadeite; ae, aegirine-augite; Wo, wollastonite; En, enstatite; Fs, ferrosilite.

Table 6 EDS analyses and recalculations of amphiboles from some of the recognised tephra layers

	SK13 295–300 cm					SK13 571 cm				
	SiO ₂	44.7	45.2	44.63	45.28	46.92	45.47	44.94	50.69	51.03
TiO ₂	1.63	1.18	1.56	1.3	1.48	1.46	1.8	0.85	0.67	
Al ₂ O ₃	17.63	18.02	18.27	16.45	17.17	16.72	15.65	11.39	12.85	
FeO _{tot}	11.31	11.22	10.87	11.06	6.91	7.79	10.67	5.98	7.02	
MnO	0.26	0.35	0.28	0.37	0.14	0.14	0.25	0.08	0.09	
MgO	3.89	3.14	2.81	4.1	6.09	7.18	5.49	10.16	8.50	
CaO	14.73	13.74	13.28	13.48	12.84	15.86	16.13	17.22	15.27	
Na ₂ O	3.41	4.12	4.15	2.82	0.27	0.25	2.54	1.47	1.86	
K ₂ O	2.07	2.54	3.66	4.39	7.56	4.69	2.22	2.01	2.53	
Total	99.63	99.51	99.51	99.25	99.38	99.56	99.69	99.85	99.82	
<i>Recalculation on the basis of 23 oxygens</i>										
Si	6.47	6.55	6.50	6.62	6.73	6.53	6.51	7.10	7.15	
Ti	0.18	0.13	0.17	0.14	0.16	0.16	0.20	0.09	0.07	
Al	3.01	3.08	3.13	2.84	2.90	2.83	2.67	1.88	2.12	
Fe ³⁺	0.00	0.00	0.00	0.00	0.00	0.00	0.00	0.00	0.00	
Fe ²⁺	1.37	1.36	1.32	1.35	0.83	0.93	1.29	0.70	0.82	
Mn	0.03	0.04	0.03	0.05	0.02	0.02	0.03	0.01	0.01	
Mg	0.84	0.68	0.61	0.89	1.30	1.54	1.19	2.12	1.78	
Ca	2.28	2.13	2.07	2.11	1.97	2.44	2.50	2.58	2.29	
Na	0.96	1.16	1.17	0.80	0.08	0.07	0.71	0.40	0.51	
K	0.38	0.47	0.68	0.82	1.38	0.86	0.41	0.36	0.45	
H	2.00	2.00	2.00	2.00	2.00	2.00	2.00	2.00	2.00	

HOLOCENE TEPHROSTRATIGRAPHIC RECORD OF LAKE SHKODRA

Table 7 EDS analyses and recalculations of olivines from SK13-540 cm tephra layer

SK 13-514 cm				
SiO ₂	38.94	38.49	41.41	38.60
TiO ₂	0.04	0.85	0.17	0.00
Al ₂ O ₃	0	0.61	3.56	0.00
FeO _{tot}	22.74	28.35	23.06	22.62
MnO	0.48	1.06	0.7	0.56
MgO	37.07	28.42	26.96	37.46
CaO	0.63	1.33	1.72	0.69
Na ₂ O	0	0	0.83	0.00
K ₂ O	0	0.38	0.65	0.00
Total	99.90	99.49	99.06	99.93
Te	0.54	1.31	0.96	0.62
Fo	73.33	61.94	64.92	73.50
Fa	25.23	34.66	31.15	24.90
Ca-Ol	0.90	2.08	2.98	0.97

Table 8 Summary of stratigraphic position, lithology, composition, chronologic constraints and proposed correlations for the recognised tephra layers in cores SK13 and SK19

	Lithology	Mineral assemblage	Glass composition	Chronological constraints	Correlation
Core SK 13					
295–300 cm	Dark-brown, vesicular, porphyritic micro-pumice	Leucite, clinopyroxenes, sanidine, amphibole	Foiditic-phonolitic	Slightly older than 1695 ± 30 ¹⁴ C a BP	AD 472 eruption, Somma-Vesuvius
514 cm	Dark-brown, poorly vesicular, porphyritic fragments	Plagioclase, clinopyroxenes, olivine	Mainly benmoreitic	Between 1695 ± 30 and 3760 ± 35 ¹⁴ C a BP	FL eruption, Mount Etna
571 cm	Dark-grey, highly vesicular, micro-pumice	Clinopyroxene, sanidine, scapolite, amphibole	Phonolitic	Between 1695 ± 30 and 3760 ± 35 ¹⁴ C a BP	Avellino eruption, Somma-Vesuvius
716–726 cm	Light-grey, highly vesicular micro-pumice and colourless glass shards	Rare clinopyroxenes	Trachytic	Older than 3760 ± 35 ¹⁴ C a BP	Agnano M.S.–Astroni group, Campi Flegrei
Core SK 19					
155–160 cm	Dark brown, vesicular, porphyritic micro-pumice	Leucite, clinopyroxenes, sanidine, amphibole	Foiditic-phonolitic	Between 775 ± 30 and 2500 ± 30 ¹⁴ C a BP	AD 472 eruption, Somma-Vesuvius
356 cm	Colourless to light grey, aphyric glass shards	Aphyric	Trachytic	Between 3220 ± 35 and 4645 ± 35 ¹⁴ C a BP	Astroni eruption, Campi Flegrei
368 cm	Colourless to light grey, aphyric glass shards	Aphyric	Trachytic	Between 3220 ± 35 and 4645 ± 35 ¹⁴ C a BP	Astroni eruption, Campi Flegrei
385–400 cm	Light grey, highly-vesicular micro-pumice and colourless glass shards	Rare clinopyroxenes	Trachytic	Between 4645 ± 35 and 6510 ± 40 ¹⁴ C a BP	Agnano M.S. eruption, Campi Flegrei
460 cm	Light grey, highly-vesicular micro-pumice	Aphyric	Trachytic	Older than 6510 ± 40 ¹⁴ C a BP	Agnano P.P. eruption, Campi Flegrei

Table 9 Comparison of EDS glass compositions of proximal deposits and the recognised tephra layers in Lake Shkodra sediments

Av. grey	SK 13 571 cm		Astroni		AMS (t)		AMS (b)		SK19 356 cm		SK19 368 cm		SK13 716-726 cm (t)		(b)		SK19 385-400 cm (t)		(m)		(b)		APP (TM7b)		SK19 460 cm		
	n=28	SD	n=12	SD	n=8	SD	n=12	SD	n=9	SD	n=12	SD	n=8	SD	n=8	SD	n=8	SD	n=10	SD	n=10	SD	n=10	SD	n=20	SD	n=9
55.63	0.60	55.59	0.44	59.21	0.14	59.79	0.26	60.16	0.48	59.87	0.47	59.91	0.59	60.33	0.93	60.11	0.26	59.37	0.60	59.56	0.28	60.37	0.66	58.38	0.88	59.87	0.47
0.31	0.10	0.36	0.11	0.52	0.07	0.55	0.09	0.52	0.07	0.54	0.09	0.51	0.10	0.44	0.13	0.49	0.06	0.55	0.09	0.51	0.12	0.45	0.07	0.49	0.05	0.54	0.09
21.85	0.50	21.79	0.65	19.31	0.13	18.94	0.16	18.76	0.11	18.98	0.09	19.09	0.31	19.20	0.43	19.10	0.32	18.91	0.13	18.99	0.16	18.91	0.13	18.78	0.44	18.98	0.09
3.07	0.46	2.98	0.56	3.42	0.12	3.71	0.19	3.54	0.32	3.54	0.19	3.52	0.24	3.31	0.53	3.58	0.34	3.88	0.35	3.72	0.17	3.40	0.23	4.17	0.46	3.54	0.19
0.00	0.00	0.14	0.06	0.13	0.10	0.01	0.02	0.05	0.06	0.12	0.09	0.14	0.08	0.10	0.07	0.12	0.04	0.12	0.10	0.11	0.09	0.07	0.07	0.13	0.04	0.12	0.09
0.09	0.08	0.59	0.40	0.61	0.06	0.59	0.09	0.50	0.12	0.87	0.16	0.80	0.16	0.70	0.13	0.83	0.08	0.94	0.14	0.84	0.11	0.72	0.15	1.00	0.53	0.87	0.16
4.46	0.92	3.78	0.78	2.57	0.09	2.90	0.13	2.73	0.34	2.58	0.27	2.63	0.27	2.39	0.40	2.52	0.29	2.95	0.33	2.79	0.17	2.43	0.27	3.50	0.85	2.58	0.27
5.57	0.52	6.49	0.68	4.60	0.10	4.02	0.14	4.39	0.45	4.23	0.26	4.07	0.26	4.43	0.68	4.15	0.51	3.89	0.21	4.06	0.17	4.43	0.26	3.89	0.21	4.23	0.26
8.23	0.49	7.74	0.34	8.92	0.13	8.90	0.16	8.67	0.21	8.67	0.25	8.85	0.28	8.57	0.78	8.52	0.43	8.86	0.23	8.87	0.14	8.60	0.24	9.02	0.49	8.67	0.25
—	—	—	—	0.02	0.03	—	—	0.01	0.03	—	—	0.01	0.02	—	—	—	—	—	—	—	—	—	—	0.16	0.06	—	—
0.63	0.13	0.54	0.04	0.70	0.05	0.59	0.04	0.68	0.07	0.61	0.06	0.57	0.07	0.56	0.06	0.59	0.04	0.53	0.03	0.56	0.08	0.62	0.05	0.62	0.06	0.61	0.06
99.84	—	100.00	—	100.00	—	100.00	—	100.00	—	100.00	—	100.10	—	100.01	—	99.99	—	99.99	—	100.00	—	100.00	—	100.14	—	100.00	—
13.80	—	14.23	—	13.52	—	12.92	—	13.05	—	12.89	—	12.93	—	13.00	—	12.66	—	12.75	—	12.92	—	13.04	—	12.91	—	12.89	—
1.48	—	1.19	—	1.94	—	2.21	—	1.98	—	2.05	—	2.17	—	1.94	—	2.05	—	2.28	—	2.19	—	1.94	—	2.32	—	2.05	—

Proximal data: AD 472 and Avellino EDS data from Santacroce *et al.* (2008); Astroni, this work; Agnano Monte Spina and Agnano Pomice Principali from Siani *et al.* (2004). FL data are EDS analyses from Lake Ohrid sediments (Wagner *et al.*, 2008). Prtg. A and Prtg. B are EDS data from Lake of Pergusa (Sadori and Narcisi, 2001). (t), top; (m), middle; (b), base.



**IV. Chapter IV: The Late Holocene to Pleistocene
tephrostratigraphic record of Lake Ohrid (Albania)**

The drilling of Lake Ohrid (Albania/Macedonia border) was supported by CNRS grants from the French ECLISPE program. A.M. Lézine and U. von Grafenstein (from LSCE, France) and N. Andersen (from Leibniz-Laboratory for Radiometric Dating and Stable Isotope Research, Germany) collected two cores. The core processing for tephra layer recovering and geochemical analyses was carried out at the Dipartimento di Scienze della Terra (University of Pisa). ^{14}C datings comes from two PhD projects (A. Boudon and S. Belmecheri from LSCE), and published in the paper of *Lezine et al. (2010)* (annexe 7). Moreover, the results of this research and the collaboration with R. Sulpizio (Univ. of Bari), G. Zanchetta (Univ. of Pisa), G. Siani (Univ. of Paris Sud XI) and R. Santacrose (Univ. of Pisa) allowed the recognition of tephra layers that encompass the last 130 ky. The results of this study were submitted to the *Comptes Rendus Geoscience* in 2009, and the paper is at present under revision.

**Tephrostratigraphie du Lac d'Ohrid (Albania) pendant le Pléistocène supérieure et
l'Holocène**

The Late Holocene to Pleistocene tephrostratigraphic record of Lake Ohrid (Albania).

Benoît Caron^{1,3,*}, Roberto Sulpizio², Giovanni Zanchetta¹, Giuseppe Siani³, Roberto Santacroce¹

¹ *Dipartimento di Scienze della Terra, via S. Maria 53, 56126, Pisa, Italy*

² *CIRISIVU, c/o Dipartimento Geomineralogico, via Orabona 4, 70125, Bari, Italy*

³ *IDES-UMR 8148, Département des Sciences de la Terre, Université Paris-XI, 91405 Orsay, France*

* Corresponding author: Benoît Caron, Dipartimento di Scienze della Terra, via S. Maria 53, 56126, Pisa, Italy, tel.: +39 050 22 15 700, fax: +39 050 22 15 800, caron@dst.unipi.it

Abstract

We present in this work a tephrostratigraphic record from a sediment piston core (JO-2004) from Lake Ohrid. Five tephra layers were recognised, all from explosive eruptions of south Italy volcanoes. A multidisciplinary study was carried out, including stratigraphy, AMS ^{14}C chronology and geochemistry. The five tephra layers were correlated with terrestrial proximal counterparts and with both marine and lacustrine tephra layers already known in the central Mediterranean area. The oldest is from Pantelleria Island (P11, 131 ka BP). Other three tephra layers are from Campanian volcanoes: X6, Campanian Ignimbrite-Y5 and SMP1-Y3 (107, 39 and 31 ka BP respectively). The youngest tephra layer corresponds to the FL eruption from Etna Volcano (3.4 ka BP). In three cases these recognitions confirm previous findings in the Balkans, while two of them were for the first time recognised in the area, with a significant enlargement of the previous assessed dispersal areas.

Résumé

Une étude tephrostratigraphique a été réalisée dans la carotte sédimentaire JO-2004 prélevée dans le Lac d'Ohrid. Cette étude bénéficie d'un cadre chronologique établi par sept datations SMA ^{14}C et par des analyses chimiques des éléments majeurs. Cinq niveaux de tephra ont été détectés et corrélés aux dépôts terrestres proximaux ainsi qu'aux tephra identifiés dans des carottes marines et lacustres de la Méditerranée Centrale. Leur origine a été attribuée au volcanisme explosif du Sud de l'Italie et corrélée à l'activité de l'île de Pantelleria (P11, 131 ka BP), à la région Campanienne (X6, 107 ka; Ignimbrite Campanienne -Y5, 39 ka; SMP1-Y3; 31 ka) et à l'éruption FL de l'Etna (3,4 ka BP). Ces résultats sont en accord avec des travaux précédemment publiés dans la région des Balkans et ont permis d'identifier pour la première fois deux tephra (X6 et P11), en élargissant significativement leurs secteurs de dispersion en Méditerranéenne Centrale.

Keywords: tephrostratigraphy, tephrochronology, Italian volcanoes, Lake Ohrid, Albania

1. Introduction:

Tephrostratigraphy is a powerful tool that is widely applied to volcanology, Quaternary Science, palaeoceanography or archaeology. This is particularly true in the central Mediterranean region, which bore witness to frequent and powerful volcanic explosive activity during both Holocene and Late Pleistocene [8, 9, 10, 15, 24, 32, 35, 36, 38, 42, 43, 44, 47, 52, 56]. Some of the tephra layers generated during these explosive eruptions have regional or extra-regional relevance (e.g. Y3, Y5, Y6, Y7, X5 and X6 tephra layers) [11, 15, 26, 39, 47, 50, 58], since they covered very wide areas facilitating correlations between different geological archives. Many other tephra layers are less dispersed but are frequently recognised in marine and lacustrine cores drilled in the central Mediterranean area [7, 20, 22, 23, 35, 37, 48, 55, 56].

Owing to its position downwind of the Italian volcanoes, the Balkans were affected by tephra deposition during Holocene and late Pleistocene [49, 55] (Fig. 1), but tephrostratigraphic studies are few. This paper deals with the study of a long core (JO 2004; 9.88 m of length), collected on the Albanian side of Lake Ohrid, which records the last 130-140 ka of sedimentation [19]. Our aim is to provide a tephrostratigraphic reconstruction of the core JO 2004, and to provide the correlation of its tephra layers with marine, lacustrine or terrestrial deposits in the central Mediterranean. The correlation among the different archives provides an updated framework of the tephra dispersion in the central Mediterranean area, and particularly in the Balkans.

Few tephra studies were carried out in the Balkans [49, 55], although their downwind position from the Italian volcanoes makes the area particularly subjected to distal ash deposition. On the other hand, the recognition of ash layers from Italian volcanoes in the Balkans contributes to shed light into the complex and poorly understood dynamics of dispersal of ash particles during and after explosive eruptions.

2. Site description

The Ohrid Lake is one of the oldest lakes in Europe [46], and is located at the border between Albania and Macedonia (40°54'- 41°10' N; 20°38'- 20°48' E) (Fig. 1). The lake is at 705 m a.s.l., and has a surface of about 360 km². Bathymetric measurements revealed that the lake has simple, tub-shaped basin morphology with a maximum water depth of 289 m (e.g. [46]). It is surrounded by two principals mountain chains: the Galiçica Mountains to the east (more

than 1750 m a.s.l.), and the Mokra Mountains to the west (around 1500 m a.s.l.). The Lake Ohrid has a NS orientation, and is located in a graben, which formed during the extension of the Albanian area during the Pleistocene [2, 55]. The Ohrid–Korca seismic zone comprises the Pliocene–Quaternary normal-fault-controlled Ohrid graben, and the Korca and Erseka half grabens, which are generally north trending [1, 3]. Active normal faulting with horst and graben structures is seen in the geomorphology and also determined from earthquake focal mechanisms [2, 12].

Carbonate rocks of Triassic and Jurassic age crop out to the north and to the east, while ophiolitic rocks of Jurassic age crop out to the south-west. The southern end of the basin connects with a small graben filled by continental mudstones and sandstones of Pliocene age, overlain by fluvio-lacustrine sediments of Holocene age [31]. Today, roughly half of its water is derived from a number of springs located in the south-east part of the lake, draining a karstic system fed by water from the nearby Lake Prespa (20 km to the south-east and 150 m higher than Lake Ohrid), and infiltration of rainwater (700 mm/yr on average) from the Galicica mountain range. The remaining water comes from rivers (e.g. the Sateska River to the north) and from direct meteoric precipitation. The Black Drin River is the only surface outflow to the north part of the Lake Ohrid [4, 19, 27, 46]. Lakes with comparable volumes and water depths, located in temperate and Mediterranean regions, are in general monomictic with a mixing of the water column during winter [54]. Complete overturn of the water column in Lake Ohrid occurs very irregularly, roughly every 7 years [14, 45]. Recent investigations have shown that in years without complete overturn the water column is mixed down to depths of 125 to 175 m during winter [27].

3. Materials and methods.

Two series of piston cores (JO 2004-1 and JO 2004-1a) were drilled in the south western part of the Lake Ohrid [19] (40° 55,000' N ; 20° 40,297' E ; WGS 84 reference ; Fig. 1), in a water depth of 100 m. The uppermost roughly 10 m of sediments were recovered using a cable-operated piston-core (63 mm in diameter and 3 m-long; Niederreiter Corer). In order to obtain a continuous sediment record, four sections were cored from a first drilling site (labelled JO 2004-1; Fig. 2), and three sections with a planed depth offset of 1.5 m from a second drilling site located at about 5 m of distance from the first (labelled JO 2004-1a; Fig. 2). The overlapping sections were correlated using marker layers clearly identified in both

cores and the resulting composite profile checked for consistency using the magnetic susceptibility record (Fig. 2b).

The magnetic susceptibility of core JO 2004 has not permitted the identification of any tephra layer, due to the high noise induced by the magnetic minerals from the drainage basin bedrocks [55]. Tephra layer were identified by both visual inspection and continuously sampling the composite profile at 1 cm-interval, and washing and sieving each sample at 125, 63 and 40 μm using distilled water. The different grain size fractions were dried in a laboratory heater at a temperature of 50°C over 24 h. The three sediment fractions were carefully inspected under a stereomicroscope, looking for volcanic particles (i.e. glass shards, pumice, magmatic crystals, volcanic lithics). At least 400 particles were counted under the stereo-microscope to obtain the glass abundance.

In samples with volcanic glass in excess of 10 %, glass shards and micro-pumice fragments were picked and sealed in resin beads. They were then polished to avoid compositional variations caused by surface alteration processes.

Major element compositions of glass was obtained using an EDAX-DX micro-analyser (EDS analyses) mounted on a Philips SEM 515 at Dipartimento di Scienze della Terra (University of Pisa). Operating conditions were: 20 kV acceleration voltage, 100 s live counting, 10^{-9} Å beam current, beam diameter ≈ 500 μm , 2100 shots per second, with ZAF correction (Z = atomic number; A = absorption; and F = fluorescence). The ZAF correction procedure does not include natural or synthetic standards for reference, and requires the analyses normalization at a given value (which is chosen at 100%). Instrument calibration and performance are described in Marianelli and Sbrana [25].

The composition of glass was classified using the Total Alkali vs. Silica diagram (TAS, [18], Fig. 3a). Major element compositions allowed the discrimination among different volcanic sources and correlation to proximal deposits of known explosive eruptions [e.g. 43, 56].

Seven ^{14}C datings were available from literature [19] (Table 3; Fig. 2a). Raw radiocarbon measurements were converted into calibrated ages using the INTCAL04 method [40] and the polynomial equation of Bard et al. [5] for ^{14}C ages older than 26 cal ka BP.

4. Results

Five tephra layers were recognised along the composite profile, and labelled JO-941 (938 – 942 cm), JO-575 (571 – 577 cm), JO-244 (235 – 252 cm), JO-187 (185.5 – 188.5 cm) and JO-42 (36.5 – 45.5 cm), respectively (Fig. 2a and b).

4.1. Cryptotephra JO-941 (938 – 942 cm)

The deepest tephra is dispersed in the sediment (cryptotephra), and glass shards were recognised in all the three sieving classes. The peak of abundance of glass particles is at 941 cm (60 %; Fig. 2c), and comprises transparent, brown-honey, cusped, thin glass shards (Fig. 4a). The groundmass is glassy, and EDS analyses show a homogeneous rhyolitic composition (Fig. 3a and b, Table 1). In the diagram Comendite-Pantellerite (FeO vs. Al₂O₃; [21]) all the analysed samples plot into the pantelleritic field.

4.2. Cryptotephra JO-575 (571 – 577 cm)

This cryptotephra mainly comprises white to light-brown, elongated and cusped glass shards and rare, white micro-pumice fragments (Fig. 4b). The peak abundance of glass shards is between 574 and 575 cm (95 %; Fig. 2c). The groundmass is glassy (Fig. 4b), and the composition shows a small variability within the trachy-phonolitic field (Fig. 3a and c; Table 1).

4.3. Tephra layer JO-244 (235 – 252 cm)

This tephra layer is composed of two distinct parts with different colours. The first one (between 244 and 244.5 cm) is Yellowish Gray (5Y 7/2; [13]), while the second one (between 247 and 248 cm) is Moderate Olive Brown (5Y 4/4; [13]). The tephra comprises white, vesicular micro-pumices and elongated glass shards with thin septa. Most of the glass shards are transparent, with few dark-brown in colour (Fig. 4c). The abundance of glass shards and micro-pumice has its maximum (100 %) between 244 and 244.5 cm (Fig. 2c). The groundmass is glassy (Fig.4c), and the glass composition is trachy-phonolitic (Fig. 3a and d; Table 1).

4.4. Tephra layer JO-187 (185.5 – 188.5 cm)

This tephra layer is Yellowish Gray in colour (5Y 4/1; [13]), and comprises transparent, tubular, elongated micro-pumice fragments and transparent, brownish glass shards (Fig. 4d). The maximum abundance (99%) is at 187 cm (Fig. 2c). The groundmass is glassy (Fig. 4d), and the glass composition is homogeneous and trachytic (Fig. 3a and e; Table 1).

4.5. Cryptotephra JO-42 (36.5 – 45.5 cm)

This cryptotephra has a peak abundance of glass particles (80%) at 42 cm of depth (Fig. 2c), and comprises dark-brown, blocky, tachylitic fragments with few spherical vesicles (Fig. 4e). The groundmass comprises small crystals of plagioclase, clinopyroxene and minor olivine (Fig. 4e). The glass composition ranges between mugearites and benmoreites (Fig. 3a and f).

5. Discussion

5.1. Correlation of tephra layers

The K- to Na-alkaline affinity of glass compositions of the five tephra layers recognised in the core JO 2004 indicate that all of them were from explosive eruptions of Italian volcanoes, since during late Quaternary the products of the Aegean arc were characterised by calc-alkaline affinity [15, 37, 50]. Two of them (JO-941 and JO-42) present peculiar glass composition that indicate a source from Pantelleria Island and from Mount Etna, respectively. The other three tephtras display trachytic to phonolitic composition, and can be correlated to the explosive activity of Campanian volcanoes. In the following, the precise correlation of each tephra layer with a specific eruption of these volcanoes will be discussed in detail. For comparison, the average compositions of the correlated tephra layers are reported in Table 2.

Cryptotephra JO-941

The pantelleritic glass composition of cryptotephra JO-941 (Table 1) indicates it was generated from Pantelleria Island. The Island of Pantelleria produced several large explosive eruptions with pantelleritic composition [24]. Among them, the most dispersed are the Green Tuff (45-50 ka), the Ignimbrite Q (113.9 ± 3.6 ka), the Ignimbrite P (133.1 ± 3.3 ka), the Welded tuff S (162-164 ka) and the Welded tuff M (174.8 ± 2.8 ka; [24]). Two other $^{40}\text{Ar}/^{39}\text{Ar}$ datings are available for the Ignimbrite P (126.8 ± 1.5 ka; [17]) and for the Welded

tuff S (174.5 ± 1.5 ka; [17]). Pantelleritic tephra layers have been found in the Ionian Sea core KET 8222 [37] (Table 2) and named P11 (estimated age at about 131 ka, 555 cm depth) and P12 (estimated age at about 164 ka, 765 cm depth), which have similar ages of Ignimbrite P and Welded tuff S. The composition of P11 and P12 is quite similar, and the two tephra layers are hardly distinguishable on the basis of major elements.

The glass composition of sample JO-941 matches well that of both tephra layers P11 and P12 (Tables 1 and 2, Fig. 3b). Indeed, the tephra layer P11 has been recognised over a wide area of the Ionian Sea while the dispersal of P12 is more limited [37]. Nevertheless, stratigraphic and paleoclimatic considerations support the correlation of the JO-941 cm tephra with P11 marine tephra layer, and then with Ignimbrite P deposits on Pantelleria Island. This is because both carbonate and pollen curves carried out on JO 2004 core sediments [19] unequivocally indicate that this tephra were emplaced close to the inception of the Last Interglacial. The onset of the Last Interglacial may have been recorded at different times in different archives [51], but, in any case, the age of 164 ka (which corresponds to P12 tephra layer) is too old of some ten thousand years with respect to that commonly accepted for the inception of Last Interglacial at Mediterranean latitudes (e.g. 126.8 and 120.3 ka; [51]).

The recognition of tephra layer P11 is the first in the Balkans, and significantly enlarges its dispersal well beyond the Ionian Sea (Fig. 5a).

Cryptotephra JO-575

This low alkali ratio (LAR) trachytic tephra layer occurs between the calibrated ^{14}C age of $44,812 \pm 1055$ cal yr BP [19] (Table 3) and the P11 tephra layer.

Composition of the tephra layer JO-575 shows a good match with marine tephra C-31 (KET 8222 and DED 8708 deep-sea cores, Fig. 3c and Table 2), which has an interpolated age of 107 ka [37]. Paterne had related the C-31 tephra with the LAR-trachyte X6 from the 22M-60 core [15]. This supports the correlation of JO-575 sample to the X6 tephra layer. The age of X6 tephra layer at 107 ka is also supported by extrapolation of the X5 tephra layer age (105 ± 2 ka; $^{40}\text{Ar}/^{39}\text{Ar}$ technique) based on sedimentation rate extrapolation. The source of the X6 eruption has been located in the Campanian volcanic zone [15]. The X6 tephra layer was for the first time described in Ionian Sea cores [15], and successively in a Tyrrhenian Sea core [37] and in the Lago Grande di Monticchio succession [57]. This is the first recognition of X6 tephra layer in the Balkans, and it considerably enlarges its dispersal area to the east (Fig. 5b).

Tephra layer JO-244

This tephra layer is 11 cm thick (Fig. 2) and comprises both glass shards and micropumice fragments. When plotted on TAS diagram the glass composition has a narrow variability within the trachytic and phonolitic fields (Fig. 3d). However, the tephra layer shows a variable alkali ratio passing from the base to the top. In particular, the basal part shows the coexistence of glasses with two different alkali ratios (Table 1), whereas the upper part has a very homogeneous LAR-trachytic glass composition (Table 1).

The glass composition indicates the Campanian area as source for this tephra that, on the basis of the peculiar variability in alkali ratio and the deposit thickness, can be confidently correlated to the Campanian Ignimbrite eruption from Campi Flegrei. The geochemical comparison of major element shown in Table 2 is applied with the ML-2 layer [26] and the TM-18 layer [56] among the many analyses available. The Campanian Ignimbrite eruption was dated at $39,280 \pm 110$ years ($^{40}\text{Ar}/^{39}\text{Ar}$ technique; [9]), and correspond to the Y5 tephra layer, widely dispersed in the central and eastern Mediterranean and in mainland Europe [11, 15, 26, 30, 34, 35, 39, 47, 53, 55, 56]. The recognition in Albanian side of Lake Ohrid succession confirms the previous finding of Wagner et al. [55] from the Macedonian side of the lake (Fig. 5c).

Tephra layer JO-187

The JO-187 tephra is chronologically constrained between the Campanian Ignimbrite (≈ 39 ka) and the ^{14}C age of $9,407 \pm 121$ cal yr BP obtained at 100 cm depth (Table 3; Fig. 2a). The homogeneous trachytic composition (Table 1, Fig. 3e) of this tephra layer suggests it was originated from the Campanian volcanic zone, and shows a good match with the composition of SMP1-e eruption from Campi Flegrei [10]. The SMP1-e eruption corresponds to the Y3 tephra layer (Table 2; [10, 47, 58]), which is widely dispersed in the central Mediterranean area [15, 29, 30, 47, 56, 58] with an estimated age between 30 and 31 cal ka BP [58]. The recognition in Albanian side of Lake Ohrid succession confirms the previous finding of Wagner et al. [55] from the Macedonian side of the lake (Fig. 5d).

Cryptotephra JO-42

This cryptotephra is stratigraphically younger than the ^{14}C age of $6,680 \pm 66$ cal yr BP (Table 3), and the mugearitic-benmoreitic composition easily indicates the Mount Etna as the source. The shallow position within the core and the glass composition indicates a correlation with the FL eruption from Mount Etna, dated at $3,370 \pm 70$ cal yr BP [8, 55]. The recognition in Lake Ohrid succession confirms the previous finding in the same lake (Macedonian side) [55] and in the Lake Shkodra successions (Albania) (Fig. 5e; [49]).

5.2. Significance of tephra layer recognition in Lake Ohrid

The recognition of tephra layers in the Lake Ohrid has relevance for both volcanology and Quaternary Sciences.

From a volcanological point of view, the five tephra layers recognised in the sediments testify for episodes of ash deposition in very distal areas with respect to the Italian volcanoes (Fig. 5), irrespective if they are from large (P11, X6, Y5 and Y3 tephra layers) or intermediate (FL tephra layer) explosive eruptions.

Three out of five tephra layers were already recognised in Lake Ohrid sediments (Y5, Y3, and FL) but from a core located in the Macedonian side of the lake [55]. Their recognition in core JO 2004, confirm their deposition was not sporadic but probably they affected all the lake area and its drainage basin. Two of them (P11 and X6) were recognised for the first time in the Balkan area, significantly enlarging to the North-East their dispersal that was previously limited to Ionian and Tyrrhenian seas [15, 37] or Lago Grande di Monticchio [57].

The distance between the studied site and the inferred source areas is 550 km for the Campanian volcanic area, 620 km for Mount Etna and 900 km for Pantelleria Island (Fig. 5). Bearing in mind that they represent minimum values, the area affected by ash deposition can be assessed at ca. 207,000 km² for P11, ca. 471,000 km² for X6, at ca. 550,000 km² for the Y3 tephra layers. The dispersal area of the Y5 was previously assessed between $1.5\text{--}3 \times 10^6$ km² [39].

The paucity of accurate studies on distal ash deposits mainly relies in their poor preservation and in their dispersal behaviour. The accumulation of volcanic ash in distal zones often represents a hazard, since most of the attention and mitigation procedures are usually devoted to proximal areas. Deposition of ash in distal sites can cause damage to infrastructures, disturbance to communications, water pollution and breathing problems. Therefore the

recognition and the collection of very distal samples can improve hazard mitigation plans and procedures over very large area far from the volcanic sources.

From a Quaternary Science point of view, the lake Ohrid represents an exceptional natural archive. A previous work [55] studied a core (Lz1120) from the Macedonian side of the lake, but analysed and discussed only the last 40 ka of sedimentation record of Lake Ohrid with a similar core length than the JO 2004. This apparent difference in sedimentation rate relies in both the presence of sedimentary hiatus in core JO 2004 (Fig. 6; [6, 19]) and the different locations of the two cores, with the Lz1120 closer to the major karstic springs than the JO 2004 [6].

The core JO 2004 offers the opportunity to study about 130 ky of the sedimentary record, which encompasses the last interglacial. In this scenario, the presence of two important regional markers like the P11 and X6 tephra layers allow the physical correlation of the deep part of the cores JO 2004 to other important archives of the central Mediterranean area.

The available ^{14}C datings (Table 3) and the tephra layers allow the drawing of a sedimentation curve (Fig. 6). The sedimentation curve was built using the seven ^{14}C datings and the tephrochronology, and shows three main rates of sedimentation. The first one between 0 and 100 cm is about 0.10 mm yr^{-1} , the second one, between 100 and 575 cm is around 0.05 mm yr^{-1} and the third one between 575 and 988 cm is about 0.15 mm yr^{-1} (Fig. 6).

These variable sedimentation rates reflect different paleo-environmental information. Below the X6 tephra layer, there is the transition between the last-glacial and the last-interglacial phases (Eemian, transition from marine isotopic stage 5 and 6, around 125 ka BP; [19]), which was characterised by a high sedimentation rate (0.15 mm yr^{-1} ; Fig. 6). Between 100 and 575 cm depth, there is a glacial period record with a low sedimentation rate (0.05 mm yr^{-1}) and low sediment dynamic. It is important to note that this sedimentation rate is probably underestimated, since it does not take into account the occurrence of the inferred sedimentary hiatus between 90 and 103 ka (Fig. 6; [6]). The upper 100 cm of core sediments (younger than 10 cal ky BP), correspond to the current interglacial period, which is characterised by a higher sedimentation rate (0.10 mm yr^{-1} ; Fig. 6).

6. Conclusions

The study of the JO 2004 cores yields some important results for the tephrostratigraphy and tephrochronology of the Balkans. Five tephra layers were recognised and described, and two

of them were for the first time discovered in the area. The tephra layer P11 is the oldest in the whole recognised succession and testifies for ash deposition at more than 900 km from its source on Pantelleria Island. Similarly, the recognition of tephra layer X6 enlarges to the east its dispersal, since it was previously described only in Ionian and Tyrrhenian Sea cores and in the Lago Grande di Monticchio. The other three tephra layers (FL, Y3 and Y5) were already recognised in Lake Ohrid succession, and the new findings testify for their extensive deposition in the area.

The recognition of the two deeper tephra layers (X6 and P11) is especially important, since they allow the establishment of a chronology for the part of the core older than 40 ka BP, and its physical link to other archives of the central Mediterranean area.

In perspective, this work will allow to obtain a better estimation of the distal tephra dispersion from Italian volcanoes. These results must be integrated in the mitigation and rescue plans that concern the population of the Central Mediterranean area.

Acknowledgements:

We acknowledge the French (INSU-CNRS) research program ECLIPSE, the French School of Athens (Greece) and the Archaeological museum of Korça (Albania) for financial support and authorizations. We thank Anne-Marie Lézine, Uli von Grafenstein and Nils Andersen for providing samples for the piston core JO 2004 and for the useful discussions. Alain Mazaud is thanked for the magnetic susceptibility. BC was partially supported by Vinci program of Université Franco-Italienne and SETCI from region of Île-de-France. Franco Colarieti (DST Pisa) is gratefully acknowledged for the preparation of samples and assistance during EDS analyses. Amandine Bordon, Soumaya Belmecheri and Sonia La Felice are thanked for helpful discussions. An anonymous reviewer provided helpful suggestions for improving the manuscript.

References

- [1] S. Aliaj, Neotectonics and seismicity in Albania. In: S. Meco, S. Aliaj, I. Turku, (Eds.), *Geology of Albania*. Gebrüder Borntrager, Berlin. *Beitrage zur regionalen Geologie der Erde*, (2000) vol. 28, pp. 135–178.
- [2] S. Aliaj, G. Baldassarre, D. Shkupi, Quaternary subsidence zones in Albania: some case studies, *Bull. Eng. Geol. Environ.* 59 (2001) 313-318.
- [3] S. Aliaj, J. Adams, S. Halchuk, E. Sulstarova, V. Peci, B. Muco, Probabilistic seismic hazard maps for Albania. In: 13th World conference earthquake engineering, Vancouver, BC, Canada, (2004) paper no. 2469, 14 pp
- [4] T. Anovski, J. Naumovski, D. Kacurkov, P. Kirkov, A study of the origin of waters of St. Naum Springs, Lake Ohrid (in Macedonian), *Fisica* 12 (1980) 76–86.
- [5] E. Bard, M. Arnold, B. Hamelin, N. Tisnerat-Laborde, G. Cabioch, Radiocarbon Calibration by Means of Mass Spectrometric $^{230}\text{Th}/^{234}\text{U}$ and ^{14}C Ages of Corals: An updated database including samples from Barbados, Mururoa, and Tahiti, In: Stuiver, M., and van der Plicht, J., eds. *INTCAL98: Calibration Issue*. *Radiocarbon* 40 (1998) 1085-1092.
- [6] S. Belmecheri, T. Namiotko, C. Robert, U. von Grafenstein, D.L. Danielopold, Climate controlled ostracod preservation in Lake Ohrid next term (Albania, Macedonia). *Palaeogeography, Palaeoclimatology, Palaeoecology* (2009) 277, 3-4, 236-245.
- [7] N. Calanchi, A. Cattaneo, E. Dinelli, G. Gasparotto, F. Lucchini, Tephra layers in Late Quaternary sediments of the central, Adriatic Sea. *Marine Geology* 149 (1998) 191–209.
- [8] M. Coltelli, P. Del Carlo, L. Vezzoli, Stratigraphic constraints for explosive activity in the past 100 ka at Etna volcano, Italy, *Int. J. Earth Sciences*. 89 (2000) 665-677.

- [9] B. De Vivo, G. Rolandi, P.B. Gans, A. Calvert, W.A. Bohrson, F.J. Spera, H.E. Belkin, News constraints on the pyroclastic eruptive history of the campagnian volcanic Plain (Italy), *Mineralogy and Petrology*. 73 (2001) 47-65.
- [10] M.A. Di Vito, R. Sulpizio, G. Zanchetta, M. D’Orazio. The late Pleistocene pyroclastic deposits of the Campanian Plain: new insights into the explosive activity of Neapolitan volcanoes, *J. Volcanol. Geotherm. Res.* 177 (2008) 19-48 doi:10.1016/j.jvolgeores.2007.11.019.
- [11] B. Giaccio, R. Isaia, F.G. Fedele, E. Di Canzio, J. Hoffecker, A. Ronchitelli, A. Sinitsyn, M. Anikovich, S.N. Lisitsyn, The Campanian Ignimbrite and Codola tephra layers: two temporal/stratigraphic markers for the Early Upper Palaeolithic in southern Italy and eastern Europe. *J. Volcanol. Geotherm. Res.* 177 (2008) 208-226 doi:10.1016/j.jvolgeores.2007.10.007.
- [12] M. Goldsworthy, J. Jackson, J. Haines, The continuity of active fault systems in Greece. *Geophys. J. Int.* (2002) 148, 596–618.
- [13] GSA Rock Color Chart (1991) The Geological Society of America Rock-Color Chart with genuine Munsell color chips. Printed by Munsell Color U.S.A.
- [14] S.D. Hadzisce, 1966. Das Mixophänomen im Ohridsee im Laufe der Jahre 1941/42-1964/65. *Verh. Internat. Verein. Limnol.* 16, 134–138.
- [15] J. Keller, W.B.F. Ryan, D. Ninkovich, R. Altherr, Explosive volcanic activity in the Mediterranean over the past 200,000 yr as recorded in deep-sea sediments. *Geol. Soc. Am. Bull.* 89 (1978) 591–604.
- [16] M. Kraml, Laser- $^{40}\text{Ar}/^{39}\text{Ar}$ -Datierungen an distalen marinen Tephren des jung-quartären mediterranen Vulkanismus (Ionisches Meer, METEOR-Fahrt 25/4), Ph.D. Thesis, Albert-Ludwigs-Universität Freiburg i.Br. (1997) 216 pp.

[17] S. La Felice, S.G. Rotolo, S. Scaillet, G. Vita, Tephrostratigraphy, petrochemistry and ^{40}Ar – ^{39}Ar age data on Pre-Green Tuff sequences, Pantelleria, Congresso FIST Geitalia 2009, I 7- Dal terreno al laboratorio: approcci multidisciplinari per lo studio del vulcanismo esplosivo.

[18] M.J. Le Bas, R.W. Le Maitre, A. Streckeisen, B. Zanettin, A chemical classification of volcanic rocks based on the total alkali-silica diagram, *J. Petrol.* 27 (1986) 745–750.

[19] A.M. Lezine, U. von Grafenstein, N. Andersen, S. Belmecheri, A. Bordon, B. Caron, J.P. Cazet, H. Erlenkeuser, E. Fouache, C. Grenier, P. Huntsman-Mapila, D. Hureau-Mazaudier, D. Manelli, A. Mazaud, C. Robert, R. Sulpizio, J.J. Tiercelin, G. Zanchetta, Z. Zeqollari, Lake Ohrid, Albania, provides an exceptional multi-proxy record of environmental changes during the last glacial-interglacial cycle, *Palaeogeography, Palaeoclimatology, Palaeoecology* (2010) doi: 10.1016/j.palaeo.2010.01.016

[20] J.J. Lowe, S. Blockley, F. Trincardi, A. Asioli, A. Cattaneo, I.P. Matthews, M. Pollard, S. Wulf, Age modelling of late Quaternary marine sequences in the Adriatic: towards improved precision and accuracy using volcanic event stratigraphy, *Continental Shelf Research* 27 (2007) 560–582.

[21] R. Macdonald, Nomenclature and Petrochemistry of the Peralkaline Oversaturated Extrusive Rocks, *Bull. Volcanol.*, 38 (1974) 498-516.

[22] M. Magny, J.L. de Beaulieu, R. Drescher-Schneider, B. Vanni re, A.V. Walter-Simonnet, L. Millet, G. Bossuet, O. Peyron, Climatic oscillations in central Italy during the Last Glacial-Holocene transition: the record from Lake Accesa, *J. Quat. Sc.* 21 (2006) 311-320.

[23] M. Magny, J.L. de Beaulieu, R. Drescher-Schneider, B. Vanni re, A.V. Walter-Simonnet, Y. Miras, L. Millet, G. Bossuet, O. Peyron, E. Brugiapaglia, A. Leroux, Holocene climate changes in the central Mediterranean as recorded by lake-level fluctuations at Lake Accesa (Tuscany, Italy), *Quat. Sc. Rev.* 26 (2007) 1736–1758.

- [24] G.A. Mahood, W. Hildreth, Geology of the peralkaline volcano at Pantelleria, Strait of Sicily, *Bull. Volcanol.* 48 (1986) 143-172.
- [25] P. Marianelli, A. Sbrana, Risultati di misure di standard di minerali e di vetri naturali in microanalisi a dispersione di energia, *Atti Società Toscana di Scienze Naturali Memorie Serie A* 105 (1998) 57-63.
- [26] V. Margari, D.M. Pyle, C. Bryant, P.L. Gibbard, Mediterranean tephra stratigraphy revisited: Results from a long terrestrial sequence on Lesvos Island, Greece, *J. Volcanol. Geotherm. Res.* 163 (2007) 34-54.
- [27] A. Matzinger, M. Jordanoski, E. Veljanoska-Sarafiloska, M. Sturm, B. Müller, A. Wüest, Is Lake Prespa jeopardizing the ecosystem of ancient Lake Ohrid? *Hydrobiologica* 553 (2006) 89–109.
- [28] R. Munno, P. Petrosino, New constraints on the occurrence of Y3 upper Pleistocene tephra marker layer in the Tyrrhenian Sea, *Italian Journal of Quaternary Sciences*, (2004) 17(1), 11-20
- [29] R. Munno, P. Petrosino, The late Quaternary tephrostratigraphical record of the San Gregorio Magno basin (southern Italy), *J. Quat. Sc.* 22 (2006) 247-266 doi:10.1002/jqs.1025.
- [30] B. Narcisi, L. Vezzoli, Quaternary stratigraphy of distal tephra layers in the Mediterranean – an overview, *Global and Planetary Change* 21 (1999) 31-50.
- [31] J. Nicot, M. Chardon, On the morphotectonic background and the evolution of natural environments and limestone relief in Western Yugoslavian Macedoni, *Méditerranée* (1983) 37-52
- [32] L. Pappalardo, L. Civetta, M. D'Antonio, A. Deino, M.A. Di Vito, G. Orsi, A. Carandente, S. de Vita, R. Isaia, M. Piochi, Chemical and Sr-isotopical evolution of the

Phlegraen magmatic system before the Campanian Ignimbrite and the Neapolitan Yellow Tuff eruptions, *J. Volcanol. Geother. Res.* 91 (1999) 141–166.

[33] M. Paterne, Reconstruction de l'activité explosive des volcans de l'Italie du Sud par tephrochronologie marine, Ph.D. Thesis University of Paris Sud XI, Paris (1985) 144 pp.

[34] M. Paterne, F. Guichard, J. Labeyrie, P.Y. Gillot, J.C. Duplessy, [Tyrrhenian Sea tephrochronology of the oxygen isotope record for the past 60,000 years](#), *Marine Geology*, 72 (1986) 259-285.

[35] M. Paterne, F. Guichard, J. Labeyrie, Explosive activity of the South Italian volcanoes during the past 80,000 years as determined by marine tephrochronology, *J. Volcanol. Geotherm. Res.* 34, (1988) 153-172.

[36] M. Paterne, J. Labeyrie, F. Guichard, A. Massaud, F. Maitre, Fluctuation of the campanian explosive activity (South Italy) during the last 190,000 years as determined by marine tephrochronology, *Earth and Planetary Science Letters* 98 (1990) 166-174.

[37] M. Paterne, F. Guichard, J.C. Duplessy, G. Siani, R. Sulpizio, J. Labeyrie, A 90,000 – 200,000 yrs marine tephra record of Italian volcanic activity in the central Mediterranean Sea, *J. Volcanol. Geotherm. Res.* 177 (2008) 187-196 doi:10.1016/j.jvolgeores.2007.11.028.

[38] S. Poli, S. Chiesa, P.Y. Gillot, F. Guichard, Chemistry versus time in the volcanic complex of Ischia (Gulf of Naples, Italy): Evidence of successive magmatic cycles. *Contrib. Min. Petrol.* 95 (1987) 322-335.

[39] D.M. Pyle, G.D. Ricketts, V. Margari, T.H. van Andel, A.A. Sinitsyn, N. Praslov, S. Lisitsyn, Wide dispersal and deposition of distal tephra during the Pleistocene “Campanian Ignimbrite/Y5” eruption, Italy, *Quat. Sc. Rev.* 25 (2006) 2713–2728.

[40] P.J. Reimer, M.G.L. Baillie, E. Bard, A. Bayliss, J.W. Beck, C. Bertrand, P.G. Blackwell, C.E. Buck, G. Burr, K.B. Cutler, P.E. Damon, R.L. Edwards, R.G. Fairbanks, M. Friedrich,

T.P. Guilderson, K.A. Hughen, B. Kromer, F.G. McCormac, S. Manning, C. Bronk Ramsey, R.W. Reimer, S. Remmele, J.R. Southon, M. Stuiver, S. Talamo, F.W. Taylor, J. van der Plicht, C.E. Weyhenmeyer, INTCAL04 terrestrial radiocarbon age calibration, 0-26 kyrBP, *Radiocarbon* 46 (2004) 1029-1058.

[41] L. Sadori, B. Narcisi, The Postglacial record of environmental history from Lago di Pergusa, Sicily, *The Holocene* 11,6 (2001) 655-670. doi: 10.1191/09596830195681

[42] R. Santacroce, (Ed), *Somma-Vesuvius*, CNR Quaderni Ricerca Scientifica 114 (1987) 251.

[43] R. Santacroce, R. Cioni, P. Marianelli, A. Sbrana, R. Sulpizio, G. Zanchetta, D.J. Donahue, J.L. Joron, Age and whole rock-glass compositions of proximal pyroclastics from the major explosive eruptions of Somma-Vesuvius: a review as a tool for distal tephrostratigraphy, *J. Volcanol. Geotherm. Res.* 177 (2008) 1-18 doi:10.1016/j.jvolgeores.2008.06.009.

[44] G. Siani, R. Sulpizio, M. Paterne, A. Sbrana, Tephrostratigraphy study for the last 18,000 14C years in a deep-sea sediment sequence for the South Adriatic, *Quat. Sc. Rev.* 23 (2004) 2485-2500.

[45] S. Stankovic, S.D. Hadzisce, *La thermique du lac d'Ohrid. Recueil des travaux, Station hydrobiologique – Ohrid*, (1953)61 pp.

[46] S. Stankovic, *The Balkan Lake Ohrid and its living world*, *Monographiae Biologicae IX*, Dr. W. Junk, Den Haag, (1960) 357.

[47] R. Sulpizio, G. Zanchetta, M. Paterne, G. Siani, A review of tephrostratigraphy in central and southern Italy during the last 65 ka, *Il Quaternario*, 16 (2003) 91-108.

[48] R. Sulpizio, R. Bonasia, P. Dellino, M.A. Di Vito, L. La Volpe, D. Mele, G. Zanchetta, L. Sadori, Discriminating the long distance dispersal of fine ash from sustained columns or

near ground ash clouds: the example of the Pomici di Avellino eruption (Somma-Vesuvius, Italy), *J. Volcanol. Geotherm. Res.* 177 (2008) 263-276
doi:10.1016/j.jvolgeores.2007.11.012.

[49] R. Sulpizio, A. van Welden, B. Caron, G. Zanchetta, The Holocene tephrostratigraphic record of Lake Shkodra (Albania and Montenegro), *J. Quat. Sc.* (2010). doi: 10.1002/jqs.1334

[50] R. Thunnell, A. Federman, S. Sparks, D. Williams, The age, origin and volcanological significance of the Y-5 ash layer in the Mediterranean, *Quaternary Research*, 12 (1979) 241–253.

[51] P.C. Tzedakis, M.R.Frogley, T.H.E. Heaton, Last Interglacial conditions in southern Europe: evidence from Ioannina, northwest Greece, *Global and Planetary Change* 36 (2003) 157–170. doi:10.1016/S0921-8181(02)00182-0.

[52] L. Vezzoli, Island of Ischia. CNR, Quaderni della Ricerca Scientifica 114 (1988) 230.

[53] L. Vezzoli, Tephra layers in Bannock Basin (Eastern Mediterranean), *Mar. Geol.* 100 (1991) 21–34.

[54] B. Wagner, K. Reicherter, G. Daut, M. Wessels, A. Matzinger, A. Schwalb, Z. Spirkovski, M. Sanxhaku, The potential of Lake Ohrid for long-term palaeoenvironmental reconstructions, *Palaeogeography, Palaeoclimatology, Palaeoecology* 259 (2008) 341–356
doi:10.1016/j.palaeo.2007.10.015.

[55] B. Wagner, R. Sulpizio, G. Zanchetta, S. Wulf, M. Wessels, G. Daut, N. Nowaczyk, The last 40 ka tephrostratigraphic record of Lake Ohrid, Albania and Macedonia: a very distal archive for ash dispersal from Italian volcanoes, *J. Volcanol. Geotherm. Res.* 177 (2008) 71-80 doi:10.1016/j.jvolgeores.2007.08.018.

[56] S. Wulf, M. Kraml, A. Brauer, J. Keller, J.F.W. Negendank, Tephrochronology of the 100 ka lacustrine sediment record of Lago Grande di Monticchio (southern Italy), *Quaternary International*, 122 (2004) 7–30.

[57] S. Wulf, A. Brauer, J. Mingram, B. Zolitschka, J.F.W. Negendank, Distal tephtras in the sediments of Monticchio maar lakes, In: C. Principe, Editor, *La Geologia del Monte Vulture, Regione Basilicata – Consiglio Nazionale delle Ricerche*, (2007) 105–122.

[58] G. Zanchetta, R. Sulpizio, B. Giaccio, G. Siani, M. Paterne, S. Wulf, M. D'Orazio, The Y-3 tephra: A Last Glacial stratigraphic marker for the central Mediterranean basin, *J. Volcanol. Geotherm. Res.* 177 (2008) 145-154 doi:10.1016/j.jvolgeores.2007.08.017.

Figure and Table captions

Figure 1: Location map of the study area. The Italian volcanoes active in the investigated time span and the location of cores used in this study are shown: CVZ = Campanian Volcanic Zone (Campi Flegrei, Somma-Vesuvius, Ischia and Procida volcanoes), PRG = Lake of Pergusa, LGM = Lago Grande di Monticchio. The inset in the upper right angle reports the location of the core JO 2004.

Carte de localisation du site d'étude. Les principaux volcans Italiens actifs lors de la période étudiée et les sites des carottes utilisées dans cet article sont indiqués: CVZ = Campanian Volcanic Zone (Champs Phlégréens, Somma-Vesuvius, Ischia et Procida), PRG = lac de Pergusa, LGM = Lago Grande di Monticchio. En haut à droite, la position du site de forage de la carotte JO 2004.

Figure 2: Composite stratigraphy of the core JO 2004 (depth in cm): (a) lithostratigraphy (modified from [19]) with tephra layers and calibrated ^{14}C ages, (b) magnetic susceptibility curve and (c) relative glass shards abundance.

Stratigraphie recomposée de la carotte JO 2004 (profondeur en cm) : (a) lithostratigraphie (modifiée à partir de [19]) avec les niveaux de tephra et les ages ^{14}C calibrés, (b) courbe de susceptibilité magnétique et (c) abondance relative des esquilles de verres volcaniques.

Figure 3: Chemical classification of the studied tephra layers and comparison with tephra from literature using the Total Alkali vs. Silica (TAS) diagram [18]. a) General classification using average glass analyses of the five identified tephra layers (1σ error bars are also reported); b) analyses of JO-941 cryptotephra and KET 8222-563 and 555 cm tephra [37]; c) analyses of JO-575 cryptotephra and KET 8222-350, 340 cm and DED 8708-1209 cm tephra [33, 37]; d) analyses of JO-244 tephra layer. Compositions of TM-18 [56] and ML-2 [26] tephra layers are reported for comparison; e) analyses of JO-187 tephra layer. Compositions of TM-15 [56] and MD90-917 920 cm [58] tephra layers are reported for comparison; f) analyses of JO-42 cryptotephra. Compositions of SK13 514 cm [41], PRG06-03 390 cm [49], Ohrid 310-315 cm [55], and Pergusa Type A and B [41] tephra layers are reported for comparison.

Comparaison entre les compositions chimiques des niveaux de tephra identifiés et ceux issus de la littérature dans un diagramme Total Alcalin vs. Silice (TAS) [18]. a) Diagramme général des moyennes des analyses sur les verres des cinq niveaux de tephra (barre d'erreur 1σ); b) analyses du cryptotephra JO-941 comparées aux niveaux de tephra KET 8222-563 et 555 cm d'après [37]; c) analyses du cryptotephra JO-575 comparées aux niveaux de tephra KET 8222-350, 340 cm et DED 8708-1209 cm d'après [33, 37]; d) analyses du niveau de tephra JO-244 comparées aux niveaux de tephra TM-18 d'après [56] et ML-2 d'après [26]; e) analyses du niveau de tephra JO-187 comparées aux niveaux de tephra TM-15 d'après [56] et MD 90-917 d'après [58]; f) analyses du cryptotephra JO-42 comparées aux niveaux de tephra de SK13 514 cm d'après [41] et PRG06-03 390 cm d'après [49], Ohrid 310-315 cm d'après [55] et Pergusa Type A et B d'après [41].

Figure 4: Scanning Electron Microscope (SEM) pictures of volcanic particles from the five studied tephra layers and cryptotephra: a) JO-941. Note the elongated glass shards with glassy groundmass; b) JO-575. Note the coexistence of elongated glass shards and vesicular micropumices, both with glassy groundmass; c) JO-244. Note the coexistence of elongated glass shards with thin septa and vesicular micropumices, both groundmass are glassy, d) JO-187. Note the coexistence of convoluted glass shards and vesicular micropumice, both with glassy groundmass; e) JO-42. Note the blocky shape of the tachylitic fragments, which contain few spherical vesicles. The groundmass comprises small crystals of plagioclase, clinopyroxene and olivine.

Images au Microscope Electronique à Balayage (MEB) des tephra volcaniques des niveaux a) JO-941 composé d'esquilles de verre fines et allongées dont la matrice est vitreuse, b) JO-575 composé d'esquilles de verre allongées ainsi que microponces vésiculées, et dont chacune des matrices sont vitreuses, c) JO-244 composé d'esquilles de verre allongées avec de fines parois et de microponces vésiculées, et dont chacune des matrices sont vitreuses, d) JO-187 composé d'esquille de verre et de microponces allongées et fibreuses, dont chacune des matrices sont vitreuses, e) JO-42 composé de fragments de blocs et de tachylites finement vésiculées dont la matrice se compose de petits cristaux de plagioclase, de clinopyroxenes et d'olivine.

Figure 5: Reconstructed dispersal areas of the five tephra layers recognised in core JO 2004 and using previously published data. a) P11 tephra layer. The dashed line indicates the previous inferred dispersal area. KET 8222, data from [37]; b) X6 tephra layer. The dashed line indicates the previous inferred dispersal area. KET 8222 and DED 8708 data from [37]; c) Y5 tephra layer. Dispersal area from [11, 39]; d) Y3 tephra layer. C6 and C145 data from [28], V10-68, RC9-190, 22M60 data from [15], KET 8004 and KET 8011 data from [37, 58], LZ 1120 data from [55] and MD90-917 data from [34, 58]; e) FL dispersal area is from [49]. Blue dots indicate the location of the JO 2004 core. Stars indicate the volcanic sources.

Reconstruction des zones de dispersion des cinq éruptions identifiées dans la carotte JO 2004. a) les tephra de P11 ont été identifiés dans la carotte KET 8222, [37]. b) les tephra de X6 ont été identifiés dans les carottes KET 8222 et DED 8708, [37]. c) la carte de dispersion des cendres de Y5 est modifiée à partir de [11, 39]. d) les tephra de Y3 ont été identifiés dans les carottes C6 et C145, [28], V10-68, RC9-190, 22M60, [15], KET 8004 et KET 8011, [37, 58], LZ 1120, [55] et MD90-917, [34, 58]. e) la carte de dispersion des cendres de Etna FL est modifiée à partir de [49]. Les points bleus indiquent la localisation de la carotte JO 2004. Les étoiles indiquent les sources volcaniques et les précédentes surfaces de dispersion sont limitées par un trait jaune et noir.

Figure 6: Sedimentation curves for core JO 2004 calculated using the available calibrated ^{14}C (cross) and the correlated ages of tephra layers (diamonds). The grey-shaded area indicates the inferred sedimentary hiatus. P11=JO-941, X6=JO-575, Y5=JO-245, Y3=JO-187, Etna FL=JO-42. Numbers in italic underlined indicate the calculated sedimentation rate (mm.yr^{-1}) for each segment of the curve.

Courbe de sédimentation de la carotte JO 2004 calculée à partir des âges ^{14}C calibrés (croix) et des datations corrélées aux niveaux de tephra (losanges). La zone grisée indique le hiatus sédimentaire. P11=JO-941, X6=JO-575, Y5=JO-245, Y3=JO-187, Etna FL=JO-42. Les chiffres soulignés en italiques représentent le taux de sédimentation (mm.an^{-1}) pour chaque section de la courbe.

Table 1: Composition of major elements of the five tephra layers recognised in core JO 2004.

Compositions des éléments majeurs des cinq niveaux de tephra identifiés dans la carotte JO 2004.

Table 2: Comparison of the composition of the recognised tephra layers with analyses from literature: KET 8222 340 cm, 350 cm, 555 cm, 563 cm, 765 cm, DED 8708 1209 cm from [33] and [37]; ML-2 from [26]; TM-15 and TM-18 from [56]; MD90-917 920cm from [58]; tephra Ohrid 310-315 cm from [55]; Pergusa type A and B from [41] and PRG06-03 390 cm and SK13 514 cm from [49].

Comparaison des moyennes et des écarts types des compositions des niveaux de tephra identifiés aux analyses issues de la littérature: KET 8222 340 cm, 350 cm, 555 cm, 563 cm, 765 cm, DED 8708 1209 cm d'après [33] et [37]; ML-2 d'après [26]; TM-15 et TM-18 d'après [56]; MD90-917 920 cm d'après [58]; tephra Ohrid 310-315 cm d'après [55]; Pergusa type A et B d'après [41] et PRG06-03 390 cm et SK13 514 cm d'après [49].

Table 3: ^{14}C ages from JO 2004 core determined at UMS-ARTEMIS (Pelletron 3MV) AMS facilities (CNRS-CEA Saclay, France, [19]). Ages were calibrated using INTCAL04 [40] for ^{14}C age younger than 26 cal ka BP and Bard polynomial equation for age older than 26 cal ka BP [5].

Tableau des âges AMS ^{14}C de la carotte JO 2004 obtenus par UMS-ARTEMIS (Pelletron 3MV) CNRS-CEA Saclay, France, [19]. Les âges ont été calibrés avec INTCAL04 [40] pour les datations d'âge inférieur à 26 cal ka BP et avec le polynôme de Bard pour les datations d'âge supérieur à 26 cal ka [5].

Figure 1

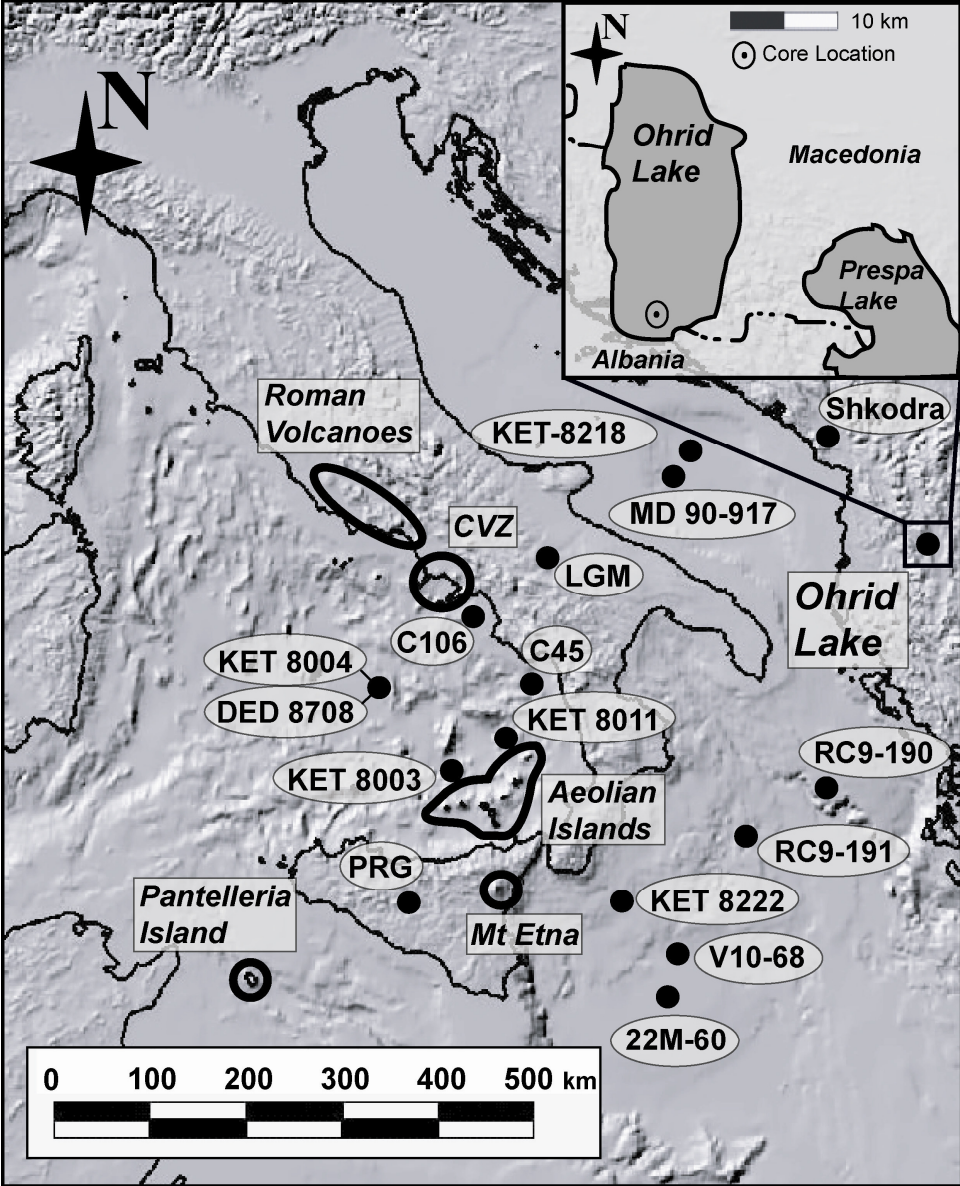


Figure 2

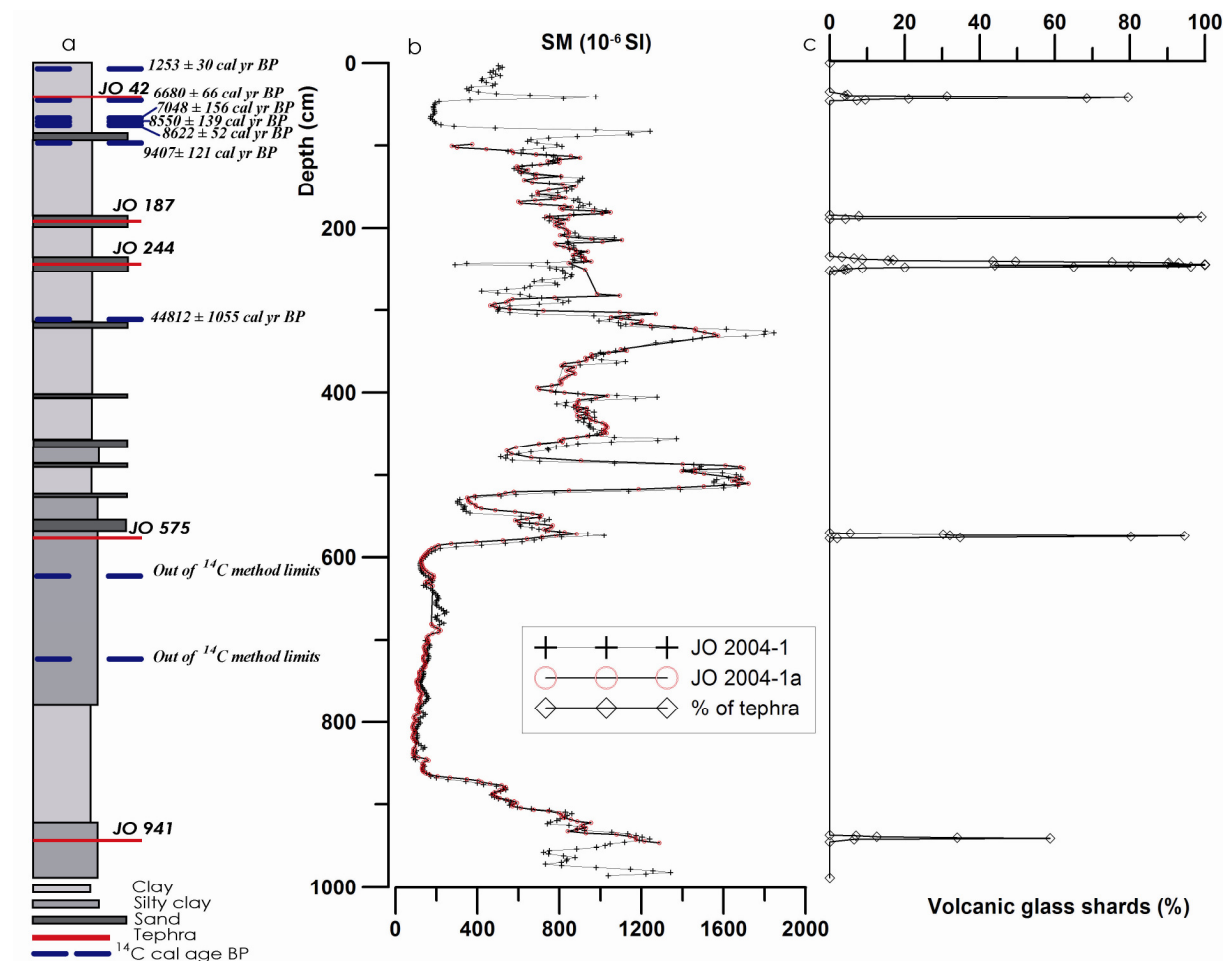


Figure 3

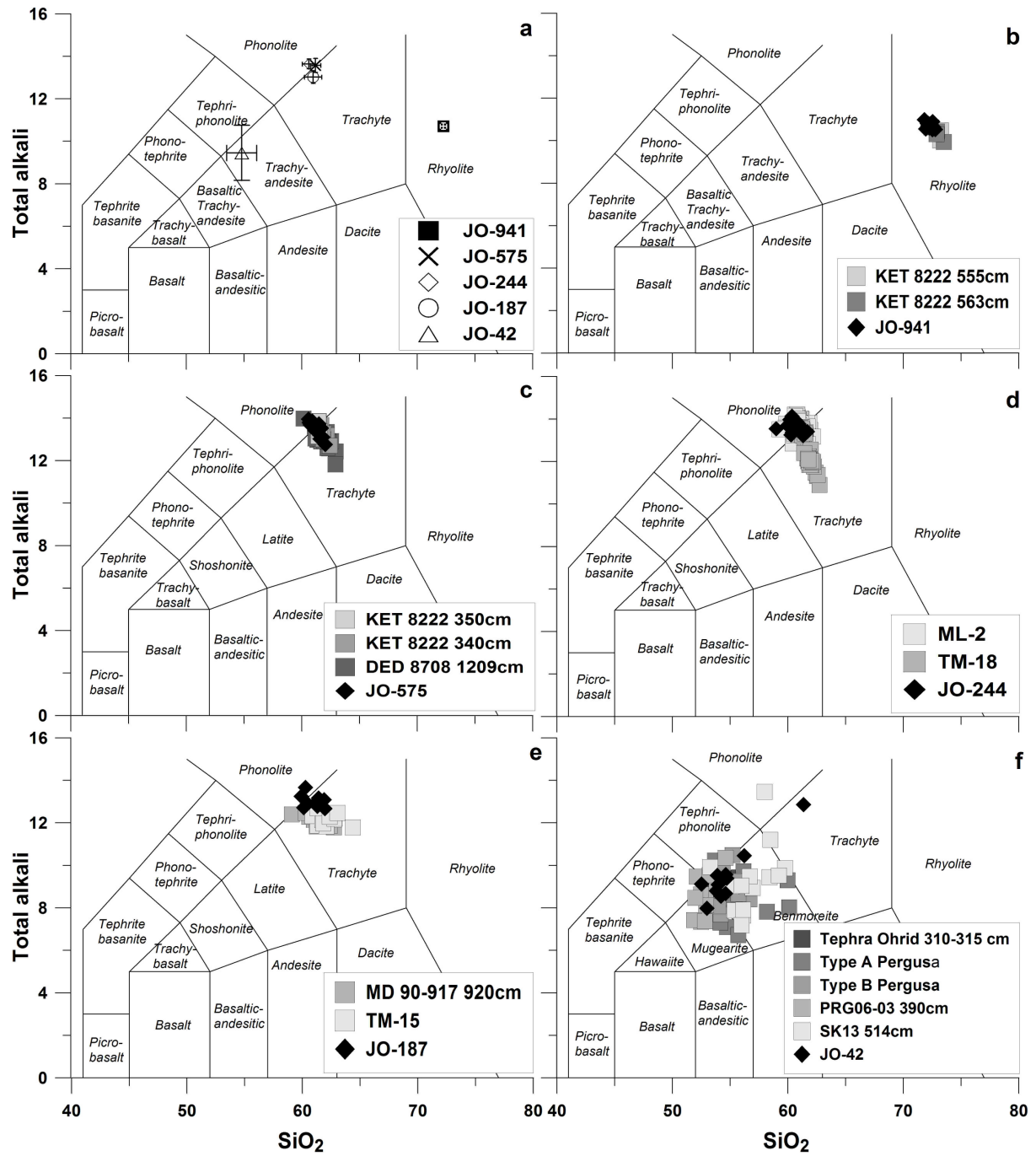


Figure 4

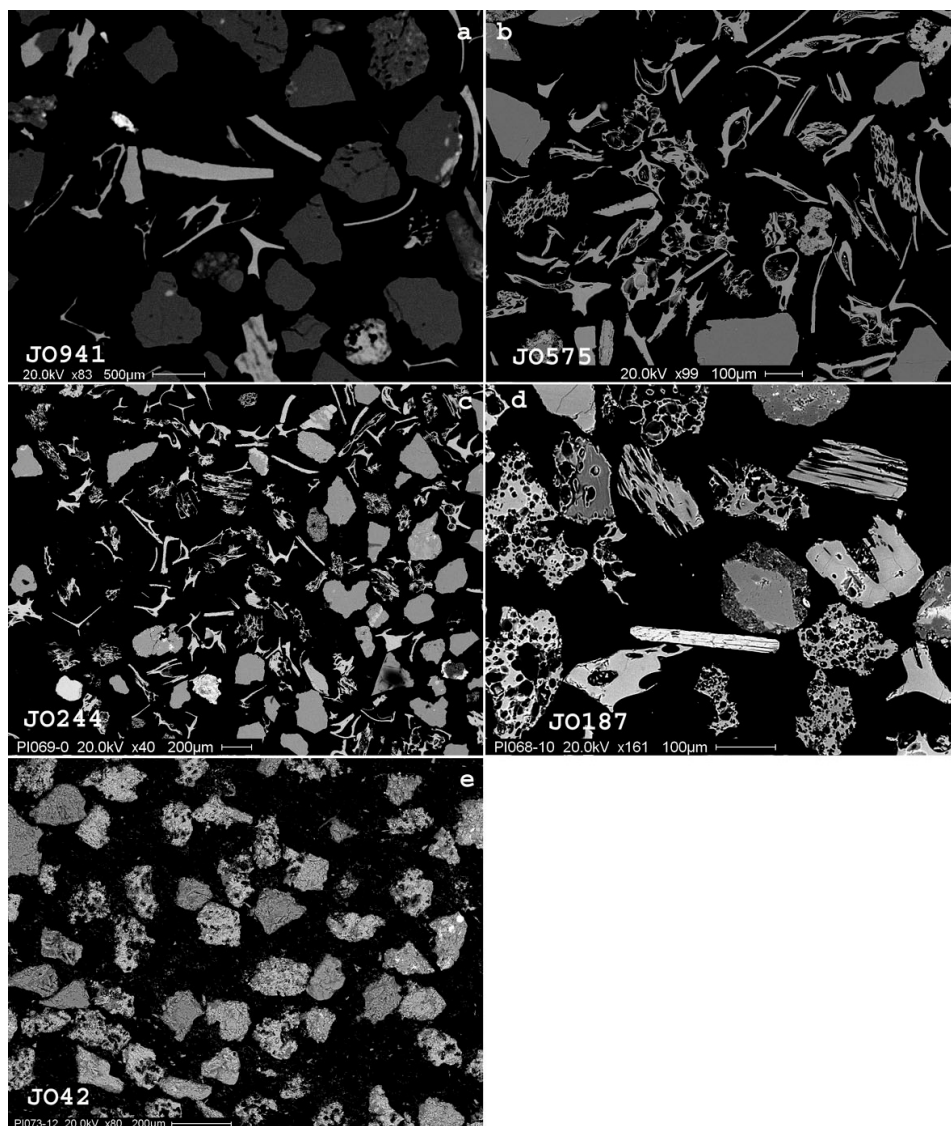


Figure 5

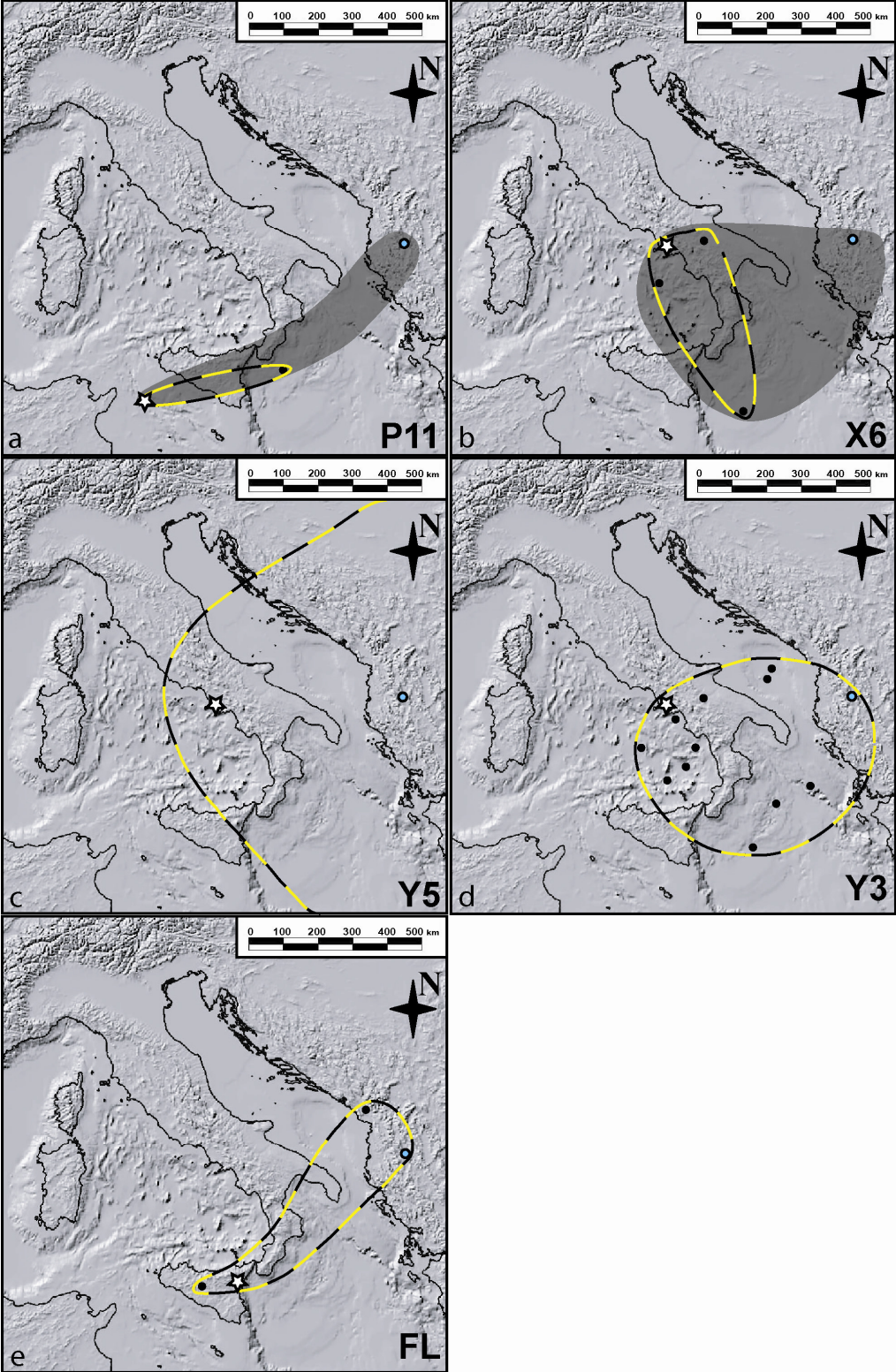


Figure 6

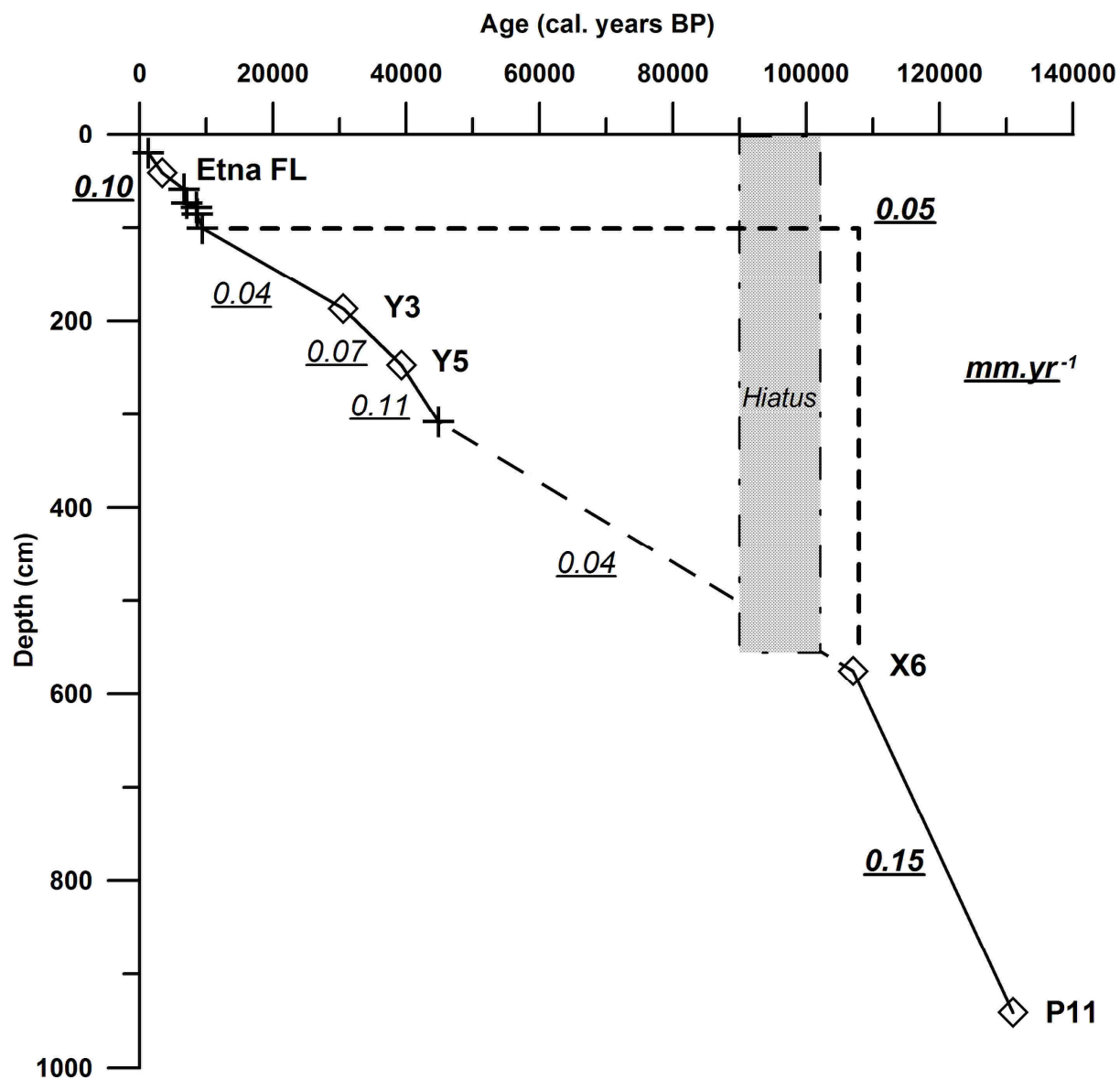


Table 1

JO941	SiO ₂	TiO ₂	Al ₂ O ₃	FeO _{tot}	MnO	MgO	CaO	Na ₂ O	K ₂ O	P ₂ O ₅	ClO	Total	Total Alkali
JO941-1	71.81	0.50	8.37	6.89	0.37	0.00	0.32	6.63	4.36	0.00	0.76	100.01	10.99
JO941-2	72.30	0.44	8.55	6.79	0.25	0.11	0.19	6.35	4.43	0.00	0.61	100.02	10.78
JO941-3	72.13	0.51	8.34	6.83	0.39	0.00	0.29	6.49	4.34	0.00	0.68	100.00	10.83
JO941-4	72.52	0.32	8.63	6.69	0.24	0.80	0.34	5.93	4.59	0.00	0.66	100.72	10.52
JO941-5	72.53	0.23	8.54	6.67	0.16	0.00	0.23	6.53	4.37	0.00	0.75	100.01	10.90
JO941-6	71.93	0.45	8.49	6.97	0.49	0.12	0.31	6.30	4.25	0.00	0.69	100.00	10.55
JO941-7	72.77	0.29	8.60	6.72	0.20	0.00	0.21	6.16	4.37	0.00	0.67	99.99	10.53
JO941-8	72.30	0.35	8.62	6.83	0.23	0.08	0.22	6.41	4.29	0.00	0.67	100.00	10.70
JO941-9	72.07	0.27	8.61	6.91	0.23	0.10	0.32	6.44	4.37	0.00	0.68	100.00	10.81
JO941-10	72.24	0.32	8.53	6.85	0.38	0.00	0.32	6.18	4.42	0.00	0.76	100.00	10.60
JO941-11	72.30	0.45	8.54	6.64	0.26	0.10	0.36	6.21	4.50	0.00	0.64	100.00	10.71
JO941-12	72.61	0.17	8.68	6.63	0.18	0.00	0.34	6.33	4.32	0.00	0.74	100.00	10.65
JO941-13	72.11	0.49	8.57	6.81	0.34	0.04	0.26	6.28	4.42	0.00	0.68	100.00	10.70
Mean	72.28	0.37	8.54	6.79	0.29	0.10	0.29	6.33	4.39	0.00	0.69	-	10.71
Sd	0.28	0.11	0.10	0.11	0.10	0.21	0.06	0.18	0.09	0.00	0.05	-	-

JO575	SiO ₂	TiO ₂	Al ₂ O ₃	FeO _{tot}	MnO	MgO	CaO	Na ₂ O	K ₂ O	P ₂ O ₅	ClO	Total	Total Alkali
JO575-1	60.59	0.53	18.42	3.24	0.39	0.27	1.78	7.29	6.66	0.00	0.82	99.99	13.95
JO575-2	61.01	0.59	18.86	2.85	0.31	0.38	1.54	6.82	6.93	0.00	0.71	100.00	13.75
JO575-3	60.90	0.44	18.46	3.13	0.20	0.31	1.84	7.08	6.76	0.00	0.87	99.99	13.84
JO575-4	60.90	0.46	18.84	2.93	0.21	0.26	1.68	7.28	6.57	0.00	0.88	100.01	13.85
JO575-5	60.71	0.50	18.63	3.08	0.40	0.47	1.63	6.85	6.94	0.00	0.78	99.99	13.79
JO575-6	61.69	0.50	18.53	2.78	0.23	0.46	1.69	5.80	7.74	0.00	0.57	99.99	13.54
JO575-7	61.48	0.36	18.74	2.80	0.13	0.36	1.84	5.62	8.11	0.00	0.57	100.01	13.73
JO575-8	61.16	0.46	18.69	3.00	0.30	0.30	1.65	6.86	6.85	0.00	0.73	100.00	13.71
JO575-9	60.69	0.61	18.54	3.21	0.40	0.39	1.59	7.20	6.56	0.00	0.81	100.00	13.76
JO575-10	61.67	0.43	18.64	2.93	0.30	0.50	1.59	6.02	7.49	0.00	0.44	100.01	13.51
JO575-11	61.68	0.64	18.79	2.82	0.42	0.35	1.50	6.33	6.81	0.00	0.65	99.99	13.14
JO575-12	61.13	0.50	18.90	3.10	0.38	0.30	1.51	6.70	6.73	0.00	0.75	100.00	13.43
JO575-13	61.83	0.52	18.69	2.95	0.27	0.43	1.56	5.56	7.54	0.00	0.64	99.99	13.10
JO575-14	61.58	0.49	19.07	2.69	0.28	0.52	1.76	5.53	7.49	0.00	0.59	100.00	13.02
JO575-15	61.11	0.37	18.85	3.00	0.24	0.43	1.59	6.73	6.87	0.00	0.80	99.99	13.60
JO575-16	60.65	0.46	18.74	3.13	0.36	0.30	1.70	7.22	6.58	0.00	0.85	99.99	13.80
JO575-17	60.73	0.35	18.92	3.02	0.34	0.35	1.73	7.08	6.60	0.00	0.88	100.00	13.68
JO575-18	61.43	0.36	18.66	2.87	0.20	0.46	1.74	6.00	7.70	0.00	0.57	99.99	13.70
JO575-19	62.04	0.38	18.96	2.86	0.24	0.42	1.61	5.87	6.89	0.00	0.73	100.00	12.76
JO575-20	60.92	0.41	18.87	3.09	0.20	0.38	1.45	6.96	6.89	0.00	0.82	99.99	13.85
Mean	61.20	0.47	18.74	2.97	0.29	0.38	1.65	6.54	7.04	0.00	0.72	-	13.58
Sd	0.45	0.08	0.17	0.15	0.08	0.08	0.11	0.63	0.46	0.00	0.13	-	-

	SiO ₂	TiO ₂	Al ₂ O ₃	FeO _{tot}	MnO	MgO	CaO	Na ₂ O	K ₂ O	P ₂ O ₅	ClO	Total	Total Alkali
JO244	60.87	0.46	19.19	2.97	0.20	0.38	1.59	6.62	7.08	0.00	0.65	100.01	13.70
JO244-1	61.16	0.33	19.08	2.93	0.20	0.34	1.81	5.98	7.49	0.00	0.68	100.00	13.47
JO244-2	60.68	0.42	19.04	2.94	0.21	0.38	1.88	6.25	7.51	0.00	0.68	99.99	13.76
JO244-3	60.60	0.52	19.17	2.85	0.25	0.35	1.69	6.53	7.24	0.00	0.80	100.00	13.77
JO244-4	60.57	0.51	19.11	2.90	0.31	0.51	1.68	6.58	7.17	0.00	0.65	99.99	13.75
JO244-5	59.96	0.36	19.47	3.14	0.23	0.40	1.92	6.10	7.60	0.00	0.82	100.00	13.70
JO244-6	61.00	0.38	19.10	2.86	0.18	0.28	1.78	6.48	7.22	0.00	0.71	99.99	13.70
JO244-7	60.62	0.55	19.09	2.99	0.26	0.47	1.75	6.37	7.31	0.00	0.61	100.02	13.68
JO244-8	60.34	0.37	19.84	2.97	0.20	0.40	1.73	6.21	7.28	0.00	0.66	100.00	13.49
JO244-9	61.67	0.44	19.08	2.65	0.15	0.36	1.68	6.07	7.34	0.00	0.58	100.02	13.41
JO244-10	58.97	0.45	19.68	3.48	0.07	0.80	2.60	5.08	8.46	0.00	0.41	100.00	13.54
JO244-11	60.93	0.36	19.00	2.99	0.21	0.22	1.73	6.42	7.35	0.00	0.79	100.00	13.77
JO244-12	60.86	0.45	19.08	2.87	0.21	0.32	1.70	6.37	7.39	0.00	0.75	100.00	13.76
JO244-13	60.78	0.45	18.97	2.93	0.19	0.42	1.80	6.33	7.39	0.00	0.75	100.01	13.72
JO244-14	61.31	0.26	19.25	2.92	0.19	0.34	1.80	5.65	7.57	0.00	0.71	100.00	13.22
JO244-15	60.16	0.49	19.13	2.98	0.28	0.42	1.87	6.13	7.84	0.00	0.71	100.01	13.97
JO244-16	60.76	0.29	18.94	2.96	0.28	0.37	1.83	6.39	7.49	0.00	0.70	100.01	13.88
JO244-18	60.35	0.46	18.97	2.97	0.20	0.40	1.72	6.31	7.82	0.00	0.81	100.01	14.13
JO244-19	60.64	0.42	19.18	2.96	0.21	0.40	1.81	6.22	7.48	0.00	0.69	-	13.69
Mean	0.58	0.08	0.25	0.16	0.05	0.12	0.21	0.37	0.32	0.00	0.10	-	-
Sd													
JO244-17	60.26	0.38	18.80	3.33	0.07	0.96	2.66	3.34	9.92	0.00	0.30	100.02	13.26
JO244-20	60.38	0.28	19.14	3.24	0.00	0.69	2.60	3.15	10.22	0.00	0.30	100.00	13.37
Mean	60.32	0.33	18.97	3.29	0.04	0.83	2.63	3.25	10.07	0.00	0.30	-	13.66
Sd	0.08	0.07	0.24	0.06	0.05	0.19	0.04	0.73	0.21	0.00	0.00	-	-
JO188	61.22	0.42	18.77	3.18	0.11	0.67	2.26	3.62	9.39	0.00	0.36	100.00	13.01
JO188-1	60.43	0.52	18.89	3.40	0.09	0.77	2.63	3.44	9.48	0.00	0.35	100.00	12.92
JO188-2	60.11	0.49	18.71	3.74	0.12	0.93	2.87	3.13	9.59	0.00	0.31	100.00	12.72
JO188-3	61.30	0.33	18.70	3.31	0.06	0.69	2.49	2.96	9.82	0.00	0.33	99.99	12.78
JO188-4	60.25	0.50	18.85	3.27	0.28	0.64	2.03	4.32	9.35	0.00	0.51	100.00	13.67
JO188-5	61.88	0.31	18.53	2.90	0.12	0.47	2.22	3.83	9.26	0.00	0.49	100.01	13.09
JO188-6	59.89	0.53	18.75	3.64	0.10	0.87	2.63	2.95	10.30	0.00	0.35	100.01	13.25
JO188-7	61.40	0.35	18.68	3.07	0.17	0.42	2.16	4.38	8.79	0.00	0.59	100.01	13.17
JO188-8	61.47	0.32	18.70	3.09	0.00	0.72	2.32	3.53	9.42	0.00	0.44	100.01	12.95
JO188-9	61.94	0.26	18.81	2.98	0.06	0.64	2.19	3.77	8.90	0.00	0.44	99.99	12.67
JO188-10	60.99	0.40	18.74	3.26	0.11	0.68	2.38	3.59	9.43	0.00	0.42	-	13.02
Mean	0.75	0.10	0.70	0.27	0.07	0.16	0.26	0.50	0.43	0.00	0.09	-	-
Sd													

JO42	SiO ₂	TiO ₂	Al ₂ O ₃	FeO _{tot}	MnO	MgO	CaO	Na ₂ O	K ₂ O	P ₂ O ₅	ClO	Total	Total Alkali
JO42-1	52.98	1.79	17.85	8.38	0.25	3.27	6.79	5.30	2.68	0.38	0.33	100.00	7.98
JO42-2	54.60	1.63	18.10	7.39	0.22	2.39	6.14	5.65	3.03	0.51	0.31	99.97	8.68
JO42-3	53.79	1.67	17.76	8.52	0.00	2.72	5.90	5.57	3.23	0.51	0.32	99.99	8.80
JO42-4	54.69	1.86	18.00	7.45	0.28	2.03	5.45	5.72	3.67	0.54	0.30	99.99	9.39
JO42-5	53.96	1.70	17.41	7.92	0.14	2.99	6.05	5.94	3.15	0.44	0.31	100.01	9.09
JO42-7	52.51	2.23	16.55	9.77	0.25	2.84	5.86	5.18	3.94	0.54	0.33	100.00	9.12
JO42-8	53.88	1.83	17.81	8.41	0.09	2.57	5.24	5.97	3.56	0.38	0.26	100.00	9.53
JO42-9	61.35	0.53	18.75	3.06	0.24	0.54	2.18	3.96	8.90	0.00	0.49	100.00	12.86
JO42-11	54.20	1.84	17.05	8.13	0.24	2.98	6.23	5.23	3.32	0.51	0.27	100.00	8.55
JO42-12	56.22	1.50	19.13	5.45	0.09	1.12	5.24	6.53	3.93	0.44	0.34	99.99	10.46
JO42-13	54.61	1.86	17.53	7.68	0.18	2.38	5.28	5.67	3.89	0.57	0.35	100.00	9.56
Mean	54.80	1.68	17.81	7.47	0.18	2.35	5.49	5.52	3.94	0.44	0.33	-	9.46
Sd	2.38	0.42	0.72	1.80	0.09	0.83	1.20	0.65	1.70	0.16	0.06	-	-

Table 2

	SiO ₂	TiO ₂	Al ₂ O ₃	FeO _{tot}	MnO	MgO	CaO	Na ₂ O	K ₂ O	P ₂ O ₅	SO ₃	ClO	F	Total Alkali
KET 8222 563cm	73.09	0.39	8.88	7.05	-	0.09	0.27	5.81	4.42	-	-	-	-	10.23
n=13	<i>sd</i> 0.36	0.08	0.13	0.12	-	0.06	0.11	0.37	0.16	-	-	-	-	-
KET 8222 555cm	72.95	0.31	8.89	7.23	-	0.05	0.20	5.90	4.48	-	-	-	-	10.38
n=13	<i>sd</i> 0.47	0.05	0.05	0.33	-	0.03	0.04	0.36	0.10	-	-	-	-	-
KET 8222 765cm	72.97	0.50	9.02	7.34	-	0.10	0.20	5.44	4.42	-	-	-	-	9.86
n=13	<i>sd</i> 0.49	0.06	0.16	0.28	-	0.07	0.02	0.30	0.06	-	-	-	-	-
KET8222 350cm	61.47	0.52	19.20	3.20	-	0.40	1.66	6.27	7.30	-	-	-	-	13.56
n=11	<i>sd</i> 0.06	0.04	0.10	0.22	-	0.06	0.10	0.53	0.77	-	-	-	-	-
KET8222 340cm	61.98	0.47	19.18	3.06	-	0.42	1.70	6.08	7.11	-	-	-	-	13.19
n=14	<i>sd</i> 0.27	0.10	0.13	0.15	-	0.09	0.10	0.68	0.46	-	-	-	-	-
DED 8708 1209cm	61.81	0.48	18.18	3.04	0.33	0.31	1.71	5.72	7.29	0.02	0.11	0.97	-	13.02
n=19	<i>sd</i> 0.68	0.10	0.31	0.23	0.12	0.07	0.32	0.91	0.86	0.04	0.08	0.28	-	-
TM-18	61.69	0.42	19.11	2.93	0.24	0.35	1.73	5.66	6.83	0.05	-	0.78	0.19	12.49
n=43	<i>sd</i> 0.46	0.02	0.21	0.09	0.02	0.02	0.07	0.71	0.29	0.03	-	0.05	0.17	-
ML-2	61.01	0.48	18.18	3.02	0.21	0.44	2.12	5.64	8.05	0.07	-	0.71	-	13.70
n=105	<i>sd</i> 0.42	0.04	0.19	0.21	0.06	0.15	0.32	1.21	1.02	0.04	-	0.20	-	-
TM-15	62.22	0.38	18.36	3.27	0.13	0.61	2.19	3.85	8.36	0.12	-	0.52	0.00	12.21
n=20	<i>sd</i> 0.78	0.03	0.21	0.29	0.04	0.15	0.22	0.44	0.55	0.06	-	0.11	0.00	-
MD90-917 920cm	61.41	0.36	18.72	3.17	0.08	0.70	2.44	3.52	9.14	-	-	0.44	-	12.66
n=20	<i>sd</i> 0.86	0.12	0.17	0.38	0.08	0.21	0.33	0.40	0.40	-	-	0.09	-	-
SK13 514cm	56.81	1.21	20.52	4.86	0.09	1.38	5.27	6.22	3.10	0.24	-	0.30	-	9.32
n=14	<i>sd</i> 1.78	0.44	2.39	2.49	0.09	1.27	1.83	1.04	1.26	0.22	-	0.11	-	-
Tephra Ohrid 310-315 cm	54.25	1.76	17.48	8.15	0.00	2.85	6.02	5.40	3.29	0.48	-	0.31	-	8.69
n=15	<i>sd</i> 0.73	0.22	0.51	0.53	0.00	0.33	0.50	0.41	0.34	0.10	-	0.06	-	-
PRG06-03 390 cm	52.82	2.04	16.86	9.43	0.23	3.21	6.13	4.99	3.58	0.47	-	0.24	-	8.57
n=11	<i>sd</i> 0.82	0.17	0.47	0.90	0.10	0.42	1.03	0.37	0.67	0.07	-	0.06	-	-
Type A Pergusa	55.61	1.58	16.97	7.25	0.15	3.98	5.62	6.02	2.37	-	-	0.46	-	8.39
n=14	<i>sd</i> 2.28	0.20	0.78	1.35	0.09	0.57	0.95	1.13	0.34	-	-	0.09	-	-
Type B Pergusa	54.91	1.61	17.65	6.83	0.15	3.90	5.65	5.79	3.06	-	-	0.45	-	8.86
n=11	<i>sd</i> 0.91	0.23	0.49	1.16	0.09	0.47	1.04	0.88	0.25	-	-	0.43	-	-

Table 3

Laboratory number (Artemis-Saclay)	Sample	Mean composite Depth (cm)	¹⁴ C age	error	age cal	final	erreur 1 s	Methods
SacA 8010	JO2004-1A020	20.5	1285	30	1253		30	intcal04 Reimer et al., 2004
SacA 8011	JO2004-1A059	59.5	5840	35	6680		66	intcal04 Reimer et al., 2004
2653	JO2004-1A074	74	6130	80	7048		156	intcal04 Reimer et al., 2004
2654	JO2004-1A078	78.5	7800	80	8550		139	intcal04 Reimer et al., 2004
SacA 8012	JO2004-1A085	85.5	7850	40	8622		52	intcal04 Reimer et al., 2004
SacA 8013	JO2004-1A100	100.5	8275	40	9407		121	intcal04 Reimer et al., 2004
2655	JO2004-1B113	307.6	39100	1200	44812		1055	Bard et al., 1998



V. Chapter V: Late Pleistocene-Holocene tephrostratigraphic record from the Ionian Sea: insights for the explosive activity of Italian volcanoes.

Here, we propose a detailed tephrostratigraphical study for the last 22 ka of the Ionian Sea core MD 90-918, which was recovered during the PROMETE II cruise of the French N/O Marion Dufrense in 1990.

The core was selected with the aim to fill a gap in the geographic distribution of available tephrostratigraphic and tephrochronologic data, which are very few in the north Ionian sea. The study was carried out using a multidisciplinary approach, which includes glass geochemistry, ^{14}C datings, stable isotope and rock magnetism.

Eight tephra layers were recognised, which encompass the last 22 ky. Three of them were related to the activity of Lipari Island (Monte Guardia, Gabelotto-Fiumebianco and Monte Pilato), while the other five are from the activity of Somma-Vesuvius. In particular, two of them were related to the Mercato eruption, while the other three testify for the existence of an interplian activity between the eruptions of Mercato and Avellino. The manuscript derived from this study will be submitted to *Marine Geology*.

Late Pleistocene-Holocene tephrostratigraphic record from the Ionian Sea: insights for the explosive activity of Italian volcanoes.

**Caron B.^{1,2*}, Siani G.², Sulpizio R.³, Zanchetta G.^{1,4,5},
Paterne M.⁶, Santacroce R.¹, Tema E.⁷, Zanella E.⁷**

¹*Dipartimento di Scienze della Terra, Via S. Maria 53, 56126 Pisa, Italy*

²*IDES-UMR 8148 CNRS-Université Paris-Sud XI, 91405 Orsay, France*

³*CIRISIVU, c/o Dipartimento Geomineralogico, via Orabona 4, 70125, Bari, Italy*

⁴*IGG-CNR Via Moruzzi, 1, 56100, Pisa, Italy*

⁵*INGV-Pisa, Via della Faggiola, 32, 56126 Pisa, Italy*

⁶*Laboratoire des Sciences du Climat et de l'Environnement, Laboratoire Mixte CEA-CNRS-UVSQ, Avenue de la Terrasse 91198 Gif-sur-Yvette Cedex, France*

⁷*Dipartimento di Scienze della Terra, Via Valperga Caluso 35, 10125 Torino, Italy*

* Corresponding author: Benoît Caron, Dipartimento di Scienze della Terra, via S. Maria 53, 56126, Pisa, Italy, tel.: +39 050 22 15 700, fax: +39 050 22 15 800, caron@dst.unipi.it ;
IDES-UMR 8148 CNRS-Université Paris-Sud XI, 91405 Orsay, France.

Abstract

A detailed tephrostratigraphy study supported by AMS ^{14}C datings, stable isotope ($\delta^{18}\text{O}$) analyses, geochemistry and rock magnetic data, has been carried out for a deep-sea core collected from the northern Ionian Sea. Eight tephra layers were recognised, all originated from explosive eruptions of southern Italian volcanoes. These tephra layers are correlated with terrestrial proximal counterparts and with both marine and lacustrine tephra layers already known in the central Mediterranean area. The oldest tephra is tentatively correlated to the Monte Guardia eruption (ca 22 ka BP, Lipari Island). Two other tephra layers are from Lipari island: Gabelotto-Fiumebianco/E-1 (8400 ± 22 cal yr BP) which is located close to the interruption of Sapropel S1 deposit, and the Monte Pilato (A.D. 1200) close to the top of the core. The Na-phonolitic composition of the other five recognised tephra layers indicates the Somma-Vesuvius as the source. The composition is quite homogeneous among the five tephra layers, and fits that of the Mercato proximal deposits (8890 ± 90 cal yr BP). Beyond the striking chemical similarity with the Mercato eruption, the recognised tephra layers spans over ca. 2000 years, and this prevents the correlation of all the tephra layers with a single Plinian eruption. Therefore, three of these tephra layers were assigned to an interplinian activity of Somma-Vesuvius between the eruptions of Mercato and Avellino, which is poorly constrained in the proximal area.

These data allow a significant update of the knowledge of the volcanic ash dispersal from Lipari and Somma-Vesuvius volcanoes.

Keywords: tephrochronology, Ionian Sea, Somma-Vesuvius, Mercato, Lipari, Gabelotto-Fiumebianco/E-1, Monte Pilato, Monte Guardia

V.1. Introduction

Pyroclastic particles can be transported over very long distances and deposited thousands of kilometers far from their sources, blanketing the landscape with thin tephra deposits. Centimeter to millimeter-thick loose ash deposits can be easily eroded by wind and rain, but in some cases they can also be preserved, under special sedimentary conditions like rapid burying and/or deposition in quiet environments with low-energy sedimentation dynamics. These deposits are commonly recognised in marine and lacustrine cores and represent a powerful tool for research on both Quaternary sciences and volcanology (e.g. *Keller et al., 1978; Sigurdsson et al., 1980; Paterne et al., 1990, 2008; Wulf et al., 2004, 2008; Le Friant et al., 2008; Giaccio et al., 2009; Zanchetta et al., 2010*).

During the last thirty years, tephrostratigraphic studies in the Mediterranean area have allowed the investigation and the reconstruction of the explosive activity of the Mediterranean volcanoes (e.g. *Keller et al., 1978; Paterne et al., 1988, 1990, 2008; Narcisi et al., 1996; Siani et al., 2004; Wulf et al., 2004, 2008; Lowe et al., 2007; Margari et al., 2007; Sulpizio et al., 2008*) and furnished support to paleoclimatic and paleoceanographic researches (e.g. *Fontugne et al., 1989; Kallel et al., 2000; Siani et al., 2001*). Magnetic measurements have also been successfully used in different environmental settings to identify and correlate tephra layers (*Oldfield et al., 1980; Andrews et al., 2002; Rousse et al., 2006; Peters et al., 2009*). Rock magnetic properties highly depend on the concentration, grain size and composition of the magnetic carriers in the sediments and can thus be further used for studying paleoceanographic and paleoclimatic changes (*Thompson and Oldfield, 1986; Verosub and Roberts, 1995*).

The Tyrrhenian, Adriatic and Ionian seas are the best studied basins of the Mediterranean area because of prevailing seasonal wind directions that mainly dispersed ash particles to the east and southeast (*Keller et al., 1978; Paterne et al., 1986, 2008; Siani et al., 2001, 2004*). However, the inspection of the location of the published cores shows an evident lacuna in the north part of the Ionian Sea, which creates a gap in the tephrostratigraphic network among the different marine basins and continental archives. In order to fill this lacuna, the deep-sea core MD 90-918 (**Figure 1**) has been selected for detailed studies, which include tephrostratigraphy, oxygen isotopes and rock magnetism. The MD 90-918 core is located in the northern part of the Ionian Sea, downwind of the Aeolian Islands, Etna and

Neapolitan volcanoes (Somma-Vesuvius, Campi Flegrei and Ischia Island). The tephrostratigraphic record of the MD 90-918 core, joined with high resolution isotopic studies, allowed its correlation with existing Adriatic (e.g. *Calanchi et al., 1998; Siani et al., 2004; Lowe et al., 2007*), Ionian (e.g. *Keller et al., 1978; Paterne et al., 1988; Fontugne et al., 1989*) and Tyrrhenian cores (*Kallel et al., 1997, 2000; Turney et al., 2004*).

V.2. Material and analytical methods

The core MD 90-918 was recovered in the Ionian Sea (39° 35,64 N, 18° 5 0,43 E; 695 m water depth, 14.77 m core length; **Figure 1**) during the 1990 PROMETE II cruise of the French N/O Marion Dufresne.

Grey to brown mud dominates the core lithology. Two dark-grey layers occur in the upper part of the core (between 204 and 231 cm depth), which represent the two parts of the Sapropel S1 (i.e. S1a and S1b) separated by a thin horizon of white hemipelagic ooze between 219 and 210 cm (**Figure 2**). These layers were deposited during the most recent period of stagnation in the East Mediterranean Sea (*Kallel et al., 1997; Mercone et al., 2000*). In addition, in the Sapropel deposits (223 cm depth) a white 2 mm thick tephra layer is visible at naked-eye. A 20 cm thick sandy layer is visible at naked-eye inspection at 992 cm (**Figure 2**), representing a turbidite deposit.

V.2.1. Tephrostratigraphy and chemical analysis

The core MD 90-918 was sampled at 5 cm interval for its entire length, with the exception of the Sapropel deposit (between 203 and 231 cm) that was sampled at 1 cm interval. Each sample was washed and sieved at 40 µm, and after at least 400 grains were counted under a stereo-microscope. Tephra layers were identified by the relative abundance of volcanic glass shards with respect to other sediments (*Fretzdorff et al., 2000*). The abundance curve of the volcanic glass allows the identification of peaks which correspond to phases of tephra deposition (**Figure 2**). Volcanic glass occurs throughout the core, and forms a background at about 4-5% of abundance for the 323 counted samples (**Figure 2**). In order to

avoid analyses of samples from the background, only abundance peaks larger than 9% were considered as representative of tephra deposition. Therefore it was assumed that the tephra layer localisation corresponds at the depth of maximum abundance of glass shards. Glass shards or micropumice fragments were morphologically and lithologically described under stereo-microscope, then hand-picked and mounted on epoxy resin beads and polished.

Two different facilities were used to analyse the major element composition of micropumice or glass shard. The first is the CAMECA-SX 100 Electron Probe Micro-Analyser (EPMA-CAMPARIS) available at Jussieu (Paris, France). Analyses were performed with an acceleration voltage of 15 kV and a beam current of 4 nÅ. Usually, analytical data show closures > 97 wt. %, which indicate a good preservation of the original composition of the analysed glass.

The second facility is the Philips SEM 515 equipped with an EDAX-DX micro-analyser available at Dipartimento di Scienze della Terra (University of Pisa). Operating conditions are 20 kV acceleration voltage, 100 s live time counting, 1 nÅ beam current, $\approx 500 \mu\text{m}$ beam diameter, 2100 shots per second, ZAF correction). The ZAF correction procedure does not include natural or synthetic standards for reference, and requires the analyses normalization at a given value (which is chosen at 100 %).

Ninety-nine analyses from 5 different tephra layers were performed on both instruments and compared to obtain instrumental calibration (**Table 1**).

The variance of analytical precision between the two instruments was calculated using the mean of the analyses from the 5 tephra layers. The geochemical compositions of these 5 tephra layers are rhyolitic or phonolitic. This difference of composition has not incidence on the variance between both instruments.

- The variance of the EDS relatively to the WDS is (**Table 1**):

- 1) 0.68 % for the SiO_2 (abundance > 59 wt. %),
- 2) 2.80 % for the Al_2O_3 (abundance between 13 and 22 wt. %),
- 3) between 1.7 and 2.7 % for Na_2O , K_2O , FeO_{tot} and CaO (abundance between 1 and 9 wt. %),
- 4) 10.73 % for ClO (abundance ca. 0.4 wt. %)
- 5) 13 %, 18 % and 74 % for TiO_2 , MnO and MgO , respectively (abundance close to the detection limit of both instruments)

Variance was not calculated for the P_2O_5 , which is under the detection limit of the EDS

The intercalibration shows the full compatibility of the EDS and WDS microanalytical facilities from DST Pisa and CAMPARIS Paris.

The different tephra layers were classified using the Total Alkali vs. Silica diagram (TAS, [Le Bas et al., 1986](#); **Figure 3**).

V.2.2. Stable isotope analysis

Oxygen isotope measurements, expressed in ‰ versus VPDB (Vienna Pee Dee Belemnite standard) were obtained on the planktonic foraminifera *Globigerinoides ruber* sampled every 10 cm along the core MD 90-918. Between 6 to 10 shells were picked in the 250-315 µm size range. The samples were cleaned in a methanol ultrasonic bath during a few seconds then roasted under vacuum at 380°C for 45 minutes, prior to isotopic analyses. Analyses were performed at Laboratoire des Sciences du Climat et de l'Environnement (LSCE, Gif-sur-Yvette, France) on Finnigan Delta+ mass-spectrometers. VPDB is defined with respect to NBS19 and NBS18 carbonate standards ([Coplen, 1988](#)). The mean external reproducibility (1σ) of carbonate standards is $\pm 0.05\text{‰}$, measured NBS18 $\delta^{18}\text{O}$ is $-23.2 \pm 0.1\text{‰}$ VPDB.

V.2.3. Radiocarbon datings

The chronology of the core MD 90-918 is based on seven ^{14}C accelerator mass spectrometry (AMS) radiocarbon datings, which were performed at UMS-ARTEMIS (Pelletron 3MV) AMS facilities (CNRS-CEA Saclay, France). ^{14}C analyses were done with the standard procedure described by [Tisnérat-Laborde et al., \(2001\)](#) (**Table 2**). Ages were calibrated using INTCAL04 ([Reimer et al., 2004](#)) for ^{14}C ages younger than 26 cal ka BP and Calpal software for age older than 26 cal ka BP ([Weninger and Jöris, 2008](#)).

V.2.4. Magnetic sampling and measurements

A total of 539 samples were collected at ≈ 3 cm interval along the total core length (14.77 m), using plastic cubic boxes of standard size (2 x 2 x 2 cm). Measurements were carried out at the ALP palaeomagnetic laboratory (Peveagno, Italy). Magnetic susceptibility (k), natural remanent magnetization (NRM) and NRM demagnetized in alternating field (AF) at 25 mT peak-field (NRM_{25}) were first measured using a KLY-3 kappabridge and a 2G cryogenic magnetometer respectively. Remanence measurements routinely done in environmental magnetism studies were then performed:

- anhysteretic remanent magnetization was given by 0.1 mT bias field during AF demagnetization at 80 mT peak-field (ARM) and then AF demagnetized at 25 mT peak-field (ARM_{25});
- isothermal remanent magnetization close to saturation (SIRM) was given in 1 T field; the samples were then magnetized in opposite direction at 0.1 T ($\text{IRM}_{0.1\text{T}}$) and 0.3 ($\text{IRM}_{0.3\text{T}}$) and the corresponding S-ratios were calculated, $S_{0.1\text{T}} = \text{IRM}_{0.1\text{T}}/\text{SIRM}$ and $S_{0.3\text{T}} = \text{IRM}_{0.3\text{T}}/\text{SIRM}$;
- isothermal remanent magnetization (IRM) acquisition and back-field curves and Lowrie-Fuller tests (*Lowrie and Fuller, 1971*) were done on representative samples.

After completion of all measurements, the samples were let to dry and weighted in order to calculate mass susceptibility (χ). The mean water content was in the order of 40-50%.

V.3. Chronological framework

The age model of the core MD 90-918 is based on seven ^{14}C AMS datings (**Table 2**) and on comparison of oxygen isotope curve with that of the Adriatic Sea core MD 90-917 (*Siani et al., 2001, 2004*; **Figure 1**). In particular, four $\delta^{18}\text{O}$ isotopic peaks (320 cm, 420 cm, 540 cm and 590 cm) supplied confident inter-correlation between the two cores, and allowed the collation of the ^{14}C ages of the MD 90-917 core into the MD 90-918 one. Using the available ^{14}C datings the age model was constructed using linear interpolation between two consecutive ages (**Figure 2**). The resulting graph can be also read as a sedimentation curve, which shows two mains slopes indicating different sedimentation rates. The first slope (from the top to 470 cm depth) indicates a sedimentation rate of ca. 31 cm/ky, while the second slopes (from 470 cm to the base) has a sedimentation rate of ca. 94 cm/ky. The last value is

calculated excluding the thickness of the turbidite deposits (20 cm). The known ages of the correlated tephra layers were inserted into the age model in order to test its consistency.

Coupling the chronology and the isotope curve, it is evident how the last glacial/interglacial transition and the Holocene encompass the upper 1470 cm of the core, with a highly detailed record of the last glacial period. Two abrupt shifts toward depleted $\delta^{18}\text{O}$ values (between 590 cm and 500 cm and between 270 cm and 230 cm; Termination IA and IB; *Duplessy et al., 1981; Bard et al., 1987a, b*) mark the two-steps of the deglaciation and the Holocene (**Figure 2**).

V.4. Results

V.4.1. Rock-magnetism

Down-core logs of the magnetic parameters are shown in Fig. 3. Mass susceptibility shows a rather uniform value along all the core. As a whole, the curve suggests that the magnetic mineralogy varies little, both in magnetic grain concentration and mineral type. The only values lower than the mean occur around 220 cm and correspond to a thin horizon made of two Sapropel levels and the white hemipelagic ooze in between. Four distinct spikes occur at 73.5 cm, 771 cm, 887 cm and 982 cm. That at 982 cm is correlated to a turbiditic sandy layers, whereas the other three do not match any clear lithological characteristic. These results are substantiated by the NRM_{25} and the SIRM curves (**Figure 3a**).

The evenness of magnetic mineralogy also results from the IRM acquisition and back-field curves, which are substantially identical irrespective of the sample depth (**Figure 4**). Saturation is approached at fields of 0.3-0.4 T and remanent coercive force is around 50 mT. These values point to a low-coercivity mineral such as Ti-magnetite as the main, if not the only remanence. This observation is also supported by the down-core constant values of the $S_{0.3\text{T}}$ ratios (**Figure 3b**) that describe the relative contributions of high-coercive to low-coercive magnetic phases (*Thompson and Oldfield, 1986*). Their values are high, very close to 1 ($S_{0.3\text{T}} > 0.9$), confirming the presence of a low coercivity magnetite-type mineral that reach saturation at 0.3 T field (**Figure 4a and b**).

NRM, SIRM and ARM were all AF demagnetized up to 100 mT peak-field. IRM and ARM have similar coercivity distribution (**Figure 4 c and d**) while NRM look a little harder. Comparison of the three normalized intensity decay curves suggests pseudosingle-domain characteristics (*Lowrie and Fuller, 1971*).

Analysis of the ARM/k curve shows a large difference between the upper (0-400 cm) and lower (400 cm-bottom) parts. The upper part is characterized by higher values, which, due to the small variation of the susceptibility k , can only result from an ARM increase. Since mineralogy is rather uniform, the increase may be reasonably referred to prevalence of fine grain in the upper part of the core (*Alvisi and Vigliotti, 1996*), because finer magnetite grains have higher ARM values than the coarser ones. This interpretation is consistent with the $S_{-0.1T}$ curve, which too shows higher values in the upper 400 cm. These point to higher coercivity, which may again be referred to the smaller size of the grains. The systematic difference in granulometry might thus reflect different depositional environments.

The most prominent features in all curves (**Figure 3**) are the large swings which occur in between 203 and 231 cm, at the same depth of the Sapropel in the core, which consist of two levels (203-210 cm and 219-231 cm). Interpretation of the magnetic measurements is made difficult by the fact that four tephra layers occur within the same interval. We remark first that no one of the tephra layers found in the core does match a distinctive change in the magnetic properties. This is probably due to both their small thickness and high content in glass and micropumice. The swings in the NRM_{25}/ARM_{25} and ARM/k curves may be regarded as the result of an ARM intensity decrease, due to the occurrence of high-coercivity iron oxides, possibly of bacterial provenance (*Tarduno et al., 1998; Passier et al., 2001*), or the increase of the mean grain size, because fine grains are most affected by reductive environment (*Kruiver and Passier, 2001*), or both.

V.4.2. Tephra layers

Eight tephra layers were recognised along the MD 90-918 core (**Figure 2 and 5**). The identified tephra layers are not evenly spaced throughout the core, occurring at 2 cm, 175 cm, 185 cm, 210 cm, 218 cm, 223 cm, 230 cm, and 820 cm. In particular, tephra layers between 210 and 230 cm form a cluster with high abundance of volcanic glass (**Figure 6**). Only the

peak at 223 cm is visible at naked eye inspection, while the other peaks were identified through the high resolution counting.

2 cm

This cryptotephra has a glass abundance of about 17.5 %, and spans between 2 and 5 cm (**Figure 2**). It contains vitric glass shards with a glassy groundmass (**Figure 7a**), and mean grain size coarser than 100 μm . The vesicles are elongated to form fibrous glass shards. The composition is homogeneous rhyolitic (**Figure 5 and 8a; Table 3**).

175 cm

This cryptotephra has a glass abundance of about 14 % (**Figure 2**), and is composed by highly vesicular, aphyric, white micropumices. They have a grain size finer than 100 μm , and a glassy groundmass (**Figure 7b**). The glass composition is homogeneous Na-phonolitic (**Figure 5 and 8b; Table 3**).

185 cm

This cryptotephra has a glass abundance of about 16 % (**Figure 2**), and contains highly vesicular, aphyric white micropumice with mean grain size finer than 100 μm (**Figure 7c**). They have a glassy groundmass and a Na-phonolitic composition (**Figure 5 and 8b; Table 3**). Differently from the previous samples, the glass analyses show a double Na-phonolitic composition, with slight differences in the CaO, Na₂O, K₂O and SiO₂ contents (**Table 3**). These two compositions were labelled 185 cm-a and 185 cm-b (**Table 3**). The 185 cm composition is quite similar composition to the tephra 175 cm.

210 cm

The glass abundance of this cryptotephra is about 88 % (**Figure 6**). Inspection under stereo-microscope shows that ca. 90 % of the volcanic glass are white micropumice and the other 10 % vitric glass shards. The first ones have grain size finer than 100 μm , are highly vesicular and aphyric, with a glassy groundmass. The second ones have grain size finer than 50 μm , small rounded bubbles and aphyric, glassy groundmass (**Figure 7d**). The composition of micropumice fragments is homogeneous Na-phonolitic (**Figure 8b and c; Table 3**), very similar to the tephra at 175 cm and 185 cm. In turn, the glass shards have a homogeneous rhyolitic composition (**Figure 5; Table 3**).

218 cm

This cryptotephra is spread between 216 and 219 cm, with a maximum abundance value around 19 % centred at 218 cm (**Figure 6**). It contains transparent glass shards with a mean

grain size finer than 50 μm which are aphyric (**Figure 7e**) with small rounded bubbles. The glass composition is homogeneous and rhyolitic (**Figure 5 and 8c; Table 3**), and similar to that of the rhyolitic tephra at 210 cm.

223 cm

This tephra layer is 2 mm thick and contains 100 % of volcanic glass (**Figure 6**). It contains exclusively highly-vesicular micro-pumices with rounded bubbles with a glassy groundmass (**Figure 7f**). The glass composition is a Na-phonolitic composition (alkali ratio lower than 1), with high Al_2O_3 content (ca. 22 wt. %; **Figure 5 and 8b; Table 3**), and similar to the tephra at 175 cm, 185 cm and 210 cm.

230 cm

This cryptotephra corresponds to a peak of glass abundance of 9.7 % (**Figure 6**), and is composed by white, aphyric micro-pumice (**Figure 7g**) with main grain size around 50 μm . The micro-pumices are highly vesicular with a glassy groundmass. The glass has Na-phonolitic composition (alkali ratio lower than 1), with high Al_2O_3 content (ca. 22 wt. %; **Figure 5 and 8b; Table 3**), and similar to the tephra at 175 cm, 185 cm, 210 cm and 223 cm..

820 cm

This cryptotephra corresponds to a peak of glass abundance of 12 % (**Figure 2**), and is composed of vitric glass shards that commonly are coarser than 100 μm (**Figure 7h**). They have a glassy groundmass and rounded bubbles. The composition straddles between the trachytic and the rhyolitic fields (**Figure 5 and 8d; Table 3**). The alkali ratio is ca. 1.2 wt. %.

V.5. Discussion

The available ^{14}C ages indicate the core sediments are Late Pleistocene to Holocene in age, and this constrains the search for the source of parent eruptions of tephra layers to the explosive activity of Mediterranean volcanoes during this period.

The recognised tephra layers show both alkaline and calc-alkaline affinity. The alkaline samples have undersaturated glass compositions with alkali ratio around or below 1 (Na-phonolites; **Figure 8; Table 3**), and are younger than 9000 years (**Figure 2; Table 2**). The composition and geochemical affinity limit their sources to Italian volcanoes, since the sources in the Aegean area during the Holocene have calc-alkaline affinity (e.g. *Keller et al.*,

1990). Sources from Massif Central (France) and Anatolia (Turkey, eastern Mediterranean) can be rejected, because both volcanisms have K-alkaline affinity (Juvigné, 1987; Druitt *et al.*, 1995). Indeed, the only known source of Na-phonolites during Holocene is the Somma-Vesuvius, and, therefore, the geochemical data indicate it as the source for tephra layers at 175 cm, 185 cm, 210 cm, 223 cm and 230 cm. The geochemistry of Holocene explosive products of Somma-Vesuvius (Santacroce *et al.*, 2008) shows that Na-phonolitic tephra characterise only the eruption of the Pomici di Mercato (Santacroce, 1987; Aulinas *et al.*, 2008; Mele *et al.*, 2010), and the initial stages of the Pomici di Avellino eruption (white pumice, Santacroce, 1987; Cioni *et al.*, 2000; Sulpizio *et al.*, 2010a, b). Because the Pomici di Mercato and Pomici di Avellino (white pumice) products have very different crystal content (almost aphyric vs. porphyritic; Santacroce *et al.*, 2008), the glassy, aphyric tephra layers of the MD 90-918 core can be confidently correlated to the Pomici di Mercato eruption. This correlation is also in agreement with the ^{14}C age measurements of the phonolitic tephra at 230 cm and 210 cm (dated at 9005 ± 45 cal yr BP and 8343 ± 56 cal yr BP, respectively; **Table 2**), which are in good agreement with the recent age (8540 ± 50 cal yr BP) obtained from charcoals sampled in the basal deposits of the Pomici di Mercato eruption on Somma-Vesuvius slopes (Zanchetta *et al.*, 2010), and with the maximum age of 8890 ± 90 cal yrs BP suggested by Santacroce *et al.* (2008).

The other phonolitic tephra layers have ^{14}C ages significantly younger than that of proximal Pomici di Mercato deposits, and their correlation with this eruption poses some problems that require a more in depth discussion. The cryptotephra at 175 cm has an age of 6989 ± 57 cal yr BP (**Table 2**), that at 185 cm has an interpolated age of 7376 cal yr BP (between 8343 ± 56 cal yr BP and 6989 ± 57 cal yr BP), and that at 210 cm is dated at 8343 ± 56 cal yr BP.

On the basis of this chronology, the correlation to a single eruption is very hard, although the Mercato eruption was recently described as a long lasting, pulsating event (Mele *et al.*, 2009). Based on field evidences, a reasonable duration of the Mercato eruption can be assessed at some decades at maximum, but in any case not to millennia. This suggest that the three tephra layers at 175 cm, 185 cm and 210 cm are the distal deposits of an interplinian activity between the eruptions of Mercato and Avellino, whose proximal counterparts are poorly constrained in the Somma-Vesuvius stratigraphy (e.g. Santacroce and Sbrana, 2003; Cioni *et al.*, 2008; Santacroce *et al.*, 2008).

Tephra layers compositionally similar to the Mercato deposits were found in lacustrine (TM6b in the Lago Grande di Monticchio; *Wulf et al., 2004, 2008*; OT02-3 in Lake Ohrid; *Vogel et al., 2010*), and marine (KET 8218, KET 8216, Adriatic Sea; *Paterne et al., 1988*; this work) (**Table 4**). The recognition in core MD 90-918 enlarges its dispersal to the south east (**Figure 9**). The surface of dispersal ash area is estimated at 250,000 km².

Homogeneous rhyolitic tephra layers with calc-alkaline affinity occur three times at 218 cm, 210 cm, and 2 cm. The available ¹⁴C age measurements constrain their deposition between 9000 cal yr BP and about 600 cal yr BP (**Table 2**). During this period of time calc-alkaline tephra were generated by explosive activity of both Aegean arc (Greece, eastern Mediterranean) and Aeolian Islands volcanoes (southern Tyrrhenian Sea, central Mediterranean). The evolved magmas from these two sources are hardly distinguishable considering major elements and even trace elements (*Clift and Blusztajn, 1999*) and, therefore, to discriminate the source of tephra basing on geochemical data is a very difficult. However, a source in the Aegean Sea is poorly probable taking into account the prevailing winds in the area, which preferentially blow from west to east (*Barberi et al., 1990; Costa et al., 2009; Folch and Sulpizio, 2010*). The tephra layers at 210 cm and 218 cm are very close in space and time, since they are separated by 8 cm of sediments and have ages of 8343 ± 56 cal yr BP (210 cm; **Table 2**) and of 8608 cal yr BP (218 cm, linear interpolation between 9005 ± 42 cal yr BP and 8343 ± 56 cal yr BP; **Table 2**). Given their identical composition, it should be reasonable to assume they are produced from the same volcano. At this period time, (i.e. Early Holocene), only one rhyolitic tephra layer occurs in the central Mediterranean tephrostratigraphy, named E-1 (*Paterne et al., 1988; Fontugne et al., 1989; Figure 8; Table 4*), which was correlated to the eruption of Gabelotto-Fiumebianco from Lipari Island (*Siani et al., 2004; Zanchetta et al., 2010*). *Siani et al (2004)* dated this eruption at 7770 ± 70 ¹⁴C yr BP (8550 ± 80 cal yr BP) through ¹⁴C AMS measurements on foraminifera, an age in good agreement with those of tephra layers at 218 cm and 210 cm in core MD 90-918. Doubling of tephra layers due to reworking or bioturbation can be rejected on the basis of core lithology, isotopic curve and magnetic analyses. Therefore, the occurrence of two rhyolitic tephra layers compositionally similar to the Gabelotto-Fiumebianco/E-1 tephra indicates a double deposition spaced by a considerable interval of time. This occurrence may be related to a delayed deposition of the younger tephra layer, or being the result of a prolonged period of

activity that lasted tens to hundreds years. The first hypothesis seems poorly probable due to the location of the MD 90-918 core far from the continental shelf (**Figure 1**), and therefore poorly influenced by paroxistic flooding events that can firstly erode the tephra blanket on land and then discharge a large amount of volcanic sediments to the sea. The second hypothesis can be related to a long lasting period of explosive activity from the same volcanic source. In the Adriatic core MD 90-917, the rhyolitic tephra layers localised at 250 cm depth and 240 cm depth are correlated to Gabelotto-Fiumebianco/E-1 eruption (*Siani et al., 2004*). The second hypothesis is a reasonable assumption for the activity of Gabelotto-Fiumebianco eruption, whose proximal deposits constitute a pumice cone at the base of Monte Pilato cone on Lipari Island and were ascribed to intermediate intensity explosive activity dominated by pyroclastic density current emplacement (*Pichler, 1980; Cortese et al., 1986; Crisci et al., 1991*).

The recognition of Gabelotto-Fiumebianco/E-1 tephra layers in core MD 90-918 enlarges its dispersal area to the east (**Figure 9**). The surface of the dispersal ash area is estimated at ca. 300,000 km².

The third rhyolitic tephra layer occurs at the very top of the core (2-5 cm; **Figure 2**), and is dated at 615 ± 20 cal yr BP (**Table 2**). Age and composition suggest a correlation with the eruption of Monte Pilato from Lipari Island (**Figure 8a; Table 4**), recently dated by archeo-magnetism between A.D. 1030-1528 (*Zanella, 2006*) or at A.D. 1200-1240 (*Arrighi et al., 2006*). This is the first recognition of Monte Pilato tephra in deep-sea cores of the Mediterranean, and suggests a prevailing dispersal of ash to the East (**Figure 9**), but it is insufficient to estimate the dispersal ash area reliably.

The cryptotephra at 820 cm is trachy-rhyolitic in composition, and is dated at $19,391 \pm 110$ cal yr BP (**Table 2**). Taking into account age and composition a correlation to the eruption of Monte Guardia from Lipari Island is the most probable. This is because among the known eruptions with trachy-rhyolitic composition occurred around 20 ky BP, like those of the Lower Pollara (Salina Island, 24 ka, *Calanchi et al., 1993*), the Lentia cycle (Vulcano Island, 15-25 ka, *De Astis et al., 1997*), and the third and fourth cycles from Pantelleria Island (*Civetta et al., 1988*), it shows the best geochemical match (**Figure 8d; Table 4**). In particular, the 820 cm tephra can be correlated to the less evolved component of the Monte

Guardia eruption (MG4 base B sample; **Table 4**), which is characterised by an important geochemical variability due to pre- and syn-eruptive processes of magma mixing and mingling (*De Rosa et al., 2003*). The Monte Guardia eruption from Lipari Island has an age comprised between 22.4 ± 1.1 and 20.3 ± 0.7 ka (*Crisci et al., 1981, 1991; De Rosa and Sheridan, 1983*), which is in fairly good agreement with that of the 820 cm tephra.

The evolved products of the Monte Guardia eruption were recognised in the sediments of the Lago di Pergusa (central Sicily; **Figure 1**; *Narcisi, 2002*), and this suggest different dispersal areas for ash produced at different times during the eruption. This effect was already observed for products of long-lasting explosive eruptions, and mainly due to the complex dynamics of the lower atmosphere (*Sulpizio et al., 2008*). The first time recognition of Monte Guardia tephra in the Ionian Sea sediments enlarges the dispersal area to the East (**Figure 9**), but prevents estimating the dispersal ash area reliably.

V.6. Conclusions

In this study, 8 tephra layers were identified: five are from Somma-Vesuvius and three from Lipari volcano. For two of them (Monte Pilato and Monte Guardia eruptions) this is the first recognition in distal cores.

Tephra layers from Somma-Vesuvius are compositionally similar to the Mercato eruption, but three out of five are too young to be correlated to this eruption. They represent an interplinian activity occurred between the Mercato and Avellino Plinian eruptions, and whose proximal deposits are poorly constrained in the Somma-Vesuvius stratigraphy. These findings point out how distal archives sometimes preserve better the traces of intermediate to weak volcanic activity than the proximal areas.

Acknowledgements: We thank the Centre National de la Recherche Scientifique (CNRS) and Commissariat à l’Energie Atomique (CEA) for basic support to the laboratory. We also thank the N/O Marion Dufresne officers and crew for support and organisation of the coring cruises. BC was partially supported by Vinci program of Université Franco-Italienne and SETCI from region of Île-de-France. Fabien Dewilde (LSCE), Franco Colarieti (DST Pisa), Michel Fialin and Frederic Couffignal (CAMPARIS) are gratefully acknowledged for the preparation of samples and assistance during analyses.

References

- Alvisi F., Vigliotti L., (1996). Magnetic signature of marine and lacustrine sediments from central Italy (PALICLAS Project). Palaeoenvironmental Analysis of Italian Crater Lake and Adriatic Sediments. Mem. Ist. Ital. Idrobiol., 55, 285-303, P. Guilizzoni and F. Oldfield (Guest Editors).
- Andrews J., Geirsdottir A., Hardardottir J., Principato S., Grönvold K., Kristjansdottir G., Helgadottir G., Drexler J., Sveinbjörnsdottir A., (2002). Distribution, sediment magnetism and geochemistry of the Saksunarvatn (10 180±60 cal. yr BP) tephra in marine, lake and terrestrial sediments, northwest Iceland. Journal of Quaternary Science, 17, 731-745.
- Arnò V., Principe C., Rosi M., Santacroce R., Sbrana A., Sheridan M.F., (1987). Eruptive history. In: Santacroce, R. (Ed.), Somma-Vesuvius, vol. 114, 8. CNR Quaderni de la Ricerca Scientifica, Roma, pp. 53–103.
- Arrighi S., Tanguy J.C., Rosi M., (2006). Eruptions of the last 2200 years at Vulcano and Vulcanello (Aeolian Islands, Italy) dated by high-accuracy archeomagnetism. Physics of the Earth and Planetary Interiors 159, 225–233. doi:10.1016/j.pepi.2006.07.010.
- Aulinas M., Civetta L., Di Vito M.A., Orsi G., Gimeno D., Fernandes-Turiel J.L., (2008). The “pomici di mercato” Plinian eruption of Somma-Vesuvius: magma chamber processes and eruption dynamics. Bulletin of Volcanology 70, 825-840.

- Bard E., Arnold M., Duprat J., Moyes J., Duplessy J.C., (1987). Reconstruction of the last deglaciation: deconvolved records of $\delta^{18}\text{O}$ profiles, micropaleontological variations and accelerator mass spectrometric ^{14}C dating. *Climate Dynamics* vol 1, pp101-112 doi: 10.1007/BF01054479.
- Calanchi N., De Rosa R., Mazzuoli R., Rossi P., Santacroce R., Ventura G., (1993). Silicic magma entering a basaltic magma chamber: eruptive dynamics and magma mixing – an example from Salina (Aeolian Islands, Southern Tyrrhenian Sea). *Bulletin of Volcanology*, 55, 504-522.
- Calanchi N., Dinelli E., (2008). Tephrostratigraphy of the last 170 ka in sedimentary successions from the Adriatic Sea. *Journal of Volcanology and Geothermal Research* 177, 81-95.
- Cioni R., Santacroce R., Sbrana A., (1999). Pyroclastic deposits as a guide for reconstructing the multi-stage evolution of the Somma-Vesuvius caldera. *Bulletin of Volcanology* 60, 207–222.
- Civetta L., Cornette Y., Gillot P.Y., Orsi G., (1988) - The eruptive history of Pantelleria (Sicily Channel) in the last 50 ka. *Bulletin of Volcanology*, 50, 47-57.
- Clift P., Blusztajn J., (1999). The trace-element characteristics of Aegean volcanic arc marine tephra. *Journal of Volcanology and Geothermal Research* 92, 321-347.
- Coplen T.B., (1988). Normalization of oxygen and hydrogen isotope data, *Chem. Geol.* 72, 293–297.
- Crisci G.M., De Rosa R., Lanzafame G., Mazzuoli R., Sheridan M.F., Zuffa G.G., (1981). Monte Guardia sequence: a late-Pleistocene eruptive cycle on Lipari. *Bull Volcanol* 44:241–255.

- Crisci G.M., Delibrias G., De Rosa R., Mazzuoli R., Sheridan M.F., (1983). Age and Petrology of the Late-Pleistocene brown tuffs of Lipari, Italy. *Bulletin Volcanologique*, 46 (4), 381-391.
- Crisci G.M., De Rosa R., Esperanca S., Mazzuoli R., Sonnino M., (1991). Temporal evolution of a three component system: the island of Lipari (Aeolian Arc, southern Italy). *Bull Volcanol* 53:207–221.
- De Astis G., La Volpe L., Peccerillo A., Civetta L., (1997). Volcanological and petrological evolution of Vulcano Island (Aeolian Arc, southern Tyrrhenian Sea). *Journal of Geophysical Research*, 102, 8021-8050.
- De Rosa R., Sheridan M.F., (1983). Evidence for magma mixing in the surge deposits of the Monte Guardia Sequence, Lipari. *J Volcanol Geotherm Res* 17:313–328.
- De Rosa R., Donato P., Gioncada A., Masetti M., Santacroce R., (2003). The Monte Guardia eruption (Lipari, Aeolian Islands): an unusual example of magma mixing sequence. *Bull. Volcanol.* 65, 530–543.
- Delibrias G., Di Paola G.M., Rosi M., Santacroce R., (1979). La storia eruttiva del complesso vulcanico Somma Vesuvio ricostruita dalle successioni piroclastiche del Monte Somma. *Rendiconti Società Italiana Mineralogia Petrologia* 35, 411–438.
- Druitt T.H., Brenchley P.J., Gökten Y.E., Francaviglia V., (1995). Late Quaternary rhyolitic eruption from the Acigöl Complex, central Turkey. *J. Geol. Soc. London.* 152, 655–667.
- Folch A., Sulpizio R., (2010). Evaluating the long-range volcanic ash hazard using supercomputing facilities. Application to Somma-Vesuvius (Italy), and consequences on civil aviation over the Central Mediterranean Area. *Bull. Volcanol.* Submitted

- Fontugne M., Paterne M., Calvert S., Murat A., Guichard F., Arnold M., (1989). Adriatic deep water formation during the Holocene: implication for the reoxygenation of the deep eastern Mediterranean sea. *Paleoceanography*, vol.4, NO.2, 199-206.
- Fretzdorff S., Paterne M., Stoffers P., Ivanova E., (2000). Explosive activity of the Reunion Island volcanoes through the past 260,000 years as recorded in deep-sea sediments. *Bulletin of Volcanology* 62, 266–277.
- Giunta S., Negri A., Morigi C., Capotondi L., Combourieu-Nebout N., Emeis K.C., Sangiorgi F., Vigliotti L., (2003). Coccolithophorid ecostratigraphy and multi-proxy paleoceanographic reconstruction in the Southern Adriatic Sea during the last deglacial time (Core AD91-17), *Palaeogeogr. Palaeoclim. Palaeoecol.* 190, pp. 39–59.
- Juvigné E., (1987). Deux retombées volcaniques tardiglaciaires dans le cézallier (Massif Central, France). *Bulletin de l'association française pour l'étude du Quaternaire*, 4, 241-249.
- Kallel N., Paterne M., Labeyrie L., Duplessy J.C., Arnold M., (1997). Temperature and salinity records of the Tyrrhenian Sea during the last 18,000 years. *Palaeogeography, Palaeoclimatology, Palaeoecology* 135 97-108.
- Kallel N., Duplessy J.C., Labeyrie L., Fontugne M., Paterne M., Montacer M., (2000). Mediterranean pluvial periods and sapropel formation over the last 200 000 years. *Palaeogeography, Palaeoclimatology, Palaeoecology* 157 45–58.
- Keller J., Ryan W.B.F., Ninkovich D., Altherr R., (1978). Explosive volcanic activity in the Mediterranean over the past 200,000 yr as recorded in deep-sea sediments. *Geol. Soc. Am. Bull.* 89, 591–604.
- Kruiver P., Passier H., (2001). Coercivity analysis of magnetic phases in sapropel S1 related to variations in redox conditions, including an investigation of the S ratio. *Geochem. Geophys. Geosyst.*, 2, 2001GC000181.

- Le Bas M.J., Le Maitre R.W., Streckeisen A., Zanettin B., (1986). A chemical classification of volcanic rocks based on the total alkali-silica diagram. *J. Petrol.* 27, 745–750.
- Le Friant A., Lock E.J., Hart M.B., Boudon G., Sparks R.S.J., Leng M.J., Smart C.W., Komorowski J.C., Deplus C., Fisher J.K., (2008). Late Pleistocene tephrochronology of marine sediments adjacent to Montserrat, Lesser Antilles volcanic arc. *Journal of the Geological Society, London*, Vol. 165, 2008, pp. 279–289.
- Lowe J.J., Blockley S., Trincardi F., Asioli A., Cattaneo A., Matthews I.P., Pollard M., Wulf S., (2007). Age modelling of late Quaternary marine sequences in the Adriatic: towards improved precision and accuracy using volcanic event stratigraphy. *Continental Shelf Research* 27: 560–582.
- Lowrie W., Fuller M., (1971). On the alternating field demagnetization characteristics of multidomain thermoremanent magnetization in magnetite. *J. Geophys. Res.*, 76, 6339-6349.
- Mele D., Sulpizio R., Dellino P., La Volpe L., (2007). A quantitative study for the reconstruction of Mercato eruption (8000 yr B.P.) of Somma-Vesuvius. IUGG XXIV General Assembly 2-13 Luglio, Perugia, Abstract volume 22-24, Italy.
- Mele D., Sulpizio R., Dellino P., La Volpe L., (2009). Stratigraphy and eruptive dynamics of a long-lasting Plinian eruption of Somma-Vesuvius: the Pomici di Mercato (8900 years BP). *Bull. volcanol.*
- Myers P.G., Rohling E.J., (2000). Modeling a 200-yr interruption of the Holocene sapropel S1. *Quat. Res.* 53, 98-104.
- Narcisi B., (1996). Tephrochronology of a Late Quaternary lacustrine record from Monticchio maar (Vulture volcano, Southern Italy). *Quat. Sci. Rev.* 15, 155-165.

- Narcisi B., Vezzoli L., (1999). Quaternary stratigraphy of distal tephra layers in the Mediterranean – an overview. *Global and Planetary Change* 21, 31-50.
- Narcisi B., (2002). Tephrostratigraphy of the Late Quaternary lacustrine sediments of Lago di Pergusa (central Sicily). *Boll. Soc. Geol. It.*, 121, 211-219, 5 ff., 1 tab.
- Negri A., Giunta S., (2001). Calcareous nannofossil paleoecology in the sapropel S1 of the eastern Ionian sea: paleoceanographic implications. *Palaeogeogr. Palaeoclimatol. Palaeoecol.* 169, 101-112.
- Oldfield F., Appleby P., Thompson R., (1980). Palaeoecological studies of lakes in the highlands of Papua New Guinea., *Journal of Ecology*, 68, 457-477.
- Passier H., De Lange G., Dekkers M., (2001). Magnetic properties and geochemistry of the active oxidation front and the youngest sapropel in the eastern Mediterranean Sea. *Geophys. J. Int.*, 145, 604-614.
- Paterne M., (1985). Reconstruction de l'activité explosive des volcans de l'Italie du sud par tephrochronologie marine. University thesis, University of Paris Sud XI, Orsay, France.
- Paterne M., Guichard F., Labeyrie J., Gillot P.Y., Duplessy J.C., (1986). Tyrrhenian Sea tephrochronology of the oxygen isotope record for the past 60,000 years. *Marine Geology*, Volume 72, Issues 3-4, Pages 259-285.
- Paterne M., Guichard F., Labeyrie J., (1988). Explosive activity of the South Italian volcanoes during the past 80,000 years as determined by marine tephrochronology. *JVGR* 34, 153-172.
- Paterne M., Labeyrie J., Guichard F., Massaud A., Maitre F., (1990). Fluctuation of the campanian explosive activity (South Italy) during the last 190,000 years as determined by marine tephrochronology. *Earth and Planetary Science Letters* 98, 166-174.

- Paterne M., Guichard F., Duplessy J.C., Siani G., Sulpizio R., Labeyrie J., (2008). A 90,000 – 200,000 yrs marine tephra record of Italian volcanic activity in the central Mediterranean Sea. *Journal of Volcanology and Geothermal Research* 177 (2008) 187–196. doi:10.1016/j.jvolgeores.2007.11.028.
- Peters C., Austin W., Walden J., Hibbert F., (2009). Magnetic characterisation and correlation of a Younger Dryas tephra in North Atlantic marine sediments. *J. Quaternary Sci.*, DOI: 10.1002/jqs.
- Roberts N., (1998). *The Holocene, an environmental history*. 2nd edition, Blackwell Publishers Inc.
- Rolandi G., Mastrolenzo G., Barrella A.M., Borrelli A., (1993). The Avellino Plinian eruption of Somma-Vesuvius (3760 y. B.P.): the progressive evolution from magmatic to hydromagmatic style. *Journal of Volcanology and Geothermal Research* 58, 67–88.
- Rohling E.J., Jorissen F.J., De Stigter H.C., (1997). 200 year interruption of Holocene sapropel formation in the Adriatic sea. *J. Micropaleontol.* 16, 97-108.
- Rousse S., Kissel C., Laj C., Eiriksson J., Knudsen K., (2006). Holocene centennial to millennial-scale climatic variability: Evidence from high-resolution magnetic analyses of the last 10 cal kyr of North Iceland (core MD99-2275). *Earth Planet. Sci. Lett.*, 242, 390-405.
- Santacroce R., Cioni R., Marianelli P., Sbrana A., Sulpizio R., Zanchetta G., Donahue D.J., Joron J.L., (2008). Age and whole rock-glass compositions of proximal pyroclastics from the major explosive eruptions of Somma-Vesuvius: a review as a tool for distal tephrostratigraphy *Journal of Volcanology and Geothermal Research* 177, 1–18. doi:10.1016/j.jvolgeores.2008.06.009.

- Siani G., Paterne M., Michel E., Sulpizio R., Sbrana A., Arnold M., Haddad G., (2001). Mediterranean sea-surface radiocarbon reservoir age changes since the last glacial maximum. *Science* 294, 1917-1920.
- Siani G., Sulpizio R., Paterne M., Sbrana A., (2004). Tephrostratigraphy study for the last 18,000 ¹⁴C years in a deep-sea sediment sequence for the South Adriatic. *Quaternary Science Review* 23 : 2485-2500.
- Sigurdsson H., Sparks R.S.J., Carey S., Huang T.C., (1980). Volcanogenic sedimentation in the Lesser Antilles arc. *J. Geol.* 88, 523–540.
- Stow D.A.V., Huc A.Y., Bertrand P., (2001). Depositional processes of black shales in deep water. *Marine and Petroleum Geology* 18, 491-498.
- Sulpizio R., Cioni R., Di Vito M.A., Mele D., Bonasia R., Dellino P., (2010a). The Pomici di Avellino eruption of Somma-Vesuvius (3.9 ka BP) part I: stratigraphy, compositional variability and eruptive dynamics. *Bull Volcanol* in press.
- Sulpizio R., Bonasia R., Dellino P., Mele D., Di Vito M.A., La Volpe L. (2010b). The Pomici di Avellino eruption of Somma-Vesuvius (3.9 ka BP) part II: Volcanic ash hazard in the central Mediterranean area. Sedimentology and physical volcanology of pyroclastic density current deposits. *Bull Volcanol* in press
- Tanguy J. C., Le Goff, M., Principe C., Arrighi S., Chillemi V., Paiotti A., La Delfa S., Patane G., (2003). Archaeomagnetic dating of Mediterranean volcanics of the last 2100 years: validity and limits. “*Earth Planet. Sci. Lett.*”, 211, 111-124.
- Tarduno J., Tian W., Wilkison S., (1998). Biogeochemical remanent magnetization in pelagic sediments of the western equatorial Pacific Ocean. *Geophys. Res. Lett.*, 25, 3987-3990.
- Thompson R., Oldfield F., (1986). *Environmental magnetism*. Allen and Unwin, London, 227.

- Tisnérat-Laborde N., Poupeau J. J., Tannau J. F., Paterne M., (2001). Development of a semi-automated system for routine preparation of carbonate samples. *Radiocarbon*, Vol 43, 2A, 299–304
- Turney C. S. M., Lowe J. J., Davies S. M., Hall V., Lowe D. J., Wastegård S., Hoek W. Z., Alloway B., (2004). Tephrochronology of Last Termination Sequences in Europe: a protocol for improved analytical precision and robust correlation procedures (a joint SCOTAV–INTIMATE proposal). *J. Quaternary Sci.*, Vol. 19 pp. 111–120. ISSN 0267-8179.
- Turney C.S.M., Blockley S.P.E., Lowe J.J., Wulf S., Branch N.P., Mastrolorenzo G., Swindle G., Nathan R., Pollard A.M., (2008). Geochemical characterization of Quaternary tephros from the Campanian province, Italy. *Quaternary International* 178, 288–305.
- Verosub K.L., Roberts A.P., (1995). Environmental magnetism: past, present and future, *J. Geophys. Res.*, 100, 2175-2192.
- Vogel H., Zanchetta G., Sulpizio R., Wagner B., Nowaczyk N., (2009). A tephrostratigraphic record for the last glacial-interglacial cycle from Lake Ohrid, Albania and Macedonia. *J. Quaternary Sci.*, (2009). ISSN 0267-8179.
- Wulf S., Kraml M., Brauer A., Keller J., Negendank J.F.W., (2004). Tephrochronology of the 100 ka lacustrine sediment record of Lago Grande di Monticchio (southern Italy). *Quaternary International* 122: 7–30.
- Wulf S., Kraml M., Keller J., (2008). Towards a detailed distal tephrostratigraphy in the Central Mediterranean: The last 20,000 yrs record of Lago Grande di Monticchio. *Journal of Volcanology and Geothermal Research* 177 (2008) 118–132.

Zanchetta G., Sulpizio R., Roberts N., Cioni R., Eastwood W.J., Siani G., Caron B., Paterne M., Santacroce R., (2010). Tephrostratigraphy, chronology and climatic events of the Mediterranean basin during the Holocene: an overview. *Holocene* in press.

Zanella E., (2006). Magnetic chronology in recent volcanic rocks: basic principles and case histories from Aeolian Islands. *Acta Vulcanologica*, Vol. 18 (1-2), 35-46.

Figure and Table captions

Figure 1: Location map of the study area, of the main Italian volcanoes and location of cores used in this study: CVZ = Campanian Volcanic Zone (Campi Flegrei, Somma-Vesuvius, Ischia and Procida), EI = Eolian Islands, LGM = Lago Grande di Monticchio.

Figure 2: Sediment magnetic properties of the MD90-918 core plotted versus core depth. The low-field susceptibility and the magnetizations are in mass units. Grey area indicates different core segments. a) χ , NRM₂₅ and SIRM curves; b) NRM₂₅/ARM₂₅, ARM/k, S_(-0.1T) and S_(-0.3T) curves.

Figure 3: a) Isothermal remanent acquisition curves and b) back-field removing curves for sediments at different depth. In c) and d) Normalized AF demagnetization curves of NRM, IRM and ARM plotted together with the IRM acquisition curve.

Figure 4: Lithostratigraphy, AMS 14C dates samples location, stable isotope $\delta^{18}O$ curve, glass shards abundance curve, magnetic susceptibility and age model of the deep sea core MD90-918.

Figure 5: General TAS with all analyses for each tephra layer from the MD90-918 core

Figure 6: Sapropel S1 stratigraphy details, abundance glass curve and % glass shards composition of the core MD90-918 core.

Figure 7: SEM pictures of volcanic glass fragments from tephra layer a) 5 cm, b) 175 cm, c) 185 cm, d) 210 cm, e) 218 cm, f) 223 cm, g) 230 cm and h) 820 cm.

Figure 8: TAS: a) TAS of the Monte Pilato eruption A.D. 1200 samples PI 134 from Lipari Island in correlation with the tephra layer 2; c) TAS of the Mercato eruption samples from the Mount Somma-Vesuvius (Wulf et al., 2004; Santacroce et al., 2008; Turney et al., 2007 and Paterne et al., 1988) in correlation with the tephra layers 230, 223, 210, 185 and 175; d) TAS of the Gabelotto-Fiumebianco eruption and E-1 tephra layer samples from the Lipari Island

(Siani et al., 2004; Paterne et al., 1988) in correlation with the tephra layers 218 and 210; e) TAS of the Monte Guardia eruption samples from the Lipari Island (De Rosa et al., 2003) in correlation with the tephra layers 820.

Figure 9: Map of the ash dispersion for a) Monte Pilato A.D. 1200 from Lipari Island, b) Mercato eruption from the Mount Somma-Vesuvius, c) Gabelotto-Fiumebianco eruption from Lipari Island and d) Monte Guardia eruption from Lipari. Stars indicate the volcanic sources.

Table 1: Intercalibration data between SEM of the University of Pisa and the microprobe of Camaparis. A set of 99 analyses of five distinct tephra layers is resumed here with: 1) the average of the mean of the analyses from the two instruments; 2) the difference between the means of the analyses from the two instruments; 3) the standard deviation of between the means of the analyses from the two instruments; 4) the variance in % of the means of analyses from the two instruments; 5) and finally the average of variance from the distinct layers.

Table 2: Conventional ^{14}C ages from MD90-918 core determined by UMS-ARTEMIS (Pelletron 3MV) AMS facilities (CNRS-CEA Gif-sur-Yvette, France). Ages were calibrated using INTCAL04 (Reimer et al., 2004) for ^{14}C age younger than 26 cal ka BP and Bard polynomial equation for age older than 26 cal ka BP (Bard et al., 1998).

Table 3: Composition of major elements of the eight tephra layers recognised in core MD90-918. Analyses performed on the SEM of the University of Pisa and the microprobe of Camaparis (Paris).

Table 4: Comparison of average and standard deviation of analyses from literature used for comparison except the analyses from PI-134 which is a sample collected on the cone Monte Pilato eruptive succession from the Lipari Island.

Figure 1

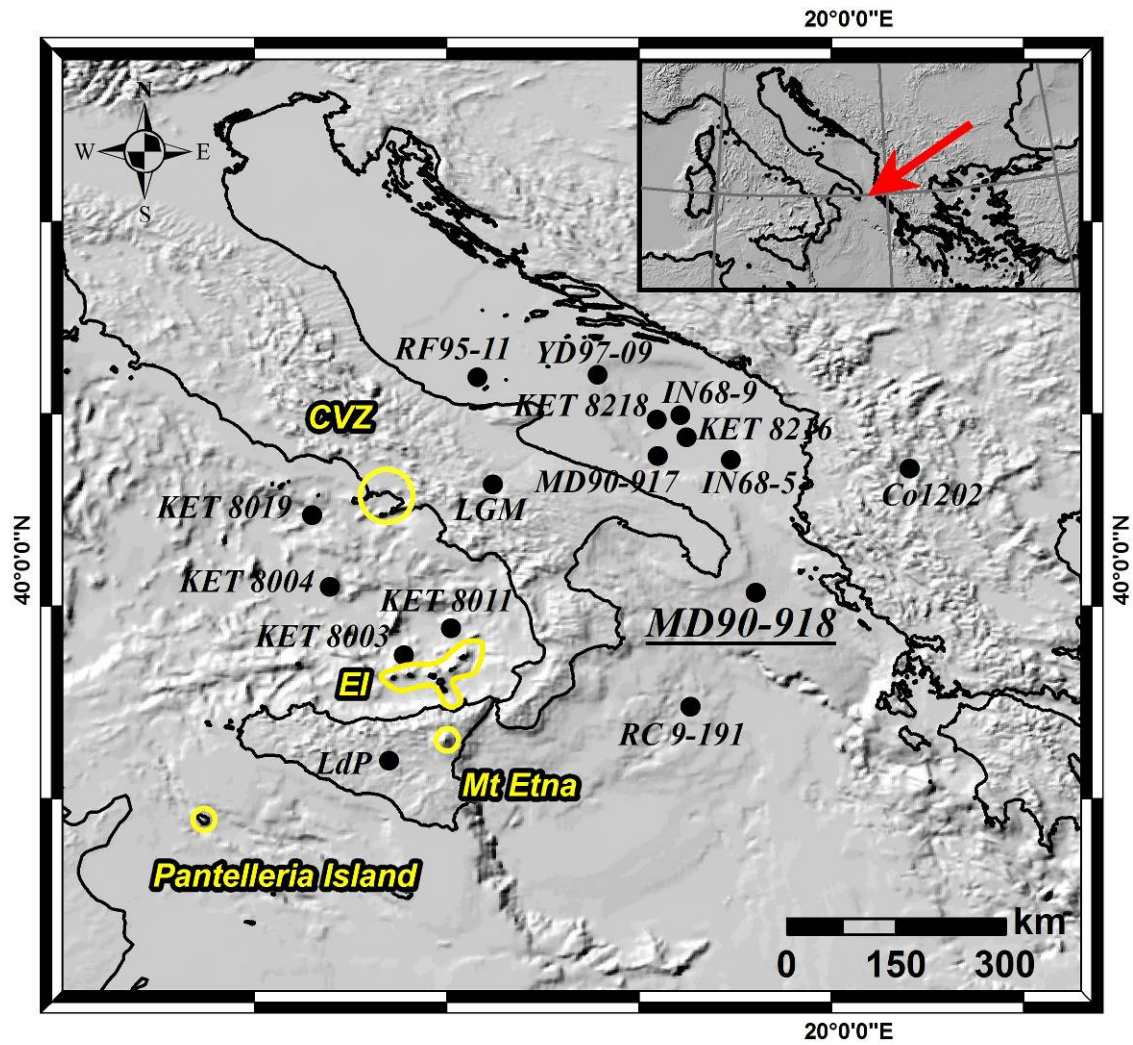


Figure 2

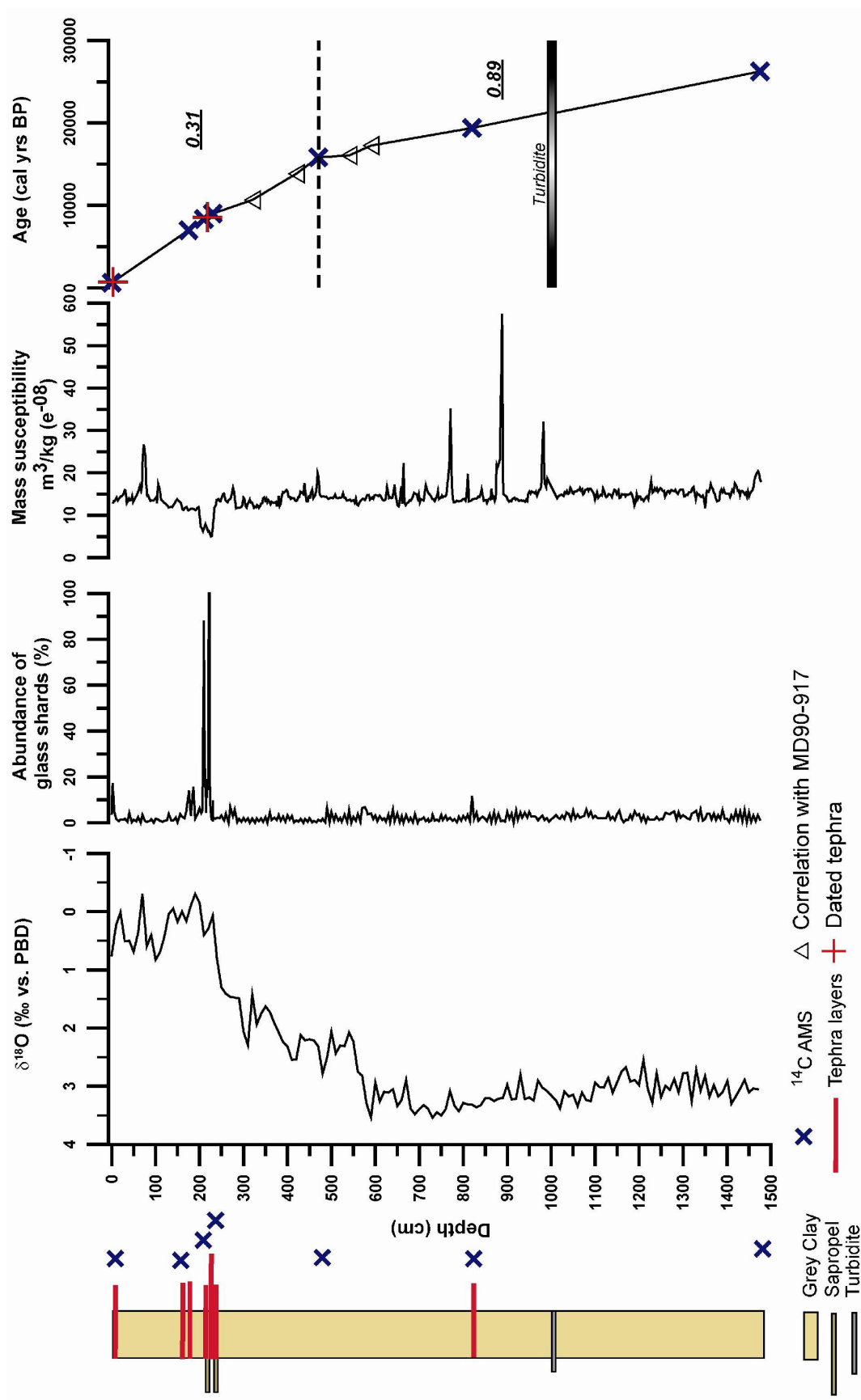


Figure 3

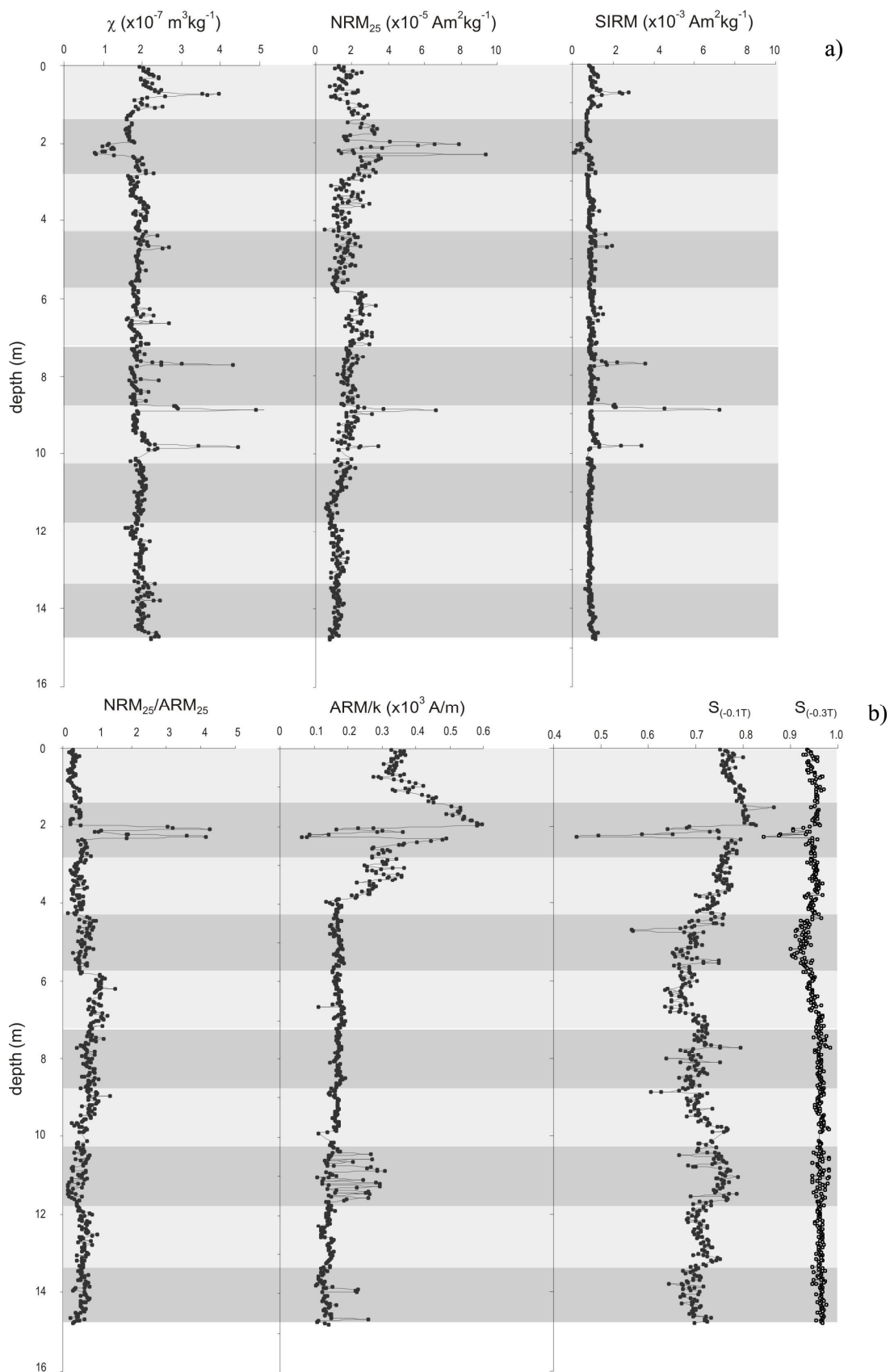


Figure 4

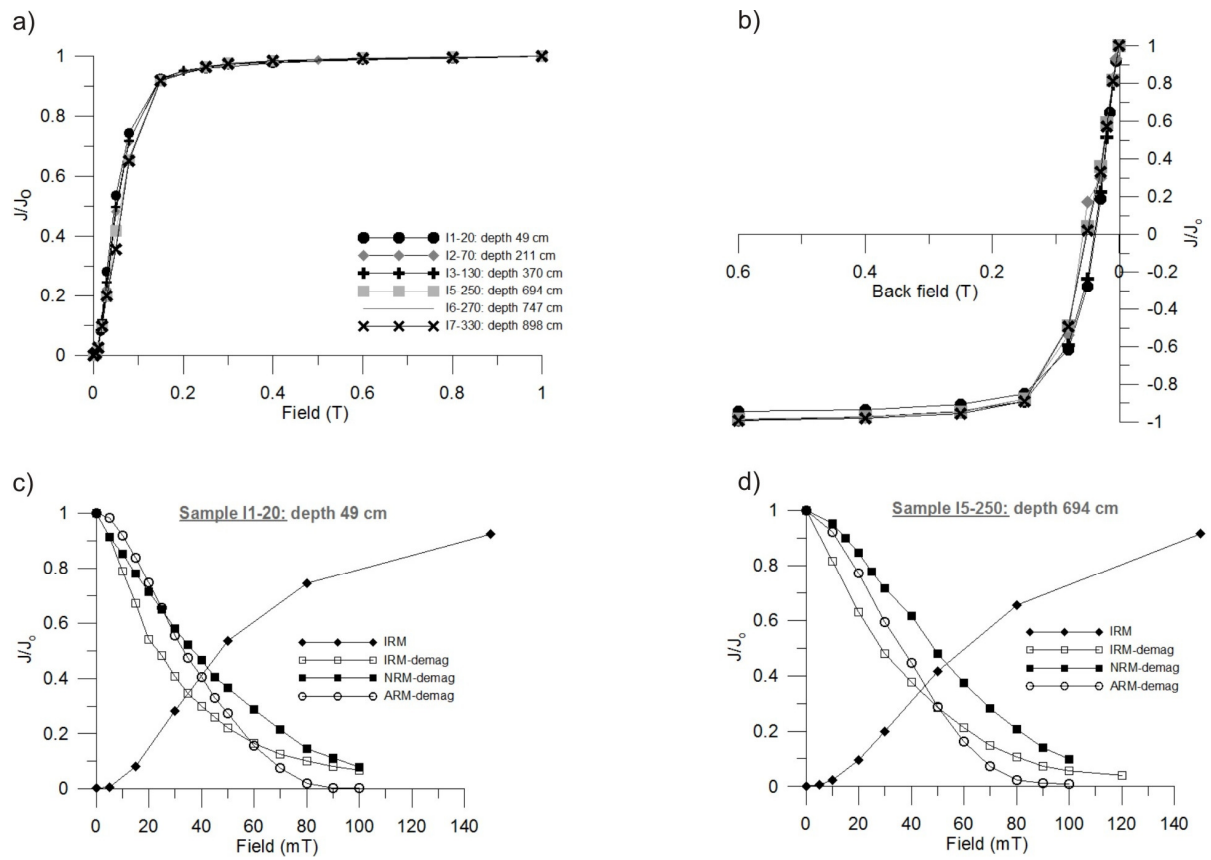


Figure 5

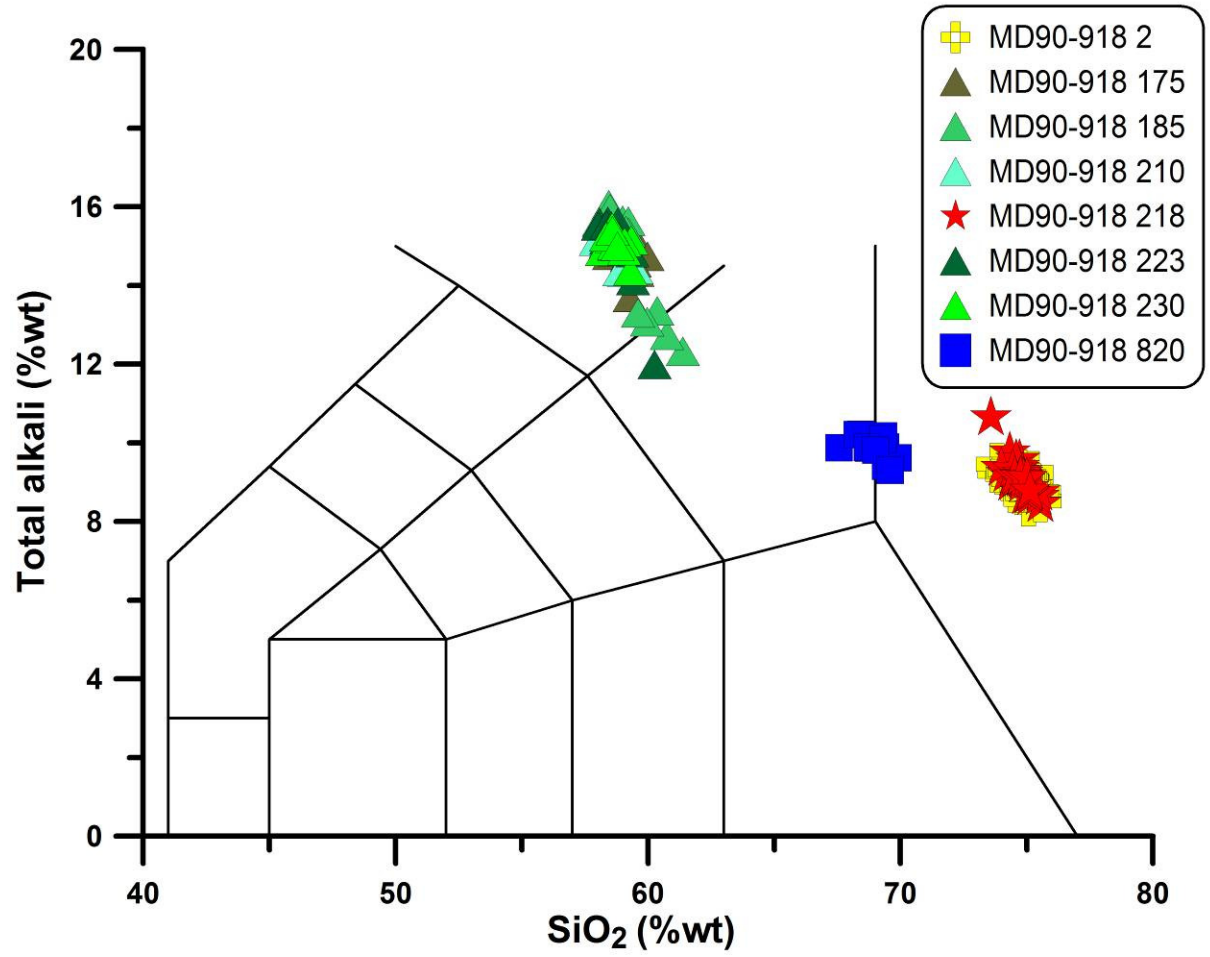


Figure 6

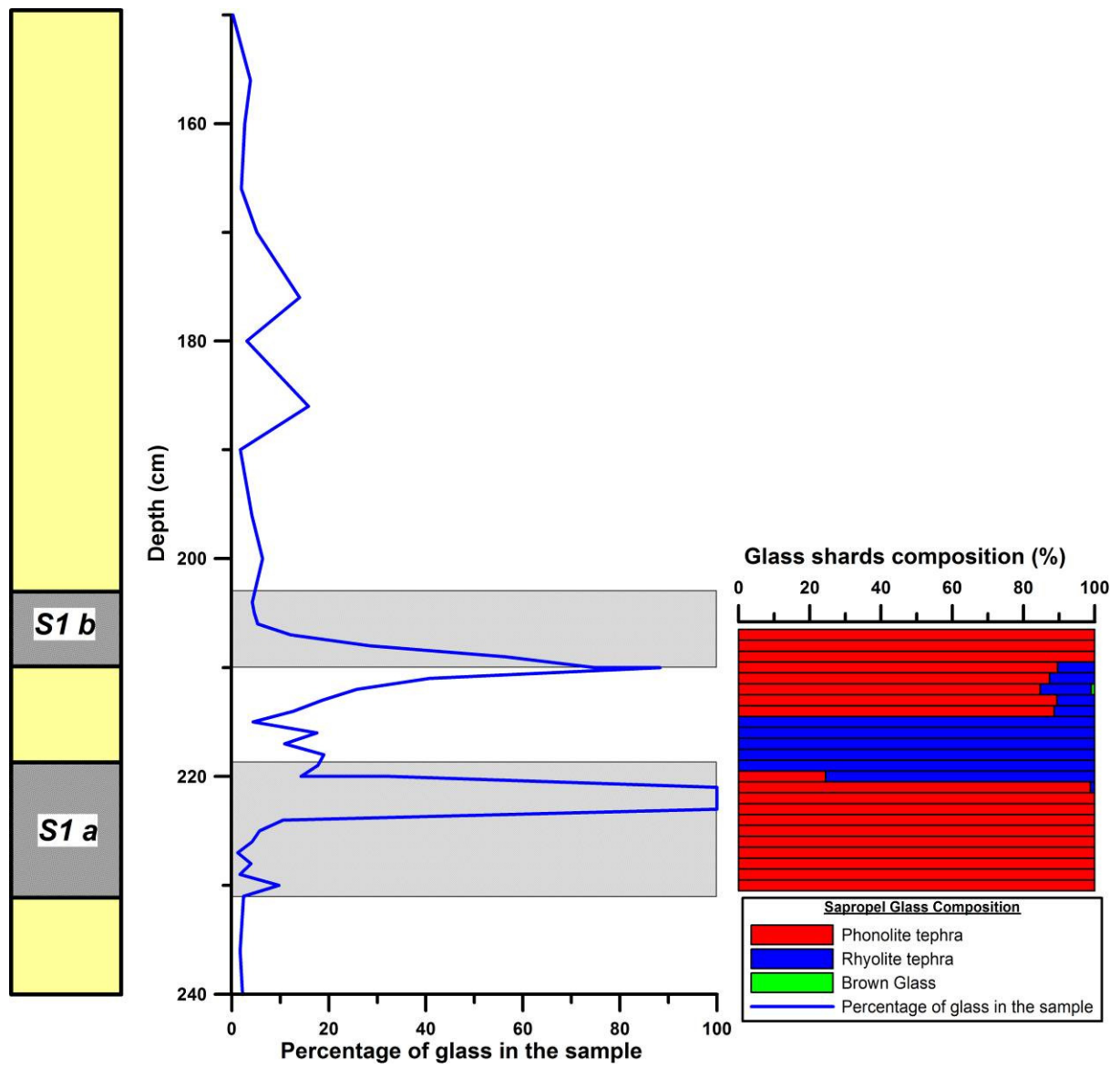


Figure 7

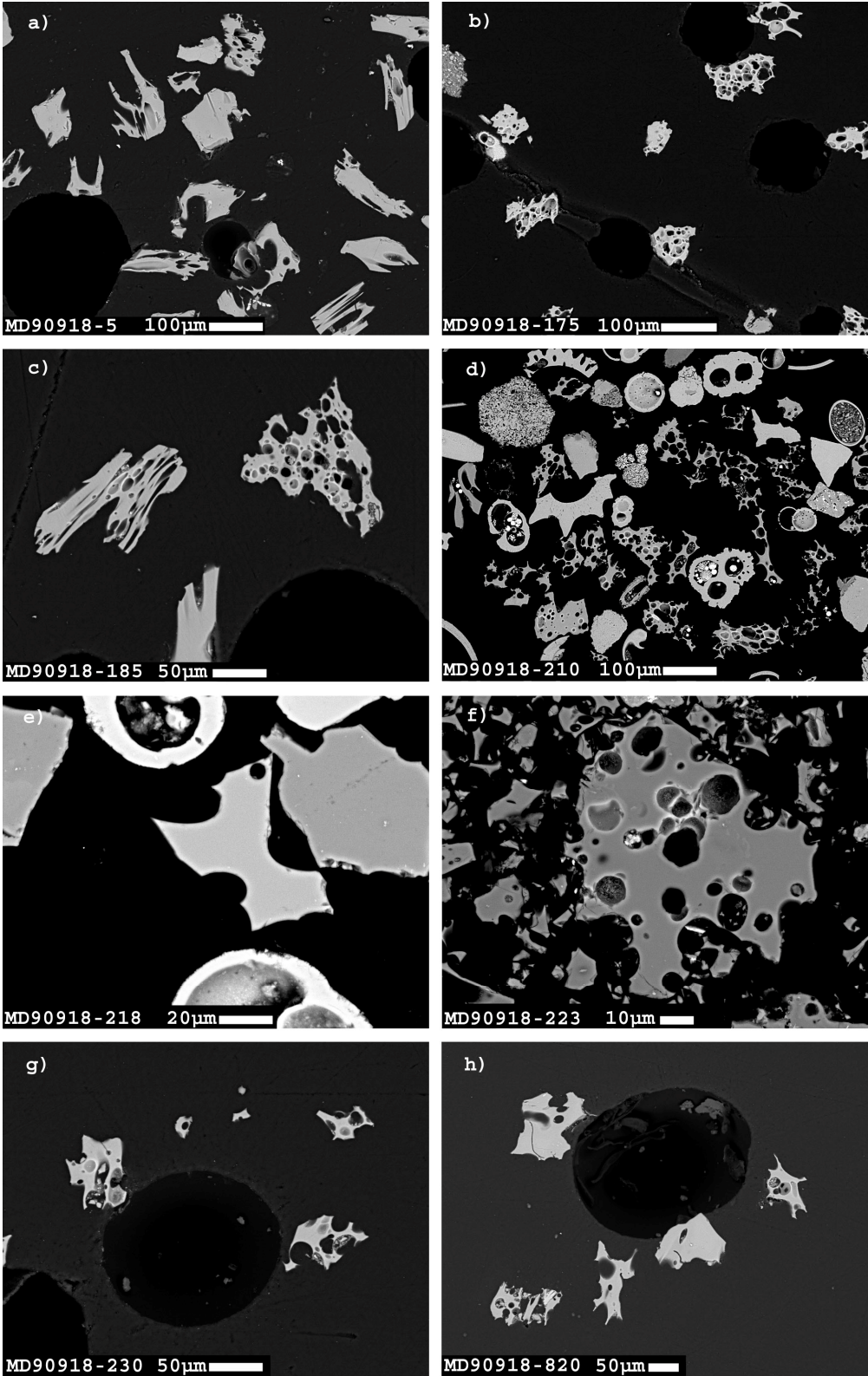


Figure 8

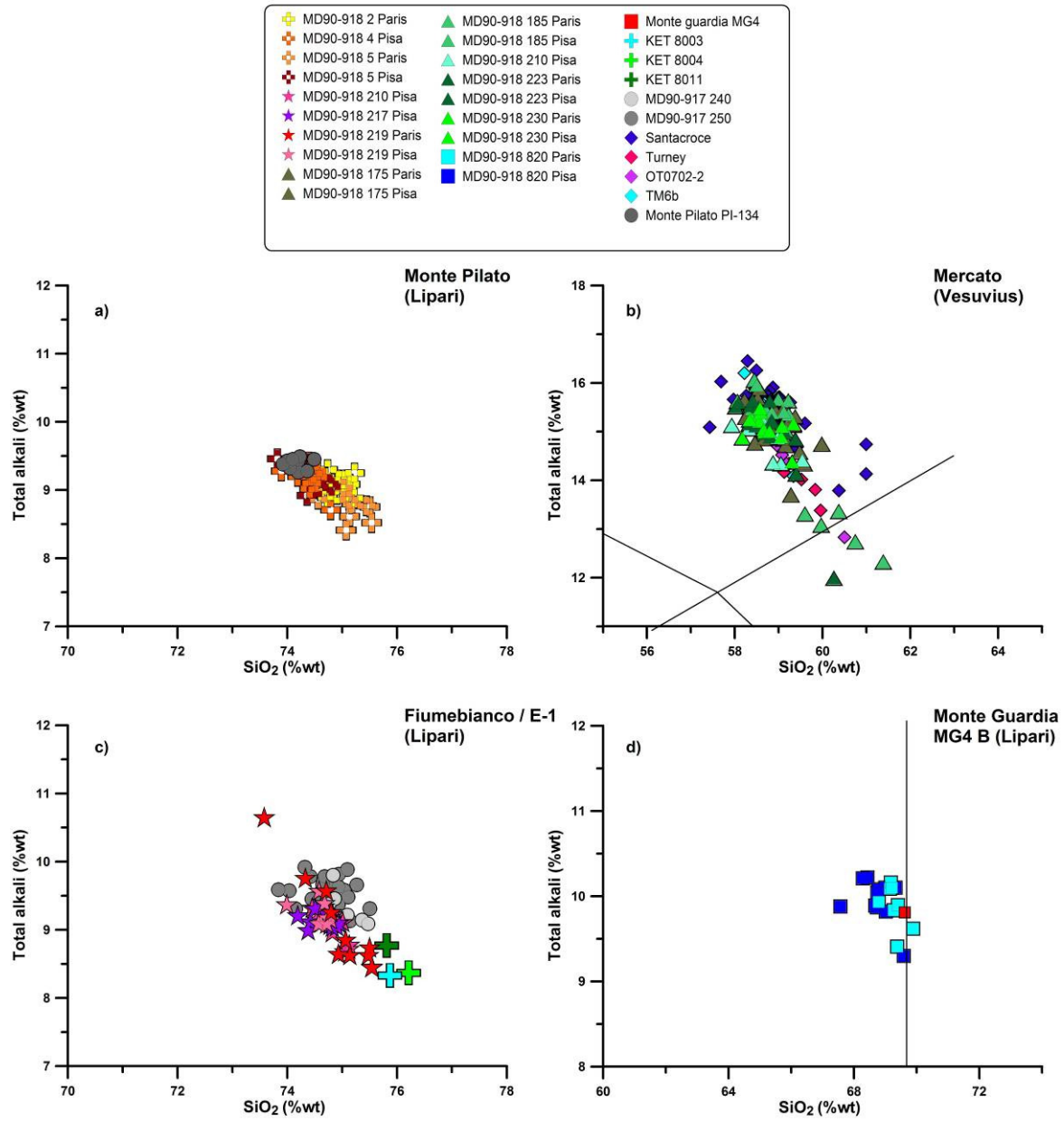


Figure 9

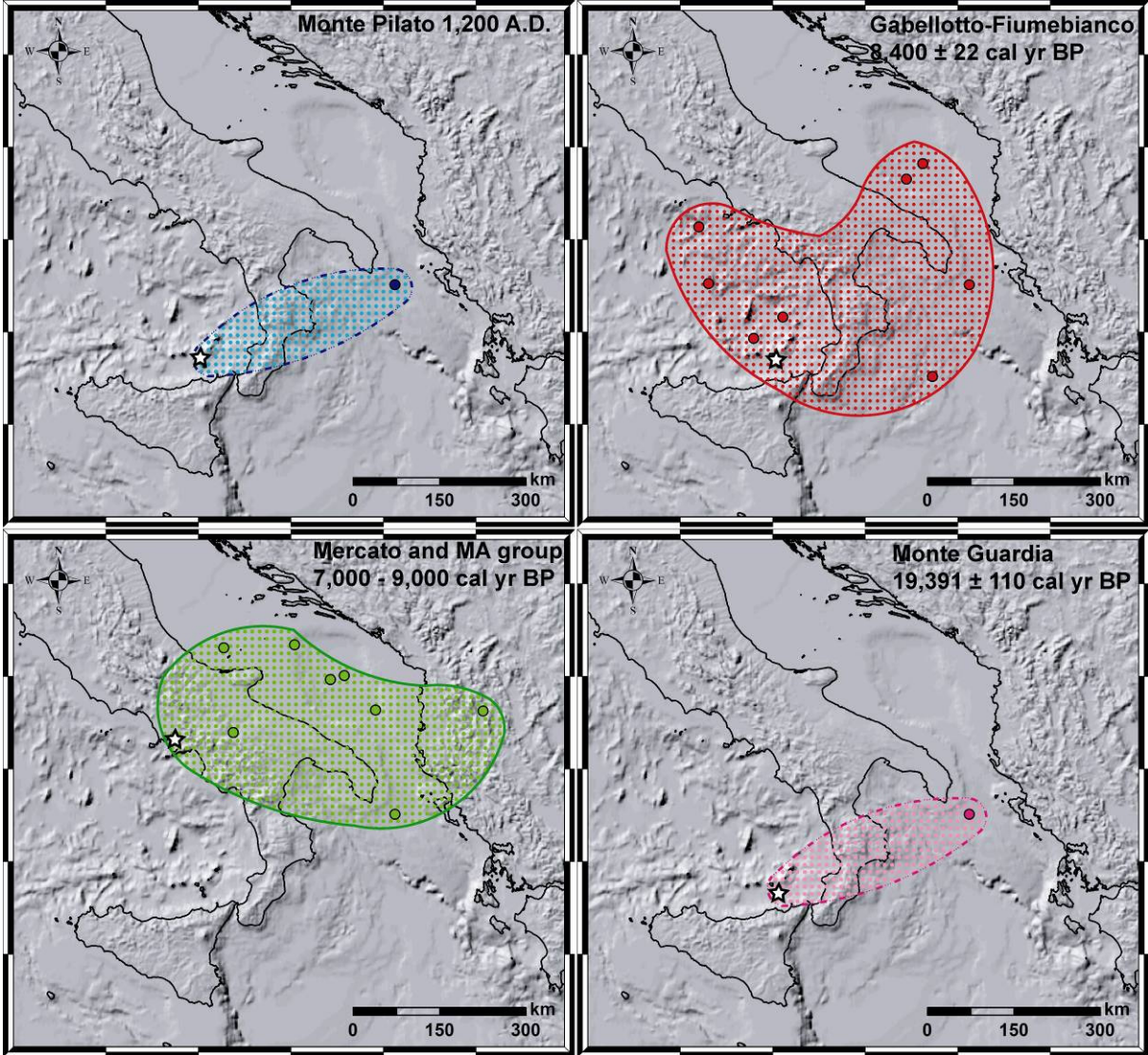


Table 1

		SiO ₂	TiO ₂	Al ₂ O ₃	FeO _{tot}	MnO	MgO	CaO	Na ₂ O	K ₂ O	P ₂ O ₅	ClO
Level 5	Mean of all analyses from the level 5	74.81	0.05	13.41	1.51	0.05	0.05	0.78	4.02	4.95	0.01	0.37
	Mean from the microsonde analyses	75.18	0.06	13.22	1.52	0.07	0.04	0.79	3.98	4.76	0.02	0.38
	Mean from the SEM analyses	74.44	0.05	13.61	1.49	0.03	0.06	0.78	4.05	5.14	0.00	0.36
	Difference between the two means	0.74	0.01	-0.39	0.03	0.04	-0.02	0.01	-0.07	-0.38	0.02	0.02
	Sd of the two means	0.52	0.01	0.27	0.02	0.03	0.01	0.00	0.05	0.27	0.01	0.01
	% variance of the two means from both instrument	0.98	15.42	2.91	2.06	59.28	48.92	0.70	1.88	7.95	100.00	4.58
Level 175	Mean of all analyses from the level 175	58.92	0.14	21.53	1.72	0.20	0.10	1.65	8.45	6.71	0.02	0.57
	Mean from the microsonde analyses	59.01	0.15	21.28	1.71	0.20	0.08	1.68	8.58	6.69	0.03	0.59
	Mean from the SEM analyses	58.79	0.13	21.87	1.74	0.19	0.13	1.60	8.28	6.73	0.00	0.55
	Difference between the two means	0.22	0.03	-0.59	-0.03	0.01	-0.05	0.08	0.30	-0.05	0.03	0.05
	Sd of the two means	0.16	0.02	0.42	0.02	0.01	0.04	0.05	0.21	0.03	0.02	0.03
	% variance of the two means from both instrument	0.38	16.87	2.77	1.49	6.51	64.84	4.62	3.46	0.70	100.00	7.86
Level 185	Mean of all analyses from the level 185	58.74	0.15	21.43	1.69	0.18	0.11	1.59	8.86	6.65	0.01	0.59
	Mean from the microsonde analyses	58.91	0.16	21.19	1.68	0.18	0.07	1.61	8.90	6.64	0.01	0.64
	Mean from the SEM analyses	58.48	0.15	21.80	1.72	0.19	0.17	1.56	8.78	6.65	0.00	0.51
	Difference between the two means	0.43	0.01	-0.61	-0.04	-0.01	-0.10	0.06	0.12	0.00	0.01	0.14
	Sd of the two means	0.30	0.01	0.43	0.03	0.01	0.07	0.04	0.08	0.00	0.01	0.10
	% variance of the two means from both instrument	0.73	4.94	2.90	2.46	4.79	138.13	3.57	1.35	0.07	100.00	21.23
Level 219	Mean of all analyses from the level 219	74.80	0.07	13.21	1.48	0.07	0.05	0.84	3.92	5.20	0.01	0.34
	Mean from the microsonde analyses	74.95	0.07	13.08	1.50	0.07	0.03	0.84	3.91	5.16	0.01	0.37
	Mean from the SEM analyses	74.58	0.07	13.40	1.46	0.06	0.07	0.83	3.95	5.28	0.00	0.31
	Difference between the two means	-0.37	0.00	0.31	-0.04	-0.01	0.03	-0.01	0.04	0.13	-0.01	-0.07
	Sd of the two means	0.26	0.00	0.22	0.03	0.01	0.02	0.01	0.03	0.09	0.01	0.05
	% variance of the two means from both instrument	0.49	5.93	2.37	2.90	11.86	101.85	1.29	1.01	2.43	100.00	18.15
Level 820	Mean of all analyses from the level 820	68.97	0.30	16.08	2.27	0.13	0.47	1.49	4.57	5.36	0.03	0.33
	Mean from the microsonde analyses	69.31	0.27	15.79	2.29	0.13	0.43	1.50	4.59	5.29	0.07	0.32
	Mean from the SEM analyses	68.74	0.32	16.27	2.27	0.13	0.49	1.48	4.56	5.40	0.00	0.33
	Difference between the two means	0.57	-0.05	-0.48	0.02	0.01	-0.06	0.02	0.03	-0.11	0.07	-0.01
	Sd of the two means	0.40	0.04	0.34	0.02	0.00	0.04	0.02	0.02	0.08	0.05	0.00
	% variance of the two means from both instrument	0.82	20.18	3.03	1.05	5.11	13.85	1.61	0.68	2.07	100.00	1.82
average of the % variance		0.68	12.67	2.80	1.99	17.51	73.52	2.36	1.68	2.65	100.00	10.73

nb=99

Table 2

Depth	Species	Size	¹⁴ C Age	error	¹⁴ C yr cal BP	error	Methods
0-6	<i>G. ruber</i>	> 150µm	960	35	615	20	intcal04 Reimer et al., 2004
175-177	<i>G. ruber</i>	> 150µm	6535	45	6989	57	intcal04 Reimer et al., 2004
210-212	<i>G. ruber</i>	> 150µm	7900	50	8342.5	56	intcal04 Reimer et al., 2004
230-232	<i>G. ruber</i>	> 150µm	8470	50	9004.5	42	intcal04 Reimer et al., 2004
470-472	<i>G. bullo</i>	> 150µm	13740	60	15823	267	intcal04 Reimer et al., 2004
820-822	<i>G. bullo + inflata</i>	> 150µm	16610	70	19391	110	intcal04 Reimer et al., 2004
1475-1477	<i>G. bullo + inflata</i>	> 150µm	22710	110	26925	563	Calpal Weninger et al., 2007

Table 3

MD90-918 2-Paris	SiO ₂	TiO ₂	Al ₂ O ₃	Fe ₂ O ₃	MnO	MgO	CaO	Na ₂ O	K ₂ O	P ₂ O ₅	ClO	Total	Total Alkali	K ₂ O/Na ₂ O
3/1.	75.14	0.09	13.14	1.27	0.03	0.05	0.79	4.09	4.99	0.00	0.39	100	9.08	1.22
5/1.	75.02	0.14	13.02	1.37	0.06	0.06	0.81	3.81	5.33	0.02	0.36	100	9.15	1.40
6/1.	75.23	0.00	12.88	1.49	0.10	0.04	0.67	3.83	5.42	0.02	0.32	100	9.25	1.41
7/1.	75.09	0.21	12.95	1.51	0.04	0.04	0.76	3.88	5.12	0.00	0.40	100	9.01	1.32
8/1.	74.57	0.01	13.40	1.46	0.13	0.03	0.87	3.90	5.22	0.03	0.37	100	9.12	1.34
9/1.	74.93	0.00	13.07	1.61	0.06	0.05	0.78	3.96	5.18	0.02	0.33	100	9.15	1.31
10/1.	75.03	0.00	13.07	1.63	0.07	0.05	0.74	4.01	5.04	0.00	0.36	100	9.06	1.26
11/1.	74.73	0.27	13.06	1.39	0.07	0.04	0.76	3.82	5.48	0.00	0.37	100	9.30	1.43
12/1.	75.21	0.05	13.09	1.49	0.12	0.04	0.75	3.98	4.89	0.00	0.37	100	8.88	1.23
14/1.	74.73	0.01	13.49	1.62	0.06	0.05	0.77	4.02	4.87	0.02	0.37	100	8.89	1.21
16/1.	74.90	0.02	13.23	1.54	0.11	0.05	0.81	3.73	5.21	0.00	0.40	100	8.94	1.40
17/1.	74.78	0.15	13.26	1.53	0.09	0.04	0.78	3.83	5.15	0.03	0.36	100	8.98	1.34
18/1.	74.69	0.01	13.27	1.58	0.06	0.05	0.77	3.97	5.21	0.01	0.38	100	9.19	1.31
19/1.	75.00	0.02	13.14	1.57	0.05	0.05	0.75	3.90	5.07	0.04	0.39	100	8.98	1.30
mean	74.93	0.07	13.15	1.50	0.07	0.05	0.77	3.91	5.16	0.01	0.37	-	9.07	1.32
sd	0.21	0.09	0.17	0.11	0.03	0.01	0.05	0.10	0.18	0.01	0.02	-	0.13	0.07
MD90-918 4-Pisa	SiO ₂	TiO ₂	Al ₂ O ₃	Fe ₂ O ₃	MnO	MgO	CaO	Na ₂ O	K ₂ O	P ₂ O ₅	ClO	Total	Total Alkali	K ₂ O/Na ₂ O
P1/151-1	74.51	0.00	13.63	1.51	0.00	0.14	0.75	3.95	5.25	0.00	0.27	100	9.20	1.33
P1/151-2	74.56	0.00	13.44	1.53	0.00	0.09	0.85	3.93	5.26	0.00	0.33	100	9.19	1.34
P1/151-3	74.55	0.00	13.52	1.48	0.00	0.00	0.88	3.98	5.30	0.00	0.29	100	9.28	1.33
P1/151-4	73.89	0.00	14.18	1.37	0.00	0.08	0.89	4.21	5.07	0.00	0.26	100	9.28	1.20
P1/151-5	74.41	0.23	13.44	1.55	0.19	0.05	0.78	3.76	5.26	0.00	0.34	100	9.02	1.40
P1/151-6	74.44	0.11	13.44	1.68	0.00	0.07	0.79	3.80	5.30	0.00	0.36	100	9.10	1.39
P1/151-7	74.79	0.07	13.65	1.57	0.00	0.08	0.72	3.68	5.03	0.00	0.42	100	8.71	1.37
P1/151-8	74.48	0.00	13.46	1.46	0.00	0.09	0.85	4.01	5.23	0.00	0.43	100	9.24	1.30
P1/151-9	74.19	0.09	13.60	1.53	0.06	0.20	0.82	3.92	5.28	0.00	0.30	100	9.20	1.35
P1/151-10	74.42	0.00	13.55	1.45	0.00	0.08	0.78	3.85	5.49	0.00	0.37	100	9.34	1.43
mean	74.42	0.05	13.59	1.51	0.03	0.09	0.81	3.91	5.25	0.00	0.34	-	9.16	1.34
sd	0.24	0.08	0.22	0.08	0.06	0.05	0.06	0.15	0.13	0.00	0.06	-	0.18	0.06

MD90-918-5-Paris	SiO ₂	TiO ₂	Al ₂ O ₃	FeO _{tot}	MnO	MgO	CaO	Na ₂ O	K ₂ O	P ₂ O ₅	ClO	Total	Total Alkali	K ₂ O/Na ₂ O
110/1.	75.02	0.00	13.18	1.54	0.09	0.02	0.73	4.00	5.03	0.00	0.38	100	9.03	1.26
111/1.	75.51	0.02	12.94	1.39	0.15	0.02	0.80	4.08	4.67	0.02	0.39	100	8.75	1.15
112/1.	74.56	0.10	13.59	1.46	0.07	0.04	0.83	3.91	4.95	0.05	0.44	100	8.87	1.27
113/1.	75.13	0.01	13.32	1.63	0.01	0.06	0.81	3.96	4.65	0.00	0.41	100	8.61	1.17
114/1.	75.07	0.00	13.69	1.61	0.00	0.03	0.83	3.97	4.44	0.00	0.34	100	8.41	1.12
115/1.	75.18	0.18	13.01	1.59	0.05	0.06	0.78	4.00	4.80	0.03	0.34	100	8.80	1.20
116/1.	75.12	0.14	13.08	1.48	0.12	0.05	0.79	3.90	4.95	0.00	0.37	100	8.85	1.27
117/1.	75.54	0.02	13.14	1.48	0.08	0.05	0.78	4.03	4.49	0.00	0.40	100	8.52	1.11
118/1.	75.44	0.06	13.03	1.53	0.03	0.05	0.74	3.93	4.84	0.04	0.31	100	8.77	1.23
mean	75.18	0.06	13.22	1.52	0.07	0.04	0.79	3.98	4.76	0.02	0.38	-	8.74	1.20
sd	0.30	0.06	0.26	0.08	0.05	0.01	0.04	0.06	0.21	0.02	0.04	-	0.19	0.06

MD90-918-5-Pisa	SiO ₂	TiO ₂	Al ₂ O ₃	FeO _{tot}	MnO	MgO	CaO	Na ₂ O	K ₂ O	P ₂ O ₅	ClO	Total	Total Alkali	K ₂ O/Na ₂ O
MD90918-5-1	74.36	0.12	13.67	1.51	0.11	0.00	0.84	3.96	4.96	0.00	0.47	100	8.92	1.25
MD90918-5-2	74.28	0.15	13.43	1.65	0.05	0.04	0.76	4.09	5.21	0.00	0.34	100	9.30	1.27
MD90918-5-3	74.58	0.00	13.64	1.63	0.04	0.04	0.73	3.81	5.22	0.00	0.32	100	9.03	1.37
MD90918-5-4	74.77	0.00	13.70	1.35	0.00	0.00	0.72	3.87	5.22	0.00	0.38	100	9.09	1.35
MD90918-5-5	73.82	0.17	13.63	1.41	0.00	0.18	0.91	4.37	5.09	0.00	0.42	100	9.46	1.16
MD90918-5-6	74.66	0.00	13.55	1.48	0.00	0.00	0.78	4.00	5.16	0.00	0.36	100	9.16	1.29
MD90918-5-7	74.81	0.00	13.55	1.49	0.00	0.11	0.69	3.82	5.23	0.00	0.31	100	9.05	1.37
MD90918-5-8	74.22	0.11	13.68	1.55	0.07	0.08	0.68	4.20	5.08	0.00	0.33	100	9.28	1.21
MD90918-5-9	74.63	0.00	13.51	1.45	0.00	0.04	0.85	4.07	5.12	0.00	0.33	100	9.19	1.26
MD90918-5-10	74.39	0.00	13.53	1.47	0.00	0.00	0.83	4.22	5.19	0.00	0.37	100	9.41	1.23
MD90918-5-11	74.43	0.00	13.71	1.44	0.00	0.11	0.93	3.93	5.13	0.00	0.32	100	9.06	1.31
MD90918-5-12	74.29	0.05	13.68	1.48	0.06	0.13	0.65	4.29	5.02	0.00	0.35	100	9.31	1.17
mean	74.44	0.05	13.61	1.49	0.03	0.06	0.78	4.05	5.14	0.00	0.36	-	9.19	1.27
sd	0.28	0.07	0.09	0.09	0.04	0.06	0.09	0.19	0.09	0.00	0.05	-	0.17	0.07

MD90-918-175-Paris	SiO₂	TiO₂	Al₂O₃	FeO_{tot}	MnO	MgO	CaO	Na₂O	K₂O	P₂O₅	ClO	Total	Total Alkali	K₂O/Na₂O
42/1.	59.14	0.23	21.62	1.72	0.12	0.06	1.66	8.26	6.60	0.01	0.58	100	14.85	0.80
43/1.	58.22	0.22	21.60	1.72	0.17	0.08	1.70	8.89	6.75	0.03	0.60	100	15.65	0.76
44/1.	58.74	0.11	21.13	1.92	0.28	0.08	1.74	8.56	6.79	0.02	0.64	100	15.35	0.79
45/1.	58.74	0.21	21.43	1.71	0.29	0.07	1.59	8.77	6.57	0.00	0.62	100	15.34	0.75
46/1.	59.33	0.18	21.16	1.79	0.02	0.10	1.73	8.62	6.51	0.02	0.54	100	15.13	0.76
47/1.	58.56	0.05	21.17	1.73	0.25	0.11	1.62	9.03	6.85	0.01	0.62	100	15.88	0.76
48/1.	58.84	0.13	21.38	1.67	0.21	0.10	1.83	8.71	6.51	0.00	0.63	100	15.21	0.75
50/1.	59.20	0.23	21.08	1.75	0.20	0.08	1.67	8.31	6.84	0.01	0.63	100	15.15	0.82
51/1.	59.38	0.18	20.97	1.66	0.26	0.07	1.62	8.68	6.63	0.01	0.55	100	15.31	0.76
52/1.	59.98	0.29	20.92	1.53	0.10	0.06	1.68	7.28	7.46	0.18	0.51	100	14.74	1.02
53/1.	59.48	0.02	21.73	1.68	0.19	0.06	1.67	8.18	6.40	0.00	0.59	100	14.58	0.78
55/1.	58.52	0.00	21.46	1.73	0.25	0.07	1.63	8.91	6.77	0.04	0.62	100	15.68	0.76
56/1.	58.93	0.18	21.15	1.71	0.22	0.07	1.72	9.10	6.32	0.07	0.54	100	15.42	0.69
58/1.	59.08	0.09	21.17	1.65	0.24	0.08	1.65	8.81	6.61	0.03	0.60	100	15.41	0.75
mean	59.01	0.15	21.28	1.71	0.20	0.08	1.68	8.58	6.69	0.03	0.59	-	15.26	0.78
sd	0.46	0.09	0.25	0.08	0.08	0.02	0.06	0.47	0.28	0.05	0.04	-	0.36	0.08
57/1.	59.28	0.19	21.78	1.61	0.15	0.07	2.75	8.35	5.35	0.00	0.47	100	13.70	0.64

MD90918-175-Pisa	SiO₂	TiO₂	Al₂O₃	FeO_{tot}	MnO	MgO	CaO	Na₂O	K₂O	P₂O₅	ClO	Total	Total Alkali	K₂O/Na₂O
MD90918-175-1	59.58	0.00	22.02	1.71	0.00	0.20	1.66	7.40	6.94	0.00	0.49	100	14.34	0.94
MD90918-175-2	58.34	0.21	21.72	1.78	0.31	0.16	1.44	8.84	6.60	0.00	0.60	100	15.44	0.75
MD90918-175-3	58.75	0.10	21.82	1.71	0.18	0.00	1.61	8.47	6.83	0.00	0.54	100	15.30	0.81
MD90918-175-4	59.09	0.15	21.86	1.55	0.12	0.00	1.54	8.55	6.56	0.00	0.59	100	15.11	0.77
MD90918-175-5	58.46	0.14	21.74	2.05	0.41	0.15	1.69	7.91	6.86	0.00	0.58	100	14.77	0.87
MD90918-175-6	58.25	0.20	22.01	1.84	0.30	0.00	1.64	8.89	6.41	0.00	0.46	100	15.30	0.72
MD90918-175-7	59.16	0.16	21.92	1.64	0.20	0.29	1.46	8.08	6.64	0.00	0.45	100	14.72	0.82
MD90918-175-8	58.80	0.13	21.87	1.69	0.18	0.11	1.58	8.16	6.93	0.00	0.55	100	15.09	0.85
MD90918-175-9	58.77	0.04	21.96	1.65	0.00	0.15	1.63	8.54	6.68	0.00	0.57	100	15.22	0.78
MD90918-175-10	58.67	0.13	21.81	1.76	0.18	0.20	1.77	7.98	6.88	0.00	0.62	100	14.86	0.86
mean	58.79	0.13	21.87	1.74	0.19	0.13	1.60	8.28	6.73	0.00	0.55	-	15.02	0.82
sd	0.40	0.07	0.10	0.14	0.13	0.10	0.10	0.46	0.18	0.00	0.06	-	0.34	0.07

MD90-918-185-Paris													
	SiO ₂	TiO ₂	Al ₂ O ₃	FeO _{tot}	MnO	MgO	CaO	Na ₂ O	K ₂ O	P ₂ O ₅	ClO	Total Alkali	K ₂ O/Na ₂ O
77/1.	58.70	0.19	21.29	1.77	0.17	0.13	1.66	8.81	6.65	0.00	0.64	15.46	0.75
79/1.	58.44	0.12	21.26	1.69	0.10	0.05	1.59	9.41	6.65	0.02	0.67	16.06	0.71
80/1.	59.16	0.21	21.39	1.63	0.13	0.10	1.71	8.60	6.42	0.03	0.63	15.02	0.75
81/1.	58.50	0.28	20.94	1.83	0.24	0.08	1.45	9.09	6.87	0.00	0.73	15.95	0.76
82/1.	58.99	0.00	21.28	1.62	0.24	0.05	1.56	8.87	6.80	0.00	0.58	15.66	0.77
83/1.	59.22	0.14	21.08	1.51	0.18	0.08	1.57	8.95	6.68	0.02	0.58	15.63	0.75
84/1.	59.23	0.31	20.91	1.64	0.14	0.08	1.69	8.68	6.67	0.00	0.66	15.35	0.77
87/1.	59.12	0.02	21.15	1.78	0.25	0.04	1.60	8.88	6.52	0.00	0.64	15.40	0.73
88/1.	58.85	0.15	21.39	1.63	0.16	0.04	1.69	8.84	6.54	0.05	0.65	15.38	0.74
mean	58.91	0.16	21.19	1.68	0.18	0.07	1.61	8.90	6.64	0.01	0.64	15.55	0.75
sd	0.31	0.10	0.18	0.10	0.05	0.03	0.08	0.24	0.14	0.02	0.05	0.32	0.02
78/1.	61.38	0.05	21.58	1.08	0.10	0.02	3.25	7.67	4.65	0.03	0.18	12.32	0.61
86/1.	60.75	0.19	21.50	1.27	0.15	0.04	2.99	7.81	4.93	0.00	0.36	12.74	0.63
mean	61.06	0.12	21.54	1.18	0.12	0.03	3.12	7.74	4.79	0.01	0.27	12.53	0.62
sd	0.45	0.10	0.06	0.14	0.04	0.02	0.18	0.10	0.20	0.02	0.12	0.30	0.02
MD90-918-185-Pisa													
	SiO ₂	TiO ₂	Al ₂ O ₃	FeO _{tot}	MnO	MgO	CaO	Na ₂ O	K ₂ O	P ₂ O ₅	ClO	Total Alkali	K ₂ O/Na ₂ O
MD90918-185-1	58.06	0.27	21.84	1.72	0.23	0.28	1.48	9.18	6.44	0.00	0.49	15.62	0.70
MD90918-185-4	58.39	0.06	21.97	1.76	0.19	0.09	1.60	8.68	6.78	0.00	0.49	15.46	0.78
MD90918-185-5	58.70	0.20	21.54	1.75	0.27	0.07	1.67	8.39	6.78	0.00	0.63	15.17	0.81
MD90918-185-6	58.57	0.21	21.73	1.61	0.17	0.19	1.59	8.83	6.59	0.00	0.50	15.42	0.75
MD90918-185-7	58.41	0.16	21.69	1.84	0.26	0.19	1.38	8.72	6.87	0.00	0.49	15.59	0.79
MD90918-185-9	58.75	0.00	22.04	1.63	0.00	0.20	1.62	8.90	6.43	0.00	0.43	15.33	0.72
mean	58.48	0.15	21.80	1.72	0.19	0.17	1.56	8.78	6.65	0.00	0.51	15.43	0.76
sd	0.25	0.10	0.19	0.09	0.10	0.08	0.11	0.26	0.19	0.00	0.07	0.17	0.04
MD90918-185-2	60.37	0.00	22.43	1.16	0.00	0.14	2.16	6.95	6.41	0.00	0.37	13.36	0.92
MD90918-185-10	59.97	0.28	22.14	1.38	0.30	0.00	2.56	7.87	5.21	0.00	0.29	13.08	0.66
MD90918-185-8	59.60	0.21	22.16	1.65	0.16	0.09	2.38	7.74	5.57	0.00	0.45	13.31	0.72
mean	59.98	0.16	22.24	1.40	0.15	0.08	2.37	7.52	5.73	0.00	0.37	13.25	0.77
sd	0.39	0.15	0.16	0.25	0.15	0.07	0.20	0.50	0.62	0.00	0.08	0.15	0.14

<u>MD90-918 210-Pisa</u>														
	SiO ₂	TiO ₂	Al ₂ O ₃	FeO _{tot}	MnO	MgO	CaO	Na ₂ O	K ₂ O	P ₂ O ₅	ClO	Total	Total Alkali	K ₂ O/Na ₂ O
P1047-1	58.32	0.22	21.54	2.01	0.28	0.14	1.92	8.11	6.95	0.00	0.50	100	15.06	0.86
P1047-4	57.93	0.15	22.39	1.86	0.23	0.12	1.65	8.15	6.98	0.00	0.55	100	15.13	0.86
P1047-7	58.58	0.07	21.81	1.65	0.00	0.16	1.71	8.62	6.68	0.00	0.73	100	15.30	0.77
P1047-8	58.49	0.26	21.68	1.86	0.30	0.20	1.62	8.35	6.76	0.00	0.48	100	15.11	0.81
P1047-9	58.98	0.17	21.86	1.70	0.12	0.22	1.54	8.05	6.82	0.00	0.55	100	14.87	0.85
P1047-10	59.54	0.00	21.74	1.71	0.07	0.29	1.64	7.49	6.92	0.00	0.60	100	14.41	0.92
P1047-13	59.05	0.14	21.76	1.72	0.18	0.12	1.89	7.74	6.60	0.00	0.81	100	14.34	0.85
P1047-14	58.87	0.18	21.80	1.75	0.18	0.21	2.03	7.75	6.61	0.00	0.63	100	14.36	0.85
P1047-20	58.63	0.11	21.80	1.78	0.19	0.10	1.70	8.26	6.88	0.00	0.56	100	15.14	0.83
mean	58.71	0.14	21.82	1.78	0.17	0.17	1.74	8.06	6.80	0.00	0.60	-	14.86	0.85
sd	0.47	0.08	0.23	0.11	0.10	0.06	0.16	0.35	0.14	0.00	0.11	-	0.38	0.04
<u>MD90-918 210-Pisa</u>														
	SiO ₂	TiO ₂	Al ₂ O ₃	FeO _{tot}	MnO	MgO	CaO	Na ₂ O	K ₂ O	P ₂ O ₅	ClO	Total	Total Alkali	K ₂ O/Na ₂ O
P1047-2	74.45	0.17	13.18	1.59	0.18	0.11	0.76	3.98	5.33	0.00	0.25	100	9.31	1.34
P1047-3	74.82	0.13	13.37	1.52	0.09	0.00	0.77	3.66	5.29	0.00	0.36	100	8.95	1.45
P1047-5	74.83	0.07	13.29	1.42	0.00	0.12	0.75	4.03	5.18	0.00	0.31	100	9.21	1.29
P1047-6	75.05	0.11	13.35	1.59	0.12	0.09	0.71	3.53	5.14	0.00	0.31	100	8.67	1.46
P1047-11	75.12	0.00	13.65	1.31	0.00	0.10	0.78	3.45	5.26	0.00	0.33	100	8.71	1.52
P1047-12	74.53	0.10	13.36	1.53	0.12	0.09	0.81	3.95	5.19	0.00	0.32	100	9.14	1.31
P1047-15	74.86	0.09	13.47	1.37	0.00	0.00	0.79	3.79	5.33	0.00	0.30	100	9.12	1.41
P1047-16	74.88	0.00	13.51	1.32	0.00	0.12	0.79	3.87	5.22	0.00	0.30	100	9.09	1.35
P1047-17	74.75	0.00	13.57	1.39	0.00	0.04	0.76	3.77	5.35	0.00	0.36	100	9.12	1.42
P1047-18	75.01	0.05	13.38	1.43	0.00	0.00	0.79	3.82	5.28	0.00	0.26	100	9.10	1.38
P1047-19	75.13	0.05	13.45	1.45	0.06	0.00	0.80	3.52	5.25	0.00	0.28	100	8.77	1.49
Media	74.86	0.07	13.42	1.45	0.05	0.06	0.77	3.76	5.26	0.00	0.31	-	9.02	1.40
sd	0.22	0.06	0.13	0.10	0.07	0.05	0.03	0.20	0.07	0.00	0.04	-	0.21	0.08

<u>MD90-918 217-Pisa</u>	SiO ₂	TiO ₂	Al ₂ O ₃	FeO _{tot}	MnO	MgO	CaO	Na ₂ O	K ₂ O	P ₂ O ₅	ClO	Total	Total Alkali	K ₂ O/Na ₂ O
<i>PI059-1</i>	74.19	0.25	13.34	1.62	0.27	0.00	0.78	3.96	5.24	0.00	0.34	100	9.20	1.32
<i>PI059-2</i>	74.67	0.06	13.24	1.54	0.00	0.00	0.85	4.01	5.32	0.00	0.30	100	9.33	1.33
<i>PI059-3</i>	74.42	0.11	13.21	1.64	0.11	0.16	0.84	3.90	5.21	0.00	0.29	100	9.11	1.34
<i>PI059-4</i>	74.82	0.09	13.20	1.61	0.00	0.00	0.87	3.88	5.15	0.00	0.37	100	9.03	1.33
<i>PI059-5</i>	74.90	0.00	13.35	1.48	0.00	0.00	0.99	3.89	5.15	0.00	0.25	100	9.04	1.32
<i>PI059-6</i>	74.38	0.32	13.36	1.68	0.24	0.06	0.66	3.93	5.05	0.00	0.32	100	8.98	1.28
<i>PI059-7</i>	74.51	0.11	13.56	1.40	0.00	0.00	0.83	3.94	5.36	0.00	0.29	100	9.30	1.36
<i>PI059-8</i>	74.78	0.00	13.45	1.50	0.00	0.07	0.82	3.97	5.09	0.00	0.33	100	9.06	1.28
<i>PI059-9</i>	74.93	0.12	13.18	1.52	0.00	0.00	0.87	3.89	5.20	0.00	0.29	100	9.09	1.34
<i>PI059-10</i>	74.68	0.00	13.55	1.41	0.00	0.06	0.77	4.08	5.17	0.00	0.27	100	9.25	1.27
<i>Media</i>	74.63	0.11	13.34	1.54	0.06	0.04	0.83	3.95	5.19	0.00	0.31	-	9.14	1.32
<i>sd</i>	0.24	0.11	0.14	0.10	0.11	0.05	0.08	0.06	0.10	0.00	0.04	-	0.12	0.03

<u>MD90-918 219-Paris</u>	SiO ₂	TiO ₂	Al ₂ O ₃	FeO _{tot}	MnO	MgO	CaO	Na ₂ O	K ₂ O	P ₂ O ₅	ClO	Total	Total Alkali	K ₂ O/Na ₂ O
<i>77/1.</i>	75.06	0.11	13.02	1.53	0.17	0.05	0.87	3.77	5.07	0.02	0.33	100	8.84	1.35
<i>78/1.</i>	74.80	0.00	13.11	1.58	0.08	0.00	0.82	4.07	5.18	0.01	0.37	100	9.25	1.27
<i>79/1.</i>	74.93	0.14	13.46	1.40	0.05	0.02	0.99	3.76	4.88	0.00	0.37	100	8.63	1.30
<i>80/1.</i>	75.14	0.01	13.51	1.42	0.00	0.00	0.92	3.63	4.99	0.00	0.38	100	8.62	1.37
<i>81/1.</i>	75.54	0.14	13.13	1.47	0.05	0.06	0.80	3.58	4.87	0.00	0.37	100	8.45	1.36
<i>82/1.</i>	74.33	0.09	12.87	1.68	0.12	0.03	0.72	4.20	5.54	0.00	0.42	100	9.75	1.32
<i>83/1.</i>	74.71	0.07	12.87	1.49	0.05	0.06	0.85	4.17	5.39	0.00	0.33	100	9.56	1.29
<i>84/1.</i>	73.58	0.13	12.51	1.65	0.08	0.04	0.93	4.61	6.03	0.03	0.40	100	10.64	1.31
<i>92/1.</i>	75.54	0.01	13.24	1.33	0.15	0.02	0.85	3.62	4.82	0.00	0.42	100	8.44	1.33
<i>93/1.</i>	75.48	0.00	13.15	1.56	0.08	0.03	0.68	3.90	4.72	0.02	0.38	100	8.62	1.21
<i>94/1.</i>	75.50	0.07	12.99	1.42	0.05	0.08	0.83	3.57	5.16	0.03	0.30	100	8.73	1.44
<i>Media</i>	74.96	0.07	13.08	1.50	0.08	0.04	0.84	3.90	5.15	0.01	0.37	-	9.05	1.32
<i>sd</i>	0.61	0.06	0.28	0.11	0.05	0.03	0.09	0.33	0.38	0.01	0.04	-	0.69	0.06

MD90-918 219-Pisa														
	SiO ₂	TiO ₂	Al ₂ O ₃	FeO _{tot}	MnO	MgO	CaO	Na ₂ O	K ₂ O	P ₂ O ₅	ClO	Total Alkali	K ₂ O/Na ₂ O	
P1060-1	74.68	0.00	13.48	1.36	0.00	0.13	0.70	4.03	5.35	0.00	0.27	100	9.38	1.33
P1060-2	74.79	0.00	13.43	1.47	0.06	0.00	0.82	3.90	5.24	0.00	0.30	100	9.14	1.34
P1060-4	74.61	0.18	13.35	1.45	0.18	0.00	0.83	3.80	5.29	0.00	0.32	100	9.09	1.39
P1060-5	74.73	0.00	13.28	1.48	0.00	0.08	0.93	3.97	5.20	0.00	0.34	100	9.17	1.31
P1060-6	74.57	0.05	13.46	1.49	0.06	0.11	0.88	3.94	5.14	0.00	0.30	100	9.08	1.30
P1060-7	74.58	0.06	13.21	1.44	0.00	0.06	0.79	4.08	5.48	0.00	0.29	100	9.56	1.34
P1060-9	73.99	0.22	13.45	1.54	0.20	0.07	0.88	4.00	5.36	0.00	0.30	100	9.36	1.34
P1060-10	74.72	0.05	13.50	1.42	0.00	0.10	0.80	3.89	5.19	0.00	0.33	100	9.08	1.33
Media	74.58	0.07	13.40	1.46	0.06	0.07	0.83	3.95	5.28	0.00	0.31	-	9.23	1.34
sd	0.25	0.08	0.10	0.05	0.08	0.05	0.07	0.09	0.11	0.00	0.02	-	0.18	0.03
MD90-918 223-Paris														
	SiO ₂	TiO ₂	Al ₂ O ₃	FeO _{tot}	MnO	MgO	CaO	Na ₂ O	K ₂ O	P ₂ O ₅	ClO	Total Alkali	K ₂ O/Na ₂ O	
85 / 1.	58.09	0.21	21.73	1.80	0.35	0.07	1.52	9.00	6.59	0.00	0.64	100	15.60	0.73
89 / 1.	58.40	0.18	21.42	1.85	0.12	0.08	1.59	8.75	6.88	0.04	0.69	100	15.63	0.79
95 / 1.	58.86	0.16	21.11	1.74	0.31	0.10	1.89	8.67	6.51	0.02	0.64	100	15.18	0.75
97 / 1.	59.15	0.02	21.42	1.76	0.30	0.08	1.59	8.23	6.73	0.01	0.70	100	14.97	0.82
mean	58.62	0.14	21.42	1.79	0.27	0.08	1.65	8.67	6.68	0.02	0.67	-	15.34	0.77
sd	0.47	0.08	0.25	0.05	0.10	0.01	0.16	0.32	0.16	0.02	0.03	-	0.32	0.04
MD90-918 223-Pisa														
	SiO ₂	TiO ₂	Al ₂ O ₃	FeO _{tot}	MnO	MgO	CaO	Na ₂ O	K ₂ O	P ₂ O ₅	ClO	Total Alkali	K ₂ O/Na ₂ O	
MD 223-1	58.33	0.21	21.77	1.79	0.24	0.11	1.82	8.17	6.99	0.00	0.57	100	15.16	0.86
MD 223-2	59.40	0.19	22.06	1.77	0.15	0.14	1.59	7.51	6.62	0.00	0.55	100	14.13	0.88
MD 223-3	58.02	0.21	21.79	1.91	0.21	0.13	1.65	8.49	7.02	0.00	0.55	100	15.51	0.83
MD 223-4	59.38	0.00	21.94	1.59	0.00	0.00	1.55	8.46	6.38	0.00	0.70	100	14.84	0.75
MD 223-5	58.35	0.19	21.78	1.81	0.24	0.11	1.41	8.85	6.68	0.00	0.58	100	15.53	0.75
MD 223-6	58.68	0.19	21.41	1.83	0.32	0.23	1.83	8.07	6.89	0.00	0.55	100	14.96	0.85
MD 223-7	58.48	0.23	21.96	1.76	0.21	0.12	1.57	8.26	6.86	0.00	0.55	100	15.12	0.83
MD 223-8	58.54	0.08	21.57	1.88	0.18	0.00	1.78	8.45	7.06	0.00	0.48	100	15.51	0.84
MD 223-9	60.26	0.11	22.40	1.39	0.00	0.10	3.44	7.87	4.12	0.00	0.31	100	11.99	0.52
MD 223-10	58.80	0.00	21.65	1.72	0.06	0.08	1.56	8.75	6.87	0.00	0.51	100	15.62	0.79
MD 223-11	58.81	0.00	22.25	1.56	0.00	0.09	1.87	8.13	6.76	0.00	0.54	100	14.89	0.83
MD 223-12	58.84	0.00	22.00	1.64	0.00	0.17	1.61	8.24	7.00	0.00	0.51	100	15.24	0.85
mean	58.82	0.12	21.88	1.72	0.13	0.11	1.81	8.27	6.60	0.00	0.53	-	14.88	0.80
sd	0.61	0.10	0.28	0.15	0.12	0.06	0.53	0.37	0.81	0.00	0.09	-	1.00	0.10

MD90-918 230-Paris	SiO ₂	TiO ₂	Al ₂ O ₃	FeO _{tot}	MnO	MgO	CaO	Na ₂ O	K ₂ O	P ₂ O ₅	ClO	Total	Total Alkali	K ₂ O/Na ₂ O
136/1.	59.34	0.12	21.07	1.77	0.19	0.06	1.68	8.76	6.39	0.02	0.59	100	15.16	0.73
138/1.	59.30	0.32	21.53	1.61	0.20	0.05	2.02	7.86	6.52	0.02	0.57	100	14.38	0.83
139/1.	58.58	0.24	21.26	1.91	0.09	0.11	1.70	8.70	6.78	0.02	0.61	100	15.48	0.78
140/1.	59.08	0.20	21.29	1.71	0.19	0.06	1.69	8.64	6.46	0.00	0.68	100	15.11	0.75
mean	59.07	0.22	21.29	1.75	0.17	0.07	1.77	8.49	6.54	0.01	0.61	-	15.03	0.77
sd	0.35	0.08	0.19	0.13	0.05	0.03	0.16	0.43	0.17	0.01	0.04	-	0.47	0.04
MD90-918 230-Pisa	SiO ₂	TiO ₂	Al ₂ O ₃	FeO _{tot}	MnO	MgO	CaO	Na ₂ O	K ₂ O	P ₂ O ₅	ClO	Total	Total Alkali	K ₂ O/Na ₂ O
MD90918-230-1	58.39	0.13	21.77	1.83	0.21	0.21	1.50	8.48	6.77	0.00	0.71	100	15.25	0.80
MD90918-230-2	58.17	0.17	21.92	1.76	0.20	0.38	1.96	8.70	6.17	0.00	0.58	100	14.87	0.71
MD90918-230-3	58.56	0.19	21.91	1.56	0.19	0.19	1.65	8.46	6.75	0.00	0.53	100	15.21	0.80
MD90918-230-4	58.67	0.22	21.96	1.77	0.15	0.00	1.64	8.25	6.74	0.00	0.60	100	14.99	0.82
MD90918-230-5	58.66	0.15	21.77	1.78	0.18	0.34	1.50	8.60	6.44	0.00	0.58	100	15.04	0.75
MD90918-230-6	58.34	0.25	21.87	1.84	0.22	0.18	1.53	8.61	6.63	0.00	0.55	100	15.24	0.77
MD90918-230-7	59.06	0.09	21.83	1.65	0.09	0.00	1.84	8.11	6.78	0.00	0.54	100	14.89	0.84
MD90918-230-8	58.59	0.14	21.76	1.72	0.19	0.23	1.38	8.78	6.61	0.00	0.61	100	15.39	0.75
MD90918-230-10	58.79	0.17	21.77	1.68	0.18	0.13	1.70	8.52	6.48	0.00	0.56	100	15.00	0.76
media	58.58	0.17	21.84	1.73	0.18	0.18	1.63	8.50	6.60	0.00	0.58	-	15.10	0.78
sd	0.26	0.05	0.08	0.09	0.04	0.13	0.18	0.21	0.20	0.00	0.05	-	0.18	0.04

MD90-918 820-Paris	SiO ₂	TiO ₂	Al ₂ O ₃	FeO _{tot}	MnO	MgO	CaO	Na ₂ O	K ₂ O	P ₂ O ₅	ClO	Total	Total Alkali	K ₂ O/Na ₂ O
119/1.	69.17	0.22	15.96	2.05	0.15	0.44	1.50	4.65	5.44	0.10	0.32	100	10.09	1.17
120/1.	69.41	0.28	15.62	2.66	0.14	0.57	1.49	4.19	5.23	0.04	0.37	100	9.41	1.25
121/1.	69.27	0.39	15.71	2.39	0.17	0.38	1.43	4.54	5.30	0.08	0.34	100	9.84	1.17
122/1.	69.40	0.25	15.77	2.20	0.18	0.40	1.50	4.66	5.24	0.08	0.31	100	9.90	1.12
124/1.	69.33	0.11	15.85	2.09	0.11	0.42	1.49	4.91	5.27	0.06	0.36	100	10.18	1.07
127/1.	69.90	0.24	15.89	2.12	0.13	0.37	1.40	4.59	5.03	0.03	0.31	100	9.62	1.09
128/1.	68.82	0.31	15.95	2.48	0.13	0.44	1.56	4.54	5.40	0.10	0.27	100	9.94	1.19
129/1.	69.21	0.34	15.56	2.33	0.05	0.42	1.62	4.67	5.43	0.06	0.32	100	10.10	1.16
media	69.31	0.27	15.79	2.29	0.13	0.43	1.50	4.59	5.29	0.07	0.32	-	9.88	1.15
sd	0.30	0.09	0.15	0.22	0.04	0.06	0.07	0.20	0.14	0.03	0.03	-	0.26	0.06
MD90-918 820-Pisa	SiO ₂	TiO ₂	Al ₂ O ₃	FeO _{tot}	MnO	MgO	CaO	Na ₂ O	K ₂ O	P ₂ O ₅	ClO	Total	Total Alkali	K ₂ O/Na ₂ O
MD90918-820-1	68.79	0.39	16.16	2.33	0.10	0.52	1.22	4.55	5.53	0.00	0.40	100	10.08	1.22
MD90918-820-2	68.73	0.33	16.50	2.19	0.13	0.58	1.35	4.60	5.27	0.00	0.30	100	9.87	1.15
MD90918-820-3	69.00	0.38	16.10	2.17	0.15	0.41	1.46	4.51	5.59	0.00	0.24	100	10.10	1.24
MD90918-820-4	68.75	0.33	16.21	2.22	0.19	0.47	1.47	4.79	5.24	0.00	0.34	100	10.03	1.09
MD90918-820-5	67.57	0.31	16.64	2.66	0.13	0.59	1.84	4.72	5.16	0.00	0.36	100	9.88	1.09
MD90918-820-6	68.43	0.30	16.05	2.47	0.17	0.46	1.57	4.58	5.64	0.00	0.33	100	10.22	1.23
MD90918-820-7	68.75	0.31	16.02	2.41	0.05	0.44	1.56	4.46	5.59	0.00	0.41	100	10.05	1.25
MD90918-820-8	68.28	0.47	16.20	2.30	0.23	0.51	1.48	4.73	5.48	0.00	0.31	100	10.21	1.16
MD90918-820-9	69.33	0.19	16.35	1.94	0.00	0.42	1.30	4.75	5.35	0.00	0.35	100	10.10	1.13
MD90918-820-10	68.68	0.31	16.18	2.00	0.06	0.61	1.84	4.61	5.28	0.00	0.43	100	9.89	1.15
MD90918-820-11	69.02	0.32	16.36	2.26	0.10	0.39	1.46	4.51	5.31	0.00	0.27	100	9.82	1.18
MD90918-820-12	69.59	0.21	16.44	2.23	0.21	0.47	1.16	3.93	5.37	0.00	0.22	100	9.30	1.37
media	68.74	0.32	16.27	2.27	0.13	0.49	1.48	4.56	5.40	0.00	0.33	-	9.96	1.19
sd	0.51	0.07	0.19	0.20	0.07	0.07	0.21	0.23	0.16	0.00	0.07	-	0.25	0.08

Table 4

Monte Pilato LP22 cycle X	SiO ₂	TiO ₂	Al ₂ O ₃	Fe ₂ O ₃	MnO	MgO	CaO	Na ₂ O	K ₂ O	P ₂ O ₅	ClO	Cr ₂ O ₃	SO ₂	F	Total	Total Alkali	K ₂ O/Na ₂ O	
bulk rock	74.32	0.09	12.75	2.07	0.11	0.16	0.67	4.14	4.69	0.01	-	-	-	-	99.01	8.83	1.13	
from Giuncada et al., 2003																		
Monte Pilato PI-134	SiO ₂	TiO ₂	Al ₂ O ₃	Fe ₂ O ₃	MnO	MgO	CaO	Na ₂ O	K ₂ O	P ₂ O ₅	ClO	Cr ₂ O ₃	SO ₂	F	Total	Total Alkali	K ₂ O/Na ₂ O	
mean	74.16	0.12	13.51	1.58	0.21	0.05	0.76	4.07	5.32	0.00	0.34	-	-	-	-	9.39	1.31	
sd	0.18	0.07	0.08	0.08	0.25	0.06	0.05	0.09	0.07	0.00	0.03	-	-	-	-	0.08	0.04	
n=10																		
Mercato-Ottaviano	SiO ₂	TiO ₂	Al ₂ O ₃	FeO _{tot}	MnO	MgO	CaO	Na ₂ O	K ₂ O	P ₂ O ₅	ClO	Cr ₂ O ₃	SO ₂	F	Total	Total Alkali	K ₂ O/Na ₂ O	
mean	59.45	0.10	22.12	1.75	0.21	0.09	1.59	7.95	6.11	0.00	0.62	-	-	-	-	14.06	0.77	
sd	0.38	0.00	0.09	0.07	0.00	0.04	0.05	0.32	0.16	0.00	0.01	-	-	-	-	0.44	0.02	
n=6, from Turney et al., 2008																		
Mercato base TM-6b	SiO ₂	TiO ₂	Al ₂ O ₃	FeO _{tot}	MnO	MgO	CaO	Na ₂ O	K ₂ O	P ₂ O ₅	ClO	Cr ₂ O ₃	SO ₂	F	Total	Total Alkali	K ₂ O/Na ₂ O	
mean	58.68	0.14	21.41	1.80	0.18	0.07	1.76	8.58	6.76	0.02	0.58	-	-	0.10	-	15.34	0.79	
sd	0.30	0.03	0.21	0.13	0.03	0.01	0.25	0.18	0.54	0.02	0.04	-	-	0.09	-	0.55	0.07	
n=10, from Wulff et al., 2004																		
Mercato base TM-6a	SiO ₂	TiO ₂	Al ₂ O ₃	FeO _{tot}	MnO	MgO	CaO	Na ₂ O	K ₂ O	P ₂ O ₅	ClO	Cr ₂ O ₃	SO ₂	F	Total	Total Alkali	K ₂ O/Na ₂ O	
mean	60.06	0.31	20.53	2.26	0.12	0.16	2.48	5.41	8.11	0.05	0.50	-	-	0.01	-	13.53	1.55	
sd	0.98	0.09	0.47	0.49	0.04	0.07	0.36	0.93	0.82	0.03	0.15	-	-	0.02	-	0.56	0.37	
n=12, from Wulff et al., 2004																		
Mercato	SiO ₂	TiO ₂	Al ₂ O ₃	FeO _{tot}	MnO	MgO	CaO	Na ₂ O	K ₂ O	P ₂ O ₅	ClO	Cr ₂ O ₃	SO ₂	F	Total	Total Alkali	K ₂ O/Na ₂ O	
mean	58.82	0.13	21.81	1.77	0.14	0.09	1.66	8.60	6.97	-	0.53	-	-	-	-	15.49	0.82	
sd	0.70	0.08	0.41	0.19	0.10	0.08	0.26	0.63	0.39	-	0.09	-	-	-	-	0.49	0.11	
n=40, from Santacroce																		
Mercato OT0702-2	SiO ₂	TiO ₂	Al ₂ O ₃	FeO _{tot}	MnO	MgO	CaO	Na ₂ O	K ₂ O	P ₂ O ₅	ClO	Cr ₂ O ₃	SO ₂	F	Total	Total Alkali	K ₂ O/Na ₂ O	
mean	59.10	0.17	21.88	1.95	0.17	0.16	1.76	7.56	7.02	0.00	0.52	-	-	-	-	14.58	0.93	
sd	0.55	0.09	0.13	0.11	0.07	0.09	0.13	0.56	0.27	0.00	0.03	-	-	-	-	0.83	0.48	
n=9, from Vogel et al., 2009																		
VES-8622	SiO ₂	TiO ₂	Al ₂ O ₃	FeO _{tot}	MnO	MgO	CaO	Na ₂ O	K ₂ O	P ₂ O ₅	ClO	Cr ₂ O ₃	SO ₂	F	Total	Total Alkali	K ₂ O/Na ₂ O	
mean	60.81	0.14	20.17	1.72	-	0.25	1.52	8.02	6.46	-	-	-	-	-	99.09	14.48	0.81	
from Paterne et al., 1988																		
KET-8218	SiO ₂	TiO ₂	Al ₂ O ₃	FeO _{tot}	MnO	MgO	CaO	Na ₂ O	K ₂ O	P ₂ O ₅	ClO	Cr ₂ O ₃	SO ₂	F	Total	Total Alkali	K ₂ O/Na ₂ O	
mean	60.04	0.10	21.49	1.74	-	0.00	1.82	7.72	7.05	-	-	-	-	-	99.96	14.77	0.91	
from Paterne et al., 1988																		

	SiO ₂	TiO ₂	Al ₂ O ₃	FeO _{tot}	MnO	MgO	CaO	Na ₂ O	K ₂ O	P ₂ O ₅	ClO	Cr ₂ O ₃	SO ₂	F	Total	Total Alkali	K ₂ O/Na ₂ O
MD90-917 240																	
mean	75.02	0.07	12.94	1.60	0.06	0.03	0.76	3.79	5.57	0.02	0.19	0.00	0.01	-	100.05	9.35	1.48
sd	0.29	0.08	0.45	0.15	0.09	0.06	0.09	0.24	0.26	0.03	0.23	0.00	0.02	-	-	0.24	0.14
n=7, from Siani et al., 2004																	
MD90-917 250																	
mean	74.74	0.12	12.93	1.59	0.12	0.04	0.79	3.89	5.63	0.16	0.03	0.00	0.04	-	100.05	9.52	1.45
sd	0.35	0.09	0.41	0.17	0.10	0.05	0.12	0.25	0.15	0.21	0.06	0.00	0.06	-	-	0.21	0.12
n=32, from Siani et al., 2004																	
E-1 Paterne et al. 1987																	
Media KEI 8004 - 8003 - 8011	75.96	0.10	13.28	1.44	-	0.00	0.69	3.25	5.24	-	-	-	-	-	99.96	8.49	1.61
from Paterne et al., 1988																	
KEI 8003																	
mean	75.87	0.08	13.38	1.62	-	0.00	0.68	2.90	5.43	-	-	-	-	-	99.96	8.33	1.87
from Paterne et al., 1988																	
KEI 8004																	
mean	76.21	0.13	13.06	1.48	-	0.01	0.72	3.30	5.07	-	-	-	-	-	99.98	8.37	1.54
from Paterne et al., 1988																	
KEI 8011																	
mean	75.81	0.08	13.40	1.22	-	0.00	0.68	3.55	5.22	-	-	-	-	-	99.96	8.77	1.47
from Paterne et al., 1988																	
Monte Guardia MG4 Base B																	
mean	69.62	0.25	16.06	1.90	0.11	0.21	1.70	4.49	5.32 bdl	-	3.260	-	-	-	-	9.81	1.18
sd	2.27	0.09	1.53	0.53	0.06	0.13	0.78	0.61	0.68 bdl	-	600	-	-	-	-	-	-
n=11, from De Rosa et al., 2003																	

VI. Chapter VI: Conclusion and Perspectives

The aim of the present study was to improve the knowledge of the past Italian volcanic activity and to improve the knowledge about volcanic ash dispersal during explosive eruptions of the last Quaternary in the Central Mediterranean area. In this way, four sedimentary cores from three various sites were studied for tephra layers and cryptotephra.

Twenty-two tephra layers were recovered from the studied cores. Among them, 17 tephra layers were correlated to well known eruptions whereas the remaining tephra layers do not have any well-known proximal counterparts.

Concerning the Shkodra site, 12 ka of volcanic activity were recorded, including the A.D. 472 and Avellino (ca. 3.9 cal ka BP) eruptions from Mount Somma-Vesuvius, FL eruption (ca. 3.4 cal ka BP) from Mount Etna, Astroni (ca. 4.2 cal. ka BP), Agnano Monte Spina (ca. 4.5 cal. ka BP) and Agnano Pomici Principali (ca. 12.3 cal. ka BP) eruptions from Phlegrean Fields caldera.

The findings from the Balkan JO 2004 core encompass the last 131 ka. Five tephra layers were correlated with the corresponding proximal deposits. All the five tephra layers are from Italian volcanoes: FL eruption (ca. 3.4 cal ka BP) from Mount Etna, SMP1-Y3 and Campanian Ignimbrite (30-31 and 39 cal ka BP respectively) from the Phlegrean Fields caldera, X6 (107 ka) of generic Campanian origin and P11 (131 ka) from Pantelleria volcano.

Results from the Ionian core MD 90-918 evidence how distal archives can preserve efficiently the traces of the past volcanic activity with respect to the proximal ones, and points out how the eruptive history of one of the most hazardous and studied volcanoes in the world, i.e. the Mount Somma-Vesuvius, is not yet completely resolved. In particular, the Ionian record encompasses the last 22 ka of volcanic activity, including the Monte Pilato (A.D. 1200), Gabelotto Fiumebianco (E-1 tephra layer, ca. 8.6 cal ka BP) and Monte Guardia (ca. 22 ka BP) eruptions from the Lipari volcano. The other five tephra layers have all Na-phonolitic composition, which clearly indicates the Somma-Vesuvius as the source. This unique composition indicates the Mercato deposits (ca. 8.9 cal ka BP) as proximal counterpart, but poses some problems with correlation of tephra layers deposited over 2000 years with a single eruption. This suggests the occurrence of interplinian activity between the eruptions of Mercato (ca. 8.9 cal ka BP) and Avellino (ca. 3.9 cal ka BP), which is poorly documented in the proximal stratigraphic succession.

The overall results show how the tephrostratigraphy is important either in the volcanological perspective or from a chronological point of view.

From a volcanological point of view these results, and the facts that some tephra layers were recognised for the first time and several hundreds kilometers far from the source, imply that the eruptive physical characteristics like the eruptive classification, the Volcanic Explosivity Index, the frequency of the volcanic activity must be revised.

All these findings were collated into a GIS data-base, together with previous data from literature, which represents a comprehensive database for the Central Mediterranean area. It includes more than three-hundred tephra layers. As an example, for each eruption is possible to extract dispersal area of the related tephra and the location of the cores from which it is recovered.

The GIS data-base can represent an important tool for future volcanic hazard investigations, since ash fragments (e.g. micropumice, glass shards...) may affect human health (e.g. respiratory problems, pollution of water resources...) and cause damage to buildings (i.e. roof collapses), the interruption of lifelines (i.e. roads, railroads), closure of airports and disturbance to the communications and powerlines.

In general, the volcanic ash accumulation in distal zones represents an underestimated hazard, and the GIS data-base can help in the assessment of the area potentially affected by volcanic ash hazard. It also represents an important tool for Civil Protection purposes, which have the responsibility to protect population and infrastructures from natural hazard through mitigation plans.

Moreover, the GIS data-base provides an useful tool for any research that includes volcanic ash layers in the Central Mediterranean area, including volcanology, paleoceanography and Quaternary Sciences.

In perspective, some questions are still outstanding and need further discussion.

1) The Mediterranean Sea is composed of many small basins which have an important capacity to record the evolution and the climatic fluctuation during the last glacial-interglacial period (*Emeis et al., 2000; Principato et al., 2003*) and to preserve the volcanic deposit in their sediment (e.g. *Keller et al., 1978; Paterne et al., 1988, 1990, 2008*).

Sediment records in the Eastern Mediterranean show that such variations induced by periodic climatic changes have occurred since at least the Pliocene: they resulted in recurring anoxic conditions in the Mediterranean Sea, during which dark-colored and organic carbon rich sediment layers were formed (*Cita et al., 1977; Thunnell et al., 1984; Emeis et al., 2000*). These layer deposits are representative of one paleoclimatic event called Sapropel. The last one of this event is the Sapropel S1 event, which is present in the marine deep core MD 90-918 was deposited in the Eastern and Central Mediterranean basins during the Early-Mid Holocene (ca 6600-9500 yr cal. BP, e.g. *Emeis et al., 2000*). The exact timing of S1 formation depends through Mediterranean basins, depends on water depth, sediment accumulation rates, organics matter flux and the position relative to intermediate and deep-water sources (e.g. *Mercone et al., 2000; Casford et al., 2003; Sperling et al., 2003; Kotthoff et al., 2008*). The **Figure 6-1** is the map of cores where was found the tephra layer Gabelotto Fiumebianco / E-1. Moreover, cores MD 90-917, KET 8216, MD 90-918 and RC 9-191, which are localised along the Adriatic and Ionian basins, have both this tephra layer and the Sapropel S1 deposit (*Paterne, 1985; Paterne et al., 1986, 1988, Fontugne et al., 1989; Siani et al., 2001, 2004*). In cores KET 8216 and RC 9-191, the sedimentation rate is very lower and it is impossible to distinct the interruption of the Sapropel S1 (**Figure 6-2**). But in cores MD 90-917 and MD 90-918, the sedimentation rate is high. In the MD 90-917 core the Sapropel interruption is between 239 and 247 cm depth, and the double tephra layers of Lipari are at 240 and 250 cm depth. In the MD 90-918 core the Sapropel interruption is between 210 and 219 cm depth, and the double tephra layers of Lipari are at 210 and 218 cm depth.

What is the exact chronological relation between the paleoclimatic event Sapropel S1 and the explosive event of Gabelotto Fiumebianco / E-1 from Lipari volcano?

The tephra of Gabelotto-Fiumebianco can represent a temporal marker of the chronological evolution of the paleoclimatic event Sapropel S1?

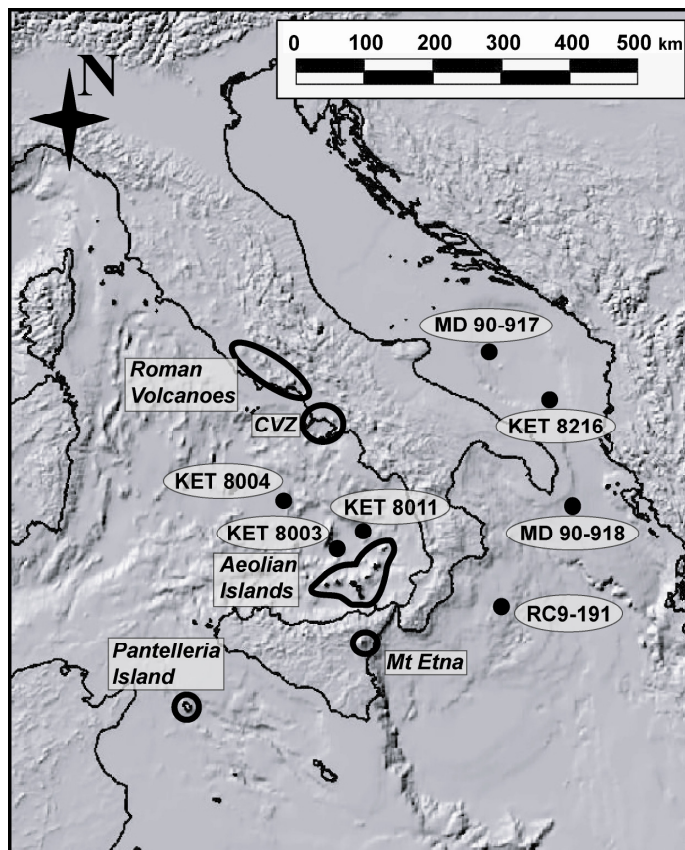
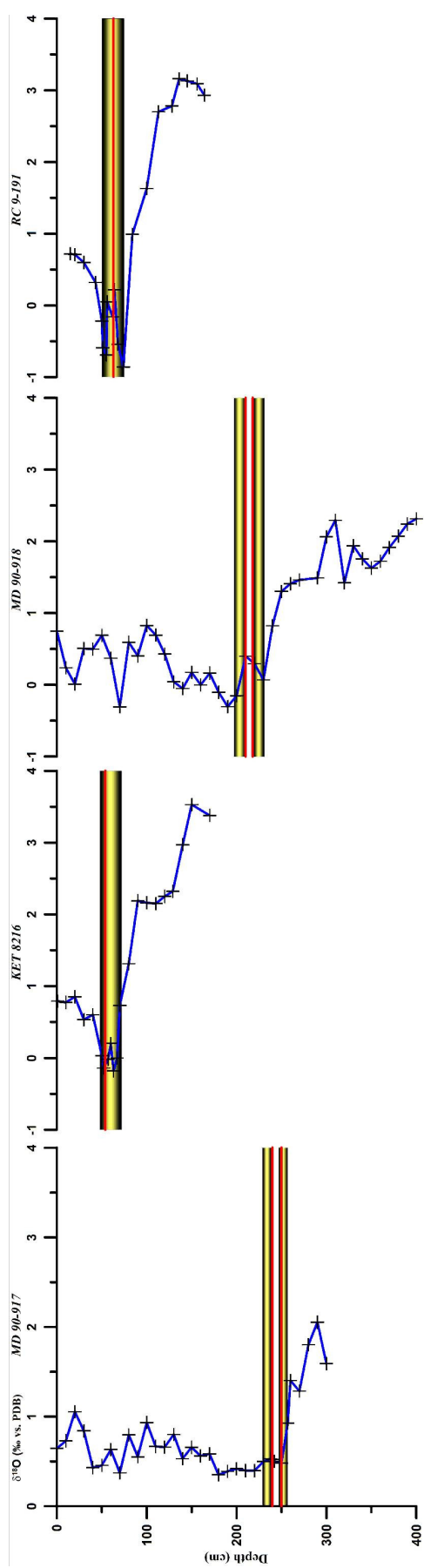


Fig. 6.1: Map of drilling cores which have the tephra layer of the Gabelotto Fiumebianco eruption.

Fig. 6.2 (next page): $\delta^{18}O$ (‰ vs. PDB) curve in blue vs depth (m) of MD 90-917, KET 8216, MD 90-918 and RC 9-191 cores. The red line represents the Gabelotto Fiumebianco / E-1 tephra layer and the black-yellow layers represents the Sapropel S1 deposits.



2) Further tephrostratigraphic studies are needed in order to fix some geographic and chronologic lacunae in the study area. In this way, the knowledge of volcanic activity and the assessment of dispersal of volcanic ash in the central Mediterranean area will be improved.

In January 2008, sediment cores were covered during the scientific cruise all around Italy on Urania (PI Insinga, Naples). At the moment only preliminary analyses were performed but a complete tephrostratigraphy of these cores can bring important data which will be added in the GIS data-base.

3) The development of the GIS data-base will be enhanced by other data like grain size distribution of tephra layers. But also, the aim is to obtain map with thickness and mass/area of the volcanic deposits. With these physical characteristics, it will be possible to improve the volcanic risk from explosive volcanic eruptions. These data will also improve the knowledge of the physical characteristics of each studied eruption (e.g. column height, volume of ejected products, Volcanic Explosive Index, duration of the eruption, eruptive frequency...). In addition, further research on proximal deposits of volcanoes will supply better constraints for correlation of distal tephra layers.



References

A

- Aliaj S.**, (2000). Neotectonics and seismicity in Albania. In: S. Meco, S. Aliaj, I. Turku, (Eds.), *Geology of Albania*. Gebrüder Borntrager, Berlin. *Beitrage zur regionalen Geologie der Erde*, 28, 135–178.
- Aliaj S., Baldassarre G., Shkupi D.**, (2001). Quaternary subsidence zones in Albania: some case studies. *Bull. Eng. Geol. Environ.* 59, 313–318.
- Aliaj, S., Adams, J., Halchuk, S., Sulstarova, E., Peci, V., Muco, B.**, (2004). Probabilistic seismic hazard maps for Albania. 13th World Conf. Earthquake Engineering, Vancouver, B.C., Canada, paper no. 2469. 14 pp.
- Alvisi F., Vigliotti L.**, (1996). Magnetic signature of marine and lacustrine sediments from central Italy (PALICLAS Project). *Palaeoenvironmental Analysis of Italian Crater Lake and Adriatic Sediments*. *Mem. Ist. Ital. Idrobiol.*, 55, 285-303, P. Guilizzoni and F. Oldfield (Guest Editors).
- Andrews J., Geirsdottir A., Hardardottir J., Principato S., Grönvold K., Kristjansdottir G., Helgadóttir G., Drexler J., Sveinbjörnsdottir A.**, (2002). Distribution, sediment magnetism and geochemistry of the Saksunarvatn ($10\,180 \pm 60$ cal. yr BP) tephra in marine, lake and terrestrial sediments, northwest Iceland. *Journal of Quaternary Science*, 17, 731-745.
- Anderson E.C., Libby W.F.**, (1947). Natural radiocarbon from cosmic radiation. *Physical Review*, 72, 10, 931–936.
- Andronico D., Calderoni G., Cioni R., Sbrana A., Sulpizio R., Santacroce R.**, (1995). Geological map of Somma-Vesuvius volcano. *Periodico di Mineralogia* 64, 77–78.
- Andronico D., Cioni R.**, (2002). Contrasting styles of Mount Vesuvius activity in the period between the Avellino and Pompeii Plinian eruptions, and some implications for assessment of future hazards. *Bull. Volcanol.* 64, 372–391.
- Anovski T., Naumovski J., Kacurkov D., Kirkov P.**, (1980). A study of the origin of waters of St. Naum Springs, Lake Ohrid (in Macedonian). *Fisica*, 12, 76–86.
- Arnò V., Principe C., Rosi M., Santacroce R., Sbrana A., Sheridan M.F.**, (1987). Eruptive history. In: Santacroce, R. (Ed.), *Somma-Vesuvius*, vol. 114, 8. CNR Quaderni de la Ricerca Scientifica, Roma, pp. 53–103.
- Argand E.**, (1916). Sur l'arc des Alpes Occidentales. *Eclogae Geol. Helv.* 14, 145–191.
- Arrighi S., Tanguy J.C., Rosi M.**, (2006). Eruptions of the last 2200 years at Vulcano and Vulcanello (Aeolian Islands, Italy) dated by high-accuracy archeomagnetism. *Physics of the Earth and Planetary Interiors* 159, 225–233. doi:10.1016/j.pepi.2006.07.010.

Aulinas M., Civetta L., Di Vito M.A., Orsi G., Gimeno D., Fernandes-Turiel J.L., (2008). The “pomici di mercato” Plinian eruption of Somma-Vesuvius: magma chamber processes and eruption dynamics. *Bull. Volcanol.* 70, 825–840.

B

Barberi F., Innocenti F., Lirer L., Munno R., Pescatore T.S., Santacroce R., (1978). The Campanian Ignimbrite: a major prehistoric eruption in the Neapolitan area (Italy). *Bull. Volcanol.* 41, 10–22.

Barberi F., Gandino A., Gioncada A., La Torre P., Sbrana A., Zenucchini C., (1994). The deep structure of the Eolian arc (Filicudi-Panarea-Vulcano sector) in light of gravity, magnetic and volcanological data. *J. Volcanol. Geotherm. Res.* 61, 189–206.

Barca D., Ventura G., (1991). Evoluzione vulcano-tettonica dell'isola di Salina (Arcipelago delle Eolie). *Mem. Soc. Geol. Ital.* 47, 401–415.

Bard E., Arnold M., Duprat J., Moyes J., Duplessy J.C., (1987). Reconstruction of the last deglaciation: deconvolved records of $\delta^{18}\text{O}$ profiles, micropaleontological variations and accelerator mass spectrometric ^{14}C dating. *Climate Dynamics*, 1, 101–112 doi: 10.1007/BF01054479.

Bard E., Arnold M., Hamelin B., Tisnerat-Laborde N., Cabioch G., (1998). Radiocarbon Calibration by Means of Mass Spectrometric $^{230}\text{Th}/^{234}\text{U}$ and ^{14}C Ages of Corals: An updated database including samples from Barbados, Mururoa, and Tahiti, In: Stuiver, M., and van der Plicht, J., eds. *INTCAL98: Calibration Issue. Radiocarbon*, 40 1085–1092.

Bard E., Rostek F., Ménot-Combes G., (2004). Radiocarbon calibration beyond 20,000 ^{14}C yr B.P. by means of planktonic foraminifera of the Iberian Margin. *Quaternary Research* 61, 204–214.

Beccaluva L., Gabbianelli G., Lucchini F., Rossi P.L., Savelli C., (1985). Petrology and K/Ar ages of volcanics dredged from the Aeolian seamounts: implications for geodynamic evolution of the Southern Tyrrhenian basin. *Earth and Planetary Science Letters*, 74, 187–208.

Beccaluva L., Bianchini G., Wilson M., (2007). Cenozoic Volcanism in the Mediterranean Area. *Geological Society of America, Special Paper* 418, 358 pp.

Beeton A., Karaman G.S., (1981). General summary. In *The Biota and Limnology of Lake Skadar*. Smithsonian Institution: Washington, DC; 429–436.

- Belmecheri S., Namiotko T., Robert C., von Grafenstein U., Danielopol D.L.,** (2009). Climate controlled ostracod preservation in Lake Ohrid (Albania, Macedonia). *Palaeogeography, Palaeoclimatology, Palaeoecology*, 277, 236–245. doi:10.1016/j.palaeo.2009.04.013.
- Blockley S.P.E., Bronk Ramsey C., Pyle D.M.,** (2008). Improved age modeling and high-precision age estimates of late Quaternary tephras, for accurate palaeoclimate reconstruction. *J. Volcanol. Geotherm. Res.* 177, 251–262.
- Bloesch J.,** (1995). Mechanisms, measurement and importance of sediment resuspension in lakes. *Marine Freshwater Research* 46, 295–304.
- Blong R. J.,** (1981). Some Effects of Tephra Falls on Buildings, in: *Tephra Studies: Proc. NATO Advanced Study Institute Tephra Studies as a Tool in Quaternary Research*, edited by: Self, S. and Sparks, R. S. J., held in Laugarvatn and Reykjavík, Iceland, 18–29 June 1980, D. Reidel Publishing Company, Dordrecht, Netherlands, 405–420.
- Boccaletti M., Dainelli P.,** (1982). Il sistema reumatico neogenico–quaternario nell’area mediterranea: esempio di deformazione plastico–rigida post-collisionale. *Mem. Soc. Geol. Ital.* 24, 465–482.
- Bocchini D., Principe C., Castradori D., Laurenzi M.A., Gorla L.,** (2001). Quaternary evolution of the southern sector of the Campanian Plain and early Somma-Vesuvius activity: insights from the Trecase 1 well. *Mineral. Petrol.* 73, 67–91.
- Boivin P., Camus G., De Goër A., Gourgaud A., Kieffer G., Mergoïl J., Vincent P.,** (1991). *Volcanology of the Chaîne des Puys. Parc Naturel Régional des Volcans d’Auvergne*, Imprimerie Moderne, Aurillac, 127pp.
- Brow R.J., Orsi G., de Vita S.,** (2008). New insights into Late Pleistocene explosive volcanic activity and caldera formation on Ischia (southern Italy). *Bull. Volcanol.* 70, 583–603. doi 10.1007/s00445-007-0155-0.

C

- Cadoux A., Blichert-Tolft J., Pinti D.L., Albarède F.,** (2007). A unique lower mantle source for Southern Italy volcanics. *Earth and Planetary Science Letters*, 259, 227–238.
- Calanchi N., De Rosa R., Mazzuoli R., Ricci Lucchi F., Rossi P.L., Santacroce R.,** (1988). L’attività del centro di Pollara (Salina, Isole Eolie). *Boll GNV, Pisa*, 187–213.

- Calanchi N., De Rosa R., Mazzuoli R., Rossi P., Santacroce R., Ventura G., (1993).** Silicic magma entering a basaltic magma chamber: eruptive dynamics and magma mixing – an example from Salina (Aeolian Islands, Southern Tyrrhenian Sea). *Bull. Volcanol.* 55, 504–522.
- Calanchi N., Dinelli E., Lucchini F., Mordenti A., (1996).** Chemostratigraphy of the Late sediments from Lake Albano and Central Adriatic Sea cores (PALICLAS project). *Memorie Istituto Italiano di Idrobiologia* 55, 247–263.
- Calanchi N., Cattaneo A., Dinelli E., Gasparotto G., Lucchini F., (1998).** Tephra layers in Late Quaternary sediments of the central Adriatic Sea. *Marine Geology* 149, 191–209.
- Calanchi N., Dinelli E., (2008).** Tephrostratigraphy of the last 170 ka in sedimentary successions from the Adriatic Sea. *J. Volcanol. Geotherm. Res.* 177, 81–95.
- Capaldi G., Civetta L., Gillot P.Y., (1985).** Geochronology of Plio-Pleistocene volcanic rocks from southern Italy. *Rendiconti della Società Italiana di Mineralogia e Petrologia* 40, 25–44.
- Carapezza M.L., Tarchini L., (2007).** Accidental gas emission from shallow pressurized aquifers at Alban Hills volcano (Rome, Italy): Geochemical evidence of magmatic degassing? *J. Volcanol. Geotherm. Res.* 165, 5–16. doi:10.1016/j.jvolgeores.2007.04.008.
- Casagli N., Tibaldi A., Merri A., Del Ventisette C., Apuani T., Guerri L., Fortuny-Guasch J., Tarchi D., (2009).** Deformation of Stromboli Volcano (Italy) during the 2007 eruption revealed by radar interferometry, numerical modelling and structural geological field data. *J. Volcanol. Geotherm. Res.* 182, 182–200, doi:10.1016/j.jvolgeores.2009.01.002.
- Casford J.S.L., Rohling E.J., Abu-Zied R.H., Fontanier C., Jorissen F.J., Leng M.J., Schmiedel G., Thomson J., (2003).** A dynamic concept for eastern Mediterranean circulation and oxygenation during sapropel formation. *Palaeogeography, Palaeoclimatology, Palaeoecology*, 190, 103–119.
- Cioni R., Marianelli P., Santacroce R., (1997).** Thermal and compositional evolution of the shallow magma chambers of Vesuvius: evidence from pyroxene phenocrysts and melt inclusions. *J. Geophys. Res.* 103, 18277–18294.
- Cioni R., Santacroce R., Sbrana A., (1999).** Pyroclastic deposits as a guide for reconstructing the multi-stage evolution of the Somma-Vesuvius caldera. *Bull. Volcanol.* 60, 207–222.
- Cioni R., Sulpizio R., Garruccio N., (2003).** Variability of the eruption dynamics during a subplinian event: the Greenish Pumice eruption of Somma-Vesuvius (Italy). *J. Volcanol. Geotherm. Res.* 124, 89–114.

- Cita M.B., Vergnaud-Grazzini C., Robert C., Chamley H., Ciaranfi N., D'Onofrio S.,** (1977). Paleoclimatic record of a long deep sea core from the eastern Mediterranean. *Quat. Res.* 8, 205–235.
- Civetta L., Cornette Y., Crisci G., Gillot P.Y., Orsi G., Requejo C.S.,** (1984). Geology, geochronology and chemical evolution of the island of Pantelleria. *Geol. Mag.* 121, 541–562.
- Civetta L., Cornette Y., Gillot P.Y., Orsi G.,** (1988) - The eruptive history of Pantelleria (Sicily Channel) in the last 50 ka. *Bull. Volcanol.* 50, 47–57.
- Civetta L., Gallo G., Orsi G.,** (1991). Sr- and Nd-isotope and trace element constraints on the chemical evolution of Ischia (Italy) in the last 55 ka. *J. Volcanol. Geotherm. Res.* 46, 213–230.
- Civetta L., Orsi G., Pappalardo L., Fisher R.V., Heiken G., Ort M.,** (1997). Geochemical zoning, mingling, eruptive dynamics and depositional processes—the Campanian Ignimbrite, Campi Flegrei caldera, Italy. *J. Volcanol. Geotherm. Res.* 75, 183–219.
- Clift P., Blusztajn J.,** (1999). The trace-element characteristics of Aegean volcanic arc marine tephra. *Journal of Volcanology and Geothermal Research* 92, 321–347.
- Coltelli M., Del Carlo P., Vezzoli L.,** (2000). Stratigraphic constraints for explosive activity in the past 100 ka at Etna volcano, Italy. *Int. J. Earth Sciences.* 89, 665–677.
- Connor C. B., Hill B. E., Winfrey B., Franklin N. M., La Femina P. C.,** (2001). Estimation of Volcanic Hazards from Tephra Fallout, *Nat. Hazards Rev.*, 2, 1, 33–42.
- Coplen T.B.,** (1988). Normalization of oxygen and hydrogen isotope data, *Chem. Geol.* 72, 293–297.
- Cornell W., Carey S., Sigurdsson H.,** (1983). Computer simulation of transport and deposition of Campanian Y-5 ash. *J. Volcanol. Geotherm. Res.* 17, 89–109.
- Cornette Y., Crisci G., Gillot P.Y., Orsi G.,** (1983). Recent volcanic history of Pantelleria: a new interpretation. In *Explosive Volcanism* (ed. Sheridan M.F. and Barberi F.) *J. Volcanol. Geotherm. Res.* 17, 361–373.
- Cortese M., Frazzetta G., La Volpe L.,** (1986). Volcanic history of Lipari (Aeolian Islands, Italy) during the last 10,000 years. *J. Volcanol. Geotherm. Res.* 27, 117–133.
- Cortesi C., Fornaseri M., Romano R., Alessio M., Allegri L., Azzi C., Bella F., Calderoni G., Follieri M., Improta S., Magri D., Preite Martinez M., Sadori L., Petrone V., Turi B.,** (1988). Cronologica ^{14}C di piroclastici recenti del Monte Etna identificazione e distribuzione dei fossili vegetali. *Boll Soc Geol Ital* 107, 531–545.

- Costa A., Dell’Erba F., Di Vito M., Isaia R., Macedonio G., Orsi G., Pfeiffer T., (2008).** Tephra fallout hazard assessment at the Campi Flegrei caldera (Italy). *Bull. Volcanol.* 71, 259–273.
- Crisci G.M., De Rosa R., Lanzafame G., Mazzuoli R., Sheridan M.F., Zuffa G.G., (1981).** Monte Guardia sequence: a late-Pleistocene eruptive cycle on Lipari. *Bull. Volcanol.* 44, 241–255.
- Crisci G.M., Delibrias G., De Rosa R., Mazzuoli R., Sheridan M.F., (1983).** Age and Petrology of the Late-Pleistocene brown tuffs of Lipari, Italy. *Bull. Volcanol.* 46, 381–391.
- Crisci G.M., De Rosa R., Esperanca S., Mazzuoli R., Sonnino M., (1991).** Temporal evolution of a three component system: the island of Lipari (Aeolian Arc, southern Italy). *Bull. Volcanol.* 53, 207–221.
- Cristofolini R., Romano R., (1982).** Petrologic features of the Etnean volcanic rocks. *Memorie della Società Geologica Italiana* 23, 99–115.
- Currie L.A., Klouda G.A., Elmore D., Gove H.E., (1985).** Radiocarbon dating of microgram samples: accelerator mass spectrometry and electromagnetic isotope separation. *Nuclear Instruments & Methods v B12*, 396–401.

D

- D’Antonio M., Civetta L., Orsi G., Pappalardo L., Piochi M., Carandente A., de Vita S., Di Vito M.A., Isaia R., Southon J., (1999).** The present state of the magmatic system of the Campi Flegrei caldera based on the reconstruction of its behaviour in the past 12 ka. *J. Volcanol. Geotherm. Res.* 91, 247–268.
- De Astis G., Frazzetta G., La Volpe L., (1989).** I depositi di riempimento della Caldera del Piano e i depositi della Lentia. *Boll. G.N.V.* 2, 763–778.
- De Astis G., La Volpe L., Peccerillo A., Civetta L., (1997).** Volcanological and petrological evolution of Vulcano Island (Aeolian Arc, southern Tyrrhenian Sea). *J. Geophys. Res.* 102, 8021–8050.
- De Astis G., Pappalardo L., Piochi M., (2004).** Procida volcanic history: new insights into the evolution of the Phlegrean volcanic district (Campania region, Italy). *Bull. Volcanol.* 66, 622–641.
- De Astis G., Dellino P., La Volpe L., Lucchi F., Tranne C.A., (2006).** Geological map of the island of Vulcano (Aeolian Islands). University of Bari, University of Bologna, and INGV; printed by L.A.C., Firenze.

- De Rita D., Funicello R., Corda L., Sposato A., Rossi U.,** (1993). Carta geologica del complesso Vulcanico Sabatino. Quaderni de la Ricerca Scientifica, 114, Progetto Finalizzato 'Geodinamica' Monografie Finali, vol.11, C.N.R., Rome, Italy.
- De Rita D., Faccenna C., Funicello R., Rosa C.,** (1995). Stratigraphy and volcano-tectonics. In: Trigila, R. (Ed.), *The Volcano of the Albani Hills*. Tipografia SGS, Roma, pp. 33–71.
- De Rosa R., Sheridan M.F.,** (1983). Evidence for magma mixing in the surge deposits of the Monte Guardia Sequence, Lipari. *J. Volcanol. Geotherm. Res.* 17, 313–328.
- De Rosa R., Mazzuoli R., Rossi P.L., Santacroce R., Ventura G.,** (1990). Nuovi dati per la ricostruzione della storia eruttiva dell' isola di Salina (Isole Eolie). *Boll GNV, Pisa*, 2, 809–825
- De Rosa R., Donato P., Ventura G.,** (2002). Fractal analysis of mingled/mixed magmas: an example from the Upper Pollara eruption (Salina Island, southern Tyrrhenian Sea, Italy). *Lithos* 65, 299–311.
- De Rosa R., Donato P., Gioncada A., Masetti M., Santacroce R.,** (2003). The Monte Guardia eruption (Lipari, Aeolian Islands): an unusual example of magma mixing sequence. *Bull. Volcanol.* 65, 530–543.
- de Vita S., Orsi G., Civetta L., Carandente A., D'Antonio M., Deino A., di Cesare T., Di Vito M., Fisher R.V., Isaia R., Marotta E., Necco A., Ort M., Pappalardo L., Piochi M., Southon J.,** (1999). The Agnano-Monte Spina eruption (4.1 ka) in the resurgent, nested Campi Flegrei caldera (Italy). *J. Volcanol. Geotherm. Res.* 91, 269–301.
- de Vita S., Sansivero F., Orsi G., Marotta E.,** (2006). Cyclical slope instability and volcanism related to volcano-tectonism in resurgent calderas: the Ischia island (Italy) case study. *Engen Geol* 86, 148–165.
- De Vivo B., Rolandi G., Gans P.B., Calvert A., Bohrsen W.A., Spera F.J., Belkin H.E.,** (2001). News constraints on the pyroclastic eruptive history of the Campanian volcanic Plain (Italy). *Mineralogy and Petrology.* 73, 47–65.
- Di Renzo V., Di Vito M.A., Arienzo I., Carandente A., Civetta L., D'antonio M., Giordano F., Orsi G., Tonarini S.,** (2007). Magmatic history of Somma-Vesuvius on the basis of new geochemical and isotopic data from a deep borehole (Camaldoli della Torre). *J. Petrol.* 48 (4), 753–784.
- Di Vito M.A., Isaia R., Orsi G., Southon J., de Vita S., D'Antonio M., Pappalardo L., Piochi M.,** (1999). Volcanism and deformation since 12,000 years at the Campi Flegrei (Italy) *J. Volcanol. Geotherm. Res.* 91, 221–246.
- Di Vito M.A., Sulpizio R., Zanchetta G., D'Orazio M.** (2008). The late Pleistocene pyroclastic deposits of the Campanian Plain: new insights into the explosive activity of Neapolitan volcanoes. *J. Volcanol. Geotherm. Res.* doi:10.1016/j.jvolgeores.2007.11.019.

- Delibrias G., Di Paola G.M., Rosi M., Santacroce R.,** (1979). La storia eruttiva del complesso vulcanico Somma Vesuvio ricostruita dalle successioni piroclastiche del Monte Somma. *Rendiconti Società Italiana Mineralogia Petrologia* 35, 411–438.
- Deino A.L., Orsi G., Piochi M., de Vita S.,** (2004). The age of the Neapolitan Yellow Tuff caldera-forming eruption (Campi Flegrei caldera – Italy) assessed by $^{40}\text{Ar}/^{39}\text{Ar}$ dating method. *J. Volcanol. Geotherm. Res.* 133, 157–170. doi:10.1016/S0377-0273(03)00396-2.
- Dellino P., Isaia R., La Volpe L., Orsi G.,** (2001). Statistical analysis of textural data from complex pyroclastic sequence: implication for fragmentation processes of the Agnano-Monte Spina eruption (4.1 ka), Phlegraean Fields, southern Italy. *Bull. Volcanol.* 63, 443–461
- Doglioni C., Mongelli F., Pieri P.,** (1994). The Puglia uplift (SE Italy): an anomaly in the foreland of the Apenninic subduction due to buckling of a thick continental lithosphere. *Tectonics* 13, 1309–1321.
- Doglioni C., Gueguen E., Harabaglia P., Mongelli F.,** (1999). On the origin of W-directed subduction zones and applications to the western Mediterranean. In: Durand, B., Jolivet, L., Horvath, F., Séranne, M. (Eds.), *The Mediterranean Basins: Tertiary Extension within the Alpine Orogen*. Geol. Soc. London, Spec. Publ., 156, 541–561.
- Druitt T.H., Brenchley P.J., Gökten Y.E., Francaviglia V.,** (1995). Late Quaternary rhyolitic eruptions from the Acigöl Complex, central Turkey. *Journal of the Geological Society, London* 152, 655–667.
- Drysdale R.N., Zanchetta G., Hellstrom J., Maas R., Fallick A.E., Pickett M., Cartwright I., Piccini L.,** (2006). Late Holocene drought responsible for the collapse of Old World civilizations is recorded in an Italian flowstone. *Geology* 34, 101–104.

E

- Emeis K.C., Struck U., Schulz H.M., Rosenberg R., Bernasconi S., Erlenkeuser H., Sakamoto T., Martinez-Ruiz F.,** (2000). Temperature and salinity variations of Mediterranean Sea surface waters over the last 16,000 years from records of planktonic stable oxygen isotopes and alkenone unsaturation ratios. *Palaeogeography, Palaeoclimatology, Palaeoecology* 158, 259–280.

F

- Fedele F., Giaccio B., Isaia R., Orsi G.,** (2002). Ecosystem impact of the Campanian Ignimbrite eruption in Late Pleistocene Europe. *Quaternary Research* 57, 420–424.
- Fedele F., Giaccio B., Isaia R., Orsi G.,** (2003). The Campanian Ignimbrite eruption, Heinrich Event 4, and Palaeolithic change in Europe: a high-resolution investigation. In: *Volcanism and Earth's Atmosphere*. AGU Geophys Monograph 139, 301–325.
- Federman A.N., Carey S.N.,** (1980). Electron microprobe correlation of tephra layers from Eastern Mediterranean abyssal sediments and the island of Santorini. *Quaternary Research* 13, 160–171.
- Fisher R.V., Orsi G., Ort M., Heiken G.,** (1993). Mobility of large-volume pyroclastic flow—emplacement of the Campanian Ignimbrite, Italy. *J. Volcanol. Geotherm. Res.* 56, 205–220.
- Folch A., Sulpizio R.,** (2010). Evaluating the long-range volcanic ash hazard using supercomputing facilities. Application to Somma-Vesuvius (Italy), and consequences on civil aviation over the Central Mediterranean Area. *Bull. Volcanol.* Submitted.
- Fontugne M., Paterne M., Calvert S., Murat A., Guichard F., Arnold M.,** (1989). Adriatic deep water formation during the Holocene: implication for the reoxygenation of the deep eastern Mediterranean sea. *Paleoceanography*, 4, 2, 199–206.
- Francalanci L.,** (1987). Evoluzione vulcanologica e magmatologica di Stromboli (Isole Eolie): relazioni fra magmatismo calc-alcinalo e shoshonitico. PhD Thesis, Florence, Italy, pp 350.
- Francalanci L., Manetti P., Peccerillo A.,** (1986). Evoluzione vulcanologica e magmatologica dell'isola di Stromboli. *Boll G Naz Vulcan* 2, 261–282.
- Francalanci L., Barbieri M., Manetti P., Peccerillo A., Tolomeo L.,** (1988). Sr isotopic systematics in volcanic rocks from the island of Stromboli (Aeolian Arc). *Chem Geol Isotope Geosci* 73, 109–124.
- Francalanci L., Manetti P., Peccerillo A.,** (1989). Volcanological and magmatological evolution of Stromboli volcano (Aeolian Islands): the roles of fractional crystallization, magma mixing, crustal contamination and source heterogeneity. *Bull. Volcanol.* 51, 355–378.
- Frazzetta G., Gillot P.Y., La Volpe L., Sheridan M.F.,** (1984). Volcanic hazards at Fossa of Vulcano: data from the last 6000 years. *Bull. Volcanol.* 47, 105–124.

- Freda C., Gaeta M., Karner D.B., Marra F., Renne P.R., Taddeucci J., Scarlato P., Christensen J.N., Dallai L., (2006).** Eruptive history and petrologic evolution of the Albano multiple maar (Alban Hills, Central Italy). *Bull. Volcanol.* 68, 567–591.
- Fretzdorff S., Paterne M., Stoffers P., Ivanova E., (2000).** Explosive activity of the Reunion Island volcanoes through the past 260,000 years as recorded in deep-sea sediments. *Bull. Volcanol.* 62, 266–277.
- Frisia S., Borsato A., Susini J., (2008).** Synchrotron radiation applications to past volcanism archived in speleothems: an overview. *J. Volcanol. Geotherm. Res.* 177, 96–100.

G

- Galdeano G., Rossignol J.C., (1977).** Assemblage à altitude constante des cartes d'anomalies magnétiques couvrant l'ensemble du bassin occidental de la Méditerranée. *Bull. Soc. Geol. Fr.* 7, 19 (3), 461–468.
- Gauthier C., Hatté C., (2008).** Effects of handling, storage, and chemical treatments on $\delta^{13}\text{C}$ values of terrestrial fossil organic matter, *Geochim. Geophys. Geosyst.*, 9, Q08011, doi:10.1029/2008GC001967.
- Ghisetti F., (1979).** Relazioni tra strutture e fasi trascorrenti e distensive lungo i sistemi Messina[^]Fiumefreddo, Tindari-Letojanni e Alia-Malvagna (Sicilia nord-orientale): uno studio microtettonico. *Geol. Rom.* 18, 23–56.
- Giaccio B., Isaia R., Fedele F.G., Di Canzio E., Hoffecker J., Ronchitelli A., Sinitsyn A., Anikovich M., Lisitsyn S.N., (2008).** The Campanian Ignimbrite and Codola tephra layers: two temporal/stratigraphic markers for the Early Upper Palaeolithic in southern Italy and eastern Europe. *J. Volcanol. Geotherm. Res.* doi:10.1016/j.jvolgeores.2007.10.007.
- Giaccio B., Messina P., Sposato A., Voltaggio M., Zanchetta G., Galadini F., Gori S., Santacroce R., (2009).** Tephra layers from Holocene lake sediments of the Sulmona basin, central Italy: implications for volcanic activity in Peninsular Italy and tephrostratigraphy in the central Mediterranean area. *Quaternary Science Reviews*, doi:10.1016/j.quascirev.2009.06.009.
- Gillot P.Y., Chiesa S., Pasquare G., Vezzoli L., (1982).** <33000 yr K/Ar dating of the volcano-tectonic horst of the isle of Ischia, Gulf of Naples. *Nature*, 229:242.
- Gillot P.Y., (1984).** Datation par la méthode du potassium argon des roches volcaniques récentes (pléistocènes et holocènes). Contribution à l'étude chronostratigraphique et magmatique des provinces volcaniques de Campanie, des Iles Eoliennes, de Pantelleria (Italie du Sud) et de la Réunion (Océan Indien). PhD thesis Paris, pp 225.

- Gillot P.Y.**, (1987). Histoire volcanique des Iles Eoliennes: arc insulaire ou complexe orogénique anulaire. *Doc. et Trav., Institut Géologique Albert-de-Lapparent* 11, 35–42.
- Gillot P.Y., Keller J.**, (1993). Radiochronological dating of Stromboli. *Acta Vulcanol* 3, 69–78.
- Gillot P.Y., Kieffer G., Romanj R.**, (1994). The evolution of Mount Etna in the Light of potassium-argon dating. *Acta Vulcanol* 5, 81–87.
- Gioncada A., Sbrana A.**, (1991). ‘La Fossa caldera’, Vulcano: inferences from deep drillings. *Acta Vulcanol.* 1, 115–126.
- Gioncada A., Mazzuoli R., Bisson M., Pareschi M.T.**, (2003). Petrology of volcanic products younger than 42 ka on the Lipari-Vulcano complex (Aeolian Islands, Italy): an example of volcanism controlled by tectonics. *J. Volcanol. Geotherm. Res.* 122, 191–220. doi:10.1016/S0377-0273(02)00502-4.
- Giunta S., Negri A., Morigi C., Capotondi L., Combourieu-Nebout N., Emeis K.C., Sangiorgi F., Vigliotti L.**, (2003). Coccolithophorid ecostratigraphy and multi-proxy paleoceanographic reconstruction in the Southern Adriatic Sea during the last deglacial time (Core AD91-17), *Palaeogeography, Palaeoclimatology, Palaeoecology*, 190, 39–59.
- Goldsworthy M., Jackson J., Haines J.**, (2002). The continuity of active fault systems in Greece. *Geophys. J. Int.* 148, 596–618.
- GSA Rock Color Chart**, (1991). The Geological Society of America Rock-Color Chart with genuine Munsell color chips. Printed by Munsell Color U.S.A.
- Gueguen E.**, (1995). Le Bassin Liguro-Provençal: un véritable océan. Exemple de segmentation des marges et de hiatus cinématiques. Implications sur les processus d’amincissement crustal. Ph.D. Thesis, Brest Univ., 315 pp.
- Gueguen A., Doglioni C., Fernandez M.**, (1998). On the post-25 Ma geodynamic evolution of the western Mediterranean. *Tectonophysics* 298, 259–269.

H

- Hadzisce S.D.**, (1966). Das Mixophänomen im Ohridsee im Laufe der Jahre 1941/42-1964/65. *Verh. Internat. Verein. Limnol.* 16, 134–138.
- Hornig-Kjarsgaard I., Keller J., Koberski U., Stadlbauer E., Francalanci L., Lenhart R.**, (1993). Geology, stratigraphy and volcanological evolution of the island of Stromboli, Aeolian arc, Italy. *Acta Vulcanologica* 3, 21–68.

Horwell C.J., Baxter P.J., (2006). The respiratory health hazards of volcanic ash: a review for volcanic risk mitigation. *Bull. Volcanol.* 69, 1–24. doi:10.1007/s00445-006-0052-y.

I

Ippolito F., Ortolani F., Russo M., (1973). Struttura marginale tirrenica dell'Appennino Campano: reinterpretazione dei dati di antiche ricerche di idrocarburi. *Mem. Soc. Geol. It.* 15, 227–250.

Isaia R., D'Antonio M., Dell'Erba F., Di Vito M., Orsi G., (2004). The Astroni volcano: the only example of closely spaced eruptions in the same vent area during the recent history of the Campi Flegrei caldera (Italy). *J. Volcanol. Geotherm. Res.* 133, 171–192.

J

Johnston Lavis H.J., (1884). The Geology of the Mt. Somma and Vesuvius: being a study of Volcanology. *Q. J. Geol. Soc. Lond.* 40, 35–149.

Juvigné E., (1987). Deux retombées volcaniques tardiglaciaires dans le cézallier (Massif Central, France). *Bulletin de l'association française pour l'étude du Quaternaire*, 4, 241–249.

K

Kallel N., Paterne M., Labeyrie L., Duplessy J.C., Arnold M., (1997). Temperature and salinity records of the Tyrrhenian Sea during the last 18,000 years. *Palaeogeography, Palaeoclimatology, Palaeoecology*, 135, 97–108.

Kallel N., Duplessy J.C., Labeyrie L., Fontugne M., Paterne M., Montacer M., (2000). Mediterranean pluvial periods and sapropel formation over the last 200 000 years. *Palaeogeography, Palaeoclimatology, Palaeoecology*, 157, 45–58.

Karaman G.S., Beeton A., (1981). The Biota and Limnology of Lake Skadar. Smithsonian Institution: Washington, DC/Univerzitet Veljko Vlahvic.

- Karner D.B., Marra F., Renne P.R.,** (2001). The history of the Monti Sabatini and Alban Hills volcanoes groundwork for assessing volcanic-tectonic hazards for Rome. *J. Volcanol. Geotherm. Res.* 107, 185–219.
- Keller J., Ryan W.B.F., Ninkovich D., Altherr R.,** (1978). Explosive volcanic activity in the Mediterranean over the past 200,000 yr as recorded in deep-sea sediments. *Geol. Soc. Am. Bull.* 89, 591–604.
- Keller J.,** (1980a). The island of Salina. *Rendiconti della Società Italiana di Mineralogia e Petrologia* 36, 489–524.
- Keller J.,** (1980b). The Island of Vulcano. *Rendiconti della Società Italiana di Mineralogia e Petrologia* 36, 369–414.
- Keller J., Rehren T., Stadlbauer E.,** (1990). Explosive volcanism in the Hellenic Arc: a summary and review. In *Thera and the Aegean World III*, Hardy DA, Keller J, Galanopoulos VP, Flemming NC, Druitt TH (eds). Thera Foundation: Santorini, Greece; 13–26.
- Keller J., Hornig-Kjarsgaard I., Koberski U., Stadlbauer E., Francalanci L., Lenhart R.,** (1993). Geology, stratigraphy, and volcanological evolution of the island of Stromboli, Aeolian Arc, Italy. *Acta Vulcanologica* 3, 21–68.
- Kennett J.P., Thunell R.C.,** (1975). Global increase in Quaternary explosive volcanism, *Science* 187, 497–503.
- Kennett J.P., McBirney, A.R., Thunell R.C.,** (1977). Episodes of Cenozoic volcanism in the circum Pacific region. *J. Volcanol. Geotherm. Res.* 2, 145–163.
- Kieffer G.,** (1979). L'activité de l'Etna pendant les derniers 20,000 ans. *CR Acad Sci Paris* 288D, 1023–1026.
- Kotthoff U., Pross J., Müller U.C., Peyron O., Schmiedl G., Schulz H., Bordon A.,** (2008). Climate dynamics in the borderlands of the Aegean Sea during formation of sapropel S1 deduced from a marine pollen record. *Quaternary Science Reviews*, 27, 832–845. doi:10.1016/j.quascirev.2007.12.001
- Kraml M.,** (1997). Laser- $^{40}\text{Ar}/^{39}\text{Ar}$ -Datierungen an distalen marinen Tephren des jung-quartären mediterranen Vulkanismus (Ionisches Meer, METEOR-Fahrt 25/4). Ph.D. Thesis, Albert-Ludwigs-Universität Freiburg i.Br., 216pp.
- Kromer B., Spurk M.,** (1998). Revision and tentative extension of the tree-ring based ^{14}C calibration, 9200–11 855 cal BP, *Radiocarbon*, 40, 1117–1125.
- Kruiver P., Passier H.,** (2001). Coercivity analysis of magnetic phases in sapropel S1 related to variations in redox conditions, including an investigation of the S ratio. *Geochem. Geophys. Geosyst.*, 2, 2001GC000181.

L

- La Felice S., Rotolo S.G., Scaillet S., Vita G.,** (2009). Tephrostratigraphy, petrochemistry and ^{40}Ar - ^{39}Ar age data on Pre-Green Tuff sequences, Pantelleria, Congresso Fis Geitalia 2009, I 7- Dal terreno al laboratorio: approcci multidisciplinari per lo studio del vulcanismo esplosivo.
- Le Bas M.J., Le Maitre R.W., Streckeisen A., Zanettin B.,** (1986). A chemical classification of volcanic rocks based on the total alkali-silica diagram. *J. Petrol.* 27, 745–750.
- Le Friant A., Lock E.J., Hart M.B., Boudon G., Sparks R.S.J., Leng M.J., Smart C.W., Komorowski J.C., Deplus C., Fisher J.K.,** (2008). Late Pleistocene tephrochronology of marine sediments adjacent to Montserrat, Lesser Antilles volcanic arc. *Journal of the Geological Society, London*, 165, 279–289.
- Lacroix A.,** (1904). *La Montagne Pelée et ses Eruptions*. Masson ed., Paris, 662 pp.
- Lasca N.P., Radulovic V., Ristic R.J., Cherkauer D.S.,** (1981). Geology, hydrology, climate and bathymetry of Lake Skadar. In *The Biota and Limnology of Lake Skadar*. Smithsonian Institution: Washington, DC; 17–38.
- Lee K.K.,** (1981). Application of mathematical modelling in studying of Lake Skadar circulation patterns. In *The Biota and Limnology of Lake Skadar*. Smithsonian Institution: Washington, DC; 56–65.
- Lezine A.M., von Grafenstein U., Andersen N., Belmecheri S., Bordon A., Caron B., Cazet J.P., Erlenkeuser H., Fouache E., Grenier C., Huntsman-Mapila P., Hureau-Mazaudier D., Manelli D., Mazaud A., Robert C., Sulpizio R., Tiercelin J.J., Zanchetta G., Zeqollari Z.,** (2010) Lake Ohrid, Albania, provides an exceptional multi-proxy record of environmental changes during the last glacial-interglacial cycle, *Palaeogeography, Palaeoclimatology, Palaeoecology* doi: 10.1016/j.palaeo.2010.01.016
- Libby W.F., Anderson, E.C., Arnold, J.R.,** (1949). Age determination by Radiocarbon content: world-wide assay of natural radiocarbon. *Science*, 109, 227-28.
- Lirer L., Pescatore T., Booth B., Walker G.P.L.,** (1973). Two plinian pumice-fall deposits from Somma-Vesuvius, Italy. *Geol. Soc. Amer. Bull.* 84, 759–772.
- Lirer L., Mastrolorenzo G., Rolandi G.,** (1987). Un evento pliniano nell'attività recente dei Campi Flegrei. *Boll Soc Geol It* 106, 461–473.
- Losito R.,** (1989). Stratigrafia, caratteri deposizionali e area sorgente dei Tufi Brunì delle Isole Eolie. Ph.D. Thesis, University of Bari.

- Lövstedt C.B., Hargeby A.,** (2005). Seasonal variation in resuspension in a shallow Swedish lake: potential factors. In 15th International Northern Research Basin Symposium and Workshop, Lulea to Kvikkjokk, Sweden; 101–109.
- Lowe J.J., Walker M.J.C.,** (1997). *Reconstructing Quaternary Environments*. Pearson Prentice Hall: London.
- Lowe J.J., Blockley S., Trincardi F., Asioli A., Cattaneo A., Matthews I.P., Pollard M., Wulf S.,** (2007). Age modelling of late Quaternary marine sequences in the Adriatic: towards improved precision and accuracy using volcanic event stratigraphy. *Continental Shelf Research* 27, 560–582.
- Lowrie W., Fuller M.,** (1971). On the alternating field demagnetization characteristics of multidomain thermoremanent magnetization in magnetite. *J. Geophys. Res.*, 76, 6339–6349.
- Lucchi F., Tranne C.A., Calanchi N., Keller J., Rossi P.L.,** (2003). Geological map of Panarea and minor islets (Aeolian Islands). University of Bologna, University of Freiburg, and INGV; printed by L.A.C., Firenze.
- Lucchi F., Tranne C.A., Calanchi N., Keller J., Rossi P.L.,** (2007). The stratigraphic role of marine deposits in the geological evolution of the Panarea volcano (Aeolian Islands, Italy). *Journal of the Geological Society of London* 164/5, 983–996.
- Lucchi F., Tranne C.A., De Astis G., Keller J., Losito R., Morche W.,** (2008). Stratigraphy and significance of Brown Tuffs on the Aeolian Islands (southern Italy). *J. Volcanol. Geotherm. Res.* 177, 49–70 doi:10.1016/j.jvolgeores.2007.11.006

M

- Macdonald R.,** (1974). Tectonic settings and magma associations. *Bull. Volcanol.* 38, 575–593.
- Magny M., de Beaulieu J.L., Drescher-Schneider R., Vannière B., Walter-Simonnet A.V., Millet L., Bossuet G., Peyron O.,** (2006). Climatic oscillations in central Italy during the Last Glacial-Holocene transition: the record from Lake Accesa. *Journal of Quaternary Science* 21, 311–320.
- Magny M., de Beaulieu J.L., Drescher-Schneider R., Vannière B., Walter-Simonnet A.V., Miras Y., Millet L., Bossuet G., Peyron O., Brugiapaglia E., Leroux A.,** (2007). Holocene climate changes in the central Mediterranean as recorded by lake-level fluctuations at Lake Accesa (Tuscany, Italy). *Quaternary Science Review* 26, 1736–1758.

- Mahood G.A.**, (1984). Calderas associated with strongly peralkaline volcanic rocks. *J. Geophys Res.* 89, 8540–8552.
- Mahood G. A., Hildreth W.**, (1983). Nested calderas and trapdoor uplift at Pantelleria, Strait of Sicily. *Geology* 11, 103–106.
- Mahood G. A., Hildreth W.**, (1986). Geology of the peralkaline volcano at Pantelleria, Strait of Sicily. *Bull. Volcanol.* 48, 143–172.
- Marciano R., Munno R., Petrosino P., Santangelo N., Santo A., Villa I.**, (2008). Late quaternary tephra layers along the Cilento coastline (southern Italy). *J. Volcanol. Geotherm. Res.* 177, 227–243. doi:10.1016/j.jvolgeores.2007.11.009.
- Marianelli P., Sbrana A.**, (1998). Risultati di misure di standard di minerali e di vetri naturali in microanalisi a dispersione di energia. *Atti Società Toscana di Scienze Naturali Memorie Serie A* 105, 57–63.
- Marianelli P., Proto M., Sbrana A.**, (2003). Water content variability in Ignimbrite Campana melts. New insights on magma chamber history. *GNV Gen Ass, Rome*, June 9–11, Abstracts, 208 pp.
- Margari V., Pyle D.M., Bryant C., Gibbard P.L.**, (2007). Mediterranean tephra stratigraphy revisited: Results from a long terrestrial sequence on Lesvos Island, Greece. *J. Volcanol. Geotherm. Res.* 163, 34–54.
- Marra F., Freda C., Scarlato P., Taddeucci J., Carner D.B., Renne P.R., Gaeta M., Palladino D.M., Trigilia R., Cavarretta G.**, (2003). Postcaldera activity in the Alban Hills volcanic district (Italy): $^{40}\text{Ar}/^{39}\text{Ar}$ geochronology and insights into magma evolution. *Bull. Volcanol.* 65, 227–247.
- Marra F., Taddeucci J., Freda C., Marzocchi W., Scarlato P.**, (2004). Recurrence of volcanic activity along the Roman Comagmatic Province (Tyrrhenian margin of Italy) and its tectonic significance. *Tectonics* 23, TC–4013.
- Mattauer M., Séguret M.**, (1971). Les relations entre la chaîne pyrénéenne et le golfe de Gascogne. In: *Histoire Structurale du Golfe de Gascogne*. Technip, Paris, pp. IV.4–1–IV.4–24.
- Matzinger A., Jordanoski M., Veljanoska-Sarafiloska E., Sturm M., Müller B., Wüest A.**, (2006). Is Lake Prespa jeopardizing the ecosystem of ancient Lake Ohrid? *Hydrobiologica* 553, 89–109.
- McCoy F.W.**, (1981). Areal distribution redeposition and mixing of tephra within deep-sea sediments of the Eastern Mediterranean Sea. In *Tephra Studies*, Self S, Sparks RSJ (eds). Reidel: Dordrecht; 245–254.

- Mele D., Sulpizio R., Dellino P., La Volpe L.,** (2007). A quantitative study for the reconstruction of Mercato eruption (8000 yr B.P.) of Somma-Vesuvius. IUGG XXIV General Assembly 2-13 Luglio, Perugia, Abstract volume 22–24, Italy.
- Mele D., Sulpizio R., Dellino P., La Volpe L.,** (2009). Stratigraphy and eruptive dynamics of a long-lasting Plinian eruption of Somma-Vesuvius: the Pomici di Mercato (8900 years BP). *Bull. volcanol.*
- Mercone D., Thomson J., Croudace I.W., Siani G., Paterne M., Troelstra S.,** (2000). Duration of S1, the Most Recent Sapropel in the Eastern Mediterranean Sea, as Indicated by Accelerator Mass Spectrometry Radiocarbon and Geochemical Evidence. *Paleoceanography*, 15(3), 336–347.
- Munno R., Petrosino P., Romano P., Russo Ermolli E., Juvigné E.,** (2001). A late Middle Pleistocene climatic cycle in southern Italy inferred from pollen analysis and tephrostratigraphy of the Acerno lacustrine succession. *Géographie Physique et Quaternaire* 55, 87–99.
- Munno R., Petrosino P.,** (2004). New constraints on the occurrence of Y3 upper Pleistocene tephra marker layer in the Tyrrhenian Sea, *Italian Journal of Quaternary Sciences*, 17(1), 11–20.
- Munno R., Petrosino P.,** (2006). The late Quaternary tephrostratigraphical record of the San Gregorio Magno basin (southern Italy). *J. Quat. Sc.*, doi:10.1002/jqs.1025.
- Myers P.G., Rohling E.J.,** (2000). Modeling a 200-yr interruption of the Holocene sapropel S1. *Quat. Res.* 53, 98–104.

N

- Narcisi B.,** (1996). Tephrochronology of a Late Quaternary lacustrine record from Monticchio maar (Vulture volcano, Southern Italy). *Quat. Sci. Rev.* 15, 155–165.
- Narcisi B., Vezzoli L.,** (1999). Quaternary stratigraphy of distal tephra layers in the Mediterranean – an overview. *Global and Planetary Change* 21, 31–50.
- Narcisi B.,** (2002). Tephrostratigraphy of the Late Quaternary lacustrine sediments of Lago di Pergusa (central Sicily). *Boll. Soc. Geol. It.*, 121, 211–219, 5 ff., 1 tab.
- Negri A., Giunta S.,** (2001). Calcareous nannofossil paleoecology in the sapropel S1 of the eastern Ionian sea: paleoceanographic implications. *Palaeogeography, Palaeoclimatology, Palaeoecology*, 169, 101–112.

- Nicot J., Chardon M.**, (1983). On the morphotectonic background and the evolution of natural environments and limestone relief in Western Yugoslavian Macedonia. *Méditerranée*: 37–52.
- Ninkovich D., Heezen B.C.**, (1965). Santorini tephra. Proceedings of the Seventeenth Symposium of the Colston Research Society, Colston Research Papers, 17, 413–452. Butterworths Scientific Publications, London.
- Ninkovich D., Heezen B.C.**, (1967). Physical and chemical properties of volcanic glass shards from Pozzuolana ash, Thera Island, and from upper and lower layers in eastern Mediterranean deep sea sediments. *Nature*, 213, 582–584.

O

- Oldfield F., Appleby P., Thompson R.**, (1980). Palaeoecological studies of lakes in the highlands of Papua New Guinea., *Journal of Ecology*, 68, 457–477.
- Oppenheimer C. and Pyle D.M.**, (2009). Volcanoes. In: J.C.Woodward (ed.) *The Physical Geography of the Mediterranean*. Oxford: Oxford University Press, 435–468.
- Orsi G., Chiesa S.**, (1988). The uplift of the Mt. Epomeo Block at the Island of Ischia (Gulf of Naples); geological and geochemical constraints. *Eos, Transactions, American Geophys Union*, 69 (44), 1473.
- Orsi G., Gallo G., Zanchi A.**, (1991). Simple shearing block resurgence in caldera depressions. A model from Pantelleria and Ischia. *J. Volcanol. Geotherm. Res.* 47, 1–11.
- Orsi G., D’Antonio M., de Vita S., Gallo G.**, (1992). The Neapolitan Yellow Tuff, a large-magnitude trachytic phreatoplinian eruption: eruptive dynamics, magma withdrawal and caldera collapse. *J. Volcanol. Geotherm. Res.* 53, 275–287.
- Orsi G., Civetta L., D’Antonio M., Di Girolamo P., Piochi M.**, (1995). Step-filling and development of a three-layers magma chamber: the Neapolitan Yellow Tuff case history. *J. Volcanol. Geotherm. Res.* 67, 291–312.
- Orsi G., Piochi M., Campajola L., D’Onofrio A., Gialanella L., Terrasi F.**, (1996). ¹⁴C geochronological constraints for the volcanic history of the island of Ischia (Italy) over the last 5000 years. *J. Volcanol. Geotherm. Res.* 71, 249–257.
- Orsi G., Di Vito M.A., Isaia R.**, (2004). Volcanic hazard assessment at the restless Campi Flegrei caldera. *Bull. Volcanol.* 66, 514–530.

P

- Pappalardo L., Civetta L., D'Antonio M., Deino A., Di Vito M.A., Orsi G., Carandente A., de Vita S., Isaia R., Piochi M., (1999).** Chemical and Sr-isotopical evolution of the Phlegraen magmatic system before the Campanian Ignimbrite and the Neapolitan Yellow Tuff eruptions. *J. Volcanol. Geother. Res.* 91, 141–166.
- Pappalardo L., Civetta L., De Vita S., Di Vito M.A., Orsi G., Carandente A., Fisher R.V., (2002a).** Timing of magma extraction during the Campanian Ignimbrite eruption (Campi Flegrei caldera). *J. Volcanol. Geother. Res.* 114, 479–497.
- Pappalardo L., Piochi M., D'Antonio M., Civetta L., Petrini R., (2002b).** Evidence for multi-stage magmatic evolution during the past 60 ka at Campi Flegrei (Italy) deduced from Sr, Nd and Pb isotope data. *J Petrol* 43, 1415–1434.
- Passier H., De Lange G., Dekkers M., (2001).** Magnetic properties and geochemistry of the active oxidation front and the youngest sapropel in the eastern Mediterranean Sea. *Geophys. J. Int.*, 145, 604-614.
- Paterne M., (1985).** Reconstruction de l'activité explosive des volcans de l'Italie du sud par tephrochronologie marine. Phd thesis Univ. Paris Sud XI, Orsay, France.
- Paterne M., Guichard F., Labeyrie J., Gillot P.Y., Duplessy J.C., (1986).** Tyrrhenian Sea tephrochronology of the oxygen isotope record for the past 60,000 years. *Marine Geology*, 72, 259–285.
- Paterne M., Guichard F., Labeyrie J., (1988).** Explosive activity of the South Italian volcanoes during the past 80,000 years as determined by marine tephrochronology. *J. Volcanol. Geotherm. Res.* 34, 153–172.
- Paterne M., Labeyrie J., Guichard F., Massaud A., Maitre F., (1990).** Fluctuation of the campanian explosive activity (South Italy) during the last 190,000 years as determined by marine tephrochronology. *Earth and Planetary Science Letters*, 98, 166–174.
- Paterne M., Guichard F., (1993).** Triggering of volcanic pulses in the Campanian area, South Italy, by periodic deep magma influx. *J. Geophys. Res.* 98, 1861–1873.
- Paterne M., Guichard F., Duplessy J.C., Siani G., Sulpizio R., Labeyrie J., (2008).** A 90,000 – 200,000 yrs marine tephra record of Italian volcanic activity in the central Mediterranean Sea. *J. Volcanol. Geotherm. Res.* 177, 187–196. doi:10.1016/j.jvolgeores.2007.11.028.
- Peccerillo A., (2005).** Plio-Quaternary Volcanism in Italy. Springer-Verlag, Berlin, pp. 1–365.

- Peters C., Austin W., Walden J., Hibbert F.,** (2009). Magnetic characterisation and correlation of a Younger Dryas tephra in North Atlantic marine sediments. *J. Quaternary Sci.*, DOI: 10.1002/jqs.
- Pichler H.,** (1980). The island of Lipari. *Rend Soc Ital Mineral Petrol* 36, 415–440.
- Piochi M., Civetta L., Orsi G.,** (1999). Mingling in the magmatic system of Ischia (Italy) in the past 5 ka. *Miner Petrol* 66, 227–258.
- Pioli L., Erlund E., Johnson E., Cashman K., Wallace P., Rosi M., Delgado Granados H.,** (2008). Explosive dynamics of violent Strombolian eruptions: The eruption of Parícutin Volcano 1943–1952 (Mexico). *Earth and Planetary Science Letters*, 271, 359–368.
- Poli S., Chiesa S., Gillot P.Y., Gregnanin A., Guichard F.,** (1987). Chemistry versus time in the volcanic complex of Ischia (Gulf of Naples, Italy): Evidence of successive magmatic cycles. *Contrib. Min. Petrol.* 95, 322–335.
- Principato M.S., Giunta S., Corselli C., Negri A.,** (2003). Late Pleistocene-Holocene planktonic assemblages in three box-cores from the Mediterranean Ridge area (west-southwest of Crete): palaeoecological and palaeoceanographic reconstruction of sapropel S1 interval. *Palaeogeography, Palaeoclimatology, Palaeoecology*, 190, 61-77.
- Pyle D.M., Ricketts G.D., Margari V., van Andel T.H., Sinitsyn A.A., Praslov N., Lisitsyn S.,** (2006). Wide dispersal and deposition of distal tephra during the Pleistocene “Campanian Ignimbrite/Y5” eruption, Italy. *Quaternary Science Review* 25, 2713–2728.

R

- Reimer P.J., Baillie M.G.L., Bard E., Bayliss A., Beck, J.W., Bertrand C.J.H., Blackwell P.G., Buck C.E., Burr G.S., Cutler K.B., Damon P.E., Edwards R.L., Fairbanks R.G., Friedrich M., Guilderson T.P., Hogg A.G., Hughen K.A., Kromer B., McCormac F.G., Manning S.W., Ramsey C.B., Reimer R.W., Remmele S., Southon J.R., Stuiver M., Talamo S., Taylor F.W., van der Plicht J., Weyhenmeyer C.E.,** (2004). INTCAL04 Terrestrial radiocarbon age calibration, 26 – 0 ka BP. *Radiocarbon* 46, 1029–1058.
- Rittmann A.,** (1930) *Geologie der Insel Ischia*. Z Vulk Erg Bd 6, 265.
- Rittmann A., Ippolito F.,** (1962). Saggi sulla stratigrafia del Somma-Vesuvio. In: Ippolito, F. (Ed.), *Saggi e studi di Geologia*. Neri-Pozza, Venezia.

- Roberts N.**, (1998). *The Holocene, an environmental history*. 2nd edition, Blackwell Publishers Inc.
- Robertson A.H.F., Grasso M.**, (1995). Overview of the Late Tertiary–recent tectonic and palaeo-environmental development of the Mediterranean region. *Terra Nova* 7, 114–127.
- Rolandi G., Mastrolenzo G., Barrella A.M., Borrelli A.**, (1993). The Avellino Plinian eruption of Somma-Vesuvius (3760 y. B.P.): the progressive evolution from magmatic to hydromagmatic style. *J. Volcanol. Geotherm. Res.* 58, 67–88.
- Rogers N.W., Hawkesworth C.J., Parker R.J., Marsh J.S.**, (1985). The geochemistry of potassic lavas from Vulcini, Central Italy, and implication for mantle enrichment processes beneath the Roman region. *Contrib. Mineral Petrol.* 86, 230–240.
- Rohling E.J., Jorissen F.J., De Stigter H.C.**, (1997). 200 year interruption of Holocene sapropel formation in the Adriatic sea. *J. Micropaleontol.* 16, 97–108.
- Rousse S., Kissel C., Laj C., Eiriksson J., Knudsen K.**, (2006). Holocene centennial to millennial-scale climatic variability: Evidence from high-resolution magnetic analyses of the last 10 cal kyr of North Iceland (core MD99-2275). *Earth Planet. Sci. Lett.*, 242, 390–405.
- Rosi M., Santacroce R.**, (1983). The A.D. 472 “Pollena” eruption: volcanological and petrological data for this poorly-known, plinian-type event at Vesuvius. *J. Volcanol. Geotherm. Res.* 17, 249–271.
- Rosi M., Sbrana A.** (Eds.), (1987). *Phlegrean Fields*. CNR, Quaderni Ricerca Scientifica, 114, 1–175.
- Rosi M., Sbrana A., Vezzoli L.**, (1988). Stratigraphy of Procida and Vivara islands (In Italian). *Boll GNV* 4, 500–525.
- Rosi M., Vezzoli L., Aleotti P., De Renzi M.**, (1996). Interaction between caldera collapse and eruptive dynamics during the Campanian Ignimbrite eruption, Phlegraean Fields, Italy. *Bull. Volcanol.* 57, 541–554
- Rosi M., Vezzoli L., Castelmignano A., Grieco G.**, (1999). Plinian pumice fall deposit of the Campanian Ignimbrite eruption (Phlegrean Fields, Italy), *J. Volcanol. Geotherm. Res.* 91, 179–198.
- Rosi M., Bertagnini A., Harris A.J.L., Pioli L., Pistolesi M., Ripepe M.**, (2006). A case history of paroxysmal explosion at Stromboli: Timing and dynamics of the April 5, 2003 event. *Earth and Planetary Science Letters* 243, 594–606.

S

- Sadori L., Narcisi B.,** (2001). The Postglacial record of environmental history from Lago di Pergusa, Sicily, *The Holocene* 11, 6, 655–670. doi: 10.1191/09596830195681.
- Santacroce R.,** (Ed), (1987). *Somma-Vesuvius*. CNR Quaderni Ricerca Scientifica 114 (9), 251.
- Santacroce R., Cioni R., Civetta L., Marianelli P., Metrich N., Sbrana A.,** (1994). How Vesuvius works. "Large Explosive Eruptions". *Atti dei Covegni Lincei*, 112, 185–196.
- Santacroce R., Sbrana A.,** eds., (2003). *Geological map of Vesuvius 1:15,000 scale*. SELCA, Firenze
- Santacroce R., Cristofolini R., La Volpe L., Orsi G., Rosi M.,** (2003). Italian active volcanoes. *Episodes*, 26, 3.
- Santacroce R., Cioni R., Marianelli P., Sbrana A., Sulpizio R., Zanchetta G., Donahue D.J., Joron J.L.,** (2008). Age and whole rock-glass compositions of proximal pyroclastics from the major explosive eruptions of Somma-Vesuvius: a review as a tool for distal tephrostratigraphy *J. Volcanol. Geotherm. Res.* 177, 1–18. doi:10.1016/j.jvolgeores.2008.06.009.
- Scandone P.,** (1980). Origin of the Tyrrhenian Sea and Calabrian Arc, *Boll. Soc. Geol. It.*, 98, 27-36.
- Scandone R., Bellucci F., Lirer L., Rolandi G.,** (1991). The structure of the Campanian Plain and the activity of the Neapolitan volcanoes (Italy). *J. Volcanol. Geotherm. Res.* 48, 1–31.
- Scandone R., Barberi F., Rosi M.,** (2009). The 2007 eruption of Stromboli: Preface, *J. Volcanol. Geotherm. Res.* 182, doi:10.1016/j.jvolgeores.2008.12.019.
- Scarpati C., Cole P., Perrotta A.,** (1993). The Neapolitan Yellow Tuff—A large volume mutiphase eruption from Campi Flegrei, Southern Italy. *Bull. Volcanol.* 55, 343–356.
- Scheidegger K.F.,** (1973). Volcanic ash layers in deep-sea sediments and their petrological significance. *Earth and Planetary Science Letters*, 17, 397–407.
- Scheidegger K.F., Corliss J.B., Jezek P.A., Ninkovich D.,** (1980). Composition of deep-sea ash-layers derived from North Pacific volcanics arcs: variations in time and space. *J. Volcanol. Geotherm. Res.* 4, 99–116.
- Schmincke H.U., Park C., Harms E.,** (1999). Evolution and environmental impacts of the eruption of Laacher See Volcano (Germany) 12,900 a BP. *Quaternary International* 61, 61–72. doi:10.1016/S1040-6182(99)00017-8.

- Sheridan M.F., Frazzetta G., La Volpe L.,** (1987). Eruptive histories of Lipari and Vulcano, Italy, during the past 22,000 years. *Geol. Soc. Am.* 212, 29–34.
- Siani G., Paterne M., Michel E., Sulpizio R., Sbrana A., Arnold M., Haddad G.,** (2001). Mediterranean sea-surface radiocarbon reservoir age changes since the last glacial maximum. *Science* 294, 1917–1920.
- Siani G., Sulpizio R., Paterne M., Sbrana A.,** (2004). Tephrostratigraphy study for the last 18,000 ¹⁴C years in a deep-sea sediment sequence for the South Adriatic. *Quaternary Science Review* 23, 2485–2500.
- Signorelli S., Vaggelli G., Romano C., Carroll M.R.,** (2001). Volatile element zonation in Campanian Ignimbrite magmas (Phlegrean Fields, Italy): evidence from the study of glass inclusions and matrix glasses. *Contributions to Mineralogy and Petrology* 140, 543–553.
- Sigurdsson H., Sparks R.S.J., Carey S., Huang T.C.,** (1980). Volcanogenic sedimentation in the Lesser Antilles arc. *J. Geol.* 88, 523–540.
- Sigurdsson H., Carey S., Cornell W., Pescatore T.,** (1985). The eruption of Vesuvius in A.D. 79. *Natl. Geogr. Res.* 1, 332–387.
- Smith D.E., Kolenkiewicz R., Nerem R.S., Dunn P.J., Torrence M.H., Robbins J.W., Klosko S.M., Williamson R.G., Pavlis E.C.,** (1994). Contemporary global horizontal crustal motion. *Geophys. J. Int.* 119, 511–520.
- Soligo M., De Astis G., Delitala M.C., La Volpe L., Taddeucci A., Tuccimei P.,** (1999). Disequilibri nella serie dell'uranio nei prodotti dell'isola di Vulcano: cronologia isotopica e implicazioni magmatologiche. *Plinius* 22, 347–349.
- Sottili G., Palladino D.M., Zanon V.,** (2004). Plinian activity during the early eruptive history of the Sabatini Volcanic District Central Italy. *J. Volcanol. Geotherm. Res.* 135, 361–379.
- Spakman W., Wortel R.,** (2004). A tomographic view on Western Mediterranean geodynamics. In: Cavazza, W., Roure, F., Spakman, W., Stampfli, G.M., Ziegler, P.A. (Eds.), *The TRANSMED Atlas, The Mediterranean Region from Crust to Mantle*. Springer-Verlag, Berlin Heidelberg, pp. 31–52.
- Spence R.J.S., Kelman I., Calogero E., Toyos G., Baxter P.J., Komorowski J.C.,** (2005). Modelling expected physical impacts and human casualties from explosive volcanic eruptions. *Natural Hazard and Earth System Sciences*, 5, 1003–1015.
- Spence R.J.S., Kelman I., Baxter P.J., Zuccaro G., Petrazzuoli S.,** (2005). Residential building and occupant vulnerability to tephra fall. *Natural Hazard and Earth System Sciences*, 5, 477–494.

- Sperling M., Schmiidl G., Hemlebn C., Emeis K.C., Erlenkeuser H., Grootes P.M.,** (2003). Black Sea impact on the formation of eastern Mediterranean sapropel S1? Evidence from the Marmara Sea. *Palaeogeography, Palaeoclimatology, Palaeoecology*, 190, 9–21.
- St Seymour K., Christianis K.,** (1995). Correlation of a tephra layer in Western Greece with a late Pleistocene eruption in the Campanian province of Italy. *Quaternary Research* 43, 46–54.
- St Seymour K., Christianis K., Bouzinos A., Papazisimou S., Papatheodorou G., Moran E., Denes G.,** (2004). Tephrostratigraphy and tephrochronology in the Philippi peat basin, Macedonia, Northern Hellas (Greece). *Quaternary International* 121, 53–65.
- Stankovic S., Hadzisce S.D.,** (1953). La thermique du lac d'Ohrid. *Recueil des travaux, Station hydrobiologique – Ohrid*. 61 pp.
- Stankovic S.,** (1960). The Balkan Lake Ohrid and its living world. *Monographiae Biologicae* IX. Dr. W. Junk, Den Haag. 357pp.
- Stow D.A.V., Huc A.Y., Bertrand P.,** (2001). Depositional processes of black shales in deep water. *Marine and Petroleum Geology* 18, 491–498.
- Stuiver M., Reimer P.J., Bard E., Beck W., Burr G., Hughen K., Kromer B., McCormac G., van der Plicht J., Spurk M.,** (1998). INTCAL98 radiocarbon age calibration, 24,000-0 cal B.P. *Radiocarbon* 40, 1041–1083.
- Stuiver M., Reimer P.J., Reimer R.W.,** (2005). CALIB 5.0. [WWW program and documentation]. <http://calib.qub.ac.uk/calib/>
- Sulpizio R., Zanchetta G., Paterne M., Siani G.,** (2003). A review of tephrostratigraphy in central and southern Italy during the last 65 ka. *Quaternario*. 16, 91–108.
- Sulpizio R.,** (2005). Three empirical methods for the calculation of distal volume of tephra-fall deposits. *J. Volcanol. Geotherm. Res.* 145, 315-336.
- Sulpizio R., Mele D., Dellino P., La Volpe L.,** (2005). A complex, Subpliniantype eruption from low-viscosity, phonolitic to tephri-phonolitic magma: the AD 472 (Pollena) eruption of Somma-Vesuvius (Italy). *Bull. Volcanol.* 67, 743–767. doi:10.1007/s00445-005-0414-x.
- Sulpizio R., Bonasia R., Dellino P., Di Vito M.A., La Volpe L., Mele D., Zanchetta G., Sadori L.,** (2008). Discriminating the-long distance dispersal of fine ash from sustained columns or near ground ash clouds: the example of the Pomici di Avellino eruption (Somma–Vesuvius, Italy). *J. Volcanol. Geotherm. Res.* doi:10.1016/j.jvolgeores.2007.11.012.

Sulpizio R., Van Welden A., Caron B., Zanchetta G., (2009). The Holocene tephrostratigraphic record of Lake Shkodra (Albania and Montenegro). *J. Quaternary Sci.*, ISSN 0267-8179.

T

Tanguy J. C., Le Goff, M., Principe C., Arrighi S., Chillemi V., Paiotti A., La Delfa S., Patane G., (2003). Archaeomagnetic dating of Mediterranean volcanics of the last 2100 years: validity and limits. *Earth and Planetary Science Letters*, 211, 111–124.

Tapponnier P., (1977). Evolution tectonique du système alpin en Méditerranée: poinçonnement et écrasement rigide–plastique. *Bull. Soc. Geol. Fr.* 19, 437–460.

Thompson R., Oldfield F., (1986). *Environmental magnetism*. Allen and Unwin, London, 227 pp.

Thunnell R.C., Federman A., Sparks S., Williams D., (1979). The age, origin and volcanological significance of the Y-5 ash layer in the Mediterranean. *Quaternary Research* 12, 241–253.

Thunnell R.C., Williams D.F., Belyea P.R., (1984). Anoxic events in the Mediterranean sea in relation to the evolution of late Neogene climates. *Mar. Geol.* 59. 105–134.

Tibaldi A., Vezzoli L., (1998). The space problem of caldera resurgence: an example from Ischia Island, Italy. *Geol Rund* 87, 53–66.

Tisnérat-Laborde N., Poupeau J. J., Tannau J. F., Paterne M., (2001). Development of a semi-automated system for routine preparation of carbonate samples. *Radiocarbon*, 43, 2A, 299–304.

Tranne C.A., Lucchi F., Calanchi N., Lanzafame G., Rossi P.L., (2002a). Geological map of the island of Lipari (Aeolian Islands). University of Bologna and INGV; printed by L.A.C., Firenze.

Tranne C.A., Lucchi F., Calanchi N., Rossi P.L., Campanella T., Sardella A., (2002b). Geological map of the island of Filicudi (Aeolian Islands). University of Bologna and INGV; printed by L.A.C., Firenze.

Trigila R., Agosta E., Currado C., De Benedetti A.A., Freda C., Gaeta M., Palladino D.M., Rosa C., (1995). Petrology. In: Trigila R., (Ed). *The volcano of the Alban Hills*. Università degli Studi di Roma 'La Sapienza', Rome, 283 pp.

- Turco E., Zuppetta A.,** (1998). A kinematic model for the Plio-Quaternary evolution of the Tyrrhenian–Apenninic system: implications for rifting processes and volcanism. *J. Volcanol. Geotherm. Res.* 82, 1–18.
- Turney C. S. M., Lowe J. J., Davies S. M., Hall V., Lowe D. J., Wastegård S., Hoek W. Z., Alloway B.,** (2004). Tephrochronology of Last Termination Sequences in Europe: a protocol for improved analytical precision and robust correlation procedures (a joint SCOTAV–INTIMATE proposal). *J. Quaternary Sci.*, 19, 111–120. ISSN 0267-8179.
- Turney C.S.M., Blockley S.P.E., Lowe J.J., Wulf S., Branch N.P., Mastrolorenzo G., Swindle G., Nathan R., Pollard A.M.,** (2008). Geochemical characterization of Quaternary tephra from the Campanian province, Italy. *Quaternary International* 178, 288–305.
- Tzedakis P.C., Frogley M.R., Heaton T.H.E.,** (2003). Last Interglacial conditions in southern Europe: evidence from Ioannina, northwest Greece, *Global and Planetary Change* 36 157–170. doi:10.1016/S0921-8181(02)00182-0.

V

- van den Bogaard P.,** (1995). $^{40}\text{Ar}/^{39}\text{Ar}$ ages of sanidine phenocrysts from Laacher See Tephra (12,900 yr BP): Chronostratigraphic and petrological significance. *Earth and Planetary Science Letters*, 133, 163–174.
- van der Plicht J., Beck J.W., Bard E., Baillie M.G.L., Blackwell P.G., Buck C.E., Friedrich M., Guilderson T.P., Hughen K.A., Kromer B., McCormac F.G., Bronk Ramsey C., Reimer P.J., Reimer R.W., Remmele S., Richards D.A., Southon J.R., Stuiver M., Weyhenmeyer C.E.,** (2004). NotCal04—Comparison/Calibration 14C records 26–50 cal kyr BP. *Radiocarbon*, vol. 46, 3, 1225–1238.
- van Welden A.,** (2007). Enregistrements sédimentaires imbriqués d’une activité sismique et de changements paléoenvironnementaux. Comparaison entre différents sites: Golfe de Corinthe (Grèce), Lac de Shkodra (Albanie/Monténégro) et Golfe de Cariaco (Vénézuéla). PhD dissertation, LGCA, Le Bourget du Lac, France.
- van Welden A., Beck C., Reyss J.L., Bushati S., Koci R., Jouanne F., Mugnier J.L.,** (2008). The last 500 year of sedimentation in Shkodra Lake (Albania/Montenegro): paleoenvironmental evolution and potential for paleoseismicity studies. *Journal of Paleolimnology* 40, 619–633.
- Ventura G.,** (1994). Tectonics, structural evolution and caldera formation on Vulcano island (Aeolian archipelago, southern Tyrrhenian Sea). *J. Volcanol. Geotherm. Res.* 60, 207–224.

- Verosub K.L., Roberts A.P.**, (1995). Environmental magnetism: Past, present and future. *J. Volcanol. Geotherm. Res.* 100 (B2), 2175–2192.
- Vezzoli L.**, (1988) Island of Ischia: *Quaderni de La Ricerca Scientifica*, 114(10). Consiglio Nazionale delle Ricerca, Rome, p 133.
- Vezzoli L.**, (1991). Tephra layers in Bannock Basin (Eastern Mediterranean). *Mar. Geol.* 100, 21–34.
- Viallard P.**, (1978). Tectogénèse de la chaîne ibérique: relations substratum–couverture dans une tectonique polyphasée. *C. R. Acad. Sci. Paris* 287D, 1103–1106.
- Viallard P.**, (1979). La chaîne ibérique: zone de cisaillement intracontinentale pendant la tectogénèse alpine. *C. R. Acad. Sci. Paris* 289D, 65–68.
- Vogel H., Zanchetta G., Sulpizio R., Wagner B., Nowaczyk N.**, (2009). A tephrostratigraphic record for the last glacial-interglacial cycle from Lake Ohrid, Albania and Macedonia. *J. Quaternary Sci.* ISSN 0267-8179.
- Vogel J.S., Cornell W., Nelson D.E., Southon J.R.**, (1990). Vesuvius Avellino, one possible source of seventeenth century BC climate disturbance. *Nature* 344, 534–537.
- Voltaggio M., Barbieri M., Castorina F., Taddeucci A., Tecce F., Tuccimei P., Turi B., Vesica P.**, (1997). Calcite in fractures in a volcanic environment (Vulcano Island, Italy): contribution of geochronological and isotopic studies to volcanotectonics. *J. Volcanol. Geotherm. Res.* 75, 271–282.

W

- Wagner B., Reicherter K., Daut G., Wessels M., Matzinger A., Schwalb A., Spirkovski Z., Sanxhahu M.**, (2008a). The potential of Lake Ohrid for long-term paleoenvironmental reconstructions. *Palaeogeography, Palaeoclimatology, Palaeoecology*, 259, 2–3, 341–356.
- Wagner B., Sulpizio R., Zanchetta G., Wulf S., Wessels M., Daut G., Nowaczyk N.**, (2008b). The last 40 ka tephrostratigraphic record of Lake Ohrid, Albania and Macedonia: a very distal archive for ash dispersal from Italian volcanoes, *J. Volcanol. Geotherm. Res.*, doi:10.1016/j.jvolgeores.2007.08.018.
- Wagner B., Lotter A.F., Nowaczyk N., Reed J.M., Schwalb A., Sulpizio R., Valsecchi V., Wessels M., Zanchetta G.**, (2008c). A 40,000-year record of environmental change from ancient lake Ohrid (Albania and Macedonia). *J. Paleolimnol.* 10.1007/s10933-008-9234-2

- Walker G.P.L.**, (1973). Explosive volcanic eruption – a new classification scheme. *Geol. Rundsch.* 62, 431–446.
- Walker G.P.L.**, (1977). Metodi geologici per la valutazione del rischio vulcanico. Atti del convegno: I vulcani attivi dell'area napoletana. Regione Campania, Napoli, 53–60.
- Walker M.J.C.**, (2005). *Quaternary dating methods*. John Wiley & Sons Ltd, The Atrium, Southern Gate, Chichester, West Sussex PO19 8SQ, England. ISBN 0 470 86927 5.
- Ward S.N.**, (1994). Constraints on the seismotectonics of the central Mediterranean from Very Long Baseline Interferometry. *Geophys. J. Int.* 117, 441–452.
- Washington H.S.**, (1906). *The Roman comagmatic region*. Carnegie Institute, Washington (publ. no. 57).
- Weeks R., Laj C., Endignoux L., Fuller M., Roberts A., Manganne R., Blanchard E., Goree W.**, (1993). Improvements in long-core measurement techniques: applications in palaeomagnetism and palaeoceanography, *Geophys. J. Int.* 114, 651–662.
- Weninger B., Jöris O.**, (2008). A 14C age calibration curve for the last 60 ka: the Greenland-Hulu U/Th timescale and its impact on understanding the Middle to Upper Paleolithic transition in Western Eurasia. *Journal of human evolution*, 55, 772–781 doi:10.1016/j.jhevol.2008.08.017.
- Wohletz K., Orsi G., de Vita S.**, (1995). Eruptive mechanisms of the Neapolitan Yellow Tuff interpreted from stratigraphic, chemical and granulometric data. *J. Volcanol. Geotherm. Res.* 67, 263–290.
- Wohlfarth B.**, (1996). The Chronology of the last termination: a review of radiocarbon-dated, high-resolution terrestrial stratigraphies. *Quaternary Science Reviews* 15, 267–284.
- Wölfli W., Polach H.A., Andersen H.W.**, (1984). Proceedings of the Third International Symposium on Accelerator Mass Spectrometry, Nuclear Instruments & Methods in Physics Research, Section B 5 1–448.
- Wright J.V.**, (1980). Stratigraphy and geology of the welded air fall tuffs of Pantelleria, Italy. *Geol Rundsch.* 69, 681–690.
- Wulf S., Kraml M., Brauer A., Keller J., Negendank J.F.W.**, (2004). Tephrochronology of the 100 ka lacustrine sediment record of Lago Grande di Monticchio (southern Italy). *Quaternary International* 122, 7–30.
- Wulf S., Brauer A., Mingram J., Zolitschka B., Egendank J.F.W.**, (2007). Distal tephras in the sediments of Monticchio maar lakes. In: C. Principe, Editor, *Geologia del Monte Vulture*, *Bollettino della Societa Geologica Italiana*, 105–122.

Wulf S., Kraml M., Keller J., (2008). Towards a detailed distal tephrostratigraphy in the Central Mediterranean: The last 20,000 yrs record of Lago Grande di Monticchio. *J. Volcanol. Geotherm. Res.* 177, 118–132.

Z

Zanchetta G., Sulpizio R., Giaccio B., Siani G., Paterne M., Wulf S., D'Orazio M. (2008). The Y-3 tephra: A Last Glacial stratigraphic marker for the central Mediterranean basin, *J. Volcanol. Geotherm. Res.*, doi:10.1016/j.jvolgeores.2007.08.017.

Zanchetta G., Sulpizio R., Roberts N., Cioni R., Eastwood W.J., Siani G., Caron B., Paterne M., Santacroce R., (2010). Tephrostratigraphy, chronology and climatic events of the Mediterranean basin during the Holocene: an overview. *Holocene* in press.

Zanella E., (2006). Magnetic chronology in recent volcanic rocks: basic principles and case histories from Aeolian Islands. *Acta Vulcanologica*, 18, 35–46.

Annexes

Annexe 1: $\delta^{18}\text{O}$ data of the MD 90-918 core

depth	G. ruber 250-315 μm		n° LL	date	depth	$\delta^{18}\text{O}$ GIF	$\delta^{13}\text{C}$ GIF	gaz ref	μg	volt SA	pression CO ₂	spectro
	$\delta^{18}\text{O}$ PDB	$\delta^{13}\text{C}$ PDB										
0	0.84	0.83	50061	21/02/2008	0	0.94	0.95	MONGA-1	F4	5.44	1158	Δ^+
0	0.66	0.81	50194	29/02/2008	0	0.66	0.84	MONGA-1	F4	4.29	1279	Δ^+
10	0.24	0.88	50062	21/02/2008	10	0.34	1.00	MONGA-1	F4	5.16	1131	Δ^+
20	0.01	0.99	50063	21/02/2008	20	0.11	1.11	MONGA-1	F4	4.25	1207	Δ^+
30	0.51	1.12	50065	21/02/2008	30	0.61	1.24	MONGA-1	F3	4.40	871	Δ^+
40	0.50	0.68	50066	21/02/2008	40	0.60	0.80	MONGA-1	F4	4.20	793	Δ^+
50	0.69	0.90	50067	21/02/2008	50	0.79	1.02	MONGA-1	F3	4.42	931	Δ^+
60	0.37	1.08	50068	21/02/2008	60	0.47	1.20	MONGA-1	F4	5.16	1127	Δ^+
70	-0.31	1.14	50069	21/02/2008	70	-0.21	1.26	MONGA-1	F4	5.08	1113	Δ^+
80	1.32	1.24	50070	21/02/2008	80	1.42	1.36	MONGA-1	F4	5.51	1191	Δ^+
80	-0.01	1.29	50204	29/02/2008	80	-0.01	1.32	MONGA-1	F4	3.54	998	Δ^+
80	0.48	1.18	50225	03/03/2008	80	0.48	1.21	MONGA-1	F2	2.55	735	Δ^+
90	0.40	1.04	50071	21/02/2008	90	0.50	1.16	MONGA-1	F4	5.05	1226	Δ^+
100	0.83	1.35	50072	21/02/2008	100	0.93	1.47	MONGA-1	F4	4.11	1334	Δ^+
110	0.69	0.92	50075	21/02/2008	110	0.79	1.04	MONGA-1	F4	5.14	1101	Δ^+
120	0.43	1.09	50076	21/02/2008	120	0.53	1.21	MONGA-1	F4	5.59	1232	Δ^+
130	0.04	1.11	50112	27/02/2008	130	0.04	1.14	MONGA-1	F3	3.16	795	Δ^+
140	-0.05	0.71	50077	21/02/2008	140	0.05	0.83	MONGA-1	F4	4.78	925	Δ^+
150	0.17	1.32	50078	21/02/2008	150	0.27	1.44	MONGA-1	F3	4.85	1064	Δ^+
160	0.00	0.86	50079	21/02/2008	160	0.10	0.98	MONGA-1	F4	2.60	689	Δ^+
170	0.16	1.15	50080	21/02/2008	170	0.26	1.27	MONGA-1	F3	3.71	810	Δ^+
180	-0.10	0.62	50114	27/02/2008	180	-0.10	0.65	MONGA-1	F3	3.09	800	Δ^+
190	-0.30	1.09	50111	27/02/2008	190	-0.30	1.12	MONGA-1	F4	5.25	1355	Δ^+
200	-0.15	0.64	50113	27/02/2008	200	-0.15	0.67	MONGA-1	F4	3.56	984	Δ^+
210	0.40	0.23	50141	28/02/2008	210	0.40	0.26	MONGA-1	F3	2.69	738	Δ^+
220	0.29	0.29	50115	27/02/2008	220	0.29	0.32	MONGA-1	F4	3.72	968	Δ^+
230	0.07	0.37	50116	27/02/2008	230	0.07	0.40	MONGA-1	F4	3.17	970	Δ^+
240	0.82	0.77	50118	27/02/2008	240	0.82	0.80	MONGA-1	F4	4.02	1047	Δ^+
250	1.30	0.53	50119	27/02/2008	250	1.30	0.56	MONGA-1	F4	2.81	749	Δ^+
260	1.41	0.68	50120	27/02/2008	260	1.41	0.71	MONGA-1	F4	3.30	820	Δ^+
270	1.46	0.65	50121	27/02/2008	270	1.46	0.68	MONGA-1	F4	2.98	764	Δ^+
290	1.49	0.74	50122	27/02/2008	290	1.49	0.77	MONGA-1	F3	2.12	659	Δ^+
300	2.06	0.57	50123	27/02/2008	300	2.06	0.60	MONGA-1	F4	4.08	1052	Δ^+
310	2.29	0.20	50124	27/02/2008	310	2.29	0.23	MONGA-1	F4	3.31	799	Δ^+
320	1.32	0.02	50125	27/02/2008	320	1.32	0.05	MONGA-1	F4	3.67	949	Δ^+
320	1.53	0.49	50196	29/02/2008	320	1.53	0.52	MONGA-1	F3	2.21	702	Δ^+
330	1.94	0.60	50128	27/02/2008	330	1.94	0.63	MONGA-1	F4	4.18	1050	Δ^+
340	1.76	0.50	50129	27/02/2008	340	1.76	0.53	MONGA-1	F4	2.94	777	Δ^+
350	1.63	0.17	50130	27/02/2008	350	1.63	0.20	MONGA-1	F4	4.72	1271	Δ^+
360	1.72	0.44	50131	27/02/2008	360	1.72	0.47	MONGA-1	F4	4.02	1050	Δ^+
370	1.91	0.51	50132	27/02/2008	370	1.91	0.54	MONGA-1	F4	4.87	1250	Δ^+
380	2.07	-0.13	50133	27/02/2008	380	2.07	-0.10	MONGA-1	F4	4.13	1218	Δ^+
390	2.24	0.32	50134	27/02/2008	390	2.24	0.35	MONGA-1	F4	3.37	916	Δ^+
400	2.32	0.54	50135	27/02/2008	400	2.32	0.57	MONGA-1	F4	2.96	1123	Δ^+
410	2.55	0.40	50138	27/02/2008	410	2.55	0.43	MONGA-1	F4	5.07	1353	Δ^+
420	2.55	0.40	50138	27/02/2008	420	2.55	0.43	MONGA-1	F4	5.07	1353	Δ^+
420	2.53	0.15	50142	28/02/2008	420	2.53	0.18	MONGA-1	F4	4.87	1224	Δ^+
430	2.12	0.29	50143	28/02/2008	430	2.12	0.32	MONGA-1	F4	3.22	794	Δ^+
440	2.21	0.51	50144	28/02/2008	440	2.21	0.54	MONGA-1	F4	3.96	1027	Δ^+
450	2.19	0.42	50145	28/02/2008	450	2.19	0.45	MONGA-1	F4	4.84	1322	Δ^+
460	2.21	0.69	50146	28/02/2008	460	2.21	0.72	MONGA-1	F4	2.81	768	Δ^+
470	2.32	0.63	50147	28/02/2008	470	2.32	0.66	MONGA-1	F4	3.63	1373	Δ^+
480	2.78	0.02	50198	29/02/2008	480	2.78	0.05	MONGA-1	F3	3.71	1263	Δ^+
490	2.51	0.49	50150	28/02/2008	490	2.51	0.52	MONGA-1	F4	3.47	875	Δ^+

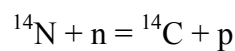
G. ruber		250-315µm										
depth	δ18O PDB	δ13C PDB	n° LL	date	depth	δ18O GIF	δ13C GIF	gaz ref	µg	volt SA	pression CO2	spectro
500	2.06	0.80	50149	28/02/2008	500	2.06	0.83	MONGA-1	F4	3.15	785	Δ+
510	2.44	0.67	50151	28/02/2008	510	2.44	0.70	MONGA-1	F4	5.09	1224	Δ+
520	2.30	0.44	50152	28/02/2008	520	2.30	0.47	MONGA-1	F3	3.66	900	Δ+
530	2.31	0.71	50154	28/02/2008	530	2.31	0.74	MONGA-1	F4	3.90	986	Δ+
540	2.08	0.50	50153	28/02/2008	540	2.08	0.53	MONGA-1	F4	4.57	1088	Δ+
550	2.23	0.63	50155	28/02/2008	550	2.23	0.66	MONGA-1	F4	3.40	1121	Δ+
560	2.75	0.23	50156	28/02/2008	560	2.75	0.26	MONGA-1	F4	2.87	1187	Δ+
570	2.82	0.48	50159	28/02/2008	570	2.82	0.51	MONGA-1	F4	3.19	796	Δ+
580	3.30	0.64	50160	28/02/2008	580	3.30	0.67	MONGA-1	F4	4.17	1068	Δ+
590	3.54	0.80	50161	28/02/2008	590	3.54	0.83	MONGA-1	F4	3.68	898	Δ+
600	2.94	0.80	50162	28/02/2008	600	2.94	0.83	MONGA-1	F4	4.80	1181	Δ+
610	3.26	0.30	50163	28/02/2008	610	3.26	0.33	MONGA-1	F4	4.17	1103	Δ+
620	3.10	0.93	50164	28/02/2008	620	3.10	0.96	MONGA-1	F4	4.07	1177	Δ+
630	3.11	0.35	50165	28/02/2008	630	3.11	0.38	MONGA-1	F4	3.50	1160	Δ+
640	3.05	0.61	50166	28/02/2008	640	3.05	0.64	MONGA-1	F4	2.93	1343	Δ+
650	3.34	0.58	50169	28/02/2008	650	3.34	0.61	MONGA-1	F4	3.82	992	Δ+
660	3.23	0.85	50170	28/02/2008	660	3.23	0.88	MONGA-1	F4	3.78	974	Δ+
670	2.89	0.73	50171	28/02/2008	670	2.89	0.76	MONGA-1	F4	5.45	1293	Δ+
680	3.39	1.02	50172	28/02/2008	680	3.39	1.05	MONGA-1	F4	5.11	1328	Δ+
690	3.48	0.77	50173	28/02/2008	690	3.48	0.80	MONGA-1	F4	4.55	1281	Δ+
700	3.40	0.67	50174	28/02/2008	700	3.40	0.70	MONGA-1	F4	3.81	1484	Δ+
710	3.33	0.89	50175	28/02/2008	710	3.33	0.92	MONGA-1	F4	3.22	1607	Δ+
720	3.39	0.87	50176	28/02/2008	720	3.39	0.90	MONGA-1	F4	2.70	1244	Δ+
730	3.54	0.63	50202	29/02/2008	730	3.54	0.66	MONGA-1	F3	4.20	1283	Δ+
740	3.45	0.69	50178	28/02/2008	740	3.45	0.72	MONGA-1	F4	5.55	1455	Δ+
750	3.50	1.06	50179	28/02/2008	750	3.50	1.09	MONGA-1	F4	5.19	1355	Δ+
760	3.40	1.03	50197	29/02/2008	760	3.40	1.06	MONGA-1	F4	4.44	1607	Δ+
770	2.58	0.66	50201	29/02/2008	770	2.58	0.69	MONGA-1	F4	5.31	1478	Δ+
770	3.36	1.09	50226	03/03/2008	770	3.36	1.12	MONGA-1	F3	4.58	1318	Δ+
770	3.31	0.59	50267	04/03/2008	770	3.31	0.62	MONGA-1	F3	3.81	1047	Δ+
780	3.34	0.25	50203	29/02/2008	780	3.34	0.28	MONGA-1	F4	3.48	978	Δ+
790	3.43	0.71	50195	29/02/2008	790	3.43	0.74	MONGA-1	F4	5.73	1554	Δ+
800	3.29	0.67	50205	29/02/2008	800	3.29	0.70	MONGA-1	F4	4.88	1664	Δ+
810	3.31	0.65	50206	29/02/2008	810	3.31	0.68	MONGA-1	F4	4.09	1603	Δ+
820	3.32	1.30	50207	29/02/2008	820	3.32	1.33	MONGA-1	F4	3.41	1500	Δ+
830	3.36	0.40	50208	29/02/2008	830	3.36	0.43	MONGA-1	F4	2.87	1234	Δ+
840	3.33	0.76	50211	29/02/2008	840	3.33	0.79	MONGA-1	F4	5.63	1402	Δ+
850	3.20	0.78	50212	29/02/2008	850	3.20	0.81	MONGA-1	F4	5.71	1511	Δ+
860	3.21	0.77	50213	29/02/2008	860	3.21	0.80	MONGA-1	F4	5.37	1504	Δ+
870	3.26	0.55	50214	29/02/2008	870	3.26	0.58	MONGA-1	F4	4.13	1300	Δ+
880	3.22	0.91	50215	29/02/2008	880	3.22	0.94	MONGA-1	F4	3.79	1347	Δ+
890	3.21	0.58	50216	29/02/2008	890	3.21	0.61	MONGA-1	F4	3.18	1332	Δ+
900	2.97	0.85	50217	29/02/2008	900	2.97	0.88	MONGA-1	F4	2.69	1496	Δ+
910	3.23	0.94	50218	29/02/2008	910	3.23	0.97	MONGA-1	F4	2.28	1513	Δ+
920	3.21	0.57	50219	29/02/2008	920	3.21	0.60	MONGA-1	F4	1.94	1134	Δ+
930	2.80	1.01	50221	29/02/2008	930	2.80	1.04	MONGA-1	F4	4.86	1326	Δ+
940	3.22	1.18	50222	29/02/2008	940	3.22	1.21	MONGA-1	F4	5.73	1572	Δ+
950	3.08	-0.06	50227	03/03/2008	950	3.08	-0.03	MONGA-1	F3	3.70	984	Δ+
950	3.36	1.00	50268	04/03/2008	950	3.36	1.03	MONGA-1	F3	3.45	914	Δ+
950	3.14	0.93	50310	05/03/2008	950	3.14	0.96	MONGA-1	F4	5.35	1422	Δ+
960	3.25	0.72	50228	03/03/2008	960	3.25	0.75	MONGA-1	F3	3.41	947	Δ+
970	2.90	1.11	50229	03/03/2008	970	2.90	1.14	MONGA-1	F3	3.26	931	Δ+
980	3.02	1.00	50230	03/03/2008	980	3.02	1.03	MONGA-1	F3	3.75	1097	Δ+
990	3.08	0.66	50231	03/03/2008	990	3.08	0.69	MONGA-1	F3	3.17	1041	Δ+

G. ruber 250-315µm												
depth	δ18O PDB	δ13C PDB	n° LL	date	depth	δ18O GIF	δ13C GIF	gaz ref	µg	volt SA	pression CO2	spectro
1011	3.25	0.80	50232	03/03/2008	1011	3.25	0.83	MONGA-1	F3	2.69	857	Δ+
1020	3.38	0.77	50235	03/03/2008	1020	3.38	0.80	MONGA-1	F3	3.50	963	Δ+
1030	3.09	1.11	50234	03/03/2008	1030	3.09	1.14	MONGA-1	F3	4.26	1140	Δ+
1040	3.18	0.43	50237	03/03/2008	1040	3.18	0.46	MONGA-1	F4	4.56	1281	Δ+
1050	3.15	0.99	50236	03/03/2008	1050	3.15	1.02	MONGA-1	F3	3.39	978	Δ+
1060	3.35	0.70	50238	03/03/2008	1060	3.35	0.73	MONGA-1	F3	3.97	1019	Δ+
1070	3.11	0.93	50239	03/03/2008	1070	3.11	0.96	MONGA-1	F3	4.16	1095	Δ+
1080	3.24	0.88	50240	03/03/2008	1080	3.24	0.91	MONGA-1	F3	3.11	794	Δ+
1090	3.26	0.47	50241	03/03/2008	1090	3.26	0.50	MONGA-1	F3	3.02	1050	Δ+
1100	2.94	0.83	50244	03/03/2008	1100	2.94	0.86	MONGA-1	F3	3.45	1011	Δ+
1110	3.02	0.81	50245	03/03/2008	1110	3.02	0.84	MONGA-1	F3	4.08	1242	Δ+
1120	3.02	0.26	50246	03/03/2008	1120	3.02	0.29	MONGA-1	F3	3.36	955	Δ+
1130	2.86	0.69	50247	03/03/2008	1130	2.86	0.72	MONGA-1	F3	4.41	1215	Δ+
1140	3.11	0.83	50248	03/03/2008	1140	3.11	0.86	MONGA-1	F3	4.10	1138	Δ+
1150	2.93	0.36	50249	03/03/2008	1150	2.93	0.39	MONGA-1	F3	3.93	1103	Δ+
1160	2.75	0.38	50250	03/03/2008	1160	2.75	0.41	MONGA-1	F3	3.66	1082	Δ+
1170	2.68	0.50	50251	03/03/2008	1170	2.68	0.53	MONGA-1	F3	3.09	1103	Δ+
1180	2.92	0.71	50269	04/03/2008	1180	2.92	0.74	MONGA-1	F3	3.49	972	Δ+
1190	2.89	1.12	50254	03/03/2008	1190	2.89	1.15	MONGA-1	F3	3.73	1066	Δ+
1200	2.98	1.12	50255	03/03/2008	1200	2.98	1.15	MONGA-1	F3	3.27	925	Δ+
1210	2.37	0.76	50256	03/03/2008	1210	2.37	0.79	MONGA-1	F3	2.89	796	Δ+
1210	2.74	0.89	50270	04/03/2008	1210	2.74	0.92	MONGA-1	F3	3.44	959	Δ+
1220	3.05	0.62	50257	03/03/2008	1220	3.05	0.65	MONGA-1	F3	3.63	888	Δ+
1230	3.29	1.07	50258	03/03/2008	1230	3.29	1.10	MONGA-1	F3	3.53	824	Δ+
1240	2.78	1.12	50259	03/03/2008	1240	2.78	1.15	MONGA-1	F3	4.39	1052	Δ+
1250	3.19	1.15	50260	03/03/2008	1250	3.19	1.18	MONGA-1	F3	3.78	992	Δ+
1260	2.99	0.66	50261	03/03/2008	1260	2.99	0.69	MONGA-1	F3	2.91	748	Δ+
1270	3.06	0.91	50263	03/03/2008	1270	3.06	0.94	MONGA-1	F3	3.76	881	Δ+
1280	2.88	0.41	50264	03/03/2008	1280	2.88	0.44	MONGA-1	F3	2.57	733	Δ+
1290	3.10	1.00	50271	04/03/2008	1290	3.10	1.03	MONGA-1	F4	4.17	1406	Δ+
1300	2.78	0.86	50272	04/03/2008	1300	2.78	0.89	MONGA-1	F3	3.00	851	Δ+
1310	2.77	0.80	50273	04/03/2008	1310	2.77	0.83	MONGA-1	F3	2.95	1095	Δ+
1320	3.30	-0.43	50274	04/03/2008	1320	3.30	-0.40	MONGA-1	F3	2.02	697	Δ+
1320	3.00	1.13	50311	05/03/2008	1320	3.00	1.16	MONGA-1	F2	2.87	779	Δ+
1320	3.49	-0.89	50312	05/03/2008	1320	3.49	-0.86	MONGA-1	F3	2.26	710	Δ+
1330	2.72	0.88	50276	04/03/2008	1330	2.72	0.91	MONGA-1	F3	4.74	1259	Δ+
1340	3.08	0.61	50277	04/03/2008	1340	3.08	0.64	MONGA-1	F3	4.50	1211	Δ+
1350	2.83	0.54	50278	04/03/2008	1350	2.83	0.57	MONGA-1	F3	3.23	863	Δ+
1360	3.18	0.64	50279	04/03/2008	1360	3.18	0.67	MONGA-1	F3	2.93	794	Δ+
1370	2.98	1.08	50280	04/03/2008	1370	2.98	1.11	MONGA-1	F3	4.34	1201	Δ+
1380	3.18	0.37	50281	04/03/2008	1380	3.18	0.40	MONGA-1	F3	3.35	929	Δ+
1390	3.11	0.87	50282	04/03/2008	1390	3.11	0.90	MONGA-1	F3	3.08	963	Δ+
1401	2.91	0.89	50283	04/03/2008	1401	2.91	0.92	MONGA-1	F3	2.72	1304	Δ+
1410	3.30	1.13	50286	04/03/2008	1410	3.30	1.16	MONGA-1	F3	3.87	1146	Δ+
1420	3.17	0.64	50287	04/03/2008	1420	3.17	0.67	MONGA-1	F3	4.10	1205	Δ+
1430	3.04	0.69	50288	04/03/2008	1430	3.04	0.72	MONGA-1	F3	2.98	853	Δ+
1440	2.89	1.09	50290	04/03/2008	1440	2.89	1.12	MONGA-1	F3	3.89	1215	Δ+
1450	3.11	0.92	50289	04/03/2008	1450	3.11	0.95	MONGA-1	F2	1.88	681	Δ+
1460	3.04	0.84	50291	04/03/2008	1460	3.04	0.87	MONGA-1	F3	2.84	802	Δ+
1470	3.05	0.89	50292	04/03/2008	1470	3.05	0.92	MONGA-1	F3	2.97	840	Δ+

Annexe 2: ^{14}C dating method

Carbon has three natural isotopes ^{12}C , ^{13}C and ^{14}C . ^{12}C and ^{13}C are stable, but ^{14}C is unstable or radioactive and rare in nature. The abundance of ^{14}C represents $1.2 \cdot 10^{-12} \%$ opposed to the 98.89% of the ^{12}C and of the 1.11% of the ^{13}C .

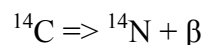
The ^{14}C isotope is continuously formed by the cosmic ray neutrons upon ^{14}N in the upper atmosphere (*Anderson and Libby, 1947*) through the reaction:



where n stays for neutron and p for proton.

The ^{14}C formed is rapidly oxidized to $^{14}\text{CO}_2$ and integrated via photosynthesis or food chain in the plant and animal life ways. During the life of organism there is an equilibrium with the ^{14}C concentration of the atmosphere and those in the photosynthetic organisms. As soon as a plant or animal dies, they cease the metabolic function of carbon uptake; there is no replenishment of radioactive carbon.

As ^{14}C decays it emits a weak beta particle (β , which is an electron with energy of ca 160 keV.)



Thus, the constant and spontaneous ^{14}C decays back to ^{14}N and there is a quantitative relationship between the decay ^{14}C and the production of a beta particle. Half of the ^{14}C quantity in the original sample has decayed after a period of 5730 ± 40 years, called half-life ($t_{1/2}$). However, following international conventions, the used half-life was determinate at 5568 ± 30 years by *Libby et al. (1949)*. After an other half-live period, half of the remaining material is decayed. After 10 half-lives, there remains a very small quantity of radioactive ^{14}C in the sample, which practically impossible to be measured. At about 50-60 ka, it is the limit of the ^{14}C dating method.

To calculate the age, that is, the period which is passed from the death of the organism, we use the exponential law

$$N = N_0 e^{-\lambda t}$$

where λ is the disintegration constant $L2/T$ (that is $0.693/T$), where T is the period, where N is number of radiocarbon atoms remaining after radioactive decay during the time t and where N_0 is the number of radiocarbon atoms at $t=0$ (that is the dead time of the organism). It is clear that this method assume that the quantity of ^{14}C produced in the atmosphere is constant over time.

The Accelerator Mass Spectrometry (AMS) allows to obtain a greater precision in the method with samples containing only a few milligrams of carbon (*Wölfli et al., 1984; Currie et al., 1985*). In this method relative abundance of ^{14}C are directly measured (compared to the $^{12}\text{C}/^{13}\text{C}$) instead of the β particles.

In order to calculate accurate ages, any atmospheric ^{14}C fluctuations must be corrected using a calibration curve (*Bard et al., 2004*). Several approaches have been devised to construct the ^{14}C calibration curves. For the Holocene period, abundant fossil trees have been used to produce a high-resolution atmospheric curve by comparing ^{14}C levels and tree-ring counts forming the tree section (*Stuiver et al., 1998; Kromer and Spurk, 1998*).

A new calibration curve for the conversion of radiocarbon ages to calibrated (cal) ages has been constructed and internationally ratified to replace INTCAL98 which extended from 0-24 ka cal BP (Before Present, 0 cal BP = A.D. 1950). The new calibration dataset for terrestrial samples extends from 0 to 26 ka cal BP, with much higher resolution beyond 11.4 ka cal BP than INTCAL98. Dendrochronologically dated tree-ring samples cover the period from 0 to 12.4 ka cal BP. Beyond the end of the tree-rings, data from marine records (corals and foraminifera) are converted to the atmospheric equivalent with a site-specific marine reservoir correction to establish a common chronological framework for marine and continental paleoproxies. A substantial enhancement relative to INTCAL98 is the introduction of a coherent statistical approach based on a random walk model, which takes into account the uncertainty in both the calendar age and the radiocarbon age to calculate the underlying calibration curve (*Reimer et al., 2004*).

For most non-marine radiocarbon samples from the Northern Hemisphere, the INTCAL04 curve is the preferred choice (*Stuiver et al., 2005*).

For ^{14}C ages older than 26 ka BP, *van der Plicht et al. (2004)* advice not to use INTCAL04. So, for the range of ^{14}C ages between 26 and 50 cal ka BP, we will use the polynomial equation of *Bard et al. (1998)* or the Calpal software (*Weninger and Jöris, 2008*).

Annexe 3: Paleomagnetism data of MD 90-918 core

Specimen	Sect. Depth (m)	Abs.Depth (m)	Weight (gr)	Net weight (gr)	Bulk susceptibility (E-06)	Mass susc.E-08 (m3/Kgr)	Absolute Depth (m)	Mass susc.E-08 (m3/Kgr)
I1_1	0.035	0.035	18.276	12.517	163.3	13.05	0.035	13.05
I1_2	0.055	0.055	17.925	12.166	163.7	13.46	0.055	13.46
I1_3	0.075	0.075	17.956	12.197	164.3	13.47	0.075	13.47
I1_4	0.115	0.115	18.372	12.613	179.2	14.21	0.115	14.21
I1_5	0.14	0.14	18.546	12.787	172.3	13.47	0.14	13.47
I1_6	0.16	0.16	18.005	12.246	169.3	13.82	0.16	13.82
I1_7	0.18	0.18	18.276	12.517	176.3	14.08	0.18	14.08
I1_8	0.2	0.2	18.505	12.746	184.2	14.45	0.2	14.45
I1_9	0.222	0.222	18.276	12.517	180.7	14.44	0.222	14.44
I1_10	0.247	0.247	18.924	13.165	194.2	14.75	0.247	14.75
I1_11	0.272	0.272	18.545	12.786	193.5	15.13	0.272	15.13
I1_12	0.297	0.297	18.033	12.274	195.9	15.96	0.297	15.96
I1_13	0.318	0.318	17.874	12.115	192.1	15.86	0.318	15.86
I1_14	0.344	0.344	18.207	12.448	160.5	12.89	0.344	12.89
I1_15	0.369	0.369	18.534	12.775	171.6	13.43	0.369	13.43
I1_16	0.394	0.394	18.352	12.593	176.1	13.98	0.394	13.98
I1_17	0.417	0.417	17.479	11.720	158.6	13.53	0.417	13.53
I1_18	0.443	0.443	18.058	12.299	166.9	13.57	0.443	13.57
I1_19	0.465	0.465	18.828	13.069	189.4	14.49	0.465	14.49
I1_20	0.489	0.489	19.216	13.457	176.6	13.12	0.489	13.12
I1_21	0.513	0.513	17.723	11.964	163.4	13.66	0.513	13.66
I1_22	0.551	0.551	17.574	11.815	170.5	14.43	0.551	14.43
I1_23	0.57	0.57	17.580	11.821	173.3	14.66	0.57	14.66
I1_24	0.595	0.595	18.406	12.647	195.5	15.46	0.595	15.46
I1_25	0.618	0.618	18.300	12.541	200.6	16.00	0.618	16.00
I1_26	0.643	0.643	18.637	12.878	218.4	16.96	0.643	16.96
I1_27	0.67	0.67	18.723	12.964	205.5	15.85	0.67	15.85
I1_28	0.69	0.69	18.761	13.002	216.7	16.67	0.69	16.67
I1_29	0.71	0.71	18.890	13.131	318.3	24.24	0.71	24.24
I1_30	0.735	0.735	18.969	13.210	353.6	26.77	0.735	26.77
I1_31	0.77	0.77	18.464	12.705	299.4	23.57	0.77	23.57
I1_32	0.785	0.785	16.628	10.869	191.4	17.61	0.785	17.61
I1_33	0.809	0.809	17.685	11.926	174.8	14.66	0.809	14.66
I1_34	0.831	0.831	18.670	12.911	190.3	14.74	0.831	14.74
I1_35	0.856	0.856	18.965	13.206	184.4	13.96	0.856	13.96
I1_36	0.881	0.881	18.889	13.130	176.8	13.47	0.881	13.47
I1_37	0.959	0.959	18.870	13.111	177.4	13.53	0.959	13.53
I1_38	0.985	0.985	18.126	12.367	171.7	13.88	0.985	13.88
I1_39	1.04	1.04	18.123	12.364	181.1	14.65	1.04	14.65
I1_40	1.03	1.03	18.114	12.355	158.9	12.86	1.03	12.86
I1_41	1.058	1.058	18.472	12.713	221.2	17.40	1.058	17.40
I1_42	1.095	1.095	17.954	12.195	197.3	16.18	1.095	16.18
I1_43	1.124	1.124	18.977	13.218	181.5	13.73	1.124	13.73
I1_44	1.197	1.197	18.349	12.590	162.6	12.92	1.197	12.92
I1_45	1.222	1.222	18.777	13.018	167.1	12.84	1.222	12.84
I1_46	1.246	1.246	19.128	13.369	167.1	12.50	1.246	12.50
I1_47	1.272	1.272	18.412	12.653	155.7	12.31	1.272	12.31
I1_48	1.297	1.297	18.832	13.073	155.2	11.87	1.297	11.87
I1_49	1.35	1.35	19.066	13.307	159.1	11.96	1.35	11.96
I1_50	1.377	1.377	18.800	13.041	155.5	11.92	1.377	11.92
I2_51	0.067	1.487	20.230	14.471	200	13.82	1.487	13.82
I2_52	0.082	1.502	15.722	9.963	135.7	13.62	1.502	13.62
I2_53	0.155	1.575	18.468	12.709	164.5	12.94	1.575	12.94
I2_54	0.19	1.61	19.070	13.311	152.9	11.49	1.61	11.49
I2_55	0.215	1.635	17.381	11.622	131.3	11.30	1.635	11.30
I2_56	0.26	1.68	19.240	13.481	160.2	11.88	1.68	11.88
I2_57	0.284	1.704	18.964	13.205	157.7	11.94	1.704	11.94
I2_58	0.322	1.742	18.873	13.114	146.2	11.15	1.742	11.15
I2_59	0.35	1.77	18.085	12.326	139.3	11.30	1.77	11.30
I2_60	0.379	1.799	17.482	11.723	135.2	11.53	1.799	11.53
I2_61	0.41	1.83	18.379	12.620	146.4	11.60	1.83	11.60
I2_62	0.43	1.85	17.481	11.722	135.5	11.56	1.85	11.56
I2_63	0.488	1.908	17.183	11.424	128.5	11.25	1.908	11.25
I2_64	0.512	1.932	16.514	10.755	123.5	11.48	1.932	11.48
I2_65	0.537	1.957	16.596	10.837	127.9	11.80	1.957	11.80
I2_66	0.562	1.982	18.215	12.456	148.9	11.95	1.982	11.95
I2_67	0.605	2.025	17.545	11.786	86.45	7.33	2.025	7.33
I2_68	0.63	2.05	17.955	12.196	85.62	7.02	2.05	7.02
I2_69	0.66	2.08	18.034	12.275	77.09	6.28	2.08	6.28
I2_70	0.69	2.11	16.870	11.111	79.46	7.15	2.11	7.15
I2_71	0.715	2.135	17.666	11.907	93.84	7.88	2.135	7.88
I2_72	0.722	2.142	17.237	11.478	88.43	7.70	2.142	7.70
I2_73	0.775	2.195	17.962	12.203	75.85	6.22	2.195	6.22
I2_74	0.795	2.215	16.713	10.954	69.04	6.30	2.215	6.30
I2_75	0.837	2.257	18.264	12.505	62.77	5.02	2.257	5.02
I2_76	0.862	2.282	17.928	12.169	62.57	5.14	2.282	5.14
I2_77	0.89	2.31	17.957	12.198	100.1	8.21	2.31	8.21
I2_78	0.922	2.342	17.296	11.537	136.8	11.86	2.342	11.86
I2_79	0.948	2.368	17.294	11.535	142.8	12.38	2.368	12.38
I2_80	0.97	2.39	18.103	12.344	168.1	13.62	2.39	13.62
I2_81	1.01	2.43	18.338	12.579	173.8	13.82	2.43	13.82
I2_82	1.035	2.455	18.431	12.672	169.2	13.35	2.455	13.35
I2_83	1.057	2.477	17.822	12.063	160.4	13.30	2.477	13.30
I2_84	1.11	2.53	19.012	13.253	198.3	14.96	2.53	14.96
I2_85	1.135	2.555	20.142	14.383	217.8	15.14	2.555	15.14
I2_86	1.168	2.588	18.803	13.044	177.4	13.60	2.588	13.60
I2_87	1.192	2.612	18.600	12.841	171.1	13.32	2.612	13.32
I2_88	1.218	2.638	19.626	13.867	181.9	13.12	2.638	13.12
I2_89	1.248	2.668	19.113	13.354	182.5	13.67	2.668	13.67
I2_90	1.272	2.692	18.681	12.922	178.5	13.81	2.692	13.81
I2_91	1.295	2.715	19.755	13.986	198.6	14.19	2.715	14.19
I2_92	1.342	2.762	16.969	11.210	185	16.50	2.762	16.50
I2_93	1.367	2.787	18.708	12.949	200.3	15.47	2.787	15.47
I3_94	0.02	2.83	17.280	11.521	134.2	11.65	2.83	11.65
I3_95	0.045	2.855	18.677	12.918	152.3	11.79	2.855	11.79
I3_96	0.07	2.88	18.339	12.580	147.8	11.75	2.88	11.75
I3_97	0.093	2.903	19.009	13.250	156.6	11.82	2.903	11.82
I3_98	0.118	2.928	16.701	10.942	130	11.88	2.928	11.88

Specimen	Sect. Depth (m)	Abs.Depth (m)	Weight (gr)	Net weight (gr)	Bulk susceptibility (E-06)	Mass susc.E-08 (m3/Kgr)	Absolute Depth (m)	Mass susc.E-08 (m3/Kgr)
I3_99	0.142	2.952	17.841	12.082	145	12.00	2.952	12.00
I3_100	0.165	2.975	17.365	11.606	143.9	12.40	2.975	12.40
I3_101	0.188	2.998	19.132	13.373	189.8	14.19	2.998	14.19
I3_102	0.212	3.022	18.256	12.497	173.5	13.88	3.022	13.88
I3_103	0.237	3.047	16.979	11.220	136.7	12.18	3.047	12.18
I3_104	0.26	3.07	19.011	13.252	156.7	11.82	3.07	11.82
I3_105	0.285	3.095	18.349	12.590	160.3	12.73	3.095	12.73
I3_106	0.308	3.118	19.446	13.687	179.6	13.12	3.118	13.12
I3_107	0.332	3.142	19.495	13.736	188.8	13.74	3.142	13.74
I3_108	0.356	3.166	19.455	13.696	178.3	13.02	3.166	13.02
I3_109	0.38	3.19	19.475	13.716	179.4	13.08	3.19	13.08
I3_110	0.404	3.214	19.603	13.844	171.9	12.42	3.214	12.42
I3_111	0.428	3.238	19.210	13.451	158.4	11.78	3.238	11.78
I3_112	0.45	3.26	18.284	12.525	150.8	12.04	3.26	12.04
I3_113	0.474	3.284	16.999	11.240	133.7	11.90	3.284	11.90
I3_114	0.498	3.308	17.460	11.701	145.6	12.44	3.308	12.44
I3_115	0.525	3.335	17.913	12.154	148.3	12.20	3.335	12.20
I3_116	0.54	3.35	17.143	11.384	134	11.77	3.35	11.77
I3_117	0.565	3.375	17.303	11.544	139.8	12.11	3.375	12.11
I3_118	0.59	3.4	16.601	10.842	138	12.73	3.4	12.73
I3_119	0.614	3.424	19.119	13.360	172.1	12.88	3.424	12.88
I3_120	0.637	3.447	19.569	13.810	193.5	14.01	3.447	14.01
I3_121	0.662	3.472	19.466	13.707	194.6	14.20	3.472	14.20
I3_122	0.685	3.495	18.620	12.861	173.6	13.50	3.495	13.50
I3_123	0.709	3.519	18.508	12.749	178.4	13.99	3.519	13.99
I3_124	0.734	3.544	18.590	12.831	168	13.09	3.544	13.09
I3_125	0.757	3.567	18.118	12.359	167.7	13.57	3.567	13.57
I3_126	0.782	3.592	17.803	12.044	158.3	13.14	3.592	13.14
I3_127	0.805	3.615	17.443	11.684	147.6	12.63	3.615	12.63
I3_128	0.828	3.638	16.878	11.119	146.6	13.18	3.638	13.18
I3_129	0.865	3.675	15.689	9.930	128.6	12.95	3.675	12.95
I3_130	0.89	3.7	18.063	12.304	159.6	12.97	3.7	12.97
I3_131	0.93	3.74	17.424	11.665	153.7	13.18	3.74	13.18
I3_132	0.944	3.754	18.431	12.672	157	12.39	3.754	12.39
I3_133	0.968	3.778	18.831	13.072	161.9	12.39	3.778	12.39
I3_134	0.99	3.8	19.392	13.633	199.2	14.61	3.8	14.61
I3_135	1.015	3.825	19.502	13.743	168.8	12.28	3.825	12.28
I3_136	1.038	3.848	18.539	12.780	163.8	12.82	3.848	12.82
I3_137	1.062	3.872	19.289	13.530	197.4	14.59	3.872	14.59
I3_138	1.088	3.898	19.262	13.503	209.3	15.50	3.898	15.50
I3_139	1.11	3.92	18.926	13.167	202.1	15.35	3.92	15.35
I3_140	1.14	3.95	17.391	11.632	182.5	15.69	3.95	15.69
I3_141	1.168	3.978	20.451	14.692	235.1	16.00	3.978	16.00
I3_142	1.192	4.002	20.210	14.451	225.3	15.59	4.002	15.59
I3_143	1.215	4.025	19.980	14.221	204.6	14.39	4.025	14.39
I3_144	1.24	4.05	19.726	13.967	201.1	14.40	4.05	14.40
I3_145	1.264	4.074	19.709	13.950	193.5	13.87	4.074	13.87
I3_146	1.288	4.098	19.476	13.717	193.4	14.10	4.098	14.10
I3_147	1.314	4.124	19.387	13.628	191.3	14.04	4.124	14.04
I3_148	1.338	4.148	19.610	13.851	194.6	14.05	4.148	14.05
I3_149	1.36	4.17	19.500	13.741	186.2	13.55	4.17	13.55
I3_150	1.385	4.195	19.644	13.885	186.1	13.40	4.195	13.40
I3_151	1.408	4.218	19.441	13.682	184.8	13.51	4.218	13.51
I3_152	1.438	4.248	20.009	14.250	203.7	14.29	4.248	14.29
I3_153	1.46	4.27	19.540	13.781	197.8	14.35	4.27	14.35
I3_154	1.485	4.295	19.340	13.581	211.6	15.58	4.295	15.58
I4_155	0.02	4.36	19.623	13.864	208.2	15.02	4.36	15.02
I4_156	0.047	4.387	19.298	13.539	237.3	17.53	4.387	17.53
I4_157	0.074	4.414	18.183	12.424	182.3	14.67	4.414	14.67
I4_158	0.098	4.438	19.683	13.924	184.8	13.27	4.438	13.27
I4_159	0.12	4.46	19.533	13.774	183	13.29	4.46	13.29
I4_160	0.145	4.485	19.574	13.815	199.3	14.43	4.485	14.43
I4_161	0.171	4.511	20.410	14.651	208.5	14.23	4.511	14.23
I4_162	0.196	4.536	20.240	14.481	222.6	15.37	4.536	15.37
I4_163	0.22	4.56	20.682	14.923	239.4	16.04	4.56	16.04
I4_164	0.247	4.587	19.777	14.018	196.9	14.05	4.587	14.05
I4_165	0.271	4.611	19.349	13.590	195.9	14.42	4.611	14.42
I4_166	0.295	4.635	21.310	15.551	231.2	14.87	4.635	14.87
I4_167	0.32	4.66	19.800	14.041	227.8	16.22	4.66	16.22
I4_168	0.345	4.685	19.709	13.950	277.6	19.90	4.685	19.90
I4_169	0.368	4.708	19.083	13.324	253.7	19.04	4.708	19.04
I4_170	0.395	4.735	19.956	14.197	212.2	14.95	4.735	14.95
I4_171	0.42	4.76	20.017	14.258	207.3	14.54	4.76	14.54
I4_172	0.434	4.774	20.258	14.499	209.1	14.42	4.774	14.42
I4_173	0.466	4.806	19.598	13.839	200	14.45	4.806	14.45
I4_174	0.492	4.832	18.509	12.750	184.1	14.44	4.832	14.44
I4_175	0.515	4.855	20.367	14.608	209.8	14.36	4.855	14.36
I4_176	0.54	4.88	20.039	14.280	206	14.43	4.88	14.43
I4_177	0.566	4.906	20.437	14.678	207	14.10	4.906	14.10
I4_178	0.59	4.93	20.334	14.575	202.1	13.87	4.93	13.87
I4_179	0.614	4.954	18.801	13.042	182.8	14.02	4.954	14.02
I4_180	0.641	4.981	20.205	14.446	203.9	14.11	4.981	14.11
I4_181	0.668	5.008	20.718	14.959	210.9	14.10	5.008	14.10
I4_182	0.693	5.033	19.931	14.172	199	14.04	5.033	14.04
I4_183	0.72	5.06	20.467	14.708	211.9	14.41	5.06	14.41
I4_184	0.744	5.084	19.254	13.495	201	14.89	5.084	14.89
I4_185	0.767	5.107	19.979	14.220	201.6	14.18	5.107	14.18
I4_186	0.795	5.135	19.043	13.284	187	14.08	5.135	14.08
I4_187	0.818	5.158	19.433	13.674	192	14.04	5.158	14.04
I4_188	0.844	5.184	18.986	13.227	188	14.21	5.184	14.21
I4_189	0.868	5.208	19.941	14.182	200.5	14.14	5.208	14.14
I4_190	0.894	5.234	19.354	13.595	193.8	14.26	5.234	14.26
I4_191	0.925	5.265	19.742	13.983	212.5	15.20	5.265	15.20
I4_192	0.95	5.29	18.427	12.668	179.5	14.17	5.29	14.17
I4_193	0.977	5.317	19.565	13.806	196.3	14.22	5.317	14.22
I4_194	1.005	5.345	19.426	13.667	184.9	13.53	5.345	13.53
I4_195	1.032	5.372	18.997	13.238	178.7	13.50	5.372	13.50
I4_196	1.057	5.397	19.745	13.986	190.9	13.65	5.397	13.65
I4_197	1.085	5.425	19.034	13.275	182.1	13.72	5.425	13.72

Annexes

Specimen	Sect. Depth (m)	Abs.Depth (m)	Weight (gr)	Net weight (gr)	Bulk susceptibility (E-06)	Mass susc.E-08 (m3/Kgr)	Absolute Depth (m)	Mass susc.E-08 (m3/Kgr)
I4_198	1.113	5.453	19.163	13.404	179.3	13.38	5.453	13.38
I4_199	1.138	5.478	19.396	13.637	183.8	13.48	5.478	13.48
I4_200	1.165	5.505	18.932	13.173	178.5	13.55	5.505	13.55
I4_201	1.192	5.532	19.772	14.013	181.7	12.97	5.532	12.97
I4_202	1.217	5.557	19.411	13.652	190.5	13.95	5.557	13.95
I4_203	1.243	5.583	19.622	13.863	174.1	12.56	5.583	12.56
I4_204	1.27	5.61	19.225	13.466	166.3	12.35	5.61	12.35
I4_205	1.295	5.635	19.725	13.966	180.8	12.95	5.635	12.95
I4_206	1.32	5.66	20.422	14.663	196.8	13.42	5.66	13.42
I4_207	1.373	5.713	20.392	14.633	203.7	13.92	5.713	13.92
I4_208	1.42	5.76	19.222	13.463	183	13.59	5.76	13.59
I5_209	0.017	5.787	19.909	14.150	199.5	14.10	5.787	14.10
I5_210	0.043	5.813	19.631	13.872	205.1	14.79	5.813	14.79
I5_211	0.082	5.852	19.095	13.336	197.5	14.81	5.852	14.81
I5_212	0.107	5.877	18.732	12.973	178	13.72	5.877	13.72
I5_213	0.134	5.904	18.834	13.075	183.1	14.00	5.904	14.00
I5_214	0.157	5.927	17.343	11.584	164.5	14.20	5.927	14.20
I5_215	0.183	5.953	18.817	13.058	181.6	13.91	5.953	13.91
I5_216	0.209	5.979	19.112	13.353	196.4	14.71	5.979	14.71
I5_217	0.233	6.003	18.586	12.827	189.8	14.80	6.003	14.80
I5_218	0.274	6.044	19.367	13.608	200.3	14.72	6.044	14.72
I5_219	0.299	6.069	20.133	14.374	209.1	14.55	6.069	14.55
I5_220	0.325	6.095	19.897	14.138	208.7	14.76	6.095	14.76
I5_221	0.351	6.121	19.484	13.725	200.2	14.59	6.121	14.59
I5_222	0.39	6.16	18.878	13.119	180.2	13.74	6.16	13.74
I5_223	0.416	6.186	17.848	12.089	163.3	13.51	6.186	13.51
I5_224	0.448	6.218	18.528	12.769	173.5	13.59	6.218	13.59
I5_225	0.47	6.24	18.778	13.019	183.2	14.07	6.24	14.07
I5_226	0.495	6.265	18.449	12.690	212.1	16.71	6.265	16.71
I5_227	0.542	6.312	19.215	13.456	190.1	14.13	6.312	14.13
I5_228	0.566	6.336	18.825	13.066	186.7	14.29	6.336	14.29
I5_229	0.593	6.363	18.917	13.158	184.8	14.04	6.363	14.04
I5_230	0.617	6.387	19.548	13.789	194.5	14.11	6.387	14.11
I5_231	0.644	6.414	18.430	12.671	194.4	15.34	6.414	15.34
I5_232	0.666	6.436	18.956	13.197	227.6	17.25	6.436	17.25
I5_233	0.692	6.462	18.322	12.563	184	14.65	6.462	14.65
I5_234	0.735	6.505	18.427	12.668	156.7	12.37	6.505	12.37
I5_235	0.76	6.53	18.703	12.944	157	12.13	6.53	12.13
I5_236	0.785	6.555	19.439	13.680	180.8	13.22	6.555	13.22
I5_237	0.82	6.59	19.809	14.050	237.7	16.92	6.59	16.92
I5_238	0.845	6.615	19.368	13.609	173.7	12.76	6.615	12.76
I5_239	0.87	6.64	17.945	12.186	272.1	22.33	6.64	22.33
I5_240	0.895	6.665	18.783	13.024	168.1	12.91	6.665	12.91
I5_241	0.92	6.69	18.750	12.991	161.2	12.41	6.69	12.41
I5_242	0.945	6.715	18.489	12.730	163.9	12.88	6.715	12.88
I5_243	0.988	6.758	20.136	14.377	188.7	13.13	6.758	13.13
I5_244	1.012	6.782	19.553	13.794	187.3	13.58	6.782	13.58
I5_245	1.038	6.808	19.294	13.535	182.7	13.50	6.808	13.50
I5_246	1.062	6.832	19.079	13.320	185.9	13.96	6.832	13.96
I5_247	1.088	6.858	20.212	14.453	209.9	14.52	6.858	14.52
I5_248	1.112	6.882	18.738	12.979	198.6	15.30	6.882	15.30
I5_249	1.142	6.912	18.338	12.579	189.8	15.09	6.912	15.09
I5_250	1.168	6.938	19.639	13.880	207.5	14.95	6.938	14.95
I5_251	1.192	6.962	19.869	14.110	198.2	14.05	6.962	14.05
I5_252	1.218	6.988	19.034	13.275	199.1	15.00	6.988	15.00
I5_253	1.242	7.012	19.703	13.944	182.6	13.10	7.012	13.10
I5_254	1.268	7.038	17.680	11.921	164.3	13.78	7.038	13.78
I5_255	1.302	7.072	19.683	13.924	190.4	13.67	7.072	13.67
I5_256	1.328	7.098	18.604	12.845	173.8	13.53	7.098	13.53
I5_257	1.352	7.122	19.335	13.576	206.7	15.23	7.122	15.23
I5_258	1.378	7.148	19.468	13.709	234.6	17.11	7.148	17.11
I5_259	1.402	7.172	19.041	13.282	214.3	16.13	7.172	16.13
I5_260	1.428	7.198	18.385	12.626	194.2	15.38	7.198	15.38
I5_261	1.452	7.222	18.303	12.544	189.5	15.11	7.222	15.11
I6_262	0.015	7.275	20.516	14.757	211.7	14.35	7.275	14.35
I6_263	0.04	7.3	20.142	14.383	197.9	13.76	7.3	13.76
I6_264	0.065	7.325	19.696	13.937	191.9	13.77	7.325	13.77
I6_265	0.09	7.35	19.663	13.904	186	13.38	7.35	13.38
I6_266	0.105	7.365	19.849	14.090	193.8	13.75	7.365	13.75
I6_267	0.14	7.4	18.750	12.991	188	14.47	7.4	14.47
I6_268	0.164	7.424	19.075	13.316	209.3	15.72	7.424	15.72
I6_269	0.188	7.448	19.150	13.91	185.3	13.84	7.448	13.84
I6_270	0.212	7.472	19.007	13.248	186.3	14.06	7.472	14.06
I6_271	0.238	7.498	18.932	13.173	187.3	14.22	7.498	14.22
I6_272	0.255	7.515	19.404	13.645	200.1	14.66	7.515	14.66
I6_273	0.278	7.538	20.194	14.435	206.2	14.28	7.538	14.28
I6_274	0.304	7.564	18.655	12.896	186.9	14.49	7.564	14.49
I6_275	0.328	7.588	19.346	13.587	196.5	14.46	7.588	14.46
I6_276	0.354	7.614	18.358	12.599	187	14.84	7.614	14.84
I6_277	0.378	7.638	18.803	13.044	223.1	17.10	7.638	17.10
I6_278	0.402	7.662	19.217	13.458	258.3	19.19	7.662	19.19
I6_279	0.425	7.685	19.538	13.779	314	22.79	7.685	22.79
I6_280	0.45	7.71	18.879	13.120	460.9	35.13	7.71	35.13
I6_281	0.475	7.735	18.159	12.400	242.5	19.56	7.735	19.56
I6_282	0.498	7.758	17.965	12.206	174.9	14.33	7.758	14.33
I6_283	0.522	7.782	19.235	13.476	175.7	13.04	7.782	13.04
I6_284	0.546	7.806	19.042	13.283	172.9	13.02	7.806	13.02
I6_285	0.573	7.833	19.641	13.882	183.5	13.22	7.833	13.22
I6_286	0.597	7.857	18.690	12.931	174	13.46	7.857	13.46
I6_287	0.646	7.906	19.087	13.328	176.6	13.25	7.906	13.25
I6_288	0.67	7.93	18.909	13.150	176.9	13.45	7.93	13.45
I6_289	0.695	7.955	18.653	12.894	173	13.42	7.955	13.42
I6_290	0.72	7.98	19.073	13.314	183	13.74	7.98	13.74
I6_291	0.743	8.003	19.535	13.776	189.7	13.77	8.003	13.77
I6_292	0.767	8.027	18.466	12.707	176.3	13.87	8.027	13.87
I6_293	0.792	8.052	18.768	13.009	175.3	13.48	8.052	13.48
I6_294	0.815	8.075	19.644	13.885	202.3	14.57	8.075	14.57
I6_295	0.846	8.106	18.694	12.935	256.3	19.81	8.106	19.81
I6_296	0.87	8.13	18.104	12.345	163.8	13.27	8.13	13.27

Specimen	Sect. Depth (m)	Abs.Depth (m)	Weight (gr)	Net weight (gr)	Bulk susceptibility (E-06)	Mass susc.E-08 (m3/Kgr)	Absolute Depth (m)	Mass susc.E-08 (m3/Kgr)
16_297	0.895	8.155	19.684	13.925	186.2	13.37	8.155	13.37
16_298	0.92	8.18	18.969	13.210	178.5	13.51	8.18	13.51
16_299	0.945	8.205	18.788	13.029	179	13.74	8.205	13.74
16_300	0.983	8.243	19.518	13.759	190.7	13.86	8.243	13.86
16_301	1.007	8.267	18.827	13.068	182.6	13.97	8.267	13.97
16_302	1.033	8.293	20.245	14.486	202.1	13.95	8.293	13.95
16_303	1.058	8.318	19.569	13.810	194.6	14.09	8.318	14.09
16_304	1.082	8.342	19.370	13.611	197	14.47	8.342	14.47
16_305	1.107	8.367	19.407	13.648	195.5	14.32	8.367	14.32
16_306	1.13	8.39	18.505	12.746	190.1	14.91	8.39	14.91
16_307	1.157	8.417	19.128	13.369	215.6	16.13	8.417	16.13
16_308	1.182	8.442	18.068	12.309	182	14.79	8.442	14.79
16_309	1.205	8.465	19.249	13.490	181.6	13.46	8.465	13.46
16_310	1.23	8.49	17.270	11.511	156.5	13.60	8.49	13.60
16_311	1.258	8.518	17.906	12.147	165.1	13.59	8.518	13.59
16_312	1.28	8.54	19.499	13.740	177.7	12.93	8.54	12.93
16_313	1.308	8.568	20.142	14.383	196.3	13.65	8.568	13.65
16_314	1.332	8.592	19.043	13.284	185	13.93	8.592	13.93
16_315	1.358	8.618	19.338	13.579	187.3	13.79	8.618	13.79
16_316	1.38	8.64	19.308	13.549	221	16.31	8.64	16.31
16_317	1.408	8.668	19.475	13.716	192.8	14.06	8.668	14.06
16_318	1.43	8.69	19.778	14.019	200.6	14.31	8.69	14.31
16_319	1.455	8.715	19.885	14.126	189	13.38	8.715	13.38
16_320	1.48	8.74	19.867	14.108	201.1	14.25	8.74	14.25
16_321	1.5	8.76	18.747	12.988	285.3	21.97	8.76	21.97
17_322	0.012	8.782	19.720	13.961	298.2	21.36	8.782	21.36
17_323	0.038	8.808	19.506	13.747	304.9	22.18	8.808	22.18
17_324	0.062	8.832	19.462	13.703	317.2	23.15	8.832	23.15
17_325	0.088	8.858	19.048	13.289	520.2	39.15	8.858	39.15
17_326	0.112	8.882	17.822	12.063	694.2	57.55	8.882	57.55
17_327	0.14	8.91	18.686	12.927	194.5	15.05	8.91	15.05
17_328	0.168	8.938	19.267	13.508	199.9	14.80	8.938	14.80
17_329	0.19	8.96	18.557	12.798	186.3	14.56	8.96	14.56
17_330	0.215	8.985	18.370	12.611	181.9	14.42	8.985	14.42
17_331	0.24	9.01	18.055	12.296	168.8	13.73	9.01	13.73
17_332	0.268	9.038	18.345	12.586	167	13.27	9.038	13.27
17_333	0.29	9.06	18.714	12.955	174.6	13.48	9.06	13.48
17_334	0.322	9.092	18.718	12.959	172.3	13.30	9.092	13.30
17_335	0.348	9.118	19.573	13.814	191.4	13.86	9.118	13.86
17_336	0.374	9.144	19.366	13.607	191.2	14.05	9.144	14.05
17_337	0.399	9.169	19.233	13.474	190.7	14.15	9.169	14.15
17_338	0.425	9.195	19.012	13.253	181.4	13.69	9.195	13.69
17_339	0.448	9.218	18.820	13.061	180.9	13.85	9.218	13.85
17_340	0.472	9.242	18.734	12.975	178	13.72	9.242	13.72
17_341	0.498	9.268	18.764	13.005	174.6	13.43	9.268	13.43
17_342	0.522	9.292	18.644	12.885	174.2	13.52	9.292	13.52
17_343	0.545	9.315	17.901	12.142	164.5	13.55	9.315	13.55
17_344	0.57	9.34	19.099	13.340	179.2	13.43	9.34	13.43
17_345	0.595	9.365	18.953	13.194	177.9	13.48	9.365	13.48
17_346	0.635	9.405	18.879	13.120	173.3	13.21	9.405	13.21
17_347	0.66	9.43	19.588	13.829	188.9	13.66	9.43	13.66
17_348	0.685	9.455	19.730	13.971	187	13.38	9.455	13.38
17_349	0.71	9.48	18.966	13.207	199.9	15.14	9.48	15.14
17_350	0.734	9.504	18.157	12.398	193.2	15.58	9.504	15.58
17_351	0.76	9.53	17.356	11.597	175.6	15.14	9.53	15.14
17_352	0.784	9.554	17.471	11.712	183	15.63	9.554	15.63
17_353	0.809	9.579	19.371	13.612	211.3	15.52	9.579	15.52
17_354	0.83	9.6	18.303	12.544	193.2	15.40	9.6	15.40
17_355	0.859	9.629	19.222	13.463	204.9	15.22	9.629	15.22
17_356	0.882	9.652	19.654	13.895	216.8	15.60	9.652	15.60
17_357	0.908	9.678	18.727	12.968	190.1	14.66	9.678	14.66
17_358	0.932	9.702	18.482	12.723	195.1	15.33	9.702	15.33
17_359	0.957	9.727	18.672	12.913	206	15.95	9.727	15.95
17_360	0.982	9.752	18.690	12.931	208.8	16.15	9.752	16.15
17_361	1.005	9.775	18.881	13.122	225	17.15	9.775	17.15
17_362	1.03	9.8	18.632	12.873	329.5	25.60	9.8	25.60
17_363	1.054	9.824	19.075	13.316	427.3	32.09	9.824	32.09
17_364	1.08	9.85	18.683	12.924	227.5	17.60	9.85	17.60
17_365	1.118	9.888	17.753	11.994	198.8	16.57	9.888	16.57
17_366	1.141	9.911	20.962	15.203	284.1	18.69	9.911	18.69
17_367	1.365	10.135	19.177	13.418	188.2	14.03	10.135	14.03
17_368	1.384	10.154	20.020	14.261	203.5	14.27	10.154	14.27
17_369	1.412	10.182	19.883	14.124	207	14.66	10.182	14.66
17_370	1.438	10.208	18.538	12.779	189	14.79	10.208	14.79
17_371	1.462	10.232	19.309	13.550	202.1	14.92	10.232	14.92
18_372	0.012	10.282	19.680	13.921	202.6	14.55	10.282	14.55
18_373	0.038	10.308	19.922	14.163	219.1	15.47	10.308	15.47
18_374	0.064	10.334	19.179	13.420	204	15.20	10.334	15.20
18_375	0.088	10.358	19.390	13.631	214.5	15.74	10.358	15.74
18_376	0.114	10.384	17.952	12.193	184.1	15.10	10.384	15.10
18_377	0.139	10.409	18.268	12.509	190.3	15.21	10.409	15.21
18_378	0.164	10.434	18.057	12.298	203.3	16.53	10.434	16.53
18_379	0.189	10.459	17.611	11.852	191.4	16.15	10.459	16.15
18_380	0.214	10.484	20.316	14.557	222	15.25	10.484	15.25
18_381	0.238	10.508	19.197	13.438	203	15.11	10.508	15.11
18_382	0.262	10.532	18.325	12.566	196.4	15.63	10.532	15.63
18_383	0.286	10.556	17.988	12.229	191.8	15.68	10.556	15.68
18_384	0.31	10.58	17.658	11.899	186.3	15.66	10.58	15.66
18_385	0.332	10.602	19.856	14.097	225.1	15.97	10.602	15.97
18_386	0.358	10.628	19.402	13.643	217	15.91	10.628	15.91
18_387	0.382	10.652	19.064	13.305	218.9	16.45	10.652	16.45
18_388	0.408	10.678	19.587	13.828	219.4	15.87	10.678	15.87
18_389	0.432	10.702	19.016	13.257	214.1	16.15	10.702	16.15
18_390	0.454	10.724	18.488	12.729	190.3	14.95	10.724	14.95
18_391	0.478	10.748	19.074	13.315	202.6	15.22	10.748	15.22
18_392	0.503	10.773	20.614	14.855	236.9	15.95	10.773	15.95
18_393	0.527	10.797	19.906	14.147	227.8	16.10	10.797	16.10
18_394	0.553	10.823	21.460	15.701	255.1	16.25	10.823	16.25
18_395	0.579	10.849	20.243	14.484	228.6	15.78	10.849	15.78

Annexes

Specimen	Sect. Depth (m)	Abs.Depth (m)	Weight (gr)	Net weight (gr)	Bulk susceptibility (E-06)	Mass susc.E-08 (m3/Kgr)	Absolute Depth (m)	Mass susc.E-08 (m3/Kgr)
I8_396	0.603	10.873	19.783	14.024	228.9	16.32	10.873	16.32
I8_397	0.627	10.897	20.554	14.795	241.7	16.34	10.897	16.34
I8_398	0.654	10.924	19.857	14.098	224.3	15.91	10.924	15.91
I8_399	0.677	10.947	20.052	14.293	221.6	15.50	10.947	15.50
I8_400	0.704	10.974	20.916	15.157	226.6	14.95	10.974	14.95
I8_401	0.728	10.998	19.930	14.171	194.2	13.70	10.998	13.70
I8_402	0.752	11.022	20.567	14.808	216	14.59	11.022	14.59
I8_403	0.775	11.045	21.033	15.274	235	15.39	11.045	15.39
I8_404	0.801	11.071	20.551	14.792	209.7	14.18	11.071	14.18
I8_405	0.827	11.097	20.052	14.293	207.6	14.52	11.097	14.52
I8_406	0.858	11.128	21.149	15.390	228.2	14.83	11.128	14.83
I8_407	0.885	11.155	20.754	14.995	220	14.67	11.155	14.67
I8_408	0.91	11.18	20.044	14.285	232.9	16.30	11.18	16.30
I8_409	0.935	11.205	21.407	15.648	245.7	15.70	11.205	15.70
I8_410	0.96	11.23	21.027	15.268	224.8	14.72	11.23	14.72
I8_411	0.985	11.255	19.444	13.685	195.4	14.28	11.255	14.28
I8_412	1.008	11.278	20.137	14.378	208.1	14.47	11.278	14.47
I8_413	1.041	11.311	19.247	13.488	202.8	15.04	11.311	15.04
I8_414	1.066	11.356	19.226	13.467	199.6	14.82	11.356	14.82
I8_415	1.112	11.382	20.349	14.590	208.5	14.29	11.382	14.29
I8_416	1.138	11.408	19.031	13.272	200	15.07	11.408	15.07
I8_417	1.168	11.438	19.590	13.831	221.8	16.04	11.438	16.04
I8_418	1.195	11.465	18.767	13.008	206.4	15.87	11.465	15.87
I8_419	1.223	11.493	18.278	12.519	188.5	15.06	11.493	15.06
I8_420	1.26	11.53	18.088	12.329	194.9	15.81	11.53	15.81
I8_421	1.286	11.556	19.912	14.153	199.3	14.08	11.556	14.08
I8_422	1.313	11.583	20.213	14.454	205.8	14.24	11.583	14.24
I8_423	1.34	11.61	18.818	13.059	196.3	15.03	11.61	15.03
I8_424	1.37	11.64	19.391	13.632	203.3	14.91	11.64	14.91
I8_425	1.396	11.666	19.979	14.220	212.7	14.96	11.666	14.96
I8_426	1.421	11.691	19.377	13.618	197.1	14.47	11.691	14.47
I8_427	1.447	11.717	19.130	13.371	199.3	14.91	11.717	14.91
I8_428	1.476	11.746	20.611	14.852	219.9	14.81	11.746	14.81
I9_429	0.016	11.786	20.843	15.084	226.7	15.03	11.786	15.03
I9_430	0.045	11.815	17.306	11.547	176.7	15.30	11.815	15.30
I9_431	0.072	11.842	18.705	12.946	190.8	14.74	11.842	14.74
I9_432	0.096	11.866	17.591	11.832	164.7	13.92	11.866	13.92
I9_433	0.123	11.893	19.113	13.354	164.1	12.29	11.893	12.29
I9_434	0.15	11.92	20.189	14.430	188.3	13.05	11.92	13.05
I9_435	0.174	11.944	19.852	14.093	211.3	14.99	11.944	14.99
I9_436	0.201	11.971	18.745	12.986	180.3	13.88	11.971	13.88
I9_437	0.229	11.999	20.201	14.442	208.8	14.46	11.999	14.46
I9_438	0.256	12.026	20.471	14.712	212	14.41	12.026	14.41
I9_439	0.282	12.052	20.020	14.712	195.7	13.72	12.052	13.72
I9_440	0.306	12.076	19.220	13.461	186.1	13.83	12.076	13.83
I9_441	0.335	12.105	18.933	13.174	176	13.36	12.105	13.36
I9_442	0.361	12.131	18.798	13.039	180.4	13.84	12.131	13.84
I9_443	0.387	12.157	18.986	13.227	188.4	14.24	12.157	14.24
I9_444	0.412	12.182	19.934	14.175	205.3	14.48	12.182	14.48
I9_445	0.44	12.21	19.037	13.278	183.4	13.81	12.21	13.81
I9_446	0.466	12.236	19.058	13.299	206.4	15.52	12.236	15.52
I9_447	0.506	12.276	19.339	13.580	244.9	18.03	12.276	18.03
I9_448	0.532	12.302	19.817	14.058	215.3	15.32	12.302	15.32
I9_449	0.559	12.329	19.832	14.073	219.2	15.58	12.329	15.58
I9_450	0.585	12.355	18.546	12.787	209.4	16.38	12.355	16.38
I9_451	0.61	12.38	19.603	13.844	220.2	15.91	12.38	15.91
I9_452	0.636	12.406	19.472	13.713	224.6	16.38	12.406	16.38
I9_453	0.661	12.431	18.550	12.791	199.4	15.59	12.431	15.59
I9_454	0.688	12.458	19.744	13.985	223.8	16.00	12.458	16.00
I9_455	0.715	12.485	17.726	11.967	196.3	16.40	12.485	16.40
I9_456	0.742	12.512	19.008	13.249	215.3	16.25	12.512	16.25
I9_457	0.768	12.538	17.900	12.141	191.5	15.77	12.538	15.77
I9_458	0.796	12.566	18.541	12.782	202.1	15.81	12.566	15.81
I9_459	0.822	12.592	19.093	13.334	192.1	14.41	12.592	14.41
I9_460	0.848	12.618	19.453	13.694	205.8	15.03	12.618	15.03
I9_461	0.875	12.645	18.748	12.989	203.5	15.67	12.645	15.67
I9_462	0.9	12.67	20.472	14.713	231.6	15.74	12.67	15.74
I9_463	0.926	12.696	19.560	13.801	211.3	15.31	12.696	15.31
I9_464	0.962	12.732	19.264	13.505	215.5	15.96	12.732	15.96
I9_465	0.99	12.76	19.163	13.404	212.3	15.84	12.76	15.84
I9_466	1.03	12.8	19.319	13.560	212.6	15.68	12.8	15.68
I9_467	1.055	12.825	18.538	12.779	204.7	16.02	12.825	16.02
I9_468	1.082	12.852	19.348	13.589	209.3	15.40	12.852	15.40
I9_469	1.112	12.882	18.262	12.503	188.5	15.08	12.882	15.08
I9_470	1.146	12.916	19.065	13.306	209.4	15.74	12.916	15.74
I9_471	1.174	12.944	18.078	12.319	197.9	16.06	12.944	16.06
I9_472	1.2	12.97	18.249	12.490	201.2	16.11	12.97	16.11
I9_473	1.228	12.998	19.191	13.432	216.3	16.10	12.998	16.10
I9_474	1.256	13.026	18.134	12.375	178.7	14.44	13.026	14.44
I9_475	1.28	13.05	19.304	13.545	196.9	14.54	13.05	14.54
I9_476	1.306	13.076	17.593	11.834	176.3	14.90	13.076	14.90
I9_477	1.335	13.105	18.365	12.606	186.5	14.79	13.105	14.79
I9_478	1.36	13.13	18.290	12.531	192.8	15.39	13.13	15.39
I9_479	1.388	13.158	17.224	11.465	176.9	15.43	13.158	15.43
I9_480	1.414	13.184	18.872	13.113	203.6	15.53	13.184	15.53
I9_481	1.44	13.21	18.055	12.296	201.1	16.35	13.21	16.35
I9_482	1.469	13.239	19.700	13.941	232.3	16.66	13.239	16.66
I10_483	0.012	13.292	19.269	13.510	187	13.84	13.292	13.84
I10_484	0.038	13.318	18.753	12.994	197.9	15.23	13.318	15.23
I10_485	0.062	13.342	17.455	11.696	174.7	14.94	13.342	14.94
I10_486	0.088	13.368	16.376	10.617	157.7	14.85	13.368	14.85
I10_487	0.114	13.394	17.318	11.559	167.6	14.50	13.394	14.50
I10_488	0.138	13.418	17.773	12.014	172	14.32	13.418	14.32
I10_489	0.17	13.45	17.672	11.913	174.8	14.67	13.45	14.67
I10_490	0.195	13.475	17.016	11.257	156.2	13.88	13.475	13.88
I10_491	0.222	13.502	18.753	12.994	151.8	11.68	13.502	11.68
I10_492	0.248	13.528	18.731	12.972	190.8	14.71	13.528	14.71
I10_493	0.264	13.544	18.509	12.750	201	15.76	13.544	15.76
I10_494	0.3	13.58	17.100	11.341	176.3	15.55	13.58	15.55

Specimen	Sect. Depth (m)	Abs.Depth (m)	Weight (gr)	Net weight (gr)	Bulk susceptibility (E-06)	Mass susc.E-08 (m3/Kgr)	Absolute Depth (m)	Mass susc.E-08 (m3/Kgr)
I10_495	0.325	13.605	16.656	10.897	175.2	16.08	13.605	16.08
I10_496	0.35	13.63	16.357	10.598	183.6	17.32	13.63	17.32
I10_497	0.375	13.655	17.144	11.385	187.3	16.45	13.655	16.45
I10_498	0.4	13.68	16.739	10.980	178.2	16.23	13.68	16.23
I10_499	0.419	13.699	18.036	12.277	189.7	15.45	13.699	15.45
I10_500	0.441	13.721	18.619	12.860	193.1	15.02	13.721	15.02
I10_501	0.469	13.749	18.841	13.082	182.5	13.95	13.749	13.95
I10_502	0.494	13.774	16.660	10.901	145	13.30	13.774	13.30
I10_503	0.517	13.797	15.957	10.198	137	13.43	13.797	13.43
I10_504	0.541	13.821	16.200	10.441	141.3	13.53	13.821	13.53
I10_505	0.566	13.846	17.994	12.235	188.9	15.44	13.846	15.44
I10_506	0.593	13.873	18.505	12.746	205.6	16.13	13.873	16.13
I10_507	0.618	13.898	16.899	11.140	172.8	15.51	13.898	15.51
I10_508	0.644	13.924	16.278	10.519	169.7	16.13	13.924	16.13
I10_509	0.669	13.949	17.253	11.494	177.3	15.43	13.949	15.43
I10_510	0.695	13.975	16.857	11.098	167.6	15.10	13.975	15.10
I10_511	0.765	14.045	17.934	12.175	183.8	15.10	14.045	15.10
I10_512	0.79	14.07	16.769	11.010	158	14.35	14.07	14.35
I10_513	0.815	14.095	17.258	11.499	173.7	15.11	14.095	15.11
I10_514	0.84	14.12	17.560	11.801	188.8	16.00	14.12	16.00
I10_515	0.87	14.15	17.511	11.752	182.7	15.55	14.15	15.55
I10_516	0.898	14.178	17.484	11.725	205.4	17.52	14.178	17.52
I10_517	0.938	14.218	16.184	10.425	174.9	16.78	14.218	16.78
I10_518	0.964	14.244	17.912	12.153	192.6	15.85	14.244	15.85
I10_519	0.988	14.268	18.663	12.904	205.2	15.90	14.268	15.90
I10_520	1.016	14.296	18.230	12.471	183.4	14.71	14.296	14.71
I10_521	1.042	14.322	18.380	12.621	198.2	15.70	14.322	15.70
I10_522	1.068	14.348	18.413	12.654	199	15.73	14.348	15.73
I10_523	1.1	14.38	18.527	12.768	196.1	15.36	14.38	15.36
I10_524	1.125	14.405	19.816	14.057	209.8	14.92	14.405	14.92
I10_525	1.15	14.43	20.212	14.453	221.4	15.32	14.43	15.32
I10_526	1.175	14.455	20.144	14.385	207.3	14.41	14.455	14.41
I10_527	1.198	14.478	19.267	13.508	211.5	15.66	14.478	15.66
I10_528	1.224	14.504	19.137	13.378	194.5	14.54	14.504	14.54
I10_529	1.248	14.528	18.775	13.016	197.4	15.17	14.528	15.17
I10_530	1.274	14.554	19.218	13.459	210.6	15.65	14.554	15.65
I10_531	1.298	14.578	18.980	13.221	210.2	15.90	14.578	15.90
I10_532	1.324	14.604	19.493	13.734	230.2	16.76	14.604	16.76
I10_533	1.348	14.628	19.640	13.881	257.1	18.52	14.628	18.52
I10_534	1.37	14.65	17.865	12.106	234	19.33	14.65	19.33
I10_535	1.399	14.679	18.155	12.396	246.9	19.92	14.679	19.92
I10_536	1.424	14.704	15.940	10.181	207.3	20.36	14.704	20.36
I10_537	1.449	14.729	17.882	12.123	240.8	19.86	14.729	19.86
I10_538	1.475	14.755	16.824	11.065	202.4	18.29	14.755	18.29
I10_539	1.49	14.77	15.459	9.700	175.3	18.07	14.77	18.07

Annexe 4: Carbon Organic data of MD 90-918 core

nom ech	weight (mg)	% N/dec	Δ % N/dec	%Corg/ dec	Δ %Corg/ dec
195	5.41	0.91	0.20	2.26	0.97
196	5.669	1.66	0.26	2.34	0.70
197	5.009	0.22	0.14	1.97	1.00
198	7.922	1.04	0.18	1.95	0.94
200	6.239	0.168	0.021	1.50	0.20
202	8.232	0.133	0.016	1.52	0.16
204	8.246	0.177	0.017	1.63	0.16
205	6.314	0.159	0.021	1.38	0.19
206	5.791	0.157	0.023	1.49	0.21
207	9.344	0.132	0.015	1.19	0.14
208	9.581	0.125	0.014	1.05	0.13
209	6.454	0.122	0.020	0.97	0.18
210	6.356	0.119	0.020	0.93	0.18
213.5	8.372	0.093	0.015	0.65	0.14
214.2	6.344	0.102	0.020	0.79	0.18
215	7.215	0.108	0.018	0.86	0.16
217	6.507	0.115	0.020	0.89	0.18
218	8.37	0.117	0.016	0.91	0.14
219	8.884	0.135	0.015	1.12	0.14
220	9.988	0.155	0.014	1.49	0.13
221	6.396	0.185	0.021	1.64	0.20
224	9.367	0.167	0.015	1.51	0.14
225	8.408	0.204	0.017	1.97	0.16
226	7.765	0.198	0.018	1.92	0.17
227	8.726	0.182	0.017	1.76	0.15
228	4.718	0.187	0.028	1.76	0.26
229	7.177	0.167	0.019	1.56	0.18
230	8.471	0.157	0.016	1.51	0.15
231	8.448	0.093	0.015	0.77	0.14
234.2	8.28	0.075	0.015	0.48	0.14
236.8	5.227	0.059	0.023	0.23	0.21
239	8.653	0.067	0.014	0.40	0.13
243	8.4	0.063	0.015	0.31	0.13

Annexe 5: SEM and EPMA intercalibration data

MD90-918 2-Paris														
	SiO ₂	TiO ₂	Al ₂ O ₃	Fe ₂ O ₃	MnO	MgO	CaO	Na ₂ O	K ₂ O	P ₂ O ₅	ClO	Total	Total Alkali	K ₂ O/Na ₂ O
3/1/1.	75.14	0.09	13.14	1.27	0.03	0.05	0.79	4.09	4.99	0.00	0.39	100.00	9.08	1.22
5/1/1.	75.02	0.14	13.02	1.37	0.06	0.06	0.81	3.81	5.33	0.02	0.36	100.00	9.15	1.40
6/1/1.	75.23	0.00	12.88	1.49	0.10	0.04	0.67	3.83	5.42	0.02	0.32	100.00	9.25	1.41
7/1/1.	75.09	0.21	12.95	1.51	0.04	0.04	0.76	3.88	5.12	0.00	0.40	100.00	9.01	1.32
8/1/1.	74.57	0.01	13.40	1.46	0.13	0.03	0.87	3.90	5.22	0.03	0.37	100.00	9.12	1.34
9/1/1.	74.93	0.00	13.07	1.61	0.06	0.05	0.78	3.96	5.18	0.02	0.33	100.00	9.15	1.31
10/1/1.	75.03	0.00	13.07	1.63	0.07	0.05	0.74	4.01	5.04	-0.01	0.36	100.00	9.06	1.26
11/1/1.	74.73	0.27	13.06	1.39	0.07	0.04	0.76	3.82	5.48	0.00	0.37	100.00	9.30	1.43
12/1/1.	75.21	0.05	13.09	1.49	0.12	0.04	0.75	3.98	4.89	0.00	0.37	100.00	8.88	1.23
14/1/1.	74.73	0.01	13.49	1.62	0.06	0.05	0.77	4.02	4.87	0.02	0.37	100.00	8.89	1.21
16/1/1.	74.90	0.02	13.23	1.54	0.11	0.05	0.81	3.73	5.21	0.00	0.40	100.00	8.94	1.40
17/1/1.	74.78	0.15	13.26	1.53	0.09	0.04	0.78	3.83	5.15	0.03	0.36	100.00	8.98	1.34
18/1/1.	74.69	0.01	13.27	1.58	0.06	0.05	0.77	3.97	5.21	0.01	0.38	100.00	9.19	1.31
19/1/1.	75.00	0.02	13.14	1.57	0.05	0.05	0.75	3.90	5.07	0.04	0.39	100.00	8.98	1.30
mean	74.93	0.07	13.15	1.50	0.07	0.05	0.77	3.91	5.16	0.01	0.37	-	9.07	1.32
sd	0.21	0.09	0.17	0.11	0.03	0.01	0.05	0.10	0.18	0.02	0.02	-	0.13	0.07
MD90-918 4-Pisa														
	SiO ₂	TiO ₂	Al ₂ O ₃	Fe ₂ O ₃	MnO	MgO	CaO	Na ₂ O	K ₂ O	P ₂ O ₅	ClO	Total	Total Alkali	K ₂ O/Na ₂ O
P1151-1	74.51	0.00	13.63	1.51	0.00	0.14	0.75	3.95	5.25	0.00	0.27	100.01	9.2	1.33
P1151-2	74.56	0.00	13.44	1.53	0.00	0.09	0.85	3.93	5.26	0.00	0.33	99.99	9.19	1.34
P1151-3	74.55	0.00	13.52	1.48	0.00	0.00	0.88	3.98	5.30	0.00	0.29	100	9.28	1.33
P1151-4	73.89	0.00	14.18	1.37	0.00	0.08	0.89	4.21	5.07	0.00	0.26	99.95	9.28	1.20
P1151-5	74.41	0.23	13.44	1.55	0.19	0.05	0.78	3.76	5.26	0.00	0.34	100.01	9.02	1.40
P1151-6	74.44	0.11	13.44	1.68	0.00	0.07	0.79	3.80	5.30	0.00	0.36	99.99	9.1	1.39
P1151-7	74.79	0.07	13.65	1.57	0.00	0.08	0.72	3.68	5.03	0.00	0.42	100.01	8.71	1.37
P1151-8	74.48	0.00	13.46	1.46	0.00	0.09	0.85	4.01	5.23	0.00	0.43	100.01	9.24	1.30
P1151-9	74.19	0.09	13.60	1.53	0.06	0.20	0.82	3.92	5.28	0.00	0.30	99.99	9.2	1.35
P1151-10	74.42	0.00	13.55	1.45	0.00	0.08	0.78	3.85	5.49	0.00	0.37	99.99	9.34	1.43
mean	74.42	0.05	13.59	1.51	0.03	0.09	0.81	3.91	5.25	0.00	0.34	-	9.16	1.34
sd	0.24	0.08	0.22	0.08	0.06	0.05	0.06	0.15	0.13	0.00	0.06	-	0.18	0.06
MD90-918 5-Paris														
	SiO ₂	TiO ₂	Al ₂ O ₃	Fe ₂ O ₃	MnO	MgO	CaO	Na ₂ O	K ₂ O	P ₂ O ₅	ClO	Total	Total Alkali	K ₂ O/Na ₂ O
110/1.	75.02	0.00	13.18	1.54	0.09	0.02	0.73	4.00	5.03	0.00	0.38	100.00	9.03	1.26
111/1.	75.51	0.02	12.94	1.39	0.15	0.02	0.80	4.08	4.67	0.02	0.39	100.00	8.75	1.15
112/1.	74.56	0.10	13.59	1.46	0.07	0.04	0.83	3.91	4.95	0.05	0.44	100.00	8.87	1.27
113/1.	75.13	0.01	13.32	1.63	0.01	0.06	0.81	3.96	4.65	0.00	0.41	100.00	8.61	1.17
114/1.	75.07	0.00	13.69	1.61	0.00	0.03	0.83	3.97	4.44	0.00	0.34	100.00	8.41	1.12
115/1.	75.18	0.18	13.01	1.59	0.05	0.06	0.78	4.00	4.80	0.03	0.34	100.00	8.80	1.20
116/1.	75.12	0.14	13.08	1.48	0.12	0.05	0.79	3.90	4.95	0.00	0.37	100.00	8.85	1.27
117/1.	75.54	0.02	13.14	1.48	0.08	0.05	0.78	4.03	4.49	0.00	0.40	100.00	8.52	1.11
118/1.	75.44	0.06	13.03	1.53	0.03	0.05	0.74	3.93	4.84	0.04	0.31	100.00	8.77	1.23
mean	75.18	0.06	13.22	1.52	0.07	0.04	0.79	3.98	4.76	0.02	0.38	-	8.74	1.20
sd	0.30	0.06	0.26	0.08	0.05	0.01	0.04	0.06	0.21	0.02	0.04	-	0.19	0.06

<u>MD90-918-5-Pisa</u>	SiO ₂	TiO ₂	Al ₂ O ₃	FeO _{tot}	MnO	MgO	CaO	Na ₂ O	K ₂ O	P ₂ O ₅	ClO	Total	Total Alkali	K ₂ O/Na ₂ O
MD90918-5-1	74.36	0.12	13.67	1.51	0.11	0	0.84	3.96	4.96	0	0.47	100	8.92	1.25
MD90918-5-2	74.28	0.15	13.43	1.65	0.04	0.04	0.76	4.09	5.21	0	0.34	100	9.3	1.27
MD90918-5-3	74.58	0	13.64	1.63	0.04	0.04	0.73	3.81	5.22	0	0.32	100.01	9.03	1.37
MD90918-5-4	74.77	0	13.7	1.35	0	0	0.72	3.87	5.22	0	0.38	100.01	9.09	1.35
MD90918-5-5	73.82	0.17	13.63	1.41	0	0.18	0.91	4.37	5.09	0	0.42	99.99	9.46	1.16
MD90918-5-6	74.66	0	13.55	1.48	0	0	0.78	4	5.16	0	0.36	99.99	9.16	1.29
MD90918-5-7	74.81	0	13.55	1.49	0	0.11	0.69	3.82	5.23	0	0.31	100.01	9.05	1.37
MD90918-5-8	74.22	0.11	13.68	1.55	0.07	0.08	0.68	4.2	5.08	0	0.33	100	9.28	1.21
MD90918-5-9	74.63	0	13.51	1.45	0	0.04	0.85	4.07	5.12	0	0.33	100	9.19	1.26
MD90918-5-10	74.39	0	13.53	1.47	0	0	0.83	4.22	5.19	0	0.37	100	9.41	1.23
MD90918-5-11	74.43	0	13.71	1.44	0	0.11	0.93	3.93	5.13	0	0.32	100	9.06	1.31
MD90918-5-12	74.29	0.05	13.68	1.48	0.06	0.13	0.65	4.29	5.02	0	0.35	100	9.31	1.17
mean	74.44	0.05	13.61	1.49	0.03	0.06	0.78	4.05	5.14	0.00	0.36	100	9.19	1.27
sd	0.28	0.07	0.09	0.09	0.04	0.06	0.09	0.19	0.09	0.00	0.05	100	0.17	0.07

<u>MD90-918-175-Paris</u>	SiO ₂	TiO ₂	Al ₂ O ₃	FeO _{tot}	MnO	MgO	CaO	Na ₂ O	K ₂ O	P ₂ O ₅	ClO	Total	Total Alkali	K ₂ O/Na ₂ O
42 / 1.	59.14	0.23	21.62	1.72	0.12	0.06	1.66	8.26	6.60	0.01	0.58	100.00	14.85	0.80
43 / 1.	58.22	0.22	21.60	1.72	0.17	0.08	1.70	8.89	6.75	0.03	0.60	100.00	15.65	0.76
44 / 1.	58.74	0.11	21.13	1.92	0.28	0.08	1.74	8.56	6.79	0.02	0.64	100.00	15.35	0.79
45 / 1.	58.74	0.21	21.43	1.71	0.29	0.07	1.59	8.77	6.57	0.00	0.62	100.00	15.34	0.75
46 / 1.	59.33	0.18	21.16	1.79	0.02	0.10	1.73	8.62	6.51	0.02	0.54	100.00	15.13	0.76
47 / 1.	58.56	0.05	21.17	1.73	0.25	0.11	1.62	9.03	6.85	0.01	0.62	100.00	15.88	0.76
48 / 1.	58.84	0.13	21.38	1.67	0.21	0.10	1.83	8.71	6.51	0.00	0.63	100.00	15.21	0.75
50 / 1.	59.20	0.23	21.08	1.75	0.20	0.08	1.67	8.31	6.84	0.01	0.63	100.00	15.15	0.82
51 / 1.	59.38	0.18	20.97	1.66	0.26	0.07	1.62	8.68	6.63	0.01	0.55	100.00	15.31	0.76
52 / 1.	59.98	0.29	20.92	1.53	0.10	0.06	1.68	7.28	7.46	0.18	0.51	100.00	14.74	1.02
53 / 1.	59.48	0.02	21.73	1.68	0.19	0.06	1.67	8.18	6.40	0.00	0.59	100.00	14.58	0.78
55 / 1.	58.52	0.00	21.46	1.73	0.25	0.07	1.63	8.91	6.77	0.04	0.62	100.00	15.68	0.76
56 / 1.	58.93	0.18	21.15	1.71	0.22	0.07	1.72	9.10	6.32	0.07	0.54	100.00	15.42	0.69
58 / 1.	59.08	0.09	21.17	1.65	0.24	0.08	1.65	8.81	6.61	0.03	0.60	100.00	15.41	0.75
mean	59.01	0.15	21.28	1.71	0.20	0.08	1.68	8.58	6.69	0.03	0.59	100.00	15.26	0.78
sd	0.46	0.09	0.25	0.08	0.08	0.02	0.06	0.47	0.28	0.05	0.04	100.00	0.36	0.08
57 / 1.	59.28	0.19	21.78	1.61	0.15	0.07	2.75	8.35	5.35	0.00	0.47	100.00	13.70	0.64

<u>MD90918-175-Pisa</u>	SiO ₂	TiO ₂	Al ₂ O ₃	FeO _{tot}	MnO	MgO	CaO	Na ₂ O	K ₂ O	P ₂ O ₅	ClO	Total	Total Alkali	K ₂ O/Na ₂ O
MD90918-175-1	59.58	0	22.02	1.71	0	0.2	1.66	7.4	6.94	0	0.49	100	14.34	0.94
MD90918-175-2	58.34	0.21	21.72	1.78	0.31	0.16	1.44	8.84	6.6	0	0.6	100	15.44	0.75
MD90918-175-3	58.75	0.1	21.82	1.71	0.18	0	1.61	8.47	6.83	0	0.54	100.01	15.3	0.81
MD90918-175-4	59.09	0.15	21.86	1.55	0.12	0	1.54	8.55	6.56	0	0.59	100.01	15.11	0.77
MD90918-175-5	58.46	0.14	21.74	2.05	0.41	0.15	1.69	7.91	6.86	0	0.58	99.99	14.77	0.87
MD90918-175-6	58.25	0.2	22.01	1.84	0.3	0	1.64	8.89	6.41	0	0.46	100	15.3	0.72
MD90918-175-7	59.16	0.16	21.92	1.64	0.2	0.29	1.46	8.08	6.64	0	0.45	100	14.72	0.82
MD90918-175-8	58.8	0.13	21.87	1.69	0.18	0.11	1.58	8.16	6.93	0	0.55	100	15.09	0.85
MD90918-175-9	58.77	0.04	21.96	1.65	0	0.15	1.63	8.54	6.68	0	0.57	99.99	15.22	0.78
MD90918-175-10	58.67	0.13	21.81	1.76	0.18	0.2	1.77	7.98	6.88	0	0.62	100	14.86	0.86
mean	58.79	0.13	21.87	1.74	0.19	0.13	1.60	8.28	6.73	0.00	0.55	100	15.02	0.82
sd	0.40	0.07	0.10	0.14	0.13	0.10	0.10	0.46	0.18	0.00	0.06	100.00	0.34	0.07

MD90-918-185-Paris														
	SiO ₂	TiO ₂	Al ₂ O ₃	FeO _{tot}	MnO	MgO	CaO	Na ₂ O	K ₂ O	P ₂ O ₅	ClO	Total	Total Alkali	K ₂ O/Na ₂ O
77/1.	58.70	0.19	21.29	1.77	0.17	0.13	1.66	8.81	6.65	0.00	0.64	100.00	15.46	0.75
79/1.	58.44	0.12	21.26	1.69	0.10	0.05	1.59	9.41	6.65	0.02	0.67	100.00	16.06	0.71
80/1.	59.16	0.21	21.39	1.63	0.13	0.10	1.71	8.60	6.42	0.03	0.63	100.00	15.02	0.75
81/1.	58.50	0.28	20.94	1.83	0.24	0.08	1.45	9.09	6.87	0.00	0.73	100.00	15.95	0.76
82/1.	58.99	0.00	21.28	1.62	0.24	0.05	1.56	8.87	6.80	0.00	0.58	100.00	15.66	0.77
83/1.	59.22	0.14	21.08	1.51	0.18	0.08	1.57	8.95	6.68	0.02	0.58	100.00	15.63	0.75
84/1.	59.23	0.31	20.91	1.64	0.14	0.08	1.69	8.68	6.67	0.00	0.66	100.00	15.35	0.77
87/1.	59.12	0.02	21.15	1.78	0.25	0.04	1.60	8.88	6.52	0.00	0.64	100.00	15.40	0.73
88/1.	58.85	0.15	21.39	1.63	0.16	0.04	1.69	8.84	6.54	0.05	0.65	100.00	15.38	0.74
mean	58.91	0.16	21.19	1.68	0.18	0.07	1.61	8.90	6.64	0.01	0.64		15.55	0.75
sd	0.31	0.10	0.18	0.10	0.05	0.03	0.08	0.24	0.14	0.02	0.05		0.32	0.02
78/1.	61.38	0.05	21.58	1.08	0.10	0.02	3.25	7.67	4.65	0.03	0.18	100.00	12.32	0.61
86/1.	60.75	0.19	21.50	1.27	0.15	0.04	2.99	7.81	4.93	0.00	0.36	100.00	12.74	0.63
mean	61.06	0.12	21.54	1.18	0.12	0.03	3.12	7.74	4.79	0.01	0.27		12.53	0.62
sd	0.45	0.10	0.06	0.14	0.04	0.02	0.18	0.10	0.20	0.02	0.12		0.30	0.02
MD90-918-185-Pisa														
	SiO ₂	TiO ₂	Al ₂ O ₃	FeO _{tot}	MnO	MgO	CaO	Na ₂ O	K ₂ O	P ₂ O ₅	ClO	Total	Total Alkali	K ₂ O/Na ₂ O
MD90918-185-1	58.06	0.27	21.84	1.72	0.23	0.28	1.48	9.18	6.44	0	0.49	99.99	15.62	0.70
MD90918-185-4	58.39	0.06	21.97	1.76	0.19	0.09	1.6	8.68	6.78	0	0.49	100.01	15.46	0.78
MD90918-185-5	58.7	0.2	21.54	1.75	0.27	0.07	1.67	8.39	6.78	0	0.63	100	15.17	0.81
MD90918-185-6	58.57	0.21	21.73	1.61	0.17	0.19	1.59	8.83	6.59	0	0.5	99.99	15.42	0.75
MD90918-185-7	58.41	0.16	21.69	1.84	0.26	0.19	1.38	8.72	6.87	0	0.49	100.01	15.59	0.79
MD90918-185-9	58.75	0	22.04	1.63	0	0.2	1.62	8.9	6.43	0	0.43	100	15.33	0.72
mean	58.48	0.15	21.80	1.72	0.19	0.17	1.56	8.78	6.65	0.00	0.51		15.43	0.76
sd	0.25	0.10	0.19	0.09	0.10	0.08	0.11	0.26	0.19	0.00	0.07		0.17	0.04
MD90918-185-2	60.37	0	22.43	1.16	0	0.14	2.16	6.95	6.41	0	0.37	99.99	13.36	0.92
MD90918-185-10	59.97	0.28	22.14	1.38	0.3	0	2.56	7.87	5.21	0	0.29	100	13.08	0.66
MD90918-185-8	59.6	0.21	22.16	1.65	0.16	0.09	2.38	7.74	5.57	0	0.45	100.01	13.31	0.72
mean	59.98	0.16	22.24	1.40	0.15	0.08	2.37	7.52	5.73	0.00	0.37		13.25	0.77
sd	0.39	0.15	0.16	0.25	0.15	0.07	0.20	0.50	0.62	0.00	0.08		0.15	0.14
MD90-918-210-Pisa														
	SiO ₂	TiO ₂	Al ₂ O ₃	FeO _{tot}	MnO	MgO	CaO	Na ₂ O	K ₂ O	P ₂ O ₅	ClO	Total	Total Alkali	K ₂ O/Na ₂ O
P1047-1	58.32	0.22	21.54	2.01	0.28	0.14	1.92	8.11	6.95	0.00	0.50	99.99	15.06	0.86
P1047-4	57.93	0.15	22.39	1.86	0.23	0.12	1.65	8.15	6.98	0.00	0.55	100.01	15.13	0.86
P1047-7	58.58	0.07	21.81	1.65	0.00	0.16	1.71	8.62	6.68	0.00	0.73	100.01	15.30	0.77
P1047-8	58.49	0.26	21.68	1.86	0.30	0.20	1.62	8.35	6.76	0.00	0.48	100.00	15.11	0.81
P1047-9	58.98	0.17	21.86	1.70	0.12	0.22	1.54	8.05	6.82	0.00	0.55	100.01	14.87	0.85
P1047-10	59.54	0.00	21.74	1.71	0.07	0.29	1.64	7.49	6.92	0.00	0.60	100.00	14.41	0.92
P1047-13	59.05	0.14	21.76	1.72	0.18	0.12	1.89	7.74	6.60	0.00	0.81	100.01	14.34	0.85
P1047-14	58.87	0.18	21.80	1.75	0.18	0.21	2.03	7.75	6.61	0.00	0.63	100.01	14.36	0.85
P1047-20	58.63	0.11	21.80	1.78	0.19	0.10	1.70	8.26	6.88	0.00	0.56	100.01	15.14	0.83
mean	58.71	0.14	21.82	1.78	0.17	0.17	1.74	8.06	6.80	0.00	0.60		14.86	0.85
sd	0.47	0.08	0.23	0.11	0.10	0.06	0.16	0.35	0.14	0.00	0.11		0.38	0.04

MD90-918-210-Pisa														
	SiO ₂	TiO ₂	Al ₂ O ₃	FeO _{tot}	MnO	MgO	CaO	Na ₂ O	K ₂ O	P ₂ O ₅	ClO	Total Alkali	K ₂ O/Na ₂ O	
P1047-2	74.45	0.17	13.18	1.59	0.18	0.11	0.76	3.98	5.33	0.00	0.25	100.00	9.31	1.34
P1047-3	74.82	0.13	13.37	1.52	0.09	0.00	0.77	3.66	5.29	0.00	0.36	100.01	8.95	1.45
P1047-5	74.83	0.07	13.29	1.42	0.00	0.12	0.75	4.03	5.18	0.00	0.31	100.00	9.21	1.29
P1047-6	75.05	0.11	13.35	1.59	0.12	0.09	0.71	3.53	5.14	0.00	0.31	100.00	8.67	1.46
P1047-11	75.12	0.00	13.65	1.31	0.00	0.10	0.78	3.45	5.26	0.00	0.33	100.00	8.71	1.52
P1047-12	74.53	0.10	13.36	1.53	0.12	0.09	0.81	3.95	5.19	0.00	0.32	100.00	9.14	1.31
P1047-15	74.86	0.09	13.47	1.37	0.00	0.00	0.79	3.79	5.33	0.00	0.30	100.00	9.12	1.41
P1047-16	74.88	0.00	13.51	1.32	0.00	0.12	0.79	3.87	5.22	0.00	0.30	100.01	9.09	1.35
P1047-17	74.75	0.00	13.57	1.39	0.00	0.04	0.76	3.77	5.35	0.00	0.36	99.99	9.12	1.42
P1047-18	75.01	0.05	13.38	1.43	0.00	0.00	0.79	3.82	5.28	0.00	0.26	100.02	9.10	1.38
P1047-19	75.13	0.05	13.45	1.45	0.06	0.00	0.80	3.52	5.25	0.00	0.28	99.99	8.77	1.49
Media	74.86	0.07	13.42	1.45	0.05	0.06	0.77	3.76	5.26	0.00	0.31	-	9.02	1.40
sd	0.22	0.06	0.13	0.10	0.07	0.05	0.03	0.20	0.07	0.00	0.04	-	0.21	0.08

MD90-918-217-Pisa														
	SiO ₂	TiO ₂	Al ₂ O ₃	FeO _{tot}	MnO	MgO	CaO	Na ₂ O	K ₂ O	P ₂ O ₅	ClO	Total Alkali	K ₂ O/Na ₂ O	
P1059-1	74.19	0.25	13.34	1.62	0.27	0.00	0.78	3.96	5.24	0.00	0.34	99.99	9.20	1.32
P1059-2	74.67	0.06	13.24	1.54	0.00	0.00	0.85	4.01	5.32	0.00	0.30	99.99	9.33	1.33
P1059-3	74.42	0.11	13.21	1.64	0.11	0.16	0.84	3.90	5.21	0.00	0.29	99.89	9.11	1.34
P1059-4	74.82	0.09	13.20	1.61	0.00	0.00	0.87	3.88	5.15	0.00	0.37	99.99	9.03	1.33
P1059-5	74.90	0.00	13.35	1.48	0.00	0.00	0.99	3.89	5.15	0.00	0.25	100.01	9.04	1.32
P1059-6	74.38	0.32	13.36	1.68	0.24	0.06	0.66	3.93	5.05	0.00	0.32	100	8.98	1.28
P1059-7	74.51	0.11	13.56	1.40	0.00	0.00	0.83	3.94	5.36	0.00	0.29	100	9.30	1.36
P1059-8	74.78	0.00	13.45	1.50	0.00	0.07	0.82	3.97	5.09	0.00	0.33	100.01	9.06	1.28
P1059-9	74.93	0.12	13.18	1.52	0.00	0.00	0.87	3.89	5.20	0.00	0.29	100	9.09	1.34
P1059-10	74.68	0.00	13.55	1.41	0.00	0.06	0.77	4.08	5.17	0.00	0.27	99.99	9.25	1.27
Media	74.63	0.11	13.34	1.54	0.06	0.04	0.83	3.95	5.19	0.00	0.31	-	9.14	1.32
sd	0.24	0.11	0.14	0.10	0.11	0.05	0.08	0.06	0.10	0.00	0.04	-	0.12	0.03

MD90-918-219-Paris														
	SiO ₂	TiO ₂	Al ₂ O ₃	FeO _{tot}	MnO	MgO	CaO	Na ₂ O	K ₂ O	P ₂ O ₅	ClO	Total Alkali	K ₂ O/Na ₂ O	
77/1.	75.06	0.11	13.02	1.53	0.17	0.05	0.87	3.77	5.07	0.02	0.33	100.00	8.84	1.35
78/1.	74.80	0.00	13.11	1.58	0.08	0.00	0.82	4.07	5.18	0.01	0.37	100.00	9.25	1.27
79/1.	74.93	0.14	13.46	1.40	0.05	0.02	0.99	3.76	4.88	0.00	0.37	100.00	8.63	1.30
80/1.	75.14	0.01	13.51	1.42	0.00	0.00	0.92	3.63	4.99	0.00	0.38	100.00	8.62	1.37
81/1.	75.54	0.14	13.13	1.47	0.05	0.06	0.80	3.58	4.87	0.00	0.37	100.00	8.45	1.36
82/1.	74.33	0.09	12.87	1.68	0.12	0.03	0.72	4.20	5.54	0.00	0.42	100.00	9.75	1.32
83/1.	74.71	0.07	12.87	1.49	0.05	0.06	0.85	4.17	5.39	0.00	0.33	100.00	9.56	1.29
84/1.	73.58	0.13	12.51	1.65	0.08	0.04	0.93	4.61	6.03	0.03	0.40	100.00	10.64	1.31
92/1.	75.54	0.01	13.24	1.33	0.15	0.02	0.85	3.62	4.82	0.00	0.42	100.00	8.44	1.33
93/1.	75.48	0.00	13.15	1.56	0.08	0.03	0.68	3.90	4.72	0.02	0.38	100.00	8.62	1.21
94/1.	75.50	0.07	12.99	1.42	0.05	0.08	0.83	3.57	5.16	0.03	0.30	100.00	8.73	1.44
Media	74.96	0.07	13.08	1.50	0.08	0.04	0.84	3.90	5.15	0.01	0.37	-	9.05	1.32
sd	0.61	0.06	0.28	0.11	0.05	0.03	0.09	0.33	0.38	0.01	0.04	-	0.69	0.06

MD90-918 219-Pisa														
	SiO ₂	TiO ₂	Al ₂ O ₃	FeO _{tot}	MnO	MgO	CaO	Na ₂ O	K ₂ O	P ₂ O ₅	ClO	Total	Total Alkali	K ₂ O/Na ₂ O
Pi060-1	74.68	0.00	13.48	1.36	0.00	0.13	0.70	4.03	5.35	0.00	0.27	100.00	9.38	1.33
Pi060-2	74.79	0.00	13.43	1.47	0.06	0.00	0.82	3.90	5.24	0.00	0.30	100.01	9.14	1.34
Pi060-4	74.61	0.18	13.35	1.45	0.18	0.00	0.83	3.80	5.29	0.00	0.32	100.01	9.09	1.39
Pi060-5	74.73	0.00	13.28	1.48	0.00	0.08	0.93	3.97	5.20	0.00	0.34	100.01	9.17	1.31
Pi060-6	74.57	0.05	13.46	1.49	0.06	0.11	0.88	3.94	5.14	0.00	0.30	100.00	9.08	1.30
Pi060-7	74.58	0.06	13.21	1.44	0.00	0.06	0.79	4.08	5.48	0.00	0.29	99.99	9.56	1.34
Pi060-9	73.99	0.22	13.45	1.54	0.2	0.07	0.88	4	5.36	0	0.3	100.01	9.36	1.34
Pi060-10	74.72	0.05	13.50	1.42	0.00	0.10	0.80	3.89	5.19	0.00	0.33	100.00	9.08	1.33
Media	74.58	0.07	13.40	1.46	0.06	0.07	0.83	3.95	5.28	0.00	0.31	100.00	9.23	1.34
sd	0.25	0.08	0.10	0.05	0.08	0.05	0.07	0.09	0.11	0.00	0.02		0.18	0.03
MD90-918 223-Paris														
	SiO ₂	TiO ₂	Al ₂ O ₃	FeO _{tot}	MnO	MgO	CaO	Na ₂ O	K ₂ O	P ₂ O ₅	ClO	Total	Total Alkali	K ₂ O/Na ₂ O
85 / 1 .	58.09	0.21	21.73	1.80	0.35	0.07	1.52	9.00	6.59	0.00	0.64	100.00	15.60	0.73
89 / 1 .	58.40	0.18	21.42	1.85	0.12	0.08	1.59	8.75	6.88	0.04	0.69	100.00	15.63	0.79
95 / 1 .	58.86	0.16	21.11	1.74	0.31	0.10	1.89	8.67	6.51	0.02	0.64	100.00	15.18	0.75
97 / 1 .	59.15	0.02	21.42	1.76	0.30	0.08	1.59	8.23	6.73	0.01	0.70	100.00	14.97	0.82
mean	58.62	0.14	21.42	1.79	0.27	0.08	1.65	8.67	6.68	0.02	0.67	100.00	15.34	0.77
sd	0.47	0.08	0.25	0.05	0.10	0.01	0.16	0.32	0.16	0.02	0.03		0.32	0.04
MD90-918 223-Pisa														
	SiO ₂	TiO ₂	Al ₂ O ₃	FeO _{tot}	MnO	MgO	CaO	Na ₂ O	K ₂ O	P ₂ O ₅	ClO	Total	Total Alkali	K ₂ O/Na ₂ O
MD 223-1	58.33	0.21	21.77	1.79	0.24	0.11	1.82	8.17	6.99	0.00	0.57	100	15.16	0.86
MD 223-2	59.40	0.19	22.06	1.77	0.15	0.14	1.59	7.51	6.62	0.00	0.55	99.98	14.13	0.88
MD 223-3	58.02	0.21	21.79	1.91	0.21	0.13	1.65	8.49	7.02	0.00	0.55	99.98	15.51	0.83
MD 223-4	59.38	0.00	21.94	1.59	0.00	0.00	1.55	8.46	6.38	0.00	0.70	100	14.84	0.75
MD 223-5	58.35	0.19	21.78	1.81	0.24	0.11	1.41	8.85	6.68	0.00	0.58	100	15.53	0.75
MD 223-6	58.68	0.19	21.41	1.83	0.32	0.23	1.83	8.07	6.89	0.00	0.55	100	14.96	0.85
MD 223-7	58.48	0.23	21.96	1.76	0.21	0.12	1.57	8.26	6.86	0.00	0.55	100	15.12	0.83
MD 223-8	58.54	0.08	21.57	1.88	0.18	0.00	1.78	8.45	7.06	0.00	0.48	100.02	15.51	0.84
MD 223-9	60.26	0.11	22.40	1.39	0.00	0.10	3.44	7.87	4.12	0.00	0.31	100	11.99	0.52
MD 223-10	58.80	0.00	21.65	1.72	0.06	0.08	1.56	8.75	6.87	0.00	0.51	100	15.62	0.79
MD 223-11	58.81	0.00	22.25	1.56	0.00	0.09	1.87	8.13	6.76	0.00	0.54	100.01	14.89	0.83
MD 223-12	58.84	0.00	22.00	1.64	0.00	0.17	1.61	8.24	7.00	0.00	0.51	100.01	15.24	0.85
mean	58.82	0.12	21.88	1.72	0.13	0.11	1.81	8.27	6.60	0.00	0.53	100.01	14.88	0.80
sd	0.61	0.10	0.28	0.15	0.12	0.06	0.53	0.37	0.81	0.00	0.09		1.00	0.10
MD90-918 230-Paris														
	SiO ₂	TiO ₂	Al ₂ O ₃	FeO _{tot}	MnO	MgO	CaO	Na ₂ O	K ₂ O	P ₂ O ₅	ClO	Total	Total Alkali	K ₂ O/Na ₂ O
136 / 1 .	59.34	0.12	21.07	1.77	0.19	0.06	1.68	8.76	6.39	0.02	0.59	100.00	15.16	0.73
138 / 1 .	59.30	0.32	21.53	1.61	0.20	0.05	2.02	7.86	6.52	0.02	0.57	100.00	14.38	0.83
139 / 1 .	58.58	0.24	21.26	1.91	0.09	0.11	1.70	8.70	6.78	0.02	0.61	100.00	15.48	0.78
140 / 1 .	59.08	0.20	21.29	1.71	0.19	0.06	1.69	8.64	6.46	0.00	0.68	100.00	15.11	0.75
mean	59.07	0.22	21.29	1.75	0.17	0.07	1.77	8.49	6.54	0.01	0.61	100.00	15.03	0.77
sd	0.35	0.08	0.19	0.13	0.05	0.03	0.16	0.43	0.17	0.01	0.04		0.47	0.04

MD90-918 230-Pisa	SiO ₂	TiO ₂	Al ₂ O ₃	FeO _{tot}	MnO	MgO	CaO	Na ₂ O	K ₂ O	P ₂ O ₅	ClO	Total	Total Alkali	K ₂ O/Na ₂ O
MD90918-230-1	58.39	0.13	21.77	1.83	0.21	0.21	1.50	8.48	6.77	0.00	0.71	100.00	15.25	0.80
MD90918-230-2	58.17	0.19	21.92	1.76	0.20	0.38	1.96	8.70	6.17	0.00	0.58	100.00	14.87	0.71
MD90918-230-3	58.56	0.17	21.91	1.56	0.19	0.19	1.65	8.46	6.75	0.00	0.53	99.99	15.21	0.80
MD90918-230-4	58.67	0.22	21.96	1.77	0.15	0.00	1.64	8.25	6.74	0.00	0.60	100.00	14.99	0.82
MD90918-230-5	58.66	0.15	21.77	1.78	0.18	0.34	1.50	8.60	6.44	0.00	0.58	100.00	15.04	0.75
MD90918-230-6	58.34	0.25	21.87	1.84	0.22	0.18	1.53	8.61	6.63	0.00	0.55	100.02	15.24	0.77
MD90918-230-7	59.06	0.09	21.83	1.65	0.09	0.00	1.84	8.11	6.78	0.00	0.54	99.99	14.89	0.84
MD90918-230-8	58.59	0.14	21.76	1.72	0.19	0.23	1.38	8.78	6.61	0.00	0.61	100.01	15.39	0.75
MD90918-230-10	58.79	0.17	21.77	1.68	0.18	0.13	1.70	8.52	6.48	0.00	0.56	99.98	15.00	0.76
<i>media</i>	58.58	0.17	21.84	1.73	0.18	0.18	1.63	8.50	6.60	0.00	0.58	-	15.10	0.78
<i>sd</i>	0.26	0.05	0.08	0.09	0.04	0.13	0.18	0.21	0.20	0.00	0.05	-	0.18	0.04

MD90-918 820-Paris	SiO ₂	TiO ₂	Al ₂ O ₃	FeO _{tot}	MnO	MgO	CaO	Na ₂ O	K ₂ O	P ₂ O ₅	ClO	Total	Total Alkali	K ₂ O/Na ₂ O
119 / 1 .	69.17	0.22	15.96	2.05	0.15	0.44	1.50	4.65	5.44	0.10	0.32	100.00	10.09	1.17
120 / 1 .	69.41	0.28	15.62	2.66	0.14	0.57	1.49	4.19	5.23	0.04	0.37	100.00	9.41	1.25
121 / 1 .	69.27	0.39	15.71	2.39	0.17	0.38	1.43	4.54	5.30	0.08	0.34	100.00	9.84	1.17
122 / 1 .	69.40	0.25	15.77	2.20	0.18	0.40	1.50	4.66	5.24	0.08	0.31	100.00	9.90	1.12
124 / 1 .	69.33	0.11	15.85	2.09	0.11	0.42	1.49	4.91	5.27	0.06	0.36	100.00	10.18	1.07
127 / 1 .	69.90	0.24	15.89	2.12	0.13	0.37	1.40	4.59	5.03	0.03	0.31	100.00	9.62	1.09
128 / 1 .	68.82	0.31	15.95	2.48	0.13	0.44	1.56	4.54	5.40	0.10	0.27	100.00	9.94	1.19
129 / 1 .	69.21	0.34	15.56	2.33	0.05	0.42	1.62	4.67	5.43	0.06	0.32	100.00	10.10	1.16
<i>media</i>	69.31	0.27	15.79	2.29	0.13	0.43	1.50	4.59	5.29	0.07	0.32	100.00	9.88	1.15
<i>sd</i>	0.30	0.09	0.15	0.22	0.04	0.06	0.07	0.20	0.14	0.03	0.03	-	0.26	0.06

MD90-918 820-Pisa	SiO ₂	TiO ₂	Al ₂ O ₃	FeO _{tot}	MnO	MgO	CaO	Na ₂ O	K ₂ O	P ₂ O ₅	ClO	Total	Total Alkali	K ₂ O/Na ₂ O
MD90918-820-1	68.79	0.39	16.16	2.33	0.10	0.52	1.22	4.55	5.53	0.00	0.40	99.99	10.08	1.22
MD90918-820-2	68.73	0.33	16.50	2.19	0.13	0.58	1.35	4.60	5.27	0.00	0.30	99.98	9.87	1.15
MD90918-820-3	69.00	0.38	16.10	2.17	0.15	0.41	1.46	4.51	5.59	0.00	0.24	100.01	10.10	1.24
MD90918-820-4	68.75	0.33	16.21	2.22	0.19	0.47	1.47	4.79	5.24	0.00	0.34	100.01	10.03	1.09
MD90918-820-5	67.57	0.31	16.64	2.66	0.13	0.59	1.84	4.72	5.16	0.00	0.36	99.98	9.88	1.09
MD90918-820-6	68.43	0.30	16.05	2.47	0.17	0.46	1.57	4.58	5.64	0.00	0.33	100.00	10.22	1.23
MD90918-820-7	68.75	0.31	16.02	2.41	0.05	0.44	1.56	4.46	5.59	0.00	0.41	100.00	10.05	1.25
MD90918-820-8	68.28	0.47	16.20	2.30	0.23	0.51	1.48	4.73	5.48	0.00	0.31	99.99	10.21	1.16
MD90918-820-9	69.33	0.19	16.35	1.94	0.00	0.42	1.30	4.75	5.35	0.00	0.35	99.98	10.10	1.13
MD90918-820-10	68.68	0.31	16.18	2.00	0.06	0.61	1.84	4.61	5.28	0.00	0.43	100.00	9.89	1.15
MD90918-820-11	69.02	0.32	16.36	2.26	0.10	0.39	1.46	4.51	5.31	0.00	0.27	100.00	9.82	1.18
MD90918-820-12	69.59	0.21	16.44	2.23	0.21	0.47	1.16	3.93	5.37	0.00	0.22	99.83	9.30	1.37
<i>media</i>	68.74	0.32	16.27	2.27	0.13	0.49	1.48	4.56	5.40	0.00	0.33	99.96	9.96	1.19
<i>sd</i>	0.51	0.07	0.19	0.20	0.07	0.07	0.21	0.23	0.16	0.00	0.07	-	0.25	0.08

Annexe 6: GIS data base

SIGLA_CARO	ID	LUNGH	AUTORI1	Y_GRDEC	X_GRDEC	Chemistry	Location	asl_m_tephra_nam	tephra_col	Origin
monticchio	0	0	Wuif et al., 2008	40.93333	15.58333	P/TP	Monticchio	556 TM-1	Grey	SV
monticchio	0	0	Wuif et al., 2008	40.93333	15.58333	PT/TrA	Monticchio	556 TM-1-1	Dark	SV
monticchio	0	0	Wuif et al., 2008	40.93333	15.58333	PT/TrA	Monticchio	556 TM-1-2	Dark	SV
monticchio	0	0	Wuif et al., 2008	40.93333	15.58333	TP/PT	Monticchio	556 TM-2a	Dark Grey	SV
monticchio	0	0	Wuif et al., 2008	40.93333	15.58333	F/P-BtrA	Monticchio	556 TM-2b	Dark Grey	SV
monticchio	0	0	Wuif et al., 2008	40.93333	15.58333	Tr	Monticchio	556 TM-2-1	Light Brown	IS
monticchio	0	0	Wuif et al., 2008	40.93333	15.58333	TP	Monticchio	556 TM-2-2	Grey	SV
monticchio	0	0	Wuif et al., 2008	40.93333	15.58333	TP/P	Monticchio	556 TM-3a	Grey	SV
monticchio	0	0	Wuif et al., 2008	40.93333	15.58333	P	Monticchio	556 TM-3b	Light Grey	SV
monticchio	0	0	Wuif et al., 2008	40.93333	15.58333	P	Monticchio	556 TM-3c	White Grey	SV
monticchio	0	0	Wuif et al., 2008	40.93333	15.58333	P	Monticchio	556 TM-4	White Grey	SV
monticchio	0	0	Wuif et al., 2008	40.93333	15.58333	P/Tr	Monticchio	556 TM-5a	White	CF
monticchio	0	0	Wuif et al., 2008	40.93333	15.58333	Tr	Monticchio	556 TM-5b	White	CF
monticchio	0	0	Wuif et al., 2008	40.93333	15.58333	P	Monticchio	556 TM-5c	Grey	CF
monticchio	0	0	Wuif et al., 2008	40.93333	15.58333	P/Tr	Monticchio	556 TM-5d	Grey	CF
monticchio	0	0	Wuif et al., 2008	40.93333	15.58333	Tr	Monticchio	556 TM-5-1	Grey Brownish	IS
monticchio	0	0	Wuif et al., 2008	40.93333	15.58333	Tr	Monticchio	556 TM-5-2	Grey Brownish	IS
monticchio	0	0	Wuif et al., 2008	40.93333	15.58333	P/Tr	Monticchio	556 TM-6a	Grey	SV
monticchio	0	0	Wuif et al., 2008	40.93333	15.58333	P-P/TP-Tr	Monticchio	556 TM-6b	White Grey Green	SV
monticchio	0	0	Wuif et al., 2008	40.93333	15.58333	Tr/TrD	Monticchio	556 TM-6-1a	Ochre Brownish	CF
monticchio	0	0	Wuif et al., 2008	40.93333	15.58333	Tr-P	Monticchio	556 TM-6-1b	Ochre Brownish	CF
monticchio	0	0	Wuif et al., 2008	40.93333	15.58333	Tr-P	Monticchio	556 TM-6-2	White	CF
monticchio	0	0	Wuif et al., 2008	40.93333	15.58333	Tr	Monticchio	556 TM-6-3	Light Brownish	IS?
monticchio	0	0	Wuif et al., 2008	40.93333	15.58333	TP-P/TrA	Monticchio	556 TM-6-4a	Brown	CF
monticchio	0	0	Wuif et al., 2008	40.93333	15.58333	TP-P/TrA	Monticchio	556 TM-6-4b	Brown	CF
monticchio	0	0	Wuif et al., 2008	40.93333	15.58333	TP-P/TrA	Monticchio	556 TM-6-4c	Brown	CF
monticchio	0	0	Wuif et al., 2008	40.93333	15.58333	L/TP	Monticchio	556 TM-7a	Brown	CF
monticchio	0	0	Wuif et al., 2008	40.93333	15.58333	P	Monticchio	556 TM-7b	Grey Brownish	CF
monticchio	0	0	Wuif et al., 2008	40.93333	15.58333	P	Monticchio	556 TM-7-1	White	CF
monticchio	0	0	Wuif et al., 2008	40.93333	15.58333	P	Monticchio	556 TM-7-2	White	CF
monticchio	0	0	Wuif et al., 2008	40.93333	15.58333	P	Monticchio	556 TM-7-3	White	CF
monticchio	0	0	Wuif et al., 2008	40.93333	15.58333	P	Monticchio	556 TM-7-4	White	CF
monticchio	0	0	Wuif et al., 2008	40.93333	15.58333	T	Monticchio	556 TM-7-5	White	?
monticchio	0	0	Wuif et al., 2008	40.93333	15.58333	Tr-L/TP	Monticchio	556 TM-8	Light Brown	CF
monticchio	0	0	Wuif et al., 2008	40.93333	15.58333	Tr	Monticchio	556 TM-9	White	CF
monticchio	0	0	Wuif et al., 2008	40.93333	15.58333	Tr	Monticchio	556 TM-10a	Pink Brownish	CF
monticchio	0	0	Wuif et al., 2008	40.93333	15.58333	Tr/P	Monticchio	556 TM-10b	Pink Grey	CF
monticchio	0	0	Wuif et al., 2008	40.93333	15.58333	Tr	Monticchio	556 TM-10c	Grey Brownish	CF
monticchio	0	0	Wuif et al., 2008	40.93333	15.58333	Tr	Monticchio	556 TM-10d	Light Grey	CF
monticchio	0	0	Wuif et al., 2008	40.93333	15.58333	Tr	Monticchio	556 TM-10-1	Dark Brown	ET
monticchio	0	0	Wuif et al., 2008	40.93333	15.58333	TrD-TrA	Monticchio	556 TM-11	Dark Brown	ET
monticchio	0	0	Wuif et al., 2008	40.93333	15.58333	P	Monticchio	556 TM-12	Grey	SV

0	Wulf et al., 2008	40.93333	15.58333	Bemmo-R	Monticchio	656 TM-12-1	Dark Brown	ET
0	Wulf et al., 2008	40.93333	15.58333	T	Monticchio	656 TM-12-2a	Grey	CF
0	Wulf et al., 2008	40.93333	15.58333	T	Monticchio	656 TM-12-2b	Grey	CF
0	Wulf et al., 2008	40.93333	15.58333	Tr-L/TP-BtrA	Monticchio	656 TM-13	White Black	SV
0	Wulf et al., 2004	40.93333	15.58333	BtrA	Monticchio	656 TM-14	Dark Brown	Procida
0	Wulf et al., 2004	40.93333	15.58333	Tr	Monticchio	656 TM-15	Beige	CF
0	Wulf et al., 2004	40.93333	15.58333	TP-Tr	Monticchio	656 TM-16a	Dark Brown	SV
0	Wulf et al., 2004	40.93333	15.58333	Tr/P	Monticchio	656 TM-16b	White Dark Brown	SV
0	Wulf et al., 2004	40.93333	15.58333	PT	Monticchio	656 TM-17a	Brown	AH
0	Wulf et al., 2004	40.93333	15.58333	PT	Monticchio	656 TM-17b	Brown Black	AH
0	Wulf et al., 2004	40.93333	15.58333	TP	Monticchio	656 TM-17c	Grey Brown	AH
0	Wulf et al., 2004	40.93333	15.58333	PT-TP	Monticchio	656 TM-17d	Dark Brown	AH
0	Wulf et al., 2004	40.93333	15.58333	PT-TP/L	Monticchio	656 TM-17e	Grey Brown	AH
0	Wulf et al., 2004	40.93333	15.58333	-	Monticchio	656 TM-17f	Grey Brown	AH
0	Wulf et al., 2004	40.93333	15.58333	Tr-P	Monticchio	656 TM-18	Beige Grey	CF
0	Wulf et al., 2004	40.93333	15.58333	Tr	Monticchio	656 TM-19	Beige Greenish	IS
0	Wulf et al., 2004	40.93333	15.58333	Tr	Monticchio	656 TM-20	Beige	IS
0	Wulf et al., 2004	40.93333	15.58333	TrA-TD	Monticchio	656 TM-21	Pale Brown Pink	Strom
0	Wulf et al., 2004	40.93333	15.58333	TrD/R	Monticchio	656 TM-22	Pale Brown	P antelleria
0	Wulf et al., 2004	40.93333	15.58333	-	Monticchio	656 TM-23	Light Brown	Sabatini
0	Wulf et al., 2004	40.93333	15.58333	Tr	Monticchio	656 TM-24a	Pink Brownish	Campanian
0	Wulf et al., 2004	39.59400	18.84050	R	Monticchio	656 TM-24b	Pale Brown	Campanian
0	Wulf et al., 2004	39.59400	18.84050	P	Ionian Sea	-695 tephra 2	Lipari	Lipari
0	Wulf et al., 2004	39.59400	18.84050	P	Ionian Sea	-695 tephra 175	SV	SV
0	Wulf et al., 2004	39.59400	18.84050	P	Ionian Sea	-695 tephra 185	SV	SV
0	Wulf et al., 2004	39.59400	18.84050	P	Ionian Sea	-695 tephra 210	SV	SV
0	Wulf et al., 2004	39.59400	18.84050	R	Ionian Sea	-695 tephra 218	Lipari	Lipari
0	Wulf et al., 2004	39.59400	18.84050	P	Ionian Sea	-695 tephra 223	SV	SV
0	Wulf et al., 2004	39.59400	18.84050	P	Ionian Sea	-695 tephra 230	SV	SV
0	Wulf et al., 2004	39.59400	18.84050	R	Ionian Sea	-695 tephra 820	CF	CF
0	Siani et al., 2004	41.28333	17.63000	T	Adriatic Sea	-1010 140	CF	CF
0	Siani et al., 2004	41.28333	17.63000	T	Adriatic Sea	-1010 167	CF	CF
0	Siani et al., 2004	41.28333	17.63000	T	Adriatic Sea	-1010 175	-	-
0	Siani et al., 2004	41.28333	17.63000	R-T	Adriatic Sea	-1010 240	Lipari	Lipari
0	Siani et al., 2004	41.28333	17.63000	R	Adriatic Sea	-1010 250	-	-
0	Siani et al., 2004	41.28333	17.63000	T	Adriatic Sea	-1010 275	-	-
0	Siani et al., 2004	41.28333	17.63000	T	Adriatic Sea	-1010 305-310	CF	CF
0	Siani et al., 2004	41.28333	17.63000	T	Adriatic Sea	-1010 395	CF	CF
0	Siani et al., 2004	41.28333	17.63000	T	Adriatic Sea	-1010 405	CF	CF
0	Siani et al., 2004	41.28333	17.63000	T	Adriatic Sea	-1010 423	CF	CF
0	Siani et al., 2004	41.28333	17.63000	T	Adriatic Sea	-1010 435	CF	CF
0	Siani et al., 2004	41.28333	17.63000	T	Adriatic Sea	-1010 530	SV	SV
0	Siani et al., 2004	41.28333	17.63000	T	Adriatic Sea	-1010 595	SV	SV
0	Siani et al., 2004	41.28333	17.63000	T	Adriatic Sea	-1010 490	ET	ET
0	Calanchi et al., 1998 Marine Geology	42.06683	15.66761	?	Adriatic Sea	-77 530	?	?

IN68-22	0	Calanchi et al., 1998	Marine Geology	15.00000 T	42.38333	15.00000 T	-129 133	CF	
PAL94-77	0	Calanchi et al., 1998	Marine Geology	15.08603 P	42.42569	15.08603 P	-148 550	CF	
PAL94-77	0	Calanchi et al., 1998	Marine Geology	15.08603 T	42.42569	15.08603 T	-148 140	CF	
RF93-77	0	Calanchi et al., 1998	Marine Geology	15.11658 T	42.44350	15.11658 T	-152 797	Campanian	
RF93-77	0	Calanchi et al., 1998	Marine Geology	15.11658 T	42.44350	15.11658 T	-152 449	IS	
RF93-77	0	Calanchi et al., 1998	Marine Geology	15.11658 ?	42.44350	15.11658 ?	-152 384	?	
RF93-77	0	Calanchi et al., 1998	Marine Geology	15.11658 P	42.44350	15.11658 P	-152 364	?	
RF93-77	0	Calanchi et al., 1998	Marine Geology	15.11658 P	42.44350	15.11658 P	-152 208	CF	
RF93-77	0	Calanchi et al., 1998	Marine Geology	15.11658 T	42.44350	15.11658 T	-152 83	CF	
CM92-42	0	Calanchi et al., 1998	Marine Geology	15.20122 T	42.62294	15.20122 T	-161 710	Campanian	
CM92-42	0	Calanchi et al., 1998	Marine Geology	15.20122 T	42.62294	15.20122 T	-161 450	IS	
CM92-43	0	Calanchi et al., 1998	Marine Geology	14.73244 P	42.88678	14.73244 P	-252 605	CF	
CM92-43	0	Calanchi et al., 1998	Marine Geology	14.73244 T	42.88678	14.73244 T	-252 150	CF	
CM92-42	0	Calanchi et al., 1998	Marine Geology	15.20122 Tr-P	42.62294	15.20122 Tr-P	-161 400	CF	
PAL94-8	0	Calanchi et al., 1998	Marine Geology	14.61844 Benmoreite - T	42.66642	14.61844 Benmoreite - T	-150 353	ET	
PAL94-8	0	Calanchi et al., 1998	Marine Geology	14.61844 P	42.66642	14.61844 P	-150 208	CF	
PAL94-8	0	Calanchi et al., 1998	Marine Geology	14.61844 T	42.66642	14.61844 T	-150 128	CF	
CM92-41	0	Calanchi et al., 1998	Marine Geology	15.09661 Benmoreite - T	42.56786	15.09661 Benmoreite - T	-173 420	ET	
CM92-41	0	Calanchi et al., 1998	Marine Geology	15.09661 ?	42.56786	15.09661 ?	-173 270	?	
CM92-41	0	Calanchi et al., 1998	Marine Geology	15.09661 P	42.56786	15.09661 P	-173 260	CF	
CM92-41	0	Calanchi et al., 1998	Marine Geology	15.09661 T	42.56786	15.09661 T	-173 70	CF	
CM92-41	0	Calanchi et al., 1998	Marine Geology	15.09661 ?	42.56786	15.09661 ?	-173 60	?	
PAL94-66	0	Calanchi et al., 1998	Marine Geology	14.93928 Benmoreite - T	42.87386	14.93928 Benmoreite - T	-214 358	ET	
PAL94-66	0	Calanchi et al., 1998	Marine Geology	14.93928	42.87386	14.93928	-214 266	?	
PAL94-66	0	Calanchi et al., 1998	Marine Geology	14.93928 P	42.87386	14.93928 P	-214 214	CF	
PAL94-66	0	Calanchi et al., 1998	Marine Geology	14.93928 T	42.87386	14.93928 T	-214 64	CF	
IN68-21	0	Calanchi et al., 1998	Marine Geology	14.92500 P	42.18500	14.92500 P	-252 402	CF	
IN68-21	0	Calanchi et al., 1998	Marine Geology	14.92500 T	42.18500	14.92500 T	-252 100	CF	
JO 2004	0	Caron et al., 2009		20.67162 Benmoreite - Mugearitic	40.91667	20.67162 Benmoreite - Mugearitic	705 JO42	Dark Brown	
JO 2004	0	Caron et al., 2009		20.67162 T	40.91667	20.67162 T	705 JO187	Yellowish Grey	Campanian
JO 2004	0	Caron et al., 2009		20.67162 TP	40.91667	20.67162 TP	705 JO244	Yellowish Grey and Moderat	CF
JO 2004	0	Caron et al., 2009		20.67162 TP	40.91667	20.67162 TP	705 JO575	White to Light Brown	Campanian
JO 2004	0	Caron et al., 2009		20.67162 R	40.91667	20.67162 R	705 JO941	Brown Honey	Pantelleria
KET 8003	0	Thbse Parterne, 1985		14.48417 R - TLP	38.81700	14.48417 R - TLP	-1900 0	?	
KET 8003	0	Thbse Parterne, 1985		14.48417 T	38.81700	14.48417 T	-1900 10	Campanian	
KET 8003	0	Thbse Parterne, 1985		14.48417 R	38.81700	14.48417 R	-1900 60 E-1	Lipari	
KET 8003	0	Thbse Parterne, 1985		14.48417 R	38.81700	14.48417 R	-1900 110-130 E-2	Salina	
KET 8003	0	Thbse Parterne, 1985		14.48417 T	38.81700	14.48417 T	-1900 154	?	
KET 8003	0	Thbse Parterne, 1985		14.48417 Benmoreite	38.81700	14.48417 Benmoreite	-1900 163-170 Et-1	ET	
KET 8003	0	Thbse Parterne, 1985		14.48417 T	38.81700	14.48417 T	-1900 163-170 C-3	?	
KET 8003	0	Thbse Parterne, 1985		14.48417 R	38.81700	14.48417 R	-1900 260	?	
KET 8003	0	Thbse Parterne, 1985		14.48417 TLP	38.81700	14.48417 TLP	-1900 290-300 C-10	SV	
KET 8003	0	Giaccio et al., 2008		14.48417 TLP	38.81700	14.48417 TLP	-1900 300 E-10	?	
KET 8003	0	Thbse Parterne, 1985		14.48417 R	38.81700	14.48417 R	-1900 340 E-11	?	
KET 8003	0	Thbse Parterne, 1985		14.48417 TP	38.81700	14.48417 TP	-1900 350-360 C-13	CF	
KET 8003	0	Thbse Parterne, 1985		14.48417 T	38.81700	14.48417 T	-1900 380 C-14	?	

KET 8003	0	Thbse Parteme, 1985	38.81700	14.48417 R - TLP	Tyrrenian	-1900 414	?
KET 8003	0	Thbse Parteme, 1985	38.81700	14.48417 D	Tyrrenian	-1900 473	?
KET 8003	0	Thbse Parteme, 1985	38.81700	14.48417 T	Tyrrenian	-1900 480 C-16	IS
KET 8003	0	Thbse Parteme, 1985	38.81700	14.48417 D	Tyrrenian	-1900 554	?
KET 8003	0	Thbse Parteme, 1985	38.81700	14.48417 T	Tyrrenian	-1900 562 C-17	IS
KET 8003	0	Thbse Parteme, 1985	38.81700	14.48417 D	Tyrrenian	-1900 592	?
KET 8003	0	Thbse Parteme, 1985	38.81700	14.48417 D	Tyrrenian	-1900 615	?
KET 8003	0	Thbse Parteme, 1985	38.81700	14.48417 D	Tyrrenian	-1900 632	?
KET 8003	0	Thbse Parteme, 1985	38.81700	14.48417 T	Tyrrenian	-1900 652 C-18	IS
KET 8003	0	Thbse Parteme, 1985	38.81700	14.48417 D-RD	Tyrrenian	-1900 694	?
KET 8003	0	Thbse Parteme, 1985	38.81700	14.48417 A	Tyrrenian	-1900 703	?
KET 8003	0	Thbse Parteme, 1985	38.81700	14.48417 RD	Tyrrenian	-1900 710	?
KET 8003	0	Thbse Parteme, 1985	38.81700	14.48417 A - RD	Tyrrenian	-1900 754	?
KET 8003	0	Thbse Parteme, 1985	38.81700	14.48417 T	Tyrrenian	-1900 761 C-20	?
KET 8003	0	Thbse Parteme, 1985	38.81700	14.48417 RD	Tyrrenian	-1900 855	?
KET 8004	0	Thbse Parteme, 1985	39.66683	13.56667 T	Tyrrenian	-1900 860	?
KET 8004	0	Thbse Parteme, 1985	39.66683	13.56667 T	Tyrrenian	-2909 10	Campanian
KET 8004	0	Thbse Parteme, 1985	39.66683	13.56667 T	Tyrrenian	-2909 40 C-0	?
KET 8004	0	Thbse Parteme, 1985	39.66683	13.56667 T	Tyrrenian	-2909 60 C(i)-1	Campanian
KET 8004	0	Thbse Parteme, 1985	39.66683	13.56667 T	Tyrrenian	-2909 70	Campanian
KET 8004	0	Thbse Parteme, 1985	39.66683	13.56667 T	Tyrrenian	-2909 85	?
KET 8004	0	Thbse Parteme, 1985	39.66683	13.56667 T	Tyrrenian	-2909 110	Campanian
KET 8004	0	Thbse Parteme, 1985	39.66683	13.56667 P	Tyrrenian	-2909 115 C-2	CF
KET 8004	0	Thbse Parteme, 1985	39.66683	13.56667 T	Tyrrenian	-2909 125	Campanian
KET 8004	0	Thbse Parteme, 1985	39.66683	13.56667 T	Tyrrenian	-2909 142	Campanian
KET 8004	0	Thbse Parteme, 1985	39.66683	13.56667 T	Tyrrenian	-2909 150 C-3	?
KET 8004	0	Thbse Parteme, 1985	39.66683	13.56667 T	Tyrrenian	-2909 207 C-4 C-5	?
KET 8004	0	Thbse Parteme, 1985	39.66683	13.56667 T	Tyrrenian	-2909 242 C-6	Campanian
KET 8004	0	Thbse Parteme, 1985	39.66683	13.56667 T	Tyrrenian	-2909 260	Campanian
KET 8004	0	Zanchetta et al., 2008	39.66683	13.56667 T	Tyrrenian	-2909 274 C-7	Campanian
KET 8004	0	Giaccio et al., 2008	39.66683	13.56667 T	Tyrrenian	-2909 320 C-10	SV
KET 8004	0	Thbse Parteme, 1985	39.66683	13.56667 T	Tyrrenian	-2909 332	Campanian
KET 8004	0	Thbse Parteme, 1985	39.66683	13.56667 T	Tyrrenian	-2909 350	Campanian
KET 8004	0	Thbse Parteme, 1985	39.66683	13.56667 D	Tyrrenian	-2909 358 C(i)-5	?
KET 8004	0	Thbse Parteme, 1985	39.66683	13.56667 T	Tyrrenian	-2909 370 C-9	?
KET 8004	0	Thbse Parteme, 1985	39.66683	13.56667 T	Tyrrenian	-2909 390 C-11	Campanian
KET 8004	0	Thbse Parteme, 1985	39.66683	13.56667 T	Tyrrenian	-2909 406 C-12	Campanian
KET 8004	0	Thbse Parteme, 1985	39.66683	13.56667 TP	Tyrrenian	-2909 445 C-13	CF
KET 8004	0	Thbse Parteme, 1985	39.66683	13.56667 T	Tyrrenian	-2909 460	Campanian
KET 8004	0	Thbse Parteme, 1985	39.66683	13.56667 T	Tyrrenian	-2909 470 C-14	?
KET 8004	0	Thbse Parteme, 1985	39.66683	13.56667 T	Tyrrenian	-2909 515 C-15	IS
KET 8004	0	Thbse Parteme, 1985	39.66683	13.56667 T	Tyrrenian	-2909 560 C-16	IS
KET 8004	0	Thbse Parteme, 1985	39.66683	13.56667 T	Tyrrenian	-2909 590 C-17	IS

KET 8004	0	Thbse Parterne, 1985	39.66683	13.56667 T	Tyrrenian	-2909 611 C(i)-6	?
KET 8004	0	Thbse Parterne, 1985	39.66683	13.56667 T	Tyrrenian	-2909 640 C-18	IS
KET 8004	0	Thbse Parterne, 1985	39.66683	13.56667 T	Tyrrenian	-2909 644	Campanian
KET 8004	0	Thbse Parterne, 1985	39.66683	13.56667 T	Tyrrenian	-2909 654	Campanian
KET 8004	0	Thbse Parterne, 1985	39.66683	13.56667 T	Tyrrenian	-2909 666	?
KET 8004	0	Thbse Parterne, 1985	39.66683	13.56667 T	Tyrrenian	-2909 690 C(i)-7	?
KET 8004	0	Thbse Parterne, 1985	39.66683	13.56667 T	Tyrrenian	-2909 707 C-20	?
KET 8004	0	Thbse Parterne, 1985	39.66683	13.56667 T	Tyrrenian	-2909 717	Campanian
KET 8004	0	Thbse Parterne, 1985	39.66683	13.56667 T	Tyrrenian	-2909 735 C(i)-8	?
KET 8004	0	Thbse Parterne, 1985	39.66683	13.56667 T	Tyrrenian	-2909 745	Campanian
KET 8004	0	Thbse Parterne, 1985	39.66683	13.56667 T	Tyrrenian	-2909 770	Campanian
KET 8004	0	Thbse Parterne, 1985	39.66683	13.56667 T	Tyrrenian	-2909 784 P-10	Pantelleria
KET 8011	0	Thbse Parterne, 1985	39.15083	15.06750 T - TLP	Tyrrenian	-2111 20	?
KET 8011	0	Thbse Parterne, 1985	39.15083	15.06750 TLP	Tyrrenian	-2111 35	?
KET 8011	0	Thbse Parterne, 1985	39.15083	15.06750 R	Tyrrenian	-2111 50 E-1	Lipari
KET 8011	0	Thbse Parterne, 1985	39.15083	15.06750 T	Tyrrenian	-2111 80	?
KET 8011	0	Thbse Parterne, 1985	39.15083	15.06750 T	Tyrrenian	-2111 94	?
KET 8011	0	Thbse Parterne, 1985	39.15083	15.06750 T	Tyrrenian	-2111 116 Et-1	ET
KET 8011	0	Thbse Parterne, 1985	39.15083	15.06750 T	Tyrrenian	-2111 118,5 C-3	?
KET 8011	0	Thbse Parterne, 1985	39.15083	15.06750 T	Tyrrenian	-2111 170 C-5	?
KET 8011	0	Zanchetta et al., 2008	39.15083	15.06750 T - TLP	Tyrrenian	-2111 204 C-7	Campanian
KET 8011	0	Thbse Parterne, 1985	39.15083	15.06750 L	Tyrrenian	-2111 220	?
KET 8011	0	Giaccio et al., 2008	39.15083	15.06750 T	Tyrrenian	-2111 258 C-10	SV
KET 8011	0	Thbse Parterne, 1985	39.15083	15.06750 TLP	Tyrrenian	-2111 275 E-10	?
KET 8011	0	Thbse Parterne, 1985	39.15083	15.06750 T	Tyrrenian	-2111 287 C-9	?
KET 8011	0	Thbse Parterne, 1985	39.15083	15.06750 R	Tyrrenian	-2111 300 E-11	?
KET 8011	0	Thbse Parterne, 1985	39.15083	15.06750 TP	Tyrrenian	-2111 325 C-13	CF
KET 8011	0	Thbse Parterne, 1985	39.15083	15.06750 T	Tyrrenian	-2111 335 C-14	?
KET 8011	0	Thbse Parterne, 1985	39.15083	15.06750 T	Tyrrenian	-2111 357 C-15	?
KET 8011	0	Thbse Parterne, 1985	39.15083	15.06750 T	Tyrrenian	-2111 450 C-17	IS
KET 8011	0	Thbse Parterne, 1985	39.15083	15.06750 T	Tyrrenian	-2111 457	IS
KET 8011	0	Thbse Parterne, 1985	39.15083	15.06750 T	Tyrrenian	-2111 480 C-18	Campanian
KET 8011	0	Thbse Parterne, 1985	39.15083	15.06750 T	Tyrrenian	-2111 500	IS
KET 8011	0	Thbse Parterne, 1985	39.15083	15.06750 T	Tyrrenian	-2111 522,5 C(i)-7	Campanian
KET 8011	0	Thbse Parterne, 1985	39.15083	15.06750 T	Tyrrenian	-2111 547 C(i)-8	?
Scutari SK13	0	Sulpizio et al., 2009	42.16667	19.40000 F/P -TP	Scutari	5 SK13 295-300	SV
Scutari SK13	0	Sulpizio et al., 2009	42.16667	19.40000 Benmoreitic	Scutari	5 SK13 514	ET
Scutari SK13	0	Sulpizio et al., 2009	42.16667	19.40000 P	Scutari	5 SK13 571	SV
Scutari SK19	0	Sulpizio et al., 2009	42.16667	19.40000 F/P	Scutari	5 SK13 716-726	CF
Scutari SK19	0	Sulpizio et al., 2009	42.16667	19.40000 T	Scutari	5 SK19 155-160	SV
Scutari SK19	0	Sulpizio et al., 2009	42.16667	19.40000 T	Scutari	5 SK19 356	CF
Scutari SK19	0	Sulpizio et al., 2009	42.16667	19.40000 T	Scutari	5 SK19 368	CF
Scutari SK19	0	Sulpizio et al., 2009	42.16667	19.40000 T	Scutari	5 SK19 385-400	CF
Scutari SK19	0	Sulpizio et al., 2009	42.16667	19.40000 T	Scutari	5 SK19 460	CF
LZ1120	0	Wagner et al., 2008 JVGR	40.94111	20.76500 Benmoreitic	Orhid	693 LZ1120 310-315	ET

LZ1120	0	Wagner et al., 2008 JVGR	40.94111	20.76500 Tr	Orhid	693 LZ1120 896-897	Yellowish-grey	CF
LZ1120	0	Wagner et al., 2008 JVGR	40.94111	20.76500 Tr	Orhid	693 LZ1120 1070-1075	Light olive grey colored to daCF	CF
ML00	0	Margari et al., 2007	39.10247	26.33086 TP	Greece	323 ML-2		Campanian
ML00	0	Margari et al., 2007	39.10247	26.33086 R	Greece	323 ML-3		Agean Arc
ML01	0	Margari et al., 2007	39.10247	26.33086 R	Greece	323 ML-1		Agean Arc
ML01	0	Margari et al., 2007	39.10247	26.33086 TP	Greece	323 ML-2		Campanian
ML01	0	Margari et al., 2007	39.10247	26.33086 R	Greece	323 ML-3		Agean Arc
ML01	0	Margari et al., 2007	39.10247	26.33086 R	Greece	323 ML-4		Agean Arc
ML01	0	Margari et al., 2007	39.10247	26.33086 R-TrD	Greece	323 ML-5		Pantellerite
ML01	0	Margari et al., 2007	39.10247	26.33086 R	Greece	323 ML-6		?
RC 9-191	0	Keller et al., 1978	38.18333	18.03333 Leucite-Tephritic	Ionian	-2345 Z-1		SV
RC 9-191	0	Keller et al., 1978	38.18333	18.03333 T	Ionian	-2345 Y-3		Campanian
RC 9-191	0	Keller et al., 1978	38.18333	18.03333 TP	Ionian	-2345 Y-5		CF
RC 9-191	0	Keller et al., 1978	38.18333	18.03333 R	Ionian	-2345 Y-6		Pantelleria
RC 9-191	0	Keller et al., 1978	38.18333	18.03333 T	Ionian	-2345 Y-7		IS
RC 9-191	0	Keller et al., 1978	38.18333	18.03333 A	Ionian	-2345 X-1		Hellenic Arc
RC 9-191	0	Keller et al., 1978	38.18333	18.03333 T	Ionian	-2345 X-2		?
RC 9-191	0	Keller et al., 1978	38.18333	18.03333 Tephritic	Ionian	-2345 W-1		?
RC 9-191	0	Keller et al., 1978	38.18333	18.03333 Tephritic	Ionian	-2345 V-2		?
RC 9-191	0	Keller et al., 1978	38.18333	18.03333 D	Ionian	-2345 V-3		Hellenic Arc
V10 69	0	Keller et al., 1978	37.16222	17.03583 Leucite-Tephritic	Ionian	0 Z-1		SV
V10 69	0	Keller et al., 1978	37.16222	17.03583 Basaltic	Ionian	0 Y-1		ET
V10 69	0	Keller et al., 1978	37.16222	17.03583 TP	Ionian	0 Y-5		CF
V10 69	0	Keller et al., 1978	37.16222	17.03583 A	Ionian	0 X-1		Hellenic Arc
V10 69	0	Keller et al., 1978	37.16222	17.03583 A	Ionian	0 X-3		?
V10 69	0	Keller et al., 1978	37.16222	17.03583 Tephritic	Ionian	0 W-1		?
V10 69	0	Keller et al., 1978	37.16222	17.03583 Tephritic	Ionian	0 V-2		?
V10 69	0	Keller et al., 1978	37.16222	17.03583 D	Ionian	0 V-3		Hellenic Arc
RC9 183	0	Keller et al., 1978	34.54083	23.15611 Leucite-Tephritic	Ionian	0 Z-1		SV
RC9 183	0	Keller et al., 1978	34.54083	23.15611 TP	Ionian	0 Y-5		CF
RC9 183	0	Keller et al., 1978	34.54083	23.15611 R	Ionian	0 Y-6		Pantelleria
RC9 183	0	Keller et al., 1978	34.54083	23.15611 A	Ionian	0 X-1		Hellenic Arc
RC9 183	0	Keller et al., 1978	34.54083	23.15611 Tephritic	Ionian	0 W-1		?
RC9 183	0	Keller et al., 1978	34.54083	23.15611 RD	Ionian	0 V-1		Hellenic Arc
RC9 183	0	Keller et al., 1978	34.54083	23.15611 D	Ionian	0 V-3		Hellenic Arc

RC9 181	0	Keller et al., 1978	32.97278	24.82972	Leucite-Tephritic	Orhid	0 Z-1	SV
RC9 181	0	Keller et al., 1978	32.97278	24.82972	TP	Orhid	0 Y-5	CF
RC9 181	0	Keller et al., 1978	32.97278	24.82972	A	Orhid	0 X-1	Hellenic Arc
RC9 181	0	Keller et al., 1978	32.97278	24.82972	Tephritic	Orhid	0 V-1	?
V10 58	0	Keller et al., 1978	32.97278	24.82972	RD	Orhid	0 V-3	Hellenic Arc
V10 58	0	Keller et al., 1978	35.50056	26.08167	RD	Orhid	0 Z-2	Hellenic Arc
V10 58	0	Keller et al., 1978	35.50056	26.08167	RD	Orhid	0 Y-2	Hellenic Arc
V10 58	0	Keller et al., 1978	35.50056	26.08167	AD	Orhid	0 Y-4	Hellenic Arc
V10 58	0	Keller et al., 1978	35.50056	26.08167	TP	Orhid	0 Y-5	CF
OT0702	0	Vogel	41.12889	20.75000	foiditic/TP	Orhid	693 OT0702-1	SV
OT0702	0	Vogel	41.12889	20.75000	P	Orhid	693 OT0702-2	SV
OT0702	0	Vogel	41.12889	20.75000	T-P	Orhid	693 OT0702-3	SV
OT0702	0	Vogel	41.12889	20.75000	Lattic	Orhid	693 OT0702-4	Campanian
OT0702	0	Vogel	41.12889	20.75000	T-P	Orhid	693 OT0702-5	?
OT0702	0	Vogel	41.12889	20.75000	R/T	Orhid	693 OT0702-6	CF
OT0702	0	Vogel	41.12889	20.75000	P-TP	Orhid	693 OT0702-7	Pantelleria
OT0702	0	Vogel	41.12889	20.75000	T-T-P	Orhid	693 OT0702-8	Campanian
OT0702	0	Vogel	41.12889	20.75000	D/R	Orhid	693 OT0702-9	Campanian
RC 9-191	0	Fontugne et al., 1989	38.18333	18.03333	R	Ionian	-2345 63	Pantelleria
KET 8019	0	Kallel et al., 1997	40.55000	13.35000	P	Tyrrenian	-1900 45	Lipari
KET 8019	0	Kallel et al., 1997	40.55000	13.35000	R	Tyrrenian	-1900 80	Lipari
KET 8019	0	Kallel et al., 1997	40.55000	13.35000	?	Tyrrenian	-1900 140	CF
KET 8019	0	Kallel et al., 1997	40.55000	13.35000	P	Tyrrenian	-1900 180	CF
KET 8019	0	Kallel et al., 1997	40.55000	13.35000	T	Tyrrenian	-1900 220	?
KET 8216	0	Fontugne et al., 1989	41.51667	17.98333	TLP	Adriatic	-1166 10	SV
KET 8216	0	Fontugne et al., 1989	41.51667	17.98333	R	Adriatic	-1166 54	Lipari
KET 8216	0	Fontugne et al., 1989	41.51667	17.98333	T	Adriatic	-1166 90	CF
KET 8216	0	Fontugne et al., 1989	41.51667	17.98333	T	Adriatic	-1166 117	CF
KET 8004	0	Thise Parterme, 1985	39.66683	13.56667	R	Tyrrenian	-2909 40 E-1	Lipari
KET 8218	0	Pateme et al., 1988	41.73483	17.61800	P	Adriatic	-1166 V-1	SV
YD97-09	0	Lowe et al., 2007	42.28972	16.88306	P	Adriatic	-502	SV
RF95-11	0	Calanchi et Dinelli 2008	42.25983	15.39381	P	Adriatic	-720	SV
RF95-12	0	Calanchi et Dinelli 2008	42.19292	15.47683	P	Adriatic	-850	SV
RF95-13	0	Calanchi et Dinelli 2008	42.23750	14.90528	P	Adriatic	-840	SV
RF95-14	0	Calanchi et Dinelli 2008	42.23261	14.89506	P	Adriatic	-758	SV
RF95-7	0	Calanchi et Dinelli 2008	42.59275	15.31778	P	Adriatic	-715	SV
IN68-5	0	Calanchi et Dinelli 2008	41.23333	18.53333	P	Adriatic	-643	SV
IN68-9	0	Calanchi et Dinelli 2008	41.79000	17.91000	P	Adriatic	-627	SV
Pergusa	0	Narcisi, 2002	37.51667	14.30000	R	Sicily	-667 T2	Lipari
Pergusa	0	Narcisi, 2002	37.51667	14.30000	Tr-A Benmoreite	Sicily	-667 T1	Etna
								transparent colourless brownish and black

volc_event	S_L_O	Age_method	Age_yr	AgecalBPyr	error_yr	Obs	Depthcor_m	thick_mm
1631 AD	Lake	varve	0	90	5	5	0.060	9
?	Lake	varve	0	820	40	40	0.500	0
Ilime	Lake	varve	0	1070	50 ?	50 ?	0.760	0
512 AD PM1	Lake	varve	0	1420	70	70	1.120	3
472 AD Pollena	Lake	varve	0	1440	70	70	1.170	35
Cannavale/Chiarfo	Lake	varve	0	3040	150 ?	150 ?	2.530	0
AP5	Lake	varve	0	3940	200	200	3.110	1
AP4	Lake	varve	0	3990	200	200	3.160	22
AP3	Lake	varve	0	4020	200	200	3.200	24
AP2	Lake	varve	0	4150	210	210	3.340	31
Avellino	Lake	varve	0	4310	220	220	3.530	6
Astroni	Lake	varve	0	4620	230 units 1-3	230 units 1-3	3.740	11
Astroni	Lake	varve	0	4660	230 units 1-3	230 units 1-3	3.780	3
Agnano Monte Spina	Lake	varve	0	5390	270	270	4.270	1
Averno1	Lake	varve	0	5640	280 ?	280 ?	4.450	1
Averno1	Lake	varve	0	5680	280 ?	280 ?	4.480	1
Puzzillo	Lake	varve	0	6590	330 units 1-3?	330 units 1-3?	5.090	3
Maisto	Lake	varve	0	7150	360 ?	360 ?	5.440	1
Mercato top	Lake	varve	0	9620	480	480	6.450	1
Mercato base	Lake	varve	0	9680	480	480	6.590	106
Fondi di Baia	Lake	varve	0	9890	490	490	6.670	1
Fondi di Baia	Lake	varve	0	9960	500	500	6.690	3
Casle	Lake	varve	0	11210	560	560	7.260	0
?	Lake	varve	0	11520	580	580	7.380	1
Soccavo 5	Lake	varve	0	11670	580 ?	580 ?	7.460	17
Soccavo 4	Lake	varve	0	11890	590 ?	590 ?	7.600	1
Soccavo 4	Lake	varve	0	11980	600 ?	600 ?	7.650	3
Agnano Pomici Principali	Lake	varve	0	12170	610	610	7.750	6
Agnano Pomici Principali	Lake	varve	0	12180	610	610	7.810	47
Gaiola	Lake	varve	0	12590	630 ?	630 ?	8.050	0
La Pigna LP	Lake	varve	0	12640	630	630	8.080	0
La Pigna - NYT	Lake	varve	0	12770	640 units 1-6	640 units 1-6	8.130	0
?	Lake	varve	0	12910	650	650	8.180	0
?	Lake	varve	0	13170	660	660	8.360	1
Neapolitan Yellow Tuff NYT	Lake	varve	0	14120	710 C2	710 C2	8.600	22
Tuff Biancastri GM1	Lake	varve	0	14560	730	730	8.770	18
Lagno Amendolare LA	Lake	varve	0	15030	750	750	8.970	4
Lagno Amendolare LA	Lake	varve	0	15220	760	760	9.040	7
Lagno Amendolare LA	Lake	varve	0	15300	770	770	9.100	1
Lagno Amendolare LA	Lake	varve	0	15550	780	780	9.180	4
St Angelo Tuff	Lake	varve	0	15820	790 ?	790 ?	9.270	12
Biancavilla	Lake	varve	0	16440	820	820	9.530	1
Verdoline	Lake	varve	0	17560	880	880	10.020	55

Ante Biancavilla	Lake	varve	0	17980	900		10,190	1
Tuffi Biancastri	Lake	varve	0	18500	920 ?		10,430	0
Tuffi Biancastri	Lake	varve	0	18540	930 ?		10,440	0
Pomici di Base	Lake	varve	0	19280	960		11,070	182
Solchiaro	Lake	varve	0	20150	0		11,770	2
Y-3	Lake	varve	0	23930	0		14,720	286
Codola	Lake	varve	0	26130	0	Codola top	16,510	16
Codola	Lake	varve	0	26790	0	Codola base	17,100	68
Peperino Albano Ignimbrite	Lake	varve	0	25930	0		16,380	9
Peperino Albano Ignimbrite	Lake	varve	0	25990	0		16,380	7
Peperino Albano - IV	Lake	varve	0	29690	0		19,180	9
Peperino Albano - III	Lake	varve	0	29870	0		19,490	12
Peperino Albano - II	Lake	varve	0	29900	0		19,630	9
Peperino Albano - I	Lake	varve	0	30530	0		22,700	97
Campanina Ignimbrite Y-5	Lake	varve	0	32970	0	Cl - Y5	24,950	257
Tufo Verde Epomeo ss.	Lake	varve	0	56250	0		38,640	332
UMSA, Y-7	Lake	varve	0	57570	0		39,540	6
Petrazza Tuffs, Y-9	Lake	varve	0	74540	0		50,040	2
Ante Green Ignimbrite P-10	Lake	varve	0	85320	0		58,240	1
Tufo di Baccano	Lake	varve	0	85670	0		59,650	66
X-5	Lake	varve	0	97770	0	X-5 pumice fallout	69,300	70
X-5	Lake	varve	0	98750	0	X-5 Co-Ignimbrite	70,200	97
Monte Pilato	Sea		0	0	0		0,020	0
Mercato	Sea		0	0	0		1,750	0
Mercato	Sea		0	0	0		1,850	0
Mercato	Sea		0	0	0		2,100	0
Mercato	Sea		0	0	0		2,180	0
Gabellotto-Fiumebianco-E1	Sea		0	0	0		2,230	0
Mercato	Sea		0	0	0		2,300	0
Mercato	Sea		0	0	0		8,200	0
Astroni 1,2,3	Sea	14C G. ruber	0	3780	70		1,400	0
Agnano Monte Spina	Sea	14C G. ruber	0	4350	70		1,670	0
-	Sea	14C G. bulloides	0	4600	70		1,750	0
Gabellotto-Fiumebianco-E1	Sea	14C G. bulloides	0	7530	80		2,400	0
Capo Palnuro	Sea	14C G. ruber	0	7770	70		2,500	0
Agnano Pomici Principali	Sea	14C G. bulloides	0	9990	90		2,750	0
Neapolitan Yellow Tuff NYT	Sea	14C G. bulloides	0	10430	90		3,100	50
Tuffi Biancastri GM1	Sea	14C N. pachyderma	0	12260	110		3,950	0
Lagno Amendolare	Sea	14C G. bulloides	0	12600	110		4,050	0
Verdoline	Sea	14C G. bulloides	0	12870	100		4,230	0
Pomici di Base	Sea	14C G. bulloides	0	13480	90		4,350	0
Biancavilla	Sea	14C G. bulloides	0	15920	130		5,300	0
?	Sea	Interpolated	0	18280	250		5,950	0
	Sea	14C G. bulloides	0	14650	90	Biancavilla Ignimbrite	4,900	0
	Sea		0	0	0		5,300	0

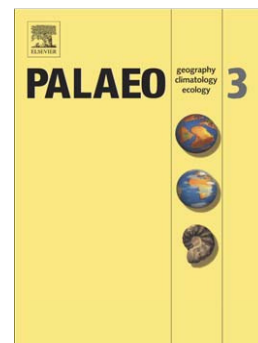
Agnano Monte Spina	Sea	0	0	0	0	1,330	0
Neapolitan Yellow Tuff NYT	Sea	0	0	0	0	5,500	0
Agnano Monte Spina	Sea	0	0	0	0	1,400	0
C-20	Sea	0	0	0	0	7,970	0
C-14 Citara	Sea	0	0	0	0	4,490	0
	Sea	0	0	0	0	3,840	0
	Sea	0	0	0	0	3,640	0
	Sea	0	0	0	0	2,080	0
	Sea	0	0	0	0	0,830	0
	Sea	0	0	0	0	7,100	0
	Sea	0	0	0	0	4,500	0
	Sea	0	0	0	0	6,050	0
	Sea	0	0	0	0	1,500	0
	Sea	0	0	0	0	4,000	0
	Sea	0	0	0	0	2,000	0
	Sea	0	0	0	0	3,530	0
	Sea	0	0	0	0	2,080	0
	Sea	0	0	0	0	1,280	0
	Sea	0	0	0	0	4,200	0
	Sea	0	0	0	0	2,700	0
	Sea	0	0	0	0	2,600	0
	Sea	0	0	0	0	0,700	0
	Sea	0	0	0	0	0,600	0
	Sea	0	0	0	0	3,580	0
	Sea	0	0	0	0	2,660	0
	Sea	0	0	0	0	2,140	0
	Sea	0	0	0	0	0,640	0
	Sea	0	0	0	0	4,020	0
	Sea	0	0	0	0	1,000	0
	Sea	0	0	0	0	0,420	0
	Lake	0	0	0	0	1,870	0
	Lake	0	0	0	0	2,440	0
	Lake	0	0	0	0	5,750	0
	Lake	0	0	0	0	9,410	0
	Sea	1700	0	0	0	0,000	0
	Sea	2550	0	0	0	0,100	0
	Sea	6900	0	0	0	0,600	0
	Sea	12970	0	0	0	1,300	200
	Sea	13900	0	0	0	1,540	0
	Sea	14180	0	0	0	1,700	70
	Sea	14400	0	0	0	1,700	70
	Sea	27600	0	0	0	0,000	0
	Sea	33500	0	0	0	3,000	100
	Sea	35800	0	0	0	3,000	0
	Sea	37800	0	0	0	3,400	0
	Sea	40000	0	0	0	3,630	0
	Sea	41800	0	0	0	3,800	0
	Interpollation						
	Interpollation						
	Interpollation						
	14C						
	Interpollation						
	14C						
	Interpollation						
	14C						
	Interpollation						
	14C or K/Ar						
	Interpollation						
	?						
	?						
	Gabelotto-Fiumebianco-E1						
	Pollara						
	?						
	Biancavilla - Y1						
	?						
	?						
	Codola						
	?						
	?						
	Y-5						
	?						

?	Sea	Interpolation	44800	0	0	Two distinct eruptions with a Eolian origin	4.140	0
?	Sea	Interpolation	50400	0	0	Eolian source.	4.730	0
Barano tuff	Sea	K/Ar	51000	0	2200	Formazione superiore della Scarpinata di Barano, Green Tuff Series of Mount Epomeo k	4.800	0
?	Sea	Interpolation	54700	0	0	Eolian source.	5.540	0
Epomeo tuff	Sea	K/Ar	55400	0	2200	Peraikalic Trachyte, Formazione superiore della Scarpinata di Barano, Green Tuff Series	5.620	0
?	Sea	Interpolation	56800	0	0	Eolian source.	5.920	0
?	Sea	Interpolation	58100	0	0	Eolian source.	6.150	0
?	Sea	Interpolation	59300	0	0	Eolian source.	6.320	0
Y-7	Sea	Interpolation	60300	0	2200	Peraikalic Trachyte, Green Tuff Series of Mount Epomeo Ischia, dans 8004 640cm; 8011	6.520	0
?	Sea	Interpolation	65000	0	0	Eolian origin	6.940	0
?	Sea	Interpolation	65300	0	0	Eolian origin	7.030	0
?	Sea	Interpolation	65600	0	0	Eolian origin	7.100	0
?	Sea	Interpolation	67200	0	0	Two distinct eruptions with a Eolian origin	7.540	0
?	Sea	Interpolation	67500	0	0	? dans KET 8004	7.610	0
?	Sea	Interpolation	76800	0	0	Eolian origin	8.550	0
?	Sea	Interpolation	77100	0	0	Eolian origin	8.600	0
?	Sea	Interpolation	5700	0	0	Two distinct eruptions with Campanian source, Trachytic and Peraikalic trachyte	0.100	0
?	Sea	Interpolation	7000	0	0	C0, Peraikalic trachyte	0.400	0
?	Sea	Interpolation	8400	0	0	CF origin?	0.600	0
?	Sea	Interpolation	8900	0	0		0.700	0
?	Sea	Interpolation	9780	0	0		0.850	0
?	Sea	Interpolation	11900	0	0	Peraikalic Trachyte	1.100	0
?	Sea	14C or K/Ar	12300	0	0	C2	1.150	0
?	Sea	Interpolation	13200	0	0		1.250	0
?	Sea	Interpolation	13900	0	0		1.420	0
?	Sea	Interpolation	14400	0	0	C3 Peraikalic trachyte dans 8003 170cm et 8011 118,5cm	1.500	0
?	Sea	14C or K/Ar	19620	0	0	Peraikalic Trachyte and Trachytic dans 8011 170cm	2.070	0
?	Sea	Interpolation	24100	0	0		2.420	0
?	Sea	Interpolation	26400	0	0	Peraikalic Trachyte	2.600	0
?	Sea	Interpolation	26900	0	0	dans 8011 204cm et 8218 310cm	2.740	0
Y-3	Sea	14C or K/Ar	33500	0	0	attention, cf Zanchetta et al., 2008 and Ton-That et al., 2001 // dans 8003 300cm; 8011 2:	3.200	0
Codola	Sea	Interpolation	33700	0	0	Peraikalic Trachyte and Trachytic	3.320	0
?	Sea	Interpolation	35200	0	0	Chira-Cigliio-Serrara formation attention described like C-13, that is recently Y5	3.500	0
?	Sea	Interpolation	36000	0	0	dans 8011 287cm	3.580	0
?	Sea	Interpolation	36600	0	0	Chira-Cigliio-Serrara formation, attention described like C-13, that is recently Y5, Peraikalic	3.700	0
?	Sea	Interpolation	38700	0	0	Y-3 or Y-5??	4.060	0
Y-5	Sea	14C or K/Ar	40000	0	0	dans 8003 363cm; 8011 335cm; 8022 320cm; 8218 485cm.	4.450	0
?	Sea	Interpolation	40500	0	0	Peraikalic Trachyte	4.600	0
?	Sea	Interpolation	41800	0	0	Peraikalic Trachyte and Trachytic, dans 8003 380cm; 8011 335cm; 8218 510cm.	4.700	0
?	Sea	Interpolation	46700	0	0	Peraikalic Trachyte, End of Green Tuff Series, dans 8011 357cm.	5.150	0
Barano tuff	Sea	14C or K/Ar	51000	0	0	Formazione superiore della Scarpinata di Barano, Green Tuff Series of Mount Epomeo k	5.600	0
Epomeo tuff	Sea	14C or K/Ar	55400	0	0	Peraikalic Trachyte, Formazione superiore della Scarpinata di Barano, Green Tuff Series	5.900	0

Neapolitan Yellow Tuff NYT

Annexe 7:**Lake Ohrid, Albania, provides an exceptional multi-proxy record of environmental changes during the last glacial-interglacial cycle**

A.-M. Lézine, U. von Grafenstein, N. Andersen, S. Belmecheri, A. Bordon, B. Caron, J.-P. Cazet, H. Erlenkeuser, E. Fouache, C. Grenier, P. Huntsman-Mapila, D. Hureau-Mazaudier, D. Manelli, A. Mazaud, C. Robert, R. Sulpizio, J.-J. Tiercelin, G. Zanchetta, Z. Zeqollari



PII: S0031-0182(10)00017-9
DOI: doi: [10.1016/j.palaeo.2010.01.016](https://doi.org/10.1016/j.palaeo.2010.01.016)
Reference: PALAEO 5240

To appear in: *Palaeogeography*

Received date: 28 July 2009
Revised date: 8 January 2010
Accepted date: 11 January 2010

Please cite this article as: Lézine, A.-M., von Grafenstein, U., Andersen, N., Belmecheri, S., Bordon, A., Caron, B., Cazet, J.-P., Erlenkeuser, H., Fouache, E., Grenier, C., Huntsman-Mapila, P., Hureau-Mazaudier, D., Manelli, D., Mazaud, A., Robert, C., Sulpizio, R., Tiercelin, J.-J., Zanchetta, G., Zeqollari, Z., Lake Ohrid, Albania, provides an exceptional multi-proxy record of environmental changes during the last glacial-interglacial cycle, *Palaeogeography* (2010), doi: [10.1016/j.palaeo.2010.01.016](https://doi.org/10.1016/j.palaeo.2010.01.016)

This is a PDF file of an unedited manuscript that has been accepted for publication. As a service to our customers we are providing this early version of the manuscript. The manuscript will undergo copyediting, typesetting, and review of the resulting proof before it is published in its final form. Please note that during the production process errors may be discovered which could affect the content, and all legal disclaimers that apply to the journal pertain.

Lake Ohrid, Albania, provides an exceptional multi-proxy record of environmental changes during the last glacial-interglacial cycle.

A.-M. Lézine¹, U. von Grafenstein¹, N. Andersen², S. Belmecheri¹, A. Bordon¹, B. Caron³, J.P. Cazet¹, H. Erlenkeuser², E. Fouache⁴, C. Grenier¹, P. Huntsman-Mapila⁵, D. Hureau-Mazaudier⁶, D. Manelli⁷, A. Mazaud¹, C. Robert⁸, R. Sulpizio⁹, J.-J. Tiercelin¹⁰, G. Zanchetta³, Z. Zeqollari⁷

¹ Laboratoire des Sciences du Climat et de l'Environnement, CNRS, CEA, UVSQ-Orme des Merisiers bâtiment 701, 91191 Gif-Sur-Yvette cedex, France

² Leibniz-Laboratory for Radiometric Dating and Stable Isotope Research, 24118 Kiel, Germany

³ Dipartimento di Scienze della Terra, University of Pisa, via S. Maria 53, 56126, Pisa, Italy .

⁴ Université de Paris 12, EA 435 Géonat, UMR 8591 CNRS/Paris 1, 61 Avenue du Général de Gaulle 94010 Créteil cedex, France.

⁵ Harry Oppenheimer Okavango Research Centre, University of Botswana, P/Bag 285, Maun, Botswana

⁶ IUEM, Université de Bretagne occidentale de Brest, Technopôle Brest Iroise, Place Copernic, 29280 Plouzane, France

⁷ Geological Survey, Pogradec, Albania

⁸ CEREGE, Europôle méditerranéen de l'Arbois, BP 80, 13545 Aix-en-Provence cedex 4, France

⁹ CIRISIVU Dipartimento Geomineralogico, University of Bari, via Orabona 4, 70125, Bari, Italy

¹⁰ Géosciences Rennes, Université Rennes 1, bat. 15 - campus de Beaulieu, 263 Avenue du général Leclerc, BP 74205, 35042 Rennes Cedex, France.

Abstract

Multi-proxy analyses on core JO2004-1 recovered from Lake Ohrid (40°55.000N, 20°40.297E, 705 m a.s.l.) provide the first environmental and climate reconstruction in a mountainous area in Southern Europe over the last 140, 000 years. The response of both lacustrine and terrestrial environments to climate change has been amplified by the peculiar geomorphological and hydrological setting, with a steep altitudinal gradient in the catchment and a karstic system feeding the lake. The karstic system was active during interglacials, leading to high carbonate production in the lake, and blocked during glacials as a result of extremely cold climate conditions with permafrost in the mountains. At the Riss-Eemian transition (Termination 2) the increase in lacustrine productivity predated forest expansion by about 10,000 years. In contrast, the Late Glacial-Holocene transition (Termination 1) was characterized by the dramatic impact of the Younger Dryas, which initially prevented interglacial carbonate production and delayed its maximum until the mid-Holocene. In contrast, forest expansion was progressive, starting as early as ca. 38,000 ago. The proximity of high mountains and the probable moderating lake effect on local climate conditions promoted forest expansion, and contributed to make the surroundings of Lake Ohrid favourable to forest refugia during the last glacial, usually steppic, period. Our study of sedimentology, mineralogy, geochemistry, magnetism, palynology and isotopes illustrates the non-linear response of terrestrial and lacustrine ecosystems to similar climate events, and demonstrates the potential of Lake Ohrid as an excellent paleoclimatic archive during the Quaternary.

Keywords

Ohrid, Albania, Last Climatic Cycle, multi-proxy approach, palaeoenvironments

1. Introduction

Lake Ohrid, Albania, is an exceptional site for reconstruction of regional climate history over repeated glacial-interglacial fluctuations and its impact on terrestrial and lacustrine ecosystems. Not only the largest southern-European freshwater body (358 km², 289 m depth), it is likely the oldest in Europe and is renowned for a high level of endemism, with at least 200 lacustrine species described (Stankovic, 1960). The exceptional thickness of sedimentary deposits (Dumurdzanov et al., 2005) makes it directly comparable to the Mediterranean lowland site of Tenaghi Philippon in NE Greece which provides a continuous 1.35-million-year pollen record (Tzedakis et al., 2006). Its location at middle altitudes in a rift basin surrounded by high escarpments, within a key area at the confluence of central-European and Mediterranean climatic influences, provides a unique opportunity to study the impact of climate changes on middle-to high-altitude forest ecosystems. Particularly, Lake Ohrid is on exceptional location which allows testing of the “glacial refugia” hypothesis for southern Europe bordering the Mediterranean (e.g., Denèfle et al., 2000; Tzedakis et al., 2002a). Previous studies of the Lake Ohrid sediment record focussed on paleolimnological and sedimentological aspects during a 40,000 years period (Roelofs and Kilham, 1983; Wagner et al., 2008a; 2008b). Here we present for the first time a record of environmental and climate change over the last 140,000 years. Attention is paid to selected proxies to discuss the influence of climate change on the karstic system and lake hydrology, as well as on regional vegetation response to glacial-interglacial variations.

2. Modern Setting

Lake Ohrid lies in a strongly asymmetric, N-S oriented half-graben at the Macedonia-Albania border. It is bounded by faults running N to NNE which affect, to the north and east, carbonate rocks of Triassic and Jurassic age, and ophiolitic rocks of Jurassic age to the southwest (Figure 1). The southern end of the basin connects with a small graben filled by Pliocene continental mudstones and sandstones, overlain by fluvio-lacustrine sediments of Holocene age (Nicot and Chardon, 1983). The basin is filled by several hundred meters of sediments deposited since around 8.5 Ma (Dumurdzanov et al., 2005). The modern lake is holomictic. Today roughly half of its water is derived from a number of springs located in the SE part of

the lake, draining a karstic system which, in turn, is fed by water from nearby Lake Prespa and infiltration of rainwater (700 mm/yr on average) in the Galicica mountain range. The remaining water comes from rivers (e.g., the Sateska River to the north) and direct precipitation. A single outlet (the Black Drin River) to the north and significant evaporation (estimated at 1145 mm/yr) complete the water budget (Matzinger et al., 2006). The small size of the Lake Ohrid drainage basin (2600 km²) and its large volume (55.4 km³) lead to a water residence time of about 70 yrs (Matzinger et al., 2006). The catchment area covers a large altitudinal range, from 700 m to more than 2200 m. The mean annual temperature is 11.5°C, with winter temperatures varying from -2.3°C to 6.6°C and summer temperatures from 10.5°C to 22.3°C. Precipitation is principally during winter and spring. As a result of the high topography, the vegetation is distributed in altitudinal belts with mixed deciduous forests including *Carpinus orientalis*, *Quercus trojana*, *Q. frainetto*, *Q. cerris* at lake level, followed by *Fagus moesiaca*, *Abies alba*, *A. borisii-regis* at the upper limit of the forest, and a sub-alpine grassland with *Juniperus excelsa* above 1800 m in the Mali i Thate mountains to the south-east.

3. Material and methods

3.1. Core JO2004-1

Core JO2004-1 consists of two series of core sections (each up to 3 m long) recovered ca. 5 m apart from a single site in the southwestern part of the lake (40°55.000 N, 20°40.297 E, 705 m a.s.l.). The uppermost ca. 10 meters of sediment were recovered in consecutive 3-m long sections using a hammer-driven Niederreiter piston corer of 63 mm diameter. To obtain a continuous sedimentary record four sections were recovered from the first hole (JO2004-1), and three sections with a planned depth offset of 1.5 m from the second hole (JO2004-1a). The overlapping sections were visually cross-correlated using marker layers clearly identified in both sequences, and the resulting composite profile was checked for consistency using the magnetic susceptibility record. The depth information used in the paper refers to a composite linear master depth scale (MCD). In addition to the core sediments, 15 samples taken from a variety of rocks and sediments outcropping in the catchment basin of Lake Ohrid have been studied for mineralogical investigations of the bulk and clay fractions and geochemical analyses.

3.2. Magnetic susceptibility

Core sections were sub-sampled with U-channels at the core repository of the Laboratoire des Sciences du Climat et de l'Environnement (LSCE) at Gif-sur-Yvette (France). The volume low-field susceptibility (κ) was measured at a high resolution. κ is determined by the amount of ferro/ferri magnetic grains, but mineralogical changes and grain size variations may also influence the susceptibility signal. Paramagnetic material (clay) and diamagnetism also contribute to κ when the magnetic grain content is low. Measurements of the low field bulk susceptibility (κ) were performed using a small diameter Bartington sensor loop mounted in line with a track system designed for u-channel.

3.3. Sedimentology, mineralogy and sediment geochemistry

Sediment facies were visually described on bulk samples. In addition, one hundred and ninety samples were analysed for bulk and clay mineral investigations. Each sample was divided into two sub-samples: one sub-sample was crushed in a grinder and pressed into a holder for bulk mineral analyses. The other sub-sample was washed on a 63 μm mesh sieve. The <63 μm fraction was decalcified using a solution of 10% HCl, rinsed with de-ionized water, and deflocculated through repeated centrifugation. The clay fraction (<2 μm) was decanted and deposited onto a glass slide. X-ray diffraction (XRD) analyses were conducted on natural clay slides after ethylene-glycol solvation and heating at 490 °C for 2 h. Determination of percent bulk and clay minerals was based on the respective XRD peak areas, using MacDiff version 3 software (Petschick, 1998); the relative error is ~5%.

Samples subjected to bulk geochemical analyses were processed at UMR 6538 "Domaines Océaniques", IUEM-UBO, Brest, France. Major elements were measured by ICP-AES with an ISA Jobin-Yvon JY 70 Plus apparatus. Calibrations were checked using the GIT-IWG (Groupe International de Travail-International Working Group) BE-N, WS-E, PM-S, AC-E and the CCRMP (Canadian Certified Reference Materials Project) LKSD-1 international standards. Trace element and rare earth element (REE) measurements were conducted by ICP-MS using a Finnigan Element 2 ICP-MS. Results obtained for the CCRMP (Canadian Certified Reference Materials Project) LKSD-1 were reproducible with precisions for trace elements < 5%, except for Zr and Hf which were not used to characterize the samples.

3.4. Dating procedures

3.4.1. Radiocarbon measurements

Seven AMS radiocarbon measurements were performed on terrestrial organic matter and charcoal remains. The ^{14}C activity was determined by UMS-ARTEMIS (Pelletron 3MV) AMS Facilities. Raw ^{14}C dates were converted to calibrated ages using CALIB 5 (Stuiver et al., 2005) except for the oldest radiocarbon age, for which polynomial equations (Bard, 1998) have been used.

3.4.2. Tephrochronology

For tephrochronology, the core was continuously screened at 1-cm intervals for volcanic particles (glass shards, magmatic crystals, volcanic lithics). The sediment was washed and sieved at 125 μm and 40 μm using distilled water. The sediment fraction less than 40 μm was collected using a paper filter and progressively dried through a water pump. The sediment fraction 40-125 μm was carefully inspected under stereo microscope. Chemical analyses on glass shards from tephra were performed at the Dipartimento di Scienze della Terra (University of Pisa), using an EDAX-DX micro-analyser (EDS analyses) mounted on a Philips SEM 515 (operating conditions: 20 kV acceleration voltage, 100s live time counting, 10^{-9} A beam current, ZAF correction). Instrument calibration and performance are described in Marianelli and Sbrana (1998). The major-element chemistry of crystal-free glass shards were used to classify the individual tephra layers and correlate them to different archives. SEM back-scattering images were used to describe the texture of the ground mass and to select micro-crystals for micro-analyses.

3.5. Pollen analysis

One hundred and fifty five samples were taken at 1 to 15-cm intervals for pollen analyses. Samples were processed using the standard HF method (Faegri and Iversen, 1989) and sieved on a 5- μm mesh. Addition of a known amount of exotic makers (*Lycopodium*) allowed calculation of pollen concentrations (grains per cm^3 of dry sediment) and influx values (grains per cm^2 per year). In total 110 different pollen types were identified for a mean pollen sum of 450 grains per sample (maximum count = 1480 grains). Pollen data are expressed as percentages calculated against a sum of all the determined pollen types except aquatics, spores (bryophytes and ferns) and damaged grains. Pollen grains were determined using regional pollen atlases from Europe and the Mediterranean (Reille, 1992; Chester and

Raine, 2001).

3.6. Ostracod isotope studies

Ostracod shells were extracted from 1-cm sediment slices taken at 5-cm intervals throughout the core, with the exception of a few continuously sampled sections at major lithostratigraphic transitions (Belmecheri et al, 2009). For sample preparation, the sediment was disaggregated with H₂O₂ and gently wet-sieved. The >125µm fraction was washed with ethanol and dried at room temperature. Ostracod shells were extracted and cleaned. Ostracod species identification follows Klie (1939a and b; 1942) and Mikulić (1961). The stable-isotope composition of the shells was analyzed at the Leibniz Laboratory in Kiel using a Finnigan MAT 251 mass spectrometer equipped with an automatic carbo-Kiel CO₂ preparation device. Isotope ratios are given relative to the PDB standard in the usual notation with a total accuracy on the order of 0.05 ‰ and 0.08 ‰ for δ¹³C and δ¹⁸O, respectively.

4. Data (Figure 2)

4.1. The sedimentary record

4.1.1. The present-day catchment basin of Lake Ohrid

Mineralogical investigations of the bulk and clay fractions have been conducted on a variety of rocks and sediments outcropping in the catchment basin of Lake Ohrid (Table 1). Lizardite and clinocllore are the main constituents of the ophiolites, which weather primarily into smectite. The bulk composition of molasse deposits, Neogene and Quaternary sediments are largely dominated by quartz, associated with feldspars, clay minerals and, locally, a proportion of ophiolite minerals (lizardite and clinocllore). Clay minerals include irregular mixed-layers of illite-smectite and chlorite-smectite types, illite, smectite and kaolinite. However, the relative proportions of the minerals vary strongly according to the nature of the substrates in the different parts of the drainage basin. In addition, irregular mixed-layered clays of illite-smectite type contain a high proportion of illite layers and probably reflect subsequent weathering of illite in the porous terrigenous sediments. The carbonates that outcrop in the drainage basin consist of calcite but do not contain other types of minerals and are not weathered into clay minerals. It is remarkable that calcite is absent or occurs in very minor abundances of less than 5% in molasse deposits and other terrigenous sediments of Pliocene and Quaternary age.

Geochemically, the ophiolitic formations are dominated by SiO₂ and MgO, with minor amounts of Fe₂O₃, CaO and Al₂O₃. The Triassic-Jurassic carbonates are purely formed by Mg-calcite (56 wt% CaO and 0,45 wt% Mg), and the continental mudstones and sandstones of Pliocene age at the southern end of the Ohrid basin are characterized by Al₂O₃ and CaO, with minor quantities of Fe₂O₃ and K₂O.

4.1.2. Core JO2004-1

The sediment series generally includes calcareous and siliciclastic elements. Calcareous elements occur principally in the form of clay-sized to sand-sized aggregates and biogenic remains (ostracods), which are especially abundant from the top of the core to 75cm (calcareous clay and sand to calcareous mud) and from 470 to 924 cm (calcareous clay to sandy calcareous mud). Siliciclastic elements are especially abundant from 75 to 470 cm (clay, silty clay and sand) and from 924 cm to the bottom of the core (silty clay). Sandy intervals at 188 cm and 240-246 cm are conspicuous tephra layers. The sediment color ranges from beige to grey, the darkest colors being associated with occurrences of organic remains, principally plant debris.

Mineralogical assemblages of the core's bulk sediment are dominated by quartz and calcite. Quartz is associated with smaller proportions of feldspars and clay minerals. Similar, quartz dominated mineralogical assemblages are also found in alluvial deposits and other Neogene and Quaternary sediments of the region. Mineral particles are typically terrigenous and originate from erosion from the adjacent drainage basin by running waters. However, feldspars significantly increase at several intervals, where they may result from in-situ alteration of tephra layers. Other terrigenous elements include pyroxenes and ophiolite minerals (principally lizardite and clinocllore), derived from ophiolitic formations which largely outcrop in the drainage basin. When present, calcite may represent up to 90% of the bulk sediment. Calcite occurs as biogenic elements (ostracods principally) or silt-sized to clay-sized aggregates.

Clay mineral assemblages are dominated by illite, which occurs in significant amounts in alluvial deposits and other terrigenous sediments of the drainage basin. In both cases, illite is associated to variable percentages of chlorite, kaolinite, and random mixed-layered clays. The association of minerals derived from poorly weathered substrates (illite, chlorite, random mixed-layered clays) and from areas of intense chemical weathering (kaolinite) probably

results from intense erosion of soils and substrates in adjacent mountain areas by run-off. It is noteworthy that maximum abundances of illite and associated minerals coincide with occurrences of calcite. Maximum abundances in illite and chlorite alternate with intervals of abundant smectite. In the modern world, abundant smectite is often found in warm areas of seasonal precipitation (Chamley, 1989; Weaver, 1989). Its formation is strongly enhanced on mafic substrates, and small proportions of the mineral have even been described in the weathering profiles of basaltic substrates of cold areas, for example in modern West Antarctica (Campbell and Claridge, 1982). Ophiolite outcrops of the drainage basin of lake Ohrid have shown to weather into smectite. Maximum abundances of smectite coincide with maximum contents of clay minerals and quartz in the bulk sediment, indicating significant development of weathering and erosion in the catchment.

4.2. Datations

4.2.1. Radiocarbon measurements

Radiocarbon measurements (Table 2) from the uppermost part of the core are in chronological order from 8275 ± 40 (100,5 cm) to 1285 ± 30 ¹⁴C yr BP (20.5 cm). However, it was impossible to obtain sufficient organic matter for reliable dating below 100,5cm. The age of $39,100 \pm 1200$ ¹⁴C yr BP (307,6 cm) is therefore only indicative.

4.2.2. Tephra

Volcanic material was recognised at 188, 240-246, 575-576 cm and 939-941 cm (Table 3). Two of these tephra layers (at 188 cm and 240-246 cm) were visible as discrete sandy-silty layers, whereas the other two are crypto-tephra (575-576 cm and 939-941 cm) mixed with lake and clastic sediments. A detailed description of the tephra layers of the studied core sequence and in-depth discussion of their correlation and origin can be found in Caron et al. (submitted). The chemical composition of glass shards and micro-pumice fragments permitted the correlation of Lake Ohrid samples to other tephra layers already recognised in the Mediterranean basin: the tephra layer at 188 cm has been correlated with the Y3 tephra layer dated at $30,670 \pm 230$ yr BP (Keller et al., 1978, Zanchetta et al., 2008). The base of the tephra at 240-246 cm has been correlated with the Y5/Campanian Ignimbrite tephra layer, widely recognised in the central-eastern Mediterranean and Eastern Europe mainland (Keller et al., 1978; Pyle et al., 2006; Giaccio et al., 2008; Aksu et al., 2008;

Calanchi and Dinelli, 2008) and dated to $39,280 \pm 110$ yr BP (De Vivo et al., 2001). The crypto-tephra material at 575-576 cm depth is correlated with the X6 tephra layer (Keller et al., 1978) on the basis of the good compositional match with analyses from Lago Grande di Monticchio (Wulf et al., 2006) and the C-31 marine tephra layer (Brauer et al., 2007; Paterne et al., 2008) (Figure 3). The $^{40}\text{Ar}/^{39}\text{Ar}$ age of $107,000 \pm 2000$ yr BP for the X-6 tephra (Keller et al., 1978) is in good agreement with the suggested age of 108,430 yr BP obtained from the varve-supported Monticchio chronology and with the suggested age of C-31 tephra layer at 107,000 yr BP (Paterne et al., 2008). The volcanic fragments of the crypto-tephra at 939-941 cm depth are a Pantellerite (Civetta et al., 1984; Civetta et al., 1988). In marine cores from the Mediterranean (Paterne et al., 2008), two tephra layers match the lithology and composition of this tephra layer, namely P11 (131,000 yr BP) and P12 (164,000 yr BP). Both tephra layers originate from Pantelleria Island, and correspond to the Ignimbrite P (dated at $133,100 \pm 3300$ yr BP) and to the Welded Tuff S (dated at ca. 163,000 yr BP), respectively (Mahood and Hildreth, 1986). Stratigraphic considerations support correlation of the 943-941 cm Ohrid tephra with the P11 marine tephra layer, and thus with Ignimbrite P deposits on Pantelleria. The tephra at 943-941 cm is located within the rising calcite content and increasing arboreal pollen values which unequivocally indicate that this tephra was deposited close to the inception of the Last Interglacial. Although the onset of the Last Interglacial may have been recorded at different times in different archives (e.g., Sánchez Gõni et al., 2005), a putative age of 164,000 yr BP (which correspond to P12 tephra layer) is several ten of thousands of years too old for the inception of the Last Interglacial around the Mediterranean (e.g. Sánchez Gõni et al., 1999; 2005).

4.3. Pollen

The Ohrid pollen record shows the classical opposition between Arboreal Pollen (AP) and Non Arboreal Pollen (NAP) percentages throughout the last climatic cycle (Bordon, 2009). AP pollen dominate with percentages higher than 80% between 879 and 597 cm, 566 and 537 cm, at 477 cm, and then from 100.5 cm to the top of the sequence. A minor peak of 77 % is recorded between 335 and 280 cm. Trees and shrubs are mainly *Pinus* (maximum = 73%), *Abies* (54%), *Quercus robur* (36%), *Carpinus* (14%), *Juniperus* (13%), *Quercus ilex* (12%), *Hippophae rhamnoides* (8.6%), *Tilia* (7.7%), *Fagus* (7%), *Betula* (4.6%), *Olea* (3%) and *Corylus* (1.7%) recording distinct influences from Mediterranean and temperate middle-

and high-elevation forests. Three pollen types of steppic origin dominate the herbaceous plant communities (*Artemisia*, *Poaceae* and *Chenopodiaceae*) with maximum percentages of 46% (228 cm), 30% (213 cm) and 15% (516.9 cm), respectively.

In detail, changes in forest vegetation record the spread of *Pinus* and *Quercus robur*, associated, to a lesser extent, with *Quercus ilex* and *Tilia* during the first phase of forest expansion (878.9-791 cm). These taxa strongly decline (*Pinus*, *Q. robur*, *Q. ilex*) or disappear (*Tilia*) to the benefit of *Abies* which massively expands (791-596.9 cm), in association with *Carpinus* (peak reached at 737.9 cm) then with *Picea* (peak reached at 666.9 cm). *Abies* and *Pinus* strongly increase during the following forest phases at levels centred at 556.9 cm and 476.9 cm, then between 125.5-50.5 cm in association with *Q. robur*. The forest phase recorded between 329.6 and 279.6 cm displays a slightly different pattern with *Pinus* dominating the pollen assemblage and *Q. robur*, *Picea* and *Abies* reaching 10% or less, only.

4.4. Ostracods

The lowermost part of the core, from the base to 940 cm, is devoid of ostracod valves. At 940 cm the ostracod valves appear and reach a maximum of high species diversity at 880 cm. Ostracod valves are well preserved and taxonomically diversified during the whole the interval from 940 cm to 470 cm. No ostracod valves are found during the following interval from 470 cm to 120 cm, apart from some broken valves found in a short 10-cm-thick interval between 320 cm and 340 cm. At 120 cm, we record the re-occurrence of the ostracod valves which are present until the top of the core.

The mean candonid species $\delta^{13}\text{C}$ record starts with values around 0.5 ‰ at 940 cm followed by an increasing trend which continues until 890 cm reaching a maximum of 2 ‰. After 890 cm, $\delta^{13}\text{C}$ decreases rapidly to -0.5 ‰ and drop to a minimum of -2 ‰ around 780 cm. The period between 750 cm and 550 cm is marked by two consecutive positive excursions, with a first maximum of 2 ‰ at 570cm and a second maximum of 0.5 ‰ at 550.5 cm. The period after the hiatus is marked by a single positive excursion starting with -1 ‰ at 530 cm, increasing to 1.2 ‰ between 520 cm and 490 cm to end with -1 ‰ just after 480 cm. The candonid valve fragments found in the short 10-cm interval at 340 cm show high $\delta^{13}\text{C}$ values around 1 ‰ close to the values before 890 cm and the positive excursion around 750 cm and 550.5 cm.

In the upper most part of the record, $\delta^{13}\text{C}$ values of the candonid valves start with

moderately low values between 0 ‰ and -1 ‰ at 110 cm. However, during this period ostracod mean $\delta^{13}\text{C}$ values scatter around -0.5 ‰, interrupted by a very short excursion to very low $\delta^{13}\text{C}$ values below -3 ‰ around 70 cm.

5. Environmental reconstruction

5.1. A sedimentological record controlled by a karstic system

The most striking characteristic of the Lake Ohrid sediment sequence is the strong variation in calcite, which dominates from 870 to 590 cm and from 80 to 0 cm, and is absent from other intervals (Figure 2). When present, calcite may represent up to 90% of the bulk sediment. Besides biogenic remains such as ostracod shells (not exceeding more than 0.1% of the sample mass), calcite principally occurs as angular to sub-angular, generally silt-sized particles. Calcite is either absent, or only occurs as trace amounts of less than 5%, in alluvial and molasse sediments that outcrop in the adjacent drainage basin. In addition, sandy intervals of the core which may indicate some degree of reworking from shallower, nearshore areas of the lake which are closer to limestone outcrops, generally contain smaller proportions of calcite than adjacent silt and clay sediments. Therefore, we consider the contribution of terrigenous calcite as limited. Calcite aggregates of similar morphology have been described in modern low salinity to fresh water environments of temperate and tropical latitudes (Stabel, 1986; Talbot and Allen, 1996) saturated in CO_3^{2-} (Eugster and Kelts, 1983) where they are considered of authigenic origin. Similar calcite aggregates also characterize Holocene paleolake deposits of Yemen where matching carbon isotope distribution in bivalve shells and bulk sediment suggest coeval, in-situ formation of biogenic and abiotic calcite (Lézine et al, 1978). Based on identical mineralogy, morphology, and occurrence of the latter calcite aggregates, we consider calcite particles in Lake Ohrid sediments to be of predominantly authigenic origin. Limestone outcrops in the drainage basin of Lake Ohrid are probably dissolved by rain water and soil acids. Calcium and carbonate ions are transported to the lake by run-off and via the karst aquifer. There, carbonate/bicarbonate reactions and photosynthesis progressively decrease the availability of free hydrogen ions and raise the pH. Dissolved carbonate and calcium ions are used by aquatic biota (ostracodes, molluscs) to build their mineral parts, or precipitate directly in the epilimnion when at high concentrations, for example during spring and summer algae blooms. At long time scales, calcite formation may either occur during intervals of high precipitation when transport of dissolved calcium

and carbonate ions to the lake increase; high evaporation, which increases their concentration in the water; and/or elevated temperature, which lowers the saturation threshold for calcite. These conditions most likely occur during interglacials. Conversely, calcite deposition is hampered under dry/cold climatic conditions due to decreased influence of running waters and the cessation of the karstic flow. In addition, cold conditions increase the capacity of lake waters to absorb carbon dioxide and reduce photosynthesis. This in turn fosters the concentration of hydrogen ions and decreases the pH of the lake waters. Such conditions likely correspond to glacial intervals.

In the absence of dilution by calcite particles, siliciclastics dominate during cold/dry intervals. Siliciclastic assemblages are diversified. They include typically terrigenous elements such as quartz, feldspars, clay minerals (mainly illite, associated with variable percentages of chlorite, kaolinite, random mixed-layered clays and smectite), pyroxenes, and ophiolite minerals (lizardite and clinochlore). Lacustrine siliciclastic assemblages are very similar in composition to those found in molasse and alluvial deposits, suggesting that they are derived from the erosion of the catchment basin by running waters. The presence of clay minerals of diverse origins indicates concomitant erosion of soils, sediments, and substrates. It is remarkable that maximum abundances in illite and chlorite coincide with intervals of highest calcite contents, indicating that strong precipitation also favoured an intense erosion of poorly weathered substrates in the drainage basin of the lake. Intervals of increased smectite contents (which coincide with low calcite and high quartz contents) suggest that dry/cold climatic conditions nevertheless allowed some degree of chemical weathering of the ophiolitic substrates. Such a transient interval of chemical weathering with smectite formation and erosion, is recognized around 490-530cm. However, climate improvement (in terms of precipitation and/or temperature) was insufficient during this interval to allow an extensive precipitation of authigenic calcite in the lake.

5.2. A complex chronological framework

The age model (see discussion in Belmecheri et al., 2009) (Figure 4) shows that the Ohrid sequence extends back to about 140,000 yr BP. It fits remarkably well with the orbitally-tuned environmental history of southern Europe (Tzedakis, 2005; Sirocko et al., 2007; Sanchez-Goni, 2007) (Figure 5) from terrestrial pollen records in Greece (e.g., Tenaghi Philippon) and marine isotope records along the southern European margin (e.g., ODP 980).

It also fits with the chronology of pollen events at Monticchio in Italy (Brauer et al., 2007) (Figure 6). According to this, the Eemian interglacial started at 127,000 yr BP and lasted roughly 17,000 yr which corroborates earlier estimations in southern Europe (Tzedakis et al. 2002b; Brauer et al., 2007; Brewer et al., 2008).

A major hiatus of roughly 12,000 years corresponds to a large part of the St. Germain I period. The stratigraphical and chronological position of this hiatus is confirmed by the absence in our record of tephra layer X5, dated at 105,000 \pm 2000 yr BP (Keller et al., 1978; Kraml, 1998; Wulf et al., 2004; Di Vito et al., 2008; Paterne et al., 2008). This tephra has been found in marine sediments from the Ionian Sea (Paterne et al., 2008) and in the lower part of the St. Germain I period at Monticchio (Brauer et al., 2007). Dating uncertainties remain for the Melisey 2 interstadial, which is dated to ca. 87,000 yr BP at Ohrid and ca. 89,000 yr BP at Monticchio. The phase of forest expansion within the last glacial period, which is dated to around 50-45,000 yr ago at Ohrid, closely corresponds to a warm event recorded in speleothem data from Villars in Southern France (Genty et al., 2003; 2005). This likely corresponds to the forest phase dated slightly earlier at Monticchio (Brauer et al., 2007), Ioannina (Tzedakis et al., 2002a), and Kopais (Okuda et al., 2001). At Villars, this event has been correlated with Dansgaard-Oeschger event 12 with exceptionally high speleothem growth rate and very low $\delta^{13}\text{C}$ values (as low as -11‰) attributed to dense vegetation growth. Based on 12 TIMS U-series dates, the optimum recorded by $\delta^{13}\text{C}$ values is dated to 45,300 \pm 400 cal yr BP. The climate improvement responsible for forest expansion at Ohrid at that time is also reflected in the temporary increase of dissolved calcium concentrations that can be inferred from the discrete occurrence of good ostracode preservation (Fig.4). It was however not sufficient to significantly revive the formation of authigenic calcite.

5.3. Regional environmental changes

Our multi-proxy record suggests that in response to an improvement of climate conditions, Lake Ohrid switched from a less to more productive ecosystem as early as 136,000 cal yr BP. The predominance of steppic herbaceous pollen types (mainly *Artemisia* and *Chenopodiaceae*) before that time indicates that steppe vegetation had dominated the immediate surroundings of the lake under a climate characterized by strong seasonal moisture deficiency. Marked seasonality in precipitation and runoff was responsible for the erosion of

regional substrates (abundant illite, chlorite, SiO₂ and Al₂O₃) as well as the development and removal of ophiolitic weathering profiles (smectite). From 136,000 to 127,000 yr BP a first prominent increase in calcite reflects the intensification of regional karst activity. The concomitant decrease in steppic vegetation elements, with mesic trees and smectite increase, suggests that climate conditions became progressively warmer and wetter. However, soils were still poorly developed as indicated by the relatively high values of $\delta^{13}\text{C}$ in ostracode calcite. At 128,000 yr BP, a slight decrease in total arboreal pollen percentages together with an abrupt positive shift in ostracod $\delta^{13}\text{C}$ of more than 1‰ and a plateau in calcite content suggest a short episode of climate deterioration interrupting the long-term warming trend. This pattern of environmental change has been recorded in several other climate-proxy records from southern Europe (e.g., Tzedakis et al., 2002a; Brauer et al., 2007; Gouzy et al., 2004). An abrupt, simultaneous shift in most proxies at 127,000 yr BP marks the true beginning of the Last Interglacial period. The episode between 126,000 and 122,000 yr BP is characterized by increased calcite precipitation within the lake as recorded by peak CaCO₃ content (>85%) and the large positive excursion of Sr/Ti. At that same time, Mediterranean trees expanded at the altitude of Lake Ohrid whereas cold steppes disappeared. Mesic forests developed on the adjacent slopes and conifer forest at higher altitude. This indicates that this period was unambiguously the warmest of the entire last interglacial. According to our data the thermal maximum was reached around 124,700 yr BP when Mediterranean vegetation elements widely expanding in southern European lowlands (e.g., Rousseau et al., 2006) reached the Lake Ohrid area at 800 m altitude. The end of this climatic optimum at 122,000 yr BP is marked by a dramatic shift in forest composition. Temperate and Mediterranean forest trees declined, whereas *Carpinus*- and *Abies*-dominated mixed forests, then *Abies*- and *Picea*-dominated conifer forests widely expanded with *Abies* proportion higher than those recorded anywhere in southern Europe (e.g., Reille et al., 2000; Tzedakis et al., 2002a; Pini et al., 2009; Allen and Huntley 2009), indicating the incursion of mountain environments into the lake basin and a progressive cooling. This is supported by the decreasing trend of calcite and increasing trend of detrital quartz during this interval. However, remarkably stable ostracode $\delta^{13}\text{C}$ values around -2‰ throughout the period 127,000-110,000 yr BP indicate that tree cover and related soil stability in this mountain environment were not affected by climate variations within the Last Interglacial.

Calcite minima and significant expansion of herbaceous steppic plant types at the

expense of forest signal significant regional climate deterioration from 110,000 to 107,000 yr BP and around 87,000 yr BP, i.e. coeval with the Melisey 1 and 2 stadials, respectively. The cold climate conditions during stadials were responsible for poor soil development and enhanced erosion as recorded by the ostracod-isotope and mineralogical records. The Saint Germain 1 and 2 interstadials are only partly recorded in Core JO2004-1 (Figure 6). Although all proxies record climate improvement around 106,000 and 82,000 yr BP, continued predominance of conifers at the expense of mesic trees in regional forests, and lower calcite content compared to that attained during the Last Interglacial suggest less favourable climate conditions and lower winter temperatures. This differs from what is observed at Ioannina (470 m altitude) in Northern Greece (Tzedakis et al., 2002a) where the two interstadials appear to have been remarkably similar in vegetation and climate conditions.

The abrupt fall in calcite content at the end of Saint Germain 2 (around 79,000 yr BP) shows that a lower temperature threshold was crossed, leading to at least seasonally frozen soil conditions at the elevation of the lake and probably permafrost in a large part of the mountain system. This is supported by the occurrence of periglacial landforms observed near the top of the Galicica mountain range (Belmecheri et al., 2009). Cold-tolerant trees such as *Juniperus* and *Betula* expanded together with steppic herbaceous plant types, similar to what occurred widely in southern Europe during the last glacial period (e.g., Allen et al., 1999; Allen and Huntley, 2009). However, the continuous presence of deciduous trees (albeit in low percentages) suggests that the forest refugia for mesic trees present at lower elevation at Ioannina (Tzedakis et al., 2002a) and in the nearby Maliq Basin (Denèfle et al., 2000) expanded up to 700-800 m in altitude to the shores of lake Ohrid. The moderating lake effect on regional climatic conditions probably favored their development at middle altitudes in southern Albania. High-amplitude variation in the mineralogical composition of Ohrid sediments deposited between 50,000 and 18,000 cal yr BP indicate unstable environmental conditions during the glacial period. For example, alternating maxima of illite and smectite in the clay-mineral assemblages suggest variable erosion and weathering rates due to fluctuation of precipitation and/or temperature, with illite maxima corresponding to intervals of enhanced precipitation and erosion.

The presence of refugia for mesic trees originating from the forest phase developed around 50-45,000 yr likely explain the surprisingly progressive last glacial-interglacial

transition (Termination I) observed at Ohrid and Ioannina (Tzedakis, 2005) with mesic tree pollen types increasing regularly from 38,000 BP to the Holocene (8800 cal yr BP). Authigenic calcite precipitation started to increase only at 17,000 cal yr BP, illustrating the delayed response of the lacustrine system to late-glacial warming. The increase of calcite was interrupted during the Younger Dryas, and then restarted from ca. 11,000 cal yr BP to reach a maximum at 6000 cal yr BP. This rising trend was interrupted by an abrupt event of forest degradation probably coeval with the “8.2 kyr” cold event already recorded at Maliq (Bordon et al., 2009), corresponding to a -2°C cooling of annual temperature compared to mean Holocene values.

6. Concluding remarks

The most prominent feature in the recorded history of Lake Ohrid is the contrast between the responses of lacustrine and terrestrial environments to climate change throughout the last climatic cycle. Abrupt hydrological changes were controlled by the karstic system, which was active during interglacials and completely blocked during glacials in response to drastic deterioration of climate conditions. The abundance and strontium content of authigenic calcite and the $\delta^{13}\text{C}$ of ostracod calcite appear to be sensitive proxies of temperature change during interglacials and help to detect and characterize the main fluctuations of climate within the interglacials and at the glacial-interglacial transitions. In contrast, the terrestrial environment recorded a more gradual evolution, particularly at the last glacial-interglacial transition. The Riss-Eemian (Termination II) and Würm-Holocene (Termination I) climate transitions significantly differ from one another, with the lacustrine system reacting well before (by about 10,000 years) local vegetation change at the Riss-Eemian transition, and peak lake productivity lagging forest expansion by several thousand years at the Würm-Holocene transition. The interruption of the Würm glaciation by a moderate forest phase around 50-45 kyr, is probably one of the main causes of the presence of forest refugia which enabled, together with probable moderating effect of a large lake on local climate, the early expansion of forests during the Würm-Holocene transition. We suggest that during the Riss glaciation no such moderate forest phase existed. The Riss glaciation is well known to have developed larger glaciated areas around the Alpes than the Würm (van Husen, 2004) and there is some evidence of larger, prewürm, glaciations in the area of Lake Ohrid. However, the corresponding moraines are not yet dated and continuous pollen records for the Riss

glaciation are still lacking. In contrast, the delayed lake response to global warming at the last glacial-interglacial transition, shown by calcite production peaking at 6000 cal yr BP, illustrate the threshold response of the geochemical system which was completely blocked during the late Würm glaciation. The succession of abrupt climate changes – especially the Bölling/Alleröd-Younger Dryas sequence and the “8.2 kyr cold event” – in this mountainous area probably accentuated this delay.

By using a large range of paleoenvironmental proxies we were able to detect climate changes even during glacial phases when calcite and the associated stable isotope records are lacking. This study illustrates the great potential of Lake Ohrid as an archive of southern European/Mediterranean climate and environment over the entire Quaternary.

Acknowledgements

This work was supported by CNRS grants from the French ECLIPSE program. Thanks are due to G. Touchais (French School of Athens, Greece and Paris 1 University, France) and P. Lera (Archaeological museum of Korçë, Albania) for support during fieldwork and authorizations, to S. Desruelle (Paris XII University, France) for drawing and to A. Bitri, J.-J. Chateauneuf (BRGM, Orléans, France), A. Brauer (Potsdam, Germany), J.-L. de Beaulieu (CNRS, Aix-en-Provence, France) and D. Verschuren (University of Gent, Belgium) for helpful discussions. H. Hooghiemstra and the second anonymous reviewer are acknowledged for helpful suggestions to improve the manuscript.. AMS dating was provided by UMSARTEMIS (Saclay, France) AMS Facilities. LSCE contribution n°3902.

References

- Aksu, A.E., Jenner, G., Hiscott, R.N., Dşler, E.B., 2008. Occurrence, stratigraphy and geochemistry of Late Quaternary tephra layers in the Aegean sea and the Marmara sea. *Marine Geol.* **252**, 3-4, 174-192.
- Allen, J.R.M., Huntley, B., 2009. Last Interglacial palaeovegetation, palaeoenvironments and chronology: a new record from Lago Grande di Monticchio, southern Italy. *Quatern. Sci. Rev.s* **28**, 15-16, 1521-1538.
- Bard, E., 1998. Geochemical and geophysical implications of the radiocarbon calibration. *Geochim. Cosmochim. Acta* **62**, 2025-2038.
- Belmecheri, S., Namiotko, T., Robert, C., von Grafenstein, U., Danielopold, D.L., 2009. Climate controlled ostracod preservation in Lake Ohridnext term (Albania, Macedonia). *Palaeogeogr., Palaeoclimatol., Palaeoecol.* **277**, 3-4, 236-245.
- Berger, A., 1978. Long-term variations of caloric insolation resulting from the earth's orbital elements. *Quatern. Res.* **9**, 139–167.
- Bordon, A. 2009. *Dynamique de la vegetation et vériations climatiques dans les Balkans au cours du dernier cycle climatique à partir des séquences polliniques des lacs Maliq et Ochrid (Albanie)*. Unpublished Thesis, University of Franche-Comté.
- Bordon, A., Peyron, O., Lézine, A.-M., Brewer, S., Fouache, E. 2009. Late-Glacial and Holocene climate in southern Balkans (Lake Maliq) from pollen data. *Quatern. Intern.* **200**, 1-2, 19-30.
- Brauer, A., Allen, J.R.M., Mingram, J., Dulski, P., Wulf S., Huntley, B., 2007. Evidence for last interglacial chronology and environmental change from Southern Europe, *PNAS* **104**, 2, 450–455.
- Brewer, S., Guiot, J., Sanchez-Goni, M.-F., Klotz, S. 2008. The climate in Europe during the Eemian: a multi-method approach using pollen data. *Quatern. Sci. Rev.* **27**, 2303-2315.
- Calanchi, N., Dinelli, E., 2008. Tephrostratigraphy of the last 170 ka in sedimentary successions from the Adriatic Sea. *J. Volcanol. Geotherm. Res.* **177**, 81-95.
- Campbell, I. B., Claridge, G.G.C., 1998. The influence of moisture on the development of soils of the cold deserts of Antarctica. *Geoderma* **28**, 221-238.
- Caron, B., Sulpizio, R., Zanchetta, G., Siani, G., Santacrose, R., submitted. The Late Holocene to Pleistocene tephrostratigraphic record of Lake Ohrid (Albania). *C. R.*

Geoscience.

- Chamley, H. 1989. *Clay Sedimentology*. Springer.
- Chester, P.I., Raine, J.I. 2001. Pollen and spores keys for Quaternary deposits in the northern Pindos mountains, Greece. *Grana* **40**, 299-387.
- Civetta, L., Cornette, Y., Crisci, G., Gillot, P.Y., Orsi, G., Requejo, C.S. 1984. Geology, geochronology and chemical evolution of the island of Pantelleria. *Geol. Mag.* **121**, 541-562
- Civetta, L., Cornette, Y., Gillot, P.Y., Orsi, G. 1988. The eruptive history of Pantelleria. (Sicily Channel) in the last 50 ka. *Bull. Volcanol.* **50**, 47-57.
- De Vivo, B., Rolandi, G., Gans, P.B., Calvert, A., Bohron, W.A., Spera, F.J., Belkin, H.E. 2001. New constraints on the pyroclastic eruptive history of the Campania volcanic Plain (Italy), *Mineral. Petrol.* **73**, 47–65.
- Di Vito, M., Sulpizio, R., Zanchetta, R., D'Orazio, M. 2008. The late Pleistocene pyroclastic deposits of the Campanian Plain: new insights on the explosive activity of Neapolitan volcanoes. *J. Volcanol. Geotherm. Res.* **177**, 1, 19-48.
- Denèfle, M., Lézine, A.-M., Fouache, E., Dufaure, J.J., 2000. First pollen data from Albania: a 12,000 years history of lake Maliq. *Quatern. Res.* **54**, 423-432.
- Dumurdzanov, N., Serafimovski, T., Burchfiel, B.C., 2005. Cenozoic tectonics of Macedonia and its relation to the South Balkan extensional regime. *Geosphere* **1**, 1–22.
- Eugster, H.P., Kelts, K., 1983. Lacustrine chemical sediments, in: Goudie, G., Pye K. (Eds.), *Chemical sediments and Geomorphology*. London, Academic Press, pp. 321-368.
- Fægri, K., Iversen, J. 1989. *Textbook of pollen analysis* (4th edition). John Wiley & Sons, New York.
- Genty, D., Blamart, D., Ouahdi, R., Gilmour, M., Baker, A., Jouzel, J., Van-Exter, S., 2003. Precise dating of Dansgaard–Oeschger climate oscillations in Western Europe from stalagmite data, *Nature* **421**, 833–837.
- Genty, D., Combourieu Nebout, N., Hatté, C., Blamart, D., Ghaleb, B., Isabello, L., 2005. Rapid climatic changes of the last 90 kyrs recorded on the European continent. *C. R. Geosciences* **337**, 10-11, 970-982.
- Giaccio, B., Isaia, R., Fedele, F.G., Di Canzio, E., Hoffecker, J., Ronchitelli, A., Sinitsyn, A.A., Anikovich, M., Lisitsyn, S.N., Popov, V.V., 2008. The Campanian Ignimbrite and Codola tephra layers: two temporal/stratigraphic markers for the Early Upper Palaeolithic

- in southern Italy and eastern Europe. *J. Volcanol. Geotherm. Res.* **177**, 1, 208-226.
- Gouzy, A., Malaizé, B., Pujol, C., Charlier, K., 2004. Climatic « pause » during Terminaison II identified in shallow and intermediate waters off the Iberian margin. *Quatern. Sci. Rev.* **23**, 14-15, 1523-1528.
- Keller, J., Ryan, W.B.F., Ninkovich, D., Altherr, R., 1978. Explosive volcanic activity in the previous termMediterraneannext term over the past 200,000 yrs as recorded in deep-sea sediments, *Geol. Soc. Amer. Bull.* **89**, 591–604.
- Klie, W., 1939a. Studien über Ostracoden aus dem Ohridsee: I. Candocyprinae, *Archiv Hydrobiol.* **35**, 28–45.
- Klie, W., 1939b. Studien über Ostracoden aus dem Ohridsee: II. Limnocytherinae und Cytherinae (Nebst der Beschreibung einer neuen *Leptocythere*-Art. aus einem Flusse des Stromgebietes der Donau), *Archiv Hydrobiol.* **35**, 631–646.
- Klie, W., 1942, 1942. Studien über Ostracoden aus dem Ohridsee: III. Erster Nachtrag, *Archiv Hydrobiol.* **38**, 254–259.
- Kraml, M., 1997. *Laser-40Ar/39Ar-Datierungen an distalen marinen tephren des jungquartären mediterranen Vulkanismus (Ionisches Meer, METEOR-Fahrt 25/4)*. Ph.D. Thesis, Albert-Ludwigs Universität Freiburg i.Br.
- Lézine, A.-M., Saliège, J.-F., Robert, C., Werth, F., Inizan, M.-L., 1998. Holocene lakes from Ramlat-as Sab'atayn (Yemen) illustrate the impact of monsoon activity in Southern Arabia. *Quatern. Res.* **50**, 290-299.
- Mahood, G.A., Hildreth, W., 1986. Geology of the peralkaline volcano at Pantelleria, strait of Sicily. *Bull. Volcanol.* **48**, 143-172.
- Matzinger, A., Spirkovski, Z., Patceva, S., Wüest, A., 2006. Sensitivity of Ancient Lake Ohrid to Local Anthropogenic Impacts and Global Warming. *J. Great Lakes Res.* **32**, 158–179.
- Mikulić, F., 1961. Nove *Candona* vrste iz Ohridskog Jezera, *Bull. Mus. Hist. Nat. Belgrade* **17 B**, 87–107.
- Nicot, J., Chardon, M., 1983. On the morphotectonic background and the evolution of natural environments and limestone relief in Western Yugoslavian Macedonia. *Méditerranée*, 37-52 (in French).
- Okuda, M., Yasuda, Y., Setoguchi, T., 2001. Middle to Late Pleistocene vegetation history and climatic changes at Lake Kopais, Southeast Greece. *Boreas* **30**, 73–82.

- Paterne, M., Guichard, F., Duplessy, J.-C., Siani, G., Sulpizio, R., Labeyrie, J., 2008. A 90,000–200,000 yrs marine tephra record of Italian volcanic activity in the Central Mediterranean Sea. *J. Volcanol. Geotherm. Res.* **177**, 1, 187-196.
- Petschick, R., 1998. *Mac Diff version 3*. Online: <http://www.servermac.geologie.uni-frankfurt.de>.
- Pini, R., Ravazzi, C., Donegana, M., 2009. Pollen stratigraphy, vegetation and climate history of the last 215 ka in the Azzano Decimo core (plain of Friuli, north-eastern Italy). *Quatern. Sci. Rev.* **28**, 13-14, 1268-1290.
- Pyle, D.M., Ricketts, G.D., Margari, V., van Andel, T.H., Sinitsyn, A.A., Praslov, N.D., Lisitsyn, S., 2006. Wide dispersal and deposition of distal tephra during the Pleistocene 'Campanian Ignimbrite/Y5' eruption, Italy. *Quatern. Sci. Rev.* **25**, 21-22, 2713-2728.
- Reille, M., 1992. *Pollen and spores of Europe and North Africa*. Laboratoire de botanique historique et palynologie, Marseille (in French).
- Reille, M., de Beaulieu, J.-L., Svobodova, H., Andrieu-Ponel, V., Goeury, C., 2000. Pollen analytical biostratigraphy of the last five climatic cycles from a long continental sequence from the Velay region (Massif Central, France). *J. Quatern. Sci.* **15**, 7, 665-685.
- Roelofs, A.K., Kilham, P., 1983. The diatom stratigraphy and paleoecology of Lake Ohrid, Yugoslavia. *Palaeogeogr., Palaeoclimato., Palaeoecol.* **42**, 225-245.
- Rousseau, D.D., Hatté, C., Guiot, J., Duzer, D., Schevin, P., Kukla, G., 2006. Reconstruction of the Grande Pile Eemian using inverse modelling of biome and $\delta^{13}\text{C}$. *Quatern. Sci. Rev.* **25**, 21-22, 2806-2819.
- Sánchez Goñi, M.-F., 2007. Introduction to climate and vegetation in Europe during MIS5. *Develop. Quatern. Sci.* **7**, 197-205.
- Sánchez Goñi, M.-F., Eynaud, F., Turon, J.-L., Shackleton, N.J., 1999. High resolution palynological record off the Iberian margin: direct land-sea correlation for the Last Interglacial complex. *EPSL* **171**, 1, 123-137.
- Sánchez Goñi, M.-F., Loutre, M.-F., Crucifix, M., Peyron, O., Santos, L., Duprat, J., Malaizé, B., Turon, J.-L., Peypouquet, J.-P., 2005. Increasing vegetation and climate gradient in Western Europe over the Last Glacial Inception (122–110 ka): data-model comparison. *EPSL* **231**, 1-2, 111-130.
- Sirocko, F., Claussen, M., Litt, T., Sánchez Goñi, M.-F., Berger, A., Boettger, T., Diehl, M., Desprat, S., Delmonte, B., Degering, D., Frechen, M., Geyh, M.A., Groeger, M.,

- Kageyama, M., Kaspar, F., Kühl, N., Kubatzki, C., Lohmann, G., Loutre, M.-F., Müller, U. 2007. Chronology and climate forcing of the last four interglacials. *Develop. Quatern. Sci.* **7**, 597-614.
- Stabel, H.H., 1986. Calcite precipitation in Lake Constance: chemical equilibrium, sedimentation, and nucleation by algae. *Limnol. Oceanogr.* **31**, 1081-1093.
- Stankovic, S., 1960. The Balkan Lake Ohrid and its Living World. Den Haag.
- Stuiver, M., Reimer, P.J., Reimer, R.W., 2005. *CALIB 5.0*. [WWW program and documentation]. <http://calib.qub.ac.uk/calib/>.
- Talbot, M.R., Allen, P.A., 1996. Lakes, in: Reading, M. G. (Ed.), *Sedimentary Environments*. Blackwell, London, pp. 83-124.
- Tzedakis, P.C., 2005. Towards an understanding of the response of southern European vegetation to orbital and suborbital climate variability. *Quatern. Sci. Rev.* **24**, 1585-1599.
- Tzedakis, P.C., Lawson, I.T., Frogley, M.R., Hewitt, G.M., Preece, R.C., 2002. Buffered tree population changes in a Quaternary refugium: evolutionary implications. *Science* **297**, 2044-2047.
- Tzedakis, P.C., Frogley, M.R., Heaton, T.H.E., 2002. Duration of last interglacial conditions in Northwestern Greece. *Quatern. Res.* **58**, 53-55.
- Tzedakis, P.C., Manus, P.C., Hooghiemstra, H., Oppo, D.W., Wijmstra, T.A., 2003. Comparison of changes in vegetation in northeast Greece with records of climate variability on orbital and suborbital frequencies over the last 450,000 years. *EPSL* **212**, 197-212.
- Tzedakis, P.C., Hooghiemstra, H., Palike, H., 2006. The last 1.35 million years at Tenaghi Philippon: revised chronostratigraphy and long-term vegetation trends. *Quatern. Sci. Rev.* **25**, 3416-3430.
- van Husen, D., 2004. Quaternary glaciation in Austria. *Develop. Quatern. Sci.* **2**, 1, 1-13.
- Wagner, B., Sulpizio, R., Zanchetta, G., Wulf, S., Wessels, M., Daut, G., Nowaczyk, N., 2008. The last 40 ka teprostratigraphic record of Lake Ohrid, Albania and Macedonia: a very distal archive for ash dispersal from Italian volcanoes. *J. Volcanol. Geotherm. Res.* **177**, 71-80.
- Wagner, B., Reicherter, K., Daut, G., Wessels, M., Matzinger, A., Schwalb, A., Spirkovski, Z., Sanxhaku, M., 2008. The potential of Lake Ohrid for long-term palaeoenvironmental reconstructions. *Palaeogeogr., Palaeoclimatol., Palaeoecol.* **259**, 341-356.
- Weaver, C.E., 1989. *Clays, Muds, and Shales*. Elsevier.

- Wulf, S., Brauer, A., Mingram, J., Zolitschka, B., Negendank, J.F.W., 2006. Distal tephra in the sediments of the Monticchio maar lakes, in: Principe, C. (Ed.), *La Geologia del Monte Vulture*, pp. 115–122.
- Zanchetta, G., Sulpizio, R., Giaccio, B., Siani, G., Paterno, M., Wulf, S., D'Orazio, M. 2008. The Y-3 tephra: a stratigraphic marker for the Last Glacial successions of the Central Mediterranean Basin. *J. Volcanol. Geotherm. Res* **177**, 1, 145-154.

Figure captions:

Figure 1: Geological/geomorphological map of the Lake Ohrid basin, southern Balkan, showing the location of the core site.

Figure 2: Age-depth model for core JO2004. The figure shows, from left to right, the main granulometric units reported for the composite section (in grey), the calcite content (in blue), the radiocarbon-dated levels (in red) and the tephra layers (in dark blue) used for the construction of the age -model. The red curve shows our age model which, takes into account the gap in the sedimentary record corresponding to a large part of the St Germain I pollen zone (see Belmecheri et al., 2009 for details).

Figure 3: Total alkali vs. silica diagram of glass composition of the recognised tephra layers. (a) and (b) indicate two different compositional groups within the same tephra layer.

Figure 4: Lake Ohrid core JO2004 multiproxy record showing from left to right: radiocarbon ages, main granulometric units, magnetic susceptibility (on both cores JO2004-1 and JO2004-1a); sediment geochemistry with Sr/Ti (dark blue) ratio and majors elements Al₂O₃ (light blue), SiO₂ (purple), Fe₂O₃ (light green) and LOI (brown); bulk mineralogy with clays (purple), quartz (orange), calcite (light blue), and feldspar (black); main clay minerals with illite (dark blue), and smectite (pink); the main pollen types and the sum of arboreal pollen percentages; $\delta^{13}\text{C}$ of Candonid ostracodes (dark blue). Note the lack of ostracod isotope records during phases of calcite absence.

Figure 5: Comparison between two independent chronologies of environmental changes in southern Europe. Upper panel: (A) June insolation curves for 65°N, (B) benthic foraminiferal $\delta^{18}\text{O}$ from ODP 980 (latitude: 55°29.1'N longitude: 14°42.1'W), representing the ice volume/sea-level component of sea-water $\delta^{18}\text{O}$, planktonic-foraminiferal $\delta^{18}\text{O}$ from core ODP 980, and (C) the tree-pollen percentage curve from Tenaghi Philippon plotted on the time scale of Tzedakis et al. (2003) (redrawn from Tzedakis (2005); see references therein). Lower panel: June insolation curves for 65°N (Berger, 1978), pollen percentage curves for steppe elements and trees, and the percent calcite content of core JO-2004 1 (this study) plotted on the same time scale. Grey vertical bars show the correspondence between the two independent

data sets.

Figure 6: Comparison between Ohrid (this study) and Monticchio (Brauer et al., 2007) pollen data. The synthetic pollen diagrams show the main vegetation types encountered in the two pollen sites. The overall development of vegetation (e.g., tree percentages variations, changes in Mediterranean vegetation types) fits to a high degree, and has been used to validate our age-model. This figure highlights the near-continuous dominance of mountain vegetation types at Ohrid due to the steep altitudinal gradient in the catchment area. Note the gradual increase in tree pollen percentages at glacial-interglacial transitions.

Table captions:

Table 1: Mineralogical and Geochemical composition of the main geological outcrops in the Ohrid-Maliq basin.

Table 2: Radiocarbon measurements.

Table 3: Energy dispersive spectrometry (EDS) analyses of tephra layers, which are labelled with the corresponding reconstructed depth in cm. The sample at 240-246 cm shows two analyses with a different alkali ratio from the main group, and are reported along with their mean.

Figure 1:

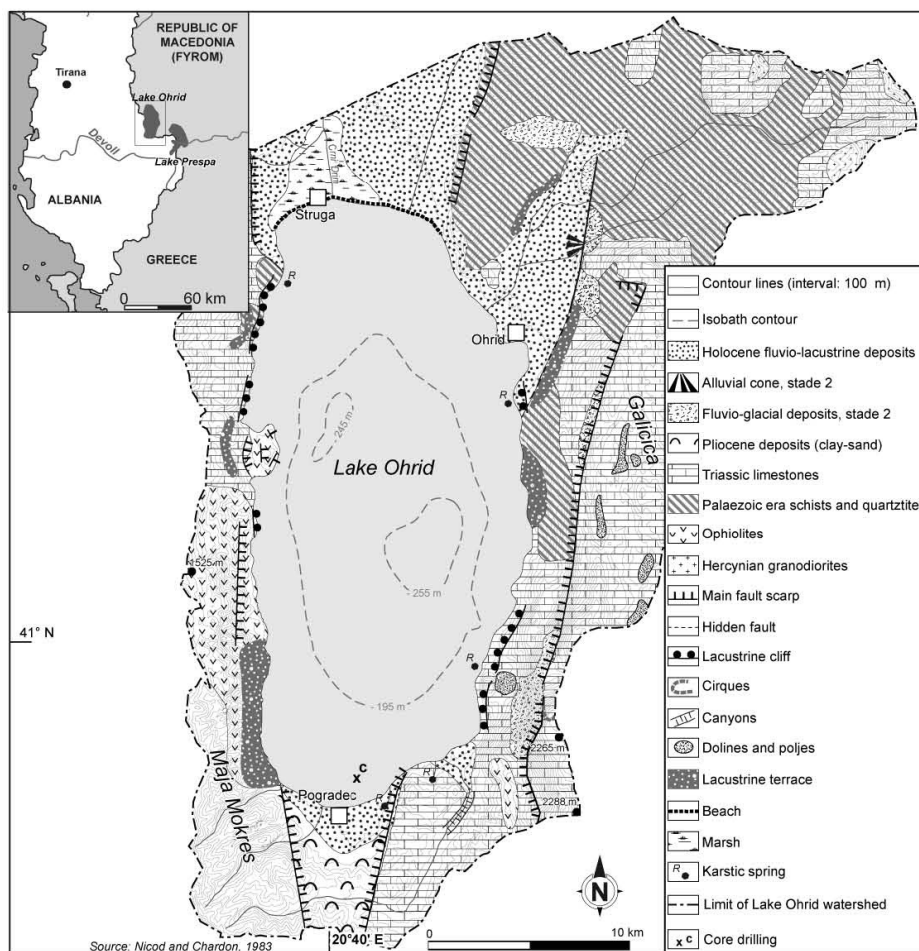


Figure 2:

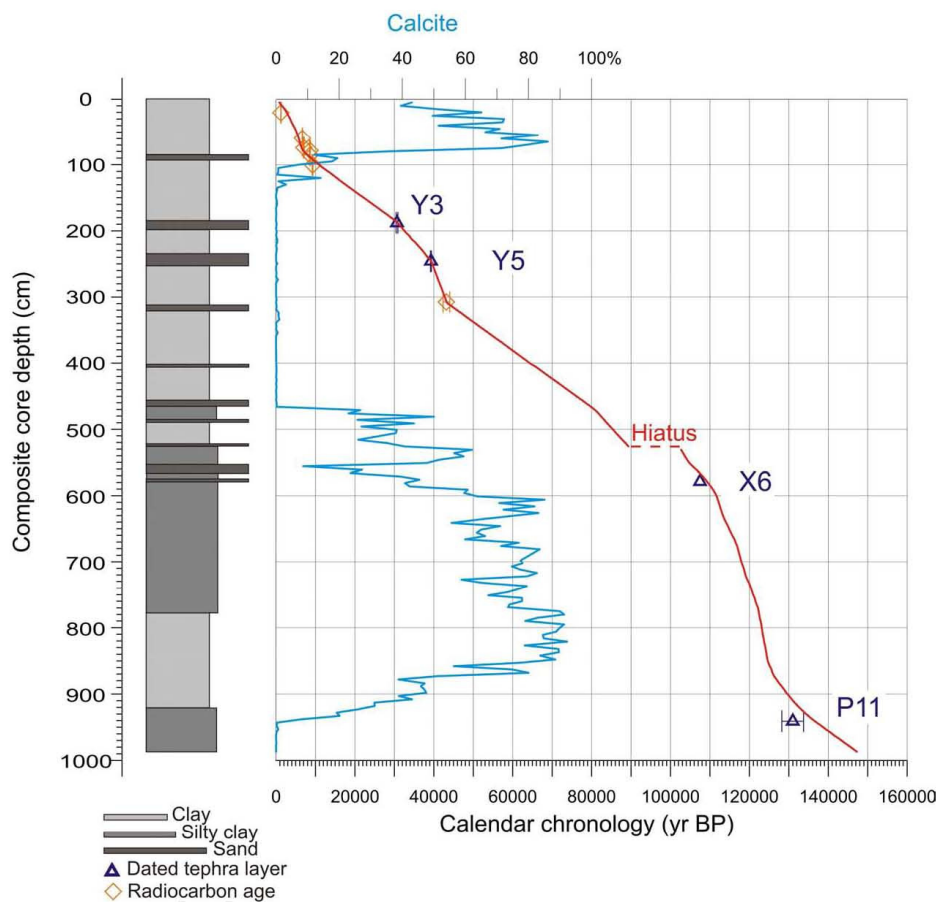


Figure 3:

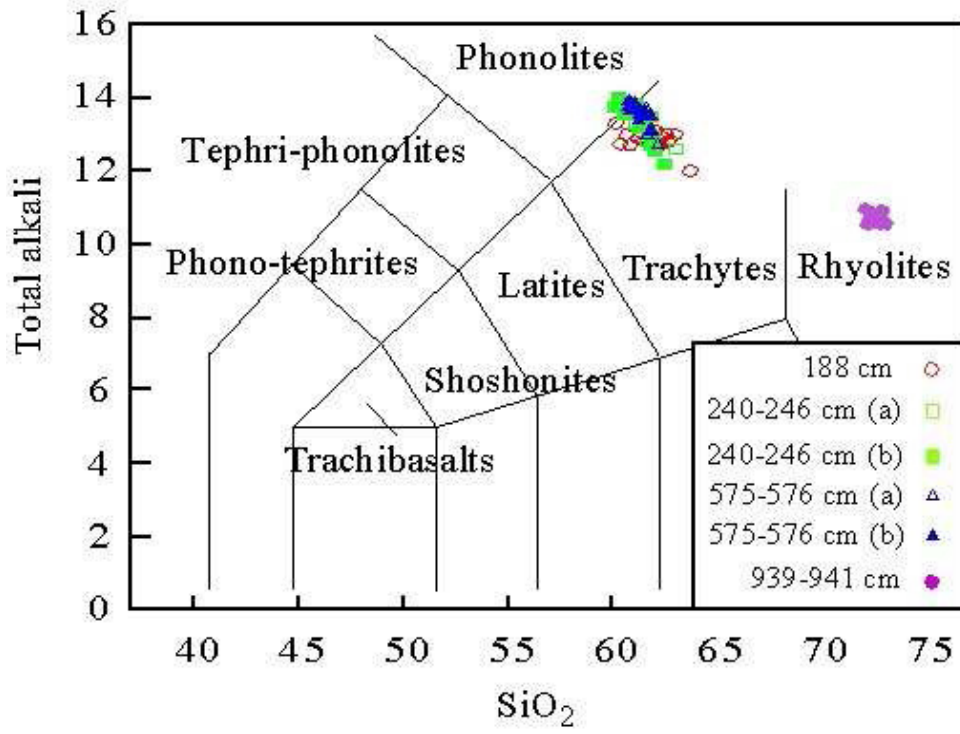


Figure 4:

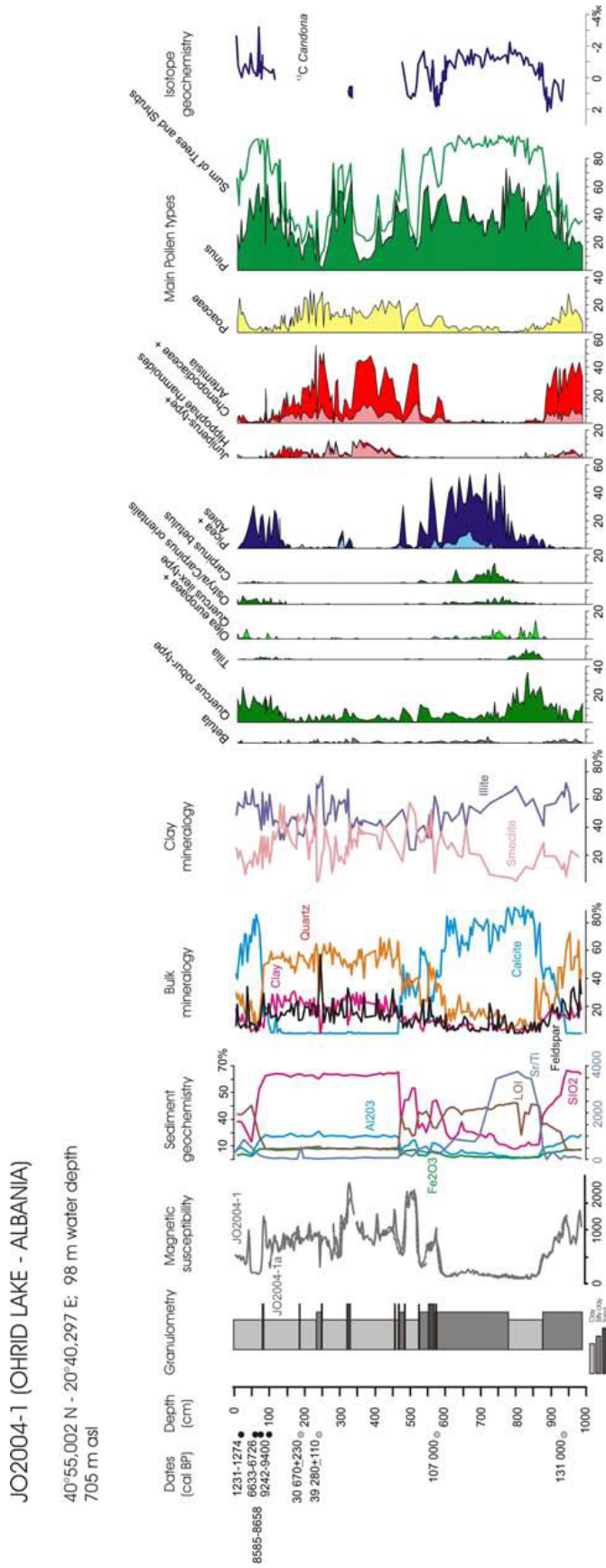


Figure 5:

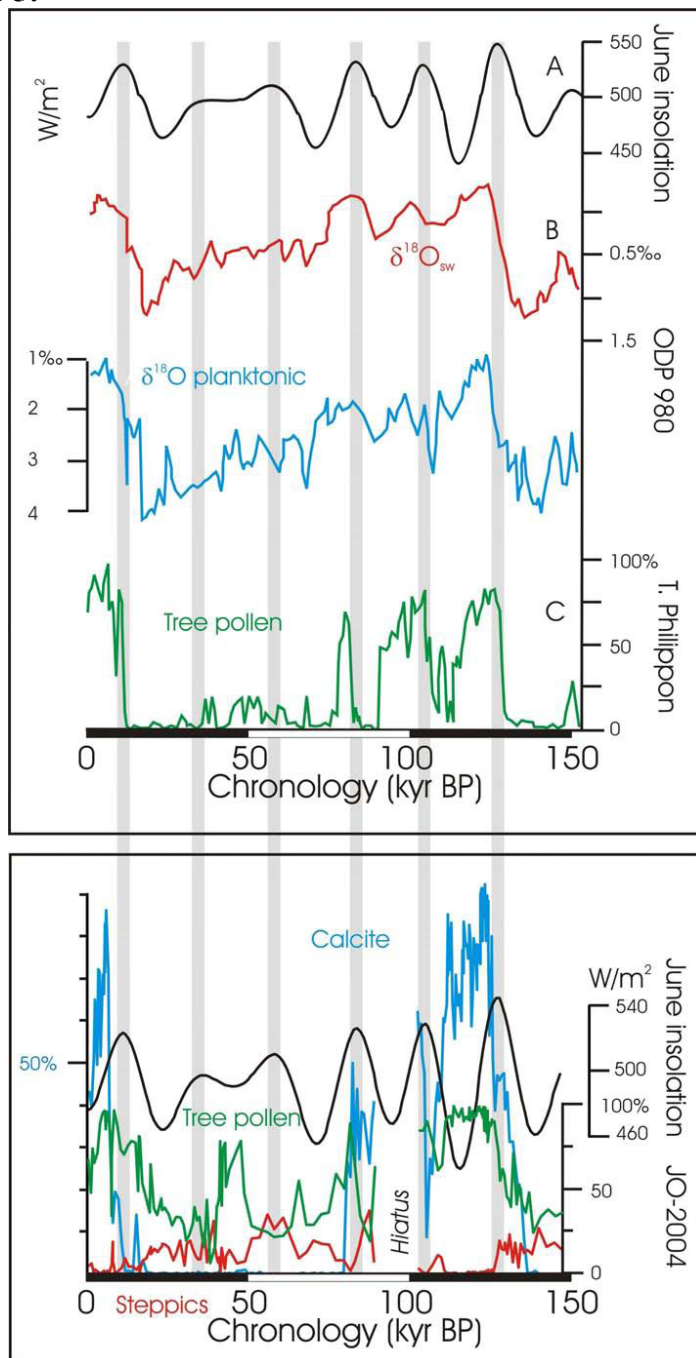


Figure 6:

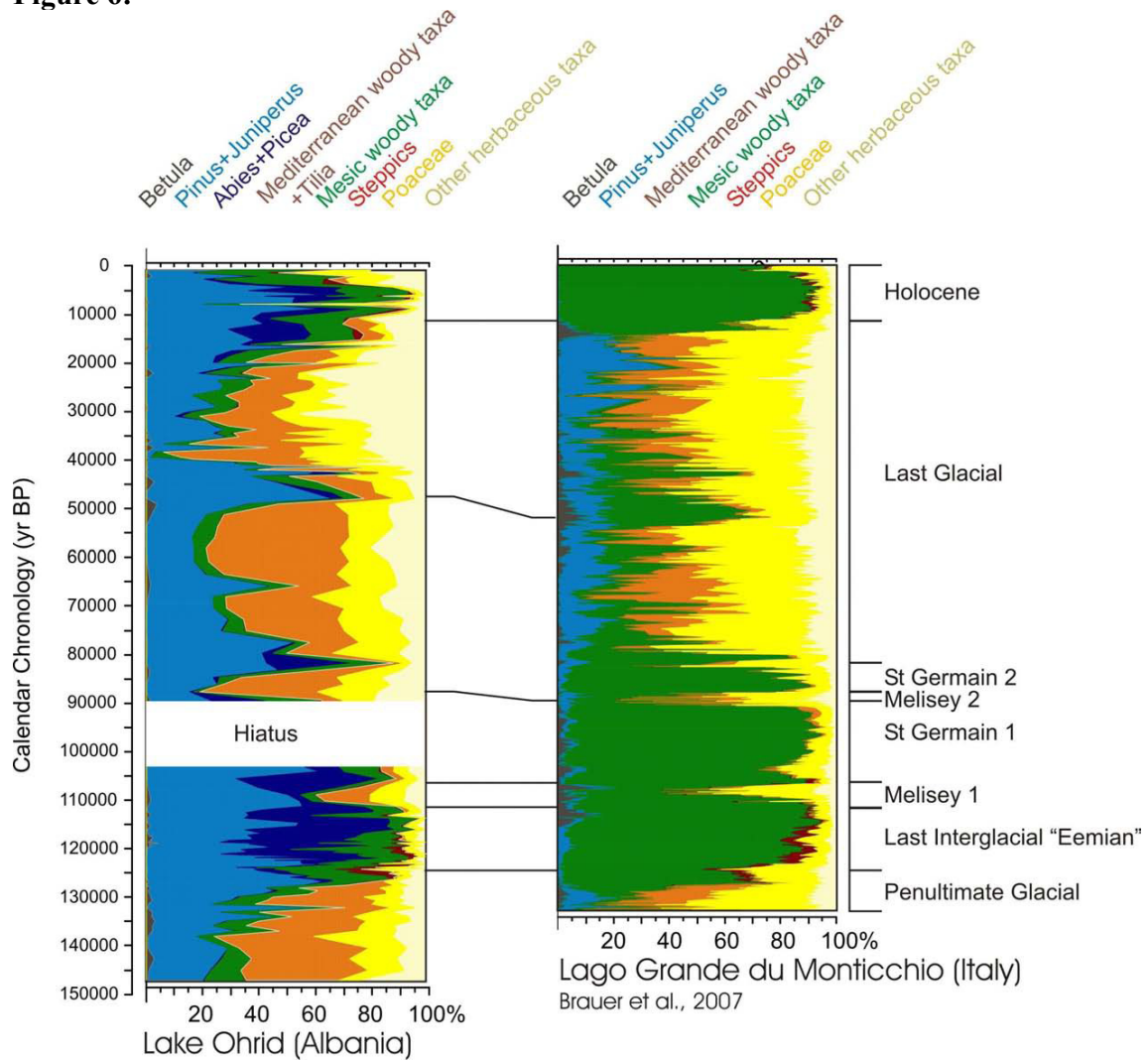


Table 1:

nature of substrate	Clay minerals (%)	Quartz (%)	Feldspars (%)	Pyroxenes (%)	Ophiolite mine	Calcite (%)	Dolomite (%)	Gypsum (%)
Pliocene fluvial deposits	10	77	12	1	0	0	0	0
Triassic limestones	0	0	0	0	0	100	0	0
molasse	25	52	10	0	2	0	0	2
ophiolite (weathered)	2	0	8	0	67	2	21	0
Middle Miocene claystones and limestones	20	44	8	0	0	24	0	4
Pliocene claystones and sandstones	18	54	10	0	8	4	0	0
ophiolite	0	0	0	1	99	0	0	0
Triassic limestones	1	0	0	0	0	99	0	0
Late Cretaceous limestones	2	1	0	0	0	97	0	0
ophiolite	2	0	0	1	65	0	2	0
Lower Miocene claystones and limestones	22	38	10	0	0	15	15	0
ophiolite	0	0	0	0	100	0	0	0

nature of substrate	Lizardite (%)	Chlorite (%)	Illite (%)	Mixed-layered Cl	Smectite (%)	Kaolinite (%)
Pliocene fluvial deposits	0	0	17	63	4	14
molasse	0	0	7	73	0	20
ophiolite (weathered)	81	0	0	0	19	0
Middle Miocene claystones and limestones	0	11	25	64	0	0
Pliocene claystones and sandstones	0	0	17	0	40	43
Late Cretaceous limestones	0	0	51	19	0	10
ophiolite	97	0	0	0	3	0
Lower Miocene claystones and limestones	0	19	34	47	0	0
Middle Miocene claystones and limestones	5	0	11	84	0	0

nature of substrate	SiO ₂	Al ₂ O ₃	Fe ₂ O ₃	MgO	CaO	K ₂ O
Pliocene fluvial deposits	66.6	14.83	8.12	1.38	0.77	2.08
Triassic limestones	0.75	0.12	6.07	0.54	58.25	0.03
molasse	65.8	13.1	5.26	1.18	0.42	1.71
ophiolite (weathered)	41.5	0.5	8.3	35.5	0.75	0.01
Middle Miocene claystones and limestones	47.8	9.7	4.57	3.17	14.1	1.97
Pliocene claystones and sandstones	67.2	11.25	4.78	1.03	4.88	3.00
ophiolite	38.7	0.15	7.4	37.8	0.20	0.01
Triassic limestones	0.3	0.015	0.04	0.45	56.00	0.03
Late Cretaceous limestones	1.15	0.24	0.16	0.59	56.00	0.09
ophiolite	38.65	0.44	8.2	36.4	0.16	0.00
Lower Miocene claystones and limestones	44.5	11.09	6.25	5.72	10.50	3.18
ophiolite	38	0.26	7.7	36.8	0.15	0.01
Middle Miocene claystones and limestones	1.35	0.28	0.16	3.84	55.00	0.07

Table 2:

Laboratory number (Artemis-Saclay)	Sample	Mean Composite Depth (cm)	¹⁴ C age	error	Calendar ages BP (one sigma)	Material
SacA 8010	JO2004-1A020	20.5	1285	± 30	1181-1274	terrestrial plant remains
SacA 8011	JO2004-1A059	59.5	5840	± 35	6572-6726	terrestrial plant remains
002653	JO2004-1A074	74	6130	± 80	6837-7158	terrestrial plant remains
002654	JO2004-1A078	78.5	7800	± 80	8451-8803	terrestrial plant remains
SacA 8012	JO2004-1A085	85.5	7850	± 40	8588-8700	terrestrial plant remains
SacA 8013	JO2004-1A100	100.5	8275	± 40	9141-9400	terrestrial plant remains
002655	JO2004-1B113	307.6	39100	± 1200	42000	terrestrial plant remains

Table 3a:

188 cm Sample	1	2	3	4	5	6	7	8	9	10	11	12	mean	sd
SiO ₂	63.42	60.62	61.46	62.23	61.64	62.08	62.29	62.77	62.37	62.42	61.02	61.22	63.42	0.79
TiO ₂	0.25	0.38	0.21	0.2	0.35	0.26	0.21	0.31	0.35	0.28	0.43	0.53	0.28	0.20
Al ₂ O ₃	18.49	18.8	18.75	18.41	18.51	18.74	18.73	18.48	18.58	18.51	18.81	18.61	18.49	0.14
Fe (total)	2.58	3.51	3.03	2.84	3.22	2.77	2.75	2.5	2.86	2.77	3.22	3.09	2.88	0.29
MnO	0.13	0.13	0.08	0	0.17	0.11	0	0	0.08	0.14	0	0	0.13	0.07
MgO	0.31	0.89	0.57	0.55	0.44	0.39	0.37	0.41	0.38	0.42	0.72	0.6	0.31	0.17
CaO	2.17	2.71	2.42	2.16	2.33	2.17	2	1.95	2.14	2.06	2.47	2.37	2.17	0.22
Na ₂ O	4.06	3.27	3.8	4.35	3.93	4.05	4.74	4.89	3.97	4.69	3.71	3.7	4.06	0.48
K ₂ O	7.91	9.4	9.23	8.65	8.94	8.82	8.25	8.05	8.77	8.1	9.15	9.45	7.91	0.54
P ₂ O ₅	0	0	0	0	0	0	0	0	0	0	0	0	0.00	0.00
Cl	0.69	0.29	0.45	0.61	0.47	0.61	0.66	0.65	0.5	0.61	0.46	0.44	0.69	0.12
Total	100.01	100	100	100	100	100	100	99.99	100	100	99.99	100.01	100.01	0.02
Total alkali K ₂ O/Na ₂ O	11.97	12.67	13.03	13.00	12.87	12.87	12.99	12.94	12.74	12.79	12.86	13.15	11.97	
	1.95	2.87	2.43	1.99	2.27	2.18	1.74	1.65	2.21	1.73	2.47	2.55	1.95	



